frontiers | Research Topics

Paradigm shifts and innovations in cellular neuroscience

Edited by
Enrico Cherubini, Dirk M. Hermann, Arianna Maffei, Marie-Ève Tremblay, Egidio D'Angelo and Christian Hansel

Published in
Frontiers in Cellular Neuroscience

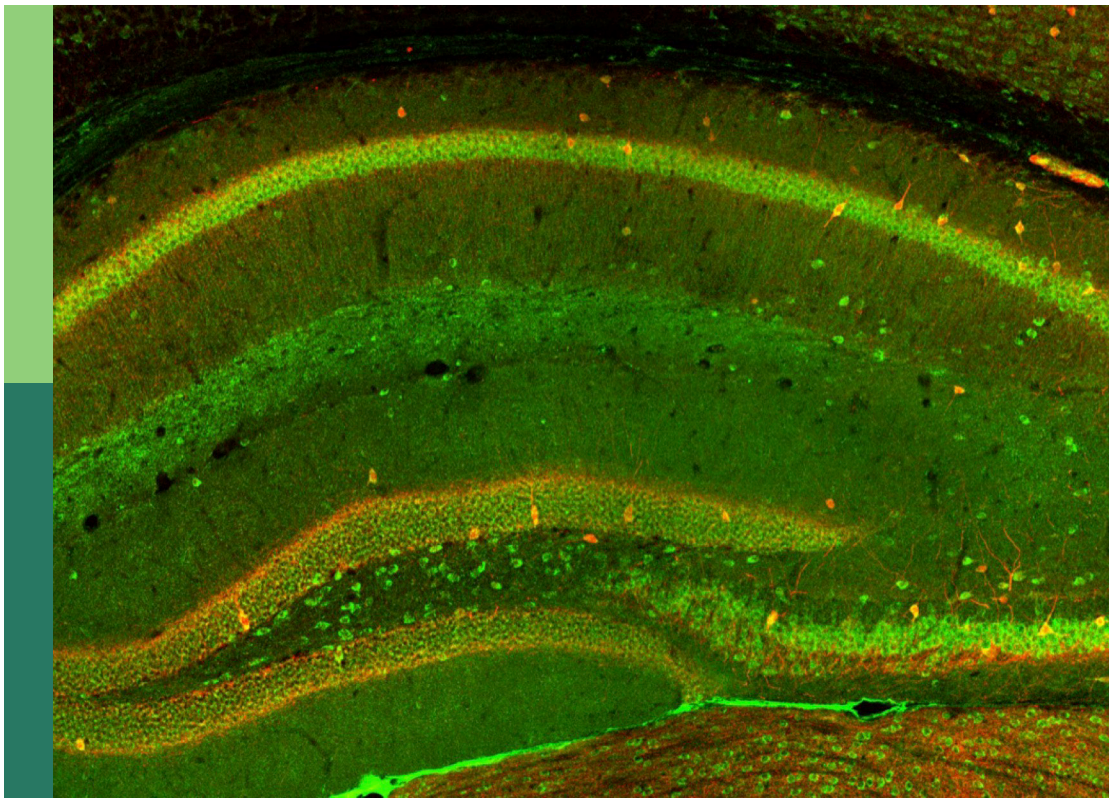

ISSN 1664-8714
ISBN 978-2-8325-6647-3
DOI 10.3389/978-2-8325-6647-3

Generative AI statement
Any alternative text (Alt text) provided alongside figures in the articles in this ebook has been generated by Frontiers with the support of artificial intelligence and reasonable efforts have been made to ensure accuracy, including review by the authors wherever possible. If you identify any issues, please contact us.

About Frontiers

Frontiers is more than just an open access publisher of scholarly articles: it is a pioneering approach to the world of academia, radically improving the way scholarly research is managed. The grand vision of Frontiers is a world where all people have an equal opportunity to seek, share and generate knowledge. Frontiers provides immediate and permanent online open access to all its publications, but this alone is not enough to realize our grand goals.

Frontiers journal series

The Frontiers journal series is a multi-tier and interdisciplinary set of open-access, online journals, promising a paradigm shift from the current review, selection and dissemination processes in academic publishing. All Frontiers journals are driven by researchers for researchers; therefore, they constitute a service to the scholarly community. At the same time, the *Frontiers journal series* operates on a revolutionary invention, the tiered publishing system, initially addressing specific communities of scholars, and gradually climbing up to broader public understanding, thus serving the interests of the lay society, too.

Dedication to quality

Each Frontiers article is a landmark of the highest quality, thanks to genuinely collaborative interactions between authors and review editors, who include some of the world's best academicians. Research must be certified by peers before entering a stream of knowledge that may eventually reach the public - and shape society; therefore, Frontiers only applies the most rigorous and unbiased reviews. Frontiers revolutionizes research publishing by freely delivering the most outstanding research, evaluated with no bias from both the academic and social point of view. By applying the most advanced information technologies, Frontiers is catapulting scholarly publishing into a new generation.

What are Frontiers Research Topics?

Frontiers Research Topics are very popular trademarks of the *Frontiers journals series*: they are collections of at least ten articles, all centered on a particular subject. With their unique mix of varied contributions from Original Research to Review Articles, Frontiers Research Topics unify the most influential researchers, the latest key findings and historical advances in a hot research area.

Find out more on how to host your own Frontiers Research Topic or contribute to one as an author by contacting the Frontiers editorial office: frontiersin.org/about/contact

Paradigm shifts and innovations in cellular neuroscience

Topic editors

Enrico Cherubini — European Brain Research Institute, Italy
Dirk M. Hermann — University of Duisburg-Essen, Germany
Arianna Maffei — Stony Brook University, United States
Marie-Ève Tremblay — University of Victoria, Canada
Egidio D'Angelo — University of Pavia, Italy
Christian Hansel — The University of Chicago, United States

Citation

Cherubini, E., Hermann, D. M., Maffei, A., Tremblay, M.-È., D'Angelo, E., Hansel, C., eds. (2025). *Paradigm shifts and innovations in cellular neuroscience*. Lausanne: Frontiers Media SA. doi: 10.3389/978-2-8325-6647-3

Table of contents

frontiers | Frontiers in Cellular Neuroscience

TYPE Editorial
PUBLISHED 14 July 2025
DOI 10.3389/fncel.2025.1644329

OPEN ACCESS

EDITED AND REVIEWED BY
Ulises Gomez-Pinedo,
Health Research Institute of Hospital Clínico San Carlos, Spain

*CORRESPONDENCE
Enrico Cherubini
✉ cher@sissa.it

RECEIVED 10 June 2025
ACCEPTED 26 June 2025
PUBLISHED 14 July 2025

CITATION
Cherubini E, Maffei A, D'Angelo E, Hermann DM, Tremblay M-È and Hansel C (2025) Editorial: Paradigm shifts and innovations in cellular neuroscience. *Front. Cell. Neurosci.* 19:1644329. doi: 10.3389/fncel.2025.1644329

Editorial: Paradigm shifts and innovations in cellular neuroscience

Enrico Cherubini[1]*, Arianna Maffei[2], Egidio D'Angelo[3], Dirk M. Hermann[4], Marie-Ève Tremblay[5] and Christian Hansel[6]

[1]European Brain Research Institute, Rome, Italy, [2]Stony Brook University, Stony Brook, NY, United States, [3]University of Pavia, Pavia, Italy, [4]Department of Neurology, University Hospital Essen, University of Duisburg-Essen, Essen, Germany, [5]University of Victoria, Victoria, BC, Canada, [6]University of Chicago, Chicago, IL, United States

KEYWORDS

neurotransmitter release, neuronal ensembles, synaptopodin, primary visual cortex, HiPSCs, focal cortical dyslasia type II, tuberous sclerosis, dendritic integration

Editorial on the Research Topic
Paradigm shifts and innovations in cellular neuroscience

In recent years, significant advances in the field of Cellular Neurosciences have contributed to translating basic science into ways to ameliorate diseases affecting the nervous system that carry high economic and social burdens such as neurodevelopmental and neurodegenerative disorders. This has been made possible by emerging technologies such as machine learning and artificial intelligence, humanized mouse and human iPSC models, imaging innovations, brain-computer interfaces, non-invasive brain stimulation, gene editing, identification of biomarkers for drug discovery, etc.

The aim of this Research Topic is to understand the paradigm shifts that have shaped and continue to shape Cellular Neuroscience. This Research Topic includes six Reviews, one Opinion, and four Research Articles.

Reviews

According to the seminal work at the neuromuscular junction by Del Castillo and Katz (1954), transmitter release occurs in packets of relatively constant size (quanta), which are equal to the content of a single vesicle fused to the presynaptic membrane. Fusion is favored by a complex network of mutually interacting proteins including synaptotagmin. Fesce reports how, with the advent of optogenetics, it has been possible to demonstrate that transmitter release can occur also through the transient opening of a pore between the vesicle and the plasma membrane, without the need for the vesicle to completely fuse with the latter (Harata et al., 2006), as already suggested by Bruno Ceccarelli, who called this event "kiss and run."

Long lasting, activity-dependent changes in synaptic strength such as those occurring in Long Term Potentation (LTP) are thought to be the cellular correlates of learning and memory (Bliss and Lomo, 1973). Here, Hansel and Yuste suggest that activity-dependent increases in neuronal excitability can recruit neurons into ensembles and maintain them active. They propose *a permissive gate model* by which the enhanced excitability facilitates ensemble integration by converting subthreshold into supra-threshold connections and

by promoting the propagation of dendritic potentials toward the soma, thus allowing to enhance the EPSP/spike coupling. This cellular plasticity mechanism can take place in the absence of LTP and thus leaves the synaptic weight distribution unchanged.

Learning and memory processes are associated with morphological modifications of dendritic spines (Bourne and Harris, 2007) which are recognized as the loci of synaptic plasticity expression. Wu et al. highlight recent findings on the functional role of synaptopodin, an actin-associated protein found in a subset of dendritic spines of telencephalic neurons, in various forms of Hebbian synaptic plasticity where it plays a central role in regulating postsynaptic calcium dynamics.

Of particular interest are synaptic plasticity processes occurring in the primary visual cortex (V1), which, as demonstrated by anatomical and molecular studies, develop over multiple time windows, from the first trimester to aging (Siu and Murphy, 2018). Murphy and Monteiro provide an overview of human primary visual cortex development, highlighting the molecular mechanisms regulating the expression of glutamatergic and GABAergic receptors involved in V1 Excitatory/Inhibitory balance and experience-dependent plasticity, including the late shift of GluN2A/GluN2B balance, consequent to the loss of GluN2B subunits in adulthood (Siu et al., 2017).

Emerging technologies such as human induced pluripotent stem cell (hiPSCs) are poised to play a crucial role in identifying the cellular and molecular mechanisms underlying genetic neuropathologies such as neurodegenerative diseases and epilepsy. Toward a precision/personalized medicine, Farahani et al. highlights how hiPSCs derived from somatic cells can produce various neuronal cell types in which non-neuronal immune cell types like microglia can be incorporated to develop new therapeutic tools to prevent and treat these disorders. The use of machine learning/artificial intelligence and quantitative neuroimaging representations would enhance precision by integrating hiPSC-neuronal models with patients' biophysical data (Vo et al., 2024).

Molecular analysis of hiPSC from pediatric patients affected by Focal Cortical Dysplasia Type II and Tuberous Sclerosis has facilitated the identification of several dysregulated genes involved in neuronal migration and differentiation which are responsible for cortical malformations and drug-resistant forms of epilepsy (Afshar Saber and Sahin, 2020; Lu et al., 2024). The review by Zhang et al. focuses on balloon/giant cells (BC/GC), commonly found in these malformations, which are unable to generate action potentials, with special emphasis to their electrophysiological and morphological glial-like properties similar to astrocytes. BC/GC express a range of glial markers, such as GFAP, vimentin, and nestin, indicating a heterogeneous population of cells with mixed neuronal and glial characteristics.

Opinion

In different brain areas, distinct synaptic input converging onto Pyramidal neurons (Pn) show a macroscale distribution across large dendritic compartments. In this Opinion paper, Cupolillo et al. discuss how spatially distributed excitatory and inhibitory signals converge and integrate onto Pn to shape the neuronal output. The authors provide experimental and computational evidence that these events closely rely on the ability of neurons to generate different forms of local dendritic spikes. The impact of clustering and cooperative plasticity among glutamatergic synapses and the specific spatial organization of GABAergic inputs on dendritic branches are key determinants for shaping dendritic excitability.

Research articles

Transient elevations of intracellular calcium by voltage-gated calcium channels (VGCCs) activated by back-propagating action potentials play a crucial role in dendritic integration (Stuart and Sakmann, 1994). Using ultrafast membrane potential recordings and calcium imaging techniques, Blömer et al., investigated the kinetics of back-propagating action potentials and associated calcium currents in apical dendrites of layer 5 neocortical pyramidal neurons. In addition, using a realistic NEURON model, they clearly demonstrate that large conductance calcium-dependent potassium channels (BK) are rapidly and selectively activated by N type of VGCCs. Activation of these channels at the dendritic level leads to reduced neuronal excitability.

Early sharp waves (eSPWs) are the earliest network activity observed in the developing rodent hippocampus. In neonates, eSPWs lack high frequency oscillations, called ripples, characteristic of adult SPWs (Leinekugel et al., 2002). Using silicon probes electrodes to record neuronal activity in deep and superficial layers of neonatal medial entorhinal cortex (MEC), Shipkov et al. found that eSPWs are primarily driven by layer 2/3 inputs of the MEC, triggered, *via* sensory feedback, by myoclonic movements. These findings contrast previous results from adult animals, showing that SPWs originating from the hippocampus spread to the entorhinal cortex, thus contributing to memory consolidation.

Recent studies highlighted the physiological role of the ventromedial nucleus of hypothalamus (VMH) in controlling energy and glucose homeostasis (Choi et al., 2013). Using a previously generated BAC transgenic line expressing Cre recombinase under cholecystokinin (CCK) promoter and pharmacological tools, Eftychidis et al. investigated the role of CCK containing neurons, highly expressed in VMH, in regulating food intake, body weight and glucose homeostasis. They found that silencing CCK neurons with DREADDS, or removing them with diphtheria toxin, resulted in increased feeding behavior. Therefore, this approach unveiled new potential targets for obesity treatment.

Finally, Girasole et al. used a nanomotion sensor to monitor, at micro and nanoscale level, the interaction-dependent movements between two clusters of neuroblastoma cells, one of which was growing on a neuro-mechanical oscillator suspended a few hundreds of microns from a Petri dish containing the other. The study reports that cell movements in one compartment are able to influence the other one, located hundreds of microns away. These bidirectional interactions occur *via* acoustic fields produced by vibrations of neuroblastoma cells movements, which, in this way, play a crucial role in cell/cell communication processes.

We thank all those who have contributed to the realization of this Research Topic. We hope that this work will stimulate further studies on new advances in the rapidly growing field of Cellular Neuroscience.

Author contributions

EC: Writing – original draft. AM: Writing – review & editing. ED'A: Writing – review & editing. DH: Writing – review & editing. M-ÈT: Writing – review & editing. CH: Writing – review & editing.

Funding

The author(s) declare that financial support was received for the research and/or publication of this article. This work was supported by the Fondo Ordinario Enti (FOE, DM571/2022) to EC; by the National Institutes of Health grants R01DC019827, R01DC013770, and R01DC015234 to AM; by #NEXTGENERATIONEU (NGEU) and Ministry of University and Research (MUR), National Recovery and Resilience Plan (NRRP), project MNESYS (PE0000006)—A Multiscale integrated approach to the study of the nervous system in health and disease (DN. 155311.10.2022) to ED'A; by the German Research Foundation [grants 389030878, 405358801/428817542 (within FOR2879), 449437943 (within TRR332, project C06), and 514990328] to DH; by the Canada Research Chair program to M-ÈT; and by NIH grant NS062771 to CH.

Conflict of interest

The authors declare that the research was conducted in the absence of any commercial or financial relationships that could be construed as a potential conflict of interest.

The author(s) declared that they were an editorial board member of Frontiers, at the time of submission. This had no impact on the peer review process and the final decision.

Generative AI statement

The author(s) declare that no Gen AI was used in the creation of this manuscript.

Publisher's note

References

Afshar Saber, W., and Sahin, M. (2020). Recent advances in human stem cell-based modeling of tuberous sclerosis complex. *Mol. Autism* 11, 16–24. doi: 10.1186/s13229-020-0320-2

Bliss, T. V., and Lomo, T. (1973). Long-lasting potentiation of synaptic transmission in the dentate area of the anaesthetized rabbit following stimulation of the perforant path. *J. Physiol.* 232, 331–356. doi: 10.1113/jphysiol.1973.sp010273

Bourne, J., and Harris, K. M. (2007). Do thin spines learn to be mushroom spines that remember? *Curr. Opin. Neurobiol.* 17, 381–386. doi: 10.1016/j.conb.2007.04.009

Choi, Y. H., Fujikawa, T., Lee, J., Reuter, A., and Kim, K. W. (2013). Revisiting the ventral medial nucleus of the hypothalamus: the roles of SF-1 neurons in energy homeostasis. *Front Neurosci.* 7:71. doi: 10.3389/fnins.2013.00071

Del Castillo, J., and Katz, B. (1954). Quantal components of the end-plate potential. *J. Physiol.* 124, 560–573. doi: 10.1113/jphysiol.1954.sp005129

Harata, N. C., Choi, S., Pyle, J. L., Aravanis, A. M., and Tsien, R. W. (2006). Frequency-dependent kinetics and prevalence of kiss-and-run and reuse at hippocampal synapses studied with novel quenching methods. *Neuron* 49, 243–256. doi: 10.1016/j.neuron.2005.12.018

Leinekugel, X., Khazipov, R., Cannon, R., Hirase, H., Ben-Ari, Y., and Buzsáki, G. (2002). Correlated bursts of activity in the neonatal hippocampus in vivo. *Science* 296, 2049–2052. doi: 10.1126/science.1071111

Lu, R., Xu, Y., Li, H., Xiong, M., Zhou, W., Feng, W., et al. (2024). Identifying the pathogenicity of a novel NPRL3 missense mutation using personalized cortical organoid model of focal cortical dysplasia. *J. Mol. Neurosci.* 75:3. doi: 10.1007/s12031-024-02304-5

Siu, C. R., Beshara, S. P., Jones, D. G., and Murphy, K. M. (2017). Development of glutamatergic proteins in human visual cortex across the lifespan. *J. Neurosci.* 37, 6031–6042. doi: 10.1523/JNEUROSCI.2304-16.2017

Siu, C. R., and Murphy, K. M. (2018). The development of human visual cortex and clinical implications. *Eye Brain*. 10, 25–36. doi: 10.2147/EB.S130893

Stuart, G. J., and Sakmann, B. (1994). Active propagation of somatic action potentials into neocortical pyramidal cell dendrites. *Nature* 367, 69–72. doi: 10.1038/367069a0

Vo, Q. D., Saito, Y., Ida, T., Nakamura, K., and Yuasa, S. (2024). The use of artificial intelligence in induced pluripotent stem cell-based technology over 10-year period: a systematic scoping review. *PLoS ONE* 19:e0302537. doi: 10.1371/journal.pone.0302537

frontiers | Frontiers in Cellular Neuroscience

TYPE Original Research
PUBLISHED 14 February 2024
DOI 10.3389/fncel.2024.1353895

OPEN ACCESS

EDITED BY
Enrico Cherubini,
European Brain Research Institute, Italy

REVIEWED BY
Kunal Shah,
The University of Texas MD Anderson Cancer Center, United States
Emilio Carbone,
University of Turin, Italy

*CORRESPONDENCE
Marco Canepari
✉ marco.canepari@univ-grenoble-alpes.fr

RECEIVED 11 December 2023
ACCEPTED 24 January 2024
PUBLISHED 14 February 2024

CITATION
Blömer LA, Giacalone E, Abbas F, Filipis L, Tegolo D, Migliore M and Canepari M (2024) Kinetics and functional consequences of BK channels activation by N-type Ca^{2+} channels in the dendrite of mouse neocortical layer-5 pyramidal neurons. *Front. Cell. Neurosci.* 18:1353895. doi: 10.3389/fncel.2024.1353895

Kinetics and functional consequences of BK channels activation by N-type Ca^{2+} channels in the dendrite of mouse neocortical layer-5 pyramidal neurons

Laila Ananda Blömer[1,2], Elisabetta Giacalone[3,4], Fatima Abbas[1,2], Luiza Filipis[1,2], Domenico Tegolo[4], Michele Migliore[3] and Marco Canepari[1,2,5]*

[1]LIPhy, CNRS, Université Grenoble Alpes, Grenoble, France, [2]Laboratories of Excellence, Ion Channel Science and Therapeutics, Valbonne, France, [3]Institute of Biophysics, National Research Council, Palermo, Italy, [4]Dipartimento Matematica e Informatica, Universitá degli Studi di Palermo, Palermo, Italy, [5]Institut National de la Santé et Recherche Médicale, Paris, France

The back-propagation of an action potential (AP) from the axon/soma to the dendrites plays a central role in dendritic integration. This process involves an intricate orchestration of various ion channels, but a comprehensive understanding of the contribution of each channel type remains elusive. In this study, we leverage ultrafast membrane potential recordings (V_m) and Ca^{2+} imaging techniques to shed light on the involvement of N-type voltage-gated Ca^{2+} channels (VGCCs) in layer-5 neocortical pyramidal neurons' apical dendrites. We found a selective interaction between N-type VGCCs and large-conductance Ca^{2+}-activated K^+ channels (BK CAKCs). Remarkably, we observe that BK CAKCs are activated within a mere 500 μs after the AP peak, preceding the peak of the Ca^{2+} current triggered by the AP. Consequently, when N-type VGCCs are inhibited, the early broadening of the AP shape amplifies the activity of other VGCCs, leading to an augmented total Ca^{2+} influx. A NEURON model, constructed to replicate and support these experimental results, reveals the critical coupling between N-type and BK channels. This study not only redefines the conventional role of N-type VGCCs as primarily involved in presynaptic neurotransmitter release but also establishes their distinct and essential function as activators of BK CAKCs in neuronal dendrites. Furthermore, our results provide original functional validation of a physical interaction between Ca^{2+} and K^+ channels, elucidated through ultrafast kinetic reconstruction. This insight enhances our understanding of the intricate mechanisms governing neuronal signaling and may have far-reaching implications in the field.

KEYWORDS

N-type voltage-activated Ca^{2+} channel, BK Ca^{2+}-activated K^+ channel, dendrite, action potential, neocortical layer-5 pyramidal neuron, neuron modelling

1 Introduction

In neocortical pyramidal neurons, action potentials (APs) actively propagate back into the dendritic tree (Stuart and Sakmann, 1994; Stuart et al., 1997), where they elicit transient elevations of intracellular Ca^{2+} concentration (Markram et al., 1995; Schiller et al., 1995). Analyses performed in dissociated pyramidal neurons (Stewart and Foehring, 2000) and in Layer-5 (L5) pyramidal neurons from brain slices (Markram et al., 1995; Almog and Korngreen, 2009) have shown that all high-voltage activated (HVA) VGCCs, namely L-type (Ca_v1), P/Q-type ($Ca_v2.1$), N-type ($Ca_v2.2$) and R-type ($Ca_v2.3$), contribute to the AP-mediated dendritic Ca^{2+} transient, but low-voltage activated (LVA) VGCCs (T-type, Ca_v3) may also contribute (Talley et al., 1999). Following the Ca^{2+} transient, Ca^{2+}-binding proteins can be activated by indistinct cytosolic Ca^{2+} elevation (Ghosh and Greenberg, 1995), and in this case these proteins are equally activated by Ca^{2+} ions from any contributing source. Alternatively, the proteins are selectively activated by a physically-coupled Ca^{2+} source. In this case, the protein experiences a larger Ca^{2+} elevation in a nanodomain adjacent to the Ca^{2+} source. This type of multi-protein structure is characterized in the synaptic cleft (Gandini and Zamponi, 2022).

Voltage-gated Ca^{2+} channels (VGCCs) in pyramidal neuron dendrites can target Ca^{2+}-activated K^+ channels (CAKCs), in particular SK and BK CAKCs (Sah and Davies, 2000). Both channels can be coupled with a Ca^{2+} source (Vierra and Trimmer, 2022), but it was suggested that BK CAKCs must localize closer to the Ca^{2+} source to ensure reliable Ca^{2+}-dependent activation because they have lower affinity for Ca^{2+} (Fakler and Adelman, 2008; Shah et al., 2022). In cell-attached patches from isolated CA1 hippocampal pyramidal neurons it was shown that L-type VGCCs activate exclusively SK CAKCs whereas N-type VGCCs activate BK CAKCs (Marrion and Tavalin, 1998). In contrast, whole-cell patch-clamp recordings from freshly dissociated neocortical pyramidal neurons showed that BK CAKCs are activated both by L-type and N-type VGCCs (Sun et al., 2003), consistently with the findings that both L-type VGCCs (Grunnet and Kaufmann, 2004) and N-type VGCCs (Loane et al., 2007) molecularly co-assemble with BK CAKCs. From the functional side, both CAKCs participate in shaping the AP, but with different kinetics (Sah and Davies, 2000) as also reproduced by computer modeling (Almog and Korngreen, 2014). Specifically, SK CAKCs regulate the AP waveform during the medium and late phase of the AP re-polarization with a variability that depends on the different Ca^{2+} source and neuronal types (Bond et al., 2004; Villalobos et al., 2004; Pedarzani and Stocker, 2008). Interestingly, dendritic excitability is impacted by SK CAKC activation in unpredictable manner (Bock et al., 2019). In contrast, BK CAKCs, which are functionally expressed in the dendrites L5 neocortical pyramidal neurons (Kang et al., 1996; Benhassine and Berger, 2005) regulate the AP in the early phase of re-polarization (Sun et al., 2003) when the membrane potential (V_m) is depolarized, consistently with the voltage dependence of the channel (Vergara et al., 1998; Cui, 2010).

The close interaction between the Ca^{2+} source and the BK CAKC implies the activation of the K^+ channel at sub-millisecond time scale (Berkefeld et al., 2006). In the present study, performed in L5 pyramidal neurons of the somatosensory cortex, we used ultrafast optical measurements of V_m (Popovic et al., 2015) and Ca^{2+} currents (Jaafari et al., 2014) to investigate in parallel the kinetics of the dendritic back-propagating AP (bAP) and that of the associated Ca^{2+} current. We found that BK CAKCs are selectively activated by N-type VGCCs. Yet, whereas the peak of the Ca^{2+} current is delayed by >500 µs with respect to the bAP peak, consistently with the kinetics of activation and deactivation of VGCCs in the order of 1 ms (Kay and Wong, 1987), the activation of BK CAKCs occurs in the first 500 µs, providing a negative feedback to the cytosolic Ca^{2+} elevation (Shah et al., 2022). We built a realistic NEURON model showing that experimental results could be reproduced by the only when N-type VGCCs and BK CAKCs were physically interacting.

2 Materials and methods

2.1 Brain slices preparation and maintenance

All experiments were performed in the "Laboratory of Interdisciplinary Physics" and mice manipulations previous to euthanasia were done in accordance with European Directives 2010/63/UE on the care, welfare and treatment of animals. Specifically, procedures were reviewed by the ethics committee affiliated to the animal facility of the university (D3842110001). Mice (C57BL/6j, 21-35 postnatal days old) purchased from Janvier Labs (Le Genest-Saint-Isle, France) were anesthetised by isofluorane inhalation and decapitated to extract the entire brain. Neocortical slices (350 µm thick) were prepared as described in recent previous reports (Filipis and Canepari, 2021; Montnach et al., 2022; Filipis et al., 2023), using a Leica VT1200 vibratome (Wetzlar, Germany). The extracellular solution contained (in mM): 125 NaCl, 26 $NaHCO_3$, 1 $MgSO_4$, 3 KCl, 1 NaH_2PO_4, 2 $CaCl_2$ and 20 glucose, bubbled with 95% O_2 and 5% CO_2. Slices were incubated at 37°C for 45 min and maintained at room temperature before being transferred to the recording chamber where the temperature was maintained at 32−34°C.

2.2 Electrophysiology and imaging

Slices with L5 pyramidal neurons in the somato-sensory cortex having the initial part of the apical dendrite parallel to the surface were used for the experiments. Patch-clamp (whole-cell) recordings were made using a Multiclamp 700A (Molecular Devices, Sannyvale, CA) with a basic intracellular solution containing (in mM): 125 $KMeSO_4$, 5 KCl, 8 $MgSO_4$, 5 Na_2-ATP, 0.3 Tris-GTP, 12 Tris-Phosphocreatine, 20 HEPES, adjusted to pH 7.35 with KOH. To this basic solution, one or more indicators were added according to the type of optical recording. In V_m imaging experiments without concomitant Ca^{2+} recordings, cell membranes were loaded with the voltage-sensitive dye D-2-ANEPEQ (JPW1114, 0.2 mg/mL, Thermo Fisher Scientific) for 30 min using a first patch clamp recording and then re-patched a second time with dye free solution. In V_m imaging experiments with concomitant Ca^{2+} recordings, the intracellular solution in the second patch contained a Ca^{2+} indicator at the concentration of

2 mM which was either Cal-520FF (AAT Bioquest, Sunnyvale, CA, USA, see Blömer et al., 2021) in 2 cells or Fura2FF (Santa Cruz Biotechnology) in 6 cells. The choice of using, in some experiments, a UV-excitable indicator is motivated by the need to obtain, in the majority of cells, both V_m and Ca^{2+} signals with a combination of spectrally non-overlapping indicators (Vogt et al., 2011a). Finally, in exclusive Ca^{2+} imaging experiments, the Ca^{2+} indicator added to the intracellular solution at the concentration of 2 mM was either Oregon Green BAPTA-5N (Thermo Fisher Scientific) or the most sensitive low-affinity dye Cal-520FF. Ca^{2+} recordings started 30 min after achieving the whole cell configuration, a time necessary for full dye equilibration in the initial 200 μm segment of the apical dendrite. Somatic APs were elicited by short current pulses of 1.5−2.5 nA through the patch pipette in current clamp mode. Electrical somatic V_m transients were acquired at 20 kHz and the bridge associated with the current pulse was corrected offline by using the recorded injected current. Finally, the measured V_m was corrected for −11 mV junction potential. Experiments were performed using an imaging system described in several previous reports (Jaafari et al., 2014; Jaafari and Canepari, 2016; Ait Ouares et al., 2019; Ait Ouares and Canepari, 2020). This system is based on an Olympus BX51 microscope equipped with a 60X/1.0 NA Nikon objective where whole-field fluorescence illumination is provided either with an OPTOLED system (Cairn Research, Faversham, UK) or with an LDI-7 laser (89 North, Williston, VT). Fluorescence emission was demagnified by 0.5X and acquired with a NeuroCCD camera (Redshirt Imaging, Decatur, GA). Signals were sampled at 20 kHz (for 8 ms) with a resolution of 4X26 pixels except in V_m imaging calibration experiments where signals were sampled at 5 kHz with a resolution of 26X26 pixels (for 160 ms). In V_m imaging recordings, JPW1114 fluorescence was excited using the 528 nm line of an LDI-7 laser (89 North, Williston, VT) and the emitted fluorescence was long-pass filtered at >610 nm before being acquired. In Ca^{2+} imaging recordings, OG5N or Cal-520FF were excited by the 470 nm line of the OPTOLED and the emitted fluorescence was band-pass filtered at 530 ± 21 nm before being acquired. Finally, in Ca^{2+} imaging recordings with Fura2FF, fluorescence was excited by the 385 nm line of the OPTOLED and the emitted fluorescence was band-pass filtered at 510 ± 41 nm before being acquired.

2.3 Pharmacology of Ca^{2+} and K^+ channels

Channels blockers used in this study were either peptides (animal toxins), purchased from Smartox Biotechnology (Saint Egrève, France), or smaller organic molecules. Peptides, dissolved in water and used at the final concentration of 1 μM, were: ω-agatoxin-IVA (P/Q-type VGCC blocker), ω-conotoxin-GVIA (N-type VGCC blocker), snx-482 (R-type VGCC blocker), apamin (SK CAKC blocker) and iberiotoxin (BK CAKC blocker). The blockade of L-type VGCCs was achieved using 4-(2,1,3-Benzoxadiazol-4-yl)-1,4-dihydro-2,6-dimethyl-3,5-pyridinecarboxylic acid methyl 1-methylethyl ester (isradipine, purchased from HelloBio, Bristol, UK) that was diluted in external solution at 20 μM concentration. To obtain an alternative blockade of N-type VGCCs we used *N*-[[4-(1,1-Dimethylethyl)phenyl]methyl]-*N*-methyl-L-leucyl-*N*-(1,1-dimethylethyl)-*O*-(phenylmethyl)-L-tyrosinamide (pd173212, purchased from TOCRIS, Bristol, UK) that was used at the final concentration of 5 μM. Finally, to block T-type VGCCs, we used a cocktail of two drugs (from TOCRIS) at the final concentrations of 30 and 5 μM, respectively: 3,5-dichloro-*N*-[[(1α,5α,6-exo,6α)-3-(3,3-dimethylbutyl)-3-azabicyclo [3.1.0]hex-6-yl]methyl]-benzamide-hydrochloride (ml218) and (1*S*,2*S*)-2-[2-[[3-(1*H*-Benzimidazol-2-yl)propyl]methylamino]ethyl]-6-fluoro-1,2,3,4-tetrahydro-1-(1-methylethyl)-2-naphthalenyl-cyclopropanecarboxylate-dihydrochloride (nnc550396). In all experiments, the blocker(s) was (were) locally delivered by gentle pressure application near the optical recording area using a pipette of 2−4 μm of diameter. The application lasted 2−4 min before recording in order to assure the stable blockade of the channel(s).

2.4 Data analysis and quantification

All data were from averages of 6−9 trials with identical somatic response in Ca^{2+} recordings, and of 4 trials with identical somatic response in V_m recordings. Raw data were converted in MATLAB format and analysed using custom-made code written in MATLAB. As a first step, fluorescence values including an AP were corrected for photo-bleaching using multi-exponential fits of fluorescence values in single trials without an AP. Then, the fractional change of fluorescence from the first image ($\Delta F/F_0$) was calculated over the mean fluorescence in regions of 20−40 μm located at ∼100 μm from the soma. It is important to state that all the conclusions reported in this study were based on comparisons of signals under control conditions and signals after the blockade of one or more channels, for which a calibration of the size of the signals was not necessary. Nevertheless, to build realistic NEURON models, the V_m ($\Delta F/F_0$) associated with the bAP was converted into mV considering an attenuation of the somatic AP size, which was 4% on average. This value was obtained in a set of experiments in which the V_m ($\Delta F/F_0$) associated with the bAP was calibrated in mV using a previously reported method (Vogt et al., 2011b). As shown in the example of **Figure 1A**, the V_m $\Delta F/F_0$ signal associated with an AP was measured in the apical dendrite at ∼100 μm from the soma. Then, in the presence of 1 μM tetrodotoxin to block APs and 50 μM cyclothiazide to inhibit AMPA receptors desensitization, L-glutamate was locally photo-released from 1 mM 4-Methoxy-7-nitroindolinyl-caged-L-glutamate (MNI-glutamate, TOCRIS) using an OPTOLED pulse of 1 ms at 365 nM wavelength. As this procedure brings the dendritic V_m to the reversal potential of ionotropic glutamate receptors (i.e., to 0 mV), the associated V_m $\Delta F/F_0$ signal was used to calibrate the V_m $\Delta F/F_0$ signal associated with the bAP. This assessment was repeated in $N = 8$ cells obtaining a consistent result (**Figure 1A**). For the quantification of Ca^{2+} signals, the dendritic Ca^{2+} $\Delta F/F_0$ signal associated with the bAP, normalized to its asymptotic value, was initially fitted with a 4-sigmoid function Y(t):

$$Y(t) \prod_{j1}^{4} \frac{1}{1+e^{-\varphi_j \cdot (t-\theta_j)}}$$

where t is time and φ_j and θ_j are the parameters to be determined by the fit. The time derivative of Y(t) was then used

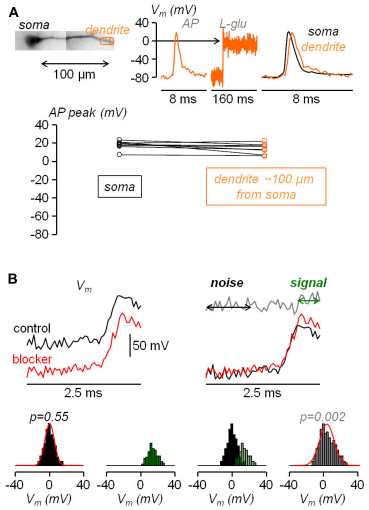

FIGURE 1
Calibration of dendritic AP and statistical assessment of the AP widening following pharmacological manipulation. **(A)** Top-left, reconstruction of L5 pyramidal neuron with dendritic compartment at ~100 µm distance from the soma outlined by a cylinder (orange). Top-right, V_m optical signal associated with an AP in the region on the left, calibrated using a depolarization to 0 mV obtained by uncaging L-glutamate (see Materials and Methods), showing a slight attenuation of the dendritic bAP with respect to the somatic AP (black trace). Bottom, AP peak in the soma and in the dendrite at ~100 µm distance from the soma measured in $N = 8$ cells. **(B)** Top, to simulate an experimental widening two sets of normally distributed random values with 5 mV standard deviation are added to a somatic AP recorded at 20 kHz, once in control conditions (black traces) and once in the presence of the channel blocker (red traces); the normal distributions are centered at 0 mV except for the 10 points (500 µs) following the AP peak in the red trace for which the distribution is centered at +15 mV; the gray trace on the right shows the difference between the red and black trace; the analysis is performed over the 20 points (1 ms) preceding the current injection (noise) and the 10 points following the AP peak (signal). Bottom, following the procedure illustrated above applied to $N = 8$ cells to obtain 160 points for the noise and 80 points for the signal, histograms of noise (black columns), of the signal (green columns) and of the noise+signal (240 points, gray columns); to qualitatively visualize the consistency with normality, normal distributions with mean and standard deviation calculated from noise and from the noise+signal are superimposed to the respective histograms (red traces); the p values of the two Lilliefors tests are indicated.

as measurement of the Ca^{2+} current (I_{Ca}). The maxima of Y(t) and of its derivative were used to quantify the fractional change of the signals produced by the channel blockers.

2.5 Statistics

To assess the consistency of the experimental results obtained in groups of cells, three statistical tests were performed and in all tests we considered 0.01 as the threshold for significance.

1. To assess the effect of a channel blocker on the Ca^{2+} and I_{Ca} signals in the same group of experiments, the parametric paired t-test was performed on the signals maxima under two different conditions. In each cell, the maxima were measured in control conditions and in the presence of one or several channel blockers.

2. To assess the effect of a channel blocker on the Ca^{2+} and I_{Ca} signals in two different groups of experiments, the Wilcoxon rank non-parametric test was performed on the fractional changes of signals maxima under two different conditions in the two groups of cells.

3. Finally, to establish the effect of a channel blocker on the shape of the dendritic AP, we assessed the widening of the AP over the photon noise of the recording using the following statistical analysis. Assuming that the photon noise is normally distributed, the distribution of the difference between the noise samples in the presence of the channel blocker and in control condition is also normal with standard deviation equal to $\sqrt{2}$ times the standard deviation of the noise. Thus the hypothesis to test was whether or not the addition of the sample differences at given intervals after the AP peak produces a distribution that deviates from normality. The rationale of the analysis is illustrated in the simulations reported in Figure 1B. In the example reported on the top of the panel, two sets of normally distributed values with 5 mV standard deviation (~15 mV peak-to-peak noise) were added to a somatic AP recorded at 20 kHz. This was done once to simulate the control conditions and once to simulate the presence of the channel blocker. The normal distributions were centered at 0 mV except for the 500 µs following the AP peak in the red trace for which the distribution was centered at + 15 mV in order to mimic the widening. The distribution of the difference between the noise samples in the presence of the channel blocker and in control condition are also normal with standard deviation equal to $\sqrt{2}$ times the standard deviation of the original signals. The distribution of the difference between the noise + signal samples, however, deviates from normality since the two original distributions are centered at two different values. Thus, we repeated the simulations in $N = 8$ cells and we illustrate the histograms of the difference in the noise, in the signal and in the noise + signal (Figure 1B). To visualize the normal behavior of the noise difference and the deviation from normality of the noise + signal difference, we superimpose to the histograms the two normal distributions with mean and standard deviation calculated from the points. The test to obtain a quantitative assessment of the normal behavior is, in principle the Kolmogorov-Smirnov test. In practice, since in the experiments the noise varies from one cell to another, we opted for the stronger Lilliefors test, which is a generalization of the Kolmogorov-Smirnov test for unknown normal distributions (Lilliefors, 1967). The p values of this test for the above simulations are reported in Figure 1B. In the experiments, to establish the kinetics of the widening, the test was repeated over three distinct time intervals during the falling phase of the AP, namely the first 500 µs following the AP peak, the next 500 µs and the next 1.5 ms.

2.6 Computational modelling

All simulations were carried out using the NEURON simulation environment (v.8.2.0). Model and simulation files will be available in the ModelDB section of the Senselab database.[1] We used a 3D reconstructed morphology of a mouse L5 pyramidal neuron (morphology NMO_36595, Buchanan et al., 2012) downloaded from NeuroMorpho.org database (Ascoli et al., 2007), with uniform passive properties (Cm = 1 mF/cm^2,

1 https://modeldb.science/2015410

Rm = 30 kohm/cm^2, Ra = 160 ohm·cm) where we attached the axon morphology used in Filipis et al. (2023). Temperature was set at 33°C. The NEURON model, built based on the original model reported by Hallermann et al. (2012) was previously employed in our previous studies (Filipis and Canepari, 2021, Filipis et al., 2023). It was adapted to reproduce the somatic AP and dendritic bAP recordings used as a reference in this work. Active properties included two Na^+ currents, the $Na_v1.2$ and $Na_v1.6$ channels, five types of K^+ currents (a delayed rectifier conductance, A-type K^+ conductance, K_v7 conductance, SK Ca^{2+}-dependent K^+ conductance and BK SK Ca^{2+}-dependent K^+ conductance), a non-specific I_h current, Ca^{2+} conductance modelling including T-type, L-type, R-type, N-type and P/Q-type Ca^{2+} currents, and a simple Ca^{2+}-extrusion mechanism with a 20 ms time constant, to reproduce the measured Ca^{2+} transient decay. For T-type VGCCs, we used the model from Migliore et al. (2008). For R-type VGCCs, we used the model from Mandge and Manchanda (2018). For N-type, P/Q-type, and L-type VGCCs, we used the same model from Wimmer et al. (2010). For BK channel in dendrites, we modified the model in Filipis et al. (2023) to match experimental data on the bAP. In particular, we shifted the voltage dependent activation kinetic by + 10 mV and used a time constant with a sigmoidal form. All other channels were taken from Filipis et al. (2023). Relative spatial distributions of channel dendritic densities were in accordance with Migliore and Shepherd (2002) and Ramaswamy and Markram (2015); $Na_v1.2$ expression was ~50-fold lower compared to the axon initial segment (Kole et al., 2008); an inward current generated by HCN cation channels was also inserted with a density increasing exponentially to 50-fold in the distal apical dendrite compared to the soma (Harnett et al., 2015). To determine the absolute channel densities of the model, we initially used the calibrated voltage imaging recording in **Figure 1A** to reflect the action potential experimental traces in both the soma and the dendrite. Specifically, we first modified the Na^+ channels to match the somatic AP and we then modified Ca^{2+} and K^+ channels to match the dendritic bAP. After that, we refined the dendritic channel density for each individual type of VGCC and set a coupling between particular VGCCs and the BK CAKC. To mimic this coupling, we distinguished the components of Ca^{2+} influx from each individual VGCC and we introduced an affinity of the CAKC for a specific component multiplied a factor $\alpha > 0$ ($\alpha = 0$ means no coupling). In agreement with a study in neocortical pyramidal neurons (Sun et al., 2003), we established the coupling both for L-type and N-type VGCCs, using values of $\alpha = 3$ and $\alpha = 10$ to mimic "weak" and "strong" coupling, respectively. Finally, the pharmacological blockade of each channel in the experiments was mimicked by removing 90% of the channel density from the model.

3 Results

3.1 The dendritic Ca^{2+} influx associated with the bAP is mediated by diverse VGCCs

This study started with the investigation of the VGCCs that mediate the Ca^{2+} influx associated with the bAP in the apical dendrite at ~100 μm from the soma using the same approach already utilised in CA1 hippocampal pyramidal neuron (Jaafari and Canepari, 2016). In the present experiments, L5 pyramidal neurons were loaded with 2 mM of a low-affinity Ca^{2+} indicator, either OG5N or the more sensitive Cal-520FF (Blömer et al., 2021), and Ca^{2+} transients ($\Delta F/F_0$ signals) were measured at 20 kHz by averaging fluorescence from dendritic segments of 20–40 μM length at ~100 μm from the soma. To investigate the contribution of the diverse VGCCs, we locally delivered one or several channel blockers using a pipette positioned near the recording region, as already done in other studies (Ait Ouares et al., 2019; Filipis et al., 2023). Specifically, we blocked L-type VGCCs with 20 μM isradipine, P/Q-type VGCCs with 1 μM ω-agatoxin-IVA, N-type VGCCs with 1 μM ω-conotoxin-GVIA, R-type VGCCs with 1 μM of SNX482, and T-type VGCCs with 5 μM ML218 and 30 μM NNC550396. **Figure 2A** shows a Ca^{2+} transient associated with a bAP that was strongly attenuated by the cocktail of all VGCC blockers. **Figure 2A** also shows the analysis of the Ca^{2+} transient consisting in fitting the signal with a 4-sigmoid function and to calculate the time-derivative of the fit to extrapolate the kinetics of the Ca^{2+} current (I_{Ca}). As shown in the inset of **Figure 2A**, the cocktail of all VGCC blockers reduced the peak of the signal by ~80 % in 5 cells tested. We then applied this analysis on the Ca^{2+} transient recorded first in control solution and then after locally blocking each individual VGCC. The five representative examples reported in **Figure 2B** show that the blockade of L-type, P/Q-type, R-type and T-type VGCCs decreased, at different extent, the size of both $\Delta F/F_0$ and I_{Ca} signals, but surprisingly the blockade of N-type VGCCs increased the size of both $\Delta F/F_0$ and I_{Ca} signals. The test was repeated in 7–10 different cells for each channel blocker and the effect of the inhibitor was quantified by measuring the maximum of the $\Delta F/F_0$ and I_{Ca} signals (**Figure 2C**). Except for the blockade of N-type VGCCs, the individual blockade of each VGCC type produced on average a decrease of both $\Delta F/F_0$ and I_{Ca} signals, an effect that was more important for L-type and T-type VGCCs. In the case of N-type VGCCs, the blockade increased both $\Delta F/F_0$ and I_{Ca} signals in 8/11 cells tested. The unexpected result of locally delivering 1 μM ω-conotoxin-GVIA could be explained by the coupling of the N-type VGCC with a mechanism that boosts the Ca^{2+} influx associated with the bAP, or with the toxin binding to a different target. To discriminate between these two hypotheses, we repeated the analysis of the Ca^{2+} transient of **Figure 2** by blocking the N-type VGCC with another selective inhibitor, namely pd173212 (Hu et al., 1999). As shown in the two representative examples of **Figures 3A, B**, local delivery of either 5 μM pd173212 or 1 μM ω-conotoxin-GVIA increased the size of both $\Delta F/F_0$ and I_{Ca} signals in a qualitatively similar manner. Altogether, the $\Delta F/F_0$ signal increased in 7 cells tested after delivery of pd173212, and the I_{Ca} signal increased in 4/7 cells tested after delivery of pd173212 (**Figure 3C**). We concluded that the blockade N-type VGCCs boosts the Ca^{2+} influx associated with the bAP.

3.2 N-type VGCCs are coupled with BK CAKCs

The boosting of the Ca^{2+} influx observed in **Figures 2**, **3** can be due to an enhancement of the depolarisation produced by the loss of Ca^{2+} influx *via* N-type VGCCs. It was shown in freshly

10.3389/fncel.2024.1353895

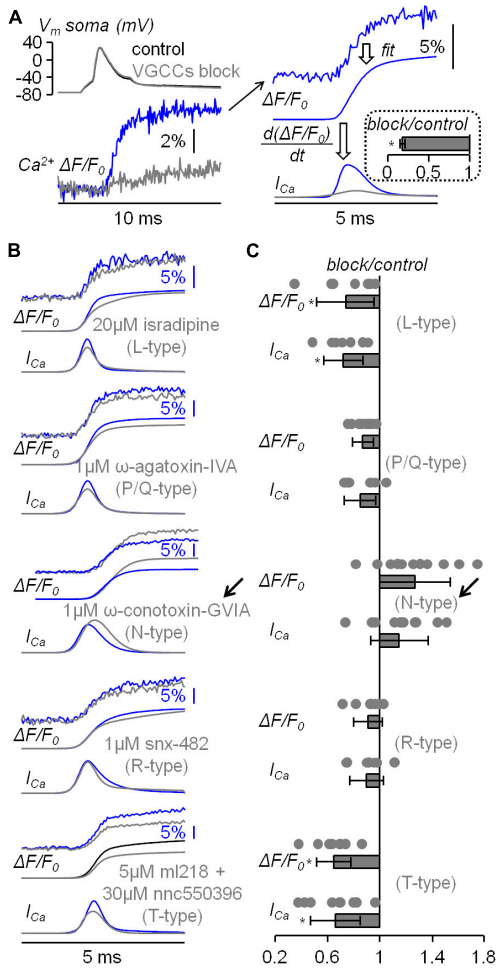

FIGURE 2
Analysis of the diverse VGCCs mediating the Ca^{2+} transient associated with the bAP. **(A)** Left V_m somatic recording (top) and Ca^{2+} transient (bottom) in control solution and after blocking all VGCCs. Right, procedure of analysis of the raw Ca^{2+} transient (top trace) with a 4-sigmoid fit (middle trace) and the calculation of the time-derivative (I_{Ca}, bottom trace). In the inset, fractional change with respect to control of the I_{Ca} maxima after blocking VGCCs (N = 5, 0.18 ± 0.03). **(B)** Five representative examples of Ca^{2+} transients with 4-sigmoid fit ($\Delta F/F_0$, top traces) and time derivative (I_{Ca}, bottom traces) in control solution and after local delivery of either 20 μM of the L-type VGCC inhibitor isradipine, 1 μM of the P/Q-type VGCC inhibitor ω-agatoxin-IVA, 1 μM of the N-type VGCC inhibitor ω-conotoxin-GVIA, 1 μM of the R-type VGCC inhibitor snx-482 or 5 and 30 μM, respectively, of the T-type VGCC inhibitors ml218 and nnc550396. The arrow indicates the unexpected boosting of the Ca^{2+} transient produced by ω-conotoxin-GVIA. **(C)** Single values and fractional change with respect to control of the maxima of the $\Delta F/F_0$ and I_{Ca} signals for the blockade of L-type VGCCs (N = 7, $\Delta F/F_0$: 0.74 ± 0.22, I_{Ca}: 0.72 ± 0.15); for the blockade of P/Q-type VGCCs (N = 8, $\Delta F/F_0$: 0.87 ± 0.08, I_{Ca}: 0.85 ± 0.12); for the blockade of N-type VGCCs (N = 11, $\Delta F/F_0$: 1.27 ± 0.27, I_{Ca}: 1.15 ± 0.22); for the blockade of R-type VGCCs (N = 7, $\Delta F/F_0$: 0.91 ± 0.11, I_{Ca}: 0.90 ± 0.13); for the blockade of T-type VGCCs (N = 7, $\Delta F/F_0$: 0.65 ± 0.13, I_{Ca}: 0.66 ± 0.19). "*" indicates that $p < 0.01$ in paired t-test performed on the signal maxima in control solution and after delivery of the channel blockers.

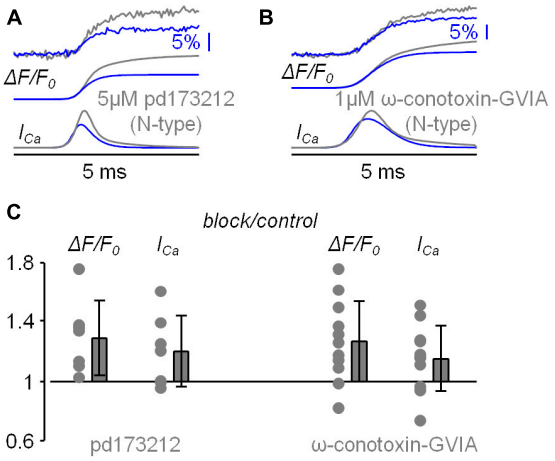

FIGURE 3
Analysis of the blockade of N-type VGCCs using pd173212. **(A)** Representative example of Ca^{2+} transient with 4-sigmoid fit ($\Delta F/F_0$, top traces) and time derivative (I_{Ca}, bottom traces) in control solution and after local delivery of 5 μM of the N-type VGCC inhibitor pd173212. **(B)** Another representative example of Ca^{2+} transient with 4-sigmoid fit ($\Delta F/F_0$, top traces) and time derivative (I_{Ca}, bottom traces) in control solution and after local delivery of 1 μM of the N-type VGCC inhibitor ω-conotoxin-GVIA. **(C)** Left, single values and fractional change with respect to control of the maxima of the $\Delta F/F_0$ and I_{Ca} signals for the blockade of N-type VGCCs with pd173212 (N = 7, $\Delta F/F_0$: 1.29 ± 0.25, I_{Ca}: 1.20 ± 0.24). The single values and fractional change with respect to control of the maxima for the blockade of N-type VGCCs with ω-conotoxin-GVIA are reported on the right for comparison.

dissociated neocortical pyramidal neurons of the mouse that BK CAKCs are activated by N-type VGCCs (Sun et al., 2003). Thus, we repeated the analysis of the Ca^{2+} transient of Figures 2, 3 by blocking in sequence first BK CAKCs with local delivery of 1 μM iberiotoxin and then BK CAKCs and N-type VGCCs together with local delivery of 1 μM iberiotoxin and 1 μM ω-conotoxin-GVIA. In the representative example of Figure 4A, the blockade of BK CAKCs increased both $\Delta F/F_0$ and I_{Ca} signals, but the further blockade of N-type VGCCs decreased both $\Delta F/F_0$ and I_{Ca} signals. Since L-type VGCCs also couple with BK CAKCs in many systems (Marcantoni et al., 2010; Vandael et al., 2010), we also performed experiments in which we blocked in sequence first BK CAKCs only and then BK CAKCs and L-type VGCCs together with local delivery of 1 μM iberiotoxin and 20 μM isradipine. As in the previous example, in the example of Figure 4B the blockade of BK CAKCs increased both $\Delta F/F_0$ and I_{Ca} signals and the further blockade of L-type VGCCs decreased both $\Delta F/F_0$ and I_{Ca} signals. These results was consistently obtained in N = 9 cells tested with blockade of N-type VGCCs and in N = 7 cells with blockade of L-type VGCCs. As shown in Figure 4C, the blockade of BK CAKCs boosted the Ca^{2+} transient similarly to the blockade of N-type VGCCs. In contrast, the blockades of N-type or of L-type VGCCs in the presence of iberiotoxin reduced the Ca^{2+} transient. To evaluate the difference between the results of blocking N-type or L-type VGCCs, either in control conditions or after blocking BK CAKS, we performed a Wilcoxon rank non-parametric test on the groups of cells where a blocker was applied under different conditions, using $p < 0.01$ as discriminator to establish whether two groups were different. As show in Table 1, the effects on both $\Delta F/F_0$ and I_{Ca} signals were similar when comparing the groups of cells where ω-conotoxin-GVIA, pd173212 or iberiotoxin were applied in control solutions, or when the effects of iberiotoxin were compared with the ensemble of cells where N-type VGCCs were

10.3389/fncel.2024.1353895

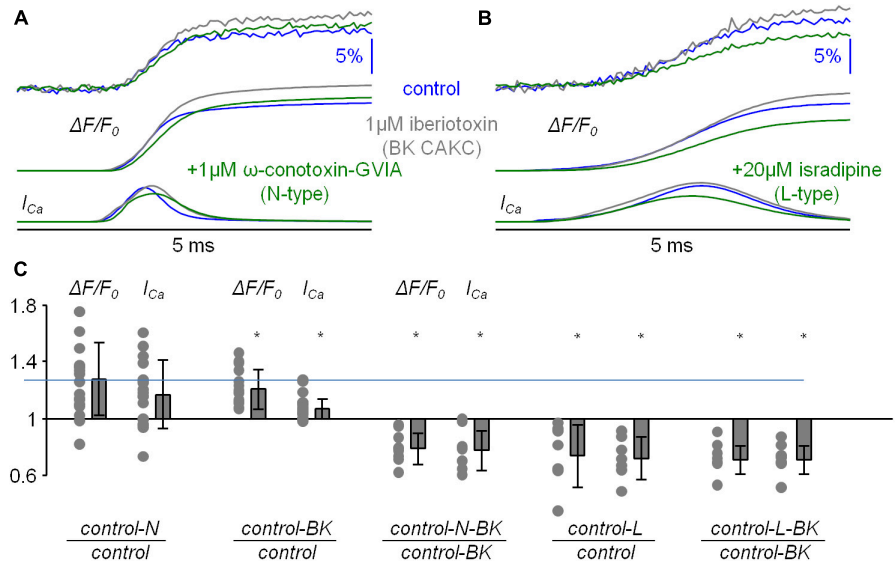

FIGURE 4
Analysis of the blockade of N-type VGCCs or L-type VGCCs after blocking BK CAKCs. **(A)** Example of Ca^{2+} transient with 4-sigmoid fit ($\Delta F/F_0$, top traces) and time derivative (I_{Ca}, bottom traces) in control solution, after local delivery of 1 μM of the BK CAKCs inhibitor iberiotoxin and after further delivery of 1 μM of the N-type VGCC inhibitor ω-conotoxin-GVIA. **(B)** Example of Ca^{2+} transient with 4-sigmoid fit ($\Delta F/F_0$, top traces) and time derivative (I_{Ca}, bottom traces) in control solution, after local delivery of 1 μM of the BK CAKCs inhibitor iberiotoxin and after further delivery of 20 μM of the L-type VGCC inhibitor isradipine. **(C)** Single values and fractional change of the maxima of the $\Delta F/F_0$ and I_{Ca} signals for the following experiments (left to right): blockade of N-type VGCCs (either with ω-conotoxin-GVIA or with pd173212) with respect to control solution (N = 18, $\Delta F/F_0$: 1.27 ± 0.26, I_{Ca}: 1.17 ± 0.22); blockade of BK CAKCs with respect to control solution (N = 16, $\Delta F/F_0$: 1.21 ± 0.14, I_{Ca}: 1.07 ± 0.07); blockade of N-type VGCCs and BK CAKCs with respect to the blockade of BK CAKCs only (N = 9, $\Delta F/F_0$: 0.79 ± 0.11, I_{Ca}: 0.78 ± 0.14); blockade of L-type VGCCs with respect to control solution (N = 7, $\Delta F/F_0$: 0.74 ± 0.22, I_{Ca}: 0.72 ± 0.15); blockade of L-type VGCCs and BK CAKCs with respect to the blockade of BK CAKCs only (N = 7, $\Delta F/F_0$: 0.71 ± 0.10, I_{Ca}: 0.71 ± 0.10); "*" indicates that $p < 0.01$ in paired t-test performed on the signal maxima.

TABLE 1 Wilcoxon rank non-parametric test performed on the effects on Ca^{2+} transients produced by blocking N-type VGCCs, L-type VGCCs and BK CAKCs.

		$p\ \Delta F/F_0$	$p\ I_{Ca}$
ω-conotoxin-GVIA/control	pd173212/control	0.8601	0.7914
ω-conotoxin-GVIA/control	iberiotoxin/control	0.9998	0.2875
ω -conotoxin-GVIA/control	**ω -conotoxin-GVIA/iberiotoxin**	**$4.74 \cdot 10^{-4}$**	**0.0024**
pd173212/control	iberiotoxin/control	0.8371	0.7577
pd173212/control	**ω -conotoxin-GVIA/iberiotoxin**	**$1.75 \cdot 10^{-4}$**	**0.0012**
(ω-conotoxin-GVIA&pd173212)/control	iberiotoxin/control	0.9385	0.3681
(ω -conotoxin-GVIA&pd173212)/control	**ω -conotoxin-GVIA/iberiotoxin**	**$6.71 \cdot 10^{-5}$**	**$4.26 \cdot 10^{-4}$**
isradipine/control	isradipine/iberiotoxin	0.6875	0.9375

The considered groups are: delivery of 1 μM ω-conotoxin-GVIA in control conditions (N = 11 cells); delivery of 5 μM pd173212 in control conditions (N = 7 cells); delivery of either 1 μM ω-conotoxin-GVIA or 5 μM pd173212 in control conditions (N = 18 cells); delivery of 1 μM iberiotoxin in control conditions (N = 9 cells); delivery of 1 μM ω-conotoxin-GVIA in the presence of 1 μM iberiotoxin (N = 9 cells); delivery of 20 μM isradipine in control conditions (N = 7 cells); delivery of 20 μM isradipine in the presence of 1 μM iberiotoxin (N = 7 cells). In each line, the two groups compared are reported in the left columns and the p values for the $\Delta F/F_0$ and I_{Ca} signals are reported on the right columns. Tests where p was < 0.01 are reported in bold characters.

blocked in control solution. In contrast, the effects on both $\Delta F/F_0$ and I_{Ca} signals were different when comparing the cells where ω-conotoxin-GVIA was applied in the presence of iberiotoxin with the groups of cells where ω-conotoxin-GVIA or pd173212 were applied in control solution, or when the comparison was done with the ensemble of cells where N-type VGCCs were blocked in control solution. Finally, the effects on both $\Delta F/F_0$ and I_{Ca} signals were similar when comparing the groups of cells where isradipine was applied in control solutions or in the presence of iberiotoxin. Since the blockade of BK CAKCs prevents the boosting of the Ca^{2+} influx when blocking N-type VGCCs, we concluded that this effect was due to the functional coupling of the two channels.

3.3 The peak of the Ca^{2+} current is delayed with respect of the bAP peak by >500 μs

Before further analyzing the interaction between N-type VGCCs and BK CAKCs, we compared the kinetics of the dendritic

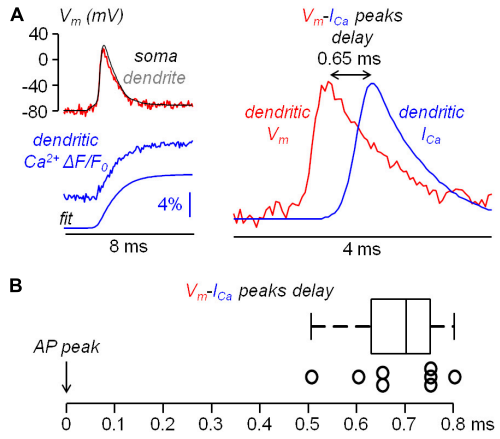

FIGURE 5
Kinetics of the Ca^{2+} current (I_{Ca}) relative to the bAP. **(A)** Left, somatic (black) and dendritic (~100 μm from the soma, red) AP and concomitant measurement Ca^{2+} transient with 4-sigmoid fit (using Cal-520FF). Right, dendritic AP superimposed to the I_{Ca} (time derivative of the fit) indicating a delay of 0.65 ms between the two signals. **(B)** Delay of the I_{Ca} peak with respect to the AP peak in N = 8 cells tested using combined V_m and Ca^{2+} imaging.

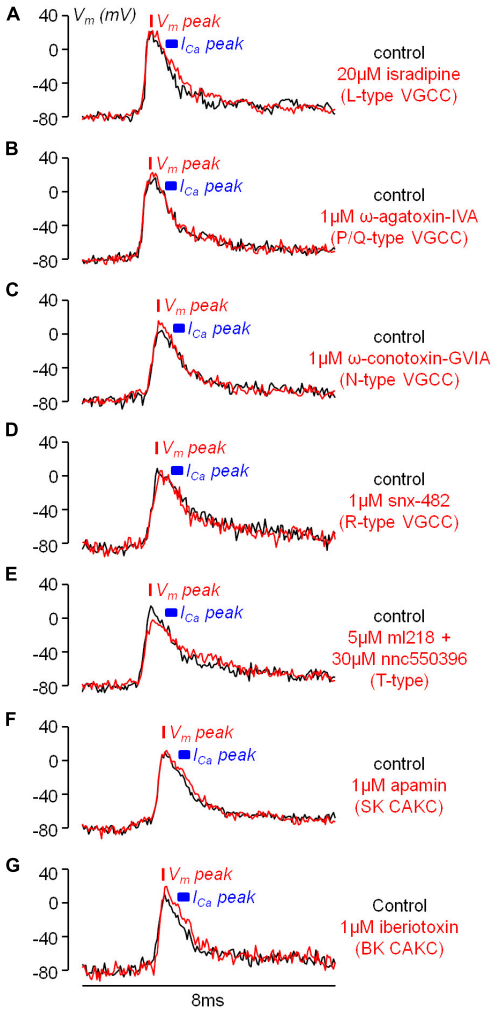

FIGURE 6
Examples of the effects of the diverse VGCC and CAKC blockades on the bAP shape. **(A)** Optical V_m transient from an apical dendrite region (~100 μm from the soma) in a representative L5 pyramidal neuron in control conditions (black trace) and after blocking L-type VGCCs with 20 μM isradipine (red trace). **(B)** Representative experiment as in *A*, but by blocking P/Q-type VGCCs with 1 μM ω-agatoxin-IVA. **(C)** Representative experiment as in *A*, but by blocking N-type VGCCs with 1 μM ω-conotoxin-GVIA. **(D)** Representative experiment as in *A*, but by blocking R-type VGCCs with 1 μM snx-482. **(E)** Representative experiment as in *A*, but by blocking T-type VGCCs with 5 μM ml218 and 30 μM nnc5503961. **(F)** Representative experiment as in *A*, but by blocking SK CAKCs with 1 μM apamin. **(G)** Representative experiment as in *A*, but by blocking BK CAKCs with 1 μM iberiotoxin. In each cell the red bar shows the timing of the AP peak and the blue segment the expected range for the peak of the I_{Ca} (500–800 μs after the AP peak).

I_{Ca} with that of the eliciting bAP at ~100 μm from the soma. In a previous study, we showed that in L5 pyramidal neurons the peak of the I_{Ca} occurs before the AP peak in the distal part of the axon initial segment whereas it is delayed in the proximal part (Filipis et al., 2023). In another study, using ultrafast combined V_m and Ca^{2+} imaging, we showed that the I_{Ca} was further delayed with respect to the AP peak in the proximal part of the apical dendrite of CA1 hippocampal pyramidal neurons (Jaafari and Canepari, 2016). Thus, we performed the same analysis in the proximal part of the apical dendrite in L5 pyramidal neurons using, as Ca^{2+} indicator, either Cal-520FF or Fura2FF (see Materials and Methods). A representative example of this type of measurement is reported in **Figure 5A**. In this particular example, the peak of the I_{Ca} corresponding to the maximal slope of the dendritic Ca^{2+} transient is delayed by 650 μs (13 samples) with respect to the dendritic AP. Consistently with the result of this experiment, a delay ranging from 500 to 800 μs was observed in N = 8 cells (**Figure 5B**). From the kinetics of the Ca^{2+} transient we concluded that VGCCs start opening during the rising phase of the AP, but they remain open during the entire falling phase of the AP increasing the cytosolic Ca^{2+} concentration over this period. As a consequence, if the activation of a Ca^{2+}-binding protein is linear with the cytosolic Ca^{2+}, the maximal effect of this activation must be observed at least 500 μs after the AP peak.

3.4 The effect of blocking N-type VGCCs or BK CAKCs occurs in the first 500 μs after the AP peak

If the inhibition of a K^+ channel occurs during an AP, then this inhibition is expected to change the shape of the AP. Thus, using ultrafast V_m imaging (Popovic et al., 2015), as shown in the examples reported in **Figure 6**, we investigated the kinetics of the dendritic bAP after blocking L-type VGCCs (panel *A*), P/Q-type VGCCs (panel *B*), N-type VGCCs (panel *C*), R-type VGCCs (panel *D*), and T-type VGCCs (panel *E*). In addition, we investigated the kinetics of the dendritic bAP after blocking the two major types of CAKCs, namely the SK channel using 1 μM apamin (panel *F*) and the BK channel (panel *G*). Consistently with the observation that the blockade of P/Q-type and R-type VGCCs caused, on average, the smallest decrease in the I_{Ca} (**Figure 2C**), in the two representative cells of **Figures 6B, D** the blockade of

these two channels did not change the AP shape. Surprisingly, in the representative cell of Figure 6E, the blockade of T-type VGCCs decreased the amplitude of the bAP, suggesting an effect on dendritic excitability. We don't have an explanation for this effect that can be in principle potentially attributed to the drugs acting on a different target other than T-type VGCC, but this result suggests that the AP weakening may contribute to the relatively large inhibition of the I_{Ca} reported in Figure 2C. In all other representative cells, the blockade of the channels caused a visually detectable widening of the AP shape. In the case of N-type VGCCs (Figure 6C) and of BK CAKS (Figure 6G), a widening seemed occurring during the first 500 μs following the AP peak, therefore during the phase of increasing of VGCC activation. In contrast, in the case of L-type VGCCs (Figure 6A) and of SK CAKS (Figure 6F), the widening seemed occurring mostly >500 μs after the AP peak, therefore during or after the expected peak of the I_{Ca}. The early widening reported in the example of Figure 6C was also observed in the example of Figure 7A. In this exceptional case, where the peak-to-peak noise was <10 mV, the widening could be visually detected by plotting the difference between the samples after blocking N-type VGCCs and the samples in control conditions. Hence, whereas the 20 differences corresponding to the noise collected before the somatic current injection were either positive or negative values, the 20 differences corresponding to the signal collected after the AP were mostly positive. In the vast majority of tested cells, however, the peak-to-peak noise was >10 mV. Thus, we performed the experiment of the examples of Figure 6 in 8−10 cells for each channel blockade and performed a statistical analysis on the ensemble of the cells tested. Figure 7B shows the averaged V_m signal of $N = 10$ cells where the individual traces were aligned with the AP peak. The analysis performed on the 200 sample differences corresponding to the noise indicate that their distribution is consistent with a normal behaviour, according to the large p value obtained by the Lilliefors test. In contrast, the 100 sample differences corresponding to the first 500 μs after the AP peak and to the following 500 μs do not follow a normal distribution. Finally, the hypothesis of deviation from the normal behaviour in the following 1.5 ms could not be rejected. The same analysis was repeated for the blockade of L-type VGCCs (Figure 7C), of P/Q-type VGCCs (Figure 7D), of R-type VGCCs (Figure 7E), of T-type VGCCs (Figure 7F), of SK CAKCs (Figure 7G) and of BK CAKCs (Figure 7H) and the p values obtained by the Lilliefors test are reported in Table 2. A significant deviation from normality in the samples collected in the first 500 μm after the AP peak was discerned in the case of blockade of BK CAKCs. Interestingly, in 4/8 cells tested for the blockade of P/Q-type VGCCs, an early widening of the AP was also observed, leading to a low value of p also in this case. Finally, the significant deviation from normality observed in the case of blockage of T-type VGCCs was due to the consistent reduction of the amplitude of the AP. In contrast to these cases, significant deviations from normality in the samples collected beyond 500 μm after the AP peak were discerned in the case of blockade of L-type VGCCs and in the case of blockade of SK CAKCs. These behaviours were due to the widening of the AP shape during or after the expected occurrence of the I_{Ca} peak. In the case of these two blockades, the time-course of the AP change is consistent with an activation of K^+ channels by cytosolic Ca^{2+}, but the hypothesis that these channels are also selectively activated by the specific Ca^{2+} source cannot be excluded since the delayed widening can be due to a slower kinetics of the K^+ channels. Yet, in the case of the blockade of N-type VGCCs or of the blockade of BK CAKCs, the results indicate that the activation of K^+ channels is not linear with the cytosolic Ca^{2+}, preceding the peak of the I_{Ca}. The fact that the AP widening occurs when only a fraction of inflowing Ca^{2+} via N-type VGCCs is detected indicates that BK channels are activated before the Ca^{2+}-dye binding reaction equilibrates. This result suggests a physical interaction between the N-type VGCC and the BK CAKC at nanoscopic domain. Thus, we further explored this hypothesis using biophysical modelling in the NEURON environment.

3.5 The coupling between N-type VGCCs and BK CAKCs is confirmed by a NEURON model

In order to reproduce the kinetics of the AP and of the I_{Ca}, we built a realistic NEURON model, and considered an apical dendrite at ∼100 μm from the soma, corresponding to the zone explored in the experiments. The model included all types of VGCCs tested, BK CAKCs and SK CAKCs. The coupling between a specific Ca^{2+} channel and the K^+ channel was modelled by introducing an activation factor (α) of the BK channel by the Ca^{2+} influx from that particular channel. This coupling was imposed both to L-type and N-type VGCCs, in agreement to what reported in the literature (Sun et al., 2003). We found that, to replicate the ensemble of experimental results, the coupling needed to be strong for N-type VGCCs (α = 10) and weak for N-type VGCCs (α = 3). Figure 8A shows the dendritic AP, which reproduces the experimental AP obtained in one cell, superimposed to the Ca^{2+} transient and of the I_{Ca}. Consistently with experimental observations, the model showed a delay of ∼0.8 ms between the peak of the AP and the peak of the I_{Ca}. Next, to mimic the pharmacological blockade of channels, from the model corresponding to the control condition we removed either 90% of N-type VGCCs, 90% of BK CAKCs or 90% of both channels (Figure 8B). The model reproduced the experimental widening of the AP preceding the peak of the I_{Ca} and the increase in the Ca^{2+} signals with all simulated pharmacological blockades. In addition, consistently with the results of the experiments reported in Figure 4, the blockade of both channels decreases the Ca^{2+} signals with respect to the simulation where only BK CAKSs are blocked. To assess whether the selective coupling between N-type VGCCs and BK CAKAs was necessary to reproduce the experimental results, we suppressed the coupling between N-type VGCCs and BK CAKCs. In this modified model, the early widening of the AP disappears and the Ca^{2+} signal and current decrease when N-type VGCCs are blocked (Figure 8C). This result supports the experimental suggestion that a strong coupling between N-type VGCCs and BK CAKAs may be in effect in these neurons.

4 Discussion

In this report we provide strong experimental evidence that BK CAKCs are selectively activated by N-type VGCCs in the apical dendrite of L5 pyramidal neurons. This activation is rapid and is

10.3389/fncel.2024.1353895

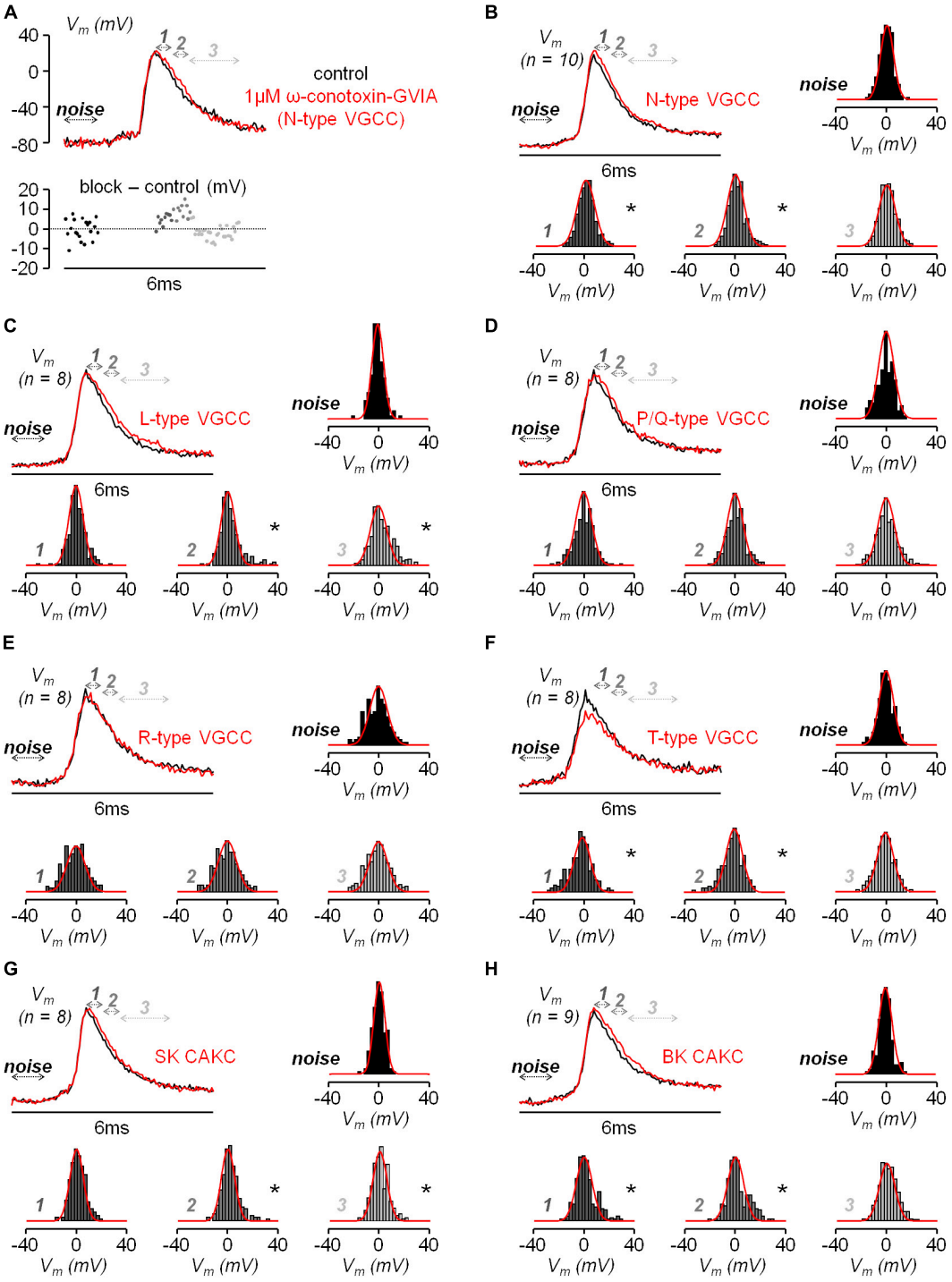

FIGURE 7

Analysis of the effect of the diverse VGCCs and CAKs on the bAP shape. **(A)** Top, optical V_m transient from an apical dendrite region (~100 μm from the soma) in a representative L5 pyramidal neuron in control conditions (black trace) and after blocking N-type VGCCs (red trace); arrows at different gray tones indicate the time windows corresponding to the noise (1 ms before current injection), signal "*1*" (first 500 μs after the AP peak), "*2*" (following 500 μs) and "*3*" (following 1.5 ms). Bottom, sample difference of the signals after the channel blockade and in control conditions in the four time windows. **(B)** Averaged signals aligned to the AP peak from *N* = 10 cells in control conditions (black trace) and after blocking N-type VGCCs (red trace) and histograms of the sample differences in the illustrated four time windows; normal distributions with mean and standard deviations calculated from the points are reported (red plots) for comparison with the histograms. **(C)** Same as in *B*, but in 8 cells where L-type VGCCs were blocked. **(D)** Same as in *B*, but in 8 cells where P/Q-type VGCCs were blocked. **(E)** Same as in *B*, but in 8 cells where R-type VGCCs were blocked. **(F)** Same as in *B*, but in 8 cells where T-type VGCCs were blocked. **(G)** Same as in *B*, but in 8 cells where SK CAKs were blocked. **(H)** Same as in *B*, but in 9 cells where BK CAKs were blocked. In panels *B-H* "*" indicates that the distribution deviates from normality ($p < 0.01$, Lilliefors test).

TABLE 2 Lilliefors test to assess whether a set of values is consistent with a normal distribution performed on sample differences in V_m imaging experiments after blocking a channel (with the name of the blocker indicated) and in control conditions.

	N cells	*p noise*	*p 1*	*p 2*	*p 3*
ω-conotoxin-GVIA (N-type VGCCs)	10	0.82	**$8.3{\cdot}10^{-4}$**	**0.0082**	0.29
isradipine (L-type VGCCs)	8	0.16	0.13	**$0.5{\cdot}10^{-5}$**	**$2.5{\cdot}10^{-5}$**
ω-agatoxin-IVA (P/Q-type VGCCs)	8	0.17	0.015	0.21	0.022
snx-482 (R-type VGCCs)	8	0.49	0.57	0.48	0.56
ml218 + nnc550396 (T-type VGCCs)	8	0.69	**$0.1{\cdot}10^{-5}$**	**0.0017**	0.012
apamin (SK CAKCs)	8	0.17	0.44	**0.0042**	**$1.3{\cdot}10^{-4}$**
iberiotoxin (BK CAKCs)	9	0.19	**$7.1{\cdot}10^{-4}$**	**0.0011**	0.18

The five columns report, for each channel tested, the total number of cells (*N*) and the values of p (*p*) for the noise (number of samples 20·*N*), for the signal *1* (first 500 μs after the AP peak, number of samples 10·*N*), for the signal *2* (following 500 μs after the AP peak, number of samples 10·*N*), for the signal *3* (following 1.5 ms after the AP peak, number of samples 30·*N*). Tests where *p* was < 0.01 are reported in bold characters and indicate a significant change of the AP shape caused by the blockade of the channel.

not linear with the increase of intracellular Ca^{2+} concentration associated with the transient activation of VGCCs. Thus, the blockade of N-type VGCCs widens the AP peak prolonging Ca^{2+} entry through the other VGCCs and boosting the increase of intracellular Ca^{2+} concentration associated with the AP. In contrast, the widening of the AP shape produced by inhibiting either L-type VGCCs or SK CAKCs occurs later in the AP falling phase, suggesting that SK channels might be uniformly activated by cytosolic Ca^{2+} from, possibly from low-threshold L channels (Vandael et al., 2012). The results reported here also indicate that our imaging approach can indirectly reveal functional protein-protein interactions that can be foreseen using structural imaging techniques such as Förster resonance energy transfer imaging (Masi et al., 2010). Indeed, in the case of VGCC nanodomains (Gandini and Zamponi, 2022), the close interaction with the Ca^{2+} target enables sub-millisecond activation of the target, as has been shown in synaptic terminals (Volynski and Krishnakumar, 2018). Here, we show that the combined analysis of cytosolic Ca^{2+} and of AP kinetics at 50 μs temporal resolution can reveal VGCC-CAKC interactions at functional level in larger structures such as neuronal dendrites.

4.1 Functional consequences of the selective coupling between BK and a specific calcium source

Overall, BK channels are known to perform multiple functions in neurons (Ancatén-González et al., 2023). Compared with other CAKCs, BK channels exhibit lower affinity to Ca^{2+} and require concomitant depolarisation (Berkefeld et al., 2010). These two biophysical properties suggest that these channels must be physically close to a specific Ca^{2+} source and that they can activate at a sub-millisecond time scale when the cell is depolarised (Berkefeld et al., 2006). It is known that BK CAKCs form macromolecular complexes with L-type, P/Q-type and N-type VGCCs and, when the two proteins were co-expressed in heterologous systems, it was found that the kinetics of activation of BK CAKCs depended on the coupled VGCCs (Berkefeld and Fakler, 2008). In presynaptic terminals, BK channel activity regulate synaptic transmission (Raffaelli et al., 2004) and can modulate both the amplitude and duration of depolarization-evoked Ca^{2+} entry as a result of the rapid repolarization and deactivation of P/Q-type and N-type VGCCs (Fakler and Adelman, 2008). In turn, reduced Ca^{2+} influx limits vesicle fusion at active zones, leading to decreased neurotransmitter release (Kyle and Braun, 2014). In the postsynaptic areas of L5 pyramidal neurons, BK channels are expressed not only in the dendritic bulk, but also in synaptic spines, and activation of BK CAKCs in small-head spines by Ca^{2+} influx through glutamate receptors reduces the size of synaptic potentials (Tazerart et al., 2022). Thus, both in synaptic terminals and spines, the selective activation of BK channels by a specific partner leads to a negative feedback of the triggering signal, which is the AP in the case of synaptic terminal and the synaptic potential in the case of spines. This negative feedback translates into a reduction of either neurotransmitter release or of neuronal excitability once the synaptic potential has reached the soma and the axon initial segment. Thus, in both cases, the functional consequences of BK CAKC activation can be tied to the underlying K^+ current that decreases the amplitude and/or the size of the triggering depolarizing event. In the apical dendrite of L5 pyramidal neurons, we found that BK CAKCs activation by N-type VGCCs anticipates the peak of the current mediated by VGCCs, providing a negative feedback to the other Ca^{2+} channels. The AP shaping produced by BK CAKCs is qualitatively similar to what we observed in the axon initial segment of L5 pyramidal neurons, where these channels are activated by the Ca^{2+} permeable voltage-gated Na^+ channel $Na_v1.2$ (Filipis et al., 2023). Compared to synaptic terminals and spines, however, the role of the regulation of the AP shape in these wider regions, produced by the K^+ current, is less straightforward.

4.2 Putative functional consequences of BK membrane conductance increase

Ion channels do not only mediate ionic currents that change the V_m, but they can also regulate the spread of V_m transient from a site to another by locally changing the membrane conductance, i.e., by "shunting" the transmission of the signal when the channels open (Blomfield, 1974). Whereas shunting inhibition is traditionally associated with localised increases of membrane conductance, the AP represents a very brief increment of membrane conductance that propagates along dendritic branches. Our realistic model shows that BK CAKCs represent a significant fraction of this

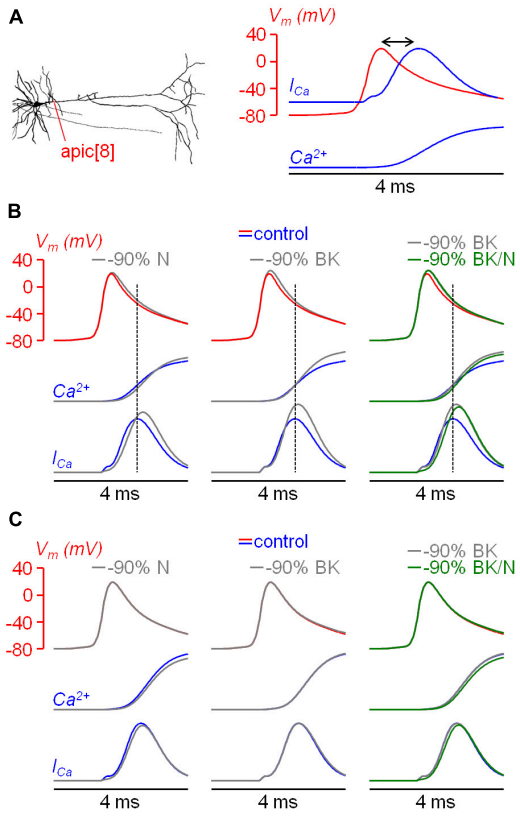

FIGURE 8
Effects of coupling between BK CAKCs and N-type VGCCs in a biophysically accurate model. **(A)** *Left,* the morphology of the L5 pyramidal neuron used in all simulations; the apical dendrite used to compare model and experiments is indicated in red. *Right*, dendritic AP evoked by a somatic current injection (red trace); time course of the associated Ca^{2+} transient and current (blue traces); the delay between the peaks of the AP and the I_{Ca} is indicated by the double arrow. **(B)** dendritic AP under control conditions (red trace) and the kinetics of the associated Ca^{2+} transient and current (blue traces); gray traces on the left are after removing 90% of N-type VGCCs; gray traces in the middle and right are after removing 90% of BK-type CAKCs; green traces on the right are after removing 90% of N-type VGCCs and BK-type CAKCs. Dotted lines indicate the timing of the I_{Ca} peak. Note the agreement with experimental recordings. **(C)** Same as in panel B, but from simulations in a model with no coupling between N-type VGCCs and BK CAKCs. Note that traces are not consistent with experimental results.

membrane conductance transient that is timely-locked to the AP. Thus, it is possible that the BK conductance transient can effectively contribute to the firing modulation produced by incoming synaptic inputs which are briefly shunted by the back-propagating AP. As for the case of localised BK channel activation in synaptic terminals and spines, the functional consequence of the spread BK channel activation is a reduction of neuronal excitability, in this case occurring at the level of dendritic integration.

4.3 Potential relevance in neurological disorders

The N-type VGCC, which is expressed in neurons predominantly at presynaptic terminals, is associated with several neurological conditions such as anxiety, addiction, and pain in correlation with its endogenous regulator nociceptin opioid peptide receptor (Caminski et al., 2022). In contrast, dysfunction of BK CAKCs encoded by the *KCNMA1* gene, which are widely expressed in many tissues, is associated with complex combinations of disorders, including seizures, movement disorders, developmental delay and intellectual disability (Bailey et al., 2019). For instance, a *KCNMA1* knock-out mouse exhibits motor impairments and suffers from learning difficulties (Typlt et al., 2013), whereas paroxysmal non-kinesigenic dyskinesia is observed in patients with gain-of-function channelopathies of BK channels (Miller et al., 2021). Notably, BK channel dysfunction is also reported in other genetic diseases such as the fragile X syndrome (Deng and Klyachko, 2016), suggesting that BK CAKCs can be a potential general target for therapeutic intervention (Griguoli et al., 2016). In the case of the signal described in the present report, the specific coupling of BK CAKCs to N-type VGCCs in the apical dendrite might be determined by alternative splicing of the channel or through auxiliary subunits. It is known that BK CAKCs are regulated by extensive alternative splicing as well as multiple auxiliary subunits, giving BK CAKCs both cell and tissue-specific properties (Kyle and Braun, 2014; Latorre et al., 2017), even within the L5 pyramidal neuron population (Guan et al., 2015). In recent years, various β and γ auxiliary subunits of BK channels have been identified which can modulate activation and inactivation dependencies (Gonzalez-Perez and Lingle, 2019), but the specific co-expression can in principle also drive the choice of the Ca^{2+} channel partner in sub-cellular compartments. We have previously reported that in the axon initial segment, BK CAKCs interact with $Na_V1.2$ channels, but this interaction seems independent of auxiliary subunits as was indicated by heterologous expression of these channels in HEK293 cells (Filipis et al., 2023). In contrast, the BK CAKCs could be guided by auxiliary subunits to form selective nanodomains with N-type VGCCs in the dendrites of L5 pyramidal neuron. This hypothesis requiring extensive investigation might be potentially important to investigate the specific function of BK CAKC characterised in this report.

Data availability statement

The datasets presented in this study can be found in online repositories. The names of the repository/repositories and accession number(s) can be found below: Repository Zenodo (https://zenodo.org/doi/10.5281/zenodo.7623897 and https://zenodo.org/records/7623898).

Ethics statement

The animal study was approved by the Ethics committee affiliated to the animal facility of the University of Grenoble (D3842110001). The study was conducted in accordance with the local legislation and institutional requirements.

Author contributions

LB: Conceptualization, Data curation, Investigation, Methodology, Writing – review & editing. EG: Data curation, Investigation, Methodology, Software, Writing – review & editing. FA: Investigation, Writing – review & editing. LF: Investigation, Supervision, Writing – review & editing. DT: Supervision, Writing – review & editing. MM: Conceptualization, Data curation, Formal analysis, Funding acquisition, Investigation, Methodology, Software, Supervision, Writing – review & editing. MC: Conceptualization, Data curation, Formal analysis, Funding acquisition, Methodology, Project administration, Software, Supervision, Validation, Writing – original draft, Writing – review & editing.

Funding

The author(s) declare financial support was received for the research, authorship, and/or publication of this article. This work was supported by the Agence Nationale de la Recherche through two grants (ANR-18-CE19-0024 – OptChemCom and Labex Ion Channels Science and Therapeutics: program number ANR-11-LABX-0015). EG was funded by the Regione Sicilia (CUP G79J21012770001). We are indebted to the Fédération pour la Recherche sur le Cerveau (FRC – Grant Espoir en tête, Rotary France) and the National Infrastructure France Life Imaging for financing part of the experimental equipment. We acknowledge a contribution from the Italian National Recovery and Resilience Plan (NRRP), M4C2, funded by the European Union – NextGenerationEU (Project IR0000011, CUP B51E22000150006, "EBRAINS-Italy") and the EU Horizon Europe Programme under the Specific Grant Agreement No. 101147319 (EBRAINS 2.0 Project).

Conflict of interest

The authors declare that the research was conducted in the absence of any commercial or financial relationships that could be construed as a potential conflict of interest.

The author(s) declared that they were an editorial board member of Frontiers, at the time of submission. This had no impact on the peer review process and the final decision.

Publisher's note

References

Ait Ouares, K., and Canepari, M. (2020). The origin of physiological local mGluR1 supralinear Ca^{2+} signals in cerebellar purkinje neurons. *J. Neurosci.* 40, 1795–1809. doi: 10.1523/JNEUROSCI.2406-19.2020

Ait Ouares, K., Filipis, L., Tzilivaki, A., Poirazi, P., and Canepari, M. (2019). Two distinct sets of Ca2+ and K+ channels are activated at different membrane potentials by the climbing fiber synaptic potential in purkinje neuron dendrites. *J. Neurosci.* 39, 1969–1981. doi: 10.1523/JNEUROSCI.2155-18.2018

Almog, M., and Korngreen, A. (2009). Characterization of voltage-gated Ca2+ conductances in layer 5 neocortical pyramidal neurons from rats. *PLoS One* 4:e4841. doi: 10.1371/journal.pone.0004841

Almog, M., and Korngreen, A. (2014). A quantitative description of dendritic conductances and its application to dendritic excitation in layer 5 pyramidal neurons. *J. Neurosci.* 34, 182–196. doi: 10.1523/JNEUROSCI.2896-13.2014

Ancatén-González, C., Segura, I., Alvarado-Sánchez, R., Chávez, A. E., and Latorre, R. (2023). Ca^{2+}- and voltage-activated K^{+} (BK) channels in the nervous system: One gene, a myriad of physiological functions. *Int. J. Mol. Sci.* 24:3407. doi: 10.3390/ijms24043407

Ascoli, G. A., Donohue, D. E., and Halavi, M. (2007). NeuroMorpho.Org: A central resource for neuronal morphologies. *J. Neurosci.* 27, 9247–9251. doi: 10.1523/JNEUROSCI.2055-07.2007

Bailey, C. S., Moldenhauer, H. J., Park, S. M., Keros, S., and Meredith, A. L. (2019). KCNMA1-linked Channelopathy. *J. Gen. Physiol.* 151, 1173–1189. doi: 10.1085/jgp.201912457

Benhassine, N., and Berger, T. (2005). Homogeneous distribution of large-conductance calcium-dependent potassium channels on soma and apical dendrite of rat neocortical layer 5 pyramidal neurons. *Eur. J. Neurosci.* 21, 914–926. doi: 10.1111/j.1460-9568.2005.03934.x

Berkefeld, H., and Fakler, B. (2008). Repolarizing responses of BKCa-Cav complexes are distinctly shaped by their Cav subunits. *J. Neurosci.* 28, 8238–8245. doi: 10.1523/JNEUROSCI.2274-08.2008

Berkefeld, H., Fakler, B., and Schulte, U. (2010). Ca2+-activated K+ channels: From protein complexes to function. *Physiol. Rev.* 90, 1437–1459. doi: 10.1152/physrev.00049.2009

Berkefeld, H., Sailer, C. A., Bildl, W., Rohde, V., Thumfart, J. O., Eble, S., et al. (2006). BKCa-Cav channel complexes mediate rapid and localized Ca2+-activated K+ signaling. *Science* 314, 615–620. doi: 10.1126/science.1132915

Blömer, L. A., Filipis, L., and Canepari, M. (2021). Cal-520FF is the present optimal Ca^{2+} indicator for ultrafast Ca^{2+} imaging and optical measurement of Ca^{2+} currents. *J. Fluoresc.* 31, 619–623. doi: 10.1007/s10895-021-02701-8

Blomfield, S. (1974). Arithmetical operations performed by nerve cells. *Brain Res.* 69, 115–124. doi: 10.1016/0006-8993(74)90375-8

Bock, T., Honnuraiah, S., and Stuart, G. J. (2019). Paradoxical excitatory impact of sk channels on dendritic excitability. *J. Neurosci.* 39, 7826–7839. doi: 10.1523/JNEUROSCI.0105-19.2019

Bond, C. T., Herson, P. S., Strassmaier, T., Hammond, R., Stackman, R., Maylie, J., et al. (2004). Small conductance Ca2+-activated K+ channel knock-out mice reveal the identity of calcium-dependent afterhyperpolarization currents. *J. Neurosci.* 24, 5301–5306. doi: 10.1523/JNEUROSCI.0182-04.2004

Buchanan, K. A., Blackman, A. V., Moreau, A. W., Elgar, D., Costa, R. P., Lalanne, T., et al. (2012). Target-specific expression of presynaptic NMDA receptors in neocortical microcircuits. *Neuron* 75, 451–466. doi: 10.1016/j.neuron.2012.06.017

Caminski, E. S., Antunes, F. T. T., Souza, I. A., Dallegrave, E., and Zamponi, G. W. (2022). Regulation of N-type calcium channels by nociceptin receptors and its possible role in neurological disorders. *Mol. Brain* 15:95. doi: 10.1186/s13041-022-00982-z

Cui, J. (2010). BK-type calcium-activated potassium channels: Coupling of metal ions and voltage sensing: BK channel activation by voltage and metal ions. *J. Physiol.* 588, 4651–4658. doi: 10.1113/jphysiol.2010.194514

Deng, P. Y., and Klyachko, V. A. (2016). Genetic upregulation of BK channel activity normalizes multiple synaptic and circuit defects in a mouse model of fragile X syndrome. *J. Physiol.* 594, 83–97. doi: 10.1113/JP271031

Fakler, B., and Adelman, J. P. (2008). Control of K(Ca) channels by calcium nano/microdomains. *Neuron* 59, 873–881. doi: 10.1016/j.neuron.2008.09.001

Filipis, L., Blömer, L. A., Montnach, J., De Waard, M., and Canepari, M. (2023). Nav1.2 and BK channels interaction shapes the action potential in the axon initial segment. *J. Physiol.* 601, 1957–1979. doi: 10.1113/JP283801

Filipis, L., and Canepari, M. (2021). Optical measurement of physiological sodium currents in the axon initial segment. *J. Physiol.* 599, 49–66. doi: 10.1113/JP280554

Gandini, M. A., and Zamponi, G. W. (2022). Voltage-gated calcium channel nanodomains: Molecular composition and function. *FEBS J.* 289, 614–633. doi: 10.1111/febs.15759

Ghosh, A., and Greenberg, M. E. (1995). Calcium signaling in neurons: Molecular mechanisms and cellular consequences. *Science* 268, 239–247.

Gonzalez-Perez, V., and Lingle, C. J. (2019). Regulation of BK channels by beta and gamma subunits. *Ann. Rev. Physiol.* 81, 113–137.

Griguoli, M., Sgritta, M., and Cherubini, E. (2016). Presynaptic BK channels control transmitter release: Physiological relevance and potential therapeutic implications. *J. Physiol.* 594, 3489–3500. doi: 10.1113/JP271841

Grunnet, M., and Kaufmann, W. A. (2004). Coassembly of big conductance Ca2+-activated K+ channels and L-type voltage-gated Ca2+ channels in rat brain. *J. Biol. Chem.* 279, 36445–36453. doi: 10.1074/jbc.M402254200

Guan, D., Armstrong, W. E., and Foehring, R. C. (2015). Electrophysiological properties of genetically identified subtypes of layer 5 neocortical pyramidal neurons: Ca^{2+} dependence and differential modulation by norepinephrine. *J. Neurophysiol.* 113, 2014–2032. doi: 10.1152/jn.00524.2014

Hallermann, S., de Kock, C. P., Stuart, G. J., and Kole, M. H. (2012). State and location dependence of action potential metabolic cost in cortical pyramidal neurons. *Nat. Neurosci.* 15, 1007–1014. doi: 10.1038/nn.3132

Harnett, M., Magee, J., and Williams, S. (2015). Distribution and function of HCN channels in the apical dendritic tuft of neocortical pyramidal neurons. *J. Neurosci.* 35, 1024–1037. doi: 10.1523/JNEUROSCI.2813-14.2015

Hu, L. Y., Ryder, T. R., Rafferty, M. F., Dooley, D. J., Geer, J. J., Lotarski, S. M., et al. (1999). Structure-activity relationship of N-methyl-N-aralkyl-peptidylamines as novel N-type calcium channel blockers. *Bioorg. Med. Chem. Lett.* 9, 2151–2156. doi: 10.1016/s0960-894x(99)00359-5

Jaafari, N., and Canepari, M. (2016). Functional coupling of diverse voltage-gated Ca(2+) channels underlies high fidelity of fast dendritic Ca(2+) signals during burst firing. *J. Physiol.* 594, 967–983. doi: 10.1113/JP271830

Jaafari, N., De Waard, M., and Canepari, M. (2014). Imaging fast calcium currents beyond the limitations of electrode techniques. *Biophys. J.* 107, 1280–1288. doi: 10.1016/j.bpj.2014.07.059

Kang, J., Huguenard, J. R., and Prince, D. A. (1996). Development of BK channels in neocortical pyramidal neurons. *J. Neurophysiol.* 76, 188–198.

Kay, A. R., and Wong, R. K. (1987). Calcium current activation kinetics in isolated pyramidal neurones of the Ca1 region of the mature guinea-pig hippocampus. *J. Physiol.* 392, 603–616. doi: 10.1113/jphysiol.1987.sp016799

Kole, M. H. P., Ilschner, S. U., Kampa, B. M., Williams, S. R., Ruben, P. C., and Stuart, G. J. (2008). Action potential generation requires a high sodium channel density in the axon initial segment. *Nat. Neurosci.* 11, 178–186. doi: 10.1038/nn2040

Kyle, B. D., and Braun, A. P. (2014). The regulation of BK channel activity by pre- and post-translational modifications. *Front. Physiol.* 5:316. doi: 10.3389/fphys.2014.00316

Latorre, R., Castillo, K., Carrasquel-Ursulaez, W., Sepulveda, R. V., Gonzalez-Nilo, F., Gonzalez, C., et al. (2017). Molecular determinants of BK channel functional diversity and functioning. *Physiol. Rev.* 97, 39–87. doi: 10.1152/physrev.00001.2016

Lilliefors, H. W. (1967). On the kolmogorov-smirnov test for normality with mean and variance unknown. *J. Am. Stat. Assoc.* 62, 399–402. doi: 10.1080/01621459.1967.10482916

Loane, D. J., Lima, P. A., and Marrion, N. V. (2007). Co-assembly of N-type Ca2+ and BK channels underlies functional coupling in rat brain. *J. Cell Sci.* 120, 985–995.

Mandge, D., and Manchanda, R. (2018). A biophysically detailed computational model of urinary bladder small DRG neuron soma. *PLoS Comp. Biol.* 14:e1006293.

Marcantoni, A., Vandael, D. H., Mahapatra, S., Carabelli, V., Sinnegger-Brauns, M. J., Striessnig, J., et al. (2010). Loss of Cav1.3 channels reveals the critical role of L-type and BK channel coupling in pacemaking mouse adrenal chromaffin cells. *J. Neurosci.* 30, 491–504. doi: 10.1523/JNEUROSCI.4961-09.2010

Markram, H., Helm, P. J., and Sakmann, B. (1995). Dendritic calcium transients evoked by single back-propagating action potentials in rat neocortical pyramidal neurons. *J. Physiol.* 485, 1–20. doi: 10.1113/jphysiol.1995.sp020708

Marrion, N. V., and Tavalin, S. J. (1998). Selective activation of Ca2+- activated K+ channels by co-localized Ca2+ channels in hippocampal neurons. *Nature* 395, 900–905. doi: 10.1038/27674

Masi, A., Cicchi, R., Carloni, A., Pavone, F. S., and Arcangeli, A. (2010). Optical methods in the study of protein-protein interactions. *Adv. Exp. Med. Biol.* 674, 33–42.

Migliore, M., Novara, G., and Tegolo, D. (2008). Single neuron binding properties and the magical number 7. *Hippocampus* 18, 1122–1130. doi: 10.1002/hipo.20480

Migliore, M., and Shepherd, G. M. (2002). Emerging rules for the distributions of active dendritic conductances. *Nat. Rev. Neurosci.* 3, 362–370. doi: 10.1038/nrn810

Miller, J. P., Moldenhauer, H. J., Keros, S., and Meredith, A. L. (2021). An emerging spectrum of variants and clinical features in *KCNMA1*-linked channelopathy. *Channels* 15, 447–464. doi: 10.1080/19336950.2021.1938852

Montnach, J., Blömer, L. A., Lopez, L., Filipis, L., Meudal, H., Lafoux, A., et al. (2022). Synthetic analogues of huwentoxin-IV spider peptide with altered human $Na_V1.7/Na_V1.6$ selectivity ratios. *Nat. Commun.* 13:417. doi: 10.1038/s41467-022-27974-w

Pedarzani, P., and Stocker, M. (2008). Molecular and cellular basis of small–and intermediate-conductance, calcium-activated potassium channel function in the brain. *Cell. Mol. Life Sci.* 65, 3196–3217. doi: 10.1007/s00018-008-8216-x

Popovic, M., Vogt, K., Holthoff, K., Konnerth, A., Salzberg, B. M., Grinvald, A., et al. (2015). Imaging submillisecond membrane potential changes from individual regions of single axons, dendrites and spines. *Adv. Exp. Med. Biol.* 859, 57–101. doi: 10.1007/978-3-319-17641-3_3

Raffaelli, G., Saviane, C., Mohajerani, M. H., Pedarzani, P., and Cherubini, E. (2004). BK potassium channels control transmitter release at CA3-CA3 synapses in the rat hippocampus. *J. Physiol.* 557, 147–157. doi: 10.1113/jphysiol.2004.062661

Ramaswamy, S., and Markram, H. (2015). Anatomy and physiology of the thick-tufted layer 5 pyramidal neuron. *Front. Cell. Neurosci.* 9:233. doi: 10.3389/fncel.2015.00233

Sah, P., and Davies, P. (2000). Calcium-activated potassium currents in mammalian neurons. *Clin. Exp. Pharmacol. Physiol.* 27, 657–663. doi: 10.1046/j.1440-1681.2000.03317.x

Schiller, J., Helmchen, F., and Sakmann, B. (1995). Spatial profile of dendritic calcium transients evoked by action potentials in rat neocortical pyramidal neurones. *J. Physiol.* 487, 583–600. doi: 10.1113/jphysiol.1995.sp020902

Shah, K. R., Guan, X., and Yan, J. (2022). Structural and functional coupling of calcium-activated BK channels and calcium-permeable channels within nanodomain signaling complexes. *Front. Physiol.* 12:796540. doi: 10.3389/fphys.2021.796540

Stewart, A. E., and Foehring, R. C. (2000). Calcium currents in retrogradely labeled pyramidal cells from rat sensorimotor cortex. *J. Neurophysiol.* 83, 2349–2354. doi: 10.1152/jn.2001.85.4.1412

Stuart, G., Schiller, J., and Sakmann, B. (1997). Action potential initiation and propagation in rat neocortical pyramidal neurons. *J. Physiol.* 505, 617–632. doi: 10.1111/j.1469-7793.1997.605ba.x

Stuart, G. J., and Sakmann, B. (1994). Active propagation of somatic action potentials into neocortical pyramidal cell dendrites. *Nature* 367, 69–72. doi: 10.1038/367069a0

Sun, X., Gu, X. Q., and Haddad, G. G. (2003). Calcium influx via L- and N-type calcium channels activates a transient large-conductance Ca2+-activated K+ current in mouse neocortical pyramidal neurons. *J. Neurosci.* 23, 3639–3648. doi: 10.1523/JNEUROSCI.23-09-03639.2003

Talley, E. M., Cribbs, L. L., Lee, J. H., Daud, A., Perez-Reyes, E., and Bayliss, D. A. (1999). Differential distribution of three members of a gene family encoding low voltage-activated (T-type) calcium channels. *J. Neurosci.* 19, 1895–1911. doi: 10.1523/JNEUROSCI.19-06-01895.1999

Tazerart, S., Blanchard, M. G., Miranda-Rottmann, S., Mitchell, D. E., NaveaPina, B., Thomas, C. I., et al. (2022). Selective activation of BK channels in small-headed dendritic spines suppresses excitatory postsynaptic potentials. *J. Physiol.* 600, 2165–2187. doi: 10.1113/JP282303

Typlt, M., Mirkowski, M., Azzopardi, E., Ruettiger, L., Ruth, P., and Schmid, S. (2013). Mice with deficient BK channel function show impaired prepulse inhibition and spatial learning, but normal working and spatial reference memory. *PLoS One* 11:e81270. doi: 10.1371/journal.pone.0081270

Vandael, D. H., Marcantoni, A., Mahapatra, S., Caro, A., Ruth, P., Zuccotti, A., et al. (2010). Ca(v)1.3 and BK channels for timing and regulating cell firing. *Mol. Neurobiol.* 42, 185–198. doi: 10.1007/s12035-010-8151-3

Vandael, D. H., Zuccotti, A., Striessnig, J., and Carbone, E. (2012). Ca(V)1.3-driven SK channel activation regulates pacemaking and spike frequency adaptation in mouse chromaffin cells. *J. Neurosci.* 32, 16345–16359. doi: 10.1523/JNEUROSCI.3715-12.2012

Vergara, C., Latorre, R., Marrion, N. V., and Adelman, J. P. (1998). Calcium-activated potassium channels. *Curr. Opin. Neurobiol.* 8, 321–329. doi: 10.1016/s0959-4388(98)80056-1

Vierra, N. C., and Trimmer, J. S. (2022). Ion channel partnerships: Odd and not-so-odd couples controlling neuronal ion channel function. *Int. J. Mol. Sci.* 23:1953. doi: 10.3390/ijms23041953

Villalobos, C., Shakkottai, V. G., Chandy, K. G., Michelhaugh, S. K., and Andrade, R. (2004). SKCa channels mediate the medium but not the slow calcium-activated afterhyperpolarization in cortical neurons. *J. Neurosci.* 24, 3537–3542. doi: 10.1523/JNEUROSCI.0380-04.2004

Vogt, K. E., Gerharz, S., Graham, J., and Canepari, M. (2011a). High-resolution simultaneous voltage and Ca^{2+} imaging. *J. Physiol.* 589, 489–494. doi: 10.1113/jphysiol.2010.200220

Vogt, K. E., Gerharz, S., Graham, J., and Canepari, M. (2011b). Combining membrane potential imaging with L-glutamate or GABA photorelease. *PLoS One* 6:e24911. doi: 10.1371/journal.pone.0024911

Volynski, K. E., and Krishnakumar, S. S. (2018). Synergistic control of neurotransmitter release by different members of the synaptotagmin family. *Curr. Opin. Neurobiol.* 51, 154–162. doi: 10.1016/j.conb.2018.05.006

Wimmer, V. C., Reid, C. A., Mitchell, S., Richards, K. L., Scaf, B. B., Leaw, B. T., et al. (2010). Axon initial segment dysfunction in a mouse model of genetic epilepsy with febrile seizures plus. *J. Clin. Invest.* 120, 2661–2671. doi: 10.1172/JCI42219

frontiers | Frontiers in Cellular Neuroscience

TYPE Brief Research Report
PUBLISHED 26 April 2024
DOI 10.3389/fncel.2024.1403073

OPEN ACCESS

EDITED BY
Enrico Cherubini,
European Brain Research Institute, Italy

REVIEWED BY
Ernesto Griego,
Albert Einstein College of Medicine, United States
Heiko J. Luhmann,
Johannes Gutenberg University Mainz, Germany

*CORRESPONDENCE
Roustem Khazipov
roustem.khazipov@inserm.fr

RECEIVED 18 March 2024
ACCEPTED 15 April 2024
PUBLISHED 26 April 2024

CITATION
Shipkov D, Nasretdinov A, Khazipov R and Valeeva G (2024) Synchronous excitation in the superficial and deep layers of the medial entorhinal cortex precedes early sharp waves in the neonatal rat hippocampus. *Front. Cell. Neurosci.* 18:1403073. doi: 10.3389/fncel.2024.1403073

Synchronous excitation in the superficial and deep layers of the medial entorhinal cortex precedes early sharp waves in the neonatal rat hippocampus

Dmitrii Shipkov[1], Azat Nasretdinov[1], Roustem Khazipov[1,2]* and Guzel Valeeva[1]

[1]Laboratory of Neurobiology, Institute of Fundamental Medicine and Biology, Kazan Federal University, Kazan, Russia, [2]INMED - INSERM, Aix-Marseille University, Marseille, France

Early Sharp Waves (eSPWs) are the earliest pattern of network activity in the developing hippocampus of neonatal rodents. eSPWs were originally considered to be an immature prototype of adult SPWs, which are spontaneous top-down hippocampal events that are self-generated in the hippocampal circuitry. However, recent studies have shifted this paradigm to a bottom-up model of eSPW genesis, in which eSPWs are primarily driven by the inputs from the layers 2/3 of the medial entorhinal cortex (MEC). A hallmark of the adult SPWs is the relay of information from the CA1 hippocampus to target structures, including deep layers of the EC. Whether and how deep layers of the MEC are activated during eSPWs in the neonates remains elusive. In this study, we investigated activity in layer 5 of the MEC of neonatal rat pups during eSPWs using silicone probe recordings from the MEC and CA1 hippocampus. We found that neurons in deep and superficial layers of the MEC fire synchronously during MEC sharp potentials, and that neuronal firing in both superficial and deep layers of the MEC precedes the activation of CA1 neurons during eSPWs. Thus, the sequence of activation of CA1 hippocampal neurons and deep EC neurons during sharp waves reverses during development, from a lead of deep EC neurons during eSPWs in neonates to a lead of CA1 neurons during adult SPWs. These findings suggest another important difference in the generative mechanisms and possible functional roles of eSPWs compared to adult SPWs.

KEYWORDS

entorhinal cortex, hippocampus, sharp wave, neonatal rat, local field potentials, multiple unit activity, current-source density

1 Introduction

Early Sharp Waves (eSPWs) are the earliest network activity pattern in the developing hippocampus of neonatal rodents (Leinekugel et al., 2002; Karlsson et al., 2006; Mohns et al., 2007; Marguet et al., 2015; Unichenko et al., 2015; Valeeva et al., 2019a,b; Murata and Colonnese, 2020; Graf et al., 2021; Cossart and Khazipov, 2022; Pochinok et al., 2024). The originally proposed paradigm implies that eSPWs are an immature prototype of adult SPWs, except that eSPWs lack the high frequency oscillations (ripples, Rs) that are characteristic of adult SPWs and appear after P10 (Leinekugel et al., 2002; Buhl and Buzsaki, 2005; Pochinok

et al., 2024), and that eSPWs are reliably triggered by myoclonic movements, presumably via sensory feedback from movements (Karlsson et al., 2006; Mohns and Blumberg, 2010; Valeeva et al., 2019a,b). In addition, eSPWs, but not adult SPW-Rs, are triggered by somatosensory stimulation (Brankack and Buzsaki, 1986; Bellistri et al., 2013; Gainutdinov et al., 2023). However, recent studies have shifted this paradigm, suggesting that eSPW network mechanisms differ from adult SPW-Rs. In fact, adult SPW-Rs are endogenous, self-generated events in the hippocampal circuitry and are considered to be top-down events that transfer information to target brain regions and support the consolidation of memories acquired during exploration (Buzsaki, 2015). In contrast, eSPWs are generated in a bottom-up fashion in the entorhinal-hippocampal circuit and are primarily driven by inputs from layers 2/3 of the medial entorhinal cortex (MEC) (Valeeva et al., 2019a,b). Synchronized firing of neurons in the superficial layers of the MEC is associated with so-called sharp potentials (MEC-SPs), which precede hippocampal eSPWs and are triggered by physiological myoclonic movements (Valeeva et al., 2019a,b). Thus, the entorhinal-hippocampal MEC-SP – eSPW complexes are embedded within the large-scale network activated during twitches and startles, and which likely involves sensory feedback from myoclonic movements conveyed from somatosensory cortex to MEC and further to hippocampus (Karlsson et al., 2006; Mohns and Blumberg, 2010; Valeeva et al., 2019a,b; Gainutdinov et al., 2023). It has been suggested that entorhinal-hippocampal MEC-SP – eSPW complexes underlie the sequential, activity-dependent maturation of connections between the MEC and the hippocampus and within the hippocampal circuitry (Donato et al., 2017; Valeeva et al., 2019a,b; Cossart and Khazipov, 2022).

A hallmark of adult SPW-ripples is the relay of information from the CA1 hippocampus to target structures, including L5 of the MEC, with further transfer of transiently stored hippocampal information to long-term engrams in neocortical networks (Buzsaki, 1986; Siapas and Wilson, 1998; Girardeau et al., 2009; Nakashiba et al., 2009; Buzsaki, 2015; Squire et al., 2015). During SPW-Rs, MEC L5 neurons are activated following CA1 pyramidal cells by direct monosynaptic CA1 to L5 inputs or via intermediate activation of subicular neurons (Chrobak and Buzsaki, 1994, 1996; Isomura et al., 2006; Roth et al., 2016; Rozov et al., 2020). Whether and how deep layers of MEC are activated during eSPWs in the neonates, and whether CA1 inputs to MEC drive L5 neurons similarly to adult SPW-Rs, remains elusive. The latter scenario is supported by studies using intact limbic structures preparation from neonatal rats *in vitro*, in which kainate-induced hippocampal seizures propagated to the EC suggesting the existence of functional connections from the hippocampus to the EC as early as P4 (Khalilov et al., 1999). On the other hand, hippocampal CA3-generated giant depolarizing potentials (GDPs) (Ben-Ari et al., 1989), which have been considered as an *in vitro* counterpart of eSPWs (Leinekugel et al., 2002; Ben Ari et al., 2007; Griguoli and Cherubini, 2017), do not propagate to the EC (Khalilov et al., 1999; Namiki et al., 2013). Furthermore, the presence of spontaneous waves of activity involving both superficial and deep EC layers in neonatal mouse brain slices suggests the existence of intracortical mechanisms for horizontal and vertical synchronization in the developing EC network (Sheroziya et al., 2009; Namiki et al., 2013; Unichenko et al., 2015). Here, we investigated how activity in deep EC layers is organized in relation to MEC-SPs and hippocampal eSPWs *in vivo*. We found that neurons in deep and superficial MEC layers fire synchronously during MEC-SPs, and that neuronal firing in both superficial and deep EC layers precedes the activation of CA1 neurons during eSPWs. Thus, the sequence of activation of hippocampal CA1 neurons and deep EC neurons during sharp waves reverses during development, from a lead of deep EC neurons during eSPWs in neonates to a lead of CA1 neurons during adult SPWs. Our findings suggest another important difference between eSPWs and adult SPWs, supporting the paradigm shift in views of the function of the developing entorhinal-hippocampal network.

2 Materials and methods

2.1 Ethical approval

The animal experiments were carried out in compliance with the ARRIVE guidelines. Animal care and procedures were in accordance with EU Directive 2010/63/EU for animal experiments, and all animal-use protocols were approved by the French National Institute of Health and Medical Research (APAFIS #16992-2020070612319346 v2) and the Local Ethical Committee of Kazan Federal University (#24/22.09.2020).

2.2 Animal preparation

Wistar rats of both sexes from postnatal days (P) 4–7 were used. Preparation of the animals for head-restrained recordings was performed under isoflurane (1.5–2.5%) anesthesia. The skull of the animal was cleaned of skin and periosteum using Hemostab Al solution (Omega Dent, Russia), dried and covered with a thin layer of cyanacrylamide glue and self-curing acrylic denture repair material (Meliodent RR, Kulzer, GmbH, Germany), leaving the surface of left parietal bone open. A metal ring was fixed to the skull by dental acrylic material and via ball-joint to a magnetic stand. The wound was treated with bupivacaine (5%). The animal was then wrapped in a cotton and warmed at a thermal pad (37°C, Warner Instr., United States) and left for an hour to recover from anesthesia. None of the animals showed any signs of discomfort or pain (as evidenced by the absence of prolonged and excessive movements) during the recordings. Extracellular recordings of local field potentials (LFP) and multiple unit activity (MUA) were performed along the CA1—dentate gyrus axis of the dorsal hippocampus and the dorsal part of MEC in the left hemisphere (Figure 1) using 16-channel linear silicon probes with 50 μm separation distance between the electrodes (NeuroNexus, United States). Of note, eSPWs are expressed and highly synchronized along the longitudinal axis of the hippocampus and bilaterally in neonatal rat pups (Valeeva et al., 2019a,b, 2020). Silicon probes were placed using stereotaxic coordinates provided by an atlas of the postnatal rat brain (Khazipov et al., 2015). For hippocampal recordings, electrodes were placed at—2.1 mm posterior and 1.35 mm lateral from bregma at depth of 2,300–2,600 μm; the lateral-medial angle from the horizontal plane 75°. For MEC recordings, electrodes were placed as in (Quilichini et al., 2010), at 1.6 mm anterior and 3.7 mm lateral from lambda at depth 3,000–3,600 μm; the anterior–posterior angle from the horizontal plane 45°. In a subset of animals, electrodes were placed into MEC along the MEC layers as in Valeeva et al. (2019a,b) at the medial-lateral angle from the horizontal plane

10.3389/fncel.2024.1403073

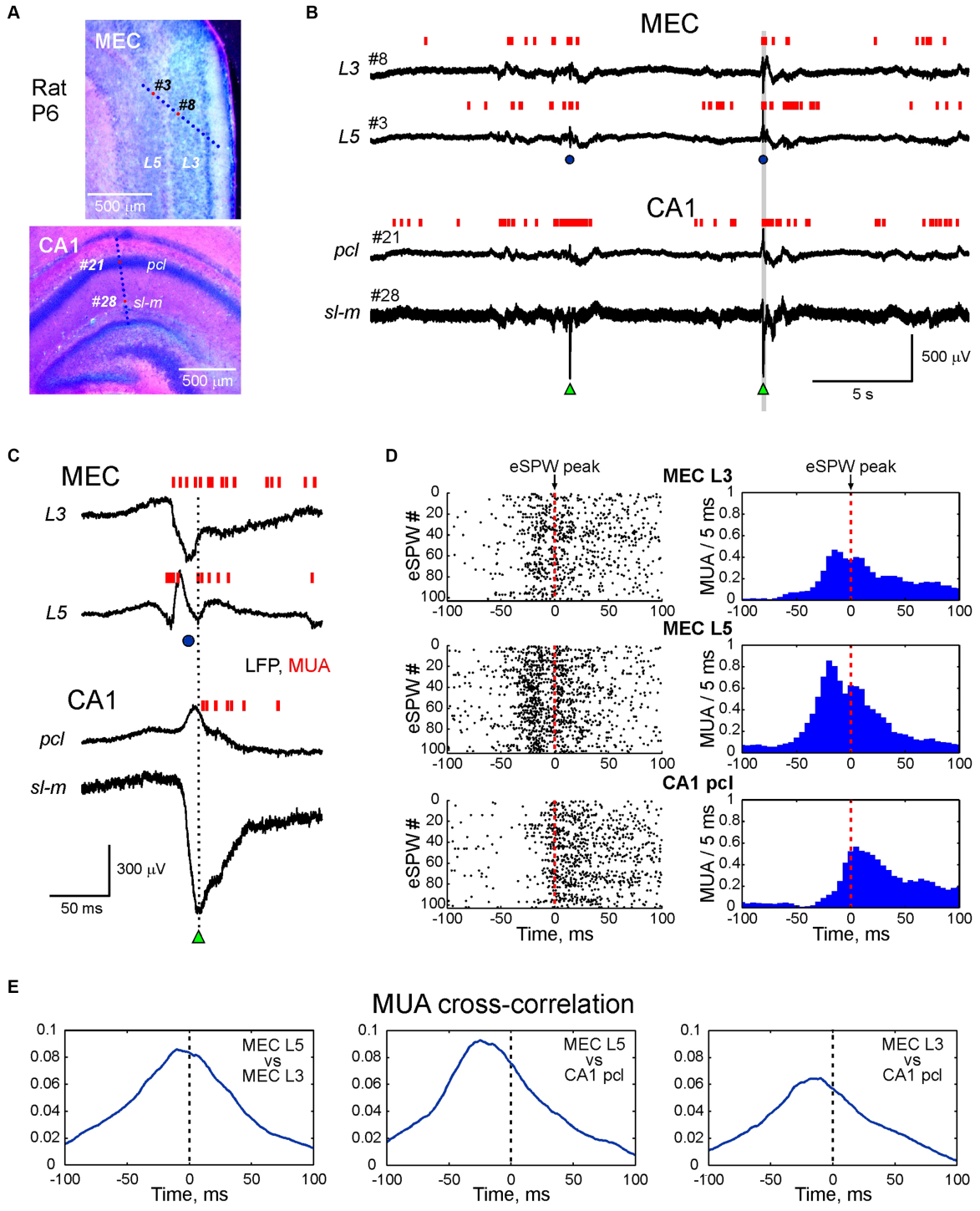

FIGURE 1
Activity bursts in MEC L3 and L5 associated with sharp potentials precede early hippocampal sharp waves in the neonatal rat. **(A)** Recording sites of multielectrode arrays overlaid on a cresyl violet stained sagittal MEC slice (top panel) and coronal hippocampal slice (bottom panel) in a P6 rat pup. **(B)** Simultaneous LFP recordings in MEC L5 and L3 (recording sites # 3 and # 8 on top panel **A**), and hippocampal CA1 pyramidal cell layer (pcl) and stratum lacunosum-moleculare (sl-m) (recording sites # 21 and # 28 on bottom panel **A**). Multiple unit activity (MUA) is represented by vertical red bars. Hippocampal early sharp waves (eSPWs) are indicated by green triangles, sharp potentials in MEC (MEC-SPs) are indicated by blue circles. **(C)** An example of MEC L3/L5 burst and eSPW complex from panel **(B)** (highlighted in a gray box) on expanded time scale. **(D)** eSPW-triggered raster plots (left) and PETHs (right) for MUA in MEC L5 and L3, and in CA1 pcl. **(E)** MUA cross-correlograms in MEC L5 vs. MEC L3 (left), MEC L5 vs. CA1 (middle) and MEC L3 vs. CA1 (right) during peri-eSPW epochs (n = 102 eSPWs).

75° (Supplementary Figure S3). For the histological reconstruction of electrode tracks, electrodes were coated with ethanol-dissolved DiI (Sigma-Aldrich, United States). A chlorided silver wire, placed in the neocortex, served as a ground electrode. Signals from extracellular recordings were amplified and filtered (10,000X; 0.15 Hz–9 kHz) using Digital Lynx SX amplifier (Neuralynx, United States), digitized at

16–32 kHz. From one to 2 h of spontaneous activity were recorded from each animal.

2.3 Histology

After recordings the animals were deeply anaesthetized with isoflurane (5%), the brains were removed and left for fixation in 4% paraformaldehyde for 2 days at room temperature. Then the brains were rinsed in PBS and mounted in agar blocks. Brains were cut into 100 µm-thick slices using Vibratome (Thermo Fisher Scientific, MA, United States) in two steps. First, coronal slices were cut in rostral-caudal direction to obtain full DiI track of the hippocampal probe. Then the two hemispheres in remaining block were separated, and sagittal slices were prepared from the left hemisphere to reveal the DiI track of the MEC probe. The location of the silicone probe in hippocampus and enthorhinal cortex was assessed through identification of the DiI track in serial 100-µm-thick sagittal sections (Supplementary Figures S1, S2). Then DiI tracks were overlaid on the microphotographs of brain slices after cresyl violet staining. In hippocampal recordings, electrode location was verified by the highest MUA rate in CA1 stratum pyramidale. In MEC recordings, electrode location was adjusted according to MEC-SP LFP reversal around L4.

2.4 Data analysis

Raw data were preprocessed using custom-written functions in MATLAB (MathWorks, United States). Hippocampal eSPWs were detected from down-sampled (1,000 Hz), bandpass filtered (3–100 Hz, Chebyshev type 2 Filter) LFPs. All troughs greater than 2–4 SD from the least active 100 s long epoch through the entire record were first detected from the channel located in the stratum lacunosum–moleculare (*sl-m*) and their peak negativity was taken as time = 0 for further analysis. Independently, LFP peaks exceeding 1–3 SD were similarly detected from the CA1 pyramidal cell layer (*pcl*). Negative *sl-m* events with a half-width ≤ 65 ms co-occurring with positive *pcl* peaks in the within ±50 ms time window were considered as eSPWs. To discard movement artifacts, LFP segments from −0.5 s to 1 s around the eSPW peak negativity for each channel were visually inspected. MEC sharp potentials (MEC-SPs) were detected from the channel displaying maximal negativity within a time window from −0.5 s to 0.5 s around the eSPW similarly to the procedure of eSPWs detection described above. Current-source density (CSD) analysis across MEC depth was performed on averaged MEC-SPs according to a differential scheme for second derivative and smoothed with a triangular kernel of length 4 (Freeman and Nicholson, 1975).

For multiple unit activity (MUA) analysis, raw LFP recordings were band-pass filtered in the range of 250–4,000 Hz (Daubechies wavelet filter). Action potentials were detected as negative peaks below 4 SD of the least active 100 s long epoch over the entire recording. Peri-event time histograms (PETHs) were calculated for MUA in 1 ms bins relative to the eSPW times followed by smoothing with the 50 ms window sliding average filter. MUA cross-correlograms were calculated in 1 ms bins for peri-eSPW epochs of [−50 + 100] ms relative to the eSPW times followed by smoothing with the 30 ms window sliding average filter.

2.5 Statistical analysis

Statistical analysis was performed using the MATLAB Statistics toolbox. Group comparisons were performed using the two-sided Wilcoxon rank sum and Wilcoxon signed rank tests. Unless otherwise noted, group data are presented as median (Q1–Q3).

3 Results

In the present study, we explored the dynamics of neuronal network activity across layers of the MEC in association with hippocampal eSPWs in neonatal rats. For this purpose, we performed simultaneous recordings of LFPs and multiple unit activity (MUA) from the dorsal CA1 hippocampus and MEC in non-anaesthetized, head-restrained postnatal day [P] 4–7 rats. The location of the recording sites was determined during *post-hoc* analysis of the DiI electrode traces in coronal slices for hippocampal recordings and sagittal slices for MEC recordings with silicone probes inserted across the MEC layers ($n = 18$ rats) (Figure 1A; Supplementary Figures S1, S2) or parallel to the MEC layers ($n = 10$ rats; Supplementary Figure S3). Consistent with previous studies, activity in the MEC and hippocampus was characterized by discontinuous temporal organization and complexes of intermittent eSPWs in the hippocampus occurring at a frequency of 1.4 (0.9–1.8) per minute ($n = 18$ rats), preceded by bursts of MEC activity often associated with large amplitude sharp potentials (MEC-SPs) (Leinekugel et al., 2002; Karlsson et al., 2006; Mohns et al., 2007; Marguet et al., 2015; Unichenko et al., 2015; Valeeva et al., 2019a,b; Murata and Colonnese, 2020; Graf et al., 2021; Pochinok et al., 2024). Example recordings from L3 and L5 of MEC and CA1 hippocampus (*pcl* and *sl-m*) are shown in Figures 1B,C. eSPWs were characterized by negativity below the CA1 pyramidal cell layer and polarity reversal at the *pcl*, whereas MEC-SPs were associated with a negative sharp potential in superficial MEC layers 2 and 3 and polarity reversal at the level of L4 (see also below) (Figure 1C). We then examined how the activity of neurons in MEC and CA1 was modulated in relation to hippocampal eSPWs (Figures 1C–E). Raster plots and peri-event histograms of MUA in L3 and L5 of MEC and CA1 *pcl* aligned by eSPW peaks revealed a strong increase in MUA and co-activation of neurons in deep and superficial MEC layers, preceding the activation of CA1 neurons (Figure 1D). This was further confirmed by cross-correlation analysis of MUA in MEC L3 and L5 and in CA1 (Figure 1E).

We further analyzed neuronal activity in MEC L3 and L5 and CA1 hippocampus during eSPWs at the population level in a group of 17 P5-7 rats (Figure 2). Action potential firing in MEC L3 and L5, and in CA1 *pcl* increased during eSPWs ($n = 17$ rats; $p < 0.001$; Figures 2A,B; Supplementary Table S1). However, the peak activation of neurons in the hippocampus was significantly delayed compared to MEC, both in L3 and L5 ($n = 17$ rats; $p < 0.001$; Figure 2C; Supplementary Table S2). Notably, although the peak of MUA relatively to eSPWs in L5 had a tendency to precede that in L3, this difference was not significant, however. A ~ 20 ms delay in activation of units in the CA1 hippocampus from MEC units in L3 and L5 was also evident from cross-correlation analysis of all units detected in a time window of −50 to +100 ms relative to eSPWs (Figures 2D,F; Supplementary Tables S3, S4). Group data analysis of paired comparisons of MUA cross-correlation peaks revealed a significant precedence of MEC units (both in L3 and L5) relative to CA1 units ($n = 17$ rats; $p < 0.05$), and a short (by ~6 ms) but

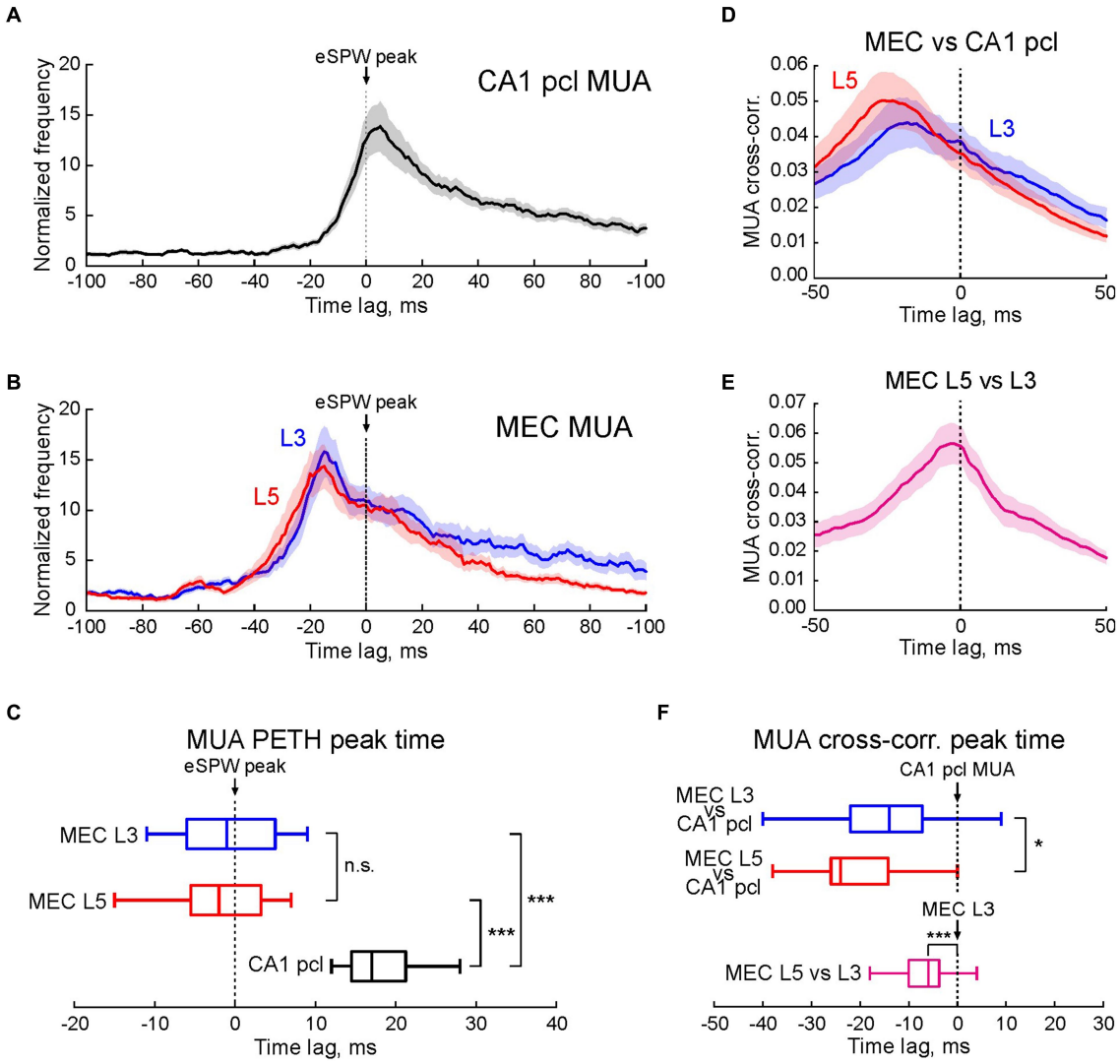

FIGURE 2
Multiple unit activity in MEC L3 and L5 and CA1 hippocampus in relation to early hippocampal sharp waves. **(A,B)** Average PETHs (mean ± SEM) of MUA in CA1 pcl **(A)** and MEC L3 and L5 **(B)** aligned to eSPW times and expressed as MUA frequency normalized to the baseline. **(C)** Horizontal boxplots of group data (center line, median; edges, Q1/Q3; whiskers, non-outlier extremes) for the time of peak firing of multiple units relatively to eSPWs (two-sided Wilcoxon rank sum test). ***p value < 0.001. **(D,E)** Average MUA cross-correlograms in MEC L3 and L5 vs. CA1 *pcl* **(D)**, and MEC L5 vs. MEC L3 **(E)** Shaded lines, SEM. **(F)** Boxplots of group data (center line, median; edges, Q1/Q3; whiskers, non-outlier extremes) for the time of cross-correlation peak of multiple units in MEC L3 and L5 vs. CA1 (top) and MEC L5 vs. MEC L3 (bottom) (two-sided Wilcoxon rank sum test). **(A–F)** Pooled data from 1,196 eSPWs recorded from $n = 17$ P5-7 rats. *p value < 0.05; ***p value < 0.001; n.s., non-significant.

significant delay in activation of neurons in L3 from L5 ($n = 17$ rats; $p < 0.001$; Figures 2E,F; Supplementary Table S4).

Next, we analyzed the LFP depth profile of MEC-SPs in 18 P5-7 animals with probe insertion across the MEC layers (Figure 3A). Consistent with previous studies *in vivo* (Valeeva et al., 2019a,b) and *in vitro* (Sheroziya et al., 2009; Namiki et al., 2013; Unichenko et al., 2015), MEC-SPs were characterized by negative LFP deflection in the superficial MEC layers (Figure 3B). In deep layers, MEC-SPs changed polarity to positive, with the reversal occurring around agranular L4. Similar LFP shapes of MEC-SPs with negativity in superficial layers and positivity in deep layers were also found at different cortical depths during "vertical" probe insertion along the MEC layers (Supplementary Figure S3), suggesting that this distinct LFP depth profile of MEC-SPs with polarity reversal around L4 may be useful for estimating electrode position in the MEC during recordings in neonatal rats. The CSD analysis of MEC-SPs revealed from two to three sinks distributed in layers 1, 2, and 3 (Figures 3B,C; Supplementary Table S5). The most superficial Sink 1 (Figures 3D,E; Supplementary Tables S5, S6) was usually located around L1/L2 border and had the largest amplitude ($n = 18$; $p < 0.001$; Figure 3F; Supplementary Table S7). The Sink 2 and Sink 3 were found within the superficial (close to L2) half of L3 and did not differ in amplitude from each other (Figures 3D–F; Supplementary Tables S5–S7). Thereby, the layerwise distribution of current sinks, reflecting areas of synaptic activation during MEC-SPs, matched the location of main external inputs to MEC (Witter et al., 2017). In addition, the most prominent Sink 1 was observed in MEC layers 1 and 2, containing the dendritic tufts of MEC neurons from all deeper layers (Canto et al., 2008).

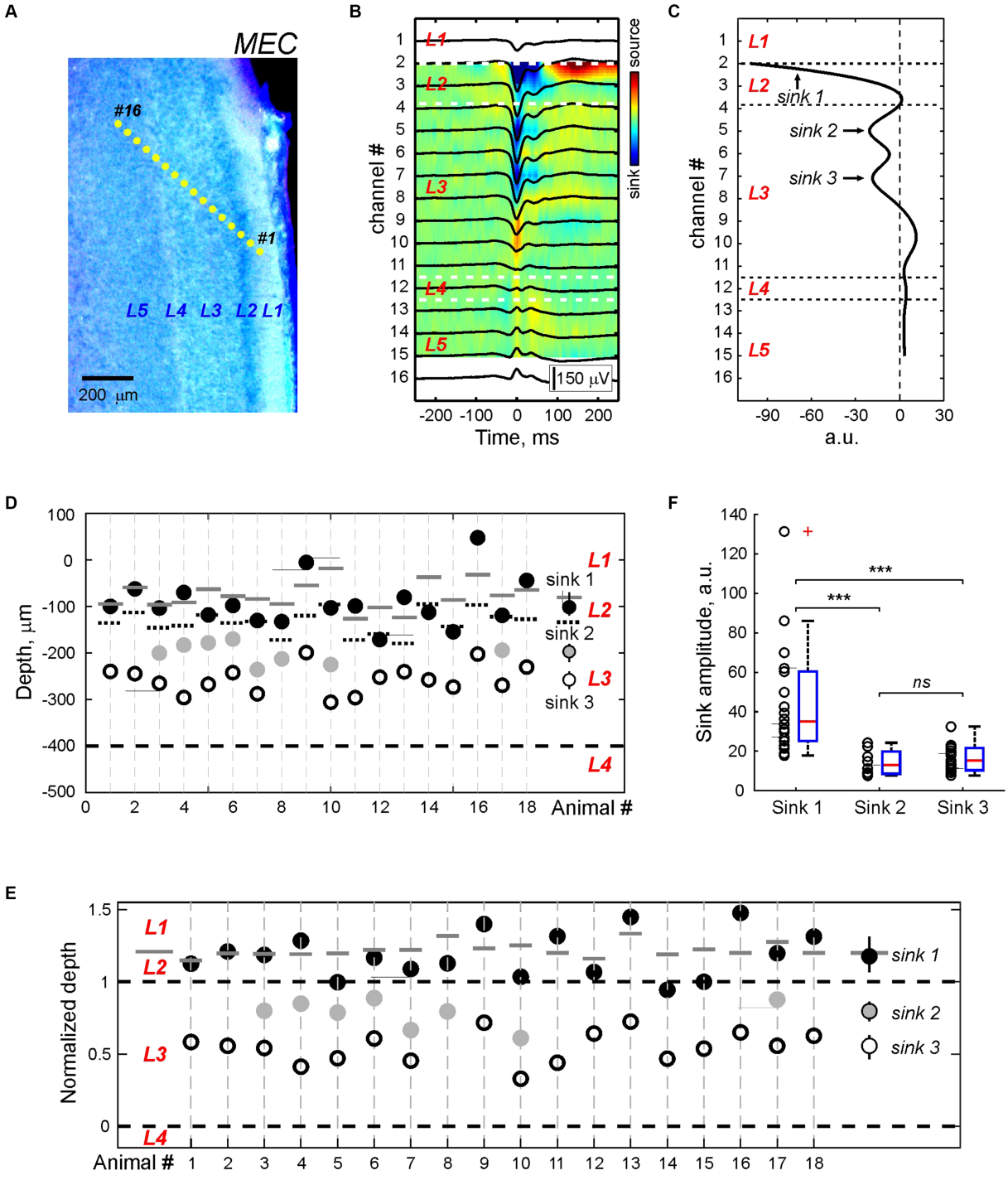

FIGURE 3
CSD profile of the MEC sharp potentials. **(A)** Recording sites of the multielectrode array overlaid on a cresyl violet stained sagittal MEC sections from a P5 rat. **(B)** Average local field potential (black traces) overlaid on the color-coded CSD map of the MEC-SP. **(C)** CSD profile at the peak of the MEC-SP shown on panel **(B)**. Note Sinks 1, 2, and 3 of the MEC-SPs in the superficial layers and a main source near L4. **(D,E)** Group data on the depth of the MEC-SP Sinks 1 (black circles), 2 (gray circles), and 3 (open circles) in relation to L3/L4 border (bottom dashed line) in absolute values **(D)** and normalized to the distance between L3/4 and L2/3 borders **(E)**. Right, group medians with Q1 and Q3. Pooled data were obtained from $n = 18$ P5–7 rats. On **(D)** and **(E)**, L2/L3 and L3/L4 borders are marked by black dashed lines, and L1/L2 border - by solid gray lines **(F)** Group data on the amplitude of current sinks associated with MEC-SPs. ***p value < 0.001; n.s., non-significant.

4 Discussion

The main findings of the present study are that in neonatal rats, deep and superficial MEC neurons are co-activated during MEC-SPs, and that neuronal firing in both superficial and deep MEC layers precedes the activation of CA1 neurons during eSPWs. Thus, the sequence of activation of hippocampal CA1 neurons and deep MEC neurons during sharp waves changes during development from

leadership of deep MEC neurons during eSPWs in neonates to leadership of CA1 neurons during SPW-Rs in adults. These results are consistent with the hypothesis that the network mechanisms underlying neonatal eSPWs are distinct from the mechanisms of adult SPWs generation, and support a paradigm shift from viewing of neonatal eSPWs as the prototype of adult SPW-Rs.

MEC-SP events, which precede hippocampal eSPWs and are triggered by myoclonic movements, have previously been described in the superficial layers of the MEC in neonatal rats (Valeeva et al., 2019a,b). In the present study, we investigated the spatiotemporal organization of MEC-SPs across cortical layers, including a description of their LFP and current-source density depth profiles and neuronal firing. We found that MEC-SPs are electronegative in superficial layers and positive in deep layers with a reversal around L4, and that their main sinks are distributed along the depth of superficial layers. The origin of the synaptic inputs that generate these sinks and drive MEC firing remains hypothetical for now. In adults, SPW-Rs cause activation of neurons in deep layers of the MEC either through direct connections from CA1 pyramidal cells or via the subiculum, whereas the activity of neurons in superficial MEC layers is weakly modulated by SPWs (Chrobak and Buzsaki, 1994, 1996). In contrast, during neonatal eSPWs, CA1 neurons are activated with a delay from neurons in MEC, and therefore the role of CA1-MEC connections in the generation of MEC-SPs is limited, at least in the initial part of MEC discharges. This raises the question of what are the generative network mechanisms of MEC-SPs? Because MEC-SPs are reliably triggered by myoclonic movements, this may involve sensory feedback conveyed from S1 cortex to the MEC. Indeed, myoclonic movements reliably trigger, via sensory feedback, thalamo-cortical oscillatory bursts of activity in the S1 cortex of newborn rodents (Khazipov et al., 2004; An et al., 2014; Akhmetshina et al., 2016; Dooley et al., 2020). Since there is no direct input from S1 to the MEC, a further transmission of sensory feedback from S1 to the MEC should involve some relay areas (Witter et al., 2017). These relay stations may include the perirhinal cortex (Burwell and Amaral, 1998), the retrosplenial cortex (Sugar and Witter, 2016), and the postrhinal cortex (Lagartos-Donate et al., 2022); noteworthy, the latter two areas already establish functional inputs to MEC during the first postnatal week. Alternatively, the link between MEC-SPs and spontaneous myoclonic movements may be supported by a non-canonical reticulo-limbic circuit via the septum, which is activated during startles (Zhang et al., 2018), consistent with a triggering role of the septum in the generation of cortical waves in cultured coronal slices *in vitro* during the first postnatal week (Conhaim et al., 2011). Generation of MEC-SPs may also involve local MEC connections including recurrent and deep to superficial synapses (Quilichini et al., 2010; Zhang et al., 2014; Witter et al., 2017; Rozov et al., 2020). Moreover, these local connections are important as evidenced by the presence of spontaneous activity, very similar to MEC-SPs *in vivo*, in the isolated entorhinal-hippocampal slices *in vitro*, and their persistence after surgical severing of connections with the hippocampus (Sheroziya et al., 2009; Namiki et al., 2013; Unichenko et al., 2015). These observations also suggest that the generation of MEC-SPs primarily involves local circuitry, whereas sensory feedback from movements plays only a triggering role in coupling MEC-SPs (and eSPWs) to movements. This is further supported by the persistence of MEC-driven eSPWs in the hippocampus of immobilized neonatal rats under general anesthesia (Leinekugel et al., 2002; Gainutdinov et al., 2023). While previous studies emphasized the pivotal role of spontaneously bursting L3 neurons in the generation of MEC-SPs in neonatal rodent MEC slices *in vitro* (Sheroziya et al., 2009; Namiki et al., 2013; Unichenko et al., 2015), here we observed that L5 neurons fire before L3 neurons during MEC-SPs *in vivo*. These observations are consistent with the highest excitability of L5 neurons, their high propensity for spontaneous firing, and with the leading role of deep layers in self-generated cortical activity such as the UP-states of slow cortical oscillations (Sanchez-Vives and Mccormick, 2000; Isomura et al., 2006; Sakata and Harris, 2009; Reyes-Puerta et al., 2015; Senzai et al., 2019). Of note, despite of the limited involvement of CA1 and subicular inputs in initiation of MEC-SPs, these connections are in place during the first postnatal week (Khalilov et al., 1999; Canto et al., 2019), and their activation during eSPWs may contribute to the late phase of population burst in MEC.

Our main finding is that neurons in deep and superficial MEC layers are activated synchronously during MEC-SPs, and that neuronal firing in both superficial and deep MEC layers precedes the activation of CA1 neurons during eSPWs. This is remarkably different from the spatiotemporal dynamics in the entorhinal-hippocampal system during SPW-Rs in the adult brain. Indeed, during adult SPW-Rs, deep MEC neurons are activated following CA1 pyramidal cells by direct monosynaptic inputs from CA1 pyramidal cells or via intermediate activation of subicular neurons, whereas neurons in superficial MEC layers are weakly modulated by SPW-Rs (Chrobak and Buzsaki, 1994, 1996; Isomura et al., 2006; Roth et al., 2016; Rozov et al., 2020). Thus, the sequence of activation of hippocampal CA1 neurons and deep MEC neurons during sharp waves changes during development from a lead of deep MEC neurons during eSPWs in neonates to a lead of CA1 neurons during adult SPW-Rs. This provides further evidence for a difference in the generative mechanisms of eSPWs versus adult SPW-Rs, despite a similarity in the electrophysiological traits of these two distinct activity patterns, and supports the transition in understanding from eSPWs as immature prototypes of adult SPWs to a bottom-up model of eSPW genesis, driven primarily by inputs from the entorhinal cortex, marking a significant paradigm shift in entorhinal-hippocampal circuitry dynamics during development. Initially, eSPWs were viewed as nascent forms of SPWs, suggesting that eSPWs emerged spontaneously within the hippocampal circuitry and represented early manifestations of the network dynamics observed in adult hippocampal function. However, recent studies and present work challenge this traditional view, proposing a bottom-up model wherein eSPWs are predominantly initiated by inputs originating from the entorhinal cortex. In this revised framework, eSPWs are seen as arising from the orchestrated interplay between the entorhinal cortex and hippocampal circuitry, with inputs from the former triggering and shaping the dynamics of the latter. This perspective emphasizes the significance of sensory inputs, particularly somatosensory feedback from myoclonic movements, in driving hippocampal network activity during development to support the activity-dependent formation of the entorhinal-hippocampal network. Our study also suggests that during eSPWs, there is a limited relay of information from the CA1 hippocampus to the deep layers of the MEC during eSPWs, in contrast to adult SPW-Rs. Adult SPW-Rs are known to support the transfer of transiently stored hippocampal information to long-term engrams in neocortical networks, contributing to memory consolidation (Buzsaki, 1986; Siapas and Wilson, 1998; Girardeau et al., 2009; Nakashiba et al., 2009; Buzsaki,

2015; Squire et al., 2015). This limited communication between CA1 and the deep MEC in newborns may contribute to delayed development of the hippocampal-dependent memory and infantile amnesia (Baram et al., 2019). Our study also raises questions for future research on the developmental stage at which the change in the temporal dynamics of neuronal activation in CA1 and EC occurs, and on the potential mechanisms and functional implications of the developmental change in the sequence of CA1 and EC activation during sharp waves, which, according to recent studies, may involve the development of inhibitory circuitry (Dard et al., 2022; Pochinok et al., 2024).

Data availability statement

The raw data supporting the conclusions of this article will be made available by the authors, without undue reservation.

Ethics statement

The animal study was approved by French National Institute of Health and Medical Research (APAFIS #16992-2020070612319346 v2) and the Local Ethical Committee of Kazan Federal University (#24/22.09.2020). The study was conducted in accordance with the local legislation and institutional requirements.

Author contributions

DS: Validation, Writing – review & editing, Data curation, Formal analysis, Investigation, Methodology, Visualization. AN: Data curation, Formal analysis, Investigation, Methodology, Validation, Visualization, Writing – review & editing, Software. RK: Validation, Writing – review & editing, Conceptualization, Writing – original draft. GV: Conceptualization, Data curation, Formal analysis, Funding acquisition, Investigation, Methodology, Project administration, Resources, Software, Supervision, Validation, Visualization, Writing – original draft, Writing – review & editing.

Funding

The author(s) declare that financial support was received for the research, authorship, and/or publication of this article. This research was supported by the Russian Science Foundation (grant #21-75-10033).

Conflict of interest

The authors declare that the research was conducted in the absence of any commercial or financial relationships that could be construed as a potential conflict of interest.

The author(s) declared that they were an editorial board member of Frontiers, at the time of submission. This had no impact on the peer review process and the final decision.

Publisher's note

Supplementary material

The Supplementary material for this article can be found online at: https://www.frontiersin.org/articles/10.3389/fncel.2024.1403073/full#supplementary-material

References

Akhmetshina, D., Nasretdinov, A., Zakharov, A., Valeeva, G., and Khazipov, R. (2016). The nature of the sensory input to the neonatal rat barrel cortex. *J. Neurosci.* 36, 9922–9932. doi: 10.1523/JNEUROSCI.1781-16.2016

An, S. M., Kilb, W., and Luhmann, H. J. (2014). Sensory-evoked and spontaneous gamma and spindle bursts in neonatal rat motor cortex. *J. Neurosci.* 34, 10870–10883. doi: 10.1523/JNEUROSCI.4539-13.2014

Baram, T. Z., Donato, F., and Holmes, G. L. (2019). Construction and disruption of spatial memory networks during development. *Learn. Mem.* 26, 206–218. doi: 10.1101/lm.049239.118

Bellistri, E., Aguilar, J., Brotons-Mas, J. R., Foffani, G., and De La Prida, L. M. (2013). Basic properties of somatosensory-evoked responses in the dorsal hippocampus of the rat. *J. Physiol.* 591, 2667–2686. doi: 10.1113/jphysiol.2013.251892

Ben Ari, Y., Gaiarsa, J. L., Tyzio, R., and Khazipov, R. (2007). GABA: a Pioneer transmitter that excites immature neurons and generates primitive oscillations. *Physiol. Rev.* 87, 1215–1284. doi: 10.1152/physrev.00017.2006

Ben-Ari, Y., Cherubini, E., Corradetti, R., and Gaïarsa, J.-L. (1989). Giant synaptic potentials in immature rat CA3 hippocampal neurones. *J. Physiol. Lond.* 416, 303–325. doi: 10.1113/jphysiol.1989.sp017762

Brankack, J., and Buzsaki, G. (1986). Hippocampal responses evoked by tooth pulp and acoustic stimulation: depth profiles and effect of behavior. *Brain Res.* 378, 303–314. doi: 10.1016/0006-8993(86)90933-9

Buhl, D. L., and Buzsaki, G. (2005). Developmental emergence of hippocampal fast-field "ripple" oscillations in the behaving rat pups. *Neuroscience* 134, 1423–1430. doi: 10.1016/j.neuroscience.2005.05.030

Burwell, R. D., and Amaral, D. G. (1998). Perirhinal and postrhinal cortices of the rat: interconnectivity and connections with the entorhinal cortex. *J. Comp. Neurol.* 391, 293–321. doi: 10.1002/(SICI)1096-9861(19980216)391:3<293::AID-CNE2>3.0.CO;2-X

Buzsaki, G. (1986). Hippocampal sharp waves: their origin and significance. *Brain Res.* 398, 242–252. doi: 10.1016/0006-8993(86)91483-6

Buzsaki, G. (2015). Hippocampal sharp wave-ripple: a cognitive biomarker for episodic memory and planning. *Hippocampus* 25, 1073–1188. doi: 10.1002/hipo.22488

Canto, C. B., Koganezawa, N., Lagartos-Donate, M. J., O'reilly, K. C., Mansvelder, H. D., and Witter, M. P. (2019). Postnatal development of functional projections from Parasubiculum and Presubiculum to medial entorhinal cortex in the rat. *J. Neurosci.* 39, 8645–8663. doi: 10.1523/JNEUROSCI.1623-19.2019

Canto, C. B., Wouterlood, F. G., and Witter, M. P. (2008). What does the anatomical Organization of the Entorhinal Cortex Tell us? *Neural Plast.* 2008:381243, 1–18. doi: 10.1155/2008/381243

Chrobak, J. J., and Buzsaki, G. (1994). Selective activation of deep layer (V-VI) retrohippocampal cortical neurons during hippocampal sharp waves in the behaving rat. *J. Neurosci.* 14, 6160–6170. doi: 10.1523/JNEUROSCI.14-10-06160.1994

Chrobak, J. J., and Buzsaki, G. (1996). High-frequency oscillations in the output networks of the hippocampal-entorhinal axis of the freely behaving rat. *J. Neurosci.* 16, 3056–3066. doi: 10.1523/JNEUROSCI.16-09-03056.1996

Conhaim, J., Easton, C. R., Becker, M. I., Barahimi, M., Cedarbaum, E. R., Moore, J. G., et al. (2011). Developmental changes in propagation patterns and transmitter dependence of waves of spontaneous activity in the mouse cerebral cortex. *J. Physiol.* 589, 2529–2541. doi: 10.1113/jphysiol.2010.202382

Cossart, R., and Khazipov, R. (2022). How development sculpts hippocampal circuits and function. *Physiol. Rev.* 102, 343–378. doi: 10.1152/physrev.00044.2020

Dard, R. F., Leprince, E., Denis, J., Rao, B. S., Suchkov, D., Boyce, R., et al. (2022). The rapid developmental rise of somatic inhibition disengages hippocampal dynamics from self-motion. *eLife* 11:e78116. doi: 10.7554/eLife.78116

Donato, F., Jacobsen, R. I., Moser, M. B., and Moser, E. I. (2017). Stellate cells drive maturation of the entorhinal-hippocampal circuit. *Science* 355:eaai8178. doi: 10.1126/science.aai8178

Dooley, J. C., Glanz, R. M., Sokoloff, G., and Blumberg, M. S. (2020). Self-generated whisker movements drive state-dependent sensory input to developing barrel cortex. *Curr. Biol.* 30, 2404–2410.e4. doi: 10.1016/j.cub.2020.04.045

Freeman, J. A., and Nicholson, C. (1975). Experimental optimization of current source-density technique for anuran cerebellum. *J. Neurophysiol.* 38, 369–382. doi: 10.1152/jn.1975.38.2.369

Gainutdinov, A., Shipkov, D., Sintsov, M., Fabrizi, L., Nasretdinov, A., Khazipov, R., et al. (2023). Somatosensory-evoked early sharp waves in the neonatal rat hippocampus. *Int. J. Mol. Sci.* 24:8721. doi: 10.3390/ijms24108721

Girardeau, G., Benchenane, K., Wiener, S. I., Buzsaki, G., and Zugaro, M. B. (2009). Selective suppression of hippocampal ripples impairs spatial memory. *Nat. Neurosci.* 12, 1222–1223. doi: 10.1038/nn.2384

Graf, J., Zhang, C., Marguet, S. L., Herrmann, T., Flossmann, T., Hinsch, R., et al. (2021). A limited role of NKCC1 in telencephalic glutamatergic neurons for developing hippocampal network dynamics and behavior. *Proc. Natl. Acad. Sci. U. S. A* 118:e2014784118. doi: 10.1073/pnas.2014784118

Griguoli, M., and Cherubini, E. (2017). Early correlated network activity in the Hippocampus: its putative role in shaping neuronal circuits. *Front. Cell. Neurosci.* 11:255. doi: 10.3389/fncel.2017.00255

Isomura, Y., Sirota, A., Ozen, S., Montgomery, S., Mizuseki, K., Henze, D. A., et al. (2006). Integration and segregation of activity in entorhinal-hippocampal subregions by neocortical slow oscillations. *Neuron* 52, 871–882. doi: 10.1016/j.neuron.2006.10.023

Karlsson, K. A., Mohns, E. J., Di Prisco, G. V., and Blumberg, M. S. (2006). On the co-occurrence of startles and hippocampal sharp waves in newborn rats. *Hippocampus* 16, 959–965. doi: 10.1002/hipo.20224

Khalilov, I., Dzhala, V., Medina, I., Leinekugel, X., Melyan, Z., Lamsa, K., et al. (1999). Maturation of kainate-induced epileptiform activities in interconnected intact neonatal limbic structures *in vitro*. *Eur. J. Neurosci.* 11, 3468–3480. doi: 10.1046/j.1460-9568.1999.00768.x

Khazipov, R., Sirota, A., Leinekugel, X., Holmes, G. L., Ben Ari, Y., and Buzsaki, G. (2004). Early motor activity drives spindle bursts in the developing somatosensory cortex. *Nature* 432, 758–761. doi: 10.1038/nature03132

Khazipov, R., Zaynutdinova, D., Ogievetsky, E., Valeeva, G., Mitrukhina, O., Manent, J. B., et al. (2015). Atlas of the postnatal rat brain in stereotaxic coordinates. *Front. Neuroanat.* 9:110.3389/fnana.2015.00161. doi: 10.3389/fnana.2015.00161

Lagartos-Donate, M. J., Doan, T. P., Girao, P. J. B., and Witter, M. P. (2022). Postnatal development of projections of the postrhinal cortex to the entorhinal cortex in the rat. *eNeuro* 9, ENEURO.0057–ENEU22.2022. doi: 10.1523/ENEURO.0057-22.2022

Leinekugel, X., Khazipov, R., Cannon, R., Hirase, H., Ben Ari, Y., and Buzsaki, G. (2002). Correlated bursts of activity in the neonatal hippocampus *in vivo*. *Science* 296, 2049–2052. doi: 10.1126/science.1071111

Marguet, S. L., Le-Schulte, V. T., Merseburg, A., Neu, A., Eichler, R., Jakovcevski, I., et al. (2015). Treatment during a vulnerable developmental period rescues a genetic epilepsy. *Nat. Med.* 21, 1436–1444. doi: 10.1038/nm.3987

Mohns, E. J., and Blumberg, M. S. (2010). Neocortical activation of the hippocampus during sleep in infant rats. *J. Neurosci.* 30, 3438–3449. doi: 10.1523/JNEUROSCI.4832-09.2010

Mohns, E. J., Karlsson, K. A., and Blumberg, M. S. (2007). Developmental emergence of transient and persistent hippocampal events and oscillations and their association with infant seizure susceptibility. *Eur. J. Neurosci.* 26, 2719–2730. doi: 10.1111/j.1460-9568.2007.05928.x

Murata, Y., and Colonnese, M. T. (2020). GABAergic interneurons excite neonatal hippocampus *in vivo*. *Sci. Adv.* 6:eaba1430. doi: 10.1126/sciadv.aba1430

Nakashiba, T., Buhl, D. L., Mchugh, T. J., and Tonegawa, S. (2009). Hippocampal CA3 output is crucial for ripple-associated reactivation and consolidation of memory. *Neuron* 62, 781–787. doi: 10.1016/j.neuron.2009.05.013

Namiki, S., Norimoto, H., Kobayashi, C., Nakatani, K., Matsuki, N., and Ikegaya, Y. (2013). Layer III neurons control synchronized waves in the immature cerebral cortex. *J. Neurosci.* 33, 987–1001. doi: 10.1523/JNEUROSCI.2522-12.2013

Pochinok, I., Stober, T. M., Triesch, J., Chini, M., and Hanganu-Opatz, I. L. (2024). A developmental increase of inhibition promotes the emergence of hippocampal ripples. *Nat. Commun.* 15:738. doi: 10.1038/s41467-024-44983-z

Quilichini, P., Sirota, A., and Buzsaki, G. (2010). Intrinsic circuit organization and theta-gamma oscillation dynamics in the entorhinal cortex of the rat. *J. Neurosci.* 30, 11128–11142. doi: 10.1523/JNEUROSCI.1327-10.2010

Reyes-Puerta, V., Sun, J. J., Kim, S., Kilb, W., and Luhmann, H. J. (2015). Laminar and columnar structure of sensory-evoked multineuronal spike sequences in adult rat barrel cortex *in vivo*. *Cereb. Cortex* 25, 2001–2021. doi: 10.1093/cercor/bhu007

Roth, F. C., Beyer, K. M., Both, M., Draguhn, A., and Egorov, A. V. (2016). Downstream effects of hippocampal sharp wave ripple oscillations on medial entorhinal cortex layer V neurons *in vitro*. *Hippocampus* 26, 1493–1508. doi: 10.1002/hipo.22623

Rozov, A., Rannap, M., Lorenz, F., Nasretdinov, A., Draguhn, A., and Egorov, A. V. (2020). Processing of hippocampal network activity in the receiver network of the medial entorhinal cortex layer V. *J. Neurosci.* 40, 8413–8425. doi: 10.1523/JNEUROSCI.0586-20.2020

Sakata, S., and Harris, K. D. (2009). Laminar structure of spontaneous and sensory-evoked population activity in auditory cortex. *Neuron* 64, 404–418. doi: 10.1016/j.neuron.2009.09.020

Sanchez-Vives, M. V., and Mccormick, D. A. (2000). Cellular and network mechanisms of rhythmic recurrent activity in neocortex. *Nat. Neurosci.* 3, 1027–1034. doi: 10.1038/79848

Senzai, Y., Fernandez-Ruiz, A., and Buzsaki, G. (2019). Layer-specific physiological features and Interlaminar interactions in the primary visual cortex of the mouse. *Neuron* 101, 500–513.e5. doi: 10.1016/j.neuron.2018.12.009

Sheroziya, M. G., Von Bohlen Und, H. O., Unsicker, K., and Egorov, A. V. (2009). Spontaneous bursting activity in the developing entorhinal cortex. *J. Neurosci.* 29, 12131–12144. doi: 10.1523/JNEUROSCI.1333-09.2009

Siapas, A. G., and Wilson, M. A. (1998). Coordinated interactions between hippocampal ripples and cortical spindles during slow-wave sleep. *Neuron* 21, 1123–1128. doi: 10.1016/S0896-6273(00)80629-7

Squire, L. R., Genzel, L., Wixted, J. T., and Morris, R. G. (2015). Memory consolidation. *Cold Spring Harb. Perspect. Biol.* 7:a021766. doi: 10.1101/cshperspect.a021766

Sugar, J., and Witter, M. P. (2016). Postnatal development of retrosplenial projections to the parahippocampal region of the rat. *eLife* 5:e13925. doi: 10.7554/eLife.13925

Unichenko, P., Yang, J. W., Luhmann, H. J., and Kirischuk, S. (2015). Glutamatergic system controls synchronization of spontaneous neuronal activity in the murine neonatal entorhinal cortex. *Pflugers Arch.* 467, 1565–1575. doi: 10.1007/s00424-014-1600-5

Valeeva, G., Janackova, S., Nasretdinov, A., Rychkova, V., Makarov, R., Holmes, G. L., et al. (2019a). Emergence of coordinated activity in the developing entorhinal-hippocampal network. *Cereb. Cortex* 29, 906–920. doi: 10.1093/cercor/bhy309

Valeeva, G., Nasretdinov, A., Rychkova, V., and Khazipov, R. (2019b). Bilateral synchronization of hippocampal early sharp waves in neonatal rats. *Front. Cell. Neurosci.* 13:29. doi: 10.3389/fncel.2019.00029

Valeeva, G., Rychkova, V., Vinokurova, D., Nasretdinov, A., and Khazipov, R. (2020). Early sharp wave synchronization along the septo-temporal axis of the neonatal rat hippocampus. *Zhurnal Vysshei Nervnoi Deyatelnosti Imeni I P Pavlova* 70, 341–350. doi: 10.31857/S0044467720030132

Witter, M. P., Doan, T. P., Jacobsen, B., Nilssen, E. S., and Ohara, S. (2017). Architecture of the entorhinal cortex a review of entorhinal anatomy in rodents with some comparative notes. *Front. Syst. Neurosci.* 11:46. doi: 10.3389/fnsys.2017.00046

Zhang, G. W., Sun, W. J., Zingg, B., Shen, L., He, J., Xiong, Y., et al. (2018). A non-canonical reticular-limbic central auditory pathway via medial septum contributes to fear conditioning. *Neuron* 97, 406–417.e4. doi: 10.1016/j.neuron.2017.12.010

Zhang, S. J., Ye, J., Couey, J. J., Witter, M., Moser, E. I., and Moser, M. B. (2014). Functional connectivity of the entorhinal - hippocampal space circuit. *Philos. Trans. R. Soc. B Biol. Sci.* 369:20120516. doi: 10.1098/rstb.2012.0516

frontiers | Frontiers in Cellular Neuroscience

TYPE Review
PUBLISHED 31 July 2024
DOI 10.3389/fncel.2024.1440588

OPEN ACCESS

EDITED BY
Lisa Mapelli,
University of Pavia, Italy

REVIEWED BY
Nazim Kourdougli,
University of California, Los Angeles, United States
Bernd Kuhn,
Okinawa Institute of Science and Technology Graduate University, Japan

*CORRESPONDENCE
Christian Hansel
✉ chansel@bsd.uchicago.edu
Rafael Yuste
✉ rmy5@columbia.edu

RECEIVED 29 May 2024
ACCEPTED 18 July 2024
PUBLISHED 31 July 2024

CITATION
Hansel C and Yuste R (2024) Neural ensembles: role of intrinsic excitability and its plasticity.
Front. Cell. Neurosci. 18:1440588.
doi: 10.3389/fncel.2024.1440588

Neural ensembles: role of intrinsic excitability and its plasticity

Christian Hansel[1]* and Rafael Yuste[2]*

[1]Department of Neurobiology and Neuroscience Institute, University of Chicago, Chicago, IL, United States, [2]NeuroTechnology Center, Department of Biological Sciences, Columbia University, New York, NY, United States

Synaptic connectivity defines groups of neurons that engage in correlated activity during specific functional tasks. These co-active groups of neurons form ensembles, the operational units involved in, for example, sensory perception, motor coordination and memory (then called an *engram*). Traditionally, ensemble formation has been thought to occur via strengthening of synaptic connections via long-term potentiation (LTP) as a plasticity mechanism. This synaptic theory of memory arises from the learning rules formulated by Hebb and is consistent with many experimental observations. Here, we propose, as an alternative, that the intrinsic excitability of neurons and its plasticity constitute a second, *non-synaptic* mechanism that could be important for the initial formation of ensembles. Indeed, enhanced neural excitability is widely observed in multiple brain areas subsequent to behavioral learning. In cortical structures and the amygdala, excitability changes are often reported as transient, even though they can last tens of minutes to a few days. Perhaps it is for this reason that they have been traditionally considered as modulatory, merely supporting ensemble formation by facilitating LTP induction, without further involvement in memory function (memory allocation hypothesis). We here suggest—based on two lines of evidence—that beyond modulating LTP allocation, enhanced excitability plays a more fundamental role in learning. First, enhanced excitability constitutes a signature of active ensembles and, due to it, subthreshold synaptic connections become suprathreshold in the absence of synaptic plasticity (*iceberg model*). Second, enhanced excitability promotes the propagation of dendritic potentials toward the soma and allows for enhanced coupling of EPSP amplitude (LTP) to the spike output (and thus ensemble participation). This *permissive gate model* describes a need for permanently increased excitability, which seems at odds with its traditional consideration as a short-lived mechanism. We propose that longer modifications in excitability are made possible by a low threshold for intrinsic plasticity induction, suggesting that excitability might be on/off-modulated at short intervals. Consistent with this, in cerebellar Purkinje cells, excitability lasts days to weeks, which shows that in some circuits the duration of the phenomenon is not a limiting factor in the first place. In our model, synaptic plasticity defines the information content received by neurons through the connectivity network that they are embedded in. However,

the plasticity of cell-autonomous excitability could dynamically regulate the ensemble participation of individual neurons as well as the overall activity state of an ensemble.

KEYWORDS

engram, ensemble, excitability, intrinsic plasticity, learning, memory, memory allocation, synaptic plasticity

Introduction

Synaptic long-term potentiation (LTP; Bliss and Lømo, 1973) translates experiences via its activity-dependence into enhanced synaptic efficacy. LTP may also be accompanied by the emergence of new dendritic spines (Engert and Bonhoeffer, 1999; Yuste and Bonhoeffer, 2001) and spine growth (Holtmaat and Svoboda, 2009) making it the ideal plasticity mechanism to establish and update synaptic connectivity in an experience-dependent manner in neural ensembles. The ultimate proof for a causal relationship between synaptic plasticity and memory was provided in 2014, when Malinow et al. optogenetically induced long-term depression (LTD) and LTP to inactivate and reactivate, respectively, a fear memory that was previously established using a fear-conditioning paradigm in the amygdala (Nabavi et al., 2014). In fear-conditioning, a tone is often used as the neutral conditioned stimulus (CS), which is paired with an electric footshock as the unconditioned stimulus (US). Nabavi et al. replaced the tone presentation with optical stimulation (channelrhodopsin 2; ChR2) of axons in an auditory relay nucleus that projects to the amygdala. Application of LTD- and LTP- inducing stimuli (tested separately *in vivo*), respectively, was sufficient to disconnect/connect the CS pathway to the fear memory engram in the amygdala. This is a critical finding due to the immediate optical control of synaptic weight and its impact on behavioral learning.

However, conditioning experiments have revealed a second parameter that changes with learning and might be causally related to engram formation as well. *Ex vivo* recordings from CA1 hippocampal pyramidal neurons following eyeblink conditioning revealed that the intrinsic membrane excitability was enhanced in neurons from conditioned, but not pseudoconditioned or naïve rabbits (Disterhoft et al., 1986). Similar findings were made previously following associative learning in the mollusk *Hermissenda* (Alkon, 1984) and subsequently following eyeblink conditioning in cerebellar Purkinje cells (Schreurs et al., 1998). In line with these and other findings, it has been suggested that there could be a "Memory from the dynamics of intrinsic membrane currents" (Marder et al., 1996), an idea that was followed up by several investigators soon after (Hansel et al., 2001; Daoudal and Debanne, 2003; Frick et al., 2004). How have these ideas been implemented into modern theories of memory? Surprisingly, intrinsic plasticity plays a relatively minor role in current learning models. In the memory allocation hypothesis, the learning model with closest focus on cellular mechanisms of engram formation and recall, neurons are allocated to an engram that show high excitability at the time of learning, facilitating subsequent integration via LTP (Rogerson et al., 2014; Yiu et al., 2014; Josselyn and Frankland, 2018; Josselyn and Tonegawa, 2020). Perhaps the disregard for a deeper involvement of intrinsic plasticity stems from the observation that excitability changes are often short-lived. A memory engram related to fear-conditioning in the dentate gyrus was characterized by a state of enhanced neuronal excitability, but this effect faded within two hours (Pignatelli et al., 2019). In prior *ex vivo* recordings from CA3 hippocampal pyramidal neurons following eyeblink conditioning in rabbits, enhanced excitability was observed for longer periods of time, but began to decline three days after learning (the conditioned behavior, in contrast, lasted for the full 180 days of recordings; Thompson et al., 1996). These findings seem to suggest that enhanced excitability cannot play a more permanent role in engram physiology, for example in memory recall. Here, we argue that despite of its transient nature enhanced excitability via intrinsic plasticity is necessary and, in some scenarios sufficient, for the formation and reactivation of ensembles in general, including ensembles that serve as memory engrams.

Enhanced excitability in cortical ensembles: the iceberg model

As mentioned, neuronal ensembles (often referred to as assemblies) are coactive groups of neurons that have been shown to mediate perception and behavior (Buzsaki, 2010; Yuste et al., 2024). In mouse primary visual cortex, ensembles are formed by a small group (~10%) of imaged neurons, which become coactive in a significant manner, within a small temporal window (Cossart et al., 2003: Miller et al., 2014; Carrillo-Reid et al., 2015). Neurons can participate in several ensembles, demonstrating that ensembles can form a multineuronal code (Miller et al., 2014). Indeed, ensembles are formed by both neurons that are specifically co-activated (onsembles) as well as neurons that are specifically silenced (offsemble), further indicating that they generate an emergent code (Pérez-Ortega et al., 2024). Offsemble neurons have shorter calcium decay kinetics than onsemble cells, suggesting that their activity is curtailed by GABAergic inhibition. Different classes of interneurons may dynamically control dendritic and somatic compartments of target pyramidal neurons. Interneuron activity itself may be controlled by synaptic and intrinsic plasticity mechanisms. Individual ensembles are activated by visual stimuli, both moving gratings and naturalistic videos. Activity in similar groups of neurons can be observed in the absence of external stimuli (ongoing activity), as if these circuits were internal building blocks of cortical activity that can be allocated to become

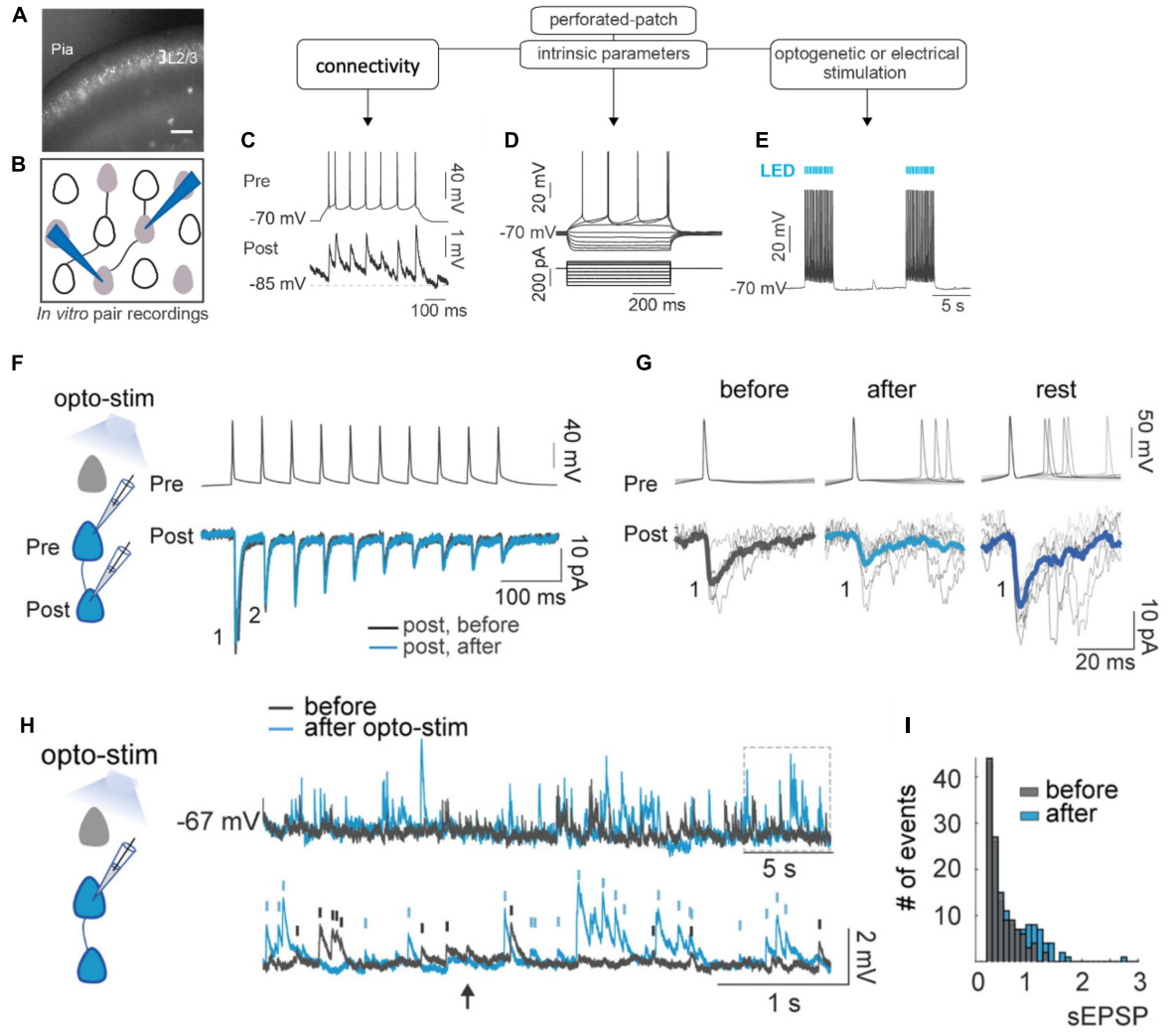

FIGURE 1
Ensemble formation leads to increased excitability. **(A)** Experimental design. Image of brain slice from mouse in primary visual cortex with ST-ChroMe opsin expression in pyramidal neurons. Scale bar: 200 μm. **(B)** Illustration of in-vitro paired recording for evaluating monosynaptic connectivity between neurons. **(C)** Perforated patch-clamp recording of presynaptic action potentials elicited by current injections (500 ms), followed by identification of a monosynaptic connection, generating postsynaptic potentials time-locked to presynaptic spikes. **(D)** Intrinsic parameters were tested, such as firing rate, input resistance, and firing threshold with the changes in membrane voltage in response to current steps. **(E)** Perforated current-clamp recording under optogenetic stimulation protocol: 1 to 30 min of 10 Hz train, 5 ms light pulses for 4 s followed by 10 s of rest. **(F)** Representative paired whole-cell recording of synaptically connected neurons. Top: current-clamp recording of presynaptic action potentials in response to 10 current injections (2 ms each; 20 Hz). Bottom: voltage-clamp recording of evoked EPSC before (black) and after (blue) 30 min of optogenetic stimulation. Each trace is average of 30 successive responses evoked by presynaptic current injection. **(G)** Representative paired recording of evoked EPSCs (perforated patch–clamp). Top: current-clamp recording of presynaptic action potentials induced by positive current steps of the I–V curve (20–120 pA). Bottom: voltage-clamp recording of evoked EPSCs before and after optogenetic stimulation and after 20 min of rest post-stimulation. Thick line is average of successive responses to the first presynaptic action potentials, for every current step of the I–V curve. **(H)** Increase in spontaneous activity after optogenetic stimulation. Representative perforated patch-clamp recording of a neuron in current-clamp before (black) and after (blue) optogenetic stimulation protocol. Bottom: Section in the top trace shows spontaneous EPSPs amplitude > 0.3 mV identified before (black) and after (blue) optogenetic stimulation protocol in a one-minute recording. Arrows show tentative EPSPs that were not detected by the threshold (0.3 mV). **(I)** Frequency histogram of EPSPs amplitudes shows that after optogenetic stimulation, the number and amplitude of spontaneous synaptic events increased. (Modified with permission from Alejandre-García et al., 2022).

engrams. This interpretation is supported by the observation that these ongoing ensembles have statistically the same neuronal components as the ones activated by visual stimuli (Miller et al., 2014). In addition, some cortical ensembles persist for up to 46 days, albeit with a substantial rotation of individual neuronal participants anchored by a group of more persistent core neurons (Perez-Ortega et al., 2021). The general feature of (relative) permanency is consistent with the possibility that ensembles serve as repositories of perceptual and memory states. In agreement with this, the optogenetic reactivation of ensembles can recall previous visual stimuli, and lead to a behavioral outcome (Carrillo-Reid et al., 2019; Marshel et al., 2019). Thus, ensembles are not an epiphenomenon of cortical activity but are causally linked to perceptual states (Carrillo-Reid et al., 2017).

Interestingly, cortical ensembles can also be created *de novo*: optogenetic co-activation of neurons leads to their joint ongoing

co-activation, forming a new ensemble which can last for days (Carrillo-Reid et al., 2016). This result can explain the concordance between visually evoked and ongoing ensembles: one can posit that sensory stimulation can imprint ensembles into the cortex and these ensembles can then be recalled internally, manifesting themselves later in the ongoing activity. Consistent with this, stimulus-evoked ensembles are recalled during sleep (Lines and Yuste, 2023). This result can also explain the concordance between ensembles and engrams, whereby engrams could represent the recalling of previously imprinted ensembles. Importantly, the optogenetics imprinting of ensembles by coactive activation of neurons initially strongly suggested that ensembles were generated by Hebbian synaptic plasticity, whereby neurons that fire together strengthen their synaptic connectivity.

To better understand the mechanisms that lead to the formation of ensembles, we co-activated optogenetically and electrically layer 2/3 pyramidal neurons in brain slices, replicating *in vitro* the optogenetic protocol to generate ensembles in vivo (Carrillo-Reid et al., 2016; Alejandre-García et al., 2022; Figures 1A–E). Using whole-cell and perforated patch-clamp pair recordings we found, to our surprise, that, after optogenetic or electrical stimulation, there were only minor changes in synaptic plasticity (Figures 1F–H). In fact, instead of synaptic potentiation, co-activated neurons actually showed an initial depression, followed by a small rebound potentiation after a recovery period. There was also no evidence that new connections formed after optogenetic stimulation in previously unconnected neurons (Alejandre-García et al., 2022). Thus, synaptic plasticity could not explain the emergence of neuronal ensembles in this protocol. But, unexpectedly, optogenetic and electrical stimulation induced major increases in amplitude and frequency of spontaneous EPSPs, even after single-cell stimulation (Figures 1I, J). Consistent with this, we observed strong and persistent increases in neuronal excitability after stimulation, along with increases in membrane resistance and reduction in spike threshold (Alejandre-García et al., 2022). Similar increases in ongoing activity had also been noticed after ensemble imprinting *in vivo* (Carrillo-Reid et al., 2016). We concluded that intrinsic excitability, rather than Hebbian plasticity, mediates the establishment of neuronal ensembles.

To explain how neuronal ensembles are generated, we propose an "iceberg" model, by which the increased neuronal excitability that results from repeated input stimulation makes subthreshold connections become suprathreshold, enhancing the postsynaptic effect of already existing synapses, and generating a neuronal ensemble (Figure 2; Alejandre-García et al., 2022). This increase in synaptic efficacy is in fact strictly consistent with the original Hebbian postulate, which relates to the effect that a synapse has on the postsynaptic cell (Hebb, 1949), but did not necessarily imply increase in synaptic transmission or strength.

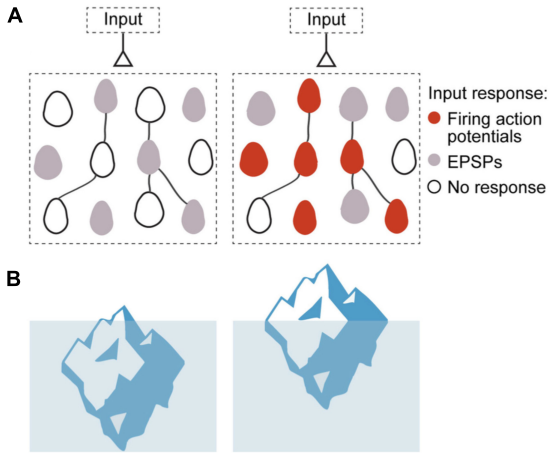

FIGURE 2
Iceberg model of ensemble formation. **(A)** Emergence of ensembles after increases in neuronal excitability, illustration circuit response before (left) and after (right) ensemble generation. Color corresponds to membrane potential response to a synaptic input: white is resting membrane potentials, gray are subthreshold responses, and red are suprathreshold ones, with firing of action potentials. Stimulated neurons become more excitable, so the same inputs induce some of them to fire (red cells), while other cells have increased subthreshold responses (gray cells). The model explains how an ensemble is formed but does not assume any changes in numbers or strength of local synapses. **(B)** Left: Iceberg emergence: An iceberg keeps underwater. Right: But if its density decreases, the iceberg emerges above water. Density is an intrinsic property of the iceberg and, by changing it, the iceberg changes its response to the same environment. Likewise, for a neuronal ensemble, membrane resistance and firing threshold are intrinsic neuronal properties that can be modified, and they enhance its response to the same excitatory input intensity, resulting in an increased depolarization and generation of action potentials (Modified with permission from Alejandre-García et al., 2022).

Permanent role for enhanced excitability despite transient nature: role for an on/off modulation

Let us assume for a moment that enhanced neuronal excitability is essential for ensemble function (in a later paragraph, we will present evidence to support this claim). Would not the transient nature of excitability potentiation make such essential contribution impossible? To begin with, it should be noted that intrinsic plasticity is not in all brain structures and neuron types short-lived. In cerebellar Purkinje cells, enhanced excitability was observed one month after eyeblink conditioning (Schreurs et al., 1998). This finding suggests that there could be more cell types, in which intrinsic plasticity is long-lasting. It further suggests the possibility that the underlying mechanism is the same or similar in different cell types, with the potential for a long effect duration, but that in some and not others specific activity patterns curtail duration. The second, perhaps more general, point is that enhanced excitability does not need to last permanently to play a permanent role in ensemble function as long as it can be readily recruited under the right conditions (on/off modulation). This criterion is fulfilled when a (transient) excitability increase results from attention-related signaling. Indeed, as illustrated in Figure 3, intrinsic plasticity is evoked in cortical pyramidal neurons upon activation of muscarinic acetylcholine receptors (mAChRs).

Intrinsic plasticity in L5 pyramidal neurons (Sourdet et al., 2003), L2/3 pyramidal neurons (Gill and Hansel, 2020) and cerebellar Purkinje cells (Belmeguenai et al., 2010) depends on the downregulation of small-conductance calcium-dependent SK-type K^+ channels. In L5 pyramidal neurons, this downregulation was driven by activation of type 5 metabotropic glutamate receptors

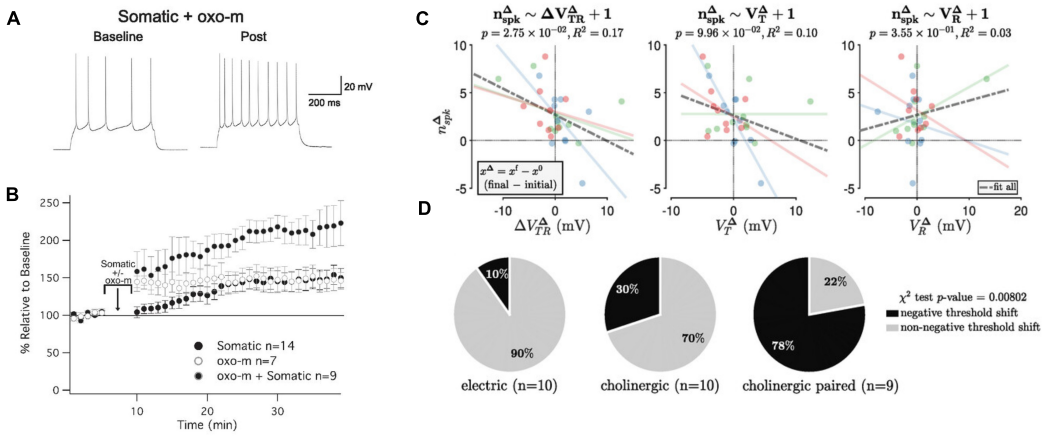

FIGURE 3
Cholinergic modulation promotes intrinsic plasticity in L2/3 pyramidal neurons of mouse primary somatosensory cortex (S1). **(A)** Example recording of a neuron that received somatic depolarization (10 Hz; 5 min) while the muscarinic agonist oxotremorine-1 (oxo-m; 7 μM) is applied to the bath during these *in vitro* recordings. **(B)** Time graph showing changes in spiking relative to baseline; the three conditions shown are oxo-m bath-application alone, somatic depolarization alone, and both stimuli combined. **(C)** Cholinergic modulation shifts the neuronal threshold potential. Relationship between the functional change (number of evoked spikes; n_{spk}) and the membrane potential change (V_R = resting potential; V_T = threshold potential; V_{TR} = difference between the two potentials). Blue dots: electric stimulation alone; green dots: cholinergic modulation alone; red dots: paired stimulation. There is a significant negative association between the changes in spike number and threshold-to-rest distance changes, but not with changes in the threshold or resting potential changes. **(D)** Distribution of S1 recordings from the three experimental groups according to category membership, based on δV_{TR}, to either 'negative threshold shift' or 'non-negative threshold shift' categories. Only paired electric and cholinergic activation causes a significant negative threshold shift. **(A,B)** are taken from Gill and Hansel (2020), *eNeuro* 7. **(C,D)** are taken from Pham and Hansel (2023), *J. Physiol*. 601.15.

(mGluR5; Sourdet et al., 2003), while in L2/3 pyramidal neurons, it was achieved by activation of mAChRs (Gill and Hansel, 2020; Figure 3). Both are Gαq-coupled metabotropic receptors. For M1 mAChRs, it has indeed been demonstrated that their activation inhibits SK-type K^+ channels (Buchanan et al., 2010; Giessel and Sabatini, 2010). These findings show that cholinergic signaling may promote enhanced excitability via the inhibition of SK channels.

The observation that intrinsic plasticity may be triggered by cholinergic signaling is important for our claim that there is no strict need for permanency in ensemble plasticity (as long as the participating neurons are synaptically connected). We postulate two requirements for a non-permanent mechanism that instead rests on the availability to readily re-activate the ensemble and thus be on/off-modulated (Figure 4). First, ensemble re-activation needs to be triggered by a 'meaningful' signal; that is to say that a cellular mechanism should link ensemble re-activation to a context that can be expected to recruit and engage ensembles. Cholinergic signaling fulfills this requirement as it occurs in the context of attention (Everitt and Robbins, 1997). Second, a mechanism for ensemble re-activation would need to be readily available and fast without affecting synaptic connectivity. This is the case for intrinsic plasticity, which—at least in the hippocampus—has been shown to have a lower induction threshold than synaptic plasticity (Lopez-Rojas et al., 2016). These considerations show that—once a second plasticity mechanism comes into play—there is no need for one mechanism whose long-duration (permanency) would guarantee longevity of memory itself. Instead, one plasticity mechanism (synaptic) would establish connectivity and ensemble identity but does not need to be further modulated upon re-activation, while the other (intrinsic) enhances excitability and ensures ensemble function as long as required. On/off modulation as described in Figure 4 furthermore guarantees that flexibility in the activation of various—potentially competing—ensembles is not jeopardized. In addition, intrinsic plasticity can be depressed in an activity-dependent manner (e.g., Paz et al., 2009) and this bidirectionality prevents saturation.

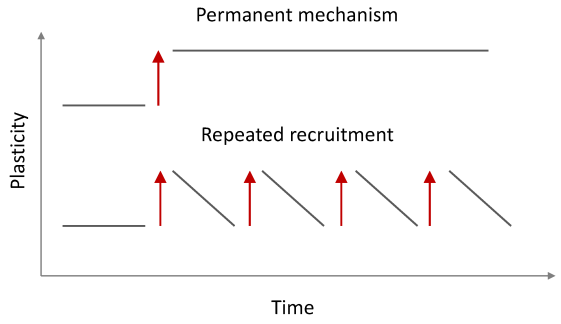

FIGURE 4
Ensemble availability for recall via permanent (top) and non-permanent (bottom) on/off modulation. A synaptically connected ensemble does not require a permanent plasticity mechanism to enhance the probability for recall as long as the ensemble can be readily reactivated (red arrows). This activation involves synaptic drive, but not synaptic plasticity.

Role of enhanced excitability in ensemble formation and function

The memory allocation hypothesis describes a transient role for intrinsic plasticity in the formation of memory engrams. In this conceptual framework, enhanced excitability promotes LTP

induction and thus contributes to engram formation by stabilizing synaptic connectivity. This scenario fits to the participation of SK channels reported in the studies described above. It has indeed been shown in hippocampal recordings that SK channel downregulation boosts calcium signaling and enhances the probability for LTP induction (Ngo-Anh et al., 2005).

What then are lasting roles of (SK-mediated) enhanced excitability? First, SK channels regulate dendritic plateau potentials, in particular their duration, and therefore adjust the integration of local synaptic potentials (Cai et al., 2004). Second, intrinsic plasticity may adjust the somatic spike threshold, and at least in L2/3 pyramidal neurons of the mouse S1 cortex, this effect is obtained by cholinergic co-activation (Pham and Hansel, 2023). In L2/3 pyramidal neurons of the rat barrel cortex, the resting potential sits 15–40 mV below the spike threshold, resulting in a low evoked spike rate of 0.031 spikes per whisker stimulus (Brecht et al., 2003). It is thus conceivable that threshold plasticity in individual neurons adjusts the spike threshold, resulting in circuit-specific response probabilities and spike patterns. A consequence of threshold plasticity further is that it alters how input patterns are processed. A high spike threshold is optimal for the discrimination of distinct patterns, while a reduced threshold is more easily reached when a subset of (driver) synapses are active and thus enables recognition of previously learned patterns, even when inputs are incompletely presented (Pham and Hansel, 2023). Here, too, threshold adjustment equals a shift in the optimal coding strategy and may represent an example where plasticity is meant to last at least until another event necessitates a change in strategy.

While these are lasting functions / consequences of enhanced excitability and its plasticity, they do not describe an essential contribution to memory engram formation. Such an essential contribution is described in the permissive gate hypothesis. Simultaneous patch-clamp recordings from the distal dendrite, proximal dendrite and the soma of L2/3 pyramidal neurons have shown that the amplitude of distally recorded excitatory postsynaptic potentials (EPSPs) is poorly correlated with more proximal EPSP amplitudes and somatic spike output (Larkum et al., 2001; Figure 5). During propagation toward the soma, the dendritic potential is exposed to conductances that may amplify or attenuate these potentials. The density and functional availability of SK-type K^+ conductances, for example, could regulate EPSP forward propagation and thus EPSP-spike coupling. Intrinsic plasticity may regulate the surface expression of SK channels (Ren et al., 2006) and / or their calcium sensitivity (Allen et al., 2007). It is therefore conceivable that SK channel plasticity constitutes a permissive gate for EPSP propagation.

What is the experimental evidence that supports the hypothesis that intrinsic (SK channel-mediated) plasticity gates EPSP-spike coupling and that without it LTP cannot efficiently control postsynaptic responsiveness? Recordings from cerebellar Purkinje cells have provided evidence for both claims. In somato-dendritic patch-clamp recordings from Purkinje cells *in vitro*, it was observed that either triggering intrinsic plasticity or bath-application of the SK channel antagonist apamin (10 nM) would enhance excitability and turn EPSP amplitude into a better predictor of spike output (Ohtsuki and Hansel, 2018). This finding is consistent with the first claim that SK channel plasticity modulates dendritic EPSP propagation.

To examine whether intrinsic plasticity is essential as an enabler (permissive gate) for LTP in learning, one of us and his team tested the involvement of LTP and intrinsic plasticity, respectively, in receptive field plasticity of Purkinje cells in awake mice (Lin et al., 2024). Two-photon recordings of GCaMP6f-encoded calcium signals were used to measure the amplitude of Purkinje cell responses to parallel fiber stimulation, or tactile activation of the ipsilateral forelimb. Repeated stimulation of a parallel fiber bundle caused a potentiation of the dendritic calcium response (Figure 6). This dendritic signal and a simultaneously recorded calcium signal in the axon initial segment (AIS) are positively correlated (not shown). When the PF tetanization is applied in mice that lack SK2 channels (L7-SK2 KO), no potentiation is observed (Figure 6). When it is applied in CaMKII-TT305/6VA mice (this mutation blocks the inhibitory autophosphorylation of CaMKII; Elgersma et al., 2002), the potentiation is reduced but a significant component remains (Figure 6). In L7-SK2 KO mice, Purkinje cell intrinsic plasticity is absent, but LTP is intact (Grasselli et al., 2020). In contrast, in CaMKII-TT305/6VA mice, parallel fiber LTP is impaired, but intrinsic plasticity is intact (Belmeguenai et al., 2010; Piochon et al., 2016a). These mouse lines therefore enable an isolated impairment of LTP and intrinsic plasticity, respectively. The results of this two-photon study using awake mice suggest that both processes are needed to complete proper plasticity, but that in the absence of LTP some potentiation is still available. This is likely the result of applying a permissive gate to synapses at their given synaptic strength. Repetitive activation of tactile stimuli to a forelimb similarly potentiates dendritic responses with comparable outcomes in the two lines of genetically modified mice (Lin et al., 2024). When a PF bundle is tetanized and responses to tactile stimuli are tested before and after tetanization, response amplitudes are enhanced, and responses are even observed in cells that did not respond before tetanization. This finding shows that this type of plasticity indeed updates the receptive field of individual Purkinje cells, showing that here the interaction of synaptic and non-synaptic plasticity occurs in the context of receptive field memory in the intact animal.

Summary and outlook

We here suggest that ensembles—including memory engrams—can be activated without significant synaptic plasticity (Figure 7). Instead, activity-dependent increases in neuronal excitability can recruit neurons into ensembles and maintain them active. There are many potential mechanisms, including cholinergic transmission, that modulate intrinsic excitability, and they are found to be quite robust and even long lasting. It is possible that this intrinsic plasticity may first occur in core neurons that anchor a wider net of participants. In this case, the core neurons could synaptically drive other participant neurons without engaging synaptic plasticity, equivalent to their own initial activation by synaptic drive, but in the strict absence of synaptic plasticity. Regardless of whether or not the intrinsic upregulation of excitability is restricted to a few core neurons or not, the underlying cellular mechanism that enables this intrinsic drive is the opening of a permissive gate that in individual neurons enhances the EPSP—spike output

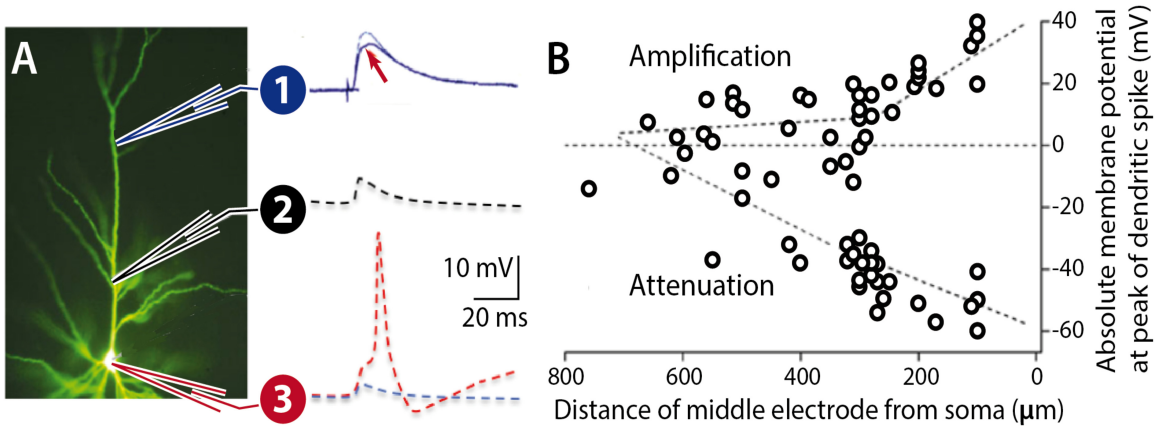

FIGURE 5
Forward propagation of dendritic EPSPs. **(A)** Pyramidal neuron filled with Lucifer Yellow. An EPSP at a distal location (1) may undergo LTP (arrow), but the dendritic potential may nevertheless experience attenuation during propagation along the proximal dendrite (2) towards the soma (3). The probability for spike firing (red) depends on the dendrite-soma coupling strength. **(B)** L5 pyramidal cell recordings show that proximal zones control forward propagation of dendritic potentials. **(B)** is adapted from Larkum et al. (2001), *J. Physiol.* 533.

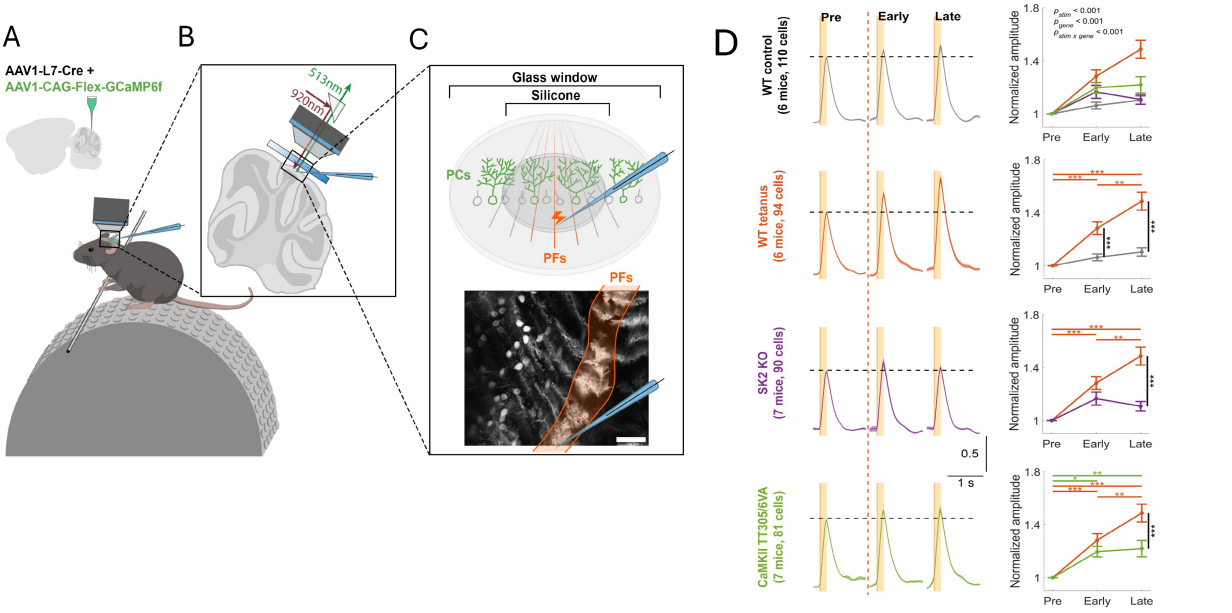

FIGURE 6
Intrinsic plasticity is an essential component of receptive field plasticity in cerebellar Purkinje cells. **(A)** Two-photon recordings from awake, head-fixed mice. AAV vectors were injected into Crus I of cerebellar cortex to express Cre-dependent GCaMP6f specifically in Purkinje cells. **(B,C)** A microelectrode was applied to stimulate a bundle of parallel fibers in Crus I. The bottom panel of **(C)** shows a representative field of view showing calcium responses in a row of Purkinje cells. In this dorsal view, each Purkinje cell is identified by a dendritic 'stripe' aligned in the rostrocaudal direction. The activated parallel fiber bundle is oriented perpendicularly to these dendrites. Scale bar: 100 µm. **(D)** Left: Normalized averaged calcium traces of different mouse genotypes for all trials before parallel fiber tetanization (pre; 20min), as well as during the first 20min after tetanization (early) and the subsequent 20 min (late). For tetanization, 1Hz stimulation is applied for 5min to the parallel fiber bundle. From top to bottom: WT control; WT tetanus; L7-SK2 KO tetanus; CaMKII TT305/6VA tetanus. Right: Normalized amplitude plotted over time. All data are shown as mean ± SEM. $*p < 0.05$; $**p < 0.01$, $***p < 0.001$. The figure is adapted from Lin et al. (2024).

coupling (permissive gate theory). A permissive gate function may be executed by a variety of voltage- or calcium-activated ion channels, not just SK channels. Indeed, we stress that the SK channel work cited is but an example of what is likely to be a complex channel ecosystem that regulates neuronal excitability. Our observation that SK2 channel modulation assumes this role in both L2/3 pyramidal neurons as well as Purkinje cells underlines the role of these channels in spike burst control, but it does not exclude the participation of other channel types. In addition, permissive gate control may link functions to ensemble integration, such as reinforcement signaling (Schiess et al., 2016). The experiments described here therefore highlight only a subset of scenarios that are potentially physiologically relevant.

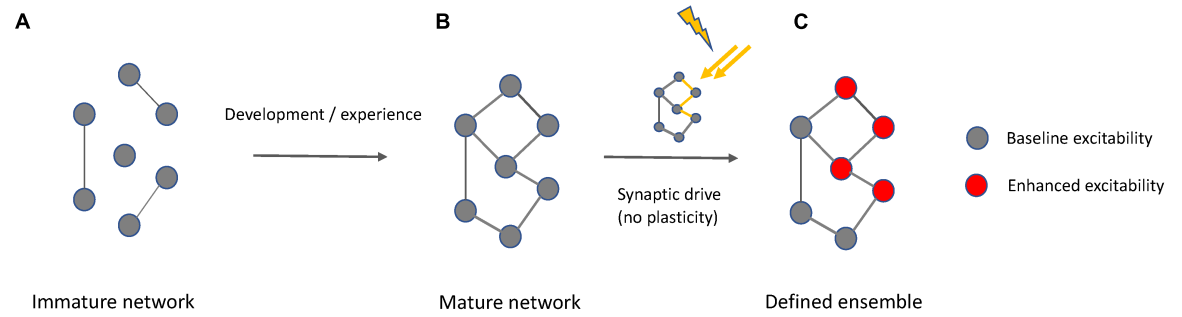

FIGURE 7
Interplay of synaptic and intrinsic mechanisms in ensemble formation. **(A)** At an immature state, a network is incompletely connected. **(B)** A mature network results from experience-dependent synapse formation and pruning during development, but also at later stages in life. Synaptic connectivity defines meaningful groups of neurons reflecting statistically relevant input relationships (e.g., in shared receptive fields). **(C)** When a mature network exists that is fully synaptically connected and encodes defined input, context-dependent activation of an ensemble based on this underlying network is possible by activity-driven enhancement of intrinsic excitability that may be transient or lasting, depending on the type of neuron and the activation conditions. This excitability enhancement requires synaptic drive but does not involve synaptic plasticity. Synaptic plasticity remains an active learning mechanism that is recruited to stabilize synapses with new information content and to adjust their input weights.

It is important to note that the view on ensemble activation presented here (illustrated by the iceberg model) is compatible with synaptic plasticity playing a role in circuit formation and modifications (Figure 7). The iceberg model assumes the *prior* existence of a synaptic connectivity matrix, perhaps via competitive synaptic plasticity processes and also it is consistent with the idea that synaptic weights can be adjusted in an experience-dependent manner throughout lifetime. The synaptic plasticity machinery for these processes is available from early postnatal development onwards and the molecular pathways involved in LTD and LTP remain similar across these developmental stages (Piochon et al., 2016b). When we emphasize the importance of intrinsic plasticity in ensemble and engram function, we do not suggest that synaptic plasticity is not important. Synaptic plasticity mechanisms may be the main mechanism that neurons use to detect and learn associative input relationships and establish neural circuits based on connectivity principles informed by such associative structures (Hansel, 2024). The synchronous activation of excitatory inputs, due to firing of an ensemble, could generate a "synaptoensemble", as a group of coactive inputs that could bring postsynaptic neurons to threshold (Buzsaki, 2010). Furthermore, postsynaptic mechanisms may also contribute to gate control, particularly when changes in dendritic integration over short time periods are considered. An example are somato-dendritic gradients of chloride that change with ongoing synaptic activity and can alter the efficacy of dendritic propagation (Currin et al., 2020; see also Doyon et al., 2014; Weilinger et al., 2022). Given the specific positioning of GABAergic interneuronal input on dendritic shafts (Kwon et al., 2018), a role for this mechanism in ensemble integration needs to be further explored. However, in contrast to any synaptic mechanism, intrinsic plasticity is in principle not associative, but cell autonomous, and it is activity-dependent and reflects the activation history of a neuron. In this way, intrinsic excitability and its plasticity may act as a constant driver for drifts in neural ensemble composition and activity (Delamore et al., 2023). This view also explains why the neuronal composition of ensembles is not stable, because it keeps changing with the passing of time, since the constant barrage of neuronal activity, through intrinsic excitability, changes the circuit.

A key prediction of the model presented here is that neuronal ensembles whose activity is meaningful for brain and organismal function are signified by synaptic connectivity and enhanced excitability. Being connected is a basic requirement; it is the enhanced excitability that signifies the importance and primacy of the signal that is conveyed. Experimental and computational future work will be required to further test the model, in particular in cortical structures. This work on plasticity mechanisms needs to go hand-in-hand with attempts to better understand the nature and signaling consequences of ensembles themselves.

Author contributions

CH: Conceptualization, Funding acquisition, Investigation, Resources, Validation, Visualization, Writing—original draft, Writing—review and editing. RY: Conceptualization, Funding acquisition, Project administration, Resources, Supervision, Validation, Visualization, Writing—original draft, Writing—review and editing.

Funding

The author(s) declare financial support was received for the research, authorship, and/or publication of the article. This work was supported by the National Institutes of Health (NINDS R01NS62771 to CH, NINDS RM1NS132981 and NEI R01EY035248 to RY).

Acknowledgments

We would like to thank members of the Hansel and Yuste laboratories for ongoing discussions that helped to shape our thoughts and perspectives on intrinsic and synaptic plasticity.

Conflict of interest

The authors declare that the research was conducted in the absence of any commercial or financial relationships that could be construed as a potential conflict of interest.

The author(s) declared that they were an editorial board member of Frontiers, at the time of submission. This had no impact on the peer review process and the final decision.

Publisher's note

References

Alejandre-García, T., Kim, S., Pérez-Ortega, J., and Yuste, R. (2022). Intrinsic excitability mechanisms of neuronal ensemble formation. *Elife* 11:e77470.

Alkon, D. L. (1984). Calcium-mediated reduction of ionic currents: A biophysical memory trace. *Science* 226, 1037–1045. doi: 10.1126/science.6093258

Allen, D., Fakler, B., Maylie, J., and Adelman, J. P. (2007). Organization and regulation of small-conductance Ca2+ -activated K+ channel multiprotein complexes. *J. Neurosci.* 27, 2369–2376. doi: 10.1523/JNEUROSCI.3565-06.2007

Belmeguenai, A., Hosy, E., Bengtsson, F., Pedroarena, C. M., Piochon, C., Teuling, E., et al. (2010). Intrinsic plasticity complements long-term potentiation in parallel fiber input gain control in cerebellar Purkinje cells. *J. Neurosci.* 30, 13630–13643. doi: 10.1523/JNEUROSCI.3226-10.2010

Bliss, T. V. P., and Lømo, T. (1973). Long-lasting potentiation of synaptic transmission in the dentate area of the anaesthetized rabbit following stimulation of the perforant path. *J. Physiol.* 232, 331–356.

Brecht, M., Roth, A., and Sakmann, B. (2003). Dynamic receptive fields of reconstructed pyramidal cells in layers 3 and 2 of rat somatosensory barrel cortex. *J. Physiol.* 553, 243–265. doi: 10.1113/jphysiol.2003.044222

Buchanan, K. A., Petrovic, M. M., Chamberlain, S. E., Marrion, N. V., and Mellor, J. R. (2010). Facilitation of long-term potentiation by muscarinic M(1) receptors is mediated by inhibition of SK channels. *Neuron* 68, 948–963. doi: 10.1016/j.neuron.2010.11.018

Buzsaki, G. (2010). Neural syntax: Cell assemblies, synapsembles, and readers. *Neuron* 68, 362–385. doi: 10.1016/j.neuron.2010.09.023

Cai, X., Liang, C. W., Muralidharan, S., Kao, J. P., Tang, C. M., and Thompson, S. M. (2004). Unique roles of SK and Kv4.2 potassium channels in dendritic integration. *Neuron* 44, 351–361. doi: 10.1016/j.neuron.2004.09.026

Carrillo-Reid, L., Han, S., Yang, W., Akrouh, A., and Yuste, R. (2019). Controlling visually guided behavior by holographic recalling of cortical ensembles. *Cell* 178, 447–457. doi: 10.1016/j.cell.2019.05.045

Carrillo-Reid, L., Miller, J.-E., Hamm, J. P., Jackson, J., and Yuste, R. (2015). Endogenous sequential cortical activity evoked by visual stimuli. *J. Neurosci.* 35, 8813–8828.

Carrillo-Reid, L., Miller, J.-E., Yang, W., Peterka, D. S., and Yuste, R. (2017). Imaging and optically manipulating neuronal ensembles. *Annu. Rev. Biophys.* 46, 271–293.

Carrillo-Reid, L., Yang, W., Bando, Y., Peterka, D. S., and Yuste, R. (2016). Imprinting and recalling cortical ensembles. *Science* 353, 691–694.

Cossart, R., Aronov, D., and Yuste, R. (2003). Attractor dynamics of network UP states in neocortex. *Nature* 423, 283–289.

Currin, C. B., Trevelyan, A. J., Akerman, C. A., and Raimondo, J. V. (2020). Chloride dynamics alter the input-output properties of neurons. *PLoS Comp. Biol.* 16:e1007932. doi: 10.1371/journal.pcbi.1007932

Daoudal, G., and Debanne, D. (2003). Long-term plasticity of intrinsic excitability: Learning rules and mechanisms. *Learn. Mem.* 10, 456–465.

Delamore, G., Zaki, Y., Cai, D. J., and Clopath, C. (2023). Drift of neural ensembles driven by slow fluctuations of intrinsic excitability. *Elife* 12:R88053. doi: 10.7554/eLife.88053

Disterhoft, J. F., Coulter, D. A., and Alkon, D. L. (1986). Conditioning-specific membrane changes of rabbit hippocampal neurons measured in vitro. *Proc. Natl. Acad. Sci. U.S.A.* 83, 2733–2737.

Doyon, N., Yinay, L., Prescott, S. A., and De Koninck, Y. (2014). Chloride regulation: A dynamic equilibrium crucial for synaptic inhibition. *Neuron* 89, 1157–1172.

Elgersma, Y., Fedorov, N. B., Ikonen, S., Choi, E. S., Elgersma, M., Carvalho, O. M., et al. (2002). Inhibitory autophosphorylation of CaMKII controls PSD association, plasticity, and learning. *Neuron* 36, 493–505. doi: 10.1016/s0896-6273(02)01007-3

Engert, F., and Bonhoeffer, T. (1999). Dendritic spine changes associated with hippocampal long-term synaptic plasticity. *Nature* 399, 66–70.

Everitt, B. J., and Robbins, T. W. (1997). Central cholinergic systems and cognition. *Annu. Rev. Psychol.* 48, 649–684.

Frick, A., Magee, J., and Johnston, D. (2004). LTP is accompanied by an enhanced local excitability of pyramidal cell dendrites. *Nat. Neurosci.* 7, 126–135.

Giessel, A. J., and Sabatini, B. L. (2010). M1 muscarinic receptors boost synaptic potentials and calcium influx in dendritic spines by inhibiting postsynaptic SK channels. *Neuron* 68, 936–947. doi: 10.1016/j.neuron.2010.09.004

Gill, D. F., and Hansel, C. (2020). Muscarinic modulation of SK2-type K+ channels promotes intrinsic plasticity in L2/3 pyramidal neurons of the mouse primary somatosensory cortex. *eNeuro* 7, 1–10. doi: 10.1523/ENEURO.0453-19.2020

Grasselli, G., Boele, H. J., Titley, H. K., Bradford, N., van Beers, L., Jay, L., et al. (2020). SK2 channels in cerebellar Purkinje cells contribute to excitability modulation in motor-learning-specific memory traces. *PLoS Biol.* 18:e3000596. doi: 10.1371/journal.pbio.3000596

Hansel, C. (2024). Contiguity in perception: Origins in cellular associative computations. *Trends Neurosci.* 47, 170–180. doi: 10.1016/j.tins.2024.01.001

Hansel, C., Linden, D. J., and D'Angelo, E. (2001). Beyond parallel fiber LTD: The diversity of synaptic and non-synaptic plasticity in the cerebellum. *Nat. Neurosci.* 4, 467–475. doi: 10.1038/87419

Hebb, D. O. (1949). *The organization of behaviour*. Hoboken, NJ: Wiley.

Holtmaat, A., and Svoboda, K. (2009). Experience-dependent structural synaptic plasticity in the mammalian brain. *Nat. Rev. Neurosci.* 10, 647–658.

Josselyn, S. A., and Frankland, P. W. (2018). Memory allocation: Mechanisms and function. *Annu. Rev. Neurosci.* 41, 389–413.

Josselyn, S. A., and Tonegawa, S. (2020). Memory engrams: Recalling the past and imagining the future. *Science* 367:eaaw4325. doi: 10.1126/science.aaw4325

Kwon, T., Merchán-Pérez, A., Rial Verde, E. M., Rodríguez, J.-R., DeFelipe, J., and Yuste, R. (2018). Ultrastructural, molecular and functional mapping of GABAergic synapses on dendritic spines and shafts of neocortical pyramidal neurons. *Cereb. Cortex* 29, 2771–2781. doi: 10.1093/cercor/bhy143

Larkum, M. E., Zhu, J. J., and Sakmann, B. (2001). Dendrite mechanisms underlying the coupling of the dendrite with the axonal action potential initiation zone of adult rat layer 5 pyramidal neurons. *J. Physiol.* 533, 447–466. doi: 10.1111/j.1469-7793.2001.0447a.x

Lin, T. F., Busch, S. E., and Hansel, C. (2024). Intrinsic and synaptic determinants of receptive field plasticity in Purkinje cells of the mouse cerebellum. *Nat. Commun.* 15:4645.

Lines, J., and Yuste, R. (2023). Visually evoked neuronal ensembles reactivate during sleep. *bioRxiv* [Preprint]. doi: 10.1101/2023.04.26.538480

Lopez-Rojas, J., Heine, M., and Kreutz, M. R. (2016). Plasticity of intrinsic excitability in mature granule cells of the dentate gyrus. *Sci. Rep.* 6:21615.

Marder, E., Abbott, L. F., Turrigiano, G. G., Liu, Z., and Golowasch, J. (1996). Memory from the dynamics of intrinsic membrane currents. *Proc. Natl. Acad. Sci. U.S.A.* 93, 13481–13486.

Marshel, J. H., Kim, Y. S., Machado, T. A., Quirin, S., Benson, B., Kadmon, J., et al. (2019). Cortical layer-specific critical dynamics triggering perception. *Science* 365:eaaw5202. doi: 10.1126/science.aaw5202

Miller, J. E., Ayzenshtat, I., Carrillo-Reid, L., and Yuste, R. (2014). Visual stimuli recruit intrinsically generated cortical ensembles. *Proc. Natl. Acad. Sci. U.S.A.* 111, 4053–4061.

Nabavi, S., Fox, R., Proulx, C. D., Lin, J. Y., Tsien, R. Y., and Malinow, R. (2014). Engineering a memory with LTD and LTP. *Nature* 511, 348–352.

Ngo-Anh, T. J., Bloodgood, B. L., Lin, M., Sabatini, B. L., Maylie, J., and Adelman, J. P. (2005). SK channels and NMDA receptors form a Ca2+-mediated feedback loop in dendritic spines. *Nat. Neurosci.* 8, 642–649. doi: 10.1038/nn1449

Ohtsuki, G., and Hansel, C. (2018). Synaptic potential and plasticity of an SK2 channel gate regulate spike burst activity in cerebellar Purkinje cells. *iScience* 1, 49–54. doi: 10.1016/j.isci.2018.02.001

Paz, J. T., Mahon, S., Tiret, P., Genet, S., Delord, B., and Charpier, S. (2009). Multiple forms of activity-dependent intrinsic plasticity in layer V cortical neurones in vivo. *J. Physiol.* 587, 3189–3205. doi: 10.1113/jphysiol.2009.169334

Pérez-Ortega, J., Akrouh, A., and Yuste, R. (2024). Stimulus encoding by specific inactivation of cortical neurons. *Nat. Commun.* 15:3192.

Perez-Ortega, J., Alejandre-Garcia, T., and Yuste, R. (2021). Long-term stability of cortical ensembles. *Elife* 10:e64449.

Pham, T., and Hansel, C. (2023). Intrinsic threshold plasticity: Cholinergic activation and role in the neuronal recognition of incomplete input patterns. *J. Physiol.* 15, 3221–3239. doi: 10.1113/JP283473

Pignatelli, M., Ryan, T. J., Roy, D. S., Lovett, C., Smith, L. M., Muralidhar, S., et al. (2019). Engram cell excitability state determines the efficacy of memory retrieval. *Neuron* 101, 274–284. doi: 10.1016/j.neuron.2018.11.029

Piochon, C., Titley, H. K., Simmons, D. H., Grasselli, G., Elgersma, Y., and Hansel, C. (2016a). Calcium threshold shift enables frequency-independent control of plasticity by an instructive signal. *Proc. Natl. Acad. Sci. U.S.A.* 113, 13221–13226. doi: 10.1073/pnas.1613897113

Piochon, C., Kano, M., and Hansel, C. (2016b). LTD-like molecular pathways in developmental synaptic pruning. *Nat. Neurosci.* 19, 1299–1310. doi: 10.1038/nn.4389

Ren, Y., Barnwell, L. F., Alexander, J. C., Lubin, F. D., Adelman, J. P., Pfaffinger, P. J., et al. (2006). Regulation of surface localization of the small conductance Ca2+ -activated potassium channel, SK2, through direct phosphorylation by cAMP-dependent protein kinase. *J. Biol. Chem.* 281, 11769–11779. doi: 10.1074/jbc.M513125200

Rogerson, T., Cai, D. J., Frank, A., Sano, Y., Shobe, J., Lopez-Aranda, M. F., et al. (2014). Synaptic tagging and memory allocation. *Nat. Rev. Neurosci.* 15, 157–169.

Schiess, M., Urbanczik, R., and Senn, W. (2016). Somato-dendritic synaptic plasticity and error-backpropagation in active dendrites. *PLoS Comp. Biol.* 12:e1004638. doi: 10.1371/journal.pcbi.1004638

Schreurs, B. G., Gusev, P. A., Tomsic, D., Alkon, D. L., and Shi, T. (1998). Intracellular correlates of acquisition and long-term memory of classical conditioning in Purkinje cell dendrites in slices of rabbit cerebellar lobule HVI. *J. Neurosci.* 18, 5498–5507. doi: 10.1523/JNEUROSCI.18-14-05498.1998

Sourdet, V., Russier, M., Daoudal, G., Ankri, N., and Debanne, D. (2003). Long-term enhancement of neuronal excitability and temporal fidelity mediated by metabotropic glutamate receptor subtype 5. *J. Neurosci.* 23, 10238–10248. doi: 10.1523/JNEUROSCI.23-32-10238.2003

Thompson, L. T., Moyer, J. R., and Disterhoft, J. F. (1996). Transient changes in excitability of rabbit CA3 neurons with a time course appropriate to support memory consolidation. *J. Neurophysiol.* 76, 1836–1849. doi: 10.1152/jn.1996.76.3.1836

Weilinger, N. L., Wicki-Stordeur, L. E., Groten, C. J., LeDue, J. M., Kahle, K. T., and MacVicar, B. A. (2022). KCC2 drives chloride microdomain formation in dendritic blebbing. *Cell Rep.* 31:111556. doi: 10.1016/j.celrep.2022.111556

Yiu, A. P., Mercaldo, V., Yan, C., Richards, B., Rashid, A. J., Hsiang, H. L., et al. (2014). Neurons are recruited to a memory trace based on relative neuronal excitability immediately before training. *Neuron* 83, 722–735. doi: 10.1016/j.neuron.2014.07.017

Yuste, R., and Bonhoeffer, T. (2001). Morphological changes in dendritic spines associated with long-term synaptic plasticity. *Annu. Rev. Neurosci.* 24, 1071–1089.

Yuste, R., Cossart, R., and Yaksi, E. (2024). Neuronal ensembles: Building blocks of neural circuits. *Neuron* 112, 875–892.

frontiers | Frontiers in Cellular Neuroscience

TYPE Review
PUBLISHED 21 August 2024
DOI 10.3389/fncel.2024.1460219

OPEN ACCESS

EDITED BY
Christian Hansel,
The University of Chicago, United States

REVIEWED BY
Simona Candiani,
University of Genoa, Italy
Aram Megighian,
University of Padua, Italy

*CORRESPONDENCE
Riccardo Fesce
riccardo.fesce@hunimed.eu

RECEIVED 05 July 2024
ACCEPTED 06 August 2024
PUBLISHED 21 August 2024

CITATION
Fesce R (2024) Old innovations and shifted paradigms in cellular neuroscience. *Front. Cell. Neurosci.* 18:1460219. doi: 10.3389/fncel.2024.1460219

Old innovations and shifted paradigms in cellular neuroscience

Riccardo Fesce*

Department of Biomedical Sciences, Humanitas University Medical School, Pieve Emanuele, Italy

Once upon a time the statistics of quantal release were fashionable: "*n*" available vesicles (fusion sites), each with probability "*p*" of releasing a quantum. The story was not so simple, a nice paradigm to be abandoned. Biophysicists, experimenting with "black films," explained the astonishing rapidity of spike-induced release: calcium can trigger the fusion of lipidic vesicles with a lipid bilayer, by masking the negative charges of the membranes. The idea passed away, buried by the discovery of NSF, SNAPs, SNARE proteins and synaptotagmin, Munc, RIM, complexin. Electrophysiology used to be a field for few adepts. Then came patch clamp, and multielectrode arrays and everybody became electrophysiologists. Now, optogenetics have blossomed, and the whole field has changed again. Nice surprise for me, when Alvarez de Toledo demonstrated that release of transmitters could occur through the transient opening of a pore between the vesicle and the plasma-membrane, no collapse of the vesicle in the membrane needed: my mentor Bruno Ceccarelli had cherished this idea ("kiss and run") and tried to prove it for 20 years. The most impressive developments have probably regarded IT, computers and all their applications; machine learning, AI, and the truly spectacular innovations in brain imaging, especially functional ones, have transformed cognitive neurosciences into a new extraordinarily prolific field, and certainly let us imagine that we may finally understand what is going on in our brains. Cellular neuroscience, on the other hand, though the large public has been much less aware of the incredible amount of information the scientific community has acquired on the cellular aspects of neuronal function, may indeed help us to eventually understand the mechanistic detail of how the brain work. But this is no more in the past, this is the future.

KEYWORDS

neurotransmitter release, electrophysiology, patch clamp, freeze-fracture, noise analysis, fluorescent dyes, kiss and run

1 Introduction

The field of Cellular Neuroscience has experienced an intense evolution for many years now, and novel approaches and techniques emerge every month. Having retired last year, the idea of "Paradigm Shifts and Innovations in Cellular Neuroscience" provoked me to look back to the old innovations I witnessed and the paradigm that shifted during my scientific career.

2 Vesicle fusion and the "fusion machine"

During my stage at the Rockefeller University in New York I joined a great group of biophysicists, headed by Alex Mauro. They had been working for quite some time on the biophysics of biological membranes (Mauro and Finkelstein, 1958) and generating artificial membrane models (the so-called "black films"). They observed that phospholipid vesicles could be induced to fuse with such films by raising calcium concentration, so that their content would be released on the other side of the membrane (Zimmerberg et al., 1980) and components of the vesicle membrane would be incorporated into the planar membrane itself (Cohen et al., 1980). It had long been known that release of neurotransmitter evoked by the presynaptic action potential depends on the presence of calcium ions (Fatt and Katz, 1952); also, the seminal work of Del Castillo and Katz (1954) had clarified that transmitter release occurs in "packets" of relatively constant size ("quanta"); when the fine structure of the neuromuscular junction was revealed by electron microscopy, the idea had come about that the fusion of a synaptic vesicle could be the structural equivalent of the recording of a "quantal" event at the postsynaptic membrane. Thus, the action of calcium in favoring phospholipid vesicle fusion with planar membranes was taken to suggest that calcium ions favor phospholipid membrane fusions, possibly by shielding the fixed – predominantly negative – charges of the phospholipids.

For several years, a silent debate went on between biochemists and physicists, about synaptic vesicle fusion: neurotransmitter release occurs in less than a ms after the action potential invades the nerve terminal, so biophysicists would not even consider the possibility that complex biochemical events be interposed between the nerve terminal depolarization and the fusion of vesicles; the instantaneous masking action by calcium ions on the fixed charges of the facing membranes seemed more likely. On the other hand, biochemists were isolating proteins specifically expressed at synapses and presumably involved in quantal release of transmitter (e.g., Südhof and Jahn, 1991); also, biochemical processes clearly influenced quantal release, and clostridial toxins (tetanus and botulinum) were known to impair neuromuscular transmission, through an unclear mechanism (see, e.g., Burgen et al., 1949; Brooks, 1954; Harris and Miledi, 1971) that clearly impaired a step between calcium entry and transmitter release (Dreyer and Schmitt, 1983; Bevan and Wendon, 1984).

The whole story was clarified by Rothman's studies on vesicular traffic in the cell (Rothman, 1994; Söllner et al., 1994), disorganized by N-ethylmaleimide. This substance interferes with an ATPase, referred to as N-ethylmaleimide sensitive factor (NSF), which is needed for the specific exo-endocytosis of vesicles at the membranes they are supposed to fuse with. Such recognition relies on complementary proteins that are expressed in intracellular vesicle membranes and in target membranes: these proteins bind cytoplasmic interactors of NSF (Soluble NSF-Attachment Protein, SNAPs), so they are called SNAP receptors, respectively vesicular (v-SNARE) and target (t-SNARE). The interaction between the tails of v- and t-SNARE proteins acts like a zip that pushes the two membranes against each other, generating a high free-energy conformation that strongly favors the fusion of the two membranes. At synapses, such fusion is prevented by a "brake" protein – presumably synaptotagmin – until a simple conformational change of the latter, produced by the interaction with calcium ions, allows the strongly thermodynamically favored fusion to occur, explosively (Figure 1).

In the meanwhile, Cesare Montecucco and his coworkers were studying clostridial toxins (Montecucco and Schiavo, 1993) and observed a curious property of theirs: they acted as zinc proteases; it turned out that tetanus toxin and botulinum toxins B and D acted on VAMP-synaptobrevin, an integral membrane protein of synaptic vesicles, which Rothman had independently identified as a synaptic v-SNARE; on the other hand, botulinum toxins A and E cleaved SNAP-25, and toxin C cleaved syntaxin, having both proteins been identified by Rothman as presynaptic membrane t-SNAREs (Montecucco and Schiavo, 1995).

This new paradigm finally reconciled the two opposed views: a complex preliminary biochemical process is actually needed for the "fusion machine" to mature around the v- and t-SNARE complex, involving other proteins, among which the N-type calcium channel; once the complete multiprotein apparatus is formed, however, the fusion and the subsequent synchronous release of neurotransmitter occurs instantly in response to the depolarization of the nerve terminal, thanks to a high free-energy conformation produced by the strong interaction between complementary proteins that push the vesicle and plasmatic membrane against each other.

The idea that the synaptic vesicle protein synaptotagmin (Syt1) could be the one triggering fusion in a calcium-dependent way was put forward quite early (Perin et al., 1990), because of its capability to interact with phospholipids in a Ca^{2+}-dependent way, although – or properly because – it has low affinity for Ca^{2+} (the local concentration of the ion in the microdomain close to the active rises high, when Ca^{2+} enters through the N-type channels opened by the action potential, and the conformational changes must occur quite quickly, presumably in less than 100 μs). Still, it took some 20 years to Nobel laureate Südhof and his group, and other laboratories involved in this research, to put the puzzle together and clarify the quite complex machinery involved in the process. Synaptotagmin was confirmed to be the key molecule, through its interaction with membrane phospholipids, especially for the synchronous secretion mediated by the action potential. However, more and more proteins were gradually shown to be involved. For example, proper conformation of syntaxin, through interaction with Munc18-1and Munc13, was shown to be needed to prime the docked vesicles for fusion; complexin was shown to be involved in the "clamping" action of Syt-1 on the SNARE complex; the G-protein Rab3 was shown to guide the vesicle to the active zone by interacting with RIM proteins, which also recruit Ca^{2+}-channels to the active zone, mediate synaptic plasticity and activate Munc13 proteins. In summary, a quite complex network of mutually interacting proteins (Südhof, 2012), something decidedly different from a simple electrostatic interaction between calcium ions and the negative charges of membrane phospholipids. . .

3 Quantal release and the "binomial" paradigm

Entering the field of Cellular Neuroscience as an electrophysiology scholar, I was fascinated by the work of

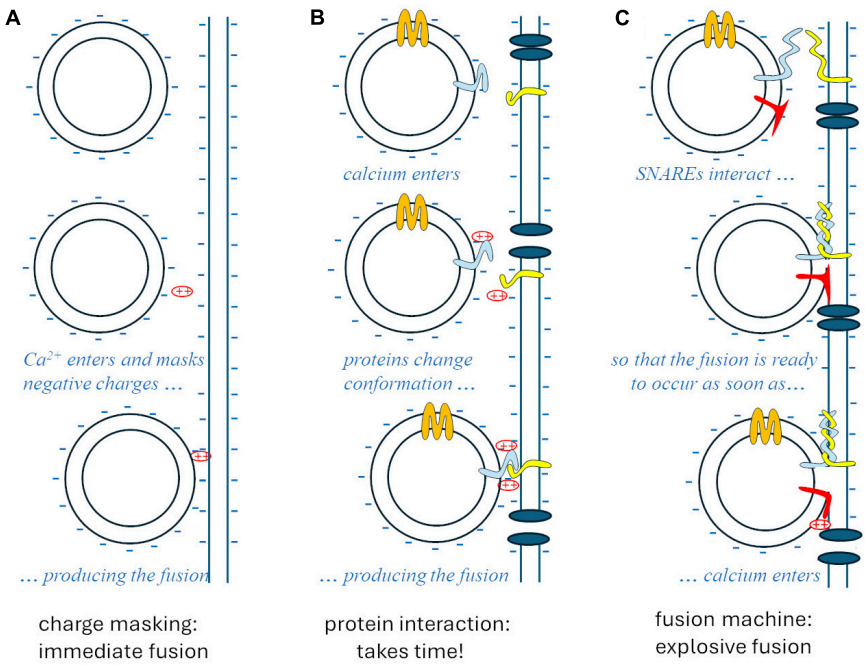

FIGURE 1
The theories of synaptic vesicle fusion. **(A)** The "biophysical" hypothesis, Ca^{2++} masking the negative charges of the membrane phospholipids, would account for the speed (<1 ms) but not for specificity and biochemical regulation. **(B)** The "biochemical" hypothesis would account for specificity and regulations but would take too long after the entry of Ca^{2+}. **(C)** The SNARE model accounts for specificity, regulation, and the explosive speed, due to the high free-energy intermediate generated by the "fusion machine."

Sir Bernard Katz and his colleagues on quantal release of neurotransmitter. At that time, our lab, directed by Bruno Ceccarelli, was mostly committed to correlating electron microscopy data with electrophysiological recordings, with the purpose of verifying what was referred to as "the vesicle hypothesis of quantal release" of neurotransmitters.

Personally, I was intrigued by the idea, quite fashionable then, that the quantal content of the end-plate potential (EPP) in successive trials could be described by binomial statistics, where the binomial parameters *n* and *p* would refer to, respectively, the number of available vesicles (or fusion sites) and the probability for the vesicles to fuse with the presynaptic membrane and release the neurotransmitter they contained. This interpretation of the binomial statistics of evoked quantal release became very popular after several processes of facilitation (a fast and a slow component of facilitation, augmentation, and post-tetanic potentiation; Magleby, 1979) and depression of quantal release were described in paired-pulse experiments, by comparing the sizes of the responses to two stimuli given in rapid sequence, or by examining the time course with which a synapse would return to the basal secretory activity following repetitive stimulation. Everything seemed consistent with the idea that stimulation increased the probability for vesicles to fuse (increasing *p* due to residual calcium ions and/or to phosphorylation of various substrates) but this effect could be counteracted by depletion of the available vesicles (decreased *n*, which may predominate on facilitation for intense quantal release).

However, some curious phenomena were apparent during repetitive stimulation: (i) in reduced calcium concentration (a situation that depresses quantal release) the EPP size would increase during the train, but binomial analysis would indicate an increase in *n* rather than release probability *p*; (ii) in normal calcium concentration, conversely, both *n* and *p* – not only *n* – would decrease during a high-frequency (50 Hz) train; (iii) the rate of occurrence of spontaneous events (miniaturized EPP, mEPP) between successive stimuli declined less than the quantal content of the EPPs (mEPP rate of occurrence even increased initially, at high stimulation frequency), suggesting that mechanisms regulating synchronous release (EPP size) and asynchronous release (mEPP rate) were somewhat different; (iv) finally, the *n-p* model would predict a strong correlation between successive responses in a train of stimuli: an EPP stochastically higher than the average should produce a momentary decrease in the number of synaptic vesicles (or sites) ready for release, *n*, and be followed by one or more responses lower than the average; but such a result was never reported. Did nobody think of this? more likely, negative results never get published, and several researchers probably wasted some time – as I did myself – in trying and detecting such kind of correlations. So, the variability of evoked quantal release did essentially follow binomial statistics, but the paradigm "*n* corresponds to the number of available vesicles (or fusion sites), while *p* represents the probability of release associated to each available vesicle (fusion site)" did not seem tenable.

Something interesting occurred when a neuromuscular preparation was subjected to "random-interval" repetitive stimulation: during a train of stimuli at 15 Hz average frequency (randomly variable intervals with average duration 67 ms), in 0.4 mM Ca^{2+} (20% of the normal Ringer's concentration), average EPP size increased with a bi-exponential time-course (time-constants: 75 and 175 s). As expected from the results of paired-pulses experiments, the size of each EPP was significantly

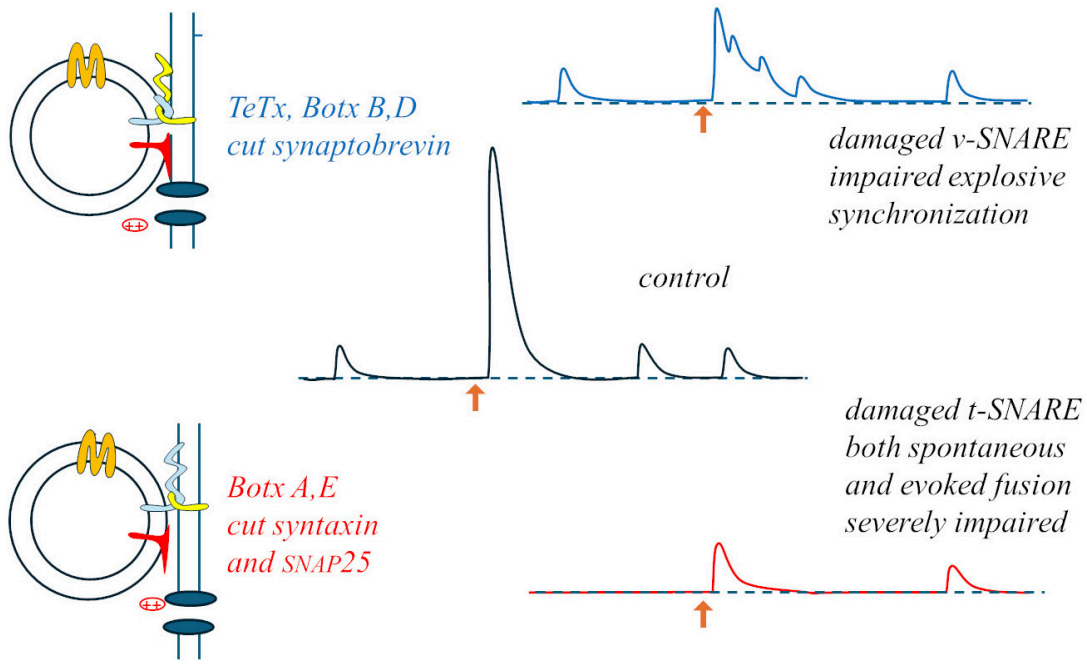

FIGURE 2
Differential effects of tetanus and botulinum toxins: damage to the v-SNARE may mostly impair the normally instantaneous and deterministic fusion upon Ca^{2+} entry **(upper part)**; the stochastic aspect may concern the formation of the fusion machine, strongly hampered by damaging the t-SNARES, and equally impairing both spontaneous and evoked release **(lower part)**.

influenced by the duration of the preceding interval (but not by the size of the previous EPP): facilitation reached a maximum for 15 ms intervals (~40% above the momentary average), waned by for 50 ms intervals, and EPP sizes fell to ~40% below average for 200 ms intervals (Fesce, 1999). This indicated that during repetitive activation each impulse was able to produce a brief silencing (few ms) followed by momentary and transient – but relevant – increase in synaptic efficiency. A similar brief silencing, followed by transient activation, was observed in mEPP occurrences after each evoked response. These observations suggest that whatever can be released is released by the arrival of the action potential to the nerve terminal, in a deterministic rather than stochastic way, and that the stochastic aspects must be related to some steps that precede the evoked response, i.e., some steps involved in the formation of the "fusion machine" through the interaction among vesicular and target SNAREs, Munc proteins, synaptotagmin and complexin, in close proximity with the calcium channels. The specific action of clostridial toxins on the various synaptic SNAREs supports this view and may lead to revise the interpretation of the binomial statistics: botulinum toxin A (BoTx A), which cleaves syntaxin and SNAP25, produces a strong decrease in both spontaneous and evoked release, but the latter remains synchronous; conversely, tetanus toxin (TeTx), that cleaves synaptobrevin, produces a milder inhibition but totally desynchronizes evoked release, transforming it into bursts of mEPPs (Figure 2). Thus, it is likely that decimating the structures on the presynaptic membrane that can host a vesicle for fusion (BoTx A) does not interfere with the capability of the few remaining ones to produce synchronous, deterministic fusions; vice versa, damaging the vesicle capability to dock (TeTx) would make the fusion upon arrival of the action potential and Ca^{2+} entry a stochastic asynchronous event.

One may wonder what are the significance and the physiological role, if any, of the spontaneous occurrence of miniature events (minis). They could have a trophic role on the synapse, as suggested by the degeneration of the endplate (the postsynaptic membrane of the neuromuscular junction) when a muscle is denervated. However, such a role is presumably played by the continuous molecular leakage of neurotransmitter that does occur at synapses, aside from the spontaneous quantal release through synaptic vesicles that produces electrophysiologically recordable minis. Since the rate of occurrence of minis is strictly related to membrane depolarization (and Ca^{2+} entry, presumably) spontaneous release may be a remnant, in spike-dependant synapses, of the mechanism of quantal release at ribbon synapses, which do not produce synchronous release but rather modulate the frequency of miniature events. On the other hand, interfering with the proteins involved in the complex organization of the fusion machine produces differential effects on spontaneous and evoked release (e.g., Südhof, 2012), as it was also mentioned above for the effects of the various clostridial toxins. This suggest that the synapse may be able to regulate the intensity of spontaneous quantal release, the ratio between basal and evoked release, and thus the dynamic range of synaptic transmission. Such an effect may be relevant at central synapses where the quantal content of the postsynaptic potential is very low (corresponding to few minis) and even single minis, typically occurring at higher rate just after a synchronous release, may have some functional (electrical) effect.

A collateral aspect is that images of vesicle fusion on the presynaptic membrane are observed when the frequency of randomly occurring minis is artificially increased at the frog neuromuscular junctions: while fusions produced by electrical stimulation (synchronous release) or hypertonic

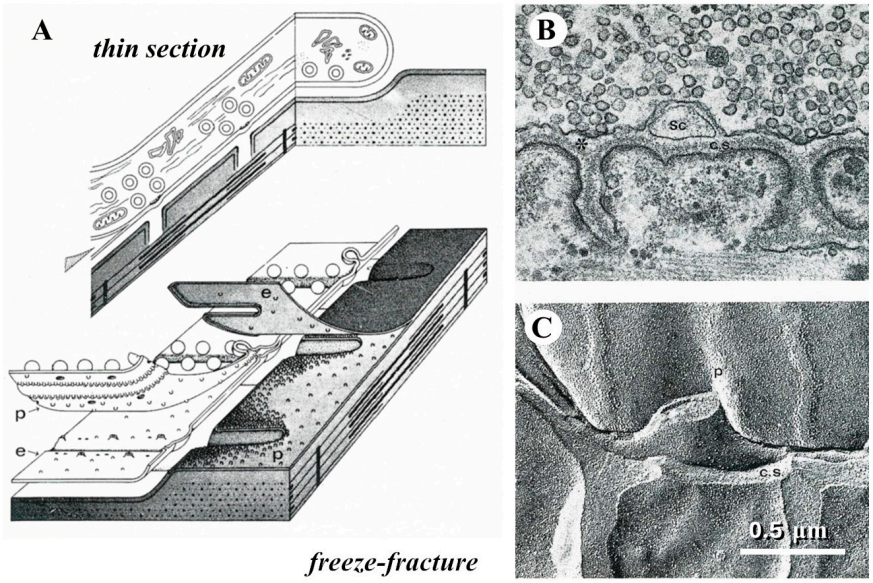

FIGURE 3
The freeze-fracture technique. **(A)** Diagrams that display how the plane of fracture tends to run in a frozen tissue; in particular, they illustrate the way a frog neuromuscular junction appears in thin section electron microscopy or after freeze-fracture. **(B)** Thin-section electron micrograph of a small portion of a frog neuromuscular junction. **(C)** freeze-fracture replica of a similar preparation, which illustrates the correspondence between the appearances of the same structures in the two kinds of electron micrographs.

solution (asynchronous release) occur at the active zone, in response to increasing depolarising concentrations of extracellular potassium they occur randomly dispersed on the membrane (Ceccarelli et al., 1988).

4 Lost in noise, or extracting information from noise?

Far back, Sir Katz and Miledi (1972) observed that the noise produced by acetylcholine (ACh) at the frog neuromuscular junction could be treated statistically by applying Campbell's theorem (Rice, 1944), to extract the elementary event produced by the activation of a receptor molecule by ACh binding and estimate how many such events would contribute to the generation of a miniature end-plate potential (mEPP; about 5,000).

This approach was applied to several physiological questions and became a standard approach in estimating the conductance and kinetics of ion channels, before single channels recording through the patch clamp technique became standard practice (see, e.g., Conti and Wanke, 1975).

During my stay at the Rockefeller, we developed, together with Paul Hurlbut, John Segal and Bruno Ceccarelli, a procedure to apply a similar principle to recordings of quantal release at the neuromuscular junction, through an extension of Campbell theorem to higher semi-invariants (Segal et al., 1985). This way we obtained an estimate of the amplitude and rate of occurrence of mEPP during the asynchronous, high frequency quantal release produced by black widow spider venom (Fesce et al., 1986a); under this condition quantal release would often occur in bursts, so that specific theoretical and analytical approaches had to be developed to treat noise nonstationarity, to resolve the synaptic noise into its elementary components (Fesce et al., 1986b; Fesce, 1990; see also Heinemann and Conti, 1992). It seemed that the approach could be profitably applied to many other experimental questions and situations but, apart from a few studies in which it was used to measure junctional activity at the cyto-neural junction in the frog posterior semicircular canal (Rossi et al., 1994), the apparently promising procedure did not yield noteworthy fruits.

5 The freezing era: freeze-fracture and quick-freezing

When I started my career a novel and intriguing morphological technique had recently been introduced, referred to as freeze-fracture or freeze-etching (Park, 1972). The procedure took advantage of the different mechanical properties of frozen aqueous vs. lipidic components of biological tissues. Breaking with a razor blade a frozen preparation, the fracture plane tended to split membrane bilayers, thus following and exposing the surface of cells; these would be diagonally sprayed with platinum, so that a replica was created that appeared like a landscape covered by snow (Figure 3).

In our laboratory, this procedure turned out particularly useful in displaying the presynaptic membrane that became marked by dimples, indicating the fusion of synaptic vesicles, if the neuromuscular preparation was fixed while intense neurotransmitter release was being elicited. However, we would have liked to be able to capture the images of vesicle fusion in real time, and that was not possible using chemical fixation techniques.

This was made possible by taking advantage of the so-called rapid-freezing (quick-freezing) technique, based on slamming a preparation on a copper block held at extremely low temperatures

with liquid helium. This approach was shown to preserve the cellular ultrastructure of a biological preparation to a depth of at least 10 μm from the impact surface. John Heuser developed a machine to deliver an electrical stimulus to the nerve during the descent of a neuromuscular preparation, mounted on a plunger, toward the copper block held at ∼4°K, so that the preparation was fixed at variable intervals (in the ms range) after the stimulus. Freeze fracture studies using this approach (Heuser et al., 1979) and thin sections obtained with the freeze-substitution procedure (Van Harreveld et al., 1965) on similarly treated preparations (Torri-Tarelli et al., 1985) were instrumental in demonstrating the temporal coincidence between synaptic vesicle fusion and spike induced neurotransmitter release.

This was another curious experience, because a lot of effort had gone in developing the instrument and the procedures and in making the experiments and analyzing the results, but once the coincidence of the electrophysiological and morphological events had been observed, little use remained for the machinery and the technique. As it had been the case for noise analysis of synaptic recordings, the innovation had become almost simultaneously promising and obsolete.

6 Here come the dyes: functional imaging using fluorescent probes

During the last 40 years innumerable functional dyes were developed and taught us a lot about physiological processes. The initial revolution were the calcium dyes, fluorescent compounds that would change their excitation or emission spectrum when bound to calcium ions. Quin2 came about in the eighties and was rapidly put to work in studying the relations between cytoplasmic Ca^{2+} and neurotransmitter release (Meldolesi et al., 1984). However, quin2 had quite low affinity for calcium, and the high concentrations needed would therefore buffer and blunt calcium transients. Higher affinity dyes were soon developed, such as fura-2 and indo-1 (Jackson et al., 1987). Systems to take the ratio between the fluorescence at two excitation (fura-2) or emission (for indo-1) wavelengths were developed to be able to measure calcium concentrations independently of the amount of dye loaded into the cells. Here, the story paralleled what was happening in many other fields: initially, several laboratories would develop mechanical devices to rapidly swap optical filters to alternate images taken with two excitation or emission wavelengths (e.g., Malgaroli et al., 1990); however this would not allow computing more than 1-2 ratios per second. Then came the monochromators, and tuneable-wavelength lasers, electronics relieving the mechanics of most of the work.

Calcium sensitive probes and proteins came as a revolution in the field of cell biology and neurobiology, especially thanks to the work of Tsien (1998), who engineered several mutants of the green fluorescent protein (GFP), from the jellyfish *Aequorea victoria*, so that it could be used as a calcium, redox, or pH sensor, or as a reporter for expression of specific proteins; this application flanked the firefly luciferase reporter gene, which has been widely applied in both transient and stable transfection protocols in eukaryotic cells to measure transcriptional regulation of DNA elements (Brasier and Ron, 1992). Specific mutations of the GFP protein also made it possible to change the emission spectrum, to obtain a turquoise form and a yellow one (YFP).

The idea that a fluorescent substance can change its light sensitivity, or emission, based on the local environment did actually give rise to innumerable applications: from sensors of each specific ion species, or of pH, to voltage sensitive dyes, lipophilic substances that migrate to cell membranes and change their fluorescence properties depending on membrane potential; or to studies of interactions, based on the capability of a substance to quench the fluorescence of another, or on the principle of FRET (Fluorescence Resonance Energy Transfer), where a fluorophore, which normally emits light at a certain wavelength, is quenched by, and excites, another fluorophore that will emit at a different wavelength, when the two are close enough (the mentioned turquoise and YFP can perform this trick).

7 Patch -clamp and its aftermaths

The procedure invented by Neher and Sakmann (1976), which earned them the Nobel prize for Medicine in 1991, was a true revolution in the field of neurobiology. Through the patch-clamp technique it became possible to obtain electrophysiological recordings without producing damage in the plasma-membrane, even in small neurons that would not tolerate the penetration of an electrode; more importantly, single channel recording in cell-attached or excised membrane patches made it possible to monitor the conformational modifications of a single protein in real time, for the first time. This essentially remained the sole technique capable of this for about three decades, until high-speed atomic force microscopy became practically usable to this purpose (Ando et al., 2007; Umeda et al., 2023).

The patch-clamp technique in its various forms – whole-cell, cell-attached, inside-out, outside-out recording – made it possible to gather an incredible amount of experimental evidence on voltage-gated as well as ligand gated channels, their gating kinetics, their conductance and their pharmacology. The properties of channels and transporters could be easily studied this way, at the single molecule level, by having them expressed in *Xenopus laevis* oocytes, a particularly versatile system, relatively poor in endogenous electrophysiologically active membrane proteins, and in the meantime an efficient expression system, which therefore also made it possible to perform mutations in channels and transporters, to clarify the contribution of specific residues to the binding, gating and conductance properties of the molecule of interest (Ivorra et al., 2022).

In addition to the unprecedented possibility to monitor and get to understand molecular dynamics, patch clamp technique opened a whole new field of study in cellular biology, thanks to the ingenuity of Erwin Neher, who realized that having a low-resistance access to the inside of a cell made it possible to determine the resistive and capacitive properties of the cell membrane, and consequently to measure its surface area (Neher and Marty, 1982). This way, secretory phenomena could be studied in quantitative terms, in real time.

Something more came out of this. In Alvarez de Toledo et al. (1993) were able, while visualizing the fusion of histamine containing granules, to measure the capacitance (and membrane

surface) changes and simultaneously determine quantitatively the release of histamine through amperometry (measuring the redox current), in real time, with time resolution in the ms range. This way, they were able to demonstrate that release from a granule can occur even without it collapsing into the plasma membrane, through a reversible fusion of the granule and cellular membranes, and a transient opening of a pore between the vesicle lumen and the extracellular space. This first demonstration was obtained using beige mouse mast-cells, which possess giant granules, but other researchers reproduced similar studies in other cells (e.g., chromaffin cells) with smaller granules. Neher (1993) proposed an extrapolation of these data, obtained with granules of variable sizes, to synaptic vesicles, and concluded that a synaptic vesicle should be able to release most of its content through a transient, sub-millisecond, opening to the synaptic cleft. My mentor, Bruno Ceccarelli, who prematurely died in 1988, would have been very excited by these data, because he had heralded the possibility of quantal neurotransmitter release through a transient, reversible fusion of the synaptic vesicle – a process that we named "kiss-and-run" release (Fesce et al., 1994) – since his first reports of the capacity of synaptic vesicle to recycle (Ceccarelli et al., 1972, 1973).

In general, patch-clamp had profoundly changed the field of electrophysiology. It used to be the world of strange people who worked in the dark, their head hidden in Faraday chambers, in perennial fight against 50-Hz (or 60-Hz) noise, masking and grounding everything, afraid that people would come in the room and touch something or simply talk too loudly, so that the electrode would imperceptibly move and lose the impalement or destroy the cell. Now, it seemed that everybody could do electrophysiology, with this new technique. And gradually came the most sophisticated piezo-controlled micromanipulators and visualization improvement, so that machines would do all the work, positioning, repositioning, contacting the membrane, and you only had to apply the appropriate suction to establish the "giga-seal" or perforate the cell membrane. Electrophysiology was gradually losing its aura of magic and mystery, when a new revolution came, the multielectrode arrays (MEA) mounted in the floor of modified Petri dishes. It was now possible to simultaneously record the activity of many neurons (or cardiomyocytes) in culture, or in a brain slice, and anybody could do it, on a simple table, in the middle of a crowded room. But if electrophysiology had become much less demanding, it certainly was even more fruitful.

More recently, the discovery in bacteria, and transfection in the cell of interest, of photosensitive channels, and more in general proteins that could change conformation in response to light ("photosensitive switches"), has generated the revolution of "optogenetics," with the possibility to activate – or shut off – cellular processes at will and with precise timing, through a laser beam (Armbruster et al., 2024). Photosensitive channels, in particular, can be transfected in specific neurons. This has added a new dimension to electrophysiological studies, making it possible to investigate the effect of the activation of specific neurons or circuits – also *in vivo* – and their involvement in particular information processing steps.

8 . . . and IT, computers, networks, AI

Possibly the most astonishing innovation that accompanied all my research life was the impressive, continuous evolution of computers. One used to need scissors and scotch tape to modify a manuscript, actual "cutting" and "pasting," not simply clicking a couple of keys; and retyping, and typing again. I loved my cupboard-sized up-to-date PDP computer, though it used to take 2 min to perform a 4096-points fast (!) Fourier transform, and we, the "scientists," had the privilege of being able to communicate with each-other, overseas, taking advantage of the ARPANET, the precursor of internet and the world-wide web. Then, every year there would be a new processor, a new storage system (can you imagine the 512 kB 8-inch floppy diskettes, now that you have a 1-TB ½-inch usb key in your pocket?), a new operating system (which however keeps taking 2 min to turn on, and crashes or decides it wants to update in the middle of your lecture or presentation). So, a geometrical increase in speed, performance, data capacity. But the most fascinating evolution in the field is possibly the idea of dynamic programming, i.e., writing software capable to modify itself – in a guided manner or even blindly – to manage to exactly produce the wanted result, or correctly classify or predict. This – changing processing mode based on previous activity, as our neurons do – is the principle of machine learning, which is making computers even more proficient than human beings in investigating, collecting data, classifying, interpreting and predicting.

It is obvious that there are differences between the way a machine learns and the way we do, and we think, although artificial intelligence (AI) systems such as ChatGPT let us think that the machine capable of passing the "Touring test" (tricking a human into thinking that it is also human) has eventually come.

In the future of AI, two quite different paths can be seen. On the one hand, AI systems still miss a sufficiently sophisticated emulation of human emotions, and somebody is trying to fill this gap, essentially pursuing a proof of principle, like alchemists in search for philosopher's stone; and this may raise quite hard questions about rights, diversity, dignity and justice, if we manage to build the "human" machine, capable of suffering. On the other hand, the capacity to handle huge sets of data and apply impeccable logic makes computers quite superior to humans, who can only analyze no more than 7–9 items at a time in their reciprocal relations, and who disagree on most interpretations and decisions – even the merely technical and scientific ones. But this is because all human interpretations and decisions arise from a process of continuous re-evaluation of the available data under different perspectives. The brain takes into consideration a limited number of aspects at a time and the relevance of each aspect changes at any moment, as a function of the other factors that are being considered and the emotional state that the evaluation process is producing at every moment; thus, our interpretations and decisions are tentative, based on likelihood, amendable. In a mathematical world artificial intelligence would certainly be much better than the human one, but the world we live in – though it certainly seems to obey the laws of physics – is full of the variability, unexpectedness, uncertainty and surprise that biology has accustomed us to, and doubting, not being so certain, may in the end be something good.

Still, machine learning and AI, on one side, and the spectacular developments in brain imaging, especially functional imaging,

have transformed cognitive neurosciences into a whole new extraordinarily prolific field and certainly have changed our perspective on the possibility of understanding how the brain works. Cellular neuroscience, on the other side, though the large public has been much less aware of the incredible amount of information the scientific community has acquired on the cellular aspects of neuronal function and neural circuit activity, may indeed help us to eventually understand the mechanistic detail of how the brain work.

But this is no more in the past, this is the future.

Author contributions

RF: Writing – original draft, Writing – review and editing.

Funding

The author(s) declare that no financial support was received for the research, authorship, and/or publication of this article.

Conflict of interest

The author declares that the research was conducted in the absence of any commercial or financial relationships that could be construed as a potential conflict of interest.

The authors declared that they were an editorial board member of Frontiers, at the time of submission. This had no impact on the peer review process and the final decision.

Publisher's note

References

Alvarez de Toledo, G., Fernández-Chacón, R., and Fernández, J. (1993). Release of secretory products during transient vesicle fusion. *Nature* 363, 554–558. doi: 10.1038/363554a0

Ando, T., Uchihashi, T., Kodera, N., Yamamoto, D., Taniguchi, M., Miyagi, A., et al. (2007). High-speed atomic force microscopy for observing dynamic biomolecular processes. *J .Mol. Recognit.* 20, 448–458. doi: 10.1002/jmr.843

Armbruster, A., Mohamed, A., Phan, H., and Weber, W. (2024). Lighting the way: Recent developments and applications in molecular optogenetics. *Curr. Opin. Biotechnol.* 87:103126. doi: 10.1016/j.copbio.2024.103126

Bevan, S., and Wendon, L. (1984). A study of the action of tetanus toxin at rat soleus neuromuscular junctions. *J. Physiol.* 348, 1–17. doi: 10.1113/jphysiol.1984.sp015095

Brasier, A., and Ron, D. (1992). Luciferase reporter gene assay in mammalian cells. *Methods Enzymol.* 216, 386–397. doi: 10.1016/0076-6879(92)16036-j

Brooks, V. (1954). The action of botulinum toxin on motor-nerve filaments. *J. Physiol.* 123, 501–515. doi: 10.1113/jphysiol.1954.sp005067

Burgen, A., Dickens, F., and Zatman, L. (1949). The action of botulinum toxin on the neuro-muscular junction. *J. Physiol.* 109, 10–24. doi: 10.1113/jphysiol.1949.sp004364

Ceccarelli, B., Fesce, R., Grohovaz, F., and Haimann, C. (1988). The effect of potassium on exocytosis of transmitter at the frog neuromuscular junction. *J. Physiol.* 401, 163–183. doi: 10.1113/jphysiol.1988.sp017156

Ceccarelli, B., Hurlbut, W., and Mauro, A. (1972). Depletion of vesicles from frog neuromuscular junctions by prolonged tetanic stimulation. *J. Cell Biol.* 54, 30–38. doi: 10.1083/jcb.54.1.30

Ceccarelli, B., Hurlbut, W., and Mauro, A. (1973). Turnover of transmitter and synaptic vesicles at the frog neuromuscular junction. *J. Cell Biol.* 57, 499–524. doi: 10.1083/jcb.57.2.499

Cohen, F., Zimmerberg, J., and Finkelstein, A. (1980). Fusion of phospholipid vesicles with planar phospholipid bilayer membranes. II. Incorporation of a vesicular membrane marker into the planar membrane. *J. Gen. Physiol.* 75, 251–270. doi: 10.1085/jgp.75.3.251

Conti, F., and Wanke, E. (1975). Channel noise in nerve membranes and lipid bilayers. *Q. Rev. Biophys.* 8, 451–506. doi: 10.1017/s0033583500001967

Del Castillo, J., and Katz, B. (1954). Quantal components of the end-plate potential. *J. Physiol.* 124, 560–573. doi: 10.1113/jphysiol.1954.sp005129

Dreyer, F., and Schmitt, A. (1983). Transmitter release in tetanus and botulinum A toxin-poisoned mammalian motor endplates and its dependence on nerve stimulation and temperature. *Pflugers Arch.* 399, 228–234. doi: 10.1007/BF00656720

Fatt, P., and Katz, B. (1952). Spontaneous subthreshold activity at motor nerve endings. *J. Physiol.* 117, 109–128.

Fesce, R. (1990). Stochastic approaches to the study of synaptic function. *Prog. Neurobiol.* 35, 85–133. doi: 10.1016/0301-0082(90)90019-d

Fesce, R. (1999). The kinetics of nerve-evoked quantal secretion. *Philos. Trans. R. Soc. Lond. B Biol. Sci.* 354, 319–329. doi: 10.1098/rstb.1999.0383

Fesce, R., Grohovaz, F., Valtorta, F., and Meldolesi, J. (1994). Neurotransmitter release: Fusion or 'kiss-and-run'? *Trends Cell Biol.* 4, 1–4. doi: 10.1016/0962-8924(94)90025-6

Fesce, R., Segal, J., Ceccarelli, B., and Hurlbut, W. (1986a). Effects of black widow spider venom and Ca2+ on quantal secretion at the frog neuromuscular junction. *J. Gen. Physiol.* 88, 59–81. doi: 10.1085/jgp.88.1.59

Fesce, R., Segal, J., and Hurlbut, W. (1986b). Fluctuation analysis of nonideal shot noise. Application to the neuromuscular junction. *J. Gen. Physiol.* 88, 25–57. doi: 10.1085/jgp.88.1.25

Harris, A., and Miledi, R. (1971). The effect of type D botulinum toxin on frog neuromuscular junctions. *J. Physiol.* 217, 497–515. doi: 10.1113/jphysiol.1971.sp009582

Heinemann, S. H., and Conti, F. (1992). Nonstationary noise analysis and application to patch clamp recordings. *Methods Enzymol.* 207, 131–148. doi: 10.1016/0076-6879(92)07009-d

Heuser, J., Reese, T., Dennis, M., Jan, Y., Jan, L., and Evans, L. (1979). Synaptic vesicle exocytosis captured by quick freezing and correlated with quantal transmitter release. *J. Cell Biol.* 81, 275–300. doi: 10.1083/jcb.81.2.275

Ivorra, I., Alberola-Die, A., Cobo, R., González-Ros, J., and Morales, A. (2022). Xenopus oocytes as a powerful cellular model to study foreign fully-processed membrane proteins. *Membranes (Basel)* 12:986. doi: 10.3390/membranes12100986

Jackson, A., Timmerman, M., Bagshaw, C., and Ashley, C. (1987). The kinetics of calcium binding to fura-2 and indo-1. *FEBS Lett.* 216, 35–39. doi: 10.1016/0014-5793(87)80752-4

Katz, B., and Miledi, R. (1972). The statistical nature of the acetycholine potential and its molecular components. *J. Physiol.* 224, 665–699. doi: 10.1113/jphysiol.1972.sp009918

Magleby, K. (1979). Facilitation, augmentation, and potentiation of transmitter release. *Prog. Brain Res.* 49, 175–182. doi: 10.1016/S0079-6123(08)64631-2

Malgaroli, A., Fesce, R., and Meldolesi, J. (1990). Spontaneous [Ca2+]i fluctuations in rat chromaffin cells do not require inositol 1,4,5-trisphosphate elevations but are generated by a caffeine- and ryanodine-sensitive intracellular Ca2+ store. *J. Biol. Chem.* 265, 3005–3008.

Mauro, A., and Finkelstein, A. (1958). Realistic model of a fixed-charge membrane according to the theory of Teorell, Meyer, and Sievers. *J. Gen. Physiol.* 42, 385–391. doi: 10.1085/jgp.42.2.385

Meldolesi, J., Huttner, W., Tsien, R., and Pozzan, T. (1984). Free cytoplasmic Ca2+ and neurotransmitter release: Studies on PC12 cells and synaptosomes exposed to alpha-latrotoxin. *Proc. Natl. Acad. Sci. U.S.A.* 81, 620–624. doi: 10.1073/pnas.81.2.620

Montecucco, C., and Schiavo, G. (1993). Tetanus and botulism neurotoxins: A new group of zinc proteases. *Trends Biochem. Sci.* 18, 324–327. doi: 10.1016/0968-0004(93)90065-u

Montecucco, C., and Schiavo, G. (1995). Structure and function of tetanus and botulinum neurotoxins. *Q. Rev. Biophys.* 28, 423–472. doi: 10.1017/s0033583500003292

Neher, E. (1993). Cell physiology. Secretion without full fusion. *Nature* 363, 497–498. doi: 10.1038/363497a0

Neher, E., and Marty, A. (1982). Discrete changes of cell membrane capacitance observed under conditions of enhanced secretion in bovine adrenal chromaffin cells. *Proc. Natl. Acad. Sci. U.S.A.* 79, 6712–6716. doi: 10.1073/pnas.79.21.6712

Neher, E., and Sakmann, B. (1976). Single-channel currents recorded from membrane of denervated frog muscle fibres. *Nature* 260, 799–802. doi: 10.1038/260799a0

Park, R. (1972). Freeze etching: A classical view. *Ann. N. Y. Acad. Sci.* 195, 262–272.

Perin, M., Fried, V., Mignery, G., Jahn, R., and Südhof, T. (1990). Phospholipid binding by a synaptic vesicle protein homologous to the regulatory region of protein kinase C. *Nature* 345, 260–263. doi: 10.1038/345260a0

Rice, S. (1944). Mathematical analysis of random noise. *Bell Tech. Syst. J.* 23, 282–332.

Rossi, M., Martini, M., Pelucchi, B., and Fesce, R. (1994). Quantal nature of synaptic transmission at the cytoneural junction in the frog labyrinth. *J. Physiol.* 478, 17–35. doi: 10.1113/jphysiol.1994.sp020227

Rothman, J. (1994). Mechanisms of intracellular protein transport. *Nature* 372, 55–63. doi: 10.1038/372055a0

Segal, J., Ceccarelli, B., Fesce, R., and Hurlbut, W. (1985). Miniature endplate potential frequency and amplitude determined by an extension of Campbell's theorem. *Biophys. J.* 47, 183–202. doi: 10.1016/s0006-3495(85)83891-1

Söllner, T., Whiteheart, S., Brunner, M., Erdjument-Bromage, H., Geromanos, S., Tempst, P., et al. (1994). SNAP receptors implicated in vesicle targeting and fusion. *Nature* 362, 318–324. doi: 10.1038/362318a0

Südhof, T. (2012). The presynaptic active zone. *Neuron* 75, 11–25. doi: 10.1016/j.neuron.2012.06.012

Südhof, T., and Jahn, R. (1991). Proteins of synaptic vesicles involved in exocytosis and membrane recycling. *Neuron* 6, 665–677. doi: 10.1016/0896-6273(91)90165-v

Torri-Tarelli, F., Grohovaz, F., Fesce, R., and Ceccarelli, B. (1985). Temporal coincidence between synaptic vesicle fusion and quantal secretion of acetylcholine. *J. Cell Biol.* 101, 1386–1399. doi: 10.1083/jcb.101.4.1386

Tsien, R. (1998). The green fluorescent protein. *Annu. Rev. Biochem.* 67, 509–544. doi: 10.1146/annurev.biochem.67.1.509

Umeda, K., McArthur, S. J., and Kodera, N. (2023). Spatiotemporal resolution in high-speed atomic force microscopy for studying biological macromolecules in action. *Microscopy* 72, 151–161. doi: 10.1093/jmicro/dfad011

Van Harreveld, A., Crowell, J., and Malhotra, S. K. (1965). A study of extracellular space in central nervous tissue by freeze-substitution. *J. Cell Biol.* 25, 117–137.

Zimmerberg, J., Cohen, F., and Finkelstein, A. (1980). Fusion of phospholipid vesicles with planar phospholipid bilayer membranes. I. Discharge of vesicular contents across the planar membrane. *J. Gen. Physiol.* 75, 241–250. doi: 10.1085/jgp.75.3.241

frontiers | Frontiers in Cellular Neuroscience

TYPE Mini Review
PUBLISHED 30 September 2024
DOI 10.3389/fncel.2024.1427515

OPEN ACCESS

EDITED BY
Arianna Maffei,
Stony Brook University, United States

REVIEWED BY
Stephen D. Van Hooser,
Brandeis University, United States
Nafiseh Atapour,
Monash University, Australia
Nicoletta Berardi,
University of Florence, Italy

*CORRESPONDENCE
Kathryn M. Murphy
✉ kmurphy@mcmaster.ca

RECEIVED 03 May 2024
ACCEPTED 10 September 2024
PUBLISHED 30 September 2024

CITATION
Murphy KM and Monteiro L (2024) Anatomical and molecular development of the human primary visual cortex. *Front. Cell. Neurosci.* 18:1427515. doi: 10.3389/fncel.2024.1427515

Anatomical and molecular development of the human primary visual cortex

Kathryn M. Murphy[1,2]* and Leanne Monteiro[1]

[1]McMaster Neuroscience Graduate Program, McMaster University, Hamilton, ON, Canada, [2]Department of Psychology, Neuroscience and Behavior, McMaster University, Hamilton, ON, Canada

The human primary visual cortex (V1) development is pivotal to understanding cortical maturation and neuroplasticity. Theories on V1 development range from early maturation models, which emphasize the early peak of synapses in infancy, to those suggesting an extended developmental timeline where key plasticity mechanisms continue to mature well into adulthood. Classic histological approaches have supported early development, while recent molecular studies highlight prolonged or multiple windows of plasticity, indicating that V1 remains susceptible to experience-dependent modifications beyond childhood. This review consolidates findings from both anatomical and molecular studies, tracing the development of V1 from prenatal stages through aging. The evidence reveals that human V1 develops across multiple timescales, with some aspects maturing early and others gradually changing across the lifespan. Reflecting on Cajal's early work, this review underscores the importance of methodological advancements in revealing the intricate details of V1's development.

KEYWORDS

human, visual cortex, V1, development, histology, neuroanatomy, molecular, plasticity

Introduction

The development of the human visual cortex (V1) has been a central theme in the two leading theories about cortical development: the system-by-system cascade, where V1 develops early (Huttenlocher and Dabholkar, 1997) and the integrated network, where V1 develops over a protracted period (Lidow et al., 1991). Classic histological investigations of V1 in infants, such as synapse counts, point to early development of human V1. Moreover, these studies suggest that the peak in synapse counts define the window of highest neuroplasticity in the human cortex (Huttenlocher, 1999; Petanjek et al., 2023). In contrast, studies using a variety of molecular approaches have shown that many of the mechanisms that regulate experience-dependent plasticity continue to mature past childhood into the second and third decades of life, suggesting that V1 has prolonged or multiple plasticity windows (Siu and Murphy, 2018). Furthermore, the protracted development of human V1 could provide a longer window for visual experience to shape its function and support plasticity-based treatments for visual disorders (Castaldi et al., 2020; Thompson et al., 2023).

In humans, more than 20 cortical areas process visual information, so the development of V1 can have a ripple effect on many cortical areas and perceptual functions. Animal models, especially those using mice, continue to reveal the unique impact of vision on the cellular landscape of the cortex (Chen et al., 2024). However, studying human V1

development using postmortem tissue is challenging because brain banks have limited cases at certain ages, and the samples are often delicate and tricky to work with. Over the past century, a growing body of anatomical and molecular research has used those rare and valuable samples to create a picture of how human V1 changes across the lifespan. This review consolidates the insights gained from classic cellular histology and modern molecular techniques, offering an overview of human V1 development covering prenatal and postnatal development and highlighting molecular mechanisms that regulate experience-dependent plasticity in V1.

Prenatal development of human V1

The detailed cytoarchitecture of the human primary visual cortex (V1) has been known since the late 19th century, as shown by Cajal's histological slides and drawing of neurons in V1 (Figure 1A; Cajal, 1899). Cajal's precise drawings of human V1 using Nissl and Golgi stained sections primarily from infants led him to conclude that:

> *The visual cortex of man and gyrencephalous mammals possesses a special structure very different from that of any other cortical area (Cajal, 1899).*

The early stages of human cortical development have been reviewed in detail (Molnár et al., 2019), so here we highlight the development of V1. Changes in the first trimester of prenatal life include extending ventricular and outer radial glia fibers to the pial surface of the developing cortical plate (Bystron et al., 2008; Nowakowski et al., 2016; Arellano et al., 2021). The maturation of radial glia cells projecting to V1 lags behind those to the prefrontal cortex by about 3 weeks (Nowakowski et al., 2017). Next, neurogenesis starts (Bhardwaj et al., 2006; Clowry et al., 2010) along with peak levels of neurogenesis-specific gene expression (Zhu et al., 2018). Newly differentiated neurons migrate from the ventricular zone into the developing cortical plate along radial glia fibers (Rakic, 1972), and the cortical layers mature in an inside-out order: the neurons that will form layer 6 are born first, followed by neurons destined for layers 5 through 2 (Rakic, 1974). The supragranular neurons (layers 2/3) use outer radial glia to migrate through the cortical plate (Nowakowski et al., 2016). During the peak of neurogenesis, maturing excitatory neurons already express a rudimentary set of V1-specific marker genes (Nowakowski et al., 2017).

Throughout the second trimester, the morphological structure of the neurons begins to develop, and thalamocortical afferents grow into the transient subplate between 22 and 26 weeks of gestation and wait briefly before entering the cortical plate (Kostovic and Rakic, 1980). The cortical layers start to differentiate before thalamic afferents invade the cortical plate with deep layers apparent by 19 weeks of gestation (Takashima et al., 1980; Flower, 1985; Burkhalter, 1993; Burkhalter et al., 1993), followed by layer IV at 28 weeks and the superficial layers II/III at 28–35 weeks (Takashima et al., 1980). By the 24–25th week of gestation, the thalamocortical afferents begin to mature and express neuronal markers (Godovalova, 2010). Just a few weeks later (29th–31st weeks), functional connectivity between the thalamus and V1 begins to strengthen (Taymourtash et al., 2022), starting the period when thalamocortical activity can influence the development of V1 and a sharp increase in genes specific to neuronal differentiation (Zhu et al., 2018).

Both excitatory glutamatergic and inhibitory GABAergic neurons are found prenatally in the developing cortical plate (Yan et al., 1992; Andersen et al., 1995; Retz et al., 1996). Many of those cells, as well as synapses and thalamocortical afferents, form a transient arrangement in the subplate zone during the second and third trimesters (Kostović and Judaš, 2007). For example, dense parvalbumin (PV+) labeling is prominent in the subplate in the second trimester and, by birth, has shifted to a cortical laminar arrangement of PV+ inhibitory interneurons (Cao et al., 1996) that continues to mature until adolescence (Letinic and Kostovic, 1998).

In addition to neurons, markers for glia are found prenatally below or in the developing cortical plate of V1. Early in the second trimester, microglia cluster in the immature white matter among the visual radiations and by the middle of the second trimester are found throughout the thickness of the developing V1 (Monier et al., 2006, 2007). Astrocytes are also found in the developing V1 by the middle of the second trimester (Honig et al., 1996; Godovalova, 2010), and astrocyte-specific gene expression in human V1 continues to increase until early childhood (Zhu et al., 2018). Myelinating oligodendrocytes begin accumulating in the white matter below V1 but do not infiltrate the cortical plate before birth (Kostović et al., 2014), leaving V1 with the translucent appearance characteristic of the neonatal cortex.

The thickness of V1 grows from 100 μm to nearly 2 mm through the prenatal period and continues to grow postnatally (Zilles et al., 1986; Molnár et al., 2019). The volume and surface area of V1 has the greatest period of growth postnatally as dendrites and spines on pyramidal neurons contribute to the increased thickness of the cortex, with spines reaching a peak at 5 months before falling to adult levels by 2 years of age (Takashima et al., 1980; Becker et al., 1984; Michel and Garey, 1984). However, V1 does not have a uniform thickness and the gyral and sulcal pattern, especially deep in the calcarine fissure, leads to large variations in thickness. Furthermore, host factors such as sex and socio-economic status are known to affect the thickness of the developing cortex (Sowell et al., 2007; Mackey et al., 2015; Gennatas et al., 2017; Leonard et al., 2019; Alncś et al., 2020; Tooley et al., 2021).

Other anatomical features, such as columnar patterns and horizontal connections, first appear in human V1 prenatally and continue to develop postnatally. Patchy cytochrome oxidase staining is visible prenatally, with distinct blobs apparent at birth (Burkhalter et al., 1993; Wong-Riley et al., 1993). The early pattern of blobs likely reflects the patchy arrangement and spontaneous activity of thalamocortical afferents projecting into the cortex. The plexus of fibers that form the stria of Gennari through layer IV of the human V1 is apparent at birth (Takashima et al., 1980), as are vertical connections between layers such as the apical dendrites of pyramidal cells drawn by Cajal (Figure 1Aii–iv). Horizontal connections emerge by layer, with long-range connections appearing in layers IV and V shortly before birth (Burkhalter et al., 1993). Those connections continue to mature postnatally, and the patchy arrangement of horizontal connections in superficial layers is found sometime after 4 months and becomes adult-like by 2 years (Burkhalter et al., 1993).

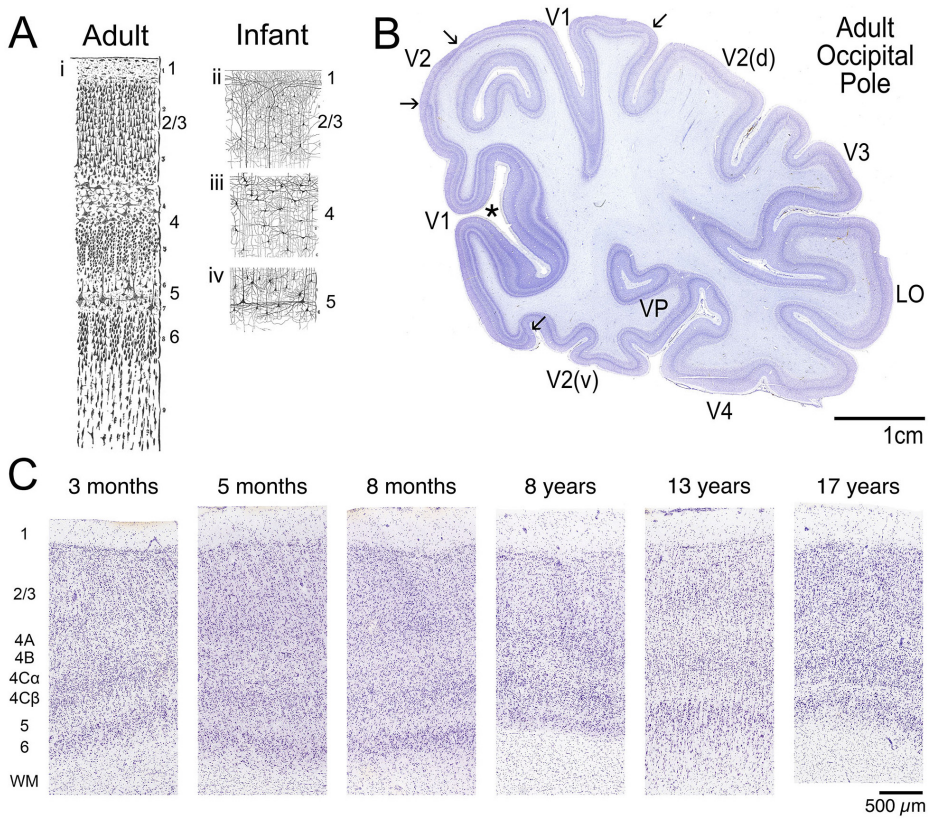

FIGURE 1
Human V1 cytoarchitecture. **(A)** Drawings by Santiago Ramón y Cajal showing the cytoarchitecture of human V1 through the full thickness of a Nissl stained section from (i) adult V1 and (ii-iv) smaller examples from Golgi stained sections of cells in layers 2/3, 4 and 5 from the infant V1. Even in the infant, the apical dendrites of pyramidal cells extend vertically across layers. Adapted from Figures 1, 4, 9 and 20 from the book "Comparative study of the sensory areas of the human cortex", pages 314, 325, 337 and 353 (Cajal, 1899). Note: the original drawings do not include scale bars so these examples could not be matched for magnification; the book is available at: https://archive.org/details/comparativestud00cajagoog/. **(B)** Nissl-stained through the occipital pole of an adult human showing the unique laminar pattern of V1 and the different appearance of the neighboring extra-striate areas. In addition, variation in thickness of V1 is apparent through the depth of the calcarine fissure (asterisk). **(C)** The postnatal appearance of human V1 is shown in a series of Nissl-stained sections from 3 months to 17 years of age. All 6 layers are visible postnatally. Layer 1 is the outermost layer and is lightly stained because it has few cell bodies. Layers 2 & 3 have many darkly stained cells including smaller pyramidal at the top of layer 2 to medium sized pyramidal cells in layer 3. Layer 4 is the recipient zone for thalamocortical afferents and has 3 main sublaminae with larger stellate cells in 4A and smaller stellate cells, often called granule cells, through layers 4B, 4Cα and 4Cβ that give rise to the appearance of the stria of Gennari. Layer 5 appears lighter than layer 4 but is distinct because it has a band of large subcortically projecting pyramidal cells. Layer 6 has medium sized pyramidal cells at the top and a dense combination of smaller cells with a range of shapes in the deeper portion of this layer. The white matter under layer 6 has tiny round cells, the oligodendrocytes that form myelin, ensheathing the axons. In one case, the 13-year-old, some interstitial cells are visible in the white matter (Kostovic and Rakic, 1980, 1990; Judaš et al., 2010). Images of the Nissl-stained sections are from: © 2010 Allen Institute for Brain Science. Allen Human Brain Atlas. Available from: atlas.brain-map.org and © 2010 Allen Institute for Brain Science. BrainSpan Reference Atlas. Available from: www.brainspan.org/static/atlas.

Feedforward and feedback connections between V1 and V2 appear to mature sequentially, with feedforward developing by 4 months, but feedback connections continue to develop, similar to the maturation of horizontal connections in superficial layers (Burkhalter, 1993). Unfortunately, a limited number of anatomical studies with just a few cases have examined feedforward and feedback connections in human V1, so it is difficult to conclude how they develop.

Postnatal development of human V1

Classic histological techniques have shown that anatomical structures of the human V1 are immature at birth. Still, some structures rapidly attain an adult-like appearance within the first few years of postnatal life (Conel, 1939, 1941, 1947, 1951, 1955, 1959, 1963, 1967; Huttenlocher et al., 1982; Burkhalter, 1993; Burkhalter et al., 1993). Cajal's drawing of the infant V1 beautifully illustrates the cytoarchitecture of different laminae shortly after birth (Cajal, 1899). Although the infant (Figure 1Aii–iv) lacks the microanatomical complexity of the adult V1 (Figure 1Ai), it already has a dense network of neuronal processes that contribute to the appearance of the cortical layers. Nissl-stained sections through the occipital pole of the adult human cortex show the unique laminar appearance of V1, with the stria of Gennari in layer 4 distinguishing V1 from adjacent extra-striate areas (Figure 1B).

The adult-like appearance of layers in Nissl-stained sections from infants (Figure 1C) could be interpreted as evidence for early maturation of human V1. However, the primary function of Nissl-stained granular organelles in cells is the synthesis of

proteins, which does not reflect all aspects of neuronal or glial maturity or plasticity. In contrast, molecular markers, especially for mechanisms that regulate experience-dependent plasticity, continue developing beyond the first few years of life.

Animal studies have shown that many neuronal and non-neuronal molecular mechanisms regulate experience-dependent plasticity in the visual system. It is beyond the scope of this mini-review to address all of those mechanisms, but there are excellent reviews that readers can use to gain a broader understanding (Huang et al., 1999; Berardi et al., 2003, 2004; Tropea et al., 2009; Takesian and Hensch, 2013; Pribiag and Stellwagen, 2014; Priebe and McGee, 2014; Sadahiro et al., 2016; Stephany et al., 2016; Hensch and Quinlan, 2018; Grieco et al., 2019; Benfey et al., 2022). Here, we focus on a set of glutamatergic and GABAergic mechanisms that are known to impact the role of excitatory and inhibitory neurotransmission in experience-dependent plasticity (Hensch, 2005; Hensch and Fagiolini, 2005; Maffei and Turrigiano, 2008; Smith et al., 2009; Tropea et al., 2009; Levelt and Hübener, 2012; Capogna et al., 2021) and have been well studied in human V1 across the lifespan (Murphy et al., 2005; Pinto et al., 2010, 2015; Williams et al., 2010; Siu et al., 2015, 2017; Siu and Murphy, 2018; Balsor et al., 2021).

Animal studies—glutamatergic and GABAergic mechanisms regulating plasticity

This section reviews findings from animal studies to introduce the role of glutamatergic and GABAergic mechanisms in regulating experience-dependent plasticity in V1.

Most neurons and synapses in V1 are excitatory (glutamatergic), while only 20% of the neurons and an even smaller percentage of the synapses are inhibitory (GABAergic) (Beaulieu et al., 1992; Jones, 1993). The thalamocortical inputs to layer 4 are excitatory; however, many parvalbumin-positive (PV+) inhibitory interneurons are found in that layer (Balaram et al., 2014). Those PV+ neurons and processes modulate feedforward inputs to V1 (Pouille and Scanziani, 2001), thereby regulating experience-dependent plasticity (Sur et al., 2013; Capogna et al., 2021). This network of glutamatergic and GABAergic mechanisms contributes to shaping the maturation of V1 by guiding synapse development, transmitting visually-driven signals, and regulating experience-dependent plasticity to connect structure and function seamlessly.

Neurons expressing glutamatergic (NMDA and AMPA receptors) and GABAergic receptors are found in all layers of V1 (Albin et al., 1991; Hendry et al., 1994; Huntley et al., 1994; Trepel et al., 1998; Eickhoff et al., 2007, 2008), and developmental changes in those receptors contribute to experience-dependent plasticity. For example, NMDA receptors regulate how visual experience shapes the maturation of receptive field properties (e.g., ocular dominance, orientation tuning and direction selectivity) and the development of visual acuity (Kleinschmidt et al., 1987; Carmignoto and Vicini, 1992; Quinlan et al., 1999; Ramoa et al., 2001; Rivadulla et al., 2001; Fagiolini et al., 2003; Philpot et al., 2003, 2007; Smith et al., 2009). Also, GABAergic transmission and its receptors are essential for triggering the start and closure of the critical period and regulating the maturation of ocular dominance and orientation tuning in V1 (Tsumoto and Sato, 1985; Hensch et al., 1998; Huang et al., 1999; Fagiolini and Hensch, 2000; Morales et al., 2002; Fagiolini et al., 2004; Hensch, 2005). Together, glutamatergic and GABAergic mechanisms regulate the Excitatory-Inhibitory (E-I) balance. When GABAergic signaling is manipulated to shift that balance, it can either enhance or reduce visual plasticity depending on the age and in which GABAergic cells are engaged (Kirkwood and Bear, 1994; Iwai et al., 2003; Maffei et al., 2004; Hensch and Fagiolini, 2005). Importantly, even small changes in the E-I balance can dramatically alter plasticity in V1 (Fagiolini and Hensch, 2000).

NMDA receptors are key components regulating experience-dependent plasticity and are highly expressed prenatally in V1 when nascent synapses are functionally silent (Rumpel et al., 1998). NMDA receptors are tetrameric and contain two obligatory GluN1 subunits paired with two GluN2 (A-D) and/or GluN3 subunits (Monyer et al., 1994). The GluN2 subunits control the kinetics of the receptors. Nascent NMDA receptors have the slower GluN2B subunit, but visual experience drives the insertion of the faster GluN2A subunit into the receptor (Sheng et al., 1994). Furthermore, the GluN2A:GluN2B ratio controls the threshold for experience-dependent plasticity (Philpot et al., 2007; Yashiro and Philpot, 2008) and can be bidirectionally regulated by visual experience (Quinlan et al., 1999).

During the early stages of synapse development, few synapses express AMPA receptors, but visual-driven activity drives their insertion into nascent synapses, converting NMDAR-dominated silent synapses into active synapses (Rumpel et al., 1998). AMPA receptors are essential components of plasticity driven by long-term potentiation or homeostatic synaptic scaling (Gainey et al., 2009). Visual experience drives the accumulation of AMPA receptors at synapses to support visual responsiveness (Heynen et al., 2003; Lambo and Turrigiano, 2013), while deprivation leads to a loss of AMPA receptor expression in V1 (Williams et al., 2015).

Other glutamatergic mechanisms, such as the receptor scaffolding protein postsynaptic density 95 (PSD95), contribute to the experience-dependent refinement of V1. A mobile pool of PSD95 rapidly moves among active synapses, and that pool is dramatically reduced by sensory deprivation (Gray et al., 2006). Furthermore, a spike in PSD95 expression contributes to ending the critical period (Huang et al., 2015). Finally, PSD95, along with the scaffolding protein for $GABA_A$ receptors, gephyrin, mediate the E-I balance (Prange et al., 2004; Lardi-Studler et al., 2007; Keith and El-Husseini, 2008) that is crucial for regulating experience-dependent plasticity in V1 (Hensch, 2004; Hensch and Fagiolini, 2005; Hensch and Quinlan, 2018).

The $GABA_A$ receptor is the most abundant ionotropic GABA receptor in V1. More than 20 subunits combine to make a wide range of different $GABA_A$ receptors (Sieghart, 1995; Cherubini and Conti, 2001) and three of those subunits, α1, α2 and α3, are developmentally regulated (Laurie et al., 1992; Hendrickson et al., 1994; Chen et al., 2001; Heinen et al., 2004). Nascent $GABA_A$ receptors have more α2 and α3 subunits, but during development, there is a shift to more α1 and a faster inhibitory postsynaptic potential (IPSP) (Gingrich et al., 1995). The α1 subunit is the high-affinity interface for binding the neurotransmitter GABA and benzodiazepines, so its development has a crucial role in GABAergic neurotransmission (Pritchett et al., 1989;

Smith and Olsen, 1995; Sigel, 2002). Abnormal visual experience during the critical period accelerates the developmental shift to more $GABA_A\alpha1$ (Beston et al., 2010; Balsor et al., 2019) while GABAergic synapses containing α2 receptors regulate neuronal firing (Fagiolini et al., 2004). However, only α1-containing receptors drive experience-dependent critical period plasticity (Fagiolini et al., 2004).

In the next section, we review the pattern of developmental changes in these glutamatergic and GABAergic mechanisms in human V1 and highlight insights from those developmental trajectories that may influence the potential for experience-dependent plasticity.

Human studies—development of glutamatergic and GABAergic mechanisms

Animal studies have shown that the development of glutamatergic and GABAergic mechanisms regulates many aspects of experience-dependent plasticity in V1. Moreover, in human V1, magnetic resonance spectroscopy has been used to observe changes in glutamate and GABA linked to visual stimulation, age and plasticity (Lin et al., 2012; Lunghi et al., 2015; Pitchaimuthu et al., 2017; Wijtenburg et al., 2017; Kurcyus et al., 2018; Frank et al., 2022). Developmental transcriptome databases like the BrainSpan (Miller et al., 2014) contain information about those mechanisms, but only a few studies provide analyses of postnatal changes in human V1 (Zhu et al., 2018; Balsor et al., 2021; Natu et al., 2021). Our laboratory has a library of postmortem tissue samples from human V1 that we have used to explore the postnatal development of many glutamatergic, GABAergic proteins and a select few other plasticity-related proteins. Those studies are included in the review below.

In human V1, the development of glutamatergic and GABAergic molecular mechanisms proceeds in waves across multiple timescales that cover the lifespan (Murphy et al., 2005; Pinto et al., 2010, 2015; Williams et al., 2010; Siu et al., 2017; Siu and Murphy, 2018; Figure 2A). The obligatory subunit of NMDA receptors, GluN1, is highly expressed at birth in human V1, then quickly declines over the first 2 years of life (Murphy et al., 2005; Siu et al., 2017; Siu and Murphy, 2018). That loss is balanced by an increase in AMPA receptors (e.g., GluA2) and the maturational shift from more NMDA (GluN1) in infancy to more AMPA receptors in older children (Murphy et al., 2005; Siu et al., 2017; Siu and Murphy, 2018). The rapid response properties of AMPA receptors imbue synapses with strong feedforward responses to visually driven activity, while the slower NMDA receptors contribute to feedback modulation of visual processing in adult V1 (Self et al., 2012). So the early shift in the AMPA:NMDA (GluA2:GluN1) balance suggests the rapid establishment of feedforward connections to human V1, followed by an extended period when feedback and other connections are established (Figure 2B).

Through infancy and young childhood, the GluN2B subunit dominates the composition of NMDA receptors in V1, and there is little expression of GluN2A or the receptor anchoring protein PSD95 (Murphy et al., 2005; Pinto et al., 2015; Siu et al., 2017; Siu and Murphy, 2018; Figure 2A). GluN2B declines through childhood to stable levels in adolescence while expression of PSD95 peaks in older childhood when the period for susceptibility to amblyopia ends. However, GluN2A does not dominate the GluN2A:GluN2B balance until teens to young adults (Siu et al., 2017; Siu and Murphy, 2018; Figure 2B). The gradual decline of GluN2B and subsequent increase of GluN2A suggests a prolonged period of NMDA-dependent plasticity in human V1 that may impact the threshold for synaptic modification (Philpot et al., 2007; Smith et al., 2009) and ocular dominance plasticity (Cho et al., 2009). Furthermore, in older adults, the loss of GluN2A triggers a shift in the GluN2A:GluN2B balance back to the pattern observed in childhood (Siu et al., 2017), but age-related changes in other mechanisms suggest this is not a return to child-like plasticity.

Developmental changes in GABAergic mechanisms over the first few years include loss of the presynaptic proteins VGAT and cannabinoid receptor CB1 and the postsynaptic receptor subunits $GABA_A\alpha2$ and $GABA_A\alpha3$. Over those same ages there is a gradual increase in expression of the postsynaptic receptor subunit $GABA_A\alpha1$ (Murphy et al., 2005; Pinto et al., 2010; Siu and Murphy, 2018; Figure 2A). The early loss of $GABA_A\alpha2$ causes a shift in favour of the α1 subunit (Figure 2B), which is important because the α1 subunit is necessary to engage experience-dependent plasticity in V1 (Fagiolini et al., 2004). In monkey V1, the shift from more α2 to more α1 is completed during early development (Hendrickson et al., 1994). However, in humans, the expression of α2 continues to decline across the lifespan, and the shift to α1 is more gradual (Pinto et al., 2010). Other GABAergic mechanisms also have prolonged development into older childhood, adolescence and adulthood. Gephyrin (GPHN) anchors $GABA_A$ receptors at the synapse, regulates the number of excitatory and inhibitory synapses, GABAergic synapse plasticity and the physiological E-I balance (Prange et al., 2004; Lardi-Studler et al., 2007; Keith and El-Husseini, 2008; Tyagarajan and Fritschy, 2014). Gephyrin peaks from adolescence to adulthood before declining into aging (Pinto et al., 2010). The enzyme that makes the basal pool of GABA, GAD67, is relatively constant, but the enzyme that makes the on-demand pool of GABA, GAD65, increases gradually until young adulthood before declining during aging of human V1 (Pinto et al., 2010). Together, these identify both pre- and post-synaptic losses of GABAergic signaling in aging human V1. These losses may contribute to changes in visual perception (Owsley, 2011) since the age-related loss of GABA in monkey V1 underlies poor orientation tuning (Leventhal et al., 2003).

There are lifelong changes in the expression of PSD95 and gephyrin (GPHN), two of the mechanisms regulating the E-I balance (Keith and El-Husseini, 2008). In infancy, gephyrin dominates the E-I balance (PSD95:GPHN), followed by a gradual shift to roughly equal expression of PSD95 and gephyrin in adults, then in aging, a shift back to more gephyrin (Figure 2B). The changes in the ratio of PSD95:gephyrin suggest that the E-I balance is continuously shifting and changing its contribution to plasticity in human V1 across the lifespan (Figure 2B).

Developmental changes in the presynaptic proteins synapsin (SYN1) and synaptophysin (SYP) and the dendritic spine marker drebrin A (DBN1) provide additional insights into synapse development in human V1. Both synapsin and synaptophysin change through infancy and childhood but

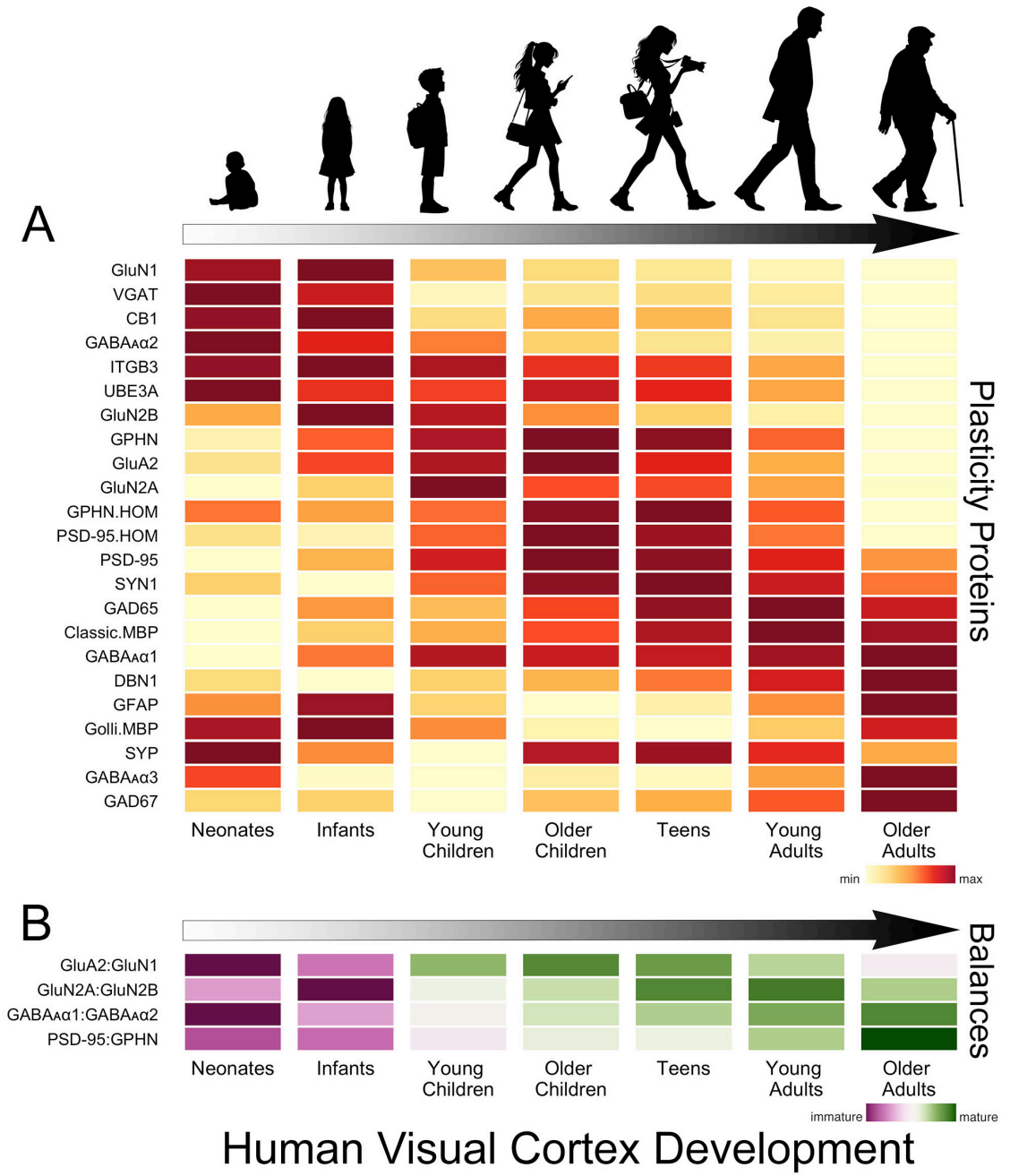

FIGURE 2
Development of plasticity proteins and balances in human V1. **(A)** The heatmap shows the development of a set of glutamatergic, GABAergic and a select few other plasticity-related proteins in human V1. The colors indicate the development of each protein across the lifespan, where yellow is the lowest and dark red is the highest expression level. There are waves of high expression (dark red) in each stage, highlighting multiple timescales for the development of these plasticity proteins. **(B)** The heatmap shows the development of a set of balances known to regulate experience-dependent plasticity in V1. The colors reflect maturation, with the purplish colors indicating that the earlier developing protein is dominant and greenish that the later developing protein dominates the balance. The proteins that develop earlier (GluN1, GluN2B, $GABA_A\alpha2$) dominate the balances in neonates and infants, but all of the balances shift toward the later developing proteins (GluA2, GluN2A, $GABA_A\alpha1$, PSD95) in childhood. The GluA2:GluN1 balance matures rapidly in childhood, but the other balances continue to mature slowly into teens, young adults and older adults. The time course of changes in these balances is significant as they indicate lifelong changes in the mechanisms regulating plasticity in human V1. The data used to create these figures are from the following papers (Murphy et al., 2005; Pinto et al., 2010, 2015; Williams et al., 2010; Siu et al., 2015, 2017).

in opposite ways; synapsin increases while synaptophysin decreases through infancy before rebounding in older childhood. However, neither of these synapse markers follows the trajectory described by electron microscopy studies that counted synapses (Huttenlocher et al., 1982). Furthermore, drebrin (DBN1), which is found in dendritic spines at excitatory synapses and supports homeostatic plasticity (Aoki et al., 2009; Takahashi and Naito, 2017), gradually increases across the lifespan, pointing to lifelong synaptic changes i human V1.

The development of a few other plasticity-related proteins has been studied in human V1. One of these mechanisms is the E3 ubiquitin ligase UBE3A, which controls ARC's degradation and regulates AMPA receptor internalization (Greer et al., 2010). Knocking out UBE3A in mouse V1 leads to a loss of experience-dependent plasticity, leaving connections rigid and unable to be fine-tuned by visual experience (Yashiro et al., 2009). In human V1, the expression of UBE3A is highest in infancy, with a smaller peak in older childhood and adolescence, followed by a steady decline into aging (Williams et al., 2010). Another mechanism that regulates the expression of AMPA receptors, beta3 integrins (ITGB3) (Cingolani et al., 2008; McGeachie et al., 2011), has a pattern of expression similar to UBE3A, suggesting that age-related declines in these mechanisms may lead to endocytosis of AMPA receptors that reduce synaptic scaling plasticity. In addition, a glial mechanism known to reduce experience-dependent plasticity, cortical myelin (classic myelin basic protein MBP) (McGee et al., 2005), gradually increases in human V1 into the fourth decade of life (Siu et al., 2015). These 3 proteins contribute to the brakes on plasticity, and their prolonged changes suggest a gradual increase in the brakes and loss of the potential for experience-dependent plasticity in human V1.

Figure 2 summarizes the changes in the proteins and balances across the lifespan. It is clear that this collection of plasticity-related proteins has peaks at different ages across the lifespan (Figure 2A). The balances also show this pattern of both early (GluA2:GluN1) and prolonged changes [E-I (PSD95:GPHN)]. These findings underscore that multiple timescales and gradual shifts in plasticity mechanisms across the lifespan characterize human V1 development.

Discussion

This review covers prenatal and postnatal development of anatomical and molecular features in human V1. Studies using various neurobiological techniques show that human V1 develops and changes over multiple timescales from the first trimester to aging, so whether human V1 is described as developing early or later depends on what is studied. Importantly, prolonged changes are found for many of the proteins that regulate plasticity, suggesting that some forms of experience-dependent plasticity in human V1 extend past childhood. Only a handful of plasticity mechanisms have been studied, so much is still unknown about the neural mechanisms that regulate plasticity in human V1.

One aspect of human V1 development that has not been explored is the impact of host factors, such as sex, genetic ancestry, and socioeconomic status. However, brain banks have small numbers of cases with limited diversity, making it challenging to do those studies. Still, it is crucial to understand the impact of host factor diversity on human V1 since those factors may account for developmental variability and the timing of plasticity.

The methods used to study the anatomy and molecular environment of human V1 continue to identify new features of its development. Molecular tools have revealed distinct aspects of human V1 (Kang et al., 2011; Carlyle et al., 2017; Jorstad et al., 2023; Wang et al., 2024) and its relationship to neurodevelopmental disorders (Gandal et al., 2022). The next wave of single-cell and spatial transcriptomic tools is poised to uncover new details about how the human cortex develops (Velmeshev et al., 2023; Qian et al., 2024). We end with a reminder from Cajal's words about the importance of the methods for studying human V1:

> *The minute anatomy of the visual cortex (region of the calcarine fissure, sulcus lobulus lingualis) has already been explored by several investigators, among whom we may make particular mention of Meynert et al. But their very incomplete researches have been performed by such insufficient methods as staining with carmine, the Weigert-Pall method, or that of Nissl with basic anilines – methods which, as is well known, do not suffice at all to demonstrate the total morphology of the elements and the organization of the most delicate nerve plexuses (Cajal, 1899).*

Author contributions

KM: Conceptualization, Visualization, Writing – original draft, Writing – review and editing. LM: Conceptualization, Visualization, Writing – original draft, Writing – review and editing.

Funding

The author(s) declare financial support was received for the research, authorship, and/or publication of this article. The research was funded by the NSERC Grant RGPIN-2020-06403, awarded to KM, and NSERC CGS-D, awarded to LM. The funder had no role in study design, data collection and analysis, publication decisions, or manuscript preparation.

Acknowledgments

We recognize that our McMaster University laboratory is located on the traditional territories of the Mississauga and Haudenosaunee nations and within the lands protected by the "Dish with One Spoon" wampum agreement. We thank Maheshwar Panday for help with figure design.

Conflict of interest

The authors declare that the research was conducted in the absence of any commercial or financial relationships that could be construed as a potential conflict of interest.

The author(s) declared that they were an editorial board member of Frontiers, at the time of submission. This had no impact on the peer review process and the final decision.

Publisher's note

References

Albin, R. L., Sakurai, S. Y., Makowiec, R. L., Higgins, D. S., Young, A. B., and Penny, J. B. (1991). Excitatory amino acid, GABAA, and GABAB binding sites in human striate cortex. *Cereb. Cortex* 1, 499–509. doi: 10.1093/cercor/1.6.499

Alnćs, D., Kaufmann, T., Marquand, A. F., Smith, S. M., and Westlye, L. T. (2020). Patterns of sociocognitive stratification and perinatal risk in the child brain. *Proc. Natl. Acad. Sci. U.S.A.* 117, 12419–12427. doi: 10.1073/pnas.2001517117

Andersen, D. L., Tannenberg, A. E. G., Burke, C. J., and Dodd, P. R. (1995). Developmental rearrangements of cortical glutamate-NMDA receptor binding sites in late human gestation. *Dev. Brain Res.* 88, 178–185. doi: 10.1016/0165-3806(95)00101-i

Aoki, C., Kojima, N., Sabaliauskas, N., Shah, L., Ahmed, T. H., Oakford, J., et al. (2009). Drebrin a knockout eliminates the rapid form of homeostatic synaptic plasticity at excitatory synapses of intact adult cerebral cortex. *J. Comp. Neurol.* 517, 105–121. doi: 10.1002/cne.22137

Arellano, J. I., Morozov, Y. M., Micali, N., and Rakic, P. (2021). Radial glial cells: New views on old questions. *Neurochem. Res.* 46, 2512–2524. doi: 10.1007/s11064-021-03296-z

Balaram, P., Kaas, J., and Young, N. (2014). Histological features of layers and sublayers in cortical visual areas V1 and V2 of chimpanzees, macaque monkeys, and humans. *Eye Brain* 6, 5–18. doi: 10.2147/eb.s51814

Balsor, J. L., Arbabi, K., Singh, D., Kwan, R., Zaslavsky, J., Jeyanesan, E., et al. (2021). A practical guide to sparse k-means clustering for studying molecular development of the human brain. *Front. Neurosci.* 15:668293. doi: 10.3389/fnins.2021.668293

Balsor, J. L., Jones, D. G., and Murphy, K. M. (2019). Classification of visual cortex plasticity phenotypes following treatment for amblyopia. *Neural Plast.* 2019, 2564018–2564023. doi: 10.1155/2019/2564018

Beaulieu, C., Kisvarday, Z., Somogyi, P., Cynader, M., and Cowey, A. (1992). Quantitative distribution of GABA-immunopositive and-immunonegative neurons and synapses in the monkey striate cortex (area 17). *Cereb. Cortex* 2, 295–309.

Becker, L. E., Armstrong, D. L., Chan, F., and Wood, M. M. (1984). Dendritic development in human occipital cortical neurons. *Dev. Brain Res.* 315, 117–124. doi: 10.1016/0165-3806(84)90083-x

Benfey, N., Foubert, D., and Ruthazer, E. S. (2022). Glia regulate the development, function, and plasticity of the visual system from retina to cortex. *Front. Neural Circuits* 16:826664. doi: 10.3389/fncir.2022.826664

Berardi, N., Pizzorusso, T., and Maffei, L. (2004). Extracellular matrix and visual cortical plasticity freeing the synapse. *Neuron* 44, 905–908. doi: 10.1016/j.neuron.2004.12.008

Berardi, N., Pizzorusso, T., Ratto, G. M., and Maffei, L. (2003). Molecular basis of plasticity in the visual cortex. *Trends Neurosci.* 26, 369–378. doi: 10.1016/s0166-2236(03)00168-1

Beston, B. R., Jones, D. G., and Murphy, K. M. (2010). Experience-dependent changes in excitatory and inhibitory receptor subunit expression in visual cortex. *Front. Synapt. Neurosci.* 2:138. doi: 10.3389/fnsyn.2010.00138

Bhardwaj, R. D., Curtis, M. A., Spalding, K. L., Buchholz, B. A., Fink, D., Björk-Eriksson, T., et al. (2006). Neocortical neurogenesis in humans is restricted to development. *Proc. Natl. Acad. Sci. U.S.A.* 103, 12564–12568. doi: 10.1073/pnas.0605177103

Burkhalter, A. (1993). Development of forward and feedback connections between areas V1 and V2 of human visual cortex. *Cereb. Cortex* 3, 476–487. doi: 10.1093/cercor/3.5.476

Burkhalter, A., Bernardo, K. L., and Charles, V. (1993). Development of local circuits in human visual cortex. *J. Neurosci.* 13, 1916–1931.

Bystron, I., Blakemore, C., and Rakic, P. (2008). Development of the human cerebral cortex: Boulder Committee revisited. *Nat. Rev. Neurosci.* 9, 110–122. doi: 10.1038/nrn2252

Cajal, S. R. (1899). *Comparative study of the sensory areas of the human cortex*. Worcester, MA: Clark University.

Cao, Q. L., Yan, X. X., Luo, X. G., and Garey, L. J. (1996). Prenatal development of parvalbumin immunoreactivity in the human striate cortex. *Cereb. Cortex* 6, 620–630. doi: 10.1093/cercor/6.4.620

Capogna, M., Castillo, P. E., and Maffei, A. (2021). The ins and outs of inhibitory synaptic plasticity: Neuron types, molecular mechanisms and functional roles. *Eur. J. Neurosci.* 54, 6882–6901. doi: 10.1111/ejn.14907

Carlyle, B. C., Kitchen, R. R., Kanyo, J. E., Voss, E. Z., Pletikos, M., Sousa, A. M. M., et al. (2017). A multiregional proteomic survey of the postnatal human brain. *Nat. Neurosci.* 20, 1–15. doi: 10.1038/s41593-017-0011-2

Carmignoto, G., and Vicini, S. (1992). Activity-dependent decrease in NMDA receptor responses during development of the visual cortex. *Science* 258, 1007–1011. doi: 10.1126/science.1279803

Castaldi, E., Lunghi, C., and Morrone, M. C. (2020). Neuroplasticity in adult human visual cortex. *Neurosci. Biobehav. Rev.* 112, 542–552. doi: 10.1016/j.neubiorev.2020.02.028

Chen, L. L., Yang, C. C., and Mower, G. D. G. (2001). Developmental changes in the expression of GABA(A) receptor subunits (alpha(1), alpha(2), alpha(3)) in the cat visual cortex and the effects of dark rearing. *Mol. Brain Res.* 88, 135–143. doi: 10.1016/s0169-328x(01)00042-0

Chen, X., Fischer, S., Rue, M. C. P., Zhang, A., Mukherjee, D., Kanold, P. O., et al. (2024). Whole-cortex in situ sequencing reveals input-dependent area identity. *Nature* 56, 1–10. doi: 10.1038/s41586-024-07221-6

Cherubini, E., and Conti, F. (2001). Generating diversity at GABAergic synapses. *Trends Neurosci.* 24, 155–162.

Cho, K. K. A., Khibnik, L., Philpot, B. D., and Bear, M. F. (2009). The ratio of NR2A/B NMDA receptor subunits determines the qualities of ocular dominance plasticity in visual cortex. *Proc. Natl. Acad. Sci. U.S.A.* 106, 5377–5382. doi: 10.1073/pnas.0808104106

Cingolani, L. A., Thalhammer, A., Yu, L. M. Y., Catalano, M., Ramos, T., Colicos, M. A., et al. (2008). Activity-dependent regulation of synaptic AMPA receptor composition and abundance by β3 integrins. *Neuron* 58, 749–762. doi: 10.1016/j.neuron.2008.04.011

Clowry, G., Molnár, Z., and Rakic, P. (2010). Renewed focus on the developing human neocortex. *J. Anat.* 217, 276–288. doi: 10.1111/j.1469-7580.2010.01281.x

Conel, J. L. (1939). *The cortex of the newborn*. Cambridge, MA: Harvard University Press, 58–60. doi: 10.4159/harvard.9780674187641.c12

Conel, J. L. (1941). *The cortex of the one-month infant*. Cambridge, MA: Harvard University Press, 145–146. doi: 10.4159/harvard.9780674187658.c39

Conel, J. L. (1947). *The cortex of the three-month infant*. Cambridge, MA: Harvard University Press, 3–3. doi: 10.4159/harvard.9780674187672.intro

Conel, J. L. (1951). *The cortex of the six-month infant*. Cambridge, MA: Harvard University Press, 123–126. doi: 10.4159/harvard.9780674187689.c21

Conel, J. L. (1955). *The cortex of the fifteen-month infant*. Cambridge, MA: Harvard University Press, 121–125. doi: 10.4159/harvard.9780674187696.c16

Conel, J. L. (1959). *The cortex of the twenty-four-month infant*. Cambridge, MA: Harvard University Press, 165–170. doi: 10.4159/harvard.9780674187702.c13

Conel, J. L. (1963). *The cortex of the four-year child*. Cambridge, MA: Harvard University Press, 188–195. doi: 10.4159/harvard.9780674187719.c17

Conel, J. L. (1967). *The cortex of the six-year child*. Cambridge, MA: Harvard University Press, 113–179. doi: 10.4159/harvard.9780674187733.c3

Eickhoff, S. B., Rottschy, C., and Zilles, K. (2007). Laminar distribution and co-distribution of neurotransmitter receptors in early human visual cortex. *Brain Struct. Funct.* 212, 255–267. doi: 10.1007/s00429-007-0156-y

Eickhoff, S. B., Rottschy, C., Kujovic, M., Palomero-Gallagher, N., and Zilles, K. (2008). Organizational principles of human visual cortex revealed by receptor mapping. *Cereb. Cortex* 18, 2637–2645. doi: 10.1093/cercor/bhn024

Fagiolini, M., and Hensch, T. K. (2000). Inhibitory threshold for critical-period activation in primary visual cortex. *Nature* 404, 183–186. doi: 10.1038/35004582

Fagiolini, M., Fritschy, J.-M., Löw, K., Möhler, H., Rudolph, U., and Hensch, T. K. (2004). Specific GABAA circuits for visual cortical plasticity. *Science* 303, 1681–1683. doi: 10.1126/science.1091032

Fagiolini, M., Katagiri, H., Miyamoto, H., Mori, H., Grant, S. G. N., Mishina, M., et al. (2003). Separable features of visual cortical plasticity revealed by N-methyl-D-aspartate receptor 2A signaling. *Proc. Natl. Acad. Sci. U.S.A.* 100, 2854–2859. doi: 10.1073/pnas.0536089100

Flower, M. J. (1985). Neuromaturation of the human fetus. *J. Med. Philos.* 10, 237–251. doi: 10.1093/jmp/10.3.237

Frank, S. M., Becker, M., Qi, A., Geiger, P., Frank, U. I., Rosedahl, L. A., et al. (2022). Efficient learning in children with rapid GABA boosting during and after training. *Curr. Biol.* 32:5022–5030.e7. doi: 10.1016/j.cub.2022.10.021

Gainey, M. A., Hurvitz-Wolff, J. R., Lambo, M. E., and Turrigiano, G. G. (2009). Synaptic scaling requires the GluR2 subunit of the AMPA receptor. *J. Neurosci.* 29, 6479–6489. doi: 10.1523/jneurosci.3753-08.2009

Gandal, M. J., Haney, J. R., Wamsley, B., Yap, C. X., Parhami, S., Emani, P. S., et al. (2022). Broad transcriptomic dysregulation occurs across the cerebral cortex in ASD. *Nature* 611, 532–539. doi: 10.1038/s41586-022-05377-7

Gennatas, E. D., Avants, B. B., Wolf, D. H., Satterthwaite, T. D., Ruparel, K., Ciric, R., et al. (2017). Age-related effects and sex differences in gray matter density, volume, mass, and cortical thickness from childhood to young adulthood. *J. Neurosci.* 37, 5065–5073. doi: 10.1523/jneurosci.3550-16.2017

Gingrich, K. J., Roberts, W. A., and Kass, R. S. (1995). Dependence of the GABAA receptor gating kinetics on the alpha-subunit isoform: Implications for structure-function relations and synaptic transmission. *J. Physiol.* 489, 529–543. doi: 10.1113/jphysiol.1995.sp021070

Godovalova, O. S. (2010). Expression of nervous tissue nuclear protein and glial fibrillary acidic protein during morphogenesis of the neocortex. *Bull. Exp. Biol. Med.* 149, 655–658. doi: 10.1007/s10517-010-1017-x

Gray, N. W., Weimer, R. M., Bureau, I., and Svoboda, K. (2006). Rapid redistribution of synaptic PSD-95 in the neocortex in vivo. *PLoS Biol.* 4:e370. doi: 10.1371/journal.pbio.0040370

Greer, P. L., Hanayama, R., Bloodgood, B. L., Mardinly, A. R., Lipton, D. M., Flavell, S. W., et al. (2010). The Angelman syndrome protein Ube3A regulates synapse development by ubiquitinating arc. *Cell* 140, 704–716. doi: 10.1016/j.cell.2010.01.026

Grieco, S. F., Holmes, T. C., and Xu, X. (2019). Neuregulin directed molecular mechanisms of visual cortical plasticity. *J. Comp. Neurol.* 527, 668–678. doi: 10.1002/cne.24414

Heinen, K., Bosman, L. W. J., Spijker, S., Pelt, J., van, Smit, A. B., et al. (2004). Gabaa receptor maturation in relation to eye opening in the rat visual cortex. *Neuroscience* 124, 161–171. doi: 10.1016/j.neuroscience.2003.11.004

Hendrickson, A., March, D., Richards, G., Erickson, A., and Shaw, C. (1994). Coincidental appearance of the α1 subunit of the gaba-a receptor and the type ibenzodiazepine receptor near birth in macaque monkey visual cortex. *Int. J. Dev. Neurosci.* 12, 299–314. doi: 10.1016/0736-5748(94)90078-7

Hendry, S., Huntsman, M., Vinuela, A., Mohler, H., Blas, A., de, et al. (1994). GABAA receptor subunit immunoreactivity in primate visual cortex: Distribution in macaques and humans and regulation by visual input in adulthood. *J. Neurosci.* 14, 2383–2401. doi: 10.1523/jneurosci.14-04-02383.1994

Hensch, T. K. (2004). Critical period regulation. *Annu. Rev. Neurosci.* 27, 549–579. doi: 10.1146/annurev.neuro.27.070203.144327

Hensch, T. K. (2005). Critical period plasticity in local cortical circuits. *Nat. Rev. Neurosci.* 6, 877–888. doi: 10.1038/nrn1787

Hensch, T. K., and Fagiolini, M. (2005). Excitatory-inhibitory balance and critical period plasticity in developing visual cortex. *Prog. Brain Res.* 147, 115–124. doi: 10.1016/s0079-6123(04)47009-5

Hensch, T. K., and Quinlan, E. M. (2018). Critical periods in amblyopia. *Vis. Neurosci.* 35:E014. doi: 10.1017/s0952523817000219

Hensch, T., Stryker, M., and Kash, S. (1998). Local GABA circuit control of experience-dependent plasticity in developing visual cortex. *Science* 282, 1504–1508. doi: 10.1126/science.282.5393.1504

Heynen, A. J., Yoon, B.-J., Liu, C.-H., Chung, H. J., Huganir, R. L., and Bear, M. F. (2003). Molecular mechanism for loss of visual cortical responsiveness following brief monocular deprivation. *Nat. Neurosci.* 6, 854–862. doi: 10.1038/nn1100

Honig, L. S., Herrmann, K., and Shatz, C. J. (1996). Developmental changes revealed by immunohistochemical markers in human cerebral cortex. *Cereb. Cortex* 6, 794–806. doi: 10.1093/cercor/6.6.794

Huang, X., Stodieck, S. K., Goetze, B., Cui, L., Wong, M. H., Wenzel, C., et al. (2015). Progressive maturation of silent synapses governs the duration of a critical period. *Proc. Natl. Acad. Sci. U.S.A.* 112, E3131–E3140. doi: 10.1073/pnas.1506488112

Huang, Z. J., Kirkwood, A., Pizzorusso, T., Porciatti, V., Morales, B., Bear, M. F., et al. (1999). BDNF regulates the maturation of inhibition and the critical period of plasticity in mouse visual cortex. *Cell* 98, 739–755. doi: 10.1016/s0092-8674(00)81509-3

Huntley, G. W., Vickers, J. C., Janssen, W., Brose, N., Heinemann, S. F., and Morrison, J. H. (1994). Distribution and synaptic localization of immunocytochemically identified NMDA receptor subunit proteins in sensory-motor and visual cortices of monkey and human. *J. Neurosci.* 14, 3603–3619. doi: 10.1523/jneurosci.14-06-03603.1994

Huttenlocher, P. R. (1999). Dendritic and synaptic development in human cerebral cortex: Time course and critical periods. *Dev. Neuropsychol.* 16, 347–349. doi: 10.1207/s15326942dn1603_12

Huttenlocher, P. R., and Dabholkar, A. S. (1997). Regional differences in synaptogenesis in human cerebral cortex. *J. Comp. Neurol.* 387, 167–178. doi: 10.1002/(sici)1096-9861(19971020)387:2<167::aid-cne1>3.0.co;2-z

Huttenlocher, P. R., Courten, C., de Garey, L. J., and Loos, H. V. (1982). Synaptogenesis in human visual cortex–evidence for synapse elimination during normal development. *Neurosci. Lett.* 33, 247–252. doi: 10.1016/0304-3940(82)90379-2

Iwai, Y., Fagiolini, M., Obata, K., and Hensch, T. K. (2003). Rapid critical period induction by tonic inhibition in visual cortex. *J. Neurosci.* 23, 6695–6702. doi: 10.1523/jneurosci.23-17-06695.2003

Jones, E. G. (1993). GABAergic neurons and their role in cortical plasticity in primates. *Cereb. Cortex* 3, 361–372. doi: 10.1093/cercor/3.5.361-a

Jorstad, N. L., Close, J., Johansen, N., Yanny, A. M., Barkan, E. R., Travaglini, K. J., et al. (2023). Transcriptomic cytoarchitecture reveals principles of human neocortex organization. *Science* 382:eadf6812. doi: 10.1126/science.adf6812

Judaš, M., Sedmak, G., Pletikos, M., and Jovanov-Milošević, N. (2010). Populations of subplate and interstitial neurons in fetal and adult human telencephalon. *J. Anat.* 217, 381–399. doi: 10.1111/j.1469-7580.2010.01284.x

Kang, H. J., Kawasawa, Y. I., Cheng, F., Zhu, Y., Xu, X., Li, M., et al. (2011). Spatio-temporal transcriptome of the human brain. *Nature* 478, 483–489. doi: 10.1038/nature10523

Keith, D., and El-Husseini, A. (2008). Excitation control: Balancing PSD-95 function at the synapse. *Front. Mol. Neurosci.* 1:4. doi: 10.3389/neuro.02.004.2008

Kirkwood, A., and Bear, M. (1994). Hebbian synapses in visual cortex. *J. Neurosci.* 14, 1634–1645. doi: 10.1523/jneurosci.14-03-01634.1994

Kleinschmidt, A., Bear, M. F., and Singer, W. (1987). Blockade of "NMDA" receptors disrupts experience-dependent plasticity of kitten striate cortex. *Science* 238, 355–358.

Kostović, I., and Judaš, M. (2007). Transient patterns of cortical lamination during prenatal life: Do they have implications for treatment? *Neurosci. Biobehav. Rev.* 31, 1157–1168. doi: 10.1016/j.neubiorev.2007.04.018

Kostovic, I., and Rakic, P. (1980). Cytology and time of origin of interstitial neurons in the white matter in infant and adult human and monkey telencephalon. *J. Neurocytol.* 9, 219–242. doi: 10.1007/bf01205159

Kostovic, I., and Rakic, P. (1990). Developmental history of the transient subplate zone in the visual and somatosensory cortex of the macaque monkey and human brain. *J. Comp. Neurol.* 297, 441–470. doi: 10.1002/cne.902970309

Kostović, I., Jovanov-Milošević, N., Radoš, M., Sedmak, G., Benjak, V., Kostović-Srzentić, M., et al. (2014). Perinatal and early postnatal reorganization of the subplate and related cellular compartments in the human cerebral wall as revealed by histological and MRI approaches. *Brain Struct. Funct.* 219, 231–253. doi: 10.1007/s00429-012-0496-0

Kurcyus, K., Annac, E., Hanning, N. M., Harris, A. D., Oeltzschner, G., Edden, R., et al. (2018). Opposite dynamics of GABA and glutamate levels in the occipital cortex during visual processing. *J. Neurosci.* 38, 9967–9976. doi: 10.1523/jneurosci.1214-18.2018

Lambo, M. E., and Turrigiano, G. G. (2013). Synaptic and intrinsic homeostatic mechanisms cooperate to increase L2/3 pyramidal neuron excitability during a late phase of critical period plasticity. *J. Neurosci.* 33, 8810–8819. doi: 10.1523/jneurosci.4502-12.2013

Lardi-Studler, B., Smolinsky, B., Petitjean, C. M., Koenig, F., Sidler, C., Meier, J. C., et al. (2007). Vertebrate-specific sequences in the gephyrin E-domain regulate cytosolic aggregation and postsynaptic clustering. *J. Cell Sci.* 120, 1371–1382. doi: 10.1242/jcs.003905

Laurie, D., Wisden, W., and Seeburg, P. (1992). The distribution of thirteen GABAA receptor subunit mRNAs in the rat brain. III. Embryonic and postnatal development. *J. Neurosci.* 12, 4151–4172. doi: 10.1523/jneurosci.12-11-04151.1992

Leonard, J. A., Romeo, R. R., Park, A. T., Takada, M. E., Robinson, S. T., Grotzinger, H., et al. (2019). Associations between cortical thickness and reasoning differ by socioeconomic status in development. *Dev. Cogn. Neurosci.* 36:100641. doi: 10.1016/j.dcn.2019.100641

Letinic, K., and Kostovic, I. (1998). Postnatal development of calcium-binding proteins calbindin and parvalbumin in human visual cortex. *Cereb. Cortex* 8, 660–669. doi: 10.1093/cercor/8.7.660

Levelt, C. N., and Hübener, M. (2012). Critical-period plasticity in the visual cortex. *Annu. Rev. Neurosci.* 35, 309–330. doi: 10.1146/annurev-neuro-061010-113813

Leventhal, A. G., Wang, Y., Pu, M., Zhou, Y., and Ma, Y. (2003). GABA and its agonists improved visual cortical function in senescent monkeys. *Science* 300, 812–815. doi: 10.1126/science.1082874

Lidow, M. S., Goldman-Rakic, P. S., and Rakic, P. (1991). Synchronized overproduction of neurotransmitter receptors in diverse regions of the primate cerebral cortex. *Proc. Natl. Acad. Sci. U.S.A.* 88, 10218–10221.

Lin, Y., Stephenson, M. C., Xin, L., Napolitano, A., and Morris, P. G. (2012). Investigating the metabolic changes due to visual stimulation using functional proton magnetic resonance spectroscopy at 7 T. *J. Cereb. Blood Flow Metab.* 32, 1484–1495. doi: 10.1038/jcbfm.2012.33

Lunghi, C., Emir, U. E., Morrone, M. C., and Bridge, H. (2015). Short-term monocular deprivation alters GABA in the adult human visual cortex. *Curr. Biol.* 25, 1496–1501. doi: 10.1016/j.cub.2015.04.021

Mackey, A. P., Finn, A. S., Leonard, J. A., Jacoby-Senghor, D. S., West, M. R., Gabrieli, C. F. O., et al. (2015). Neuroanatomical correlates of the income-achievement gap. *Psychol. Sci.* 26, 925–933. doi: 10.1177/0956797615572233

Maffei, A., and Turrigiano, G. (2008). The age of plasticity: Developmental regulation of synaptic plasticity in neocortical microcircuits. *Prog. Brain Res.* 169, 211–223. doi: 10.1016/s0079-6123(07)00012-x

Maffei, A., Nelson, S. B., and Turrigiano, G. G. (2004). Selective reconfiguration of layer 4 visual cortical circuitry by visual deprivation. *Nat. Neurosci.* 7, 1353–1359. doi: 10.1038/nn1351

McGeachie, A. B., Cingolani, L. A., and Goda, Y. (2011). A stabilising influence: Integrins in regulation of synaptic plasticity. *Neurosci. Res.* 70, 24–29. doi: 10.1016/j.neures.2011.02.006

McGee, A. W., Yang, Y., Fischer, Q. S., Daw, N. W., and Strittmatter, S. M. (2005). Experience-driven plasticity of visual cortex limited by myelin and Nogo receptor. *Science* 309, 2222–2226. doi: 10.1126/science.1114362

Michel, A. E., and Garey, L. J. (1984). The development of dendritic spines in the human visual cortex. *Hum. Neurobiol.* 3, 223–227.

Miller, J. A., Ding, S.-L., Sunkin, S. M., Smith, K. A., Ng, L., Szafer, A., et al. (2014). Transcriptional landscape of the prenatal human brain. *Nature* 508, 199–206. doi: 10.1038/nature13185

Molnár, Z., Clowry, G. J., Šestan, N., Alzu'bi, A., Bakken, T., Hevner, R. F., et al. (2019). New insights into the development of the human cerebral cortex. *J. Anat.* 235, 432–451. doi: 10.1111/joa.13055

Monier, A., Adle-Biassette, H., Delezoide, A.-L., Evrard, P., Gressens, P., and Verney, C. (2007). Entry and distribution of microglial cells in human embryonic and fetal cerebral cortex. *J. Neuropathol. Exp. Neurol.* 66, 372–382. doi: 10.1097/nen.0b013e3180517b46

Monier, A., Evrard, P., Gressens, P., and Verney, C. (2006). Distribution and differentiation of microglia in the human encephalon during the first two trimesters of gestation. *J. Comp. Neurol.* 499, 565–582. doi: 10.1002/cne.21123

Monyer, H., Burnashev, N., Laurie, D. J., Sakmann, B., and Seeburg, P. H. (1994). Developmental and regional expression in the rat brain and functional properties of four NMDA receptors. *Neuron* 12, 529–540. doi: 10.1016/0896-6273(94)90210-0

Morales, B., Choi, S.-Y., and Kirkwood, A. (2002). Dark rearing alters the development of GABAergic transmission in visual cortex. *J. Neurosci.* 22, 8084–8090. doi: 10.1523/jneurosci.22-18-08084.2002

Murphy, K. M., Beston, B. R., Boley, P. M., and Jones, D. G. (2005). Development of human visual cortex: A balance between excitatory and inhibitory plasticity mechanisms. *Dev. Psychobiol.* 46, 209–221. doi: 10.1002/dev.20053

Natu, V. S., Rosenke, M., Wu, H., Querdasi, F. R., Kular, H., Lopez-Alvarez, N., et al. (2021). Infants' cortex undergoes microstructural growth coupled with myelination during development. *Commun. Biol.* 4:1191. doi: 10.1038/s42003-021-02706-w

Nowakowski, T. J., Bhaduri, A., Pollen, A. A., Alvarado, B., Mostajo-Radji, M. A., Lullo, E. D., et al. (2017). Spatiotemporal gene expression trajectories reveal developmental hierarchies of the human cortex. *Science* 358, 1318–1323. doi: 10.1126/science.aap8809

Nowakowski, T. J., Pollen, A. A., Sandoval-Espinosa, C., and Kriegstein, A. R. (2016). Transformation of the radial glia scaffold demarcates two stages of human cerebral cortex development. *Neuron* 91, 1219–1227. doi: 10.1016/j.neuron.2016.09.005

Owsley, C. (2011). Aging and vision. *Vis. Res.* 51, 1610–1622. doi: 10.1016/j.visres.2010.10.020

Petanjek, Z., Banovac, I., Sedmak, D., and Hladnik, A. (2023). Dendritic spines, structure, function, and plasticity. *Adv. Neurobiol.* 34, 143–221. doi: 10.1007/978-3-031-36159-3_4

Philpot, B. D., Cho, K. K. A., and Bear, M. F. (2007). Obligatory role of NR2A for metaplasticity in visual cortex. *Neuron* 53, 495–502. doi: 10.1016/j.neuron.2007.01.027

Philpot, B. D., Espinosa, J. S., and Bear, M. F. (2003). Evidence for altered NMDA receptor function as a basis for metaplasticity in visual cortex. *J. Neurosci.* 23, 5583–5588.

Pinto, J. G. A., Hornby, K. R., Jones, D. G., and Murphy, K. M. (2010). Developmental changes in GABAergic mechanisms in human visual cortex across the lifespan. *Front. Cell. Neurosci.* 4:16. doi: 10.3389/fncel.2010.00016

Pinto, J. G. A., Jones, D. G., Williams, C. K., and Murphy, K. M. (2015). Characterizing synaptic protein development in human visual cortex enables alignment of synaptic age with rat visual cortex. *Front. Neural Circuit* 9:3. doi: 10.3389/fncir.2015.00003

Pitchaimuthu, K., Wu, Q., Carter, O., Nguyen, B. N., Ahn, S., Egan, G. F., et al. (2017). Occipital GABA levels in older adults and their relationship to visual perceptual suppression. *Sci. Rep.* 7:14231. doi: 10.1038/s41598-017-14577-5

Pouille, F., and Scanziani, M. (2001). Enforcement of temporal fidelity in pyramidal cells by somatic feed-forward inhibition. *Science* 293, 1159–1163. doi: 10.1126/science.1060342

Prange, O., Wong, T. P., Gerrow, K., Wang, Y. T., and El-Husseini, A. (2004). A balance between excitatory and inhibitory synapses is controlled by PSD-95 and neuroligin. *Proc. Natl. Acad. Sci. U.S.A.* 101, 13915–13920. doi: 10.1073/pnas.0405939101

Pribiag, H., and Stellwagen, D. (2014). Neuroimmune regulation of homeostatic synaptic plasticity. *Neuropharmacology* 78, 13–22. doi: 10.1016/j.neuropharm.2013.06.008

Priebe, N. J., and McGee, A. W. (2014). Mouse vision as a gateway for understanding how experience shapes neural circuits. *Front. Neural Circuits* 8:123. doi: 10.3389/fncir.2014.00123

Pritchett, D. B., Sontheimer, H., Shivers, B. D., Ymer, S., Kettenmann, H., Schofield, P. R., et al. (1989). Importance of a novel GABAA receptor subunit for benzodiazepine pharmacology. *Nature* 338, 582–585. doi: 10.1038/338582a0

Qian, X., Coleman, K., Jiang, S., Kriz, A. J., Marciano, J. H., Luo, C., et al. (2024). Spatial Single-cell Analysis Decodes Cortical Layer and Area Specification. *bioRxiv* [Preprint]. doi: 10.1101/2024.06.05.597673 bioRxiv: 2024.06.05.597673.

Quinlan, E. M., Philpot, B. D., Huganir, R. L., and Bear, M. F. (1999). Rapid, experience-dependent expression of synaptic NMDA receptors in visual cortex in vivo. *Nat. Neurosci.* 2, 352–357. doi: 10.1038/7263

Rakic, P. (1972). Mode of cell migration to the superficial layers of fetal monkey neocortex. *J. Comp. Neurol.* 145, 61–83. doi: 10.1002/cne.901450105

Rakic, P. (1974). Neurons in rhesus monkey visual cortex: Systematic relation between time of origin and eventual disposition. *Science* 183, 425–427. doi: 10.1126/science.183.4123.425

Ramoa, A. S., Mower, A. F., Liao, D., and Jafri, S. I. (2001). Suppression of cortical NMDA receptor function prevents development of orientation selectivity in the primary visual cortex. *J. Neurosci.* 21, 4299–4309.

Retz, W., Kornhuber, J., and Riederer, P. (1996). Neurotransmission and the ontogeny of human brain. *J. Neural Transm.* 103, 403–419. doi: 10.1007/bf01276417

Rivadulla, C. C., Sharma, J. J., and Sur, M. M. (2001). Specific roles of NMDA and AMPA receptors in direction-selective and spatial phase-selective responses in visual cortex. *J. Neurosci.* 21, 1710–1719.

Rumpel, S., Hatt, H., and Gottmann, K. (1998). Silent synapses in the developing rat visual cortex: Evidence for postsynaptic expression of synaptic plasticity. *J. Neurosci.* 18, 8863–8874.

Sadahiro, M., Sajo, M., and Morishita, H. (2016). Nicotinic regulation of experience-dependent plasticity in visual cortex. *J. Physiol.* 110, 29–36. doi: 10.1016/j.jphysparis.2016.11.003

Self, M. W., Kooijmans, R. N., Supèr, H., Lamme, V. A., and Roelfsema, P. R. (2012). Different glutamate receptors convey feedforward and recurrent processing in macaque V1. *Proc. Natl. Acad. Sci. U.S.A.* 109, 11031–11036. doi: 10.1073/pnas.1119527109/-/dcsupplemental

Sheng, M., Cummings, J., Roldan, L. A., Jan, Y. N., and Jan, L. Y. (1994). Changing subunit composition of heteromeric NMDA receptors during development of rat cortex. *Nature* 368, 144–147. doi: 10.1038/368144a0

Sieghart, W. (1995). Structure and pharmacology of gamma-aminobutyric acidA receptor subtypes. *Pharmacol. Rev.* 47, 181–234.

Sigel, E. (2002). Mapping of the benzodiazepine recognition site on GABA-A receptors. *Curr. Top. Med. Chem.* 2, 833–839. doi: 10.2174/1568026023393444

Siu, C. R., and Murphy, K. M. (2018). The development of human visual cortex and clinical implications. *Eye Brain* 10, 25–36. doi: 10.2147/eb.s130893

Siu, C. R., Balsor, J. L., Jones, D. G., and Murphy, K. M. (2015). Classic and golli myelin basic protein have distinct developmental trajectories in human visual cortex. *Front. Neurosci.* 9:138. doi: 10.3389/fnins.2015.00138

Siu, C. R., Beshara, S. P., Jones, D. G., and Murphy, K. M. (2017). Development of glutamatergic proteins in human visual cortex across the lifespan. *J. Neurosci.* 37, 6031–6042. doi: 10.1523/jneurosci.2304-16.2017

Smith, G. B., and Olsen, R. W. (1995). Functional domains of GABAA receptors. *Trends Pharmacol. Sci.* 16, 162–168. doi: 10.1016/s0165-6147(00)89009-4

Smith, G. B., Heynen, A. J., and Bear, M. F. (2009). Bidirectional synaptic mechanisms of ocular dominance plasticity in visual cortex. *Philos. Trans. R. Soc. B Biol. Sci.* 364, 357–367. doi: 10.1098/rstb.2008.0198

Sowell, E. R., Peterson, B. S., Kan, E., Woods, R. P., Yoshii, J., Bansal, R., et al. (2007). Sex differences in cortical thickness mapped in 176 healthy individuals between 7 and 87 years of age. *Cereb. Cortex* 17, 1550–1560. doi: 10.1093/cercor/bhl066

Stephany, C. -É, Frantz, M. G., and McGee, A. W. (2016). multiple roles for nogo receptor 1 in visual system plasticity. *Neuroscience* 22, 653–666. doi: 10.1177/1073858415614564

Sur, M., Nagakura, I., Chen, N., and Sugihara, H. (2013). Chapter 9 mechanisms of plasticity in the developing and adult visual cortex. *Prog. Brain Res.* 207, 243–254. doi: 10.1016/b978-0-444-63327-9.00002-3

Takahashi, H., and Naito, Y. (2017). Drebrin, from structure and function to physiological and pathological roles. *Adv. Exp. Med. Biol.* 1006, 157–181. doi: 10.1007/978-4-431-56550-5_10

Takashima, S., Chan, F., Becker, L. E., and Armstrong, D. L. (1980). Morphology of the developing visual cortex of the human infant: A quantitative and qualitative Golgi study. *J. Neuropathol. Exp. Neurol.* 39, 487–501. doi: 10.1097/00005072-198007000-00007

Takesian, A. E., and Hensch, T. K. (2013). Chapter 1 balancing plasticity/stability across brain development. *Prog. Brain Res.* 207, 3–34. doi: 10.1016/b978-0-444-63327-9.00001-1

Taymourtash, A., Schwartz, E., Nenning, K.-H., Sobotka, D., Licandro, R., Glatter, S., et al. (2022). Fetal development of functional thalamocortical and cortico–cortical connectivity. *Cereb. Cortex* 33, 5613–5624. doi: 10.1093/cercor/bhac446

Thompson, B., Morrone, M. C., Bex, P., Lozama, A., and Sabel, B. A. (2023). Harnessing brain plasticity to improve binocular vision in amblyopia: An evidence-based update. *Eur. J. Ophthalmol.* 34, 901–912. doi: 10.1177/11206721231187426

Tooley, U. A., Bassett, D. S., and Mackey, A. P. (2021). Environmental influences on the pace of brain development. *Nat. Rev. Neurosci.* 22, 372–384. doi: 10.1038/s41583-021-00457-5

Trepel, C., Duffy, K. R., Pegado, V. D., and Murphy, K. M. (1998). Patchy distribution of NMDAR1 subunit immunoreactivity in developing visual cortex. *J. Neurosci.* 18, 3404–3415.

Tropea, D., Wart, A. V., and Sur, M. (2009). Molecular mechanisms of experience-dependent plasticity in visual cortex. *Nat. Neurosci.* 364, 341–355. doi: 10.1038/nn1464

Tsumoto, T., and Sato, H. (1985). GABAergic inhibition and orientation selectivity of neurons in the kitten visual cortex at the time of eye opening. *Vis. Res.* 25, 383–388. doi: 10.1016/0042-6989(85)90063-x

Tyagarajan, S. K., and Fritschy, J.-M. (2014). Gephyrin: A master regulator of neuronal function? *Nat. Rev. Neurosci.* 15, 141–156. doi: 10.1038/nrn3670

Velmeshev, D., Perez, Y., Yan, Z., Valencia, J. E., Castaneda-Castellanos, D. R., Wang, L., et al. (2023). Single-cell analysis of prenatal and postnatal human cortical development. *Science* 382:eadf0834. doi: 10.1126/science.adf0834

Wang, L., Wang, C., Moriano, J. A., Chen, S., Zuo, G., Cebrián-Silla, A., et al. (2024). Molecular and cellular dynamics of the developing human neocortex at single-cell resolution. *bioRxiv* [Preprint]. doi: 10.1101/2024.01.16.575956 bioRxiv: 2024.01.16.575956.

Wijtenburg, S. A., West, J., Korenic, S. A., Kuhney, F., Gaston, F. E., Chen, H., et al. (2017). Glutamatergic metabolites are associated with visual plasticity in humans. *Neurosci. Lett.* 644, 30–36. doi: 10.1016/j.neulet.2017.02.020

Williams, K., Balsor, J. L., Beshara, S., Beston, B. R., Jones, D. G., and Murphy, K. M. (2015). Experience-dependent central vision deficits: Neurobiology and visual acuity. *Vis. Res.* 114, 68–78. doi: 10.1016/j.visres.2015.01.021

Williams, K., Irwin, D. A., Jones, D. G., and Murphy, K. M. (2010). Dramatic loss of Ube3A expression during aging of the mammalian cortex. *Front. Aging Neurosci.* 2:18. doi: 10.3389/fnagi.2010.00018

Wong-Riley, M. T. T., Hevner, R. F., Cutlan, R., Earnest, M., Egan, R., Frost, J., et al. (1993). Cytochrome oxidase in the human visual cortex: Distribution in the developing and the adult brain. *Vis. Neurosci.* 10, 41–58. doi: 10.1017/s0952523800003217

Yan, X. X., Zheng, D. S., and Garey, L. J. (1992). Prenatal development of GABA-immunoreactive neurons in the human striate cortex. *Dev. Brain Res.* 65, 191–204. doi: 10.1016/0165-3806(92)90179-z

Yashiro, K., and Philpot, B. D. (2008). Regulation of NMDA receptor subunit expression and its implications for LTD, LTP, and metaplasticity. *Neuropharmacology* 55, 1081–1094. doi: 10.1016/j.neuropharm.2008.07.046

Yashiro, K., Riday, T. T., Condon, K. H., Roberts, A. C., Bernardo, D. R., Prakash, R., et al. (2009). Ube3a is required for experience-dependent maturation of the neocortex. *Nat. Neurosci.* 12, 777–783. doi: 10.1038/nn.2327

Zhu, Y., Sousa, A. M. M., Gao, T., Skarica, M., Li, M., Santpere, G., et al. (2018). Spatiotemporal transcriptomic divergence across human and macaque brain development. *Science* 362:eaat8077. doi: 10.1126/science.aat8077

Zilles, K., Werners, R., Büsching, U., and Schleicher, A. (1986). Ontogenesis of the laminar structure in areas 17 and 18 of the human visual cortex. *Anat. Embryol.* 174, 339–353. doi: 10.1007/bf00698784

frontiers | Frontiers in Cellular Neuroscience

TYPE Original Research
PUBLISHED 28 October 2024
DOI 10.3389/fncel.2024.1483368

OPEN ACCESS

EDITED BY
Enrico Cherubini,
European Brain Research Institute, Italy

REVIEWED BY
Takeshi Kanda,
Nara Medical University, Japan
James Ernest Blevins,
VA Puget Sound Health Care System,
Veterans Health Administration, United States

*CORRESPONDENCE
Liliana Minichiello
✉ liliana.minichiello@pharm.ox.ac.uk

RECEIVED 19 August 2024
ACCEPTED 11 October 2024
PUBLISHED 28 October 2024

CITATION
Eftychidis V, Ellender TJ, Szymanski J and Minichiello L (2024)
Cholecystokinin-expressing neurons of the ventromedial hypothalamic nucleus control energy homeostasis.
Front. Cell. Neurosci. 18:1483368.
doi: 10.3389/fncel.2024.1483368

Cholecystokinin-expressing neurons of the ventromedial hypothalamic nucleus control energy homeostasis

Vasileios Eftychidis[1], Tommas J. Ellender[1,2], Jacek Szymanski[1] and Liliana Minichiello[1]*

[1]Department of Pharmacology, University of Oxford, Oxford, United Kingdom, [2]Department of Biomedical Sciences, University of Antwerp, Antwerp, Belgium

The hypothalamus is the primary center of the brain that regulates energy homeostasis. The ventromedial hypothalamus (VMH) plays a central role in maintaining energy balance by regulating food intake, energy expenditure, and glucose levels. However, the cellular and molecular mechanisms underlying its functions are still poorly understood. Cholecystokinin (CCK) is one of many genes expressed in this hypothalamic nucleus. Peripheral CCK regulates food intake, body weight, and glucose homeostasis. However, current research does not explain the function of CCK neurons in specific nuclei of the hypothalamus and their likely roles in network dynamics related to energy balance and food intake. This study uses genetic and pharmacological methods to examine the role of CCK-expressing neurons in the VMH (CCK^{VMH}). Namely, using a previously generated BAC transgenic line expressing Cre recombinase under the CCK promoter, we performed targeted manipulations of CCK^{VMH} neurons. Histological and transcriptomic database analysis revealed extensive distribution of these neurons in the VMH, with significant heterogeneity in gene expression related to energy balance, including co-expression with PACAP and somatostatin. Pharmacogenetic acute inhibition via Designer Receptors Exclusively Activated by Designer Drugs (DREADDs) resulted in increased food intake and altered meal patterns, characterized by higher meal frequency and shorter intermeal intervals. Furthermore, diphtheria toxin-mediated ablation of CCK^{VMH} neurons led to significant weight gain and hyperphagia over time, increasing meal size and duration. These mice also exhibited impaired glucose tolerance, indicative of disrupted glucose homeostasis. Our findings underscore the integral role of CCK^{VMH} neurons in modulating feeding behavior, energy homeostasis, and glucose regulation. This study enhances our understanding of the neurohormonal mechanisms underlying obesity and metabolic disorders, providing potential targets for therapeutic interventions.

KEYWORDS

hypothalamus, VMH, central CCK, food intake, body weight, glucose homeostasis, energy homeostasis

1 Introduction

The hypothalamus is a widely studied brain region. It is one of the most important regulators of food intake and energy homeostasis. It comprises several distinct nuclei, among which the ventromedial hypothalamic nucleus (VMH) was the first to be recognized as a site for body weight regulation and energy homeostasis (Hetherington and Ranson, 1940).

Over the years, the VMH has been associated with various physiological and behavioral functions (Hetherington and Ranson, 1940; King, 2006). The VMH, together with other hypothalamic nuclei, the lateral hypothalamus (LH), the dorsomedial hypothalamus (DMH), the arcuate nucleus of the hypothalamus (ARH), and the paraventricular hypothalamic nucleus (PVH), process incoming information and relay it to neuronal circuits beyond the hypothalamus, leading to an integrated response to food intake and energy expenditure (Kleinridders et al., 2009; Roh et al., 2016; Waterson and Horvath, 2015).

Recent studies using refined genetic tools have further highlighted the physiological role of the VMH in regulating energy and glucose homeostasis (Choi et al., 2013).

Like the rest of the hypothalamus, the VMH is highly heterogeneous in terms of cellular composition. It contains neurons responsible for sensing changes in glucose concentrations, as well as neurons equipped with receptors for various metabolic hormones (e.g., insulin and leptin) or neuropeptides associated with the regulation of energy balance (Affinati et al., 2023; Elmquist et al., 1997; Routh, 2003; Scott et al., 2009; Steuernagel et al., 2022).

The *Nr5a1* gene, which encodes steroidogenic factor 1 (SF1), is a transcription factor specifically expressed in the VMH within the adult rodent brain. However, it is also found in the adrenal gland, pituitary gonadotrophs, and gonads (Ikeda et al., 1995; Khodai and Luckman, 2021). *Nr5a1*-knockout mice were suggested as a genetic model for hypothalamic obesity. Interestingly, mice deficient in *Nr5a1* become obese due to a lack of activity and decreased energy expenditure rather than increased food intake (Flak et al., 2020; Kim et al., 2011; Majdic et al., 2002). Also, *Nr5a1*-expressing cells of the VMH are a heterogeneous group. Selective knockout of leptin receptor (Dhillon et al., 2006) or cannabinoid receptor 1 (Cardinal et al., 2014) from *Nr5a1*-expressing cells leads to high-fat diet-induced dysregulation of energy homeostasis and increased body weight. In contrast, insulin receptors (Klöckener et al., 2011), *Sirt1* (Ramadori et al., 2011), or the *Foxo1* transcription factor (Kim et al., 2012) deficient *Nr5a1*-expressing cells alleviate weight gain related to diet. Therefore, it is difficult to discern the cumulative or combined effects of this heterogeneous group of cells when targeting VMH *Nr5a1*-expressing cells to elucidate the mechanisms of satiety and energy homeostasis.

Cholecystokinin (CCK) is a pleiotropic neuropeptide, a gut hormone, and a well-known peripheral satiety signal synthesized, among others, in the intestinal tract, extraintestinal endocrine glands, and peripheral nervous system (Ahn et al., 2022; Cawthon and de La Serre, 2021; Gibbs et al., 1973; Steinert et al., 2017). Exogenous CCK reduces meal size and duration. However, a compensatory increase in meal frequency allows for regulating total food intake or body weight (Cawthon and de La Serre, 2021; Overduin et al., 2014; West et al., 1984). Peripheral injections of exogenous CCK-8 act on the cholecystokinin A receptors (CCKAR) found mainly on the vagal afferents of the stomach and liver (Reidelberger et al., 2003) but also in the hypothalamus, basal ganglia, thalamus and other areas of the CNS (Sjöstedt et al., 2020). They transmit signals through the vagal nerve to the brainstem's satiety centers, such as the nucleus tractus solitarius (NTS), resulting in a brief reduction in food intake (Bray, 2000). Antagonists for the CCKAR have been shown to modulate food consumption in a dose-dependent manner across various contexts and species, predominantly by augmenting the size of individual meals (Argueta et al., 2019; Moran et al., 1992, 1993; Reidelberger et al., 2003), while a CCKAR agonist has been shown to lower food intake and body weight of Göttingen Minipigs (Christoffersen et al., 2020).

In the central nervous system (CNS), CCK is highly expressed in the hypothalamus, hippocampus, cerebral cortex, and spinal cord. However, research on its central role in regulating energy expenditure and food intake is still limited. Small sulphated CCK-8 is the predominant form in the CNS (Rehfeld, 1978; Rehfeld and Hansen, 1986). The main CCK receptor in the brain is CCKBR, which is moderately expressed in the dorsomedial and central VMH (Flak et al., 2020). CCKAR is more commonly expressed in the ventrolateral VMH (vlVMH) (Xu et al., 2012) in females controlling their sexual behaviors. It is well known that CNS-derived CCK acts centrally to modulate energy balance by modulating the activity of hypothalamic neuronal populations. CCK-8 injections into different hypothalamic nuclei suppress feeding in rats (Blevins et al., 2000), while CCKAR-deficient rats become hyperphagic (Bi et al., 2001, 2004). Earlier studies on cats and owl monkeys have shown CCK release postprandially from the hypothalamus (Schick et al., 1986, 1987, 1989). Similar findings were reported in lean Zucker rats, where CCK was released postprandially from the PVH, though this response was diminished in obese rats (De Fanti et al., 1998).

Furthermore, injecting a CCK antibody directly into the cerebral ventricles stimulated food intake in sheep (Della-Fera et al., 1981). Following central injections of CCK receptor antagonists, a similar increase in food intake was observed in rats (Corp et al., 1997; Dorré and Smith, 1998; Ebenezer, 2002). Reidelberger and colleagues extended this research by treating vagotomised rats with devazepide and A-70104, both CCKAR antagonists that either penetrate or do not penetrate the blood–brain barrier, respectively. While both compounds stimulated food intake in non-vagotomised control rats, only devazepide increased food intake in rats with subdiaphragmatic vagotomies, underscoring the role of central CCK action in satiety regulation (Reidelberger et al., 2004).

While CCK-expressing neurons are widely distributed throughout the hypothalamus (Geibel et al., 2014; Schiffmann and Vanderhaeghen, 1991), the source of endogenous CCK that acts on distinct neuronal components has not been clarified. Current research does not explain the function of CCK neurons in specific nuclei of the hypothalamus and their likely roles in network dynamics related to energy balance and food intake.

Here, we have untangled the role of CCK-expressing neurons in the hypothalamic circuits responsible for energy homeostasis, specifically their importance in feeding circuits and regulation of body weight. The VMH contains an abundance of CCK-expressing neurons, and this nucleus has long been recognized to affect the regulation of food intake and body weight balance as well as glucose sensing and homeostasis. We have, therefore, focused our studies on the role of CCK-expressing neurons within the VMH (CCK^{VMH}).

We used a chemogenetic method to control the activity of CCK-expressing neurons in the VMH. The spatiotemporal control was achieved by using the BAC-CCK-Cre mouse line we had previously established (Geibel et al., 2014) and by intracranially injecting Cre-dependent viral particles expressing Gi-coupled Designer Receptors Exclusively Activated by Designer Drugs (DREADDs) to silence their activity specifically. This approach allowed us to assess their impact on food intake. We used a similar

approach to selectively ablate CCK^{VMH} neurons. This was achieved by intracranial injection of a Cre-dependent viral vector that expresses Diphtheria toxin A subunit (DTA) in the VMH of the BAC-CCK-Cre mouse line, leading to the specific ablation of CCK^{VMH} neurons. The latter has helped address the long-term consequences of CCK^{VMH} neuronal loss within the hypothalamus, such as body weight regulation and glucose homeostasis.

2 Materials and methods

2.1 Animals

All animal procedures conformed to the United Kingdom legislation (Scientific Procedures Act 1986) and the University of Oxford ethical review committee policy, with a final ethical review by the Animals in Science Regulation Unit (ASRU) of the United Kingdom Home Office. Mice were maintained under standard laboratory conditions with *ad libitum* access to food and water unless otherwise specified. Experimental groups consisted of mice of the same strain, sex, and similar age and body weight. Mouse lines used in this study are the BAC transgenic line (BAC-CCK-Cre) expressing Cre recombinase under the CCK promoter previously generated in our laboratory (Geibel et al., 2014) and the Gt(ROSA)26Sor$^{tm9(CAG-tdTomato)Hze}$ reporter line (Madisen et al., 2010), here called Ai9 reporter line. Crossing the BAC-CCK-Cre strain to the Ai9 reporter line generated the BAC-CCK-Cre; Ai9 (here called Ai9-CCK).

2.2 Transcriptomic database analysis

HypoMap single-cell gene expression atlas of the murine hypothalamus (Steuernagel et al., 2022) was used to characterize the *Cck*-expressing cells within the VMH of 2 months old mice. UMAP expression of selected genes relevant to energy homeostasis was highlighted specifically in the VMH region with log-normalized expression values scaled to the maximum of each gene. Only positive expression values were shown on the hypothalamus background. A co-expression analysis was performed to show cells expressing *Cck* and other relevant genes on one UMAP, highlighting the cells co-expressing *Cck* and the other gene of interest. Gene expression of relevant genes in the entire hypothalamus was analyzed using the CELLxGENE Discover platform. Specifically, the study by Steuernagel et al., 2022 was selected to analyse hypothalamic neurons. The analysis was fully performed using the toggles of the online CELLxGENE Discover platform and HypoMap atlas (Abdulla et al., 2023; Megill et al., 2021; Steuernagel et al., 2022).

2.3 Histology and immunohistochemistry

Mice were perfused as previously described (Gage et al., 2012). Briefly, mice were terminally anesthetised with 50 µL of sodium pentobarbital 200 mg/mL concentration. Brains were prefixed by cardiac perfusion with 20 mL ice-cold 4% paraformaldehyde (PFA) following blood clearance with 0.1 M phosphate buffer saline (PBS, pH 7.4). Brains were post-fixed in 4% PFA/0.1 M PBS for 3 h, then cryoprotected in 10, 20, and 30% sucrose/0.1 M PBS overnight. Brains were embedded in optimal cutting temperature (OCT) compound, snap-frozen in isopentane cooled by dry ice, and stored at −80°C. Sectioning was performed on a Leica cryostat, generating 20 µm thick sections. Sections were washed in PBS and stored at 4°C in PBS with 0.01% sodium azide.

2.3.1 Immunofluorescence and cell quantification

Free-floating sections 20 µm thick were transferred to 24-well plates and processed at room temperature. Sections from BAC-CCK-Cre intracranially injected with AAV carrying mCherry, were blocked with 5% fish gelatin and 0.5% Triton X-100 in PBS for 1 h, then incubated with rabbit anti-dsRed antibody (1:1000, Clontech, 632496) overnight. After washing, sections were incubated with Alexa-555 goat anti-rabbit antibody (1:1000, Invitrogen, 21428) for 2–3 h. DAPI counterstaining (1:10000, 5 mg/mL stock) was performed for 5 min. Sections from Ai9-CCK mouse brains were only stained with DAPI. Other antibodies used were FOXO1 [1:200, New England Biolabs, (C29H4) Rabbit mAb #2880]; anti-POMC precursor (1 : 4000, Phoenix Pharmaceuticals, H-029-30); CCK-pro-Rb-Af350 (a gift from Prof. Masayoshi Watanabe, Frontier Institute Co. Ltd); and secondary antibodies, Alexa fluor 488 goat anti-rabbit (1:1000, Invitrogen, A-11008). All sections were mounted on slides, dried overnight, coverslipped with Vectashield (Vector Labs), and stored at 4°C. Imaging was performed using a Leica DM6000B microscope (camera: DFC365FX; objectives: HCX PL APO10x/0.40 CS, HC PL 20x/0.75 CS2 and HCX PL APO 40x/0.85 CORR CS; Leica Microsystems, Wetzlar, Germany). Leica microscope Fluorescence filter cube L5 ET 504166, k; Fluorescence Filter TX2 ET 11504170, k; Leica Microsystems Filter cube LED 405 nm.

VMH Ai9-CCK (tdTomato-expressing) and mCherry-expressing cell numbers were quantified from three mice using three non-consecutive sections spaced 100 µm per mouse. Cell counts were performed manually in NIH ImageJ, with the experimenter blind to the condition.

2.3.2 DAB (3′3-diaminobenzidine) staining

DAB staining was performed on 20 µm thick floating sections. All steps were performed at RT on a rocking platform unless otherwise stated. Sections were washed three times with PBS for 15 min. Endogenous peroxidase activity was quenched by incubating for 20 min in 3% H_2O_2. Three 10-min washes in PBS were performed before blocking with 5% fish gelatine and 0.5% Triton-X 100 in PBS for 1 h. Sections were incubated with primary antibody rabbit anti-dsRed antibody (1:1000, Clontech, 632496) diluted in blocking buffer overnight at room temperature. Afterwards, sections were washed thrice with PBS 0.1% Triton for 15 min. The secondary antibody biotinylated donkey anti-rabbit (Jackson, cat. no. 703–065-155) was applied at a dilution of 1:200 in blocking buffer and incubated for 2 h at room temperature. Sections were then washed three times for 15 min with PBST. The peroxidase Vectastain ABC system from (Vector Biolabs, cat. no. PK-6100) was used to develop the staining. The sections were then mounted on gelatine-coated slides and dried overnight. Sections were dehydrated for 1 min in 90% and then 100% ethanol, incubated for 10 min in xylene and then coverslipped with Vectamount. Slides were air-dried for at least a day and then imaged as above.

2.4 Electrophysiology recording

2.4.1 Brain slice preparation

Mice were anesthetised with isoflurane and then decapitated. Brains were removed, and coronal 350–400 µm slices were cut using a vibrating microtome (Microm HM650V). Slices were prepared in artificial cerebrospinal fluid (aCSF) containing (in mM): 65 Sucrose, 85 NaCl, 2.5 KCl, 1.25 NaH_2PO_4, 7 $MgCl_2$, 0.5 $CaCl_2$, 25 $NaHCO_3$ and 10 glucose pH 7.2–7.4, bubbled with carbogen gas (95% O_2, 5% CO_2). Slices were immediately transferred to a storage chamber containing aCSF (in mM): 130 NaCl, 3.5 KCl, 1.2 NaH_2PO_4, 2 $MgCl_2$, 2 $CaCl_2$, 24 $NaHCO_3$ and 10 glucose pH 7.2–7.4, at 32°C and bubbled with carbogen gas until used for recording. Slices were transferred to a recording chamber and continuously superfused with aCSF bubbled with carbogen gas with the same composition as the storage solution (32°C and perfusion speed of 2 mL/min). Whole-cell current-clamp recordings were performed using glass pipettes, pulled from standard wall borosilicate glass capillaries and containing (in mM): 110 potassium gluconate, 40 HEPES, 2 ATP-Mg, 0.3 Na-GTP, 4 NaCl and 4 mg/mL biocytin (pH 7.2–7.3; osmolarity, 290–300 mOsmol/l). Recordings were made using Multiclamp 700B amplifiers and acquired using WinWCP software (University of Strathclyde, United Kingdom).

2.4.2 Slice recording protocols

Recordings of resting membrane potential were performed in whole-cell current-clamp mode. After a 5–10 min recording of baseline resting membrane potential, the hM4Di agonist clozapine-*N*-oxide (CNO; 10–20 µM) was superfused for 15–20 min while continuously measuring the resting membrane potential. Subsequently, CNO was washed out for more than 10 min while continuously measuring the resting membrane potential - we did not observe a significant reversal of hyperpolarisation upon washout. Hyperpolarising and depolarising current steps were used to assess further the intrinsic properties of the recorded neurons, including input resistance and action potential frequency.

2.4.3 Analysis of slice recordings

Data were analyzed offline using custom-written procedures in Igor Pro (Wavemetrics). Resting membrane potential measurements were taken from the last 10 s of the baseline recordings and the last 10 s of the CNO superfusion recordings. The input resistance was calculated from the observed membrane potential change after hyperpolarizing the membrane potential with a set current injection. The membrane time constant was taken as the time it takes for a change in potential to reach 63% of its final value. The action potential amplitude was taken from the peak amplitude of the individual action potentials relative to the average steady-state membrane depolarization during positive current injection. Action potential duration was taken as the duration between the upward and downward stroke of the action potential at 25% of the peak amplitude.

2.5 Intracranial injections

2.5.1 Adeno-associated viral particles and bregma

AAV vectors used in this study: AAV9-CAG-FLEX-DTA-IRES-mCherry (Virovek, Lot 15–335) (here called AAV-DIO-DTA) expressing Diphtheria toxin A subunit (DTA) and mCherry fluorescent protein in a Cre-dependent manner under the CAG promoter. A control vector, AAV9-CAG-mCherry (Virovek, Lot#11–148). And AAV1-CAG-FLEX-eGFP-WPRE-bGH (Penn Vector Core) (here called AAV1-DIO-eGFP). We also made use of AAV2/5-hSyn-DIO-hM4Di-mCherry (here called AAV-hM4Di) (200 nL at 5.1×10^{12} GC/ml; University of North Carolina vector core) expressing the inhibitory G protein-coupled receptor hM4Di Designer Receptors Exclusively Activated by Designer Drugs (DREADDs) in a Cre-dependent manner. Expression was driven by the hSyn promoter, and the hM4Di was fused to the mCherry protein at the C-terminus. Activation of hM4Di in neurons inhibits neuronal activity by triggering hyperpolarisation through Gβ/γ-mediated activation of G-protein inwardly rectifying potassium channels and suppressing neurotransmitter release at the presynaptic level (Armbruster et al., 2007). And the AAV2.EF1a.DIO.eYFP.WPRE.hGH (Addgene27056) (here called AAV2-DIO-YFP), with an EF1a-driven, Cre-dependent EYFP expression. Finally, FluoSpheres™ green-fluorescent 0.04 µm diameter, Invitrogen, cat no: F-8795, were used to establish VMH intracranial injection coordinates.

2.5.2 Stereotactic surgery

Mice were anesthetised with 2–3% vaporised isoflurane and placed in a stereotactic frame. An analgesic cocktail was administered, and the skull was exposed. Coordinates were adjusted based on the Allen Mouse Brain Atlas. For targeting the whole VMH nucleus, the coordinates were adjusted to AP 1.5 mm, ML ±0.6 mm and DV -6.5 mm. Burr holes were drilled, and viral particles were injected using a Hamilton syringe (34-gauge, 30 mm length) at a rate of 125 nL/min. The needle was left in place for 10 min post-injection to prevent reflux. Incisions were sutured, and mice were allowed to recover in a pre-warmed incubator before returning to their home cages. Post-operative care included Metacam administration as needed. The animals were allowed to recover for 3–4 weeks before any experiments, ensuring sufficient expression of AAVs in the brain.

2.6 Food intake measurements and analysis

2.6.1 Metabolic cages

After surgery (3 to 4 weeks), the mice were transferred into the LabMaster metabolic cages (TSE Systems). These cages were fitted with calibrated sensors capable of measuring food and water intake by calculating the average weight changes of the food hopper in ten-second intervals, with a sensitivity of 0.01 g. Food and water were provided *ad libitum*. Mice were fed the standard chow diet, Teklad Rodent Diet (60% calories from carbohydrates, 23% from protein and 17% from fat, 3.3 Kcal/g digestible energy). Two days before the experiment, mice were habituated to the new water bottle nozzle, which releases water upon touch. Mice were singly housed in the metabolic cages and allowed at least a week to habituate to the new environment before recording any food sensor measurements. Food intake was measured continuously. The cages were inspected daily for any dropped pellets, and any small pellets were removed from the food hopper to avoid drops. A meal event (meal bout) was defined as the total of all sensor measurements taken less than 15 min apart (minimum intermeal interval). The minimum meal size was set at 0.02 g, a commonly used method for defining meals in mice and rats

(Atalayer and Rowland, 2011; Bake et al., 2014; Farley et al., 2003). Meal metrics included size, duration in minutes, and intermeal interval, averaged across the experimental period, daily (average of days), or in specific hours (i.e., 6 h post hM4Di activation).

2.6.2 Pharmacogenetic hM4Di inhibition

Mice underwent stereotactic surgery as described above and were injected bilaterally with AAV2/5-hSyn-DIO-hM4Di-mCherry in the VMH region. After 3–4 weeks of recovery, the mice were habituated to handling and intraperitoneal (IP) injections. IP injections of sterile saline with 10% DMSO (dimethylsulfoxide) were administered at 10 a.m. and 6 p.m. daily for 10 days to habituate the animals to the injections. Food intake data was collected during the habituation period and was monitored and analyzed as described. Following habituation, animals received increasing doses of CNO (Tocris Biosciences, cat. no. 4936) via IP injections twice daily. Appropriate non-AAV-hM4Di injected littermate controls were used to control the CNO reverse-metabolisation to clozapine, which produces clozapine-like interoceptive stimulus effects in mice (Manvich et al., 2018). The doses were 0.75, 1.5, 2, and 3 mg/kg body weight, each administered for 3 days. Food intake measurements and meal pattern analysis were performed as described above (2.6.1 section). Before each injection, cage sensors were paused for 1 min, and animals were handled minimally to ensure consistent treatment.

2.7 Diphtheria toxin deletion of CCK^{VMH} neurons

Ai9-CCK and Ai9-Control (not expressing Cre) mice were injected bilaterally with AAV9-CAG-FLEX-DTA-IRES-mCherry in the VMH region, as described in section 2.5.2 above. Their body mass was monitored for 3 months post-surgery. A month after the surgery, the mice were singly caged in metabolic cages, and their food intake was measured starting with a 10-day habituation period and for five experimental days, after which the measurements were averaged.

2.8 Glucose tolerance test

Female Ai9-CCK and Ai9-Control mice were injected with AAV9-CAG-FLEX-DTA-IRES-mCherry in the VMH nucleus and allowed to recover for 3 months. They were fasted overnight (16 h) before the glucose tolerance test. Blood glucose levels were measured using a hand-held glucose meter (One Touch Verio). Following a baseline glucose reading, mice received an IP injection of D-glucose (200 g/L) at 2 g/kg body weight. Blood glucose levels were measured at 30- and 180 min post-injection. Mice were sacrificed by transcardial perfusion, and their brains were harvested.

2.9 Statistical analysis

Experiments and analyses were conducted blind to genotype with at least three animals per genotype. Unless stated otherwise, values were presented as mean ± standard error of the mean (s.e.m). Statistical significance was assessed using paired/unpaired two-tailed Student's t-test, one- or two-way ANOVA with appropriate post-hoc tests, either Dunnett's or Sidak's *post hoc* test or Fisher's LSD test, as appropriate for each data set and indicated in the figure legends. Significance was defined as $p < 0.05$. Analyses were performed using GraphPad Software (La Jolla, CA, United States).

3 Results

3.1 Characterization of the CCK-expressing cells in the ventromedial hypothalamus

To specifically target the CCK^{VMH} neurons, we used the BAC-CCK-Cre mouse line, previously generated and characterized in our laboratory (Geibel et al., 2014). We first confirmed this line's recombination pattern by crossing the BAC-CCK-Cre strain with the Ai9 reporter line (Madisen et al., 2010), leading to tdTomato fluorescence signal upon Cre-recombination (Ai9-CCK). Focusing in particular on the hypothalamic region and the nuclei adjacent to the VMH nucleus, we confirmed our previous findings; CCK-expressing neurons were visualised in both sagittal and coronal sections using immunohistochemical staining in 3,3′-diaminobenzidine (DAB) or direct fluorescent imaging of tdTomato (Figures 1A,B). In particular, we identified CCK + tdTomato expressing neurons in the anterior hypothalamic nucleus (AHN), DMH, and VMH nuclei, with some presence in the ARH and suprachiasmatic nucleus (SCH) and very few in the PVH.

Using the HypoMap single-cell gene expression atlas of the murine hypothalamus (Steuernagel et al., 2022), we demonstrate that at 2 months of age, the majority of CCK^{VMH} cells do not co-express the *Nr5a1* gene, which encodes SF1 (Figure 1E). Only around 10% of CCK^{VMH} cells co-express *Nr5a1*, with a varying degree of expression of both *Cck* and *Nr5a1* (Figures 1C,D). The CCK^{VMH} cells are a heterogeneous group co-expressing various genes involved in energy homeostasis. Approximately 58% of them co-express *Adcyap1* encoding PACAP, which is known to regulate metabolic rate and energy balance and has a high expression in the VMH (Bozadjieva-Kramer et al., 2021; Figures 1F,G). In addition, about 36% of CCK^{VMH} co-express somatostatin (*Sst*), which is important for regulating factors in the satiety system and obesity. This includes both central and peripheral effects, such as increasing food intake by inhibiting the release of endogenous CCK and GLP-1 (Kumar and Singh, 2020; Figures 1H,I). GLP-1 receptor agonists are at the forefront of hormone-based treatments for obesity (Müller et al., 2019). While GLP-1 is not expressed in the hypothalamus, its receptor GLP-1R is co-expressed with approximately 1.5% of CCK^{VMH} cells (Figures 1J,K). The main CCK receptor in the brain, CCKBR (Flak et al., 2020), is expressed in a greater number of cells of the VMH than CCK, but only 12% of those co-express both (Figures 1L,M). Hypothalamic *Pomc*- and *Agrp*-expressing neurons are conventionally considered to function in opposing ways, contributing to anorexigenic and orexigenic signaling, respectively (Quarta et al., 2021). *Pomc* is co-expressed with approximately 25% of *Cck*-expressing cells of the VMH and 23% in the ARH (Figure 1N,O; Supplementary Figures S1A–C). *Foxo1*, a well-known negative leptin signaling regulator (Quarta et al., 2021), is co-expressed with approximately 5% *Cck*-expressing VMH cells (Supplementary Figures S1G,H). Finally, CCK^{VMH} cells also co-express *Bdnf* (34%), *Tac1* (30%), *Esr1* (26%), *Agrp* (16%), *Mc3r*

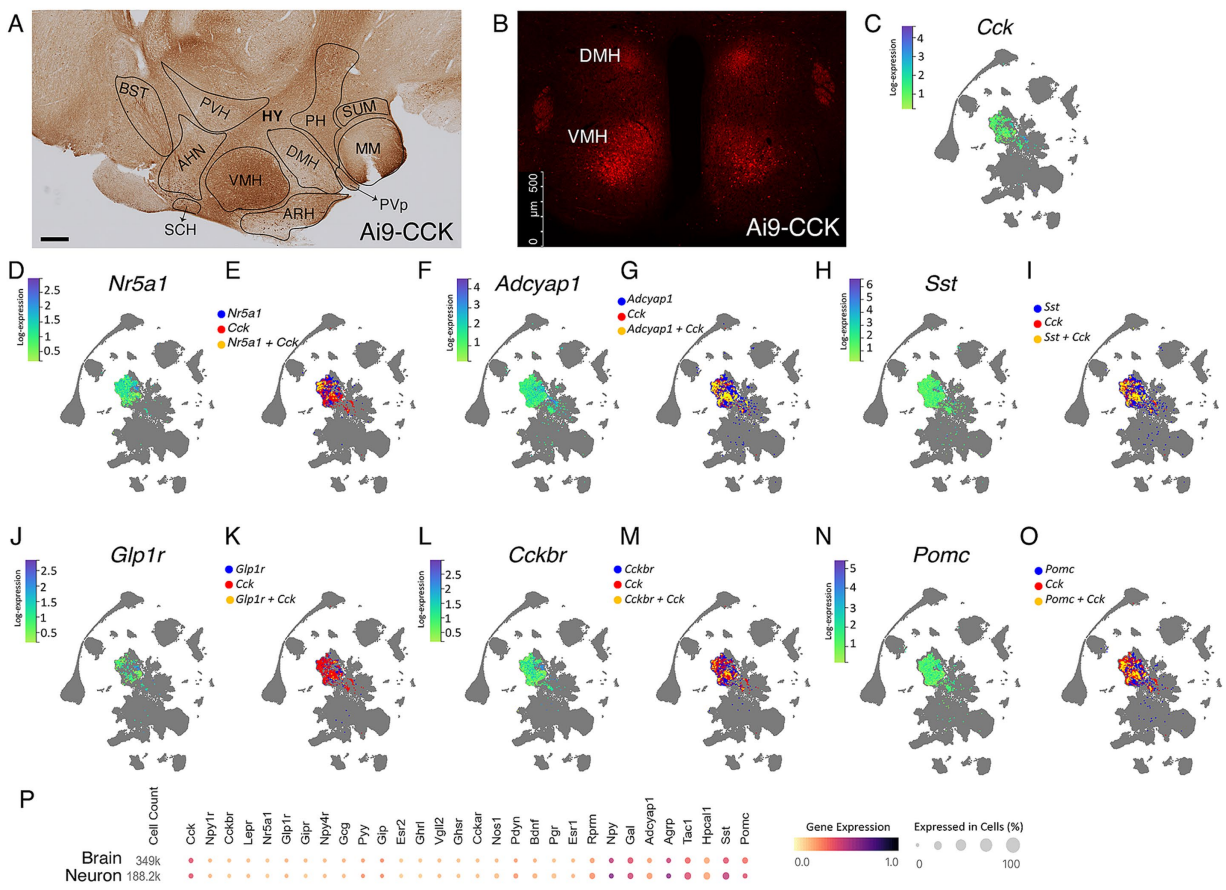

FIGURE 1
Single-cell transcriptomic analysis reveals heterogeneity of the CCK^{VMH}-expressing neurons. (A,B) Representative immunohistochemical and IF images of CCK + tdTomato expressing cells in the hypothalamic regions from the Ai9-CCK brain sections. (A) Tile image of DAB-stained sagittal section showing, in particular, the hypothalamic region highlighting the different nuclei, such as ventromedial hypothalamus (VMH), dorsomedial nucleus (DMH), anterior hypothalamic nucleus (AHN), and (B) IF image from a coronal section showing endogenously expressed td-Tomato in CCK-expressing (CCK + tdTomato) cells around the paraventricular hypothalamic nucleus (PVH) in the DMH and the VMH. (C,D,F,H,J,L,N) HypoMap (Steuernagel et al., 2022) UMAP expression of selected genes relevant to energy homeostasis in the VMH, showing a specific selection of only positive expression values in the VMH region of 2-months old mice. The color sidebar corresponds to log-normalized expression values scaled to the maximum of each gene, with the rest of the hypothalamus in gray. (E,G,I,K,M,O) HypoMap (Steuernagel et al., 2022) UMAP of cells expressing selected genes relevant to energy homeostasis in the VMH, with marked cells expressing *Cck* in red, the other selected genes in blue and cells co-expressing the relevant gene with *Cck* in yellow. Only positive expression values are shown. (P) Relevant gene expression from a study utilizing the mouse hypothalamus (Steuernagel et al., 2022), with specific data for the hypothalamic neurons highlighted, prepared using the CELLxGENE Discover platform (Abdulla et al., 2023). HY, hypothalamus, PH, posterior hypothalamic nucleus, SUM, supra mammillary nucleus, MM, medial mammillary nucleus, PVp, periventricular hypothalamic nucleus (posterior part), BST, Bed nuclei of the stria terminalis. Scale bars, panel A, 300 µm; panel B, 500 µm.

(9.5%), and *Lepr* (8%) among some of the genes related to energy homeostasis, which is paralleled in neurons on the scale of the entire hypothalamus (Figure 1P). We have validated some of these RNAseq results through immunofluorescence colocalisation studies (Supplementary Figures 1D–F,I–K), confirming a faithful BAC-CCK-Cre strain recombination pattern.

3.2 Pharmacogenetic silencing of CCK^{VMH} neurons results in increased food intake and alterations in meal patterns

To investigate the short-term role of CCK^{VMH} neurons, we employed the DREADDs pharmacogenetic approach (Roth, 2016). This technique allowed for rapid neuronal silencing following the systemic administration of CNO. Stable expression of the inhibitory hM4Di in CCK^{VMH} neurons was achieved via stereotactic delivery of AAV-hM4Di bilaterally at established VMH coordinates (Supplementary Figure S2). The AAV construct included a DIO cassette for Cre-dependent expression of the hM4D(Gi) receptor and a mCherry fluorescent protein for cell identification. Stereotactic surgery was performed on young adult BAC-CCK-Cre animals by injecting 200 nL at 5.1 × 10^{12} GC/ml of AAV-hM4Di bilaterally (Figures 2A,B). Immunohistochemical analysis confirmed hM4Di expression in CCK^{VMH} neurons of injected mice (hM4Di-CCK^{VMH}). This was determined by detecting the endogenous mCherry fluorescence, indicating that the viral spread was limited to the VMH region, as expected (Figure 2C). Quantifying the transduced hM4Di:mCherry-CCK^{VMH} neurons revealed that 76% expressed hM4Di:mCherry (Figures 2D,E).

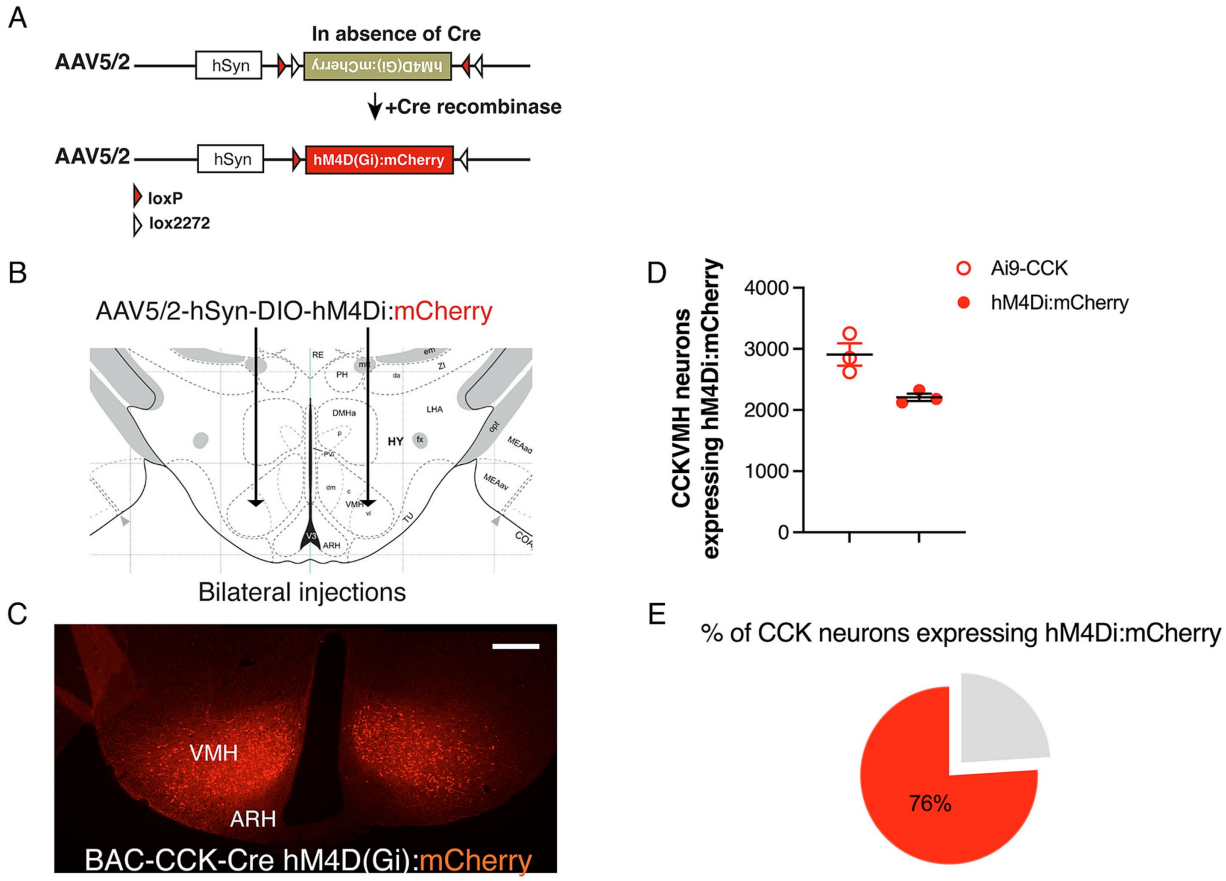

FIGURE 2
Successful Cre-dependent expression of inhibitory DREADDs in CCK^{VMH} neurons of BAC-CCK-Cre mice. (A) Diagram of the Double-floxed Inverted Orientation (DIO) AAV construct depicting the Cre-dependent recombination/inversion of the hM4D(Gi):mCherry cassette into the sense orientation to allow its expression in Cre-positive cells (Cre + ve). (B) Drawing of the bilateral stereotactic injection of the AAV-DIO-hM4Di(Gi):mCherry in the VMH region. (C) Successful expression of hM4Di(Gi):mCherry in the CCK^{VMH} neurons of BAC-CCK-Cre hypothalamic area 2 weeks after surgery. (D) Quantification of neurons expressing hM4Di compared to the CCK^{VMH} neurons of Ai9-CCK reporter line (see Figure 1B). CCK^{VMH} neurons expressing hM4Di, 2209 ± 60 mCherry-positive neurons out of 2908 ± 184 Ai9-CCK reporter line detected CCK-expressing neurons (n = 3 male mice per group). (E) About 76% of CCK^{VMH} neurons expressed hM4Di. Scale bar panel C, 200 μm.

Following the successful expression of hM4Di in the CCK^{VMH} neurons, we first validated the ability of CNO to successfully inhibit the generation of action potentials by recording their firing rate through electrophysiology upon CNO administration. Therefore, we unilaterally injected another group of BAC-CCK-Cre animals (~8 weeks old) with AAV-hM4Di on one hemisphere and a control AAV2-DIO-YFP virus on the other. Three weeks after the injection, acute brain slices containing the hypothalamus were made from these mice and analyzed electrophysiologically. We found that CCK^{VMH} neurons were spontaneously active (83.3%, 5 out of 6 neurons, Figures 3A–C) with an average firing frequency of 2.53 ± 0.37 Hz. The intrinsic properties of CCK^{VMH} neurons suggest they are excitable cells with a high input resistance (854 MΩ) but are slow to respond to inputs as they exhibit a slow membrane time-constant (26.5 ms) concomitant with their function in the hypothalamus (Figure 3D). The spontaneous firing frequency and response to depolarising current steps would suggest they have an action potential firing range roughly between 2 and 20 Hz. Neurons significantly hyperpolarise upon the superfusion of the chemogenetic actuator CNO, followed by a reduction in the spontaneous action potential frequency (Figures 3E–G). These data show that we achieved sufficient expression of hM4Di, which is capable of silencing CCK^{VMH} neurons upon CNO application.

Given the variability in CNO doses reported in the literature, we titrated the dose range for *in vivo* DREADDs applications. Three to 4 weeks post-intracranial injection, the mice were individually housed in metabolic cages for food intake analysis. Following our established 10-day habituation to saline IP injections (Supplementary Figure S3), animals received incremental CNO doses [0.75, 1.5, 2, and 3 mg/kg body weight (BW)] twice daily, each dose for three consecutive days. Food intake was recorded in hM4Di-CCK^{VMH} and control mice (Figure 4A). As hM4Di activation in neurons typically persists for 6–8 h (Roth, 2016), the CNO temporal effect was examined at 6 h and 24 h post-CNO injections. In control mice, CNO administration did not affect food intake at any concentration within 6 h post-injection or daily (Figures 4B,C).

In contrast, hM4Di-CCK^{VMH} animals, upon activation of hM4Di with 3 mg/kg of BW CNO, significantly increased daily food intake of chow pellets (Figure 4D) compared to saline baseline. Lower doses showed no significant effect (Figure 4D). Food intake analysis as a

10.3389/fncel.2024.1483368

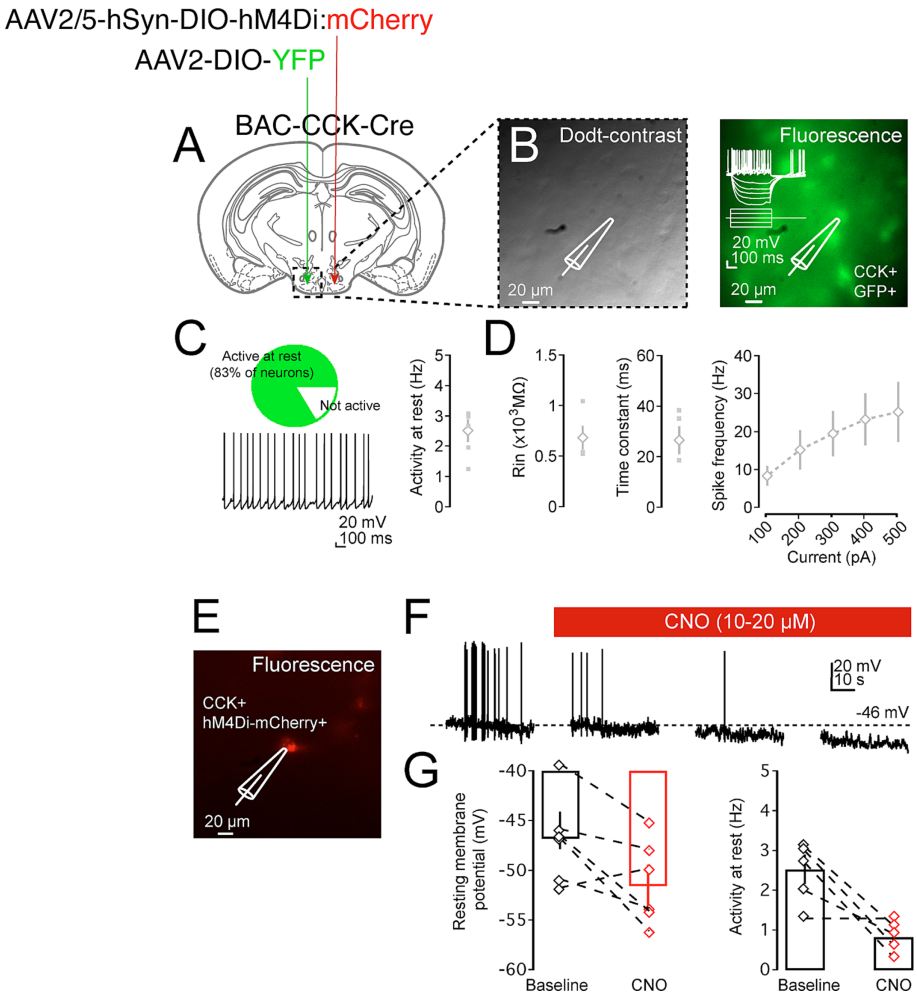

FIGURE 3
Pharmacogenetic inhibition of CCK^{VMH} neurons in brain slices. (A) A diagram of a coronal brain section showing an experimental design for a BAC-CCK-Cre injected with appropriate viruses on the two sides of the hypothalamus-VMH area. The recording area containing the VMH is indicated in the dashed box. (B) Dodt-contrast image of the VMH hypothalamic region with the placement of recording electrode and neuron during patch-clamp recordings (left). Fluorescent image indicating that the recorded neuron is a CCK+ GFP+ neuron (right). (C) CCK^{VMH} neurons are mostly spontaneously active, and further intrinsic properties suggest they are small, high Rin neurons with a firing rate of between 2 and 20 Hz (D). (E) Fluorescence image indicating a recorded neuron that is hM4Di:mCherry positive. (F) Example of recording trace of spontaneously active CCK^{VMH} neuron. Not only did CNO superfusion lead to a significant hyperpolarisation of the resting membrane action potentials, but this was also concomitant with a reduction in the frequency of spontaneous action potential. (G) Summary plot of the effect of CNO on the resting membrane voltage and firing frequency of the hM4Di-CCK^{VMH} neurons. Hyperpolarisation of recorded neuron upon washing of CNO, baseline: −45.99 ± 1.87 mV and CNO: −51.55 ± 2.10 mV, $p = 0.016$. Reduction in the spontaneous action potential frequency of the recorded neuron upon washing of CNO baseline: 2.53 ± 0.37 Hz and CNO: 0.83 ± 0.21 Hz, $p = 0.027$. $n = 5$. Values are means ± s.e.m. p statistic from two-tailed paired student t-test. Scale bar panel B, E 20 µm.

percentage change relative to baseline saline injections revealed significant increases at 2 and 3 mg/kg BW CNO doses in hM4Di-CCK^{VMH} mice compared to controls (Figure 4F). However, hM4Di-CCK^{VMH} mice showed no significant change in cumulative food intake 6 h post-CNO injection (Figure 4E). Despite the significant increase in daily food intake with 3 mg/kg BW CNO, immediate consumption remained unchanged within the first 6 h post-injection, suggesting a delayed effect. This interesting discovery sparked further questions about regulating food intake in hM4Di-CCK^{VMH} mice.

Therefore, we analyzed a meal pattern 6 h post-CNO administration (3 mg/kg BW). The results showed a significant increase in meal frequency in hM4Di-CCK^{VMH} animals and a significant decrease in intermeal interval (Figures 5A,C). Control mice showed no change in meal frequency and an increased intermeal time (Figures 5B,D). Meal size, duration, and consumption rate did not show statistically significant changes in either group (Figures 5E–H). Meal pattern changes persisted throughout the day during CNO administration. hM4Di-CCK^{VMH} animals exhibited significantly increased meal frequency and decreased intermeal time, while control animals exhibited no changes (Figures 5I–L). Daily meal size and duration remained unchanged (Figures 5M–P).

In summary, silencing CCK^{VMH} neurons via CNO-activated DREADDs significantly increased daily food intake and meal frequency, with no immediate effect on consumption within 6 h post-injection. These findings suggest that CCK^{VMH} neurons are critical in regulating meal patterns, contributing to increased cumulative food intake.

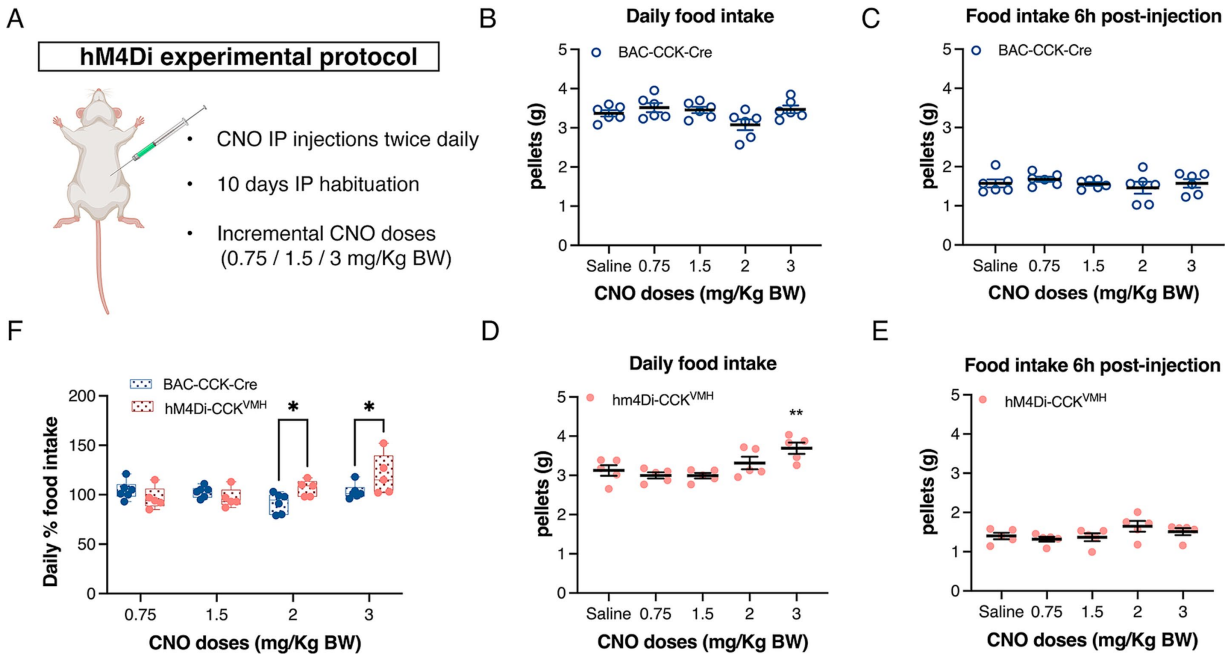

FIGURE 4
Acute inhibition of CCK^{VMH} neurons causes a gradual increase in total food intake. (A) DREADDs experimental protocol to assess food intake. Animals were singly housed for 2 days in metabolic cages and then habituated for 10 days with saline IP injections twice daily (10 a.m. and 6 p.m.). They were then injected with increasing doses of CNO (0.75/1.5/2/3 mg/kg BW). Each dose was administered for 3 days. (B,C) The plots display the daily food intake of control BAC-CCK-Cre non-injected mice and their food intake 6 h post-injection. At no point was there a significant difference from the saline baseline. (D) Plot showing the daily food intake post-injection for hM4Di-CCK^{VMH} mice. IP 3 mg/kg of BW CNO significantly increased the daily food intake of chow pellets from 3.125 ± 0.135 g to 3.693 ± 0.143 g compared to the saline baseline, $p = 0.002$. (E) Cumulative food intake 6 h post-injection with saline/CNO of hM4Di-CCK^{VMH} animals. (F) Percentage change of daily total food intake of hM4Di-CCK^{VMH} animals compared to the control BAC-CCK-Cre group. Each group was normalized to their own IP saline baseline. Significant increases in hM4Di-CCK^{VMH} mice compared to controls at 2 and 3 mg/kg BW doses (2 mg: 92 ± 4% vs. 106 ± 4%, $p = 0.032$; 3 mg: 103 ± 3% vs. 120 ± 9%, $p = 0.016$). Values are means ± s.e.m. ($n = 5–6$ mice per group, males). p statistic (B–E) from repeated measures one-way analysis of variance followed by Dunnett's *post hoc* test; (F) from two-way analysis of variance followed by Fisher's LSD test. Image in A was created with BioRender.com.

3.3 Ablation of CCK^{VMH} neurons by AAV-mediated Cre-dependent expression of diphtheria toxin A subunit leads to hyperphagia and obesity

To investigate the long-term role of CCK^{VMH} neurons in maintaining energy homeostasis, we sought to perform spatiotemporal ablation of the CCK^{VMH} neurons. Therefore, we again used a pharmacogenetic approach, performing intracranial injections to express the diphtheria toxin A subunit (DTA) via AAV-DIO-mediated expression in the CCK^{VMH} neurons. First, we determined an optimal AAV-DIO-DTA virus titre by titration performed in Ai9-CCK control animals (not expressing Cre, here called Ai9-Control/DTA). Injections with various dilutions identified 2.32×10^{11} GC/ml as the most tolerable titre, avoiding non-specific weight gain observed at higher titres. Weight monitoring up to 6 months post-surgery revealed no significant deviations in BW between Ai9-Control/DTA injected animals and non-injected controls (data not shown). Successful ablation of CCK^{VMH} neurons was confirmed by a significant reduction in tdTomato fluorescence in the VMH region 1 month after unilaterally injecting AAV-DIO-DTA in Ai9-CCK brains (Ai9-CCK/DTA) compared to the contralateral side used as control (Figure 6A). We conducted an additional experiment to further confirm AAV-DIO-DTA's specific deletion of CCK^{VMH} cells without affecting non-transduced surrounding cells. In this experiment, we intracranially injected AAV-DIO-DTA and AAV1-DIO-eGFP unilaterally into Ai9-CCK mice. The AAV1-DIO-eGFP was used to identify the location and extent of the Cre-mediated deletion (Supplementary Figure S4). This experiment confirmed a significant reduction of both CCK + tdTomato and eGFP co-expressing cells in the VMH at the site of injection (Supplementary Figures S4A–C). However, moving 200 µm away from the injection site would result in a partial deletion of tdTomato-eGFP expressing cells, suggesting that those not transduced by AAV-DIO-DTA would remain intact in the VMH (Supplementary Figures S4D–I).

We also performed a similar experiment by injecting the AAV-DIO-DTA viral construct into another brain region that expresses higher levels of CCK, specifically the hippocampal CA1 region. This was done to confirm further that the AAV-DIO-DTA targets only the transduced CCK neurons at the injection site, not the surrounding cells (Supplementary Figure S5).

Finally, using the established viral AAV-DIO-DTA titre, Ai9-CCK animals and Ai9-Control littermates (Cre negative) were intracranially injected in the VMH region (resulting in Ai9-CCK/DTA and Ai9-Control/DTA, respectively). All experimental groups underwent surgery at 3–4 months of age and had a weight ranging from 23 to 25 g. BW was recorded for about 13 weeks post-surgery. Ai9-CCK/DTA animals exhibited a significant increase in BW starting around 5 weeks

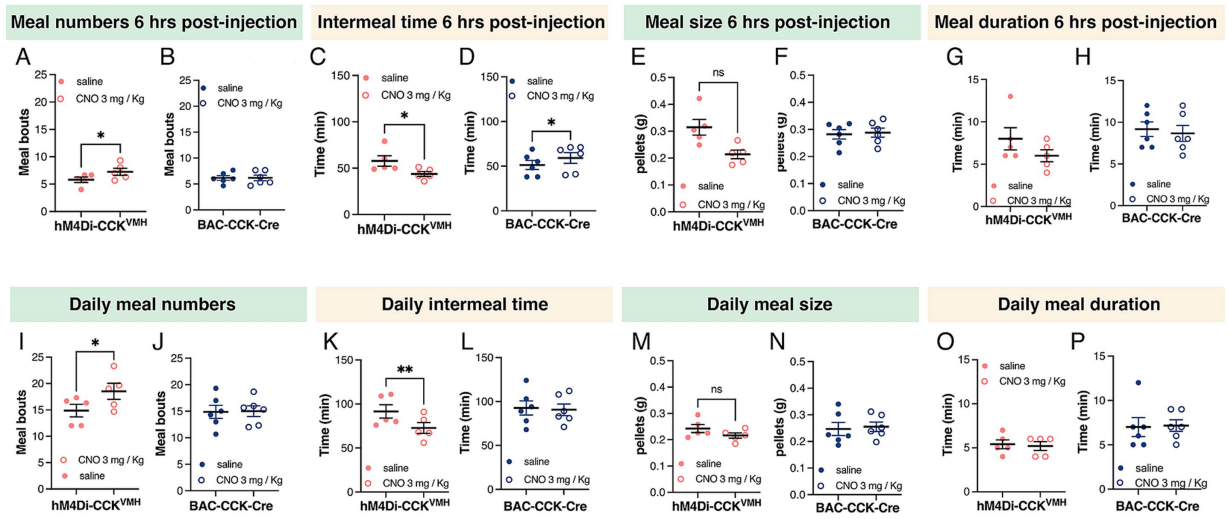

FIGURE 5
Silencing CCK^{VMH} neurons alters meal patterns. (A–D) Six hours post-CNO administration (3 mg/kg BW) revealed increased meal frequency in hM4Di-CCK^{VMH} animals, from 5.802 ± 0.4904 to 7.266 ± 0.6439 meals, $p = 0.048$ (A) and decreased intermeal time, from 57.80 ± 5.652 min to 43.80 ± 2.615 min, $p = 0.035$ (C). The control group showed no changes in meal frequency (B) and an increased intermeal time from 51.33 ± 5.057 to 59.17 ± 5.997 min, $p = 0.035$ (D). (E–H) Meal size and duration showed no difference in either group. (I–L) Meal pattern alterations persisted throughout the day under CNO administration. hM4Di-CCK^{VMH} animals showed further increased meal frequency from 14.87 ± 1.181 to 18.53 ± 1.514 meals $p = 0.014$ (I) and decreased intermeal time from 91.60 ± 7.580 to 72.80 ± 6.143 min, $p = 0.006$ (K), while control animals exhibited no changes (J,L). (M–P) Daily meal size and duration remained unchanged in both groups. Values are means ± s.e.m. ($n = 5$–6 mice per group, males). p statistic from two-tailed paired student t-test.

post-surgery, and their BW continued to increase through the experimental time compared to Ai9-Control/DTA (Figure 6B). At 13 weeks post-surgery, Ai9-CCK/DTA animals showed about a 34% increase in BW, while Ai9-Control/DTA animals showed a 19% increase, indicating about 15% difference attributed to CCK^{VMH} neuron ablation (Figure 6C).

However, to examine the effects of CCK-expressing neuron ablation on food intake and meal patterns, new cohorts of Ai9-CCK/DTA and Ai9-Control/DTA animals were singly housed in metabolic cages one-month post-surgery. After a 10-day habituation period to the cages, food intake was recorded in real-time for 5 days and averaged. Ai9-CCK/DTA animals significantly increased daily food intake compared to injected Ai9-Control/DTA animals (Figure 6D). Meanwhile, meal pattern analysis revealed a significant decrease in meal frequency, with the number of daily meals decreasing from 18 to 14 and intermeal time increasing from 70 to 90 min in Ai9-CCK/DTA animals (Figures 6E,F). Additionally, Ai9-CCK/DTA animals significantly increased average meal size from 0.2 to 0.35 g (Figure 6G) and average meal duration from 5 to 9 min (Figure 6H). In summary, the ablation of CCK-expressing neurons in the VMH region results in a long-term increase in BW, likely due to hyperphagia characterized by lengthier and larger meals occurring less frequently throughout the day. These findings underscore the critical role of CCK^{VMH} neurons in homeostatic energy regulation.

3.4 Ablation of CCK^{VMH} neurons leads to hyperglycaemia and glucose intolerance

The VMH plays a crucial role in regulating glucose balance and is closely associated with abnormalities in BW and food intake that impact blood glucose control. To explore this further, Ai9-CCK/DTA and Ai9-Control/DTA animals injected with AAV-DIO-DTA underwent a glucose tolerance test (GTT) 3 months post-surgery. Both groups experienced a 16-h overnight fast, beginning at the onset of their active period (6 p.m.), to control for variations in individual food consumption. Blood glucose levels were measured using a handheld whole blood glucometer, with samples taken from the tail vein. Baseline blood glucose levels were recorded the following morning at the start of their resting phase. Ai9-CCK/DTA animals displayed hyperglycaemia, with average glucose levels at 8.5 mmol/L, compared to 6.5 mmol/L in the Ai9-Control/DTA animals (Figure 7A). The animals were given an IP glucose injection for the GTT assay, and their glucose clearance rates were monitored (Figure 7B). Within the first 30 min post-injection, both groups showed a substantial increase in blood glucose levels to 30 mmol/L, with no significant differences observed between the two groups. However, Ai9-CCK/DTA animals maintained elevated blood glucose levels, whereas controls nearly returned to baseline glucose levels within 3 h after the glucose challenge (Figure 7B).

4 Discussion

This study provides evidence that CCK-expressing neurons of the VMH play an essential role in energy homeostasis. Acute pharmacogenetic inhibition of CCK^{VMH} neurons leads to hyperphagia by altering food intake and meal patterns. Complete ablation of CCK^{VMH} neurons leads to hyperphagia and, consequently, to obesity and hyperglycaemia.

Due to its essential roles within the hypothalamic nuclei, attempts have been made to identify genes with enriched and distinct regional expression patterns in the VMH (Kurrasch et al., 2007; Liu et al., 2003) and, through gene manipulation, shed light on the distinct role of its heterogeneous cellular composition.

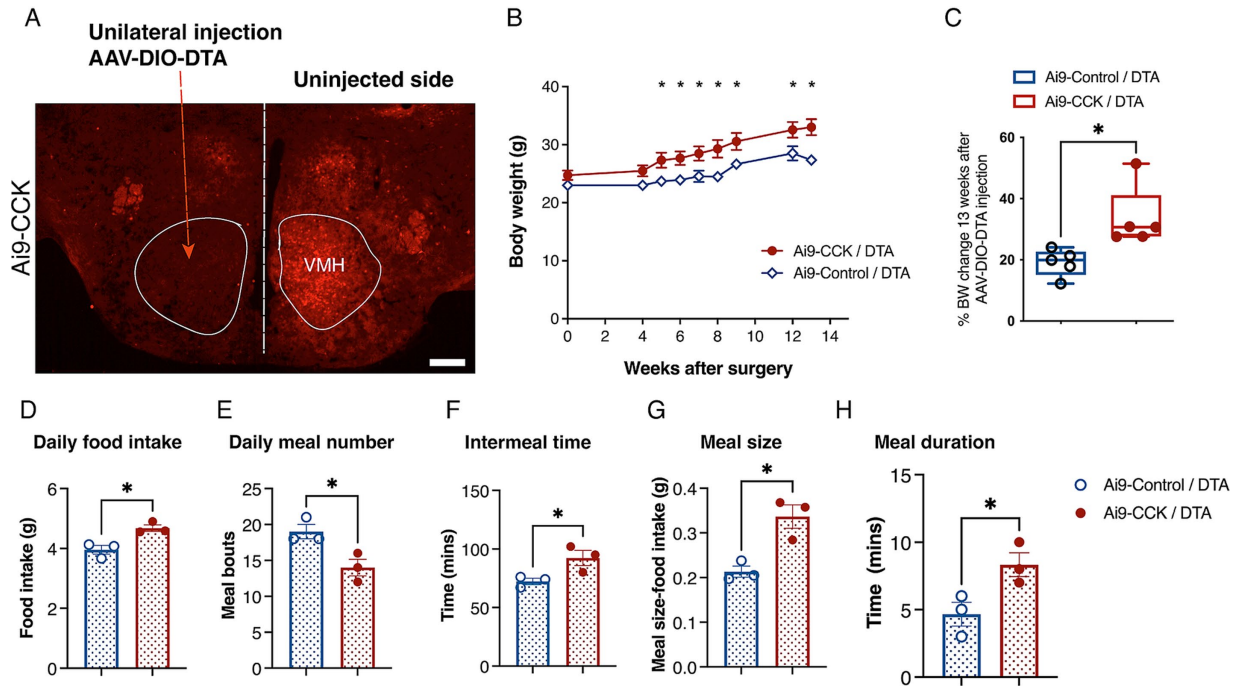

FIGURE 6
DTA-mediated ablation of CCK^{VMH} neurons in Ai9-CCK mice leads to prolonged weight gain due to increased food intake and disrupted meal patterns. (A) Coronal brain section from Ai9-CCK/DTA injected unilaterally with AAV-DIO-DTA, showing that the Ai9 fluorescent signal significantly decreased in the injected VMH region compared to the contralateral side. (B) A cohort of female mice (n = 5 per group; Ai9-CCK and Ai9-Control) aged 3–4 months were injected bilaterally with AAV-DIO-DTA. BW analysis was recorded for a total of 3 months after surgery. Ai9-CCK/DTA animals significantly increased their BW compared to the Ai9-Control /DTA group starting 5 weeks after injection (Adj $p = 0.042$), culminating with 13 weeks Adj $p = 0.00147$. (C) Three months after surgery, the percentage of BW in each group significantly changes based on its pre-surgery weight. However, there was a significant difference between Ai9-CCK/DTA and the control group (Ai9-Control/DTA, 19.09 ± 1.98 vs. Ai9-CCK/DTA, 33.6 ± 4.50, $p = 0.018$) attributable to the ablation of CCK^{VMH} neurons. (D-H) Food intake and meal pattern analysis between the two groups reveals that Ai9-CCK/DTA animals increased food intake with longer and bigger meals while decreasing their meal frequency. (D) The food intake of the CCK^{VMH}-ablated animals increased compared to the control group, as shown by the average daily intake (3.955 g ± 0.1457 vs. 4.679 g ± 0.1098, $p = 0.016$). (E) Meal bouts (19.00 ± 1.00 vs. 14.00 ± 1.15, $p = 0.0307$). (F) Intermeal time (minutes) (72.33 ± 2.72 vs. 92.33 ± 6.489, $p = 0.047$). (G) Meal size (0.2133 g ± 0.012 vs. 0.3366 g ± 0.026, $p = 0.0133$). (H) Meal duration (minutes) (4.667 ± 0.88 vs. 8.333 ± 0.88, $p = 0.0424$). Values are means ± s.e.m. p statistic (B) from multiple student t-tests corrected for multiple comparisons using the Holm-Šídák method and (C–H) from two-tailed unpaired student t-test. D-H, $n = 3$ female mice in each group. Scale bar panel A, 200 μm.

Here, using the HypoMap single-cell gene expression atlas of the murine hypothalamus (Steuernagel et al., 2022) we characterized the heterogeneity of *Cck*-expressing cells within the VMH. Although SF1 is a recognized marker to identify the VMH (Ikeda et al., 1995), it was co-expressed in only about 10% of the CCK^{VMH} cells. Notably, SF1 and CCKBR are predominantly found in the dorsomedial VMH (dmVMH) and central VMH (cVMH) regions, with minimal expression in the vlVMH (Flak et al., 2020; D. W. Kim et al., 2019). This pattern could imply a more substantial presence of CCK in the vlVMH. Yet, our immunostaining assays reveal a more uniform CCK expression across the dmVMH and cVMH, alongside a significant presence in the vlVMH. CCK^{VMH} neurons appear to be a distinct therapeutic target than the broader SF1^{VMH} neurons.

PACAP, on the other hand, is co-expressed in 58% of CCK^{VMH} neurons. Intracerebroventricular administration of PACAP has been shown to decrease food intake, promote leanness in mice (Hawke et al., 2009), and activate sympathetic nerve activity while inhibiting parasympathetic responses (Tanida et al., 2010). Conversely, ablation of PACAP from the VMH or the broader mediobasal hypothalamus results in rapid weight gain, increased adiposity, hyperinsulinemia and hyperglycaemia in mice, with only a slight and delayed rise in food intake (Bozadjieva-Kramer et al., 2021). The loss of PACAP in 58% of CCK^{VMH} neurons may partially explain the observed increases in BW and hyperglycaemia following CCK^{VMH} ablation.

Somatostatin is co-expressed in approximately 36% of CCK^{VMH} neurons and is crucial in regulating satiety and obesity factors both centrally and peripherally (Kumar and Singh, 2020). Somatostatin was found to have both orexigenic actions, for example, through inhibition of CCK (Herzig et al., 1994) and action on the somatostatin receptor 2 inducing feeding and drinking behavior (Stengel et al., 2010, 2015), and anorexigenic action, for example, when administered peripherally (Bray, 1995). Loss or acute inhibition of the CCK^{VMH} neurons expressing SST may contribute to the changes in the feeding behavior observed in our pharmacogenetic mouse model.

CCKBR is the primary CCK receptor in the brain (Flak et al., 2020) and is moderately expressed throughout the VMH, with low expression in the vlVMH. Moreover, CCKBR is found in three times as many VMH cells as CCK, indicating minimal autocrine effects of CCK. CCKBR^{VMH} neurons specifically raise the blood glucose setpoint without affecting energy expenditure and BW, both under normal conditions and during the counterregulatory response (CRR). They do so by regulating hepatic glucose production independently of islet hormones, highlighting the brain's central role in glucose homeostasis (Flak et al., 2020). When CCKBR is knocked out

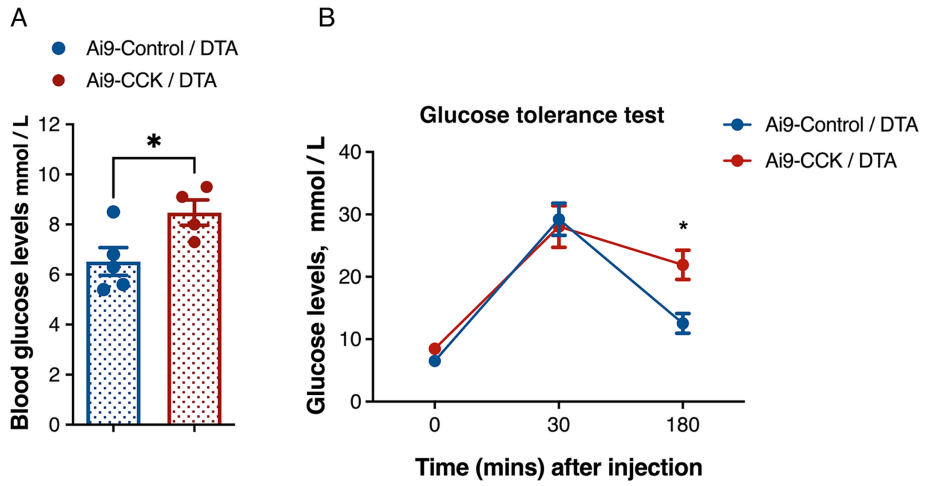

FIGURE 7
DTA-mediated ablation of CCK^{VMH} neurons results in hyperglycaemia and glucose intolerance. (A) Baseline glucose levels after 16 h fasting before glucose IP injection show that Ai9-CCK/DTA animals are hyperglycaemic (6.520 ± 0.55 vs. 8.475 ± 0.50, $p = 0.038$). (B) The plot shows the GTT of the two groups with a similar increase in blood glucose levels 30 min after IP but glucose intolerance at 180 min $p = 0.0122$. Values are means ± s.e.m. ($n = 4–5$ female mice per group). (A) p statistic from unpaired student t-test and (B) from two-way analysis of variance followed by Sidak's *post hoc* test.

systemically in mice, it leads to obesity characterized by increased food intake and fat accumulation due to adipocyte hypertrophy. This also disrupts glucose regulation, causing elevated fasting blood glucose and insulin levels, impaired glucose tolerance, and hepatic insulin resistance (Clerc et al., 2007). In contrast, the silencing of CCKBR^{VMH} neurons results in hypoglycaemia (Flak et al., 2020). In our study, acute inhibition of CCK^{VMH} neurons leads to hyperphagia, and complete ablation of these neurons leads to hyperphagia-associated obesity and hyperglycaemia. This information and the slight overlap between the two subpopulations expressing CCK and the CCKBR in the VMH suggest that they have distinct functions within their circuits. This emphasizes that CCK can still affect the CCKBR^{VMH} neurons by being produced by other cells in the hypothalamus or from the periphery.

In this study, we utilised two approaches to investigate the role of CCK-expressing cells in the VMH. The first approach involved spatiotemporal control of the activity of CCK^{VMH}-specific cells using chemogenetic cellular inhibition (hM4Di). The second approach involved ablating CCK^{VMH} cells using DTA viral transduction, which aimed to remove the cells expressing CCK in the VMH, potentially resulting in a more pronounced phenotype.

For the chemogenetic approach, incremental doses of CNO revealed a dose-dependent increase in food intake, with significant effects observed at 3 mg/kg BW. This dose-dependent response indicated that higher CNO concentrations effectively inhibited sufficient CCK^{VMH} neurons to modulate food intake. This experiment revealed that CCK^{VMH} neurons significantly influence food intake and meal patterns. The increase in daily food intake and meal frequency following hM4Di activation suggests that CCK^{VMH} neurons play a critical role in suppressing feeding behavior. This finding is consistent with the known anorexigenic effects of CCK in peripheral tissues (Ahn et al., 2022; Cawthon and de La Serre, 2021; Gibbs et al., 1973; Steinert et al., 2017), extending these effects to central mechanisms within the hypothalamus. Interestingly, the increased food intake manifested as a delayed response within the first 6 h post-injection. This delay may suggest that the CCK^{VMH} neurons are involved in a broader neural circuit activation that regulates feeding behavior, supporting a delay in phenotype manifestation.

To assess changes in food intake resulting from the inhibition of CCK^{VMH} neurons, we analyzed various meal patterns, including meal frequency, intermeal intervals, meal size, and duration. Meal frequency increased 6 h after CNO injection without affecting total food intake. The intermeal time significantly decreased with the rise in meal frequency and number of meals. Given that meal duration remained unchanged, it suggests that the increase in meal frequency was temporarily offset by a slight reduction in meal size, which may explain the unchanged cumulative food intake 6 h post-inhibition. Prolonged activation of the hM4Di and the associated GPCR signaling pathways could have long-lasting, cell-type-specific effects. Inhibition of CCK^{VMH} neurons indeed led to a sustained increase in meal frequency throughout the day. In the 24 h data analysis, meal sizes did not change, indicating that the initial compensatory mechanism in response to increased meal frequency was overridden by continued inhibition. Other components of the satiety neuronal circuitry might fine-tune the VMH neuronal circuit's sensitivity, including CCK-expressing neurons. In summary, inhibition of CCK^{VMH}-expressing neurons increases meal frequency, with meal size initially adjusted to prevent excessive energy intake. However, chronic inhibition eliminates this adjustment, increasing total food intake due to higher meal frequency. These results reveal a potential modulatory window for intervention considering the delay in phenotype manifestation.

Meanwhile, the ablation of CCK^{VMH} neurons led to a 28% increase in BW compared to controls at 14 weeks post AAV-DIO-DTA injection. The obese phenotype emerged about a month post-injection, corresponding with the typical time frame for optimal AAV expression and complete neuronal ablation. The obesity resulted from hyperphagia, with larger meal sizes and longer durations. Interestingly, meal numbers decreased, and intermeal intervals increased significantly without CCK^{VMH} neurons, suggesting dysregulated compensatory mechanisms attempting to balance increased food intake with larger, longer meals. The energy surplus might also heighten peripheral satiety signals, activating hindbrain inhibitory circuits.

The dysregulation of food intake caused by CCK^{VMH} neuron ablation differs from acute inhibition using hM4Di. DTA ablation nearly eliminates all CCK-positive neurons in the VMH, disconnecting them from local circuits. During hM4Di-mediated inhibition, neurons remain intact and continue to receive presynaptic inputs, possibly engaging in satiety signal processing (for example, glucose, leptin/insulin, ghrelin) that do not require synaptic neurotransmission, which is inhibited by hM4Di. The inhibition by hM4Di is ligand-dependent, creating a temporal inhibition window, varying based on the injection schedule. Thus, CCK^{VMH} neurons likely modulate food intake through multiple mechanisms. Inhibition of neurotransmission increases meal frequency, suggesting postsynaptic partners contribute to satiety signals by adjusting energy intake per meal. Without CCK input, meal consumption becomes disrupted, initially decreasing meal size, which normalizes over time, though meal onset becomes more frequent. Conversely, neuron ablation results in prolonged meals with increased size, indicating a role in integrating neurohormonal satiety signals independent of synaptic communication. Increased meal sizes might trigger compensatory satiety circuits from the gastrointestinal tract and vagal pathways to the brain, ultimately reducing meal frequency.

Given the VMH's role in glucose homeostasis and CRR, we found that CCK^{VMH} ablation caused hyperglycaemia, with baseline blood glucose levels higher than controls after 16 h of fasting. These animals also showed glucose intolerance, maintaining higher blood glucose levels up to 3 h post-glucose administration. These findings indicate that CCK-expressing neurons contribute to glucose sensing and homeostasis within the VMH, and their absence results in sustained high blood glucose levels.

As hormone-based obesity treatments gain prominence, GLP-1 receptor agonists have established themselves as frontrunners in this rapidly advancing field (Müller et al., 2019). While both GLP-1 and CCK have relatively short half-lives (Skibicka and Dickson, 2013), their pharmacological receptor agonists exhibit significantly prolonged effects (Christoffersen et al., 2020; Goldenberg and Steen, 2019). In pursuing more effective therapies for obesity and diabetes (Rodriguez et al., 2023), CCK analog NN9056 has emerged as a promising candidate, especially when combined with the GLP-1R agonist semaglutide (Zhou et al., 2024). Although peripheral CCK action is vital for regulating food intake and energy balance, our findings demonstrate that CCK-expressing neurons in the VMH play a pivotal role in controlling feeding behavior and influencing glucose homeostasis by integrating neurohormonal satiety signals and synaptic inputs. Understanding the neural circuits involving CCK^{VMH} neurons may lead to more targeted and effective therapies in this crucial area.

Data availability statement

The datasets presented in this study can be found in the article, source data and Supplementary material. Further inquiries can be directed to the corresponding author.

Ethics statement

The animal study was approved by The University of Oxford ethical review committee policy, with a final ethical review by the Animals in Science Regulation Unit (ASRU) of the United Kingdom Home Office. The study was conducted in accordance with the local legislation and institutional requirements.

Author contributions

VE: Conceptualization, Data curation, Formal analysis, Investigation, Methodology, Writing – review & editing. TE: Formal analysis, Investigation, Methodology, Writing – review & editing. JS: Data curation, Formal analysis, Writing – original draft, Writing – review & editing. LM: Conceptualization, Data curation, Funding acquisition, Project administration, Supervision, Writing – original draft, Writing – review & editing.

Funding

The author(s) declare that financial support was received for the research, authorship, and/or publication of this article. LM discloses support for this work from the BBSRC [BB/L021382/1] and in part from the Institutional Strategic Support Fund, the University of Oxford [ISSF-2019], and the MRC [MR/W005166/1]. VE was supported by a Medical Research Council scholarship, Ref. 13/14_MSD_OSS 682974, and the Onassis Foundation. TE was supported by an MRC Career Development Award (MR/M009599/1).

Acknowledgments

We thank the Biomedical Services at the University of Oxford for the technical support of animals. Based on the journal's policy regarding the inclusion of previously published online content in a thesis, we want to clarify that this is the case: Eftychidis (2017) Elucidating the principal role of cholecystokinin neurons of the ventromedial hypothalamic nucleus in energy homeostasis [thesis] Oxford: University of Oxford (2017). Eftychidis DPhil thesis dissemination version.pdf.

Conflict of interest

The authors declare that the research was conducted in the absence of any commercial or financial relationships that could be construed as a potential conflict of interest.

Publisher's note

Supplementary material

The Supplementary material for this article can be found online at: https://www.frontiersin.org/articles/10.3389/fncel.2024.1483368/full#supplementary-material

References

Abdulla, S., Aevermann, B., Assis, P., Badajoz, S., Bell, S. M., Bezzi, E., et al. (2023). CZ CELL×GENE discover: a single-cell data platform for scalable exploration, analysis and modeling of aggregated data. *BioRxiv* 2023:563174. doi: 10.1101/2023.10.30.563174

Affinati, A. H., Elias, C. F., Olson, D. P., and Myers, M. G. (2023). Brain regulation of feeding and energy homeostasis. In: R. S. Ahima Metabolic Syndrome. Berlin: Springer.

Ahn, W. M., Latremouille, J., and Harris, R. B. S. (2022). Leptin receptor-expressing cells in the ventromedial nucleus of the hypothalamus contribute to enhanced CCK-induced satiety following central leptin injection. *Am. J. Physiol. Endocrinol. Metab.* 323, E267–E280. doi: 10.1152/ajpendo.00088.2022

Argueta, D. A., Perez, P. A., Makriyannis, A., and Di Patrizio, N. V. (2019). Cannabinoid CB1 receptors inhibit gut-brain satiation signaling in diet-induced obesity. *Front. Physiol.* 10:704. doi: 10.3389/fphys.2019.00704

Armbruster, B. N., Li, X., Pausch, M. H., Herlitze, S., and Roth, B. L. (2007). Evolving the lock to fit the key to create a family of G protein-coupled receptors potently activated by an inert ligand. *Proc. Natl. Acad. Sci. U. S. A.* 104, 5163–5168. doi: 10.1073/pnas.0700293104

Atalayer, D., and Rowland, N. E. (2011). Structure of motivation using food demand in mice. *Physiol. Behav.* 104, 15–19. doi: 10.1016/j.physbeh.2011.04.042

Bake, T., Murphy, M., Morgan, D. G. A., and Mercer, J. G. (2014). Large, binge-type meals of high fat diet change feeding behaviour and entrain food anticipatory activity in mice. *Appetite* 77, 62–73. doi: 10.1016/j.appet.2014.02.020

Bi, S., Ladenheim, E. E., Schwartz, G. J., and Moran, T. H. (2001). A role for NPY overexpression in the dorsomedial hypothalamus in hyperphagia and obesity of OLETF rats. *Am. J. Physiol. Regul. Integr. Comp. Physiol.* 281, R254–R260. doi: 10.1152/ajpregu.2001.281.1.r254

Bi, S., Scott, K. A., Kopin, A. S., and Moran, T. H. (2004). Differential roles for cholecystokinin a receptors in energy balance in rats and mice. *Endocrinology* 145, 3873–3880. doi: 10.1210/en.2004-0284

Blevins, J. E., Stanley, B. G., and Reidelberger, R. D. (2000). Brain regions where cholecystokinin suppresses feeding in rats. *Brain Res.* 860, 1–10. doi: 10.1016/S0006-8993(99)02477-4

Bozadjieva-Kramer, N., Ross, R. A., Johnson, D. Q., Fenselau, H., Haggerty, D. L., Atwood, B., et al. (2021). The role of Mediobasal hypothalamic PACAP in the control of body weight and metabolism. *Endocrinology (United States)* 162:12. doi: 10.1210/endocr/bqab012

Bray, G. A. (1995). Nutrient intake is modulated by peripheral peptide administration. *Obes. Res.* 3:4. doi: 10.1002/j.1550-8528.1995.tb00229.x

Bray, G. A. (2000). Afferent signals regulating food intake. *Proc. Nutr. Soc.* 59, 373–384. doi: 10.1017/S0029665100000422

Cardinal, P., André, C., Quarta, C., Bellocchio, L., Clark, S., Elie, M., et al. (2014). CB1 cannabinoid receptor in SF1-expressing neurons of the ventromedial hypothalamus determines metabolic responses to diet and leptin. Molecular. *Metabolism* 3, 705–716. doi: 10.1016/j.molmet.2014.07.004

Cawthon, C. R., and de La Serre, C. B. (2021). The critical role of CCK in the regulation of food intake and diet-induced obesity. *Peptides* 138:170492. doi: 10.1016/j.peptides.2020.170492

Choi, Y. H., Fujikawa, T., Lee, J., Reuter, A., and Kim, K. W. (2013). Revisiting the ventral medial nucleus of the hypothalamus: the roles of SF-1 neurons in energy homeostasis. Frontiers in neuroscience 7, 71. doi: 10.3389/fnins.2013.00071

Christoffersen, B., Skyggebjerg, R. B., Bugge, A., Kirk, R. K., Vestergaard, B., Uldam, H. K., et al. (2020). Long-acting CCK analogue NN9056 lowers food intake and body weight in obese Göttingen Minipigs. *Int. J. Obes.* 44, 447–456. doi: 10.1038/s41366-019-0386-0

Clerc, P., Constans, M. G. C., Lulka, H., Broussaud, S., Guigné, C., Leung-Theung-Long, S., et al. (2007). Involvement of cholecystokinin 2 receptor in food intake regulation: Hyperphagia and increased fat deposition in cholecystokinin 2 receptor-deficient mice. *Endocrinology* 148, 1039–1049. doi: 10.1210/en.2006-1064

Corp, E. S., Curcio, M., Gibbs, J., and Smith, G. P. (1997). The effect of centrally administered CCK-receptor antagonist on food intake in rats. *Physiol. Behav.* 61, 823–827. doi: 10.1016/S0031-9384(96)00561-6

De Fanti, B. A., Backus, R. C., Hamilton, J. S., Gietzen, D. W., and Horwitz, B. A. (1998). Lean (fa/fa) obese (fa/fa) zucker rats release cholecystokinin at PVN after a gavaged meal. *Am. J. Physiol.* 275, E1–E5. doi: 10.1152/ajpendo.1998.275.1.E1

Della-Fera, M. A., Baile, C. A., Schneider, B. S., and Grinker, J. A. (1981). Cholecystokinin antibody injected in cerebral ventricles stimulates feeding in sheep. *Science* 212, 687–689. doi: 10.1126/science.7221559

Dhillon, H., Zigman, J. M., Ye, C., Lee, C. E., McGovern, R. A., Tang, V., et al. (2006). Leptin directly activates SF1 neurons in the VMH, and this action by leptin is required for normal body-weight homeostasis. *Neuron* 49, 191–203. doi: 10.1016/j.neuron.2005.12.021

Dorré, D., and Smith, G. P. (1998). Cholecystokinin(B) receptor antagonist increases food intake in rats. *Physiol. Behav.* 65, 11–14. doi: 10.1016/S0031-9384(98)00080-8

Ebenezer, I. S. (2002). Effects of intracerebroventricular administration of the CCK1 receptor antagonist devazepide on food intake in rats. *Eur. J. Pharmacol.* 441, 79–82. doi: 10.1016/S0014-2999(02)01485-1

Eftychidis, V. (2017) *Elucidating the principal role of cholecystokinin neurons of the ventromedial hypothalamic nucleus in energy homeostasis [dissertation thesis]*. Oxford: University of Oxford 2017. Eftychidis DPhil thesis dissemination version.pdf.

Elmquist, J. K., Ahima, R. S., Maratos-Flier, E., Flier, J. S., and Saper, C. B. (1997). Leptin activates neurons in ventrobasal hypothalamus and brainstem. *Endocrinology* 138, 839–842. doi: 10.1210/endo.138.2.5033

Farley, C., Cook, J. A., Spar, B. D., Austin, T. M., and Kowalski, T. J. (2003). Meal pattern analysis of diet-induced obesity in susceptible and resistant rats. *Obes. Res.* 11, 845–851. doi: 10.1038/oby.2003.116

Flak, J. N., Goforth, P. B., Dell'Orco, J., Sabatini, P. V., Li, C., Bozadjieva, N., et al. (2020). Ventromedial hypothalamic nucleus neuronal subset regulates blood glucose independently of insulin. *J. Clin. Invest.* 130, 2943–2952. doi: 10.1172/JCI134135

Gage, G. J., Kipke, D. R., and Shain, W. (2012). Whole animal perfusion fixation for rodents. *J. Vis. Exp.* 65, 1–9. doi: 10.3791/3564

Geibel, M., Badurek, S., Horn, J. M., Vatanashevanopakorn, C., Koudelka, J., Wunderlich, C. M., et al. (2014). Ablation of TrkB signalling in CCK neurons results in hypercortisolism and obesity. *Nat. Commun.* 5:3427. doi: 10.1038/ncomms4427

Gibbs, J., Young, R. C., and Smith, G. P. (1973). Cholecystokinin decreases food intake in rats. *J. Comp. Physiol. Psychol.* 84, 488–495. doi: 10.1037/h0034870

Goldenberg, R. M., and Steen, O. (2019). Semaglutide: review and place in therapy for adults with type 2 diabetes. In. *Can. J. Diabetes* 43, 136–145. doi: 10.1016/j.jcjd.2018.05.008

Hawke, Z., Ivanov, T. R., Bechtold, D. A., Dhillon, H., Lowell, B. B., and Luckman, S. M. (2009). PACAP neurons in the hypothalamic ventromedial nucleus are targets of central leptin signaling. *J. Neurosci.* 29, 14828–14835. doi: 10.1523/JNEUROSCI.1526-09.2009

Herzig, K. H., Louie, D. S., and Owyang, C. (1994). Somatostatin inhibits CCK release by inhibiting secretion and action of CCK-releasing peptide. *Am. J. Physiol. Gastrointest. Liver Physiol.* 266, G1156–G1161. doi: 10.1152/ajpgi.1994.266.6.g1156

Hetherington, A. W., and Ranson, S. W. (1940). Hypothalamic lesions and adiposity in the rat. *Anat. Rec.* 78, 149–172. doi: 10.1002/ar.1090780203

Ikeda, Y., Luo, X., Abbud, R., Nilson, J. H., and Parker, K. L. (1995). The nuclear receptor steroidogenic factor 1 is essential for the formation of the ventromedial hypothalamic nucleus. *Mol. Endocrinol.* 9, 478–486. doi: 10.1210/mend.9.4.7659091

Khodai, T., and Luckman, S. M. (2021). Ventromedial nucleus of the hypothalamus neurons under the magnifying glass. *Endocrinology* 162:141. doi: 10.1210/endocr/bqab141

Kim, K. W., Donato, J., Berglund, E. D., Choi, Y. H., Kohno, D., Elias, C. F., et al. (2012). FOXO1 in the ventromedial hypothalamus regulates energy balance. *J. Clin. Invest.* 122, 2578–2589. doi: 10.1172/JCI62848

Kim, K. W., Sohn, J. W., Kohno, D., Xu, Y., Williams, K., and Elmquist, J. K. (2011). SF-1 in the ventral medial hypothalamic nucleus: a key regulator of homeostasis. *Mol. Cell. Endocrinol.* 336, 219–223. doi: 10.1016/j.mce.2010.11.019

Kim, D. W., Yao, Z., Graybuck, L. T., Kim, T. K., Nguyen, T. N., Smith, K. A., et al. (2019). Multimodal analysis of cell types in a hypothalamic node controlling social behavior. *Cell* 179, 713–728.e17. doi: 10.1016/j.cell.2019.09.020

King, B. M. (2006). The rise, fall, and resurrection of the ventromedial hypothalamus in the regulation of feeding behavior and body weight. *Physiol. Behav.* 87, 221–244. doi: 10.1016/j.physbeh.2005.10.007

Kleinridders, A., Könner, A. C., and Brüning, J. C. (2009). CNS-targets in control of energy and glucose homeostasis. *Curr. Opin. Pharmacol.* 9, 794–804. doi: 10.1016/j.coph.2009.10.006

Klöckener, T., Hess, S., Belgardt, B. F., Paeger, L., Verhagen, L. A. W., Husch, A., et al. (2011). High-fat feeding promotes obesity via insulin receptor/PI3K-dependent inhibition of SF-1 VMH neurons. *Nat. Neurosci.* 14, 911–918. doi: 10.1038/nn.2847

Kumar, U., and Singh, S. (2020). Role of somatostatin in the regulation of central and peripheral factors of satiety and obesity. *Int. J. Mol. Sci.* 21:2568. doi: 10.3390/ijms21072568

Kurrasch, D. M., Cheung, C. C., Lee, F. Y., Tran, P. V., Hata, K., and Ingraham, H. A. (2007). The neonatal ventromedial hypothalamus transcriptome reveals novel markers with spatially distinct patterning. *J. Neurosci.* 27, 13624–13634. doi: 10.1523/JNEUROSCI.2858-07.2007

Liu, H., Kishi, T., Roseberry, A. G., Cai, X., Lee, C. E., Montez, J. M., et al. (2003). Transgenic mice expressing green fluorescent protein under the control of the melanocortin-4 receptor promoter. *J. Neurosci.* 23, 7143–7154. doi: 10.1523/JNEUROSCI.23-18-07143.2003

Madisen, L., Zwingman, T. A., Sunkin, S. M., Oh, S. W., Zariwala, H. A., Gu, H., et al. (2010). A robust and high-throughput Cre reporting and characterization system for the whole mouse brain. *Nat. Neurosci.* 13, 133–140. doi: 10.1038/nn.2467

Majdic, G., Young, M., Gomez-Sanchez, E., Anderson, P., Szczepaniak, L. S., Dobbins, R. L., et al. (2002). Knockout mice lacking steroidogenic factor 1 are a novel genetic model of hypothalamic obesity. *Endocrinology* 143, 607–614. doi: 10.1210/endo.143.2.8652

Manvich, D. F., Webster, K. A., Foster, S. L., Farrell, M. S., Ritchie, J. C., Porter, J. H., et al. (2018). The DREADD agonist clozapine N-oxide (CNO) is reverse-metabolized to clozapine and produces clozapine-like interoceptive stimulus effects in rats and mice. *Sci. Rep.* 8:3840. doi: 10.1038/s41598-018-22116-z

Megill, C., Martin, B., Weaver, C., Bell, S., Prins, L., Badajoz, S., et al. (2021). Cellxgene: a performant, scalable exploration platform for high dimensional sparse matrices. *BioRxiv* 2021:318. doi: 10.1101/2021.04.05.438318

Moran, T. H., Ameglio, P. J., Peyton, H. J., Schwartz, G. J., and McHugh, P. R. (1993). Blockade of type a, but not type B, CCK receptors postpones satiety in rhesus monkeys. *Am. J. Physiol. Regul. Integr. Comp. Physiol.* 265, R620–R624. doi: 10.1152/ajpregu.1993.265.3.r620

Moran, T. H., Ameglio, P. J., Schwartz, G. J., and McHugh, P. R. (1992). Blockade of type a, not type B, CCK receptors attenuates satiety actions of exogenous and endogenous CCK. *Am. J. Physiol. Regul. Integr. Comp. Physiol.* 262, R46–R50. doi: 10.1152/ajpregu.1992.262.1.r46

Müller, T. D., Finan, B., Bloom, S. R., D'Alessio, D., Drucker, D. J., Flatt, P. R., et al. (2019). Glucagon-like peptide 1 (GLP-1). *Mol. Metab.* 30, 72–130. doi: 10.1016/j.molmet.2019.09.010

Overduin, J., Gibbs, J., Cummings, D. E., and Reeve, J. R. (2014). CCK-58 elicits both satiety and satiation in rats while CCK-8 elicits only satiation. *Peptides* 54, 71–80. doi: 10.1016/j.peptides.2014.01.008

Quarta, C., Claret, M., Zeltser, L. M., Williams, K. W., Yeo, G. S. H., Tschöp, M. H., et al. (2021). POMC neuronal heterogeneity in energy balance and beyond: an integrated view. Nature. *Metabolism* 3:34. doi: 10.1038/s42255-021-0034

Ramadori, G., Fujikawa, T., Anderson, J., Berglund, E. D., Frazao, R., Michán, S., et al. (2011). SIRT1 deacetylase in SF1 neurons protects against metabolic imbalance. *Cell Metab.* 14, 301–312. doi: 10.1016/j.cmet.2011.06.014

Rehfeld, J. F. (1978). Immunochemical studies on cholecystokinin. II. Distribution and molecular heterogeneity in the central nervous system and small intestine of man and hog. *J. Biol. Chem.* 253, 4022–4030. doi: 10.1016/s0021-9258(17)34793-2

Rehfeld, J. F., and Hansen, H. F. (1986). Characterization of preprocholecystokinin products in the porcine cerebral cortex. Evidence of different processing pathways. *J. Biol. Chem.* 261, 5832–5840. doi: 10.1016/s0021-9258(17)38458-2

Reidelberger, R. D., Castellanos, D. A., and Hulce, M. (2003). Effects of peripheral CCK receptor blockade on food intake in rats. *Am. J. Physiol. Regul. Integr. Comp. Physiol.* 285, R429–R437. doi: 10.1152/ajpregu.00176.2003

Reidelberger, R. D., Hernandez, J., Fritzsch, B., and Hulce, M. (2004). Abdominal vagal mediation of the satiety effects of CCK in rats. *Am. J. Physiol. Regul. Integr. Comp. Physiol.* 286, R1005–R1012. doi: 10.1152/ajpregu.00646.2003

Rodriguez, P. J., Goodwin Cartwright, B. M., Gratzl, S., Brar, R., Baker, C., Gluckman, T. J., et al. (2023). Comparative effectiveness of Semaglutide and Tirzepatide for weight loss in adults with overweight and obesity in the US: A real-world evidence study. *MedRxiv* 2023:8775. doi: 10.1101/2023.11.21.23298775

Roh, E., Song, D. K., and Kim, M. S. (2016). Emerging role of the brain in the homeostatic regulation of energy and glucose metabolism. *Exp. Mol. Med.* 48:e216. doi: 10.1038/emm.2016.4

Roth, B. L. (2016). DREADDs for Neuroscientists. *Neuron* 89, 683–694. doi: 10.1016/j.neuron.2016.01.040

Routh, V. H. (2003). Glucosensing neurons in the ventromedial hypothalamic nucleus (VMN) and hypoglycemia-associated autonomic failure (HAAF). *Diabetes Metab. Res. Rev.* 19, 348–356. doi: 10.1002/dmrr.404

Schick, R. R., Reilly, W. M., Roddy, D. R., Yaksh, T. L., and Go, V. L. W. (1987). Neuronal cholecystokinin-like immunoreactivity is postprandially released from primate hypothalamus. *Brain Res.* 418, 20–26. doi: 10.1016/0006-8993(87)90957-7

Schick, R. R., Yaksh, T. L., and Go, V. L. W. (1986). An intragastric meal releases the putative satiety factor cholecystokinin from hypothalamic neurons in cats. *Brain Res.* 370, 349–353. doi: 10.1016/0006-8993(86)90492-0

Schick, R. R., Yaksh, T. L., Roddy, D. R., and Go, V. L. W. (1989). Release of hypothalamic cholecystokinin in cats: effects of nutrient and volume loading. *Am. J. Physiol. Regul. Integr. Comp. Physiol.* 256, R248–R254. doi: 10.1152/ajpregu.1989.256.1.r248

Schiffmann, S. N., and Vanderhaeghen, J. -J. (1991). Distribution of cells containing mRNA encoding cholecystokinin in the rat central nervous system. *J. Comp. Neurol.* 304, 219–233. doi: 10.1002/cne.903040206

Scott, M. M., Lachey, J. L., Sternson, S. M., Lee, C. E., Elias, C. F., Friedman, J. M., et al. (2009). Leptin targets in the mouse brain. *J. Comp. Neurol.* 514, 518–532. doi: 10.1002/cne.22025

Sjöstedt, E., Zhong, W., Fagerberg, L., Karlsson, M., Mitsios, N., Adori, C., et al. (2020). An atlas of the protein-coding genes in the human, pig, and mouse brain. *Science* 367:947. doi: 10.1126/science.aay5947

Skibicka, K. P., and Dickson, S. L. (2013). Enteroendocrine hormones - central effects on behavior. *Curr. Opin. Pharmacol.* 13, 977–982. doi: 10.1016/j.coph.2013.09.004

Steinert, R. E., Feinle-Bisset, C., Asarian, L., Horowitz, M., Beglinger, C., and Geary, N. (2017). Ghrelin, CCK, GLP-1, and PYY(3-36): secretory controls and physiological roles in eating and glycemia in health, obesity, and after RYGB. *Physiol. Rev.* 97, 411–463. doi: 10.1152/physrev.00031.2014

Stengel, A., Goebel, M., Wang, L., Rivier, J., Kobelt, P., Monnikes, H., et al. (2010). Selective central activation of somatostatin receptor 2 increases food intake, grooming behavior and rectal temperature in rats. *J. Physiol. Pharmacol.* 61, 399–407

Stengel, A., Karasawa, H., and Taché, Y. (2015). The role of brain somatostatin receptor 2 in the regulation of feeding and drinking behavior. *Horm. Behav.* 73, 15–22. doi: 10.1016/j.yhbeh.2015.05.009

Steuernagel, L., Lam, B. Y. H., Klemm, P., Dowsett, G. K. C., Bauder, C. A., Tadross, J. A., et al. (2022). HypoMap—a unified single-cell gene expression atlas of the murine hypothalamus. Nature. *Metabolism* 4, 1402–1419. doi: 10.1038/s42255-022-00657-y

Tanida, M., Shintani, N., Morita, Y., Tsukiyama, N., Hatanaka, M., Hashimoto, H., et al. (2010). Regulation of autonomic nerve activities by central pituitary adenylate cyclase-activating polypeptide. *Regul. Pept.* 161, 73–80. doi: 10.1016/j.regpep.2010.02.002

Waterson, M. J., and Horvath, T. L. (2015). Neuronal regulation of energy homeostasis: beyond the hypothalamus and feeding. *Cell Metab.* 22:26. doi: 10.1016/j.cmet.2015.09.026

West, D. B., Fey, D., and Woods, S. C. (1984). Cholecystokinin persistently suppresses meal size but not food intake in free-feeding rats. *Am. J. Physiol. Regul. Integr. Comp. Physiol.* 246, R776–R787. doi: 10.1152/ajpregu.1984.246.5.r776

Xu, X., Coats, J. K., Yang, C. F., Wang, A., Ahmed, O. M., Alvarado, M., et al. (2012). Modular genetic control of sexually dimorphic behaviors. *Cell* 148, 596–607. doi: 10.1016/j.cell.2011.12.018

Zhou, C., Sun, L., Guoqiang, H., Gong, B., Wang, T., Sun, X., et al. (2024). Discovery of novel glucagon-like peptide 1/cholecystokinin 1 receptor dual agonists. *Eur. J. Pharm. Sci.* 199:106818. doi: 10.1016/j.ejps.2024.106818

frontiers | Frontiers in Cellular Neuroscience

TYPE Review
PUBLISHED 06 November 2024
DOI 10.3389/fncel.2024.1482844

OPEN ACCESS

EDITED BY
Enrico Cherubini,
European Brain Research Institute, Italy

REVIEWED BY
Dongqing Shi,
University of Michigan, United States
Masaaki Kuwajima,
The University of Texas at Austin,
United States

*CORRESPONDENCE
Yanis Inglebert
✉ yanis.inglebert@umontreal.ca
R. Anne McKinney
✉ anne.mckinney@mcgill.ca

†These authors have contributed equally to this work and share first authorship

RECEIVED 18 August 2024
ACCEPTED 25 October 2024
PUBLISHED 06 November 2024

CITATION
Wu PY, Inglebert Y and McKinney RA (2024) Synaptopodin: a key regulator of Hebbian plasticity.
Front. Cell. Neurosci. 18:1482844.
doi: 10.3389/fncel.2024.1482844

Synaptopodin: a key regulator of Hebbian plasticity

Pei You Wu[1†], Yanis Inglebert[1,2,3*†] and R. Anne McKinney[1*]

[1]Department of Pharmacology & Therapeutics, McGill University, Montreal, QC, Canada, [2]Department of Neurosciences, Université de Montréal, Montreal, QC, Canada, [3]Centre Interdisciplinaire de Recherche sur le Cerveau et l'Apprentissage (CIRCA), Montreal, QC, Canada

Synaptopodin, an actin-associated protein found in a subset of dendritic spines in telencephalic neurons, has been described to influence both functional and morphological plasticity under various plasticity paradigms. Synaptopodin is necessary and sufficient for the formation of the spine apparatus, stacks of smooth endoplasmic reticulum cisternae. The spine apparatus is a calcium store that locally regulates calcium dynamics in response to different patterns of activity and is also thought to be a site for local protein synthesis. Synaptopodin is present in ~30% of telencephalic large dendritic spines *in vivo* and *in vitro* highlighting the heterogeneous microanatomy and molecular architecture of dendritic spines, an important but not well understood aspect of neuroplasticity. In recent years, it has become increasingly clear that synaptopodin is a formidable regulator of multiple mechanisms essential for learning and memory. In fact, synaptopodin appears to be the decisive factor that determines whether plasticity can occur, acting as a key regulator for synaptic changes. In this review, we summarize the current understanding of synaptopodin's role in various forms of Hebbian synaptic plasticity.

KEYWORDS

dendritic spines, synaptic plasticity, synaptopodin, mGluR-LTD, STDP, LTP, LTD

Introduction

Dendritic spines are small thorn-like protrusions found on the dendrites of most of the excitatory neurons in the brain. They are the point of contact between neurons, forming the postsynaptic side of the excitatory synapses, and hold the molecular machinery that allows the transmission of signal from the afferent neurons (Gray, 1959; Hering and Sheng, 2001; Nimchinsky et al., 2002; McKinney, 2010). Spines can grow, shrink, form *de novo* and be maintained or be eliminated, all of which contribute to the formation and experience-dependent optimization of neuronal circuits (Caroni et al., 2012; Harris, 2020). These morphological modifications of spines are widely regarded as the structural basis for learning and encoding memories (Bourne and Harris, 2007; Kasai et al., 2021). They are also recognized as the loci of synaptic plasticity expression, believed to be the cellular mechanism underlying learning and memory formation (Hering and Sheng, 2001; Runge et al., 2020; McCann and Ross, 2017; Ma and Zuo, 2022). The most well-studied form of plasticity is Hebbian plasticity, in which the firing of one neuron induces the firing of another, strengthening the connection. Conversely, if the firing is desynchronized and does not drive the other neuron, the connection weakens. These processes correspond to the classical forms of long-term potentiation (LTP) and long-term depression (LTD), respectively.

The functional aspects of synaptic plasticity have been well characterized, whereby LTP increases synaptic strength and LTD decreases synaptic strength. Strengthened synaptic transmission during LTP is typically echoed by spine volume enlargement to accommodate more glutamate receptors (Bosch et al., 2014; Nakahata and Yasuda, 2018), as well as increased

spine stability or spine density (Geinisman et al., 2001). Conversely, weakened synaptic transmission during LTD is typically associated with shrinkage and/or spine loss, synapse loss, and undesirable decreased connectivity in neuronal circuits (Nägerl et al., 2004; Zhou et al., 2004; Stein and Zito, 2019). Intriguingly not all dendritic spines will undergo similar plastic changes despite receiving a similar stimulus, highlighting a heterogeneity in synapses (Ramiro-Cortés and Israely, 2013; Szepesi et al., 2014; Thomazeau et al., 2021). In fact, spines are highly heterogeneous as they have been grouped into different subtypes based on their size and shape, which are often associated with their function in memory storage and formation (Papa et al., 1995; Hering and Sheng, 2001; Nimchinsky et al., 2002; von Bohlen und Halbach, 2009; McKinney, 2010; Rochefort and Konnerth, 2012; Pchitskaya and Bezprozvanny, 2020). Moreover, they also differ in terms of their molecular composition. Using electron microscopy (EM), Gray (1959) identified the presence of smooth endoplasmic reticulum (sER) in a subpopulation of the spines, and among those, some formed spine apparatus (SA), a more complex form of sER composed of several stacks of cisterns interconnected by electron dense materials (Frotscher et al., 2014). The formation and function of the sER in spines was a mystery, until recent live imaging experiments and 3D electron microscopy images revealed that the spine sER is continuous with the dendritic sER, which is critical for multiple forms of synaptic plasticity (Miyata et al., 2000; Holbro et al., 2009; Ostroff et al., 2010; Chirillo et al., 2019) and exhibits motility to enter or exit the spines (Špaček, 1985; Spacek and Harris, 1997; Perez-Alvarez et al., 2020).

The insertion of the sER in spines has been shown to be dependent on elevated synaptic transmission and activity and structural changes of spines after plasticity (Perez-Alvarez et al., 2020). The spines with stable sER have a longer lifetime with around 90% of these stable spines are associated with synaptopodin (SP), an actin-associated postsynaptic protein (Deller et al., 2000; Korkotian and Segal, 2011; Perez-Alvarez et al., 2020; Yap et al., 2020). While not expressed in the cerebellum, SP is found in the dendritic shaft, the dendritic spines and the axon initial segment of the excitatory neurons in the hippocampus, cerebral cortex and striatum (Mundel et al., 1997; Deller et al., 2000, 2003). In the hippocampus, SP expression is developmentally regulated as it gradually increases over the maturation of the brain circuitry, reaching its maximum in adult animals (Czarnecki et al., 2005). A similar developmentally regulated expression pattern was also observed in cultured neurons (Konietzny et al., 2019). SP is the only molecule found so far to be responsible for the formation of SA and colocalizes with it at the base of dendritic spines (Deller et al., 2003). SA is originated from sER, it is believed to act as an intracellular calcium reservoir and to help in the compartmentalization of calcium within spines (Buchs et al., 1994; Holbro et al., 2009; Korkotian and Segal, 2011; Korkotian et al., 2014; Rosado et al., 2022). Presence of ribosomes and translocon on SA also imply that it might play an essential role in local protein synthesis (Špaček, 1985; Pierce et al., 2000). Furthermore, the major glutamate receptors of the excitatory synapses, N-methyl-D-aspartate receptors (NMDAR) and α-amino-3-hydroxy-5-methyl-4-isoxazolepropionic acid receptor (AMPAR), were also found co-localizing with SA, suggesting a role in receptor turnover and trafficking (Nusser et al., 1998; Racca et al., 2000).

Studies on SP, the molecular marker of SA, have provided solid evidence that spines with or without SP are two functionally distinct groups of spines. SP is preferential localization in about 30% of the mushroom spine in adult hippocampus (Deller et al., 2003; Speranza et al., 2022b). SP expression in spines is also very dynamic and is differentially regulated by synaptic activity and various molecules such as the motor protein myosin V and miRNA (Yamazaki et al., 2001; Konietzny et al., 2019; Dubes et al., 2022). Presence or gain of SP in spines increases the spine head volume and the spine lifetime, whereas spines that lose SP have decreased spine size and survival time (Deller et al., 2000; Okubo-Suzuki et al., 2008; Zhang et al., 2013; Yap et al., 2020; Speranza et al., 2022b). Mice in which the *Synpo* gene encoding SP is deleted (SPKO) show deficits in spatial learning (Deller et al., 2003; Jedlicka et al., 2008), consistent with evidence that SP plays an important role in hippocampal structural/functional plasticity. SP regulates spine structural plasticity by supporting spine head enlargement induced by LTP (Okubo-Suzuki et al., 2008; Vlachos et al., 2009; Zhang et al., 2013; Chirillo et al., 2019). From our previous work we also know that under conditions of reduced activity, certain spines produce spine head protrusions to near by active presynaptic boutons, the stability of which depends on the presence of SP (Verbich et al., 2016). Increasing evidence in the past decade suggests that SP acts as a critical molecule for many forms of synaptic plasticity.

NMDAR-LTP

NMDAR -mediated LTP (NMDAR-LTP) is the most studied and best understood form of synaptic plasticity. It is commonly induced by either high frequency electrical stimulation (100 Hz) or chemical stimulation (e.g., NMDA, forskolin, etc.) (Dudek and Bear, 1992). The different stimulation methods may require slightly different molecular players, but NMDAR-LTP generally involves the elevation of post-synaptic calcium (Ca^{2+}) through NMDAR, followed by the activation of CAMKII and Protein Kinase A (PKA), leading to the subsequent trafficking of α-amino-3-hydroxy-5-methyl-4-isoxazolepropionic acid receptor (AMPAR) to the post-synaptic density (PSD) membrane (Figure 1) (Chetkovich and Sweatt, 1993; Lüscher and Malenka, 2012). Insertion of AMPAR to the PSD increases the synaptic strength and is associated with dendritic spine enlargement and stability (De Roo et al., 2008; Holtmaat and Svoboda, 2009; Lüscher and Malenka, 2012; Kasai et al., 2021). Ultrastructural analysis of rat hippocampal CA1 dendritic spines following theta-burst stimulation induced LTP was shown to have enlarged PSD and perforated synapse, which is more likely to contain sER and spine apparatus (Toni et al., 2001; Chirillo et al., 2019). In fact, these post-LTP ultrastructural changes in dendritic spines were further confirmed after the discovery of SP, where studies showed that SP mRNA and protein expression as well as the dendritic spine size increase following LTP (Yamazaki et al., 2001; Fukazawa et al., 2003). The first observation of NMDAR-LTP deficits in SPKO was made in the hippocampus at Schaffer Collateral-CA1 (Sc-CA1) synapses, and was also linked to impairments in spatial learning (Deller et al., 2003). These findings have been subsequently confirmed by multiple independent studies (Zhang et al., 2013; Grigoryan and Segal, 2016; Inglebert et al., 2024), including the *in vivo* study in the Dentate Gyrus (Jedlicka et al., 2009). These studies provided solid evidence for a prominent role of SP in NMDAR-LTP, however how SP participates in the molecular mechanism of the plasticity is not well understood. An interesting observation has been made by Zhang et al., where only the younger SPKO mice (P15-21), but not the older mature mice (2 months- or

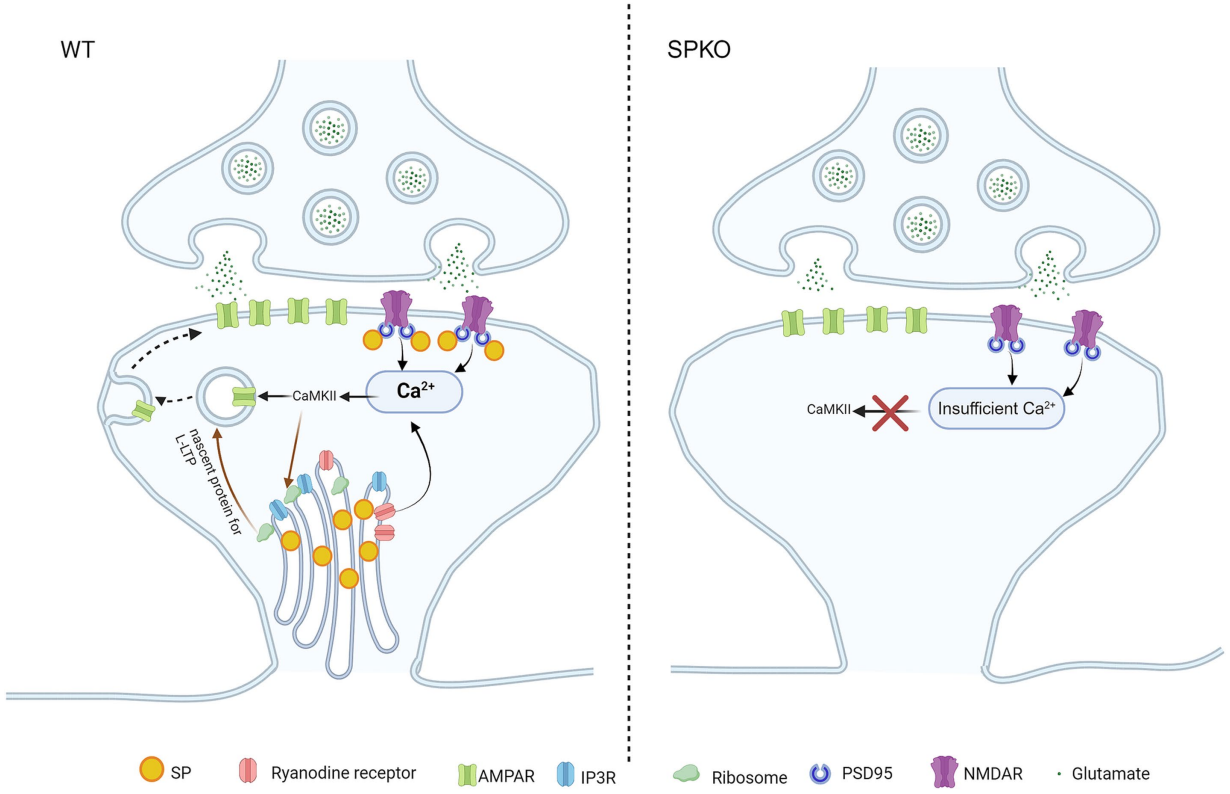

FIGURE 1
SP/SA is involved in Hebbian long-term potentiation. Presence of SP/SA in spines enables the release of Ca^{2+} from RYR and NMDAR, allowing for the build-up of high [Ca^{2+}] in spines to activate CAMKII during NMDAR-LTP and t-LTP. Subsequent phosphorylation of AMPAR by CAMKII initiates AMPAR surface insertion (signaling pathway shown in black arrow). CAMKII can equally activate signaling pathways to induce the long-lasting form of LTP (l-LTP) through ribosome-mediated local *de novo* protein synthesis in WT, as ribosomes are associated with SA (signaling pathway shown in brown arrow). In SPKO, NMDAR-LTP and t-LTP are impaired as SA is absent in spines. Lack of SA causes insufficient release of Ca^{2+} in spines to activate CaMKII. Loss of SA also lead to removal of ribosome from spines, disabling local protein synthesis for l-LTP.

6 months-old), exhibits deficiency in NMDAR-LTP. The authors reasoned that the young developing mice require PKA activation for LTP and SP is a substrate of PKA (Yasuda et al., 2003; Faul et al., 2008; Zhang et al., 2013). In kidney podocytes phosphorylation of SP by PKA and CAMKII was found to protects from proteolysis and promotes stress fiber formation by stabilizing the GTPases RhoA (Asanuma et al., 2006; Faul et al., 2008), perhaps a similar mechanism occurs in the brain. However, direct evidence of SP phosphorylation and its relevant physiological effect in brain is still lacking. Despite this interesting observation by Zhang et al. (2013), a few studies showed conflicting results that NMDAR-LTP deficit is observed in mature SPKO mice (Table 1). Such discrepancy may be due to the difference in genetic background of the SPKO mice (Jedlicka and Deller, 2017), potential unknown compensatory mechanism in the adult animal, or the use of ventral hippocampal slices from WT, which exhibits weaker LTP than dorsal hippocampal slices, occluding the deficits in SPKO (Vlachos et al., 2008; Grigoryan and Segal, 2016). Lack of NMDAR-LTP in adult SPKO mice can be attributable to impaired CAMKII activation due to the loss of intracellular calcium store SA leading to insufficient [Ca^{2+}] in spines.

In addition to electrophysiological data, SP has been shown to regulate the structural plasticity of dendritic spines. Specifically, SP is necessary for NMDA-induced spine expansion (Zhang et al., 2013) and broadly regulates dendritic spine plasticity (Vlachos et al., 2009). During NMDAR-LTP in WT mice, SP is upregulated in neurons and is specifically recruited to dendritic spines, where it promotes the enlargement of the spines and the accumulation of the AMPAR subunit GLUA1 in the spines (Yamazaki et al., 2001; Vlachos et al., 2009; Korkotian et al., 2014). It is possible that SP also regulates actin dynamics through the Rho GTPases in neurons, in a way similar to how SP regulates stress fiber formation in kidney podocytes, to mediate the structural plasticity of the spines (Asanuma et al., 2006). There is currently a lack of information of the involvement of SP in actin dynamics in the brain and will be an important area for future research.

The loss of SP also affects the long-lasting maintenance of LTP (lasting from hours to months) (l-LTP) (Zhang et al., 2013), which relies on local protein synthesis (Otani et al., 1989; Raymond et al., 2000; Kelleher et al., 2004). Electron micrographs have revealed the presence of polyribosomes and translocon in close association with SA, and that spines containing SP/SA are more likely to contain ribosomes compared to spines devoid of SP/SA, suggesting a critical role of SP in regulating local protein synthesis (Špaček, 1985; Pierce et al., 2000; Kruse et al., 2024). Complete loss of SP (e.g., SPKO) may significantly affect ribosomal trafficking and localization in spines, leading to the impairment of plasticity mechanisms that require *de novo* local protein synthesis, including l-LTP and mGluR-LTD, which will be elaborated later in this review (Figures 1, 2). Recent discovery of monosomes in synapses contributing to the local synthesis of many key synaptic

TABLE 1 The importance of synaptopodin in synaptic plasticity.

Reference	Region	Synapse	Preparation	Protocol	Plasticity observed
Deller et al. (2003)	Hippocampus	Sc – CA1	Acute slices (adult)	TBS (100 Hz, 10 × 4 pulses) or tetani (3 × 30 pulses, 200 Hz)	Reduced LTP
Zhang et al. (2013)	Hippocampus	Sc – CA1	Acute slices (P15 or 21)	TBS (100 Hz, 10 × 4 pulses)	Reduced LTP
			Acute slice (2 or 6 month-old)	TBS (100 Hz, 10 × 4 pulses)	Normal LTP
			Acute slice (P15 or 21)	2 Hz, 10 min, 1,200 stimuli	Normal LTD
Grigoryan and Segal (2016)	Hippocampus	Sc – CA1	Acute slices (2 to 3 month-old)	100 Hz, 1 s	Reduced LTP
Inglebert et al. (2024)	Hippocampus	Sc – CA1	Acute slices (P15 to P21)	10 Hz, 900 stimuli	Reduced LTP
				100 Hz, 900 stimuli	Reduced LTP
				t-LTP (+10 ms, 0,3 Hz, 100 pairings)	Absence of LTP, LTD instead
				t-LTD (−25 ms, 0.3 Hz, 100 pairings)	Absence of LTD
				2 Hz, 900 stimuli	Absence of LTD
Jedlicka et al. (2009)	Hippocampus	PP – GC	Anesthetized mice (3 month-old)	TBS (4 × 15, 200 Hz) TBS (6 series of 6 × 6, 400 Hz)	Normal LTP
				TBS (6 series of 6 × 6, 400 Hz)	Reduced LTP
Speranza et al. (2022b)	Hippocampus	Sc – CA1	Acute slices (P30 – P40)	DHPG (100 µM, 5 min)	Reduced mGluR-LTD
Wu et al. (2024)	Hippocampus	Sc – CA1	Acute slices (P30 – P40)	S-DHPG (100 µM, 5 min)	Reduced mGluR-LTD
Vlachos et al. (2009)	Hippocampus	N/A	Hippocampal cultures	cLTP (Glycine)	Reduce GluR1 function
Korkotian et al. (2014)	Hippocampus	N/A	Hippocampal cultures	cLTP (Glycine)	Absence of morphological plasticity

This table summarizes the plasticity observed in the absence of synaptopodin under various protocols. It details the region, synapses, and type of preparation used. Additionally, the frequency of stimulation and the number of repetitions are specified. For instance, "10 × 4 pulses" means that the 4 pulses are repeated 10 times. Abbreviations used include TBS for Theta Burst Stimulation, t-LTP for timing LTP, Sc for Schaffer Collateral, PP for Perforant Path, GC for granule cells and cLTP for Chemical LTP.

proteins adds an additional layer of complexity in understanding the regulation of local protein synthesis in spines (Biever et al., 2020). It would be interesting to uncover the relationship between SP and monosomes and perform an in-depth study on SP/SA's role in synapse-targeting and regulation of protein synthesis machinery in dendritic spines, the primary sites of protein production (Figure 1).

NMDAR-LTD

In contrast to LTP, the role of SP in LTD has been less explored. One primary reason is that low-frequency stimulation at 2 Hz yields conflicting results. At Sc-CA1 synapses, earlier findings indicated that LTD is normal in SPKO mice (Zhang et al., 2013), while our recent data showed that LTD is absent (Inglebert et al., 2024). This discrepancy can be attributed to variations in the number of stimulations, the extracellular Ca^{2+} concentration or the genetic background of the animals, similar to the discrepancy observed in adult LTP studies (Zhang et al., 2013; Grigoryan and Segal, 2016). It is important to note that LFS-LTD can be induced at various frequencies (usually between 1 and 10 Hz), but so far has only been explored at 2 Hz in SPKO mice. The lack of LTD in SPKO observed in Inglebert et al. (2024) is supported by the fact that ryanodine receptors (RYR) level is significantly reduced in spines of SPKO, as RYR-mediated calcium has been shown to play an important role in LTD (Arias-Cavieres et al., 2018). This could lead to insufficient Ca^{2+} entry into spines to activate calcineurin and protein phosphatase 1, resulting in disrupted signaling and impaired AMPAR endocytosis (Figure 2). This recent evidence calls for further investigation into the role of SP in activity-dependent LTD, either induced by LFS or STDP.

Metabotropic glutamate receptors-LTD (mGluR-LTD)

One specific type of LTD, known as mGluR-LTD, is mediated by group 1 metabotropic glutamate receptors (mGluR1 and mGluR5).

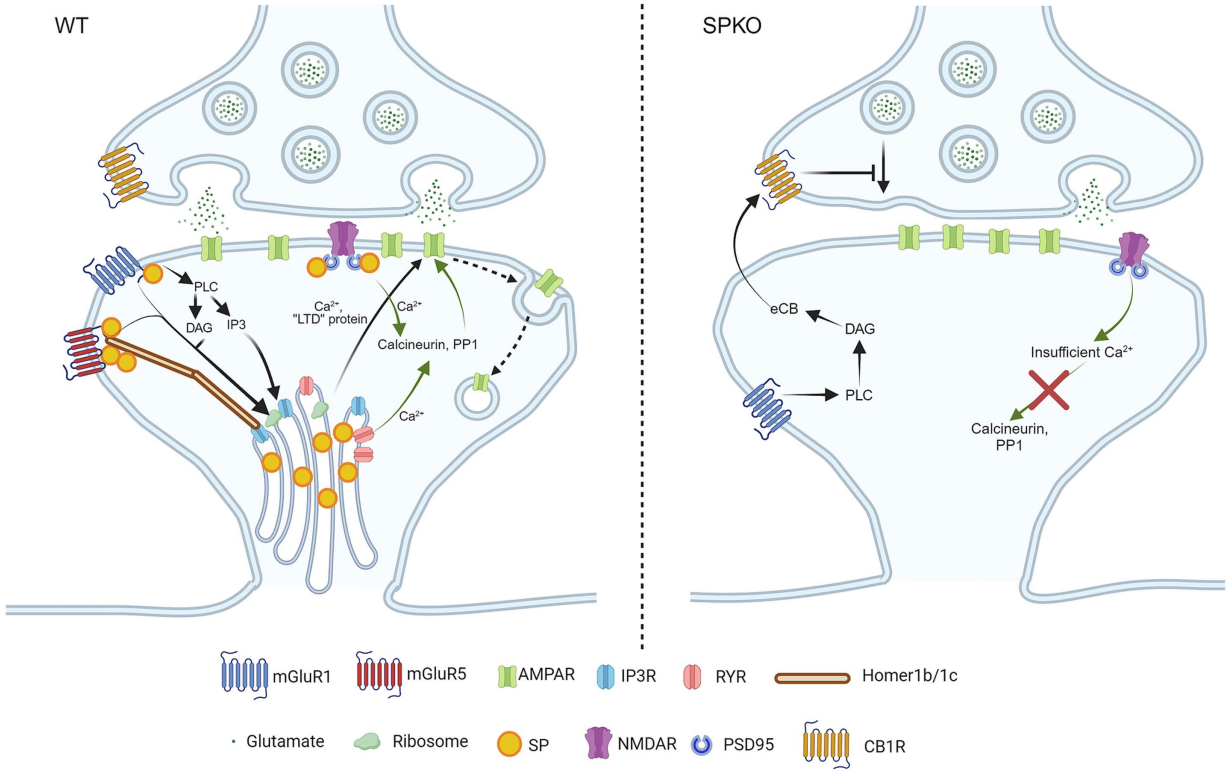

FIGURE 2
SP/SA is necessary for Hebbian long-term depressions. In WT spines that contain SP/SA, mGluR5 is stabilized by long Homers in the presence of SP. Upon activation of mGluR1/5, they trigger the release of phospholipase C (PLC), diacylglycerol (DAG) and Inositol trisphosphate (IP3) to activate IP3R and ribosomes. IP3R and ribosomes are found on SA, and they release Ca^{2+} and produce "LTD proteins" in order to promote endocytosis of AMPAR (signaling pathway shown in black arrows). NMDAR-LTD requires calcium entry from both NMDAR and RYR to activate the calcium-sensitive enzymes (calcineurin, PP1), to induce AMPAR internalization (signaling pathway shown in green arrows). In SPKO, due to the absence of SP and SA in spines, the postsynaptic mechanism of mGluR-LTD is completely switched to presynaptic mechanism through endocannabinoid signaling. The endocannabinoid is produced by mGluR1 alone, due to the loss of mGluR5 in the absence of SP, and retrograde signals back to presynaptic CB1R, leading to decreased glutamate release. As for NMDAR-LTD, the loss of RYR in the absence of SP/SA impairs intracellular Ca^{2+} release, leading to improper enzymatic signaling.

This form of LTD is observed in various brain regions, both *in vitro* and *in vivo*, including the hippocampus, amygdala, cortex, striatum and cerebellum (Bolshakov and Siegelbaum, 1994; Oliet et al., 1997; Palmer et al., 1997; Lüscher and Huber, 2010). It is typically induced by a brief application (5–10 min) of the mGluR agonist R,S-Dihydroxyphenylglycine (DHPG), which can lead to either the removal of postsynaptic AMPARs or a decrease in presynaptic release, depending on the concentration of DHPG (Sanderson et al., 2022). In mature neurons, AMPAR endocytosis by the rapid local translation of "LTD proteins" such as Arc, Map1b and STEP is a hallmark of mGluR-LTD (Figure 3) (Waung and Huber, 2009). In addition, mGluR-LTD induces structural changes which are characterized by spine shrinkage or loss (Oh et al., 2013; Ramiro-Cortés and Israely, 2013). Yet, spines loss is not always observed (Thomazeau et al., 2021). Since the ability of Gp1 mGluRs to depress synaptic transmission depends on sER (Holbro et al., 2009), It has been hypothesized that the presence of SP might explain the discrepancies observed in the literature. Indeed, in hippocampal slices from SPKO, both functional and structural mGluR-LTD is impaired (Speranza et al., 2022b; Wu et al., 2024). Notably, the application of DHPG results in the selective loss of mushroom-shaped spines that lack SP through mGluR1 but not mGluR5 activity, while spines containing SP remain stable (Speranza et al., 2022b).

Spine shrinkage/loss may occur through the mammalian target of rapamycin complex 2 (mTORC2)-signaled protein synthesis, which has been shown to regulate mGluR-LTD, actin re-organization and protein synthesis (Huang et al., 2013; Takei and Nawa, 2014; Huber et al., 2015; Zhu et al., 2018). Spines containing SP are protected from structure remodeling during mGluR-LTD due to the presence of SP in spines that physically binds and tethers the actin filaments (Figure 3). Interestingly, SPKO mice do not exhibit significant spine elimination despite unchanged mGluR1 expression. This suggests that the activation of downstream effectors, such as protein synthesis machinery, may be defective or absent in SPKO mice (Špaček, 1985; Pierce et al., 2000; Wu et al., 2024). In contrast to structural plasticity, the decrease in synaptic strength requires the combined activity of both mGluR1 and mGluR5 (Volk et al., 2006; Wu et al., 2024). Although mGluR1 surface expression is normal in SPKO mice, mGluR5 surface expression is reduced, explaining the observed impairment in mGluR-LTD. Loss of SP destabilizes the interaction between scaffolding proteins (such as long Homers) that keeps mGluR5 anchored on the surface of dendritic spines (Brakeman et al.,

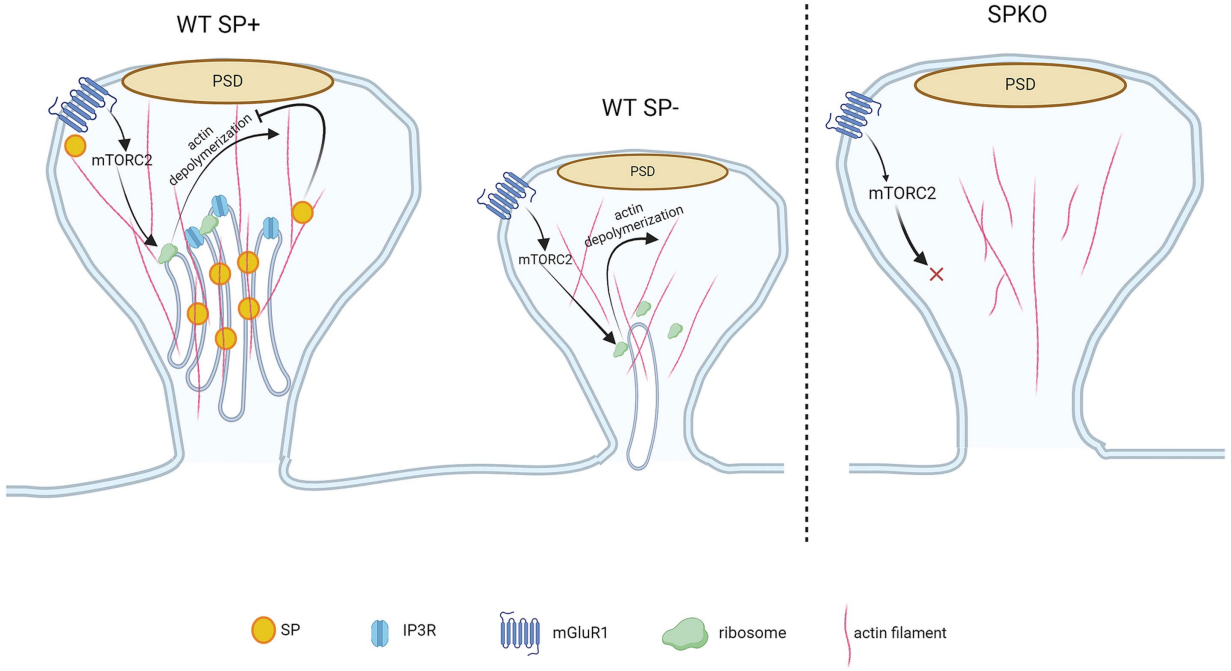

FIGURE 3
mGluR-LTD-mediated spine structural remodeling is regulated by synaptopodin. WT spines containing SP are protected from mGluR-LTD-induced shrinkage due to the presence of SP/SA that binds to F-actin and prevents actin depolymerization. WT spines lacking SP undergo spine shrinkage as SP is absent in the spine, allowing the F-actin to be depolymerized following mGluR1-induced mTORC2 signaling. Though the spine is devoid of SP/SA, they contain sER and protein synthesis machinery required for structural remodeling (i.e., mTORC2 and ribosomes). The SPKO spines do not display mGluR-LTD-dependent structural plasticity. They lack SP/SA, sER and the molecular machinery that is required for mGluR-LTD-induced structural plasticity.

1997; Wu et al., 2024) (Figure 2). More surprisingly, we found that the residual mGluR-LTD in SPKO mice is protein synthesis-independent and is instead mediated by a decrease in presynaptic release through endocannabinoid signaling as observed in neonatal animals (P8-15) (Nosyreva and Huber, 2005; Wu et al., 2024). This suggests that SP may regulate the locus of expression of mGluR-LTD and that loss of SP probably impact the normal maturation of the hippocampus.

Spike timing-dependent plasticity

Spike Timing-Dependent Plasticity (STDP) is an activity-dependent plasticity thought to be more physiological and closer to what could happen in the brain (Debanne and Inglebert, 2023). Unlike plasticity dependent on stimulation frequency, STDP relies on the precise timing between presynaptic activity (excitatory postsynaptic potential, EPSP) and postsynaptic activity (action potential, AP). Classically, timing-dependent LTP (t-LTP) is induced when an EPSP is followed by an AP in the postsynaptic neuron and timing-dependent LTD (t-LTD) is induced when AP is followed by an EPSP (Bi and Poo, 1998; Debanne et al., 1998). SP has been recently identified to be required for normal t-LTP and t-LTD at Sc-CA1 synapses (Inglebert et al., 2024). The absence of SP shifts t-LTP into t-LTD but can still be restored by adjusting the parameters of the STDP paradigm (Table 1). The higher threshold for t-LTP in SPKO mice is most likely due to the loss of AMPAR in Sc CA1 synapses, which works in conjunction with NMDAR to induce postsynaptic Ca^{2+} elevation in spines. Loss of AMPAR might have caused a reduction of Ca^{2+} in spines resulting in impaired t-LTP. A stronger STDP protocol that induced stronger NMDAR-mediated currents might have overcame the impact of AMPAR deficiency and therefore rescued the t-LTP deficit (Inglebert et al., 2024; Nevian and Sakmann, 2006) (Figure 1). In the hippocampus, at Sc-CA1 synapses, t-LTD has been described to required numerous molecular players to exist, such as calcium release from internal stores and mGluR5 activation, which are both disrupted in the absence of SP (Inglebert et al., 2024; Wu et al., 2024) (Figure 2). Since STDP can be induced at the single spine level by pairing glutamate uncaging with post-synaptic APs (Tazerart et al., 2020), it presents a compelling paradigm for studying the role of SP in morphological plasticity of dendritic spines. Remarkably, following glutamate uncaging on SP-positive spines, neighboring synapses demonstrate spine head shrinkage (Korkotian et al., 2014). *Could SP-positive spines influence neighboring spines more strongly or differently than SP-negative spines*? In support of this idea, after TBS-induced LTP, the vicinity of spines expressing sER formed larger clusters with an increased total synaptic weight. We believe that STDP provides an ideal framework for investigating both homo- and hetero-synaptic plasticity at the single-spine level, as it is highly dependent on

clustered dendritic spines. For example, t-LTP can be enhanced through the co-activation of closely clustered spines (within <5 μm) (Tazerart et al., 2020). The presence of SP in the spine could alter the rules of synaptic cooperation and is an interesting area for future studies. In addition, in some cases, STDP also necessitates activation of group 1 metabotropic glutamate receptors (Group I mGluRs), which we recently demonstrated to be down-regulated in SPKO mice (Speranza et al., 2022b; Wu et al., 2024).

Synaptopodin and calcium dynamics

SP/SA has long been identified as an important source of postsynaptic Ca^{2+} and regulates Ca^{2+} dynamics within spines. In fact, experiments involving glutamate uncaging at single spines have demonstrated that, regardless of spine shape, SP-positive spines exhibit stronger calcium transients compared to SP-negative spines (Korkotian and Segal, 2011; Korkotian et al., 2014). This elevated calcium signal likely originates from intracellular Ca^{2+} stored in the SA/sER, as the application of thapsigargin or cyclopiazonic, the sER calcium depletion agent, eliminates this difference. Specifically, RYR are considered key players in the release of Ca^{2+} from internal stores. Indeed, SP expression is correlated with the presence of RYR, and the specific application of caffeine, a RYR agonist, results in a greater Ca^{2+} increase in SP-positive spines (Vlachos et al., 2009; Segal et al., 2010). This Ca^{2+}-induced Ca^{2+}-release from internal stores has been shown important for structural plasticity as blocking the RYR or depleting the intracellular calcium store was shown to prevent the structural expansion and AMPAR accumulation in spines (Vlachos et al., 2009). In addition, blocking of RYR have been long shown to prevent the expression of different forms of LTP as well as NMDAR-LTD at Sc-CA1 synapses (Raymond and Redman, 2002; Mellentin et al., 2007; Grigoryan et al., 2012; Arias-Cavieres et al., 2018; Valdés-Undurraga et al., 2023). Similarly, t-LTP has been shown to require RYR signaling depending on the repeat number and frequency of the STDP stimulation (Cepeda-Prado et al., 2022). Furthermore, knocking down SP significantly reduces RYR-positive spines and prevents the accumulation of GLUA1 in spines (Vlachos et al., 2009). RYR are not the only molecular players expressed in the SA/sER that control calcium dynamics and affect plasticity. Inositol triphosphate receptor (IP3R) mediated Ca^{2+} transient was observed only in the SA/sER-containing spines, and is necessary for NMDAR-LTP/LTD as well as mGluR-LTD (Taufiq et al., 2005; Holbro et al., 2009; Yoshioka et al., 2010). In addition, store-operated calcium entry (SOCE) channels, Orai1/STIM1, which serve to replenish the Ca^{2+} stores when depleted, are also preferentially located in SP-positive spines and may contribute to the amplified calcium response in these SP-positive spines (Korkotian et al., 2014). Based on these experimental evidence, SP/SA plays a central role in regulating postsynaptic Ca^{2+} dynamics during activity. SP/SA-positive spines, where intracellular calcium signaling is present, appear to be the locus of expression for synaptic plasticity. The deficits in these different forms of Hebbian plasticity in SPKO that have been discussed earlier in this review can all be partially, if not completely, attributable to the impaired calcium signaling. Additionally, recent publications provided compelling evidence showing that postsynaptic calcium dynamics regulates local translation in a synaptic plasticity-specific manner, implying calcium as the central signaling molecule involved in the induction and maintenance of synaptic plasticity (Sun et al., 2021; Ramakrishna et al., 2024). This suggests that the protein synthesis pathways, which are implicated in many forms of Hebbian plasticity and often considered as an independent mechanism to the calcium signaling, are downstream effectors regulated by calcium dynamics. Based on this idea, SP/SA, the master switch of calcium in dendritic spines, would be the ultimate regulator of Hebbian plasticity. Moving forward, experiments combining calcium imaging and electrophysiology as well as biochemical analysis of calcium-dependent proteins are necessary to gain a better understanding of calcium dynamics and calcium signaling in SP-positive spines during the activity-dependent plasticity.

Synaptopodin and neuronal excitability

Synaptopodin is also expressed in the Axon Initial Segment (AIS), where action potentials are generated (Schlüter et al., 2019). Plasticity in the AIS serves as a powerful regulatory mechanism for neuronal excitability, as changes in morphology (*such as length and distance from the soma*) or ion channel expression can lead to increased or decreased excitability (Yamada and Kuba, 2016), directly affecting synaptic plasticity induction threshold. CA1 pyramidal neurons from 6-month-old SPKO mice show increased intrinsic excitability (measured by field potential recordings) and altered spike waveform properties (Aloni et al., 2021). However, the mechanisms underlying this increased excitability remain largely unknown. It is speculated that it may serve as a homeostatic compensatory mechanism to counteract reduced synaptic plasticity. Additionally, it is important to note that no study has thoroughly characterized the intrinsic excitability in SPKO mice, including parameters such as input–output curves or rheobase. Consequently, the impact of SP loss on intrinsic excitability remains uncertain. One possible explanation is that it directly influences the development of the AIS, as suggested by several studies. For instance, following LTP in hippocampal granule cells, AIS shortening is linked to a reduction in SP clusters (Jungenitz et al., 2023) and the absence of SP impairs the maturation of AIS length in the visual cortex (Schlüter et al., 2017). Furthermore, recent evidence suggests that the AIS can rapidly shorten following LTD in the hippocampus (Fréal et al., 2023), though the role of SP in this process remains unclear.

Synaptopodin in neurological disorders

While SP is heavily implicated in the cellular form of learning by mediating various forms of synaptic plasticity in brain, not much is known about SP role in the diseased state of the brain. Many neurodevelopmental and neurodegenerative disorders have been shown deficits in synaptic activities and plasticity (Usdin et al., 1999; Huber et al., 2002; Ma et al., 2010; Yoo et al., 2014; Chu, 2020). Recently, SP has been identified to be linked to autism spectrum disorder and regulates calcium dynamics as well as spine structural plasticity in a mouse model of autism (Hu et al., 2023). Furthermore, in a mouse model of Fragile X syndrome (FXS), which is the most prevalent form of intellectual disability and has enhanced mGluR-LTD,

SP was found upregulated in the dendritic spines, especially in the long thin type of immature spines that usually do not contain SP (Huber et al., 2002; Speranza et al., 2022a), As the presence of SP in spines enhance spine stability, the upregulation of SP in spines of FXS mouse model could explain the increase of in total and thin spine density in these mice (Comery et al., 1997; McKinney et al., 2005; Speranza et al., 2022a). Together with the deficit of mGluR-LTD in SPKO (Wu et al., 2024), this finding suggests that SP level requires precise regulation, too much or too little SP could both lead to abnormal synaptic plasticity and potentially neurological disorders. SP has been shown to be required for lesion-induced synaptic homeostatic changes following neuronal denervation, which is often resulted from demyelination, cells death and traumatic brain injury (Vlachos et al., 2013; Kruse et al., 2024). SP's ability to modulate calcium has been used to rescue Alzheimer's disease in mouse model. Aloni et al. (2019) has crossed SPKO mice with the 3xTg Alzheimer's mouse model in the attempt of rescuing the LTP deficit that was observed in the Alzheimer's mouse model. This was achieved by decreasing the intracellular calcium level that is elevated in the disease mouse model (Chakroborty et al., 2009). Not only did the LTP deficit was rescued, animal spatial learning was also improved in the crossed mice. Current data on SP involvement in diseases is only just beginning and is very limited, however current data suggests that SP has a significant clinical implication. Future studies on SP will reveal more exciting findings on the role of SP on memory formation and storage as well as its role in neurological diseases.

Concluding remark

This review highlighted the recent findings and discovery about SP's role in Hebbian synaptic plasticity. SP/SA, acting as the important source of Ca^{2+} in the postsynaptic compartment, regulates virtually all types of Hebbian plasticity. Increasing studies start to look at SP from different perspectives. Proteomic studies have identified novel binding partners of SP in spines, further delineating SP/SA function in spines (Falahati et al., 2022; Konietzny et al., 2023). Electrophysiological studies showed SP playing important roles in non-Hebbian plasticity as well (Vlachos et al., 2013; Dubes et al., 2022). A key question that has never been answered for SP is why it is only present in a subset of dendritic spines and what determines its presence in spines. Some may argue activity determines its presence in spines, but SP is also regulating the activity of the spines. Future studies are needed to identify the missing factor that determines the heterogeneous presence of SP in spines.

Author contributions

PW: Data curation, Investigation, Visualization, Writing – original draft, Writing – review & editing. YI: Conceptualization, Data curation, Visualization, Writing – original draft, Writing – review & editing. RM: Conceptualization, Funding acquisition, Resources, Supervision, Writing – original draft, Writing – review & editing.

Funding

The author(s) declare that financial support was received for the research, authorship, and/or publication of this article. This study was supported by Canadian Institutes of Health Research MOP 86724 to RM; NSERC Discovery RGPIN-2020-06373 to RM and the Norman Zavalkoff Family Foundation to RM; Richard and Edith Strauss Postdoctoral Fellowship in Medicine to YI.

Acknowledgments

We thank members of RM laboratories for comments on the manuscript. All figures are generated from Biorender.

Conflict of interest

The authors declare that the research was conducted in the absence of any commercial or financial relationships that could be construed as a potential conflict of interest.

Publisher's note

References

Aloni, E., Oni-Biton, E., Tsoory, M., Moallem, D. H., and Segal, M. (2019). Synaptopodin deficiency ameliorates symptoms in the 3xTg mouse model of Alzheimer's disease. *J. Neurosci.* 39, 3983–3992. doi: 10.1523/JNEUROSCI.2920-18.2019

Aloni, E., Verbitsky, S., Kushnireva, L., Korkotian, E., and Segal, M. (2021). Increased excitability of hippocampal neurons in mature synaptopodin-knockout mice. *Brain Struct. Funct.* 226, 2459–2466. doi: 10.1007/s00429-021-02346-0

Arias-Cavieres, A., Barrientos, G. C., Sánchez, G., Elgueta, C., Muñoz, P., and Hidalgo, C. (2018). Ryanodine receptor-mediated calcium release has a key role in hippocampal LTD induction. *Front. Cell. Neurosci.* 12:403. doi: 10.3389/fncel.2018.00403

Asanuma, K., Yanagida-Asanuma, E., Faul, C., Tomino, Y., Kim, K., and Mundel, P. (2006). Synaptopodin orchestrates actin organization and cell motility via regulation of RhoA signalling. *Nat. Cell Biol.* 8, 485–491. doi: 10.1038/ncb1400

Bi, G., and Poo, M. (1998). Synaptic modifications in cultured hippocampal neurons: dependence on spike timing, synaptic strength, and postsynaptic cell type. *J. Neurosci.* 18, 10464–10472. doi: 10.1523/JNEUROSCI.18-24-10464.1998

Biever, A., Glock, C., Tushev, G., Ciirdaeva, E., Dalmay, T., Langer, J. D., et al. (2020). Monosomes actively translate synaptic mRNAs in neuronal processes. *Science* 367:eaay4991. doi: 10.1126/science.aay4991

Bolshakov, V. Y., and Siegelbaum, S. A. (1994). Postsynaptic induction and presynaptic expression of hippocampal long-term depression. *Science* 264, 1148–1152. doi: 10.1126/science.7909958

Bosch, M., Castro, J., Saneyoshi, T., Matsuno, H., Sur, M., and Hayashi, Y. (2014). Structural and molecular remodeling of dendritic spine substructures during long-term potentiation. *Neuron* 82, 444–459. doi: 10.1016/j.neuron.2014.03.021

Bourne, J., and Harris, K. M. (2007). Do thin spines learn to be mushroom spines that remember? *Curr. Opin. Neurobiol.* 17, 381–386. doi: 10.1016/j.conb.2007.04.009

Brakeman, P. R., Lanahan, A. A., O'Brien, R., Roche, K., Barnes, C. A., Huganir, R. L., et al. (1997). Homer: a protein that selectively binds metabotropic glutamate receptors. *Nature* 386, 284–288. doi: 10.1038/386284a0

Buchs, P.-A., Stoppini, L., Párducz, A., Siklós, L., and Muller, D. (1994). A new cytochemical method for the ultrastructural localization of calcium in the central nervous system. *J. Neurosci. Methods* 54, 83–93. doi: 10.1016/0165-0270(94)90162-7

Caroni, P., Donato, F., and Muller, D. (2012). Structural plasticity upon learning: regulation and functions. *Nat. Rev. Neurosci.* 13, 478–490. doi: 10.1038/nrn3258

Cepeda-Prado, E. A., Khodaie, B., Quiceno, G. D., Beythien, S., Edelmann, E., and Lessmann, V. (2022). Calcium-permeable AMPA receptors mediate timing-dependent LTP elicited by low repeat coincident pre- and postsynaptic activity at Schaffer collateral-CA1 synapses. *Cereb. Cortex* 32, 1682–1703. doi: 10.1093/cercor/bhab306

Chakroborty, S., Goussakov, I., Miller, M. B., and Stutzmann, G. E. (2009). Deviant ryanodine receptor-mediated calcium release resets synaptic homeostasis in Presymptomatic 3xTg-AD mice. *J. Neurosci.* 29, 9458–9470. doi: 10.1523/JNEUROSCI.2047-09.2009

Chetkovich, D. M., and Sweatt, J. D. (1993). NMDA receptor activation increases cyclic AMP in area CA1 of the Hippocampus via calcium/calmodulin stimulation of adenylyl cyclase. *J. Neurochem.* 61, 1933–1942. doi: 10.1111/j.1471-4159.1993.tb09836.x

Chirillo, M. A., Waters, M. S., Lindsey, L. F., Bourne, J. N., and Harris, K. M. (2019). Local resources of polyribosomes and SER promote synapse enlargement and spine clustering after long-term potentiation in adult rat hippocampus. *Sci. Rep.* 9:3861. doi: 10.1038/s41598-019-40520-x

Chu, H.-Y. (2020). Synaptic and cellular plasticity in Parkinson's disease. *Acta Pharmacol. Sin.* 41, 447–452. doi: 10.1038/s41401-020-0371-0

Comery, T. A., Harris, J. B., Willems, P. J., Oostra, B. A., Irwin, S. A., Weiler, I. J., et al. (1997). Abnormal dendritic spines in fragile X knockout mice: maturation and pruning deficits. *Proc. Natl. Acad. Sci.* 94, 5401–5404. doi: 10.1073/pnas.94.10.5401

Czarnecki, K., Haas, C. A., Bas Orth, C., Deller, T., and Frotscher, M. (2005). Postnatal development of synaptopodin expression in the rodent hippocampus. *J. Comp. Neurol.* 490, 133–144. doi: 10.1002/cne.20651

De Roo, M., Klauser, P., and Muller, D. (2008). LTP promotes a selective long-term stabilization and clustering of dendritic spines. *PLoS Biol.* 6:e219. doi: 10.1371/journal.pbio.0060219

Debanne, D., Gähwiler, B. H., and Thompson, S. M. (1998). Long-term synaptic plasticity between pairs of individual CA3 pyramidal cells in rat hippocampal slice cultures. *J. Physiol.* 507, 237–247. doi: 10.1111/j.1469-7793.1998.237bu.x

Debanne, D., and Inglebert, Y. (2023). Spike timing-dependent plasticity and memory. *Curr. Opin. Neurobiol.* 80:102707. doi: 10.1016/j.conb.2023.102707

Deller, T., Korte, M., Chabanis, S., Drakew, A., Schwegler, H., Stefani, G. G., et al. (2003). Synaptopodin-deficient mice lack a spine apparatus and show deficits in synaptic plasticity. *Proc. Natl. Acad. Sci. USA* 100, 10494–10499. doi: 10.1073/pnas.1832384100

Deller, T., Mundel, P., and Frotscher, M. (2000). Potential role of synaptopodin in spine motility by coupling actin to the spine apparatus. *Hippocampus* 10, 569–581. doi: 10.1002/1098-1063(2000)10:5<569::AID-HIPO7>3.0.CO;2-M

Dubes, S., Soula, A., Benquet, S., Tessier, B., Poujol, C., Favereaux, A., et al. (2022). miR-124-dependent tagging of synapses by synaptopodin enables input-specific homeostatic plasticity. *EMBO J.* 41:e109012. doi: 10.15252/embj.2021109012

Dudek, S. M., and Bear, M. F. (1992). Homosynaptic long-term depression in area CA1 of hippocampus and effects of N-methyl-D-aspartate receptor blockade. *Proc. Natl. Acad. Sci. USA* 89, 4363–4367. doi: 10.1073/pnas.89.10.4363

Falahati, H., Wu, Y., Feuerer, V., Simon, H.-G., and De Camilli, P. (2022). Proximity proteomics of synaptopodin provides insight into the molecular composition of the spine apparatus of dendritic spines. *Proc. Natl. Acad. Sci.* 119:e2203750119. doi: 10.1073/pnas.2203750119

Faul, C., Donnelly, M., Merscher-Gomez, S., Chang, Y. H., Franz, S., Delfgaauw, J., et al. (2008). The actin cytoskeleton of kidney podocytes is a direct target of the antiproteinuric effect of cyclosporine a. *Nat. Med.* 14, 931–938. doi: 10.1038/nm.1857

Fréal, A., Jamann, N., Ten Bos, J., Jansen, J., Petersen, N., Ligthart, T., et al. (2023). Sodium channel endocytosis drives axon initial segment plasticity. *Sci. Adv.* 9:eadf3885. doi: 10.1126/sciadv.adf3885

Frotscher, M., Studer, D., Graber, W., Chai, X., Nestel, S., and Zhao, S. (2014). Fine structure of synapses on dendritic spines. *Front. Neuroanat.* 8:94. doi: 10.3389/fnana.2014.00094

Fukazawa, Y., Saitoh, Y., Ozawa, F., Ohta, Y., Mizuno, K., and Inokuchi, K. (2003). Hippocampal LTP is accompanied by enhanced F-actin content within the dendritic spine that is essential for late LTP maintenance in vivo. *Neuron* 38, 447–460. doi: 10.1016/S0896-6273(03)00206-X

Geinisman, Y., Berry, R. W., Disterhoft, J. F., Power, J. M., and Van der Zee, E. A. (2001). Associative learning elicits the formation of multiple-synapse boutons. *J. Neurosci.* 21, 5568–5573. doi: 10.1523/JNEUROSCI.21-15-05568.2001

Gray, E. G. (1959). Electron microscopy of synaptic contacts on dendrite spines of the cerebral cortex. *Nature* 183, 1592–1593. doi: 10.1038/1831592a0

Grigoryan, G., Korkotian, E., and Segal, M. (2012). Selective facilitation of LTP in the ventral hippocampus by calcium stores. *Hippocampus* 22, 1635–1644. doi: 10.1002/hipo.22000

Grigoryan, G., and Segal, M. (2016). Ryanodine-mediated conversion of STP to LTP is lacking in synaptopodin-deficient mice. *Brain Struct. Funct.* 221, 2393–2397. doi: 10.1007/s00429-015-1026-7

Harris, K. M. (2020). Structural LTP: from synaptogenesis to regulated synapse enlargement and clustering. *Curr. Opin. Neurobiol.* 63, 189–197. doi: 10.1016/j.conb.2020.04.009

Hering, H., and Sheng, M. (2001). Dendritic spines: structure, dynamics and regulation. *Nat Rev Neurosci* 2, 880–888. doi: 10.1038/35104061

Holbro, N., Grunditz, Å., and Oertner, T. G. (2009). Differential distribution of endoplasmic reticulum controls metabotropic signaling and plasticity at hippocampal synapses. *Proc. Natl. Acad. Sci. USA* 106, 15055–15060. doi: 10.1073/pnas.0905110106

Holtmaat, A., and Svoboda, K. (2009). Experience-dependent structural synaptic plasticity in the mammalian brain. *Nat. Rev. Neurosci.* 10, 647–658. doi: 10.1038/nrn2699

Hu, H.-T., Lin, Y.-J., Wang, U.-T. T., Lee, S.-P., Liou, Y.-H., Chen, B.-C., et al. (2023). Autism-related KLHL17 and SYNPO act in concert to control activity-dependent dendritic spine enlargement and the spine apparatus. *PLoS Biol.* 21:e3002274. doi: 10.1371/journal.pbio.3002274

Huang, W., Zhu, P. J., Zhang, S., Zhou, H., Stoica, L., Galiano, M., et al. (2013). mTORC2 controls actin polymerization required for consolidation of long-term memory. *Nat. Neurosci.* 16, 441–448. doi: 10.1038/nn.3351

Huber, K. M., Gallagher, S. M., Warren, S. T., and Bear, M. F. (2002). Altered synaptic plasticity in a mouse model of fragile X mental retardation. *Proc. Natl. Acad. Sci.* 99, 7746–7750. doi: 10.1073/pnas.122205699

Huber, K. M., Klann, E., Costa-Mattioli, M., and Zukin, R. S. (2015). Dysregulation of mammalian target of rapamycin signaling in mouse models of autism. *J. Neurosci.* 35, 13836–13842. doi: 10.1523/JNEUROSCI.2656-15.2015

Inglebert, Y., Wu, P. Y., Tourbina-Kolomiets, J., Dang, C. L., and McKinney, R. A. (2024). Synaptopodin is required for long-term depression at Schaffer collateral-CA1 synapses. *Mol. Brain* 17:17. doi: 10.1186/s13041-024-01089-3

Jedlicka, P., and Deller, T. (2017). Understanding the role of synaptopodin and the spine apparatus in Hebbian synaptic plasticity – new perspectives and the need for computational modeling. *Neurobiol. Learn. Mem.* 138, 21–30. doi: 10.1016/j.nlm.2016.07.023

Jedlicka, P., Schwarzacher, S. W., Winkels, R., Kienzler, F., Frotscher, M., Bramham, C. R., et al. (2009). Impairment of in vivo theta-burst long-term potentiation and network excitability in the dentate gyrus of synaptopodin-deficient mice lacking the spine apparatus and the cisternal organelle. *Hippocampus* 19, 130–140. doi: 10.1002/hipo.20489

Jedlicka, P., Vlachos, A., Schwarzacher, S. W., and Deller, T. (2008). A role for the spine apparatus in LTP and spatial learning. *Behav. Brain Res.* 192, 12–19. doi: 10.1016/j.bbr.2008.02.033

Jungenitz, T., Bird, A., Engelhardt, M., Jedlicka, P., Schwarzacher, S. W., and Deller, T. (2023). Structural plasticity of the axon initial segment in rat hippocampal granule cells following high frequency stimulation and LTP induction. *Front. Neuroanat.* 17:5623. doi: 10.3389/fnana.2023.1125623

Kasai, H., Ziv, N. E., Okazaki, H., Yagishita, S., and Toyoizumi, T. (2021). Spine dynamics in the brain, mental disorders and artificial neural networks. *Nat. Rev. Neurosci.* 22, 407–422. doi: 10.1038/s41583-021-00467-3

Kelleher, R. J., Govindarajan, A., and Tonegawa, S. (2004). Translational regulatory mechanisms in persistent forms of synaptic plasticity. *Neuron* 44, 59–73. doi: 10.1016/j.neuron.2004.09.013

Konietzny, A., González-Gallego, J., Bär, J., Perez-Alvarez, A., Drakew, A., Demmers, J. A. A., et al. (2019). Myosin V regulates synaptopodin clustering and localization in the dendrites of hippocampal neurons. *J. Cell Sci.* 132:jcs230177. doi: 10.1242/jcs.230177

Konietzny, A., Wegmann, S., and Mikhaylova, M. (2023). The endoplasmic reticulum puts a new spin on synaptic tagging. *Trends Neurosci.* 46, 32–44. doi: 10.1016/j.tins.2022.10.012

Korkotian, E., Frotscher, M., and Segal, M. (2014). Synaptopodin regulates spine plasticity: mediation by calcium stores. *J. Neurosci.* 34, 11641–11651. doi: 10.1523/JNEUROSCI.0381-14.2014

Korkotian, E., and Segal, M. (2011). Synaptopodin regulates release of calcium from stores in dendritic spines of cultured hippocampal neurons. *J. Physiol.* 589, 5987–5995. doi: 10.1113/jphysiol.2011.217315

Kruse, P., Brandes, G., Hemeling, H., Huang, Z., Wrede, C., Hegermann, J., et al. (2024). Synaptopodin regulates denervation-induced plasticity at hippocampal mossy Fiber synapses. *Cells* 13:114. doi: 10.3390/cells13020114

Lüscher, C., and Huber, K. M. (2010). Group 1 mGluR-dependent synaptic long-term depression: mechanisms and implications for circuitry and disease. *Neuron* 65, 445–459. doi: 10.1016/j.neuron.2010.01.016

Lüscher, C., and Malenka, R. C. (2012). NMDA receptor-dependent long-term potentiation and long-term depression (LTP/LTD). *Cold Spring Harb. Perspect. Biol.* 4:a005710. doi: 10.1101/cshperspect.a005710

Ma, T., Hoeffer, C. A., Capetillo-Zarate, E., Yu, F., Wong, H., Lin, M. T., et al. (2010). Dysregulation of the mTOR pathway mediates impairment of synaptic plasticity in a mouse model of Alzheimer's disease. *PLoS One* 5:e12845. doi: 10.1371/journal.pone.0012845

Ma, S., and Zuo, Y. (2022). Synaptic modifications in learning and memory – a dendritic spine story. *Semin. Cell Dev. Biol.* 125, 84–90. doi: 10.1016/j.semcdb.2021.05.015

McCann, R. F., and Ross, D. A. (2017). A fragile balance: dendritic spines, learning, and memory. *Biol. Psychiatry* 82, e11–e13. doi: 10.1016/j.biopsych.2017.05.020

McKinney, R. A. (2010). Excitatory amino acid involvement in dendritic spine formation, maintenance and remodelling. *J. Physiol.* 588, 107–116. doi: 10.1113/jphysiol.2009.178905

McKinney, B. C., Grossman, A. W., Elisseou, N. M., and Greenough, W. T. (2005). Dendritic spine abnormalities in the occipital cortex of C57BL/6 Fmr1 knockout mice. *Am. J. Med. Genet. B Neuropsychiatr. Genet.* 136B, 98–102. doi: 10.1002/ajmg.b.30183

Mellentin, C., Jahnsen, H., and Abraham, W. C. (2007). Priming of long-term potentiation mediated by ryanodine receptor activation in rat hippocampal slices. *Neuropharmacology* 52, 118–125. doi: 10.1016/j.neuropharm.2006.07.009

Miyata, M., Finch, E. A., Khiroug, L., Hashimoto, K., Hayasaka, S., Oda, S.-I., et al. (2000). Local calcium release in dendritic spines required for long-term synaptic depression. *Neuron* 28, 233–244. doi: 10.1016/S0896-6273(00)00099-4

Mundel, P., Heid, H. W., Mundel, T. M., Krüger, M., Reiser, J., and Kriz, W. (1997). Synaptopodin: an actin-associated protein in Telencephalic dendrites and renal podocytes. *J. Cell Biol.* 139, 193–204. doi: 10.1083/jcb.139.1.193

Nägerl, U. V., Eberhorn, N., Cambridge, S. B., and Bonhoeffer, T. (2004). Bidirectional activity-dependent morphological plasticity in hippocampal neurons. *Neuron* 44, 759–767. doi: 10.1016/j.neuron.2004.11.016

Nakahata, Y., and Yasuda, R. (2018). Plasticity of spine structure: local signaling, translation and cytoskeletal reorganization. *Front Synaptic Neurosci* 10:29. doi: 10.3389/fnsyn.2018.00029

Nevian, T., and Sakmann, B. (2006). Spine Ca^{2+} signaling in spike-timing-dependent plasticity. *J. Neurosci.* 26, 11001–11013. doi: 10.1523/JNEUROSCI.1749-06.2006

Nimchinsky, E. A., Sabatini, B. L., and Svoboda, K. (2002). Structure and function of dendritic spines. *Annu. Rev. Physiol.* 64, 313–353. doi: 10.1146/annurev.physiol.64.081501.160008

Nosyreva, E. D., and Huber, K. M. (2005). Developmental switch in synaptic mechanisms of hippocampal metabotropic glutamate receptor-dependent long-term depression. *J. Neurosci.* 25, 2992–3001. doi: 10.1523/JNEUROSCI.3652-04.2005

Nusser, Z., Lujan, R., Laube, G., Roberts, J. D. B., Molnar, E., and Somogyi, P. (1998). Cell type and pathway dependence of synaptic AMPA receptor number and variability in the Hippocampus. *Neuron* 21, 545–559. doi: 10.1016/S0896-6273(00)80565-6

Oh, W. C., Hill, T. C., and Zito, K. (2013). Synapse-specific and size-dependent mechanisms of spine structural plasticity accompanying synaptic weakening. *Proc. Natl. Acad. Sci. USA* 110, E305–E312. doi: 10.1073/pnas.1214705110

Okubo-Suzuki, R., Okada, D., Sekiguchi, M., and Inokuchi, K. (2008). Synaptopodin maintains the neural activity-dependent enlargement of dendritic spines in hippocampal neurons. *Mol. Cell. Neurosci.* 38, 266–276. doi: 10.1016/j.mcn.2008.03.001

Oliet, S. H. R., Malenka, R. C., and Nicoll, R. A. (1997). Two distinct forms of long-term depression coexist in CA1 hippocampal pyramidal cells. *Neuron* 18, 969–982. doi: 10.1016/S0896-6273(00)80336-0

Ostroff, L. E., Cain, C. K., Bedont, J., Monfils, M. H., and LeDoux, J. E. (2010). Fear and safety learning differentially affect synapse size and dendritic translation in the lateral amygdala. *Proc. Natl. Acad. Sci.* 107, 9418–9423. doi: 10.1073/pnas.0913384107

Otani, S., Marshall, C. J., Tate, W. P., Goddard, G. V., and Abraham, W. C. (1989). Maintenance of long-term potentiation in rat dentate gyrus requires protein synthesis but not messenger RNA synthesis immediately post-tetanization. *Neuroscience* 28, 519–526. doi: 10.1016/0306-4522(89)90001-8

Palmer, M. J., Irving, A. J., Seabrook, G. R., Jane, D. E., and Collingridge, G. L. (1997). The group I mGlu receptor agonist DHPG induces a novel form of LTD in the CA1 region of the hippocampus. *Neuropharmacology* 36, 1517–1532. doi: 10.1016/S0028-3908(97)00181-0

Papa, M., Bundman, M., Greenberger, V., and Segal, M. (1995). Morphological analysis of dendritic spine development in primary cultures of hippocampal neurons. *J. Neurosci.* 15, 1–11. doi: 10.1523/JNEUROSCI.15-01-00001.1995

Pchitskaya, E., and Bezprozvanny, I. (2020). Dendritic spines shape analysis—classification or Clusterization? Perspective. *Front. Synaptic Neurosci.* 12:31. doi: 10.3389/fnsyn.2020.00031

Perez-Alvarez, A., Yin, S., Schulze, C., Hammer, J. A., Wagner, W., and Oertner, T. G. (2020). Endoplasmic reticulum visits highly active spines and prevents runaway potentiation of synapses. *Nat. Commun.* 11:5083. doi: 10.1038/s41467-020-18889-5

Pierce, J. P., van Leyen, K., and McCarthy, J. B. (2000). Translocation machinery for synthesis of integral membrane and secretory proteins in dendritic spines. *Nat. Neurosci.* 3, 311–313. doi: 10.1038/73868

Racca, C., Stephenson, F. A., Streit, P., Roberts, J. D. B., and Somogyi, P. (2000). NMDA receptor content of synapses in stratum Radiatum of the hippocampal CA1 area. *J. Neurosci.* 20, 2512–2522. doi: 10.1523/JNEUROSCI.20-07-02512.2000

Ramakrishna, S., Radhakrishna, B. K., Kaladiyil, A. P., Shah, N. M., Basavaraju, N., Freude, K. K., et al. (2024). Distinct calcium sources regulate temporal profiles of NMDAR and mGluR-mediated protein synthesis. *Life Sci. Allian.* 7:e202402594. doi: 10.26508/lsa.202402594

Ramiro-Cortés, Y., and Israely, I. (2013). Long lasting protein synthesis- and activity-dependent spine shrinkage and elimination after synaptic depression. *PLoS One* 8:e71155. doi: 10.1371/journal.pone.0071155

Raymond, C. R., and Redman, S. J. (2002). Different calcium sources are narrowly tuned to the induction of different forms of LTP. *J. Neurophysiol.* 88, 249–255. doi: 10.1152/jn.2002.88.1.249

Raymond, C. R., Thompson, V. L., Tate, W. P., and Abraham, W. C. (2000). Metabotropic glutamate receptors trigger homosynaptic protein synthesis to prolong long-term potentiation. *J. Neurosci.* 20, 969–976. doi: 10.1523/JNEUROSCI.20-03-00969.2000

Rochefort, N. L., and Konnerth, A. (2012). Dendritic spines: from structure to in vivo function. *EMBO Rep.* 13, 699–708. doi: 10.1038/embor.2012.102

Rosado, J., Bui, V. D., Haas, C. A., Beck, J., Queisser, G., and Vlachos, A. (2022). Calcium modeling of spine apparatus-containing human dendritic spines demonstrates an "all-or-nothing" communication switch between the spine head and dendrite. *PLoS Comput. Biol.* 18:e1010069. doi: 10.1371/journal.pcbi.1010069

Runge, K., Cardoso, C., and de Chevigny, A. (2020). Dendritic spine plasticity: function and mechanisms. *Front. Synaptic Neurosci.* 12:36. doi: 10.3389/fnsyn.2020.00036

Sanderson, T. M., Ralph, L. T., Amici, M., Ng, A. N., Kaang, B.-K., Zhuo, M., et al. (2022). Selective recruitment of presynaptic and postsynaptic forms of mGluR-LTD. *Front. Synaptic Neurosci.* 14:7675. doi: 10.3389/fnsyn.2022.857675

Schlüter, A., Del Turco, D., Deller, T., Gutzmann, A., Schultz, C., and Engelhardt, M. (2017). Structural plasticity of Synaptopodin in the axon initial segment during visual cortex development. *Cereb. Cortex* 27, 4662–4675. doi: 10.1093/cercor/bhx208

Schlüter, A., Rossberger, S., Dannehl, D., Janssen, J. M., Vorwald, S., Hanne, J., et al. (2019). Dynamic regulation of Synaptopodin and the axon initial segment in retinal ganglion cells during postnatal development. *Front. Cell. Neurosci.* 13:318. doi: 10.3389/fncel.2019.00318

Segal, M., Vlachos, A., and Korkotian, E. (2010). The spine apparatus, Synaptopodin, and dendritic spine plasticity. *Neuroscientist* 16, 125–131. doi: 10.1177/1073858409355829

Špaček, J. (1985). Three-dimensional analysis of dendritic spines. *Anat. Embryol.* 171, 235–243. doi: 10.1007/BF00341418

Spacek, J., and Harris, K. M. (1997). Three-dimensional Organization of Smooth Endoplasmic Reticulum in hippocampal CA1 dendrites and dendritic spines of the immature and mature rat. *J. Neurosci.* 17, 190–203. doi: 10.1523/JNEUROSCI.17-01-00190.1997

Speranza, L., Filiz, K. D., Goebel, S., Perrone-Capano, C., Pulcrano, S., Volpicelli, F., et al. (2022a). Combined DiI and antibody labeling reveals complex dysgenesis of hippocampal dendritic spines in a mouse model of fragile X syndrome. *Biomedicines* 10:2692. doi: 10.3390/biomedicines10112692

Speranza, L., Inglebert, Y., De Sanctis, C., Wu, P. Y., Kalinowska, M., McKinney, R. A., et al. (2022b). Stabilization of spine Synaptopodin by mGluR1 is required for mGluR-LTD. *J. Neurosci.* 42, 1666–1678. doi: 10.1523/JNEUROSCI.1466-21.2022

Stein, I. S., and Zito, K. (2019). Dendritic spine elimination: molecular mechanisms and implications. *Neuroscientist* 25, 27–47. doi: 10.1177/1073858418769644

Sun, C., Nold, A., Fusco, C. M., Rangaraju, V., Tchumatchenko, T., Heilemann, M., et al. (2021). The prevalence and specificity of local protein synthesis during neuronal synaptic plasticity. *Science. Advances* 7:eabj0790. doi: 10.1126/sciadv.abj0790

Szepesi, Z., Hosy, E., Ruszczycki, B., Bijata, M., Pyskaty, M., Bikbaev, A., et al. (2014). Synaptically released matrix metalloproteinase activity in control of structural plasticity and the cell surface distribution of GluA1-AMPA receptors. *PLoS One* 9:e98274. doi: 10.1371/journal.pone.0098274

Takei, N., and Nawa, H. (2014). mTOR signaling and its roles in normal and abnormal brain development. *Front. Mol. Neurosci.* 7:28. doi: 10.3389/fnmol.2014.00028

Taufiq, A. M., Fujii, S., Yamazaki, Y., Sasaki, H., Kaneko, K., Li, J., et al. (2005). Involvement of IP3 receptors in LTP and LTD induction in guinea pig hippocampal CA1 neurons. *Learn. Mem.* 12, 594–600. doi: 10.1101/lm.17405

Tazerart, S., Mitchell, D. E., Miranda-Rottmann, S., and Araya, R. (2020). A spike-timing-dependent plasticity rule for dendritic spines. *Nat. Commun.* 11:4276. doi: 10.1038/s41467-020-17861-7

Thomazeau, A., Bosch, M., Essayan-Perez, S., Barnes, S. A., De Jesus-Cortes, H., and Bear, M. F. (2021). Dissociation of functional and structural plasticity of dendritic spines during NMDAR and mGluR-dependent long-term synaptic depression in wild-type and fragile X model mice. *Mol. Psychiatry* 26, 4652–4669. doi: 10.1038/s41380-020-0821-6

Toni, N., Buchs, P.-A., Nikonenko, I., Povilaitite, P., Parisi, L., and Muller, D. (2001). Remodeling of synaptic membranes after induction of long-term potentiation. *J. Neurosci.* 21, 6245–6251. doi: 10.1523/JNEUROSCI.21-16-06245.2001

Usdin, M. T., Shelbourne, P. F., Myers, R. M., and Madison, D. V. (1999). Impaired synaptic plasticity in mice carrying the Huntington's disease mutation. *Hum. Mol. Genet.* 8, 839–846. doi: 10.1093/hmg/8.5.839

Valdés-Undurraga, I., Lobos, P., Sánchez-Robledo, V., Arias-Cavieres, A., SanMartín, C. D., Barrientos, G., et al. (2023). Long-term potentiation and spatial memory training stimulate the hippocampal expression of RyR2 calcium release channels. *Front. Cell. Neurosci.* 17:1132121. doi: 10.3389/fncel.2023.1132121

Verbich, D., Becker, D., Vlachos, A., Mundel, P., Deller, T., and McKinney, R. A. (2016). Rewiring neuronal microcircuits of the brain via spine head protrusions-a role for synaptopodin and intracellular calcium stores. *Acta Neuropathol. Commun.* 4:38. doi: 10.1186/s40478-016-0311-x

Vlachos, A., Ikenberg, B., Lenz, M., Becker, D., Reifenberg, K., Bas-Orth, C., et al. (2013). Synaptopodin regulates denervation-induced homeostatic synaptic plasticity. *Proc. Natl. Acad. Sci.* 110, 8242–8247. doi: 10.1073/pnas.1213677110

Vlachos, A., Korkotian, E., Schonfeld, E., Copanaki, E., Deller, T., and Segal, M. (2009). Synaptopodin regulates plasticity of dendritic spines in hippocampal neurons. *J. Neurosci.* 29, 1017–1033. doi: 10.1523/JNEUROSCI.5528-08.2009

Vlachos, A., Maggio, N., and Segal, M. (2008). Lack of correlation between synaptopodin expression and the ability to induce LTP in the rat dorsal and ventral hippocampus. *Hippocampus* 18, 1–4. doi: 10.1002/hipo.20373

Volk, L. J., Daly, C. A., and Huber, K. M. (2006). Differential roles for group 1 mGluR subtypes in induction and expression of chemically induced hippocampal long-term depression. *J. Neurophysiol.* 95, 2427–2438. doi: 10.1152/jn.00383.2005

von Bohlen und Halbach, O. (2009). Structure and function of dendritic spines within the hippocampus. *Ann. Anat.* 191, 518–531. doi: 10.1016/j.aanat.2009.08.006

Waung, M. W., and Huber, K. M. (2009). Protein translation in synaptic plasticity: mGluR-LTD, fragile X. *Curr. Opin. Neurobiol.* 19, 319–326. doi: 10.1016/j.conb.2009.03.011

Wu, P. Y., Ji, L., De Sanctis, C., Francesconi, A., Inglebert, Y., and McKinney, R. A. (2024). Loss of synaptopodin impairs mGluR5 and protein synthesis–dependent mGluR-LTD at CA3-CA1 synapses. *PNAS Nexus* 3:pgae062. doi: 10.1093/pnasnexus/pgae062

Yamada, R., and Kuba, H. (2016). Structural and functional plasticity at the axon initial segment. *Front. Cell. Neurosci.* 10:250. doi: 10.3389/fncel.2016.00250

Yamazaki, M., Matsuo, R., Fukazawa, Y., Ozawa, F., and Inokuchi, K. (2001). Regulated expression of an actin-associated protein, synaptopodin, during long-term potentiation. *J. Neurochem.* 79, 192–199. doi: 10.1046/j.1471-4159.2001.00552.x

Yap, K., Drakew, A., Smilovic, D., Rietsche, M., Paul, M. H., Vuksic, M., et al. (2020). The actin-modulating protein synaptopodin mediates long-term survival of dendritic spines. *eLife* 9:e62944. doi: 10.7554/eLife.62944

Yasuda, H., Barth, A. L., Stellwagen, D., and Malenka, R. C. (2003). A developmental switch in the signaling cascades for LTP induction. *Nat. Neurosci.* 6, 15–16. doi: 10.1038/nn985

Yoo, J., Bakes, J., Bradley, C., Collingridge, G. L., and Kaang, B.-K. (2014). Shank mutant mice as an animal model of autism. *Philos. Trans. R. Soc. Lond. Ser. B Biol. Sci.* 369:20130143. doi: 10.1098/rstb.2013.0143

Yoshioka, M., Yamazaki, Y., Fujii, S., Kaneko, K., Kato, H., and Mikoshiba, K. (2010). Intracellular calcium ion dynamics involved in long-term potentiation in hippocampal CA1 neurons in mice lacking the IP3 type 1 receptor. *Neurosci. Res.* 67, 149–155. doi: 10.1016/j.neures.2010.03.002

Zhang, X., Poschel, B., Faul, C., Upreti, C., Stanton, P. K., and Mundel, P. (2013). Essential role for Synaptopodin in dendritic spine plasticity of the developing Hippocampus. *J. Neurosci.* 33, 12510–12518. doi: 10.1523/JNEUROSCI.2983-12.2013

Zhou, Q., Homma, K. J., and Poo, M. (2004). Shrinkage of dendritic spines associated with long-term depression of hippocampal synapses. *Neuron* 44, 749–757. doi: 10.1016/j.neuron.2004.11.011

Zhu, P. J., Chen, C.-J., Mays, J., Stoica, L., and Costa-Mattioli, M. (2018). mTORC2, but not mTORC1, is required for hippocampal mGluR-LTD and associated behaviors. *Nat. Neurosci.* 21, 799–802. doi: 10.1038/s41593-018-0156-7

frontiers | Frontiers in Cellular Neuroscience

TYPE Opinion
PUBLISHED 20 December 2024
DOI 10.3389/fncel.2024.1513602

OPEN ACCESS

EDITED BY
Arianna Maffei,
Stony Brook University, United States

REVIEWED BY
Chiayu Chiu,
Universidad de Valparaíso, Chile
Joanna Urban-Ciecko,
Polish Academy of Sciences, Poland
Gergely Katona,
Hungarian Academy of Sciences (MTA), Hungary

*CORRESPONDENCE
Andrea Barberis
✉ andrea.barberis@iit.it

RECEIVED 18 October 2024
ACCEPTED 03 December 2024
PUBLISHED 20 December 2024

CITATION
Cupolillo D, Regio V and Barberis A (2024) Synaptic microarchitecture: the role of spatial interplay between excitatory and inhibitory inputs in shaping dendritic plasticity and neuronal output.
Front. Cell. Neurosci. 18:1513602.
doi: 10.3389/fncel.2024.1513602

Synaptic microarchitecture: the role of spatial interplay between excitatory and inhibitory inputs in shaping dendritic plasticity and neuronal output

Dario Cupolillo, Vincenzo Regio and Andrea Barberis*

Istituto Italiano di Tecnologia, Synaptic Plasticity of Inhibitory Networks, Genova, Italy

KEYWORDS

excitatory synapses, inhibitory synapses, dendritic integration, dendritic spikes, heterosynaptic plasticity, dendritic modeling, pyramidal neurons, interneurons

Introduction

Pyramidal neurons (PNs) receive and integrate 1,000's of synaptic inputs impinging onto their dendritic arbor to shape the neuronal output. The richness and the complexity of such input-output transformation primarily relies on the ability of neurons to generate different forms of dendritic local spikes, regenerative events originating in the dendrites profoundly influencing the probability and the temporal structure of somatic spiking. Extensive work during the last two decades has identified the impact of clustering and cooperative plasticity among glutamatergic synapse in promoting dendritic spikes. However, the role of inhibitory synapses in such processes remains elusive. In this opinion paper, following a general introduction on the impact of the synaptic input spatial distribution in neuronal activity, we highlight the coordinated plasticity of excitatory and inhibitory dendritic synapses as an emerging key factor in the organization of the dendritic input architecture. In particular we will emphasize that the relative positioning of diverse excitatory and inhibitory dendritic synapses at the microscale level is a major determinant for shaping dendritic dynamics and neuronal circuit function in the brain.

Multiscale spatial arrangement of dendritic excitatory or inhibitory synaptic inputs

In different brain areas, distinct synaptic inputs converging onto PNs show a macro-scale distribution across large dendritic compartments. For instance, in the hippocampal formation, excitatory fibers from entorhinal cortex (EC) project to the distal portions of apical dendrites of CA1 PNs through the perforant path (PP), while Schaffer collaterals (SCs) from the CA3 area mainly contact the proximal dendrites (Megías et al., 2001; Figure 1). Similarly, in the neocortex, intra-cortical layer 2/3 (L2/3) PNs axons (feedforward information) contact the proximal dendrites of layer 5 (L5) PNs, with cortico-cortical inputs from high-order cortical areas (feedback information) targeting their distal dendrites (Larkum, 2012). This illustrates a large-scale connectivity scheme wherein fibers from either distant or local brain regions preferentially contact distal or proximal dendrites, respectively (Felleman and Van Essen, 1991). Such broad-scale input organization reflects important functional properties where the activation of proximal dendrites typically

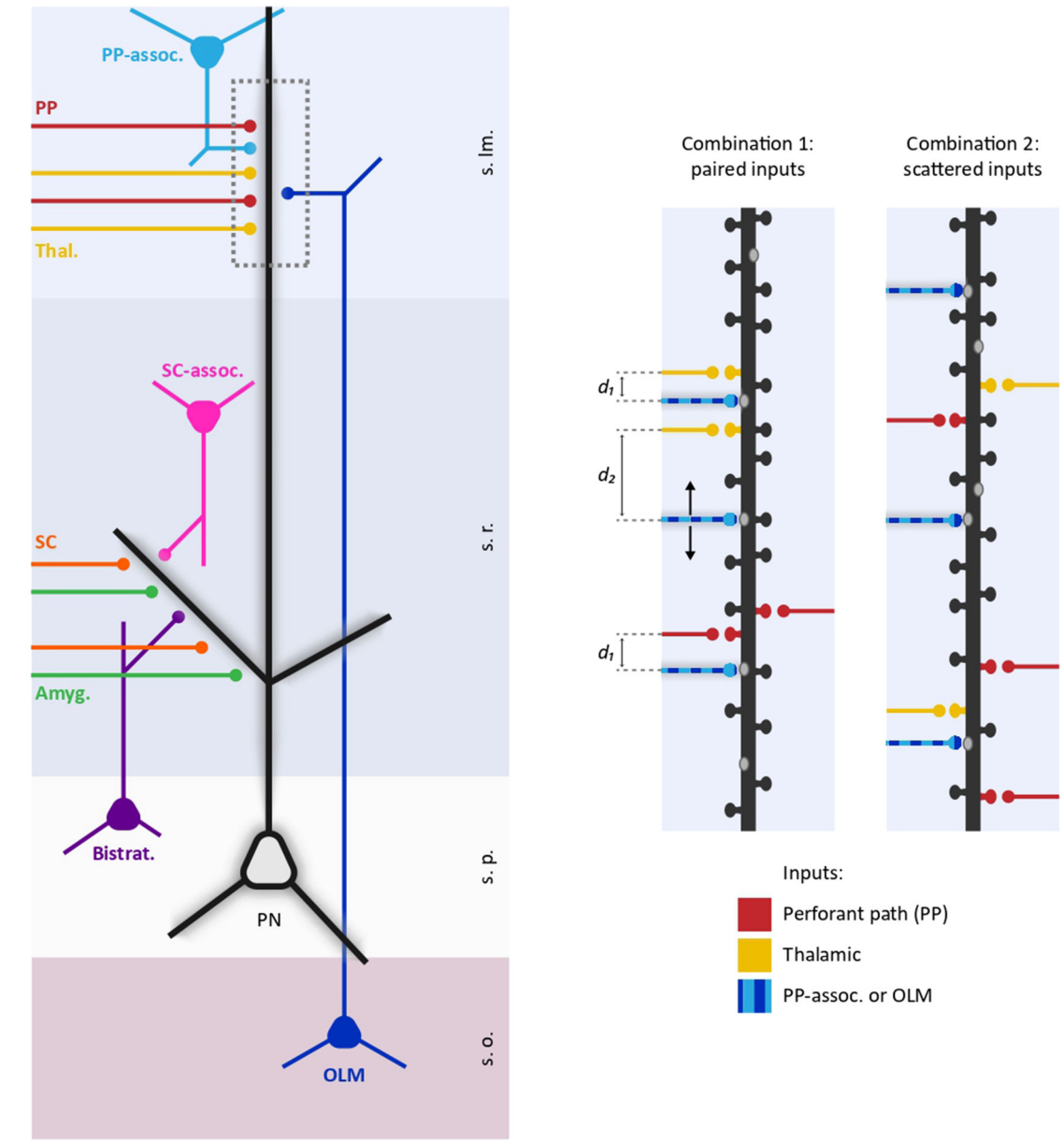

FIGURE 1
Schematic representation of proximo-distal dendritic compartmentalization of diverse GABAergic and glutamatergic inputs on a CA1 pyramidal neuron. **(A)** Representative selection of excitatory and inhibitory inputs received by CA1 dendrites. Specific subsets of excitatory inputs are aligned with distinct GABAergic fibers. Proximal dendrites in the stratum radiatum are targeted by SC (orange), amygdala projections (green), as well as local SC-associated interneurons (pink) and bistratified interneurons (purple). In contrast, distal dendrites in the stratum lacunosum moleculare receive inputs from the thalamus (yellow), the EC through the PP (red), O-LM interneurons (dark blue), and PP-associated interneurons (light blue). Dashed box delineates a distal dendritic portion represented in **(B)**. **(B)** Two different possible spatial arrangements of excitatory and inhibitory inputs on a distal dendritic segment. **(Left)** GABAergic inputs from either O-LM or PP-associated interneurons (striped light-dark blue) are positioned within an "interplay range" with thalamic or PP inputs (d1) or located beyond this range (d2). This points to the existence of excitatory-inhibitory spatial combinations, wherein certain inhibitory inputs consistently spatially paired with specific subsets of glutamatergic inputs. **(Right)** Excitatory and inhibitory inputs are randomly distributed along a dendritic segment. In this spatial arrangement, there are no consistent rules determining the pairing of specific GABAergic and glutamatergic inputs at the microscale level (s.o., stratum oriens; s.p., stratum pyramidale; s.r., stratum radiatum; s.lm., stratum lacunosum moleculare; PP, perforant path; SC, Scaffer Collaterals; Thal, Thalamic; Amyg, Amygdala).

produces single action potentials while co-activation of distal and proximal synaptic inputs can generate calcium plateau potentials—specific forms of dendritic spikes initiated in the distal dendritic region—leading the neuron to burst firing (Jarsky et al., 2005; Takahashi and Magee, 2009; Larkum et al., 1999). This supra-linear integration provides the biophysical basis for a fundamental associative process to combine and compare different types of information at the single cell level (Bittner et al., 2015; Larkum, 2012). Along the same line, the differential effect of distal feedforward inputs triggering single spikes and the combined activation of feedforward and distal feedback inputs inducing burst firing, provides the opportunity for the independent transmission of these two distinct signals through the same neuronal pathway (multiplexing; Naud and Sprekeler, 2017).

Intriguingly, GABAergic inputs are also non-randomly distributed along the axo-dendritic axis of PNs. Diverse subclasses of GABAergic interneurons (INs) target specific sub-regions of PNs including axon initial segment, soma, proximal dendrites and distal dendrites, with a specific temporal activation critically contributing to e.g., brain oscillations (Klausberger and Somogyi, 2007; Tzilivaki et al., 2023). In both hippocampus and neocortex, the proximo-distal dendritic compartmentalization of diverse GABAergic inputs creates a spatial pattern where distinct GABAergic fibers broadly align with specific subsets of excitatory inputs. For example, in the hippocampus, oriens-lacunosum-moleculare (O-LM), neurogliaform, and perforant path (PP)-associated INs target the distal dendrites of CA1 pyramidal neurons aligning with PP inputs from the EC. Comparably, bistratified, SC-associated and Ivy interneurons match glutamatergic inputs from CA3 onto proximal dendrites (Klausberger, 2009; Lovett-Barron et al., 2012; Figure 1).

The existence of structured patterns of synaptic inputs localization persists at smaller scales. At glutamatergic side, computational and experimental works showed that dendritic synaptic inputs clustering favors dendritic spikes initiation (Mel, 1993; Poirazi and Mel, 2001; Poirazi et al., 2003a,b; Larkum et al., 2009). In L5 PNs, for instance the activation of glutamatergic inputs within a $\sim 40\,\mu m$ range undergo supra-linear summation due to N-methyl-D-aspartate (NMDA) receptor-dependent regenerative mechanism, whereas inputs more than $80\,\mu m$ apart integrate linearly, indicating the key role of the spatial determinants in dendritic input summation (Polsky et al., 2004). The functional clustering of glutamatergic inputs has been observed directly in dendrites of both CA3 and L2/3 PNs, where spontaneous activity is more likely to co-activate neighboring glutamatergic spines rather than distant spines, thus forming glutamatergic synaptic "assemblets" within $\sim 10\,\mu m$ (Takahashi et al., 2012). The clustered organization of glutamatergic inputs underpins an important role at the functional level. In the visual cortex, the clustering of similarly tuned inputs aids edge detection and contour integration (Iacaruso et al., 2017), while in the motor cortex, task-related inputs cluster within $10\,\mu m$ subdomains to support decision-making (Kerlin et al., 2019). Besides the relevance of the tight spatial proximity between active glutamatergic synapses (*synaptic clustering*), the initiation of dendritic spikes strongly depends on the dendritic morphology. In thin and short dendritic branches, the high input resistance determines low attenuation of the depolarization produced by individual synapses thus promoting the signal summation within the branch (Kastellakis and Poirazi, 2019). For instance, the timely activation of ~ 20 glutamatergic inputs on a radial oblique dendritic branch of $100\,\mu m$ in CA1 PNs initiate a local sodium spike regardless of their spatial relationship along the branch, thus determining *in-branch clustering* (Losonczy and Magee, 2006). Anatomical studies of SCs synapses localization onto CA1 PNs dendrites have revealed a highly non-uniform connectivity structure. In particular, the number of short inter-spine distances as well as the number of glutamatergic inputs per branch was greater than chance level, thus supporting both synaptic clustering and in-branch clustering modes, respectively (Druckmann et al., 2014). Similar findings were observed for thalamocortical inputs onto L5 PN (Rah et al., 2013). Collectively, this evidence indicates that, at different scales, the spatial arrangement of glutamatergic synapses in dendrites of PNs crucially shapes the transfer function between synaptic activation and dendritic depolarization/spiking (Ujfalussy and Makara, 2020; Kastellakis and Poirazi, 2019). It is interesting to note that, synaptic inputs in dendrites of interneurons are less spatially structured with respect to PNs (Kwon et al., 2018), and, in contrast to PNs, synaptic inputs in small caliber dendrites of fast spiking basket cells tend to summate sub-linearly (Tzilivaki et al., 2019).

As with excitatory inputs, several lines of evidence show that synaptic inhibition in PNs dendrites depends on local spatial determinants at the microscale level, such as their fine relative positioning with respect to excitatory synapses (Boivin and Nedivi, 2018). Modeling studies suggest that GABAergic synapses positioned distally (off-path) from a cluster of glutamatergic synapses more efficiently raise the threshold for initiating a dendritic spike compared to proximally-placed ones (on-path), whereas the on-path location is more effective in shunting already-triggered dendritic spikes (Gidon and Segev, 2012). Both predictions have been corroborated experimentally *ex vivo* in L5 PNs, confirming that the specific spatial arrangement of GABAergic synapses in dendritic branches is an important determinant shaping dendritic excitability (Jadi et al., 2012). In this concern, studies report that diverse GABAergic inputs from specific interneurons are highly structured at branch and sub-branch levels. In CA1 PNs, O-LM interneurons (somatostatin+, SOM+) or neurogliaform interneurons (neural nitric oxide synthase+, nNOS+) preferentially target the ending or the intermediated region of the terminal domain of distal dendrites, respectively whereas bistratified interneurons (neuropeptide Y+, NPY+) target the origin of the terminal domain of proximal apical oblique and basal dendrites (Bloss et al., 2016). In addition, the study of the excitatory and inhibitory synapses distribution in the whole dendritic arbor in L2/3 PNs revealed that, while density of both synapses significantly vary in different neuronal sub-regions, its ratio was remarkably balanced at branch level (Iascone et al., 2020). Finally, inhibitory GABAergic synapses can be located directly on glutamatergic spines thus effectively controlling spine depolarization (Boivin and Nedivi, 2018; Chiu et al., 2013).

How does cooperative plasticity among glutamatergic synapses shape synaptic clustering?

Extensive work on glutamatergic spines reports that the expression of long-term potentiation (LTP) at an individual spine

can lower the threshold for the induction of synaptic plasticity at neighboring spines by spreading signaling molecules such as small GTPases from the potentiated spine in dendritic stretches of ~10 μm: this establishes the coordinated potentiation of a subset of contiguous spines ultimately leading to the formation of a glutamatergic synaptic cluster (Harvey and Svoboda, 2007; Harvey et al., 2008; Hedrick and Yasuda, 2017). On the other hand, the stimulation of a glutamatergic spine cluster can depress nearby spines through the diffusion of the phosphatase calcineurin, a mechanism that is expected to increase the structural and functional identity of specific clusters (Oh et al., 2017). Likewise, long-term depression (LTD) at an individual spine can either depress or potentiate neighboring spines (Chater and Goda, 2021). Overall, these observations suggest that short-range interplay between spines can define the spatial pattern of dendritic glutamatergic synapses. Nevertheless, how GABAergic synapses contribute to these processes remains largely obscure. Traditionally, inhibition has been considered poorly plastic and to take part to plasticity phenomena mainly by adjusting the threshold for the induction of glutamatergic plasticity (Steele and Mauk, 1999). In this concern, modeling studies report that specific placement of GABAergic synapses with respect to either excitatory synapses or dendritic branches can spatially constraint glutamatergic plasticity hence influencing the degree of glutamatergic synapses clustering (Bar-Ilan et al., 2012). Similarly, the activation of GABAA receptors by GABA uncaging leads to the shrinkage of nearby glutamatergic spines within a range of ~15 μm, reinforcing the spatial role of inhibition in promoting the competitive selection of dendritic spines (Hayama et al., 2013).

Nevertheless, several lines of evidence indicate that GABAergic synapses express several forms of plasticity (Chiu et al., 2019). This prompts the questions of how glutamatergic and GABAergic plasticity interact at dendritic level at the microscale level and how this can shape synaptic clustering—topics that have thus far been investigated mainly through indirect approaches (Chapman et al., 2022). After the induction of spike-timing-dependent plasticity at a specific synaptic population subset in an auditory cortex PN, the plasticity of excitatory and inhibitory plasticity at distinct unstimulated synaptic population subset was found to be co-tuned to achieve a precise excitation-to-inhibition set point (Field et al., 2020). Interestingly, the plasticity-induced remodeling of excitatory and inhibitory synapses on dendrites of L2/3 PNs in the visual cortex is spatially coordinated in dendritic portions of ~10 μm suggesting short-range interplay between inhibitory and excitatory synapses (Chen et al., 2012). In addition, the stimulation of thalamic afferents to distal dendrites of cortical L2/3 PNs induces inhibitory LTP at GABAergic synapses formed by SOM+ interneurons in the same dendritic portion, thus hinting to local interaction between excitatory and inhibitory synapses (Chiu et al., 2018). Extending this framework, a modeling study identifies the presence of plastic GABAergic synapses as important organizers of dendritic glutamatergic synaptic clustering (Kirchner and Gjorgjieva, 2022).

A more recent work investigated the spatial determinants for the interaction between individual dendritic glutamatergic and GABAergic synapses in hippocampal neurons (Ravasenga et al., 2022). By inducing single-spine LTP through the pairing of glutamate uncaging with somatic action potential train, they observed that GABAergic synapses located within a spatial range of ~3–4 μm around the potentiated spine were depressed. Although several factors could limit the generalization of this finding including the poorly physiological induction of LTP and the lack of *in vivo* data, the spatial dependence of the interaction between excitation and inhibition likely plays an important role in the organization of dendritic synaptic inputs. First, by considering the local effect of inhibition (Gidon and Segev, 2012), this heterosynaptic interplay is expected to disinhibit specific potentiated glutamatergic inputs through a winner-takes-all process, with e.g., other concurrent plasticity phenomena maintaining the global dendritic homeostatic balance. Second, the activity-dependent depression of a neighboring GABAergic synapse can contribute to the formation of glutamatergic synaptic clusters thus complementing the cooperative plasticity phenomena between glutamatergic inputs mentioned above. Finally, in the light of this short-range interplay, the convergence of diverse excitatory and inhibitory inputs within the same dendritic stretch can crucially impact at the network level, allowing, for instance, specific glutamatergic inputs to differentially control inputs from different interneuron subtypes. For example, PP and thalamic inputs contact the distal apical dendrites of CA1 PNs together with inputs from O-LM and PP-associated interneurons, which primarily mediate feed-back and feed-forward inhibition, respectively. If, differently from thalamic inputs, EC inputs are consistently located within the "interplay range" with inputs from O-LM interneurons, EC activity could weaken neighboring O-LM inputs (Figure 1). This could bias the balance of inhibition from feedback to feed-forward, thereby altering how these dendrites process and integrate incoming signals. Thus, in analogy with the aforementioned large-scale matching between excitation and inhibition in proximal and distal dendritic compartments, it is important to define the co-alignment between excitatory and inhibitory inputs at the microscale level. The spatial pattern of diverse excitatory and inhibitory inputs along the dendrites may serve as a "fingerprint" for PN subtypes, where the consistent pairing of particular excitatory inputs with inhibitory inputs from specific interneurons could act as structural "synaptic motifs." In a broader framework, the impact of excitatory-inhibitory short-range synaptic interplay can be assessed by including specific synaptic topology and plasticity rules in available biophysical computational models predicting the spiking output of PNs receiving realistic excitatory and inhibitory temporal activity patterns at cellular level. This will allow to understand how short-range plasticity contribute to modulate specific network oscillations by tuning at dendritic level the contribution of diverse interneuron subtypes, or how it could enable associative learning by differentially gating information from distinct brain areas. Importantly, this could also clarify how aberrant short-range plasticity could lead to the disruption of coordination between different interneurons subtypes activity ultimately causing pathology. In the long run, the refined information about the dendritic synaptic spatial arrangement

and short-range interaction could be integrated in computational models that include dendritic computation in large-networks functions and will also contribute designing more neuromorphic and efficient deep neuronal networks (DNNs; Pagkalos et al., 2024, 2023).

Author contributions

DC: Conceptualization, Writing – original draft, Writing – review & editing. VR: Conceptualization, Writing – original draft, Writing – review & editing. AB: Conceptualization, Writing – original draft, Writing – review & editing.

Funding

The author(s) declare financial support was received for the research, authorship, and/or publication of this article. The present work has been supported by HORIZON-MSCA-2021-PF-01 – SynEMO – (Project: 101068871).

Conflict of interest

The authors declare that the research was conducted in the absence of any commercial or financial relationships that could be construed as a potential conflict of interest.

The author(s) declared that they were an editorial board member of Frontiers, at the time of submission. This had no impact on the peer review process and the final decision.

Generative AI statement

The authors declare that no Generative AI was used in the creation of this manuscript.

Publisher's note

References

Bar-Ilan, L., Gidon, A., and Segev, I. (2012). The role of dendritic inhibition in shaping the plasticity of excitatory synapses. *Front. Neural Circ.* 6:118. doi: 10.3389/fncir.2012.00118

Bittner, K. C., Grienberger, C., Vaidya, S. P., Milstein, A. D., Macklin, J. J., Suh, J., et al. (2015). Conjunctive input processing drives feature selectivity in hippocampal CA1 neurons. *Science* 350, 448–452. doi: 10.1038/nn.4062

Bloss, E. B., Cembrowski, M. S., Karsh, B., Colonell, J., Fetter, R. D., and Spruston, N. (2016). Structured dendritic inhibition supports branch-selective integration in CA1 pyramidal cells. *Neuron* 89, 1016–1030. doi: 10.1016/j.neuron.2016.01.029

Boivin, J. R., and Nedivi, E. (2018). Functional implications of inhibitory synapse placement on signal processing in pyramidal neuron dendrites. *Curr. Opin. Neurobiol.* 51, 16–22. doi: 10.1016/j.conb.2018.01.013

Chapman, C. A., Nuwer, J. L., and Jacob, T. C. (2022). The Yin and Yang of GABAergic and glutamatergic synaptic plasticity: opposites in balance by crosstalking mechanisms. *Front. Synapt. Neurosci.* 14:911020. doi: 10.3389/fnsyn.2022.911020

Chater, T. E., and Goda, Y. (2021). My Neighbour Hetero-deconstructing the mechanisms underlying heterosynaptic plasticity. *Curr. Opin. Neurobiol.* 67, 106–114. doi: 10.1016/j.conb.2020.10.007

Chen, J. L., Villa, K. L., Cha, J. W., So, P. T., Kubota, Y., and Nedivi, E. (2012). Clustered dynamics of inhibitory synapses and dendritic spines in the adult neocortex. *Neuron* 74, 361–373. doi: 10.1016/j.neuron.2012.02.030

Chiu, C. Q., Barberis, A., and Higley, M. J. (2019). Preserving the balance: diverse forms of long-term GABAergic synaptic plasticity. *Nat. Rev. Neurosci.* 20, 272–281. doi: 10.1038/s41583-019-0141-5

Chiu, C. Q., Lur, G., Morse, T. M., Carnevale, N. T., Ellis-Davies, G. C. R., and Higley, M. J. (2013). Compartmentalization of GABAergic inhibition by dendritic spines. *Science* 340, 759–762. doi: 10.1126/science.1234274

Chiu, C. Q., Martenson, J. S., Yamazaki, M., Natsume, R., Sakimura, K., Tomita, S., et al. (2018). Input-specific NMDAR-dependent potentiation of dendritic GABAergic inhibition. *Neuron* 97, 368–377.e3. doi: 10.1016/j.neuron.2017.12.032

Druckmann, S., Feng, L., Lee, B., Yook, C., Zhao, T., Magee, J. C., et al. (2014). Structured synaptic connectivity between hippocampal regions *Neuron* 81, 629–640. doi: 10.1016/j.neuron.2013.11.026

Felleman, D. J., and Van Essen, D. C. (1991). Distributed hierarchical processing in the primate cerebral cortex. *Cerebr. Cortex* 1, 1–47. doi: 10.1093/cercor/1.1.1

Field, R. E., D'Amour, J. A., Tremblay, R., Miehl, C., Rudy, B., Gjorgjieva, J., et al. (2020). Heterosynaptic plasticity determines the set point for cortical excitatory-inhibitory balance. *Neuron* 106, 842–854.e4. doi: 10.1016/j.neuron.2020.03.002

Gidon, A., and Segev, I. (2012). Principles governing the operation of synaptic inhibition in dendrites. *Neuron* 75, 330–341. doi: 10.1016/j.neuron.2012.05.015

Harvey, C. D., and Svoboda, K. (2007). Locally dynamic synaptic learning rules in pyramidal neuron dendrites. *Nature* 450, 1195–1200. doi: 10.1038/nature06416

Harvey, C. D., Yasuda, R., Zhong, H., and Svoboda, K. (2008). The spread of Ras activity triggered by activation of a single dendritic spine. *Science* 321, 136–140. doi: 10.1126/science.1159675

Hayama, T., Noguchi, J., Watanabe, S., Takahashi, N., Hayashi-Takagi, A., Ellis-Davies, G. C., et al. (2013). GABA promotes the competitive selection of dendritic spines by controlling local Ca2+ signaling. *Nat. Neurosci.* 16, 1409–1416. doi: 10.1038/nn.3496

Hedrick, N. G., and Yasuda, R. (2017). Regulation of Rho GTPase proteins during spine structural plasticity for the control of local dendritic plasticity. *Curr. Opin. Neurobiol.* 45, 193–201. doi: 10.1016/j.conb.2017.06.002

Iacaruso, M. F., Gasler, I. T., and Hofer, S. B. (2017). Synaptic organization of visual space in primary visual cortex. *Nature* 547, 449–452. doi: 10.1038/nature23019

Iascone, D. M., Li, Y., Sümbül, U., Doron, M., Chen, H., Andreu, V., et al. (2020). Whole-neuron synaptic mapping reveals spatially precise excitatory/inhibitory balance limiting dendritic and somatic spiking. *Neuron* 106, 566–578.e8. doi: 10.1016/j.neuron.2020.02.015

Jadi, M., Polsky, A., Schiller, J., and Mel, B. W. (2012). Location-dependent effects of inhibition on local spiking in pyramidal neuron dendrites. *PLoS Comput. Biol.* 8:e1002550. doi: 10.1371/journal.pcbi.1002550

Jarsky, T., Roxin, A., Kath, W. L., and Spruston, N. (2005). Conditional dendritic spike propagation following distal synaptic activation of hippocampal CA1 pyramidal neurons. *Nat. Neurosci.* 8, 1667–1676. doi: 10.1038/nn1599

Kastellakis, G., and Poirazi, P. (2019). Synaptic clustering and memory formation. *Front. Mol. Neurosci.* 12:300. doi: 10.3389/fnmol.2019.00300

Kerlin, A., Boaz, M., Flickinger, D., MacLennan, B. J., Dean, M. B., Davis, C., et al. (2019). Functional clustering of dendritic activity during decision-making. *Nature* 569, 89–95. doi: 10.7554/eLife.46966.029

Kirchner, J. H., and Gjorgjieva, J. (2022). Emergence of synaptic organization and computation in dendrites. *Neuroforum* 28, 21–30. doi: 10.1515/nf-2021-0031

Klausberger, T. (2009). GABAergic interneurons targeting dendrites of pyramidal cells in the CA1 area of the hippocampus. *Eur. J. Neurosci.* 30, 947–957. doi: 10.1111/j.1460-9568.2009.06913.x

Klausberger, T., and Somogyi, P. (2007). Neuronal diversity and temporal dynamics: the unity of hippocampal circuit operations. *Science* 321, 53–57. doi: 10.1126/science.1149381

Kwon, O., Feng, L., Druckmann, S., and Kim, J. (2018). Schaffer collateral inputs to CA1 excitatory and inhibitory neurons follow different connectivity rules. *J. Neurosci.* 38, 5140–5152. doi: 10.1523/JNEUROSCI.0155-18.2018

Larkum, M. E. (2012). A cellular mechanism for cortical associations: an organizing principle for the cerebral cortex. *Trends Neurosci.* 36, 141–151. doi: 10.1016/j.tins.2012.11.006

Larkum, M. E., Nevian, T., Sandler, M., Polsky, A., and Schiller, J. (2009). Synaptic integration in tuft dendrites of layer 5 pyramidal neurons: a new unifying principle. *Science* 325, 756–760. doi: 10.1126/science.1171958

Larkum, M. E., Zhu, J. J., and Sakmann, B. (1999). A new cellular mechanism for coupling inputs arriving at different cortical layers. *Nature* 398, 338–341. doi: 10.1038/18686

Losonczy, A., and Magee, J. C. (2006). Integrative properties of radial oblique dendrites in hippocampal CA1 pyramidal neurons. *Neuron* 50, 291–307. doi: 10.1016/j.neuron.2006.03.016

Lovett-Barron, M., Turi, G. F., Kaifosh, P., Lee, P. H., Bolze, F., Sun, X. H., et al. (2012). Regulation of neuronal input transformations by tunable dendritic inhibition. *Nat. Neurosci.* 15, 423–430. doi: 10.1038/nn.3024

Megías, M., Emri, Z., Freund, T. F., and Gulyás, A. I. (2001). Total number and distribution of inhibitory and excitatory synapses on hippocampal CA1 pyramidal cells. *Neuroscience* 102, 527–540. doi: 10.1016/S0306-4522(00)00496-6

Mel, B. W. (1993). Synaptic integration in an excitable dendritic tree. *J. Neurophysiol.* 70, 1086–1101. doi: 10.1152/jn.1993.70.3.1086

Naud, R., and Sprekeler, H. (2017). Sparse bursts optimize information transmission in a multiplexed neural code. *Proc. Natl. Acad. Sci. U. S. A.* 114, E6329–E6338. doi: 10.1101/143636

Oh, W. C., Parajuli, L. K., and Zito, K. (2017). Heterosynaptic structural plasticity on local dendritic segments of hippocampal CA1 neurons. *Cell Rep.* 10, 162–169. doi: 10.1016/j.celrep.2014.12.016

Pagkalos, M., Chavlis, S., and Poirazi, P. (2023). Introducing the Dendrify framework for incorporating dendrites into spiking neural networks. *Nat. Commun.* 14:131. doi: 10.1038/s41467-022-35747-8

Pagkalos, M., Makarov, R., and Poirazi, P. (2024). Leveraging dendritic properties to advance machine learning and neuro-inspired computing. *Curr. Opin. Neurobiol.* 85:102853. doi: 10.1016/j.conb.2024.102853

Poirazi, P., Brannon, T., and Mel, B. W. (2003a). Arithmetic of subthreshold synaptic summation in a model CA1 pyramidal cell. *Neuron* 37, 977–987. doi: 10.1016/S0896-6273(03)00148-X

Poirazi, P., Brannon, T., and Mel, B. W. (2003b). Pyramidal neuron as two-layer neural network. *Neuron* 37, 989–999. doi: 10.1016/S0896-6273(03)00149-1

Poirazi, P., and Mel, B. W. (2001). Impact of active dendrites and structural plasticity on the memory capacity of neural tissue. *Neuron* 29, 779–796. doi: 10.1016/S0896-6273(01)00252-5

Polsky, A., Mel, B. W., and Schiller, J. (2004). Computational subunits in thin dendrites of pyramidal cells. *Nat. Neurosci.* 7, 621–627. doi: 10.1038/nn1253

Rah, J.-C., Bas, E., Colonell, J., Mishchenko, Y., Karsh, B., Fetter, R. D., et al. (2013). Thalamocortical input onto layer 5 pyramidal neurons measured using quantitative large-scale array tomography. *Front. Neural Circuits* 7:177. doi: 10.3389/fncir.2013.00177

Ravasenga, T., Ruben, M., Regio, V., Polenghi, A., Petrini, E. M., and Barberis, A. (2022). Spatial regulation of coordinated excitatory and inhibitory synaptic plasticity at dendritic synapses. *Cell Rep.* 38:110347. doi: 10.1016/j.celrep.2022.110347

Steele, P. M., and Mauk, M. D. (1999). Inhibitory control of LTP and LTD: stability of synapse strength. *J. Neurophysiol.* 81, 1559–1566 doi: 10.1152/jn.1999.81.4.1559

Takahashi, H., and Magee, J. C. (2009). Pathway interactions and synaptic plasticity in the dendritic tuft regions of CA1 pyramidal neurons. *Neuron* 62, 102–111. doi: 10.1016/j.neuron.2009.03.007

Takahashi, N., Kitamura, K., Matsuo, N., Mayford, M., Kano, M., Matsuki, N., et al. (2012). Locally synchronized synaptic inputs. *Science* 335, 353–356. doi: 10.1126/science.1210362

Tzilivaki, A., Kastellakis, G., and Poirazi, P. (2019). Challenging the point neuron dogma: FS basket cells as 2-stage nonlinear integrators. *Nat. Commun.* 10:3664. doi: 10.1038/s41467-019-11537-7

Tzilivaki, A., Tukker, J. J., Maier, N., Poirazi, P., Sammons, R. P., and Schmitz, D. (2023). Hippocampal GABAergic interneurons and memory. *Neuron* 111, 3154–3175. doi: 10.1016/j.neuron.2023.06.016

Ujfalussy, B. B., and Makara, J. K. (2020). Impact of functional dendritic synapse clustering on neuronal information processing. *Nat. Commun.* 11:1413. doi: 10.1038/s41467-020-15147-6

frontiers | Frontiers in Cellular Neuroscience

TYPE Review
PUBLISHED 06 January 2025
DOI 10.3389/fncel.2024.1486315

OPEN ACCESS

EDITED BY
Enrico Cherubini,
European Brain Research Institute, Italy

REVIEWED BY
Stéphanie Baulac,
Sorbonne Universités, France
Gabriele Ruffolo,
Sapienza University of Rome, Italy

*CORRESPONDENCE
Carlos Cepeda
✉ ccepeda@mednet.ucla.edu

RECEIVED 26 August 2024
ACCEPTED 11 December 2024
PUBLISHED 06 January 2025

CITATION
Zhang J, Argueta D, Tong X, Vinters HV, Mathern GW and Cepeda C (2025) Iconography of abnormal non-neuronal cells in pediatric focal cortical dysplasia type IIb and tuberous sclerosis complex.
Front. Cell. Neurosci. 18:1486315.
doi: 10.3389/fncel.2024.1486315

Iconography of abnormal non-neuronal cells in pediatric focal cortical dysplasia type IIb and tuberous sclerosis complex

Joyce Zhang[1], Deneen Argueta[1], Xiaoping Tong[2], Harry V. Vinters[3], Gary W. Mathern[4] and Carlos Cepeda[1]*

[1]IDDRC, Jane and Terry Semel Institute for Neuroscience and Human Behavior, University of California - Los Angeles, Los Angeles, CA, United States, [2]Department of Anatomy and Physiology, Shanghai Jiao Tong University School of Medicine, Shanghai, China, [3]Department of Pathology and Laboratory Medicine, University of California - Los Angeles, Los Angeles, CA, United States, [4]Department of Neurosurgery, David Geffen School of Medicine, University of California - Los Angeles, Los Angeles, CA, United States

Once believed to be the culprits of epileptogenic activity, the functional properties of balloon/giant cells (BC/GC), commonly found in some malformations of cortical development including focal cortical dysplasia type IIb (FCDIIb) and tuberous sclerosis complex (TSC), are beginning to be unraveled. These abnormal cells emerge during early brain development as a result of a hyperactive mTOR pathway and may express both neuronal and glial markers. A paradigm shift occurred when our group demonstrated that BC/GC in pediatric cases of FCDIIb and TSC are unable to generate action potentials and lack synaptic inputs. Hence, their role in epileptogenesis remained obscure. In this review, we provide a detailed characterization of abnormal non-neuronal cells including BC/GC, intermediate cells, and dysmorphic/reactive astrocytes found in FCDIIb and TSC cases, with special emphasis on electrophysiological and morphological assessments. Regardless of pathology, the electrophysiological properties of abnormal cells appear more glial-like, while others appear more neuronal-like. Their morphology also differs in terms of somatic size, shape, and dendritic elaboration. A common feature of these types of non-neuronal cells is their inability to generate action potentials. Thus, despite their distinct properties and etiologies, they share a common functional feature. We hypothesize that, although the exact role of abnormal non-neuronal cells in FCDIIb and TSC remains mysterious, it can be suggested that cells displaying more glial-like properties function in a similar way as astrocytes do, i.e., to buffer K^+ ions and neurotransmitters, while those with more neuronal properties, may represent a metabolic burden due to high energy demands but inability to receive or transmit electric signals. In addition, due to the heterogeneity of these cells, a new classification scheme based on morphological, electrophysiological, and gene/protein expression in FCDIIb and TSC cases seems warranted.

KEYWORDS

focal cortical dysplasia, tuberous sclerosis complex, balloon cells, electrophysiology, pediatric epilepsy

1 Introduction and pathological findings in FCDIIb and TSC

Malformations of cortical development (MCD) comprise a wide range of conditions arising from anomalies in cell differentiation, migration, and proliferation within the cerebral cortex (Barkovich et al., 2012). Although the exact prevalence of MCD remains uncertain, studies estimate their involvement in up to 40% of cases with pharmaco-resistant childhood epilepsies (Barkovich et al., 2012; Guerrini and Dobyns, 2014; Represa, 2019). In such instances, elective surgical resections not only offer a means to mitigate epileptic episodes, but also present an opportunity to explore the pathophysiology of MCD (Blumcke et al., 2017; Juric-Sekhar and Hevner, 2019; Blumcke, 2024).

A common type of MCD is Focal Cortical Dysplasia (FCD), characterized by Taylor et al. while performing microscopic analysis of lobectomy specimens from epileptic patients (Taylor et al., 1971). The study described localized disruptions in cortical laminae and the presence of large, bizarre neurons scattered throughout all but the first cortical layer. In most cases, "grotesque" cells, probably of glial origin, were also present in the depths of the affected cortex and in the subjacent white matter. These "grotesque cells" are now known as balloon cells (BC) due to their peculiar shape. The International League Against Epilepsy (ILAE) consensus classification of FCD distinguishes the pathology into three main classes: FCDI, FCDII, and FCDIII. FCDII is characterized by pronounced cortical dyslamination, the presence of dysmorphic, cytomegalic neurons (FCDIIa), and all of the above plus BC (FCD IIb) (Blumcke et al., 2011; Najm et al., 2022). On Magnetic Resonance Imaging (MRI), there is cortical thickening, aberrant sulcal and gyral patterns, subcortical white matter hyperintensity, and the occurrence of the transmantle sign, which is a funnel-shaped high T2/FLAIR correlated with the presence of abundant BC (Blumcke et al., 2011; Kimura et al., 2019). The transmantle sign is associated with abnormal radial glial progenitor cells, which normally create a framework for neuronal migration from the periventricular germinal matrix to the cortex (Castillo, 2002). Topographic characterization showed that BC are primarily clustered in the white matter and scatter diffusely into the gray-white matter junction, in line with MRI findings (Rossini et al., 2017).

Interestingly, Taylor and associates noticed that FCD with BC displayed histological similarities with tubers isolated from patients with Tuberous Sclerosis Complex (TSC, formerly known as Bourneville disease or epiloia), another rare MCD. Its clinical presentation includes a classic triad of symptoms; epilepsy (particularly infantile spasms), intellectual disability, and facial angiofibromas (Northrup et al., 2021). Other manifestations include cortical tubers, subependymal nodules, subependymal giant cell astrocytomas (SEGA), cardiac rhabdomyomas, renal angiomyolipomas, retinal hamartomas, pulmonary lymphangioleiomyomatosis, and autism spectrum disorder. TSC results from mutations in TSC1 and TSC2 genes, which code for hamartin and tuberin, respectively. TSC1 and TSC2 inhibit the mechanistic target of rapamycin (mTOR) pathway, which is a major contributor to enhanced protein synthesis and cell growth (Kwiatkowski and Manning, 2005; Liu and Sabatini, 2020; Panwar et al., 2023). Notably, classic features of FCD, such as blurred boundaries of gray and white matter, cortical thickening, and the radial band sign, can also be observed on MRI in TSC cases (Muhlebner et al., 2019). At present, it is not clear whether the radial band in TSC and the transmantle sign in FCDIIb are manifestations of the same pathology or if they are separate conditions (Matsuo et al., 2022). Importantly, in cortical tubers enlarged cells similar to the BC also abound and they have been named "giant" cells (GC). Based on similarities between histopathologic cortical abnormalities observed in FCDIIb and TSC, it has been suggested that FCD with BC represents a forme fruste or phenotypic variant of TSC, limited to selected focal regions of brain tissue (Vinters et al., 1993; Jozwiak et al., 2006). While both share morphological features and protein expression, BC and GC differ in cortical localization. BC in FCDIIb are more concentrated in deep cortical layers and white matter, while GC in TSC are more scattered throughout the tuber and they also are present in perituberal areas (Marcotte et al., 2012). Further, a gross cell count of BC vs. GC from resected tissue showed that GC were more numerous (Cepeda et al., 2012), potentially because GC concentrate within the tubers of TSC lesions and are less common in the surrounding areas (Abdijadid et al., 2015).

A 2020 study used web-based deep learning to delineate unique histopathological features of TSC vs. FCDIIb cortical tissue, two pathological entities hard to differentiate based on Hematoxylin & Eosin (H&E) staining. Although some features appeared unique to TSC samples (e.g., the matrix reaction was fibrillar and strand-like vs. diffuse and granular in FCDIIb, or larger nuclei of astrocytes with uncondensed chromatin vs. smaller nuclei and more condensed chromatin in FCDIIb), BC/GC themselves were not critical to distinguish both pathologies (Kubach et al., 2020). Apparently, the only notable difference between these cells was the presence of a "halo" effect present in GC from TSC but less prevalent in BC from FCDIIb cases (Kubach et al., 2020). The "halo" effect, visible as a ring of white background in H&E staining, is probably caused by altered synaptogenesis in BC/GC (Yamanouchi et al., 1997).

The presence of BC/GC in FCDIIb and TSC has baffled histopathologists as they have defied classification due to their ill-defined, glio-neuronal nature. With the advent of imaging techniques allowing visualization of individual cells in *ex vivo* brain slices, e.g., infrared differential interference contrast (IR-DIC) microscopy, a functional characterization of these enigmatic cells is within reach. The present review aims to provide a more detailed characterization of abnormal non-neuronal cells, e.g., BC/GC, intermediate cells, and reactive/dysmorphic astrocytes (Figure 1), in FCDIIb and TSC, with particular emphasis on our own studies in a large cohort of pediatric patients undergoing surgery for the treatment of pharmaco-resistant epilepsy.

2 Some words regarding cell nomenclature and definition of BC/GC

BC and GC are named for their substantial size and mostly spherical morphology, hypothesized to result from mutations affecting the mTOR pathway (Miyata et al., 2004; Blumcke et al., 2011). They are similar to gemistocytic astrocytes and to cells found in SEGA. Traditionally, the term "balloon" has been applied to the bizarre cells occurring in FCDIIb, while the term "giant" has been reserved to the enlarged cells observed in TSC. According to the ILAE classification of FCDs, BC are characterized by a large cell body,

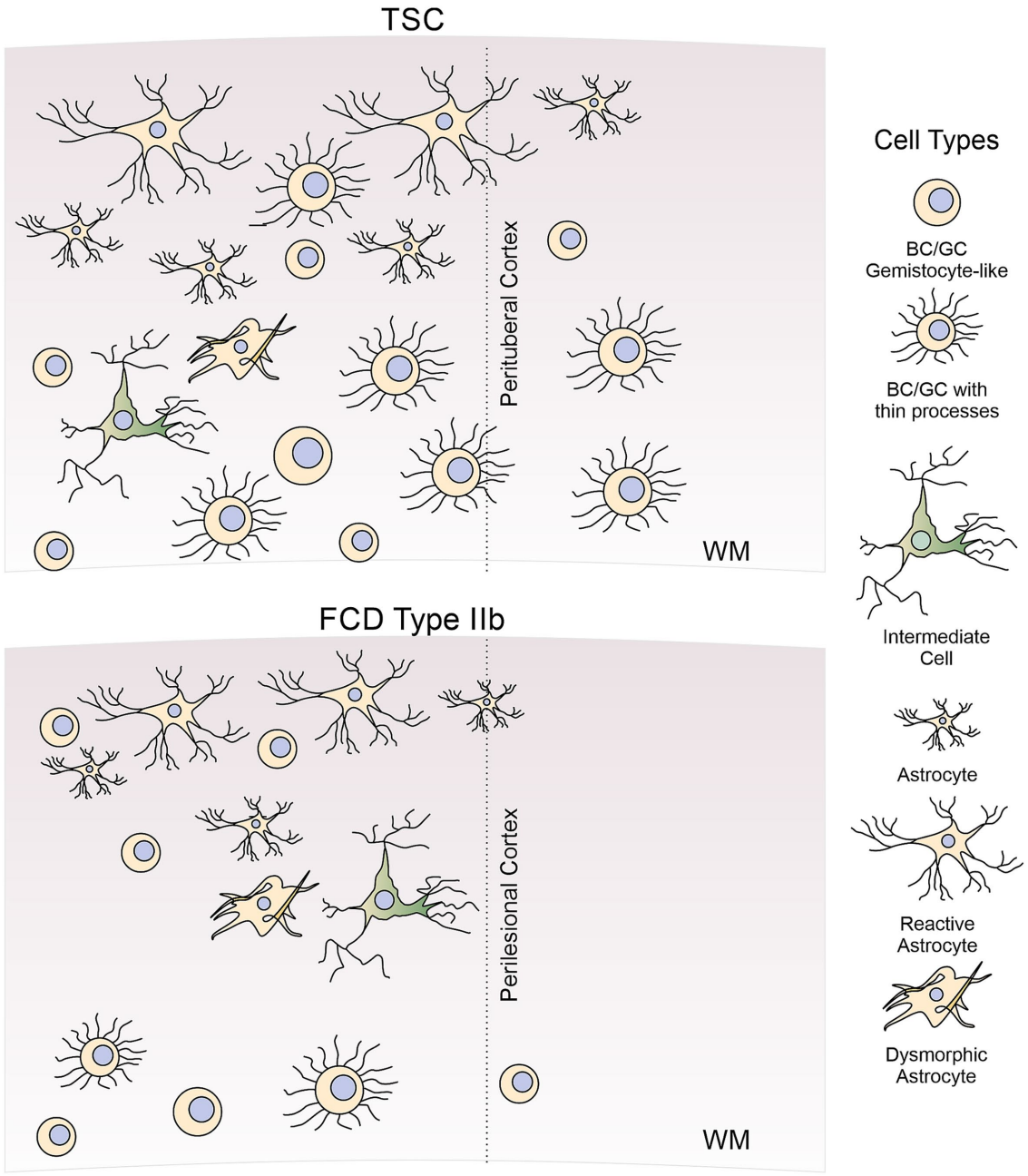

FIGURE 1
Diagram of abnormal non-neuronal cells found in FCDIIb and TSC cases. In this review, we discuss morphological, molecular, and electrophysiological properties of abnormal non-neuronal cells observed in cortical tissue from FCDIIb and TSC cases. These include BC/GC (both gemistocytic-like and BC/GC with thin processes), intermediate or hybrid cells, reactive, and dysmorphic astrocytes. For comparison, normal astrocytes are also illustrated. Not included in this review are other types of abnormal cells (e.g., dysmorphic cytomegalic neurons), oligodendrocytes or microglia.

opalescent glassy eosinophilic cytoplasm lacking Nissl substance, and the frequent occurrence of multiple nuclei (Blumcke et al., 2011). On the other hand, the term "giant" in TSC refers to a cell type that shares a large soma, as well as cytoplasmic and nuclear characteristics also encountered in BC of FCDIIb. However, the term "giant" is fraught with confusion due to its lack of specificity. There are other cells in cortical tubers that also are very large, e.g., cytomegalic neurons, but are unlike "balloon" cells. But besides their occurrence in different pathologies, is there a good reason to divide the abnormally enlarged, non-neuronal cells into "balloon" and "giant"? Probably not. In fact, some of the current literature has used BC and GC interchangeably, regardless of the associated pathology (Vinters et al., 1993; Fauser et al., 2004; Yasin et al., 2010; Kubach et al., 2020; Arceneaux et al., 2024; Liu et al., 2024). In this review we use the general term BC/GC to identify this specific type of cell regardless of underlying pathology, generally BC when applied to FCDIIb, and GC when applied to TSC cases. We reserve the term "non-neuronal" cells to encompass any cell type unable to generating action potentials including BC, GC,

intermediate cells, dysmorphic astrocytes, as well as the normal and reactive astrocytes. Not included in this review are oligodendrocytes and microglia, which also are affected in TSC and FCDIIb (Boer et al., 2006; Gruber et al., 2021).

3 A brief history of BC/GC in TSC and FCDIIb

The first detailed microscopic description of FCD, including the identification of "grotesque" cells similar to those reported in TSC, occurred relatively recently (Taylor et al., 1971). In contrast, histological observations of large, "atypical" cells in cortical tubers started in the early 20th century. It was probably G. B. Pellizzi the first neuropathologist who, in 1901, described the dysplastic nature of the tubers and the existence of heterotopias in the brains of TSC cases (Pellizzi, 1901). Abnormal cells were found inside the tubers and they were variably referred to as "atypical," "bizarre," "giant," "monstrous." From the outset, the identity of these cells was a puzzle, due to their glio-neuronal aspect. Hallervorden and Krücke, in a paper published in 1956 [cited in (Arseni et al., 1972)], maintained that the large cells in TSC represent a heterogeneous cellular group formed by both nerve and glial cells. They also mentioned that these cells are malformed, undifferentiated neurons, "indifferent" forms of transitions from glial cells to neurons. Ultrastructural studies also were published in the late 1960s and 1970s (Gruner, 1969; Ribadeau Dumas et al., 1973). Of particular interest is the case of a stillborn infant (31st week gestation) who presumably died due to a rhabdomyoma of the heart. Notably, the "atypical" cells in the cortical tuber showed ultrastructural features of reactive astrocytes adorned with innumerable microvilli-like projections on their surface and junctional complexes (Probst and Ohnacker, 1977). In addition, some features of these "atypical" cells resembled those of reactive astrocytes and gemistocytes [round to oval astrocytes with abundant, glassy, eosinophilic cytoplasm and an eccentric nucleus (Tihan et al., 2006)]. Probst and Ohnacker suggested that the "atypical" cells in this case were the manifestation of aberrant differentiation of progenitor cells. Apparent discrepancies regarding the glio-neuronal ambiguity of the "monstrous" cells described by other authors, they remarked, could be due to the localization of the tuber sample and different stage of differentiation.

The Golgi method provided invaluable information on the fine morphology of brain cells in both normal and pathological conditions, including TSC, other cortical malformations, and subcortical heterotopias (Ferrer, 2024). In 1984, three landmark papers analyzed the fine morphology of neurons and glia in cortical tubers using the Golgi technique (Ferrer et al., 1984; Huttenlocher and Heydemann, 1984; Machado-Salas, 1984). Huttenlocher and Heydemann described two principal cell types composed of astroglia and "stellate" neurons with varicose dendrites and few dendritic spines, many of those cells lacked identifiable axons. Glial cells were prominent in subpial regions and in deeper zones (Huttenlocher and Heydemann, 1984). Ferrer et al. also noticed a large number of "stellate" cells in the intermediate and deep regions of the tuber. Their main finding was aberrant cellular orientation and impaired neuronal distribution, leading them to postulate a disorder of cell migration and neuronal organization (Ferrer et al., 1984). Machado-Salas identified two main cell populations that included astrocytes, mostly of the fibrillary type, and large pyramidal neurons with misoriented apical dendrites. In addition, a small number of "bizarre" cells of questionable nature, probably pyramidal-like cells with progressive loss of pyramidal contour were observed (Machado-Salas, 1984). He concluded that two types of giant cells coexist in TSC, one type clearly displays nerve cell features, while the other displays the typical morphology of astrocytes.

Modern studies using the Golgi technique have concentrated more on the dendritic and spine morphology of normal and dysmorphic neurons in different types of FCD. Dendritic and spine abnormalities were more evident in normal and dysmorphic neurons of FCDIIb than in FCDIIa (Rossini et al., 2021). Abnormalities were manifested by reduced dendritic fields, spine loss, distortions in spine morphology, and the presence in some cells of numerous dendritic varicosities. Interestingly, in some dysmorphic neurons, the authors observed the presence of numerous short filopodia-like protrusions emerging from the soma. One may wonder if those protrusions are similar to the microvilli reported in "atypical" cells of cortical tubers by Probst and Ohnacker (op. cit.). Another important ultrastructural study of a TSC case and a subependymal tumor found, in both cases, GC with astrocytic characteristics (Trombley and Mirra, 1981). Notably, the authors also reported that, in addition to numerous glial-glial contacts, rare neuroglial junctions were encountered in the cortical tuber case, suggesting aberrant synapse formation. This unprecedented observation, they suggested, may correlate with the existence of transient axo-glia junctions, including synapses, in the developing nervous system. These contacts may promote synaptogenesis by releasing GABA from the glial processes into the neuronal milieu (Wolff et al., 1979). Other electron microscopy studies demonstrated increased intermediate filaments in BC/GC from FCDIIb and TSC cases, along with numerous mitochondria, which were centrally located, without neurosecretory granules, and of normal architecture (Yasin et al., 2010). It should be noted that mTOR is functional in mitophagy inhibition (Frauscher et al., 2017), so increased mitochondrial numbers support the hypothesis that mTOR is overactive in BC/GC.

Pioneer histopathological and IHC studies by Vinters and his group at the University of California, Los Angeles (UCLA) characterized cortical tissue associated with infantile spasms. Those studies concluded that, as already mentioned, cases of severe FCD had similarities to cerebral changes described in TSC, including the presence of blurred gray-white matter junction containing bizarre gemistocytic BC (Vinters et al., 1993). BC in FCDIIb are similar to GC observed in cortical tubers and show both neuronal and astrocytic epitopes, indicating the local proliferation of multipotential neuroectodermal cells (De Rosa et al., 1992). A further characterization of BC demonstrated their location in FCD lesions and presence of GFAP and the cytoskeletal marker tau (Vinters et al., 1999). A revealing study by the same group used autopsy material from a 20-week-old fetus with TSC, which demonstrated three tubers populated with "gemistocyte-like BC," along with scattered BC throughout the subcortical white matter. These cells were noted to be positive for both GFAP and vimentin (Park et al., 1997). In another landmark report, the development of TSC lesions in fetal brain tissue from 19 gestational weeks to term, it was found that subcortical lesions forming around the germinative zones are the first alterations detected already at 19 weeks of gestation. These lesions are characterized first by the presence of dysmorphic astrocytes and GC. The data suggested that cortical tuber formation is a long process that initiates with the presence of dysmorphic astrocytes and GC,

while the appearance of dysmorphic neurons occurs by the end of gestation (Gelot and Represa, 2020). Overall, these studies suggest BC/GC have a mixed phenotype and originate very early during brain development.

4 Immunohistological, Western blot, and mRNA expression studies provide insights into the developmental origin and identity of BC/GC

The normal process of cortical development guides the understanding of BC/GC identity. After formation of the neural tube, radial glial cells tightly anchored to each other divide to form a ventricular zone. These radial glial cells are not only the precursors to neurons and glia, but also use their processes to guide proliferating cells away from the ventricles, eventually forming the subventricular zone and the cortex (Zarzor et al., 2023).

Immunohistochemical (IHC) studies have stressed the remarkable similarities of large cells in FCDIIb and TSC, including the expression of neuronal and astrocytic markers such as microtubule-associated protein 2 (MAP2) and glial fibrillary acidic protein (GFAP) (Jozwiak et al., 2005; Ying et al., 2005). Since then, many other specific markers have been added to the list and have aided in determining the origin and identity of BC/GC.

4.1 Immature neuronal and glial cell markers

The presence of immature neuronal and glial cell markers in BC/GC (Table 1), along with their localization in the gray/white matter junction, suggest BC/GC may represent cells in a pre-differentiation state (Englund et al., 2005; Rossini et al., 2017). Hence, from the outset it has been difficult to determine if they are more neuronal or glial in origin. The demonstration that radial glia are capable of generating astrocytes as well as neurons during cortical development (Malatesta et al., 2000; Alvarez-Buylla et al., 2001; Noctor et al., 2001) provided important clues about the origin of BC/GC. It seemed possible that BC/GC were originally radial glia that, under unspecified circumstances, had an arrest in development, preventing them from reaching their final morphological and functional fate (Cepeda et al., 2006; Lamparello et al., 2007). Multiple cell markers suggest BC/GC may be arrested at the G1 stage of the cell cycle (Table 1). In BC, low levels of cyclin D and cyclin E suggested cells did not advance to S, as these cyclins facilitate progression through G1 (Thom et al., 2005; Schick et al., 2007b; DeBerardinis et al., 2008). MCM2, a G1 protein necessary for S stage initiation, was expressed in BC/GC, but exposure to stem cell mitogens in BC showed no proliferation (Yasin et al., 2010). These authors also succeeded at isolating, in culture, an undifferentiated population of BC from surgical resections of FCD and cortical tubers, and demonstrated that β1-integrin, a protein that participates in neuronal differentiation, labels a sub-population of BC with a stem cell phenotype (Yasin et al., 2010). Ki-67, another cell proliferation marker, was shown to be increased in GC but not expressed in BC (Crino et al., 1996; Munakata et al., 2013).

Neuronal-glial markers expressed in BC/GC can be separated by their stage of differentiation: neuronal stem cell, neuronal progenitor, mature neuronal, and mature glial markers (Table 1). BC/GC commonly accumulate intermediate filaments vimentin and nestin, known to function in neuronal migration and differentiation in weeks 20–30 of embryonic development (Garbelli et al., 1999; Mizuguchi et al., 2002; Urbach et al., 2002; Oh et al., 2008). General markers of cellular immaturity, SOX2, OCT4, c-myc, KLF4, FOXG, were identified in more than 75% of BC examined (Orlova et al., 2010). The neuronal progenitor cell may express MAP1B, Doublecortin, FGF-13, or GFAP-δ variant, all present in BC/GC (Crino et al., 1997; Yamanouchi et al., 1997; Mizuguchi et al., 2002; Lee et al., 2003; Martinian et al., 2009; Marin-Valencia et al., 2014; Wu et al., 2021a; Wu et al., 2021b). Finally, markers of mature neuronal (α-internexin, MAP2, NeuN, NSE) and glial (GFAP, S100 β, Cx43) lineage are positive in BC/GC (Hirose et al., 1995; Crino et al., 1996; Urbach et al., 2002; Sharma et al., 2004; Jozwiak et al., 2005; Blandini et al., 2008; Garbelli et al., 2011; Marin-Valencia et al., 2014). Notably, they have variable GFAP and neurofilament staining patterns. In rare examples, co-expression of both markers was reported suggesting glial and neuronal lineage determination, that is, intermediate cells (Englund et al., 2005; Talos et al., 2008), while another study suggested that BC/GC have a stronger neuronal heritage (Mizuguchi et al., 2002). In agreement, single-cell analysis in tubers suggested that GC are of neuronal lineage despite the persistence of embryonic markers, such as nestin (Crino et al., 1996). As stated above, these discrepancies could be due to cell heterogeneity in FCDIIb and TSC samples.

Various neuronal-glial markers positive in BC/GC have been linked to epileptic activity and histological disturbances of cortical tissue in both FCDIIb and TSC. Doublecortin, an immature neuronal marker, is primarily found in migrating cells of the fetal central nervous system and correlates well with the degree of histological abnormality of the lesion (Mizuguchi et al., 2002). Fibroblast growth factor 13 (FGF13) plays a role in the differentiation of neurons during early embryonic development and is correlated with seizure frequency in FCDIIb and TSC cases (Wu et al., 2021a). Fibroblast growth factor 2 (FGF2) upregulation in BC has been shown to positively correlate with disturbed gliogenesis and neuroblast migration (Ueda et al., 2011). A survey of FGF2 across multiple MCD showed that the percentage of FGF2-IR can reflect the timing of insult in each cortical development disorder (Sugiura et al., 2008).

Interestingly, a recent customized machine-learning workflow trained to identify BC in tissue sections using a histological stain compatible with high-dimensional cytometry (BAIDEN), reported that BC express proteins associated with progenitor-cell identity (e.g., vimentin, SOX2, CD133, and EGFR) rather than mature-cell identity (e.g., β-III-tubulin, SMI-311, GFAP, and EAAT1), which tended to be decreased (Arceneaux et al., 2024).

4.2 mTOR pathway markers

MTOR is a tumor suppressor gene which codes a protein product (mTOR) pivotal to GC pathology because functional hamartin (TSC1) and tuberin (TSC2) inactivate the mTOR pathway. The protein kinase regulates, among others, cellular growth, proliferation and differentiation, autophagy, and immune responses (Panwar et al., 2023). In line with demonstrated parallels between BC and GC, IHC studies found a loss of tuberin and hamartin expression, as well as strong immunoreactivity for mTOR in BC (Jozwiak et al., 2004;

TABLE 1 mRNA and protein expression of balloon cells (BC) and giant cells (GC) of neuro-glial markers.

Category	Cell marker	BC	GC	Function	Notes and references
Neuronal stem cell marker	CD34	+	+	Stem cell marker	Positive in BC/GC in white matter (Fauser et al., 2004) Expressed in 7.5% of BC (Oh et al., 2008)
	CD133	+	+	Stem cell marker	BC (Ying et al., 2005) GC (Yasin et al., 2010)
	SOX2	+	+	Stem cell marker	BC (Yasin et al., 2010) GC (Yasin et al., 2010; Arceneaux et al., 2024)
	β1-integrin	+	+	Neural stem cell behavior modulator	BC/GC (Yasin et al., 2010)
	Nestin	+	+	Modulator of differentiation and migration of neural stem cells	57.1% of cells in BC (Marin-Valencia et al., 2014; Oh et al., 2008; Orlova et al., 2010) 80% of cells in GC (Crino et al., 1996; Mizuguchi et al., 2002)
	Vimentin	+	+	Radial glia marker and Neuronal stem cell marker	53.1%; 63.1% of cells in BC (Urbach et al., 2002; Oh et al., 2008; Marin-Valencia et al., 2014) GC (Hirose et al., 1995; Mizuguchi et al., 2002; Arceneaux et al., 2024)
	FGF2	+	+	Regulates differentiation in neuronal stem cells	BC/GC (Ueda et al., 2011)
Neuronal progenitor marker	MAP1B	+	+	Modulates neuronal migration and dendritic outgrowth	BC (Crino et al., 1997; Marin-Valencia et al., 2014); GC (Yamanouchi et al., 1997)
	Doublecortin	+	+	Neuronal progenitor cell marker	Expressed in a smaller number of cells in BC vs. GC (Mizuguchi et al., 2002), GC (Lee et al., 2003)
	FGF13	++	++	Modulates neuronal differentiation	BC (Wu et al., 2021a), mRNA expression is also shown in GC (Wu et al., 2021b).
	GFAP-δ	+	+	GFAP isomer in neuronal stem cells	BC/GC (Martinian et al., 2009)
Mature neuronal marker	α-internexin	+	+	Maintains dendritic structure	BC (Marin-Valencia et al., 2014) Expression 50–70%; mRNA expression is also shown in GC (Crino et al., 1996)
	MAP2	+	+	Influences microtubule dynamics in neurons	BC (Oh et al., 2008) GC (Crino et al., 1996)
	NeuN	+	+	Neuronal marker expressed in cell nuclei	BC (Marin-Valencia et al., 2014) GC Heterogeneous expression (Lee et al., 2003)
	NSE (vs. GFAP)	+	+	Neuronal marker	NSE more than GFAP in BC vs. GC compared to GFAP (Jozwiak et al., 2006)
Mature glial marker	GFAP	+	+	Astrocytic marker	BC Expression heterogeneous (Urbach et al., 2002) 67% of BC (Oh et al., 2008) GC (Hirose et al., 1995; Sharma et al., 2004; Arceneaux et al., 2024)
	S100 β	n	+	Glial marker	GC (Hirose et al., 1995; Sharma et al., 2004)
	Cx43	+	n	Glial gap junction protein	BC (Garbelli et al., 2011)

n: "no study found" -: "not expressed" u: "Underexpressed"; +: Expressed (may be weakly expressed or normal expression); ++: "Overexpressed"; +++: "Strongly Expressed."
All studies examined human cortical samples. Unless otherwise noted, all studies are immunohistochemical studies of protein expression.

Grajkowska et al., 2008; Table 2). Considering the large size of BC/GC, numerous studies have also looked for evidence of increased mTOR downstream markers in BC/GC. IHC studies have shown increased expression of pS6K1, pAkt, pPDK, and p4EBP1 in both BC/GC (Baybis et al., 2004; Schick et al., 2006; Schick et al., 2007a; Rossini et al., 2017). However, in a study designed to assess whether the PI3K pathway, a modifier of the mTOR pathway, differentiates BC from GC, it was found that, when compared to GC, BC showed elevated upstream modifiers of TSC1 and TSC2, p-PDK1 and p-Akt, but similar levels of TSC1/TSC2 markers downstream the pS6 marker, suggesting recruitment of different factors in the molecular pathogenesis of GC in cortical tubers vs. BC in FCDIIb (Schick et al., 2007a). The presence of elevated upstream markers in BC that is absent in GC may suggest that the same therapy would not be effective in FCDIIb, but this has not been demonstrated yet.

Since the mTOR pathway is involved in a complex network of other protein pathways, Baybis et al. furthered their investigation by delineating transcription profiles of BC/GC in related cell growth factors. According to the study, similar expression changes in BCs and GCs included reduction of c-fos, hairy enhancer of split–1, and TGF-β1 and TGF-β2.

TABLE 2 mRNA and protein expression of balloon cells (BC) and giant cells (GC) of mTOR and cell growth markers.

Category	Cell marker	BC	GC	Function	Notes and references
	pAkt	++	+	TSC 1 and 2 suppressor	mRNA data suggest normal expression in GC but increased in BC (Rossini et al., 2017; Schick et al., 2007a)
mTOR pathway Cell growth marker	Hamartin	u	-	Tumor suppressor; mTOR suppressor	BC/GC (Jozwiak et al., 2004; Grajkowska et al., 2008)
	Tuberin	u	-		
	pPDK	++	++	Signal transduction in mTOR	mRNA expression is also shown in BC/GC (Rossini et al., 2017; Schick et al., 2007a)
	p4EBP1	+	+	Translation initiation factor	mRNA expression is also shown in BC/GC; More focal, more variable expression in BC (Yasin et al., 2010)
	pTuberin	++	++	Inactivated tuberin/TSC2	Only shown in mRNA so far (Schick et al., 2007a)
	Actin Stress Fiber	++	++	Disrupts actin skeleton	Only shown in mRNA so far (Schick et al., 2007a)
	pS6	++	++	Protein synthesis, cell proliferation, apoptosis, and metabolism	BC/GC (Rossini et al., 2017)
	p-p70(S6k)	++	++	Cell proliferation, growth, and cell cycle progression	Only shown in mRNA so far (Schick et al., 2007a)
Cell growth pathways	MCM2	+	+	G1 cell stage marker	unable to be activated with stem cell mitogens in BC/GC (Yasin et al., 2010)
	IGF2	++	+	Insulin growth factor	Only shown in mRNA so far; Normal expression in GC (Baybis et al., 2004)
	Ki67	-	+	Cell proliferation marker and immature neuronal marker	BC (Munakata et al., 2013) GC (Crino et al., 1996; Crino et al., 1997)
Inflammation markers	LILRB2	+	+++	Modulates neurite growth, synaptic plasticity, and inflammatory responses	BC/GC (Yue et al., 2019)
	TLR4	++	++	Toll-like receptor involved in neurogenesis	BC/GC (Arena et al., 2019)
	IL-1β	++	++	Proinflammatory cytokine involved in neuronal development	BC/GC (Arena et al., 2019)
	IL-6/IL-6R	+++	+++	Proinflammatory cytokine involved in neuronal development	Colocalization with GFAP in BC, but not GC (Shu et al., 2010)
	IL-17/IL17R	+	+	Activates innate and adaptive immunity	2x higher compared to cortex in BC/GC (He et al., 2013)
	TGF-β	u	u	Regulates response to cell injury, including modulating cell growth	Only shown in mRNA so far (Baybis et al., 2004)
	FPR2	+	+	Inflammatory resolution in CNS; Negatively correlated with NF-kB	Weakly shown in GC/BC (Huang et al., 2022)

-: "not expressed" u: "Under expressed"; +: Expressed (may be weakly expressed or normal expression); ++: "Overexpressed"; +++: "Strongly Expressed."
All studies examined human cortical samples. Unless otherwise noted, all studies are immunohistochemical studies of protein expression.

However, GC demonstrated increased expression of AP-1, c-ret, ICAM-1, NF-kB, TGFR2, and VEGF, and reduced expression of c-jun, CaMKII, Erb, and platelet-derived growth factor receptor in comparison to BCs. The authors also demonstrated increased IGF2 in BC compared to GC based on single-cell mRNA data (Baybis et al., 2004).

4.3 Immune system markers

Various markers positive in BC/GC reflect alterations in immune activity (Table 2). Interleukins 6 and 17 (IL-6, IL-17) and their receptors are involved in the inflammatory response and demonstrated to be elevated in BC/GC. Notably, IL-6 is also involved in neuronal development and seen to be colocalized with GFAP in BC but not GC (Shu et al., 2010; He et al., 2013). Another cytokine, IL-1β, along with TLR4, also are highly expressed in BC/GC (Arena et al., 2019). Leukocyte immunoglobulin-like receptor subfamily B member 2 (LILRB2) is a neuronal progenitor cell marker, as well as a marker of inflammatory responses. It is involved in neurite growth, synaptic plasticity, and inflammatory responses. A study demonstrated that increased protein concentration of LILRB2 in BC/GC has a negative correlation with seizure frequency (Yue et al., 2019). Increased levels of Formyl Peptide Receptor 2 (FPR2) in BC/GC is also negatively related with NF-kB and seizure frequency in TSC and FCDIIb (Huang et al., 2022). Other markers, such as TGF-β, which regulates cell response to injury, was demonstrated to

be under-expressed in BC/GC mRNA by single-cell analysis (Baybis et al., 2004).

4.4 GluR and $GABA_AR$ subunit markers, and glutamate and chloride cation transporters

The composition of $GABA_A$ and glutamate receptor ($GABA_AR$ and GluR) subunits evolves throughout neuronal/glial development. Studies have used this principle to understand the identity of abnormal FCDIIb and TSC cells (Table 3). FCDIIb lesions, defined by their BC composition, demonstrated high $GABA_A$ receptor subunit α4:α1 ratio. Comparatively, FCDIIa lesions (which lack BC) had low $GABA_AR$ α4:α1 ratio, suggesting BC may modify or directly contribute to altered $GABA_AR$ subunit composition. Investigation of TSC lesions showed analogously increased $GABA_AR$ α4:α1 ratio, further supporting similarities of BC/GC identity (Talos et al., 2012). Reduced expression of $GABA_AR$ α1 is linked to reduced sensitivity to benzodiazepines and barbiturates, which are $GABA_AR$ modulators indicated for select types of seizures, in these pathologies. Comparison of glutamate receptor expression, including AMPAR and NMDAR, have also been measured across BC/GC cells. Increases in GluA1 and GluA4 subunits are consistent with an immature GluR expression profile (Blandini et al., 2008; Talos et al., 2008). Although BC/GC express GluR and $GABA_AR$ subunits, no studies have demonstrated the ability to assemble into functional receptors.

The expression levels of protein transporters further elucidate BC/GC function (Table 3). Chloride cation transporters KCC2 and NKCC1 are downstream targets of mTOR and also the target of the drug bumetanide, respectively (Bakouh et al., 2024). Talos et al. demonstrated decreased KCC2 and increased NKCC1 levels in TSC and FCDIIb lesions. This expression profile is associated with increased neuronal excitability and enhanced seizure susceptibility (Ben-Ari, 2014). At the cellular level, high NKCC1 expression occurred in dysplastic neurons, as well as in GC and reactive astrocytes. In contrast, KCC2 was only expressed in dysplastic and normal-sized neurons, but not in undifferentiated GC or dysplastic astrocytes (Talos et al., 2012). The functional significance of increased NKCC1 in BC/GC is unknown. However, high expression of this chloride transporter could be a sign of immaturity (Rivera et al., 1999).

Glutamate homeostasis was also examined, as it is an important component of epileptogenicity regulated by glial cells. The glutamate transporter EAAT contains two isomers, each linked to a neuronal (EAAT3) versus a glial (EAAT2) lineage. In BC, there was higher EAAT2 than EAAT3 expression by IHC. Additionally, EAAT2 was associated with non-epileptic samples, while the EAAT3 stained heavily in epileptic sections. Together, the authors suggested BC may play a protective role in epileptogenesis (Gonzalez-Martinez et al., 2011). EAATs in GC have not been examined extensively. A mRNA study demonstrated increased abundance of EAAT3 in tuber slices compared to controls (White et al., 2001). After single-cell microdissection, the authors showed that EAAT3 mRNA was expressed in both dysmorphic neurons and GC, although its relative abundance was higher in dysmorphic neurons. Overall, these studies demonstrate that BC/GC are very similar in terms of gene/protein expression and that the differences are more quantitative than qualitative, reinforcing the idea of a common developmental origin.

5 Further insights into BC/GC identity from genetic studies

Single germline or somatic mutations in the mTOR pathway genes have emerged as a primary cause of FCDII (Pelorosso et al.,

TABLE 3 mRNA and protein expression of balloon cells (BC) and giant cells (GC) of glutamate and GABA subunit markers.

Category	Cell marker	BC	GC	Function	Notes and references
Glutamate receptor subunit	GluA1	++	+	Subunit of AMPAR; synaptic plasticity	BC (Oh et al., 2008); Weakly expressed in GC (Talos et al., 2008)
	GluA2	+	u	Subunit of AMPAR; synaptic plasticity	Normal expression in BC (Oh et al., 2008); GC (Talos et al., 2008)
	GluA3	++	u	Subunit of AMPAR	BC (Oh et al., 2008); GC (Talos et al., 2008)
	GluA4	+	++	Subunit of AMPAR; synaptic plasticity	Normal expression in BC (Oh et al., 2008); GC (Talos et al., 2008)
	GluN1	+++	+	Subunit of NMDAR	BC (Oh et al., 2008); Normal expression in GC (Talos et al., 2008)
	GluN2A/B	+++	+	Subunit of NMDAR	BC (Oh et al., 2008); Weak expression in GC (Talos et al., 2008)
GABA receptor subunit	$GABA_AR$ α1	u	u	Subunit of $GABA_AR$; mature neuronal cell marker	BC/GC (Talos et al., 2012; White et al., 2001)
	$GABA_AR$ α4	+	+	Subunit of $GABA_AR$; immature neuronal cell marker	Normal expression in BC/GC (Talos et al., 2012)
Transport protein	KCC2	u	u	Neuron-specific chloride potassium symporter	BC/GC (Talos et al., 2012)
	NKCC1	+	+	Na–K–Cl co-transporter in both neuron and glia	BC/GC (Talos et al., 2012)
	EAAT2	+	n	Glial marker; glutamate regulator	BC (Gonzalez-Martinez et al., 2011)
	EAAT3	u	+	Neuronal marker, glutamate regulator	BC (Gonzalez-Martinez et al., 2011) GC (White et al., 2001)

-: "not expressed" u: "Under expressed"; +: Expressed (may be weakly expressed or normal expression); ++: "Overexpressed"; +++: "Strongly Expressed."
All studies examined human cortical samples. Unless otherwise noted, all studies are immunohistochemical studies of protein expression.

2019). While genetic mutations in TSC1 and TSC2 genes have been known for a long time (European Chromosome 16 Tuberous Sclerosis Consortium, 1993; Martin et al., 2017), the contribution of genetic mutations in FCDII took much longer to be recognized [for a concise review see (Lee et al., 2022)]. In TSC, pathogenic variants for TSC1 and TSC2 genes include deletion, nonsense, and missense mutations, leading to a loss-of-function of hamartin and tuberin (Caban et al., 2017). In FCDIIb, the presence of somatic mutations was first hypothesized in a case of hemimegalencephaly (HME, a congenital MCD with similar histopathology as FCDIIb), and TSC (Salamon et al., 2006). A few years later, whole-exome sequencing in paired brain–blood samples from HME patients identified *de novo* somatic mutations in PIK3CA, AKT3 and MTOR genes in brain samples from one third of affected individuals, indicating aberrant activation of mTOR signaling (Lee et al., 2012). Exome sequencing combined with mass spectrometry analyses validated genetic findings and identified variations in mutation burden across different cortical areas. This led to the conclusion that HME is a genetic mosaic disease caused by gain-of-function in the PI3K-AKT3-mTOR signaling pathway. Soon thereafter, using similar techniques, somatic missense mutations in PIK3CA, AKT3, MTOR and other associated genes were observed in both FCDII and HME cases (Baek et al., 2015; D'Gama et al., 2015; Lim et al., 2015; Nakashima et al., 2015; Pelorosso et al., 2019; Gerasimenko et al., 2023; Lopez-Rivera et al., 2023). In another study including a large cohort of surgical cases presenting with HME and FCDIIa/b, somatic gain-of-function variants in MTOR and its activators (AKT3, PIK3CA, RHEB), as well as germline, somatic and two-hit loss-of-function variants in its repressors (DEPDC5, TSC1, TSC2) were corroborated. Importantly, in the present context, analysis of pools of laser-captured microdissected cells and whole-genome amplification demonstrated that dysmorphic neurons and BC carry those pathogenic variants (Baldassari et al., 2019). More recently, in a large multicenter international collaboration that recruited 283 individuals with FCD, HME and TSC that underwent surgical resections, whole-exome and targeted-amplicon sequencing, as well as single-nucleus RNA sequencing, identified 75 mutated genes through intensive profiling of somatic mutations. In addition, many MCD mutated genes were dysregulated in some specific cell types, particularly in the astrocyte and excitatory neuron lineages (Chung et al., 2023). In agreement, a study in a homogeneous population of FCDII cases using single-nucleus RNA sequencing in morphologically-identified cells, showed that dysmorphic neurons and BC are molecularly distinct, with glutamatergic neuron-like and astrocyte-like identities, respectively (Baldassari et al., 2024). Interestingly, the same study demonstrated that BC display stronger expression of genes coding for secreted proteins (e.g., MFAP4 and IGFBP7), which could affect neighboring cells in a paracrine manner. Finally, some rare neurons displayed an intermediate phenotype, with normal somatic size and mitochondrial numbers, but with aberrant accumulation of intermediate filaments. In terms of the timing of the mutation and the possible origin of BC, based on the fact that other cell types including interneurons and microglia are mutated, the authors suggested that the mutations occurred prior to the divergence into different cell lineages, i.e., at the time of gastrulation, during gestational weeks 2–3 (Baldassari et al., 2024).

6 Electrophysiological and morphological findings in *ex vivo* slices

To the best of our knowledge, our group at UCLA, was the first and, thus far, the only one to record, *in vitro*, the electrophysiological properties of abnormal non-neuronal cells, in particular BC/GC, in FCDIIb and TSC pediatric cases. Although the UCLA pediatric epilepsy program started in earnest around 1988, initial electrophysiological studies sampled neocortical cells from all children undergoing surgery, including a wide variety of pathological substrates (e.g., FCD, infarct, Rasmussen's encephalitis, tumors, etc.) (Wuarin et al., 1990; Wuarin et al., 1992; Dudek et al., 1995). ECoG was used sparingly to select neocortical sample sites, and cells were recorded blindly in slice preparations and categorized, a posteriori, based on electrophysiological properties and fluorescent markers or biocytin labeling. Not surprisingly, the findings were disappointing in that the electrophysiological properties of the sampled neurons were generally normal, and BC/GC cells were not observed.

Our success at recording BC/GC was the result of a number of notable factors: A selection of a homogeneous population of patients presenting with FCD and TSC, increasing the likelihood of finding abnormal cells; an improved method of neocortical sampling previous (MRI, PET) and during surgical procedures (ECoG) to determine the greatest cortical abnormality; the short period of time elapsed between sample resection and slicing (under 10 min); the use of IR-DIC optics to selectively identify abnormal-looking cells before patching; and the confirmation of the pathological substrate by an expert pathologist. Other *ex vivo* studies using human tissue samples from FCD, including FCDIIb, and TSC cases did not report electrophysiological recordings from BC/GC (Calcagnotto et al., 2005; Wang et al., 2007; Lozovaya et al., 2014; Bakouh et al., 2024; Ribierre et al., 2024).

Methods to visualize BC/GC in *ex vivo* slices: With the advent of IR-DIC microscopy (Dodt and Zieglgansberger, 1990), visualization of single cells in slices became feasible (Figure 2). This technique combines infrared light, which penetrates deeper in brain tissue, and Nomarski optics, which greatly enhances the contrast in unstained samples. One drawback of this technique when using brain slices is that, with age and increased myelination, it becomes more difficult to visualize individual cells. We were very fortunate in that our cohort comprised children as young as 2 months of age, up to 14 yr. Before 5 yr. of age, visualization is optimal, but BC/GC could be recorded even in the older cases. In addition, the younger the patient, the better the tissue preservation, the more resistance to hypoxia, and to the trauma caused by the slicing procedure. Brain slices could be maintained in good condition for up to 24 h.

Electrophysiological properties of BC/GC: The first IR-DIC images of GC (Figure 2D) from a TSC patient (3.27 yr. old) were obtained in 1997. In this case, GC were subsequently recorded using the whole-cell patch clamp technique in voltage clamp mode (Figures 3A). After breaking the gigaohm seal and applying a series of depolarizing step voltage commands, we noticed that some GC had an usually high membrane input resistance, suggesting a neuronal phenotype typically seen in immature neurons. Unexpectedly, inward (Na^+ and Ca^{2+}) or outward (delayed rectifier) currents were, respectively, absent or minimal (Figures 3B,C), suggesting the possible existence of "silent" neurons. After processing the slices for biocytin to obtain a more detailed picture

of those cells, we noticed their bizarre morphology consisting of abundant undulating processes stemming from round or oval somata, the absence of dendritic spines and instead the presence of varicosities, and, more importantly, a definite axon could not be found. We initially called these cells "atypical." IHC staining of tissue from the same case, demonstrated that many of these "atypical" cells were positive for NeuN. However, a few cells were labeled by both NeuN and GFAP, suggesting a glial or mixed phenotype (Mathern et al., 2000). In fact, the morphology appeared consistent with that of fibrillary astrocytes. As more cases of FCDIIb and TSC were examined both electrophysiologically and morphologically, we came to the realization that these "atypical" cells were indeed the "grotesque," "bizarre," "monstrous," BC/GC described in classic anatomical studies (Cepeda et al., 2003). But while BC/GC have attracted most of the attention, we have to emphasize that medium- and small-sized, variably shaped cells also abound in FCDIIb and TSC tissue. Many of these could correspond to the "stellate" or "spider" cells reported by pioneer investigators of TSC cases.

The electrophysiological membrane properties of non-neuronal cells, including BC/GC in FCDIIb and TSC, were examined in more detail in subsequent studies by our group (Cepeda et al., 2005a,

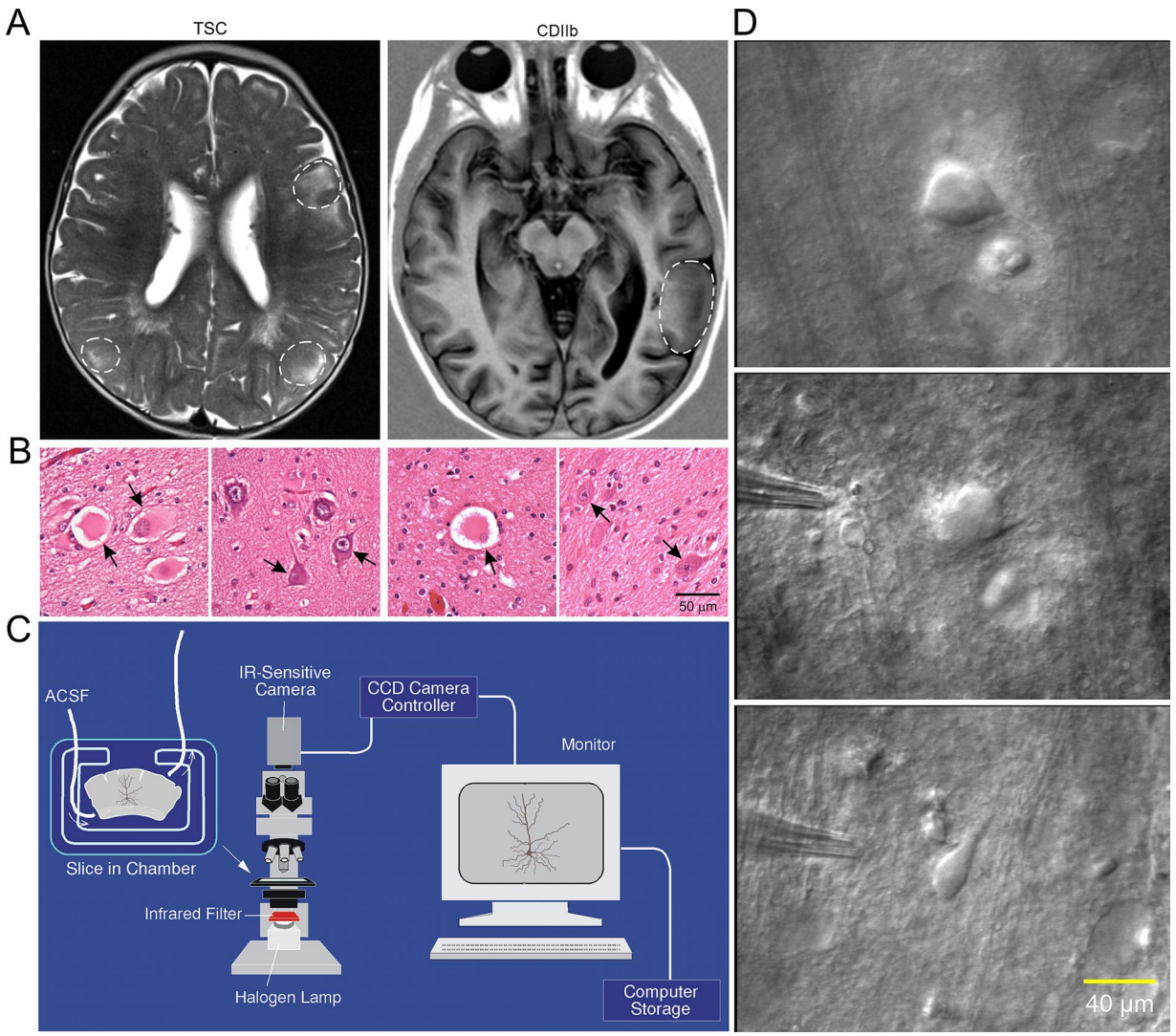

FIGURE 2
(A) Representative axial MRI scans of children (both 7 years old) with refractory epilepsy from TSC (left) and FCDIIb (right). There are multiple cortical tubers (dashed circles) in the patient with TSC and one focal area of cortical dysplasia in the left temporal lobe in the child with FCDIIb. **(B)** *Left panels*: Section of a tuber (originating from a 19-month-old male) showing abundant giant cells and disorganized collections of dysmorphic neurons. Arrows in left panel indicate giant cells in which the nucleus shows coarse chromatin, a pattern often seen in astrocytes. *Right panels*: Representative fields from a resection (originating from a 9-year-old female) showing features of FCDIIb. Note a balloon cell (arrow, left panel) with glassy eosinophilic cytoplasm, and dysmorphic neurons (arrows, right panel). The balloon cell shows "retraction" of cytoplasm from the neuropil (images are from sections stained with H&E). Scale bar represents 50 µm and applies to all panels. **(C)** Setup used for electrophysiological recordings from visualized cells in *ex vivo* brain tissue slices. An upright microscope equipped with differential interference contrast (DIC, Nomrarski) optics and infrared (IR) illumination allows visualization of individual cells. Slices are maintained in a custom-made chamber with oxygenated artificial cerebrospinal fluid (ACSF). IR images are stored in a computer. After electrophysiological recordings the slices are fixed in paraformaldehyde and processed for biocytin staining. **(D)** First ever IR-DIC images (top and middle panels) of BC/GC from a TSC patient (3.27 years). Notice the large size of BC/GC compared to a normal pyramidal neuron (bottom panel). Adapted from Cepeda et al. (2003, 2012). This and other figures use material previously published. Permission to use this material was obtained from Wiley and Elsevier Publishers.

2006, 2010). Passive membrane properties showed that most BC/GC had a large membrane capacitance, consistent with their large size, the input resistance was more variable, but it was generally high. In terms of active membrane properties, recordings in current clamp mode showed that most cells had a hyperpolarized resting membrane potential, and could not generate action potentials even at very depolarized voltages (Figures 4, 5B). Analysis of the current–voltage (IV) plots revealed that some cells had a clearly linear relationship, consistent with an astroglial phenotype, while others displayed rectification at hyperpolarized or depolarized membrane potentials, consistent with a neuronal phenotype. In addition, small outward currents usually could be appreciated, and very rarely an incipient inward current occurred (Cepeda et al., 2012).

It soon became evident that a simple categorization of non-neuronal cells as just BC/GC in FCDIIb and TSC, could not account for the wide variety of morphological and electrophysiological features of these cells.

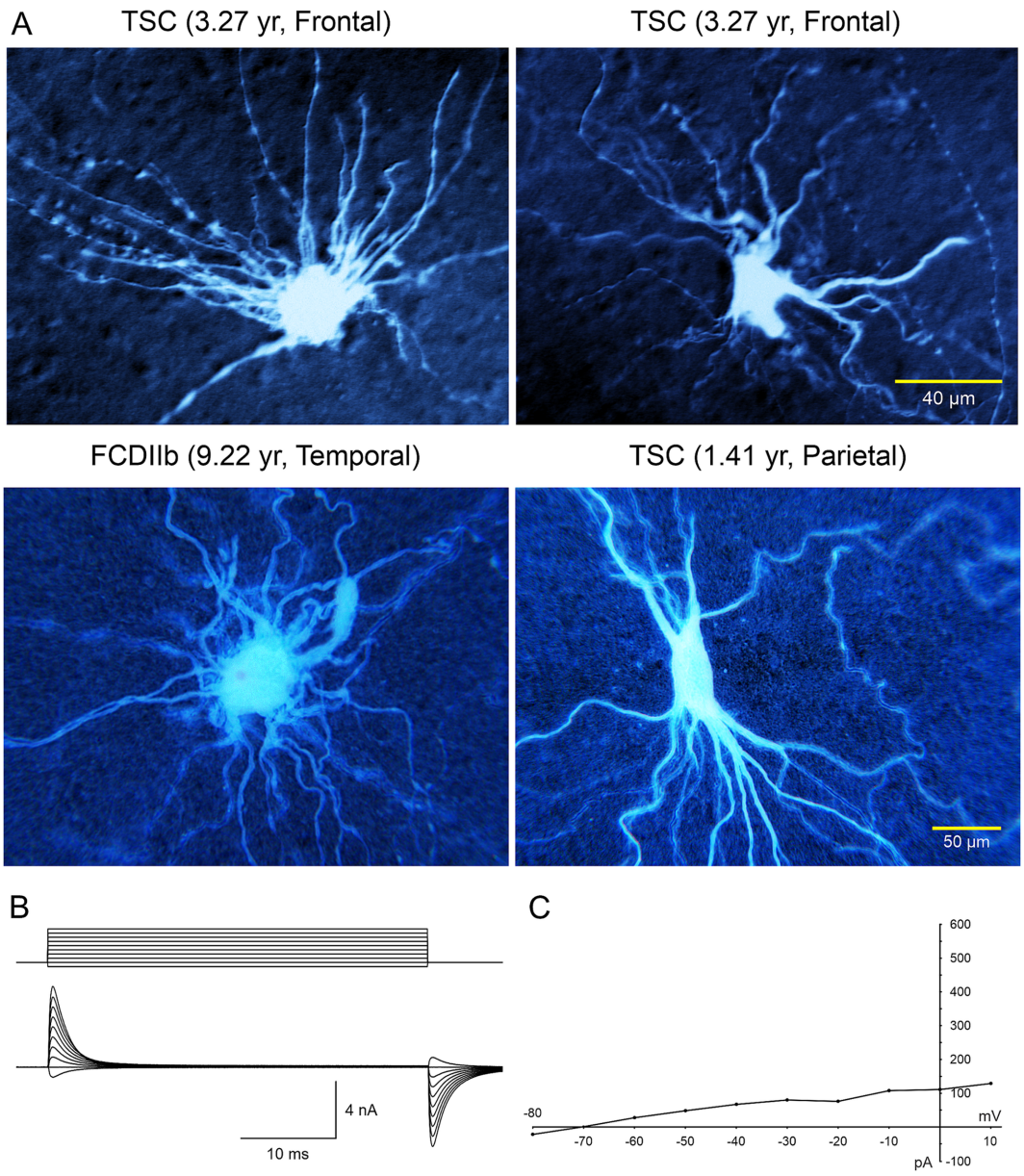

FIGURE 3
(A) Large cells recorded electrophysiologically in tissue slices from TSC and FCDIIb cases. Cells were recorded and subsequently stained with biocytin. Top left cell corresponds to the IR image in Figure 1 (top panel). The voluminous cell in the FCDIIb case had a very thick appendage and presented with an incipient Na^+ current at depolarized potentials, while the other cells displayed no inward currents and only small outward currents. **(B)** Whole-cell patch clamp recording of the cell in top left. In voltage clamp mode, a series of hyperpolarizing and depolarizing voltage commands (from –80 to +10 mV) evoked practically no inward current and very small outward currents. The high input resistance suggested a neuronal phenotype; however this was dismissed as no Na^+ or Ca^{2+} currents were observed. The patch pipette contained Cs-methanesulfonate-based internal solution. **(C)** Current–voltage plot of responses evoked by hyperpolarizing and depolarizing voltage commands in **(B)**. Only very small outward current could be measured. Calibration bar on the right also applies to left panels. The original biocytin images were modified for pseudo-color and brightness/contrast enhancement using Adobe Photoshop. Adapted from Mathern et al. (2000) and Cepeda et al. (2003, 2012).

Thus, while some of the non-neuronal cells appeared "neuronal-like" (Figure 6) and others appeared "glial-like" (Figures 7, 8), still others defied classification. Although calling non-neuronal cells "neuronal-like" seems paradoxical, it is not unprecedented. We recently recorded human neural stem cells implanted in a mouse model of Huntington's disease. Some of the cells displaying immature membrane properties, including very high input resistance, did not fire action potentials when depolarized, and received no or rare synaptic inputs (Holley et al., 2023). If we assume that BC/GC are frozen in a progenitor neural stem cell stage, it is possible that some membrane properties appear neuronal-like, while others are not yet typical of neurons.

Other types of abnormal non-neuronal cells: We later described the existence of "intermediate cells" that appear to have a clear pyramidal-shaped soma and a nascent apical dendrite, but in more distal regions they display bushy, wavy processes, reminiscent of those observed in BC/GC (Figures 9, 10; Cepeda et al., 2012). Finally, after separating cells into "neuronal-like," "glial-like," and "intermediate," still some cells could not be categorized, and we call them "undetermined" (Figure 9). Indeed, we also recorded cells that looked like dysmorphic or reactive astrocytes. This rich variety could reflect the fact that the degree of neuronal vs. glial marker expression varies from cell to cell, suggesting that these cells conform a heterogeneous group. This is consistent with observations in TSC histological samples showing a wide spectrum of abnormal cells including dysplastic neurons, giant neuroglial cells, giant and dysplastic astroglia, and reactive astrocytes (Talos et al., 2008). Indeed, based on the pediatric epilepsy material we have examined in the past 30 years we found that non-neuronal cells represent a heterogeneous group, with a wide variety of cell shapes, sizes, and dendritic elaboration, suggesting diverse function or lack thereof, as well as different roles in epileptogenesis.

In sum, before the introduction of IR-DIC microscopy, it was believed that BC/GC could play an active role in epileptogenesis, based on complex morphology and exuberant dendrites (Spreafico et al., 1998; Schwartzkroin and Walsh, 2000). A paradigm shift occurred when we demonstrated conclusively that BC/GC cells were incapable of generating action potentials, did not appear to receive synaptic inputs, and were unresponsive to iontophoretic application of excitatory aminoacids (Mathern et al., 2000; Cepeda et al., 2003). The absence of synaptic inputs is consistent with IHC studies by other groups showing that cortical tubers have reduced expression of synapsin I, as well as other synaptic markers (Lippa et al., 1993; Toering et al., 2009). Overall, our findings support the idea that non-neuronal cells in FCDIIb and TSC are a heterogenous group that can come in many flavors, similar to IHC findings in TSC cases (Talos

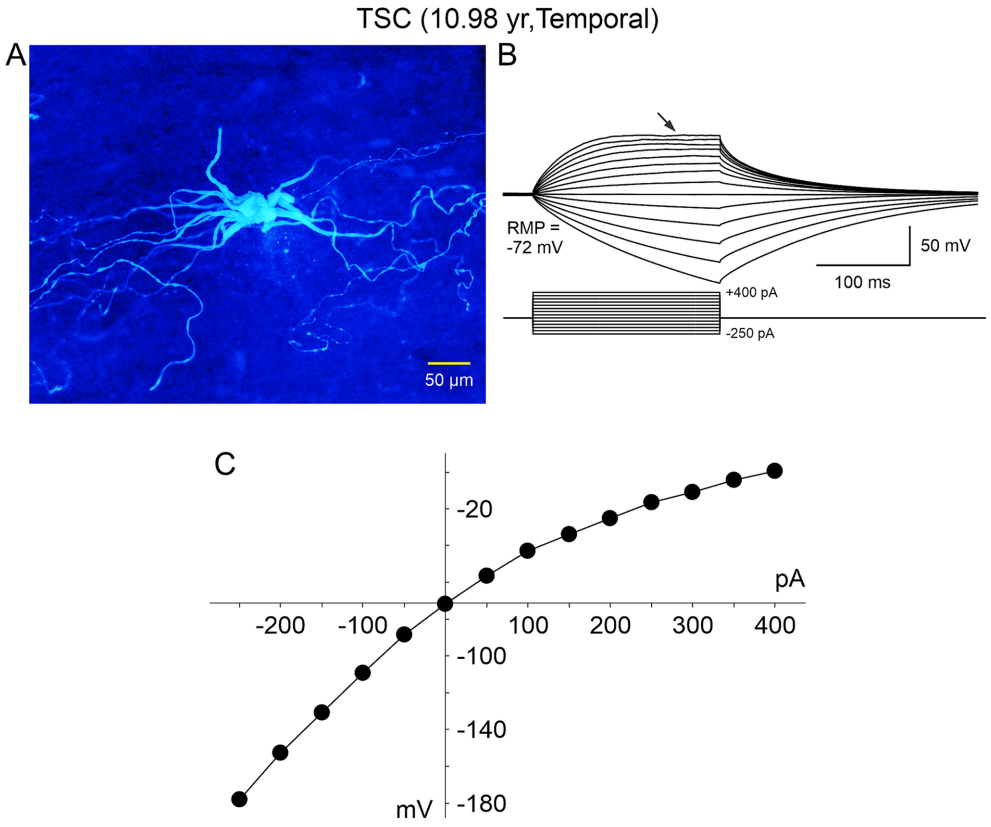

FIGURE 4
A "spider"-like cell recorded in a TSC case. **(A)** Biocytin-filled cell showed multiple thick processes emerging from an ill-defined, gnarled soma. As they distanced from the center, these processes tapered and became progressively thinner, swerving around haphazardly. The thin processes contained numerous varicosities, similar to those illustrated in Machado-Salas (1984) study (Figure 1) and speculated as being a point of neuronoglial interaction by a reactive astrocyte and a deteriorated cortical pyramidal neuron. **(B)** This cell was recorded in current clamp mode (K-gluconate as the pipette internal solution). A series of negative and positive step currents induced voltage deflections similar to those evoked in a "model" cell. However, no action potentials could be evoked even at very depolarized potentials and instead a strong rectification occurred (arrow). **(C)** Current–voltage plot of the changes in voltage evoked by increasing negative and positive current pulses. Notice that with negative current steps the current–voltage relationship is practically linear, whereas positive current steps induce strong rectification. Adapted from Cepeda et al. (2012).

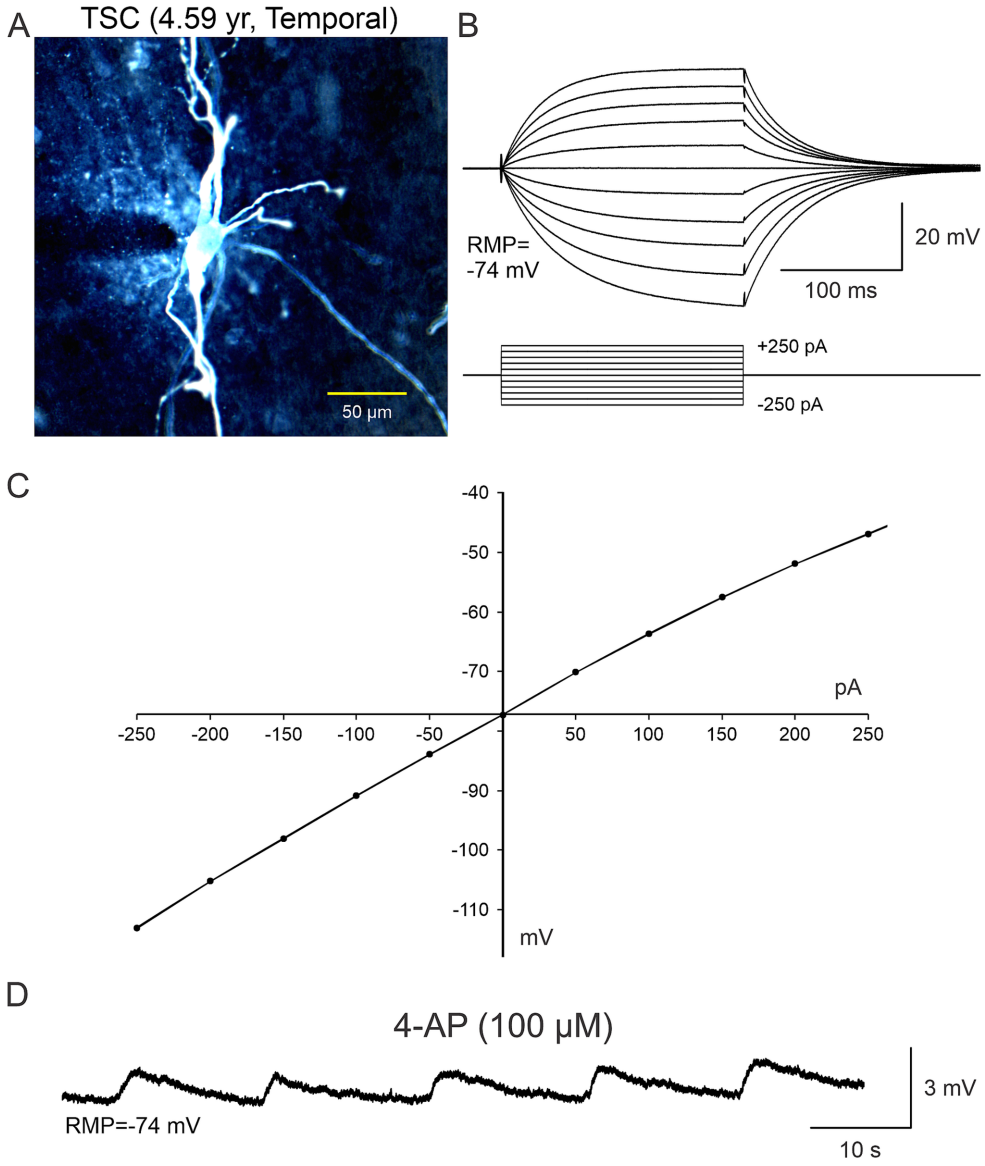

FIGURE 5
In terms of the functional role of non-neuronal cells **(A–C)**, in some electrophysiological recordings slices were bathed in ACSF solution containing 4-aminopyridine (4-AP), a K^+ channel blocker that increases neurotransmitter release as well as K^+ concentration in the extracellular milieu. It became evident that BC/GC were not completely isolated from the environment as they were capable of sensing changes in K^+ concentration, that was manifested by small, rhythmic membrane oscillations **(D)**. Adapted from Levinson et al. (2020).

et al., 2008). This heterogeneity of non-neuronal cells in FCDIIb and TSC, calls for a re-evaluation of cell classification in these pathologies.

7 Functional considerations regarding BC/GC and their role in epileptogenesis

BC are pathognomonic of FCDIIb, resemble GC found in TSC, and many of these cells are similar to fibrillary astrocytes. Indeed, some authors have suggested that TSC, and by extension FCDIIb, could be classified as a pathology of astrocytes, a group that includes, among others, subependymal tumors, SEGA, Alexander disease, and gemistocytic astrocytoma (Sosunov et al., 2008). For example, despite the name astrocytoma, the GC in SEGA also express neuronal markers (Jozwiak et al., 2005; Jozwiak et al., 2006). Similarly, in Alexander disease, a genetic disorder of astrocytes caused by a dominant gain-of-function mutation in the GFAP gene, enlarged dysmorphic and reactive astrocytes with characteristic Rosenthal fibers can be found (Brenner et al., 2001; Messing et al., 2012). They are believed to be a product of elevated GFAP, secondary to increased protein synthesis driven by the mTOR pathway. Of relevance, Rosenthal fibers also have been observed in some TSC and FCDIIb cases (Khanlou et al., 2009; Hirfanoglu and Gupta, 2010; Blumcke et al., 2021). Similar histopathologies in these disorders support the idea that FCDIIb and TSC could be considered, at least in part, a disease of astrocytes. This idea has been reinforced by recent single-cell genomic and transcriptomic profiling demonstrating that BC in FCDIIb are closely

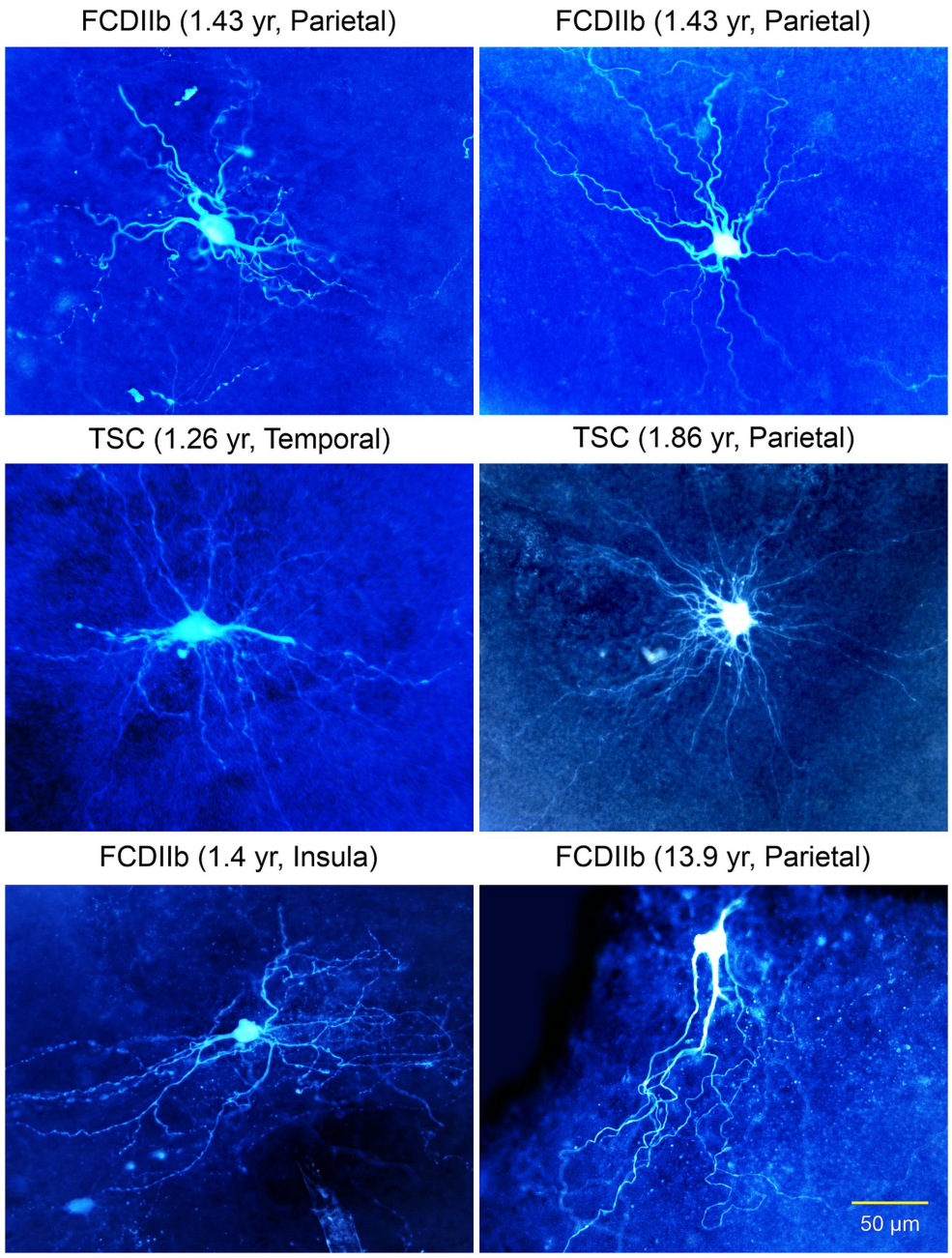

FIGURE 6
Gallery of non-neuronal cells with "neuronal"-like properties recorded in FCDIIb and TSC cases. Some commonalities included the inability to generate action potentials, lack of synaptic inputs, and absence of dendritic spines. The cell in the right middle panel appeared similar to a glial cell, however, its electrophysiological properties were more neuronal-like, e.g., high input resistance. Some of these cells appear similar to the "stellate" cells reported by Huttenlocher and Heydemann or by Ferrer et al. in 1984. Importantly, they do not have an axon. Adapted from Cepeda et al. (2003, 2005a,b, 2006).

related to astrocytes, whereas dysmorphic neurons are more akin to glutamatergic neurons (Baldassari et al., 2024).

In normal and pathological conditions, astrocytes play a critical role in, among others, buffering K^+ and glutamate, providing energy substrates, neurotransmitter precursors, purines, growth factors, and gliotransmitters (Sofroniew and Vinters, 2010). Importantly, astrocytes are an integral part of the tripartite synapse and modulate neuronal activity via feedback mechanisms. Aberrant synaptic communication between neurons and glia may thus contribute to neural pathologies (Liu et al., 2023). If some BC/GC can be considered enlarged astrocytes, what could be their significance in FCDIIb and TSC? Before attempting to answer this question, it is important to determine whether BC/GC establish direct contact with neurons and vice versa. In his landmark Golgi study, Machado-Salas noticed the existence of GC-neuron contacts, suggesting a possible substrate for interaction (Machado-Salas, 1984). Also, as noted earlier, an ultrastructural study reported the existence of rare neuroglial junctions (Trombley and Mirra, 1981). However, direct contacts between neurons and BC/GC seem to be an exception. More likely, the presence of BC/GC leads to aberrant synaptic organization.

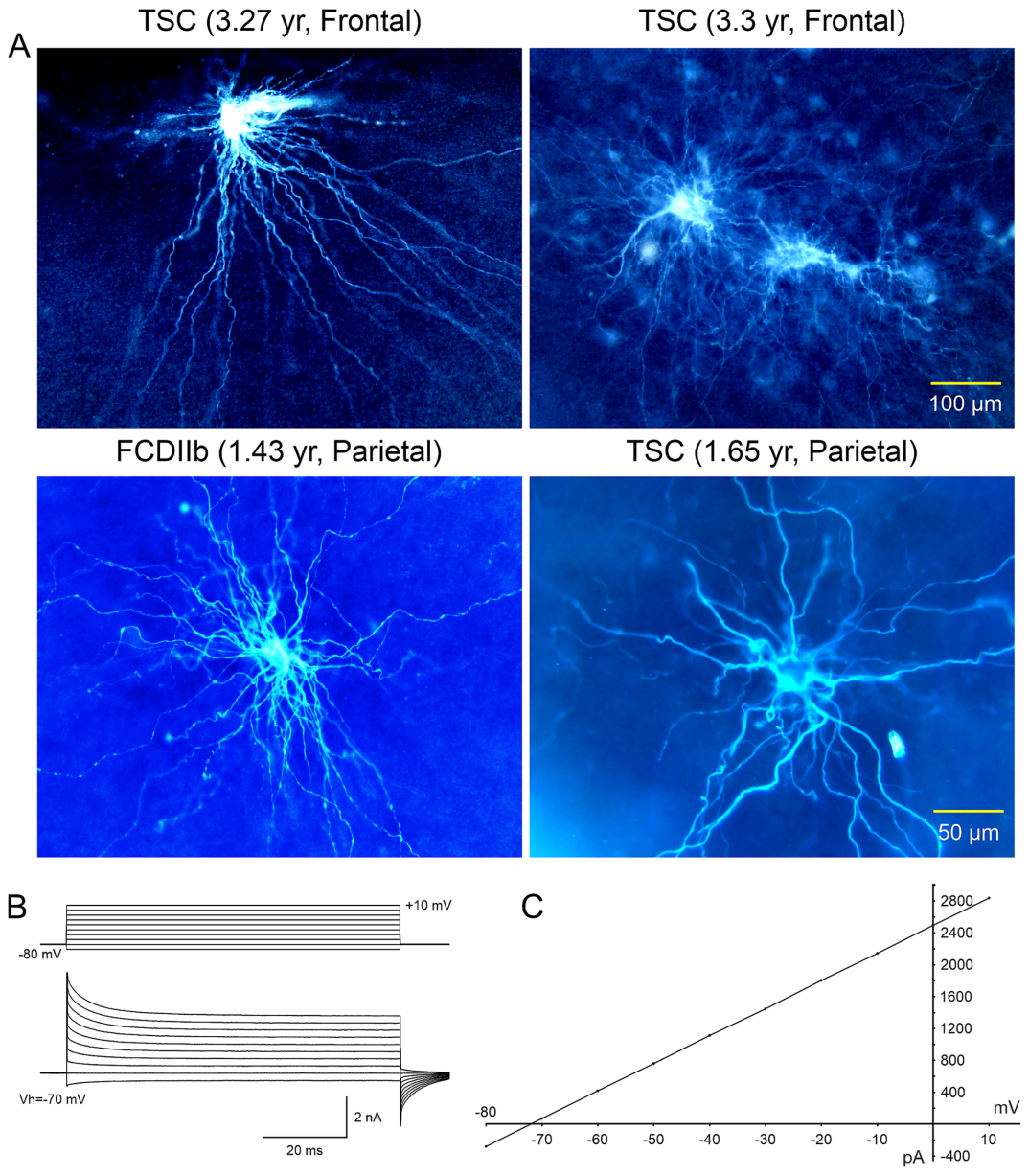

FIGURE 7
(A) Cells with glial-like properties recorded in TSC and CDIIb cases. The electrophysiology of depicted cells was more typical of those of astrocytes, except for the large size and extended space domain. The two giant cells in top right panel appear coupled via gap junctions. **(B)** One of the coupled cells (top right panel) was recorded in voltage clamp mode. It displayed a very low input resistance and large cell membrane capacitance. **(C)** The plot shows a typical linear current–voltage relationship as well as very large outward currents. Adapted from Cepeda et al. (2012).

Because axon terminals slated to innervate cortical areas are now occupied by BC/GC unable to form functional synaptic connections, those areas could become hyperexcitable (Cepeda et al., 2003; Cepeda et al., 2006; Abdijadid et al., 2015). Interestingly, studies have demonstrated that areas with larger accumulation of BC do not appear to be epileptogenic, in fact they display less paroxysmal activity than adjacent areas (Boonyapisit et al., 2003). This agrees with FDG-PET characterization of FCDIIb and TSC lesions prior to surgical resections demonstrating that BC are localized to areas of hypometabolism (Luat et al., 2007; Wang et al., 2023), likely related to the inability of BC to generate action potentials (Cepeda et al., 2006).

Investigation of glutamate clearance showed BC outside of ictal onset areas had an increased expression of glial glutamate transporters (GLT1/EAAT2) (Gonzalez-Martinez et al., 2011). Increased neuronal glutamate transporters also were found in cortical tubers (White et al., 2001). Therefore, it is possible that BC/GC play a protective role in epileptogenesis, regulating neuronal synaptic transmission via the tripartite synapse. In support, we recently demonstrated that BC/GC can sense changes in neurotransmitter and K^+ concentration and display slow rhythmic membrane oscillations during high levels of neuronal activation (Levinson et al., 2020; Figure 5). Similar to BC/GCs are intermediate cells, which display both neuronal and glial markers and do not generate action potentials (Talos et al., 2008;

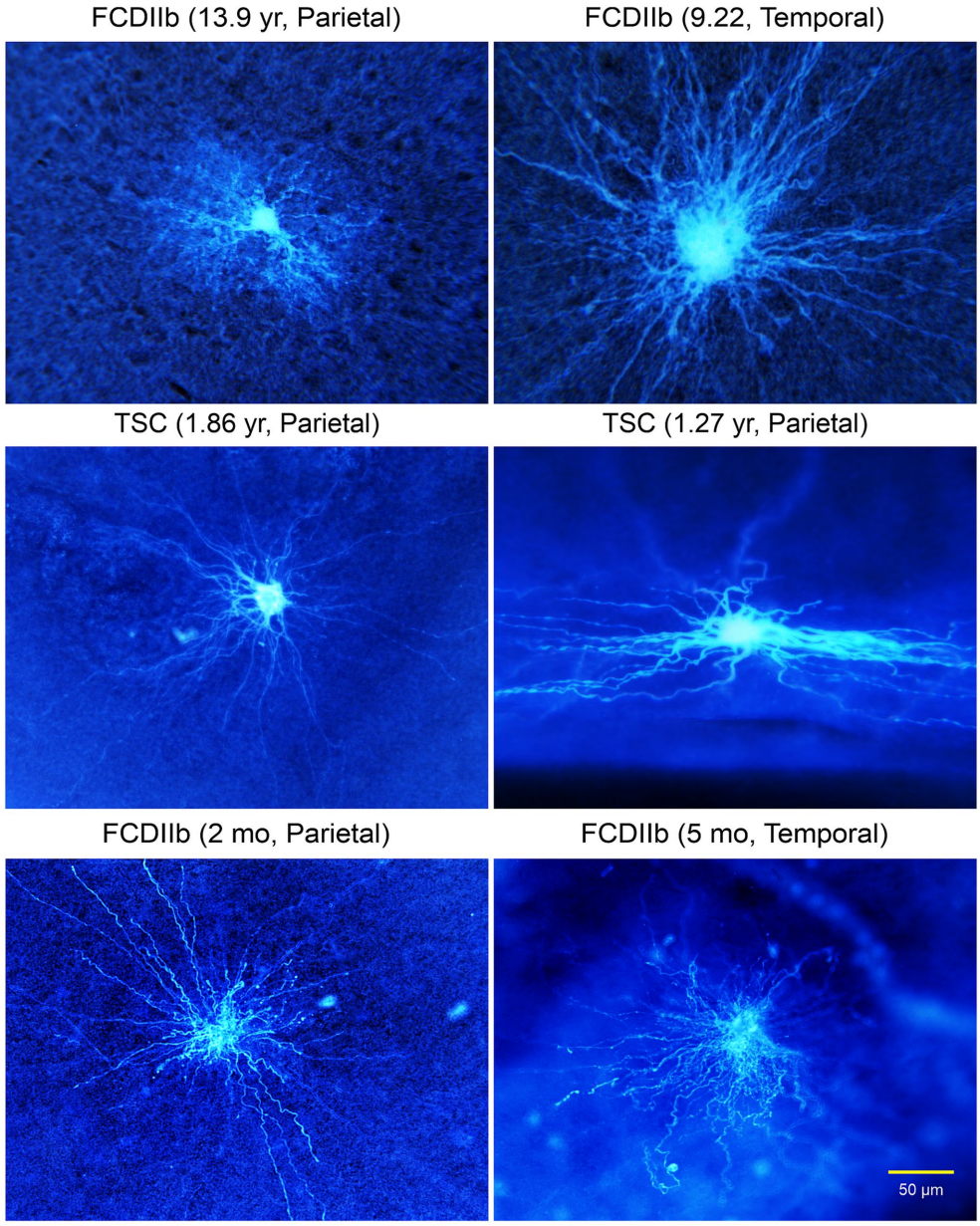

FIGURE 8
Gallery of typical glial cells. The astrocyte in top left panel looks more normal compared to the other cells, in particular the enlarged cell in the top right panel. All cells had abundant processes extending for several hundred microns. The cell in the right middle panel was recorded in the subpial area, hence the very different, flattened space domain of its processes. Adapted from Cepeda et al. (2012).

Blumcke et al., 2011; Cepeda et al., 2012). Thus, while BC/GC and intermediate cells do not appear to participate actively in epileptogenic processes, they could instead dampen epileptic activity.

A recent review article asked the question of whether BC/GC in FCDIIb, TSC, and HME are friends or foes (Liu et al., 2024). The authors are correct in that there is no simple answer and their role in these pathologies is more nuanced, which may be related to the extent to which BC/GC are more glial-like or neuronal-like. If BC can effectively dampen epileptic activity, one may think that they are friends. This would agree with the fact that epileptogenesis is associated with the density of dysmorphic cytomegalic neurons (Stephenson et al., 2021) and not with that of BC/GC. However, even though BC/GC lack an axon and classical chemical synapses, gliotransmission is still possible. For example, a study designed to examine neuron–glia interactions in cell cultures and organoids from TSC and control cases demonstrated that TSC astrocytes displayed increased proliferation and changes in gene expression consistent with an enrichment of secreted and transmembrane proteins related to EGFR signaling (Dooves et al., 2021). Surprisingly, in neurons cultured with astrocyte-conditioned medium there was an increase in the percentage of GABA synapses ($VGAT^+$) relative to glutamate synapses ($VGLUT^+$), leading to altered excitatory-inhibitory balance. Considering that KCC2 is reduced in cortical tubers and FCDIIb lesions (Talos et al., 2012), GABA gliotransmitter release from BC/GC could become excitatory. Interestingly, studies have shown increased GABA levels along with reduced benzodiazepine receptors in brain

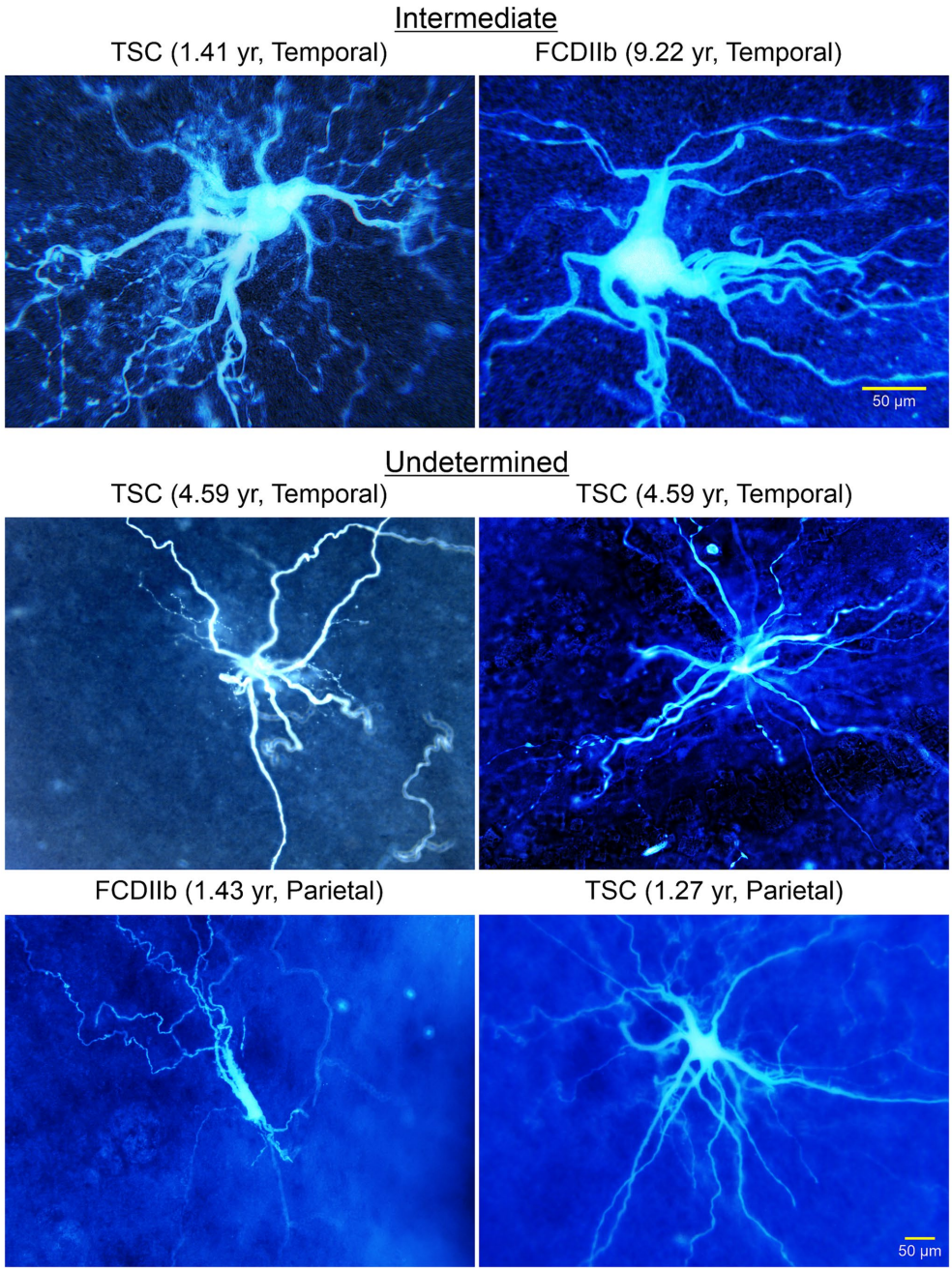

FIGURE 9
A wide variety of cells was observed in TSC and FCDIIb tissue samples. Some cells had a neuronal, even pyramidal-shaped soma (top right panel). However, the processes lacked spines and the thick (apical-looking) dendrites quickly metamorphosed into a multitude of fine branches. These cells are considered "intermediate" for their glioneuronal features. Other cells could not be determined (middle and bottom panels). Some appeared as just a few thick processes but seemingly lacking a defined soma. The cell in the bottom left panel appeared as a deteriorating cell similar to the aberrant cortical neurons observed by Machado-Salas (1984, Figure 2). Adapted from Cepeda et al. (2012).

tissue from TSC patients (Mori et al., 2012). Thus, GABA gliotransmission, if confirmed, could exacerbate the intrinsic epileptogenicity of dysmorphic cytomegalic pyramidal neurons (Cepeda et al., 2005b; Cepeda et al., 2007; Abdijadid et al., 2015). In addition, considering that BC/GC do not appear to participate in integrative functions associated with typical neurons, their energy demands could represent a metabolic burden for local neuronal circuits.

8 Therapeutic implications

Without knowing with certainty whether BC/GC and other non-neuronal cells in FCDIIb and TSC are protective or deleterious, targeting these cells specifically or the mTOR pathway in general, the possible outcomes are difficult to predict. Because of the diffuse nature of these changes affecting not only the lesion or tuber areas but also the perilesional/perituberal regions, and the fact that they

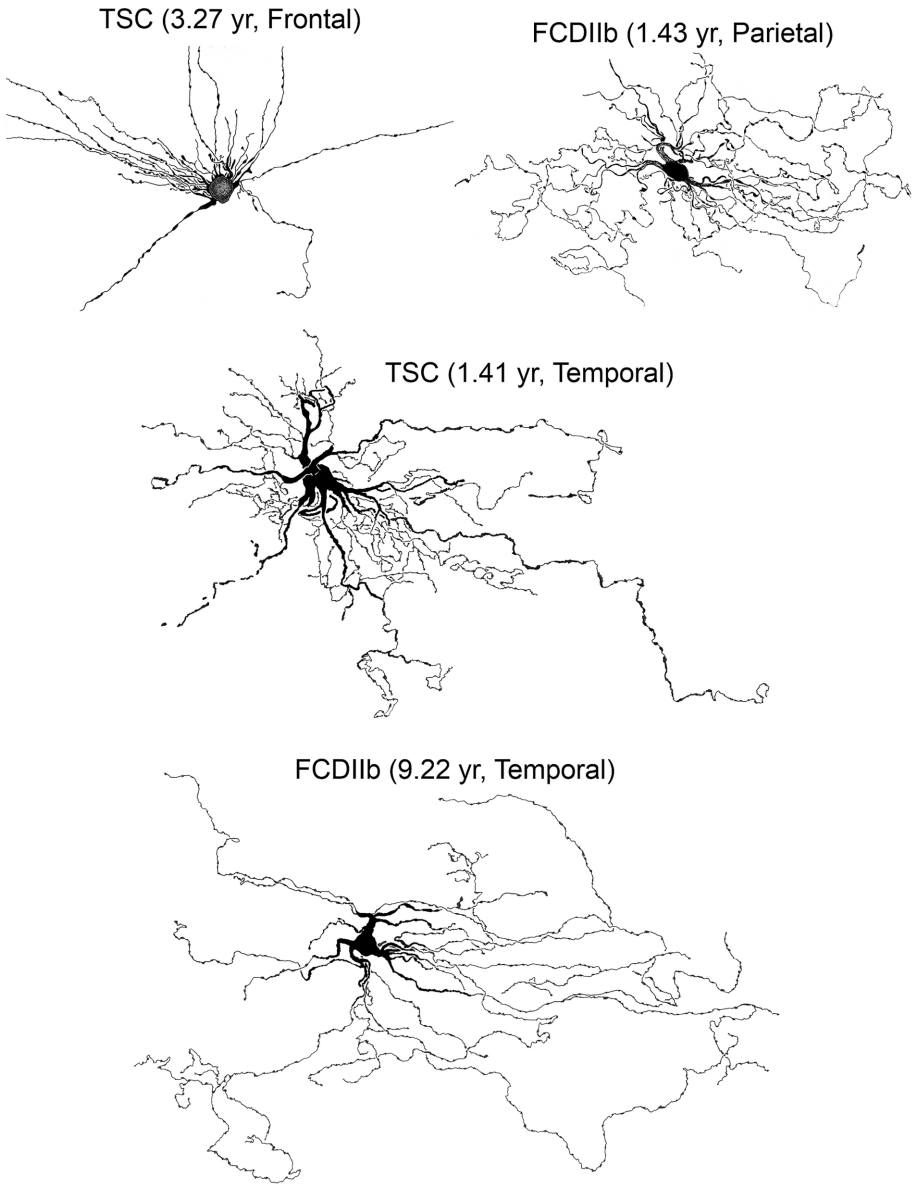

FIGURE 10
Some of the biocytin-filled cells shown in previous figures were used to construct camera lucida drawings (courtesy of the late Robin S. Fisher). Cells displayed various somatic shapes but all possessed long, waving processes with numerous varicosities. Adapted from Cepeda et al. (2003, 2006, 2012).

occur so early in brain development, it is unlikely that pharmacological manipulations will have a major impact on seizure-generation unless the lesions can be identified in utero and treatment starts immediately. A promising venue is CRISPR-based gene editing. For example, gene activation via targeting enhancers of haploinsufficient genes has been proposed as a therapeutic intervention in autism, as well other neurodevelopmental disorders (Chen et al., 2024). However, some symptoms in FCDIIb and TSC patients can be ameliorated using mTOR targeting drugs. For example, mTOR inhibitors everolimus and rapamycin have demonstrated the ability to decrease seizure activity in TSC human trials (Muncy et al., 2009; Krueger et al., 2013). Sirolimus, generic for rapamycin, also was shown to reduce the frequency of epileptic seizures in FCDII patients (Kato et al., 2022). However, no improvement was noted in another case (Hadouiri et al., 2020). A different clinical study in TSC and FCD patients showed that short-term everolimus had no adverse effects and there was a trend for lower pS6 (Leitner et al., 2022). In *ex vivo* slices, we demonstrated antiseizure effects of everolimus and these effects were more pronounced in TSC and FCD cases compared to non-mTOR-mediated pathologies (Cepeda et al., 2018). Another pharmacological target has been finding ways to reverse the depolarizing actions of GABA caused by high levels of NKCC1 and low levels of KCC2 (Talos et al., 2012), which facilitate seizure occurrence (Dzhala et al., 2005). A number of studies have demonstrated efficacy of bumetanide in the treatment of seizures and some symptoms of autism (Ben-Ari, 2017; van Andel et al., 2020; Soul et al., 2021; Ben-Ari and Cherubini, 2022). Other studies also indicate that the expression of innate immune markers is elevated in areas with high concentrations of BC in FCDIIb, particularly in the white matter (Zimmer et al., 2021).

Thus, therapies targeting inflammation could be beneficial in FCDIIb. Similarly, a recent study reported signatures of cellular senescence (e.g., p53/p16 expression and senescence-associated β-galactosidase activity) in dysmorphic neurons and BC found in FCDIIb cases, suggesting that senolytic drugs such as dasatinib and quercetincan can be used to reduce seizure activity (Ribierre et al., 2024).

9 Conclusion

Any attempt to classify BC/GC into further subcategories cannot be based on purely morphological or electrophysiological grounds. Only by integrating electrophysiological observations, morphology, protein and gene (mRNA) expression, can we determine with more accuracy cell type and potential function. Morphology alone can be misleading (e.g., BC/GC being epileptogenic or "stellate" neurons lacking an axon). By definition, neurons have the capacity to generate an action potential, they possess an axon able to transmit electric signals, integrate synaptic inputs, and release neurotransmitters and/or neuromodulators. We can conclude that BC/GC are a subtype of non-neuronal cells and are functionally similar to astrocytes. However, some BC/GC also display some neuronal properties typically found in immature neural stem cells. Thus, although definitely not neuronal, BC/GC, as well as some medium-sized cells unable to fire action potentials, can be categorized into different subgroups based on morphological and electrophysiological properties as neuronal-like or glial-like. We hope that decontextualizing these cells from their pathology may elucidate the role of BC/GC in the pathophysiology of pediatric epileptic seizures caused by FCDIIb and TSC.

Author contributions

JZ: Writing – original draft, Writing – review & editing. DA: Writing – review & editing. XT: Writing – review & editing. HV: Writing – review & editing. GM: Writing – review & editing. CC: Writing – review & editing, Writing – original draft.

Funding

The author(s) declare that no financial support was received for the research, authorship, and/or publication of this article.

Acknowledgments

The authors would like to acknowledge the critical comments from Jesus P. Machado-Salas. Daphne Marina contributed to literature search during the initial stages of this review. Joshua Barry helped with the illustrations.

Conflict of interest

The authors declare that the research was conducted in the absence of any commercial or financial relationships that could be construed as a potential conflict of interest.

The author(s) declared that they were an editorial board member of Frontiers, at the time of submission. This had no impact on the peer review process and the final decision.

Publisher's note

References

Abdijadid, S., Mathern, G. W., Levine, M. S., and Cepeda, C. (2015). Basic mechanisms of epileptogenesis in pediatric cortical dysplasia. *CNS Neurosci. Ther.* 21, 92–103. doi: 10.1111/cns.12345

Alvarez-Buylla, A., Garcia-Verdugo, J. M., and Tramontin, A. D. (2001). A unified hypothesis on the lineage of neural stem cells. *Nat. Rev. Neurosci.* 2, 287–293. doi: 10.1038/35067582

Arceneaux, J. S., Brockman, A. A., Khurana, R., Chalkley, M. L., Geben, L. C., Krbanjevic, A., et al. (2024). Multiparameter quantitative analyses of diagnostic cells in brain tissues from tuberous sclerosis complex. *Cytometry B Clin. Cytom.* doi: 10.1002/cyto.b.22194

Arena, A., Zimmer, T. S., van Scheppingen, J., Korotkov, A., Anink, J. J., Muhlebner, A., et al. (2019). Oxidative stress and inflammation in a spectrum of epileptogenic cortical malformations: molecular insights into their interdependence. *Brain Pathol.* 29, 351–365. doi: 10.1111/bpa.12661

Arseni, C., Alexianu, M., Horvat, L., Alexianu, D., and Petrovici, A. (1972). Fine structure of atypical cells in tuberous sclerosis. *Acta Neuropathol.* 21, 185–193. doi: 10.1007/BF00688497

Baek, S. T., Copeland, B., Yun, E. J., Kwon, S. K., Guemez-Gamboa, A., Schaffer, A. E., et al. (2015). An AKT3-FOXG1-reelin network underlies defective migration in human focal malformations of cortical development. *Nat. Med.* 21, 1445–1454. doi: 10.1038/nm.3982

Bakouh, N., Castano-Martin, R., Metais, A., Dan, E. L., Balducci, E., Chhuon, C., et al. (2024). Chloride deregulation and GABA depolarization in MTOR related malformations of cortical development. *Brain*. doi: 10.1093/brain/awae262

Baldassari, S., Klingler, E., Gomez Teijeiro, L., Doladilhe, M., Raoux, C., Puiggros, S. R., et al. (2024). Single-cell genotyping and transcriptomic profiling in focal cortical dysplasia. *Nat. Portf.* doi: 10.21203/rs.3.rs-4014535/v1

Baldassari, S., Ribierre, T., Marsan, E., Adle-Biassette, H., Ferrand-Sorbets, S., Bulteau, C., et al. (2019). Dissecting the genetic basis of focal cortical dysplasia: a large cohort study. *Acta Neuropathol.* 138, 885–900. doi: 10.1007/s00401-019-02061-5

Barkovich, A. J., Guerrini, R., Kuzniecky, R. I., Jackson, G. D., and Dobyns, W. B. (2012). A developmental and genetic classification for malformations of cortical development: update 2012. *Brain J. Neurol.* 135, 1348–1369. doi: 10.1093/brain/aws019

Baybis, M., Yu, J., Lee, A., Golden, J. A., Weiner, H., McKhann, G. 2nd, et al. (2004). mTOR cascade activation distinguishes tubers from focal cortical dysplasia. *Ann. Neurol.* 56, 478–487. doi: 10.1002/ana.20211

Ben-Ari, Y. (2014). The GABA excitatory/inhibitory developmental sequence: a personal journey. *Neuroscience* 279, 187–219. doi: 10.1016/j.neuroscience.2014.08.001

Ben-Ari, Y. (2017). NKCC1 chloride importer antagonists attenuate many neurological and psychiatric disorders. *Trends Neurosci.* 40, 536–554. doi: 10.1016/j.tins.2017.07.001

Ben-Ari, Y., and Cherubini, E. (2022). The GABA polarity shift and bumetanide treatment: making sense requires unbiased and undogmatic analysis. *Cells* 11:396. doi: 10.3390/cells11030396

Blandini, F., Armentero, M. T., and Martignoni, E. (2008). The 6-hydroxydopamine model: news from the past. *Parkinsonism Relat. Disord.* 14, S124–S129. doi: 10.1016/j.parkreldis.2008.04.015

Blumcke, I. (2024). Neuropathology and epilepsy surgery −2024 update. *Free Neuropathol.* 5. doi: 10.17879/freeneuropathology-2024-5347

Blumcke, I., Coras, R., Busch, R. M., Morita-Sherman, M., Lal, D., Prayson, R., et al. (2021). Toward a better definition of focal cortical dysplasia: An iterative histopathological and genetic agreement trial. *Epilepsia* 62, 1416–1428. doi: 10.1111/epi.16899

Blumcke, I., Spreafico, R., Haaker, G., Coras, R., Kobow, K., Bien, C., et al. (2017). Histopathological findings in Brain tissue obtained during epilepsy surgery. *N. Engl. J. Med.* 377, 1648–1656. doi: 10.1056/NEJMoa1703784

Blumcke, I., Thom, M., Aronica, E., Armstrong, D. D., Vinters, H. V., Palmini, A., et al. (2011). The clinicopathologic spectrum of focal cortical dysplasias: a consensus classification proposed by an ad hoc task force of the ILAE diagnostic methods commission. *Epilepsia* 52, 158–174. doi: 10.1111/j.1528-1167.2010.02777.x

Boer, K., Spliet, W. G., van Rijen, P. C., Redeker, S., Troost, D., and Aronica, E. (2006). Evidence of activated microglia in focal cortical dysplasia. *J. Neuroimmunol.* 173, 188–195. doi: 10.1016/j.jneuroim.2006.01.002

Boonyapisit, K., Najm, I., Klem, G., Ying, Z., Burrier, C., LaPresto, E., et al. (2003). Epileptogenicity of focal malformations due to abnormal cortical development: direct electrocorticographic-histopathologic correlations. *Epilepsia* 44, 69–76. doi: 10.1046/j.1528-1157.2003.08102.x

Brenner, M., Johnson, A. B., Boespflug-Tanguy, O., Rodriguez, D., Goldman, J. E., and Messing, A. (2001). Mutations in GFAP, encoding glial fibrillary acidic protein, are associated with Alexander disease. *Nat. Genet.* 27, 117–120. doi: 10.1038/83679

Caban, C., Khan, N., Hasbani, D. M., and Crino, P. B. (2017). Genetics of tuberous sclerosis complex: implications for clinical practice. *Appl. Clin. Genet.* 10, 1–8. doi: 10.2147/TACG.S90262

Calcagnotto, M. E., Paredes, M. F., Tihan, T., Barbaro, N. M., and Baraban, S. C. (2005). Dysfunction of synaptic inhibition in epilepsy associated with focal cortical dysplasia. *J. Neurosci. Off. J. Soc. Neurosci.* 25, 9649–9657. doi: 10.1523/JNEUROSCI.2687-05.2005

Castillo, M. (2002). The Core curriculum: Neuroradiology: Lippincott Williams & Wilkins.

Cepeda, C., André, V. M., Flores-Hernández, J., Nguyen, O. K., Wu, N., Klapstein, G. J., et al. (2005a). Pediatric cortical dysplasia: correlations between neuroimaging, electrophysiology and location of cytomegalic neurons and balloon cells and glutamate/GABA synaptic circuits. *Dev. Neurosci.* 27, 59–76. doi: 10.1159/000084533

Cepeda, C., Andre, V. M., Hauptman, J. S., Yamazaki, I., Huynh, M. N., Chang, J. W., et al. (2012). Enhanced GABAergic network and receptor function in pediatric cortical dysplasia type IIB compared with Tuberous Sclerosis complex. *Neurobiol. Dis.* 45, 310–321. doi: 10.1016/j.nbd.2011.08.015

Cepeda, C., André, V. M., Levine, M. S., Salamon, N., Miyata, H., Vinters, H. V., et al. (2006). Epileptogenesis in pediatric cortical dysplasia: the dysmature cerebral developmental hypothesis. *Epil. Behav.* 9, 219–235. doi: 10.1016/j.yebeh.2006.05.012

Cepeda, C., André, V. M., Vinters, H. V., Levine, M. S., and Mathern, G. W. (2005b). Are cytomegalic neurons and balloon cells generators of epileptic activity in pediatric cortical dysplasia? *Epilepsia* 46, 82–88. doi: 10.1111/j.1528-1167.2005.01013.x

Cepeda, C., André, V. M., Wu, N., Yamazaki, I., Uzgil, B., Vinters, H. V., et al. (2007). Immature neurons and GABA networks may contribute to epileptogenesis in pediatric cortical dysplasia. *Epilepsia* 48, 79–85. doi: 10.1111/j.1528-1167.2007.01293.x

Cepeda, C., André, V. M., Yamazaki, I., Hauptman, J. S., Chen, J. Y., Vinters, H. V., et al. (2010). Comparative study of cellular and synaptic abnormalities in brain tissue samples from pediatric tuberous sclerosis complex and cortical dysplasia type II. *Epilepsia* 51, 160–165. doi: 10.1111/j.1528-1167.2010.02633.x

Cepeda, C., Hurst, R. S., Flores-Hernández, J., Hernández-Echeagaray, E., Klapstein, G. J., Boylan, M. K., et al. (2003). Morphological and electrophysiological characterization of abnormal cell types in pediatric cortical dysplasia. *J. Neurosci. Res.* 72, 472–486. doi: 10.1002/jnr.10604

Cepeda, C., Levinson, S., Yazon, V. W., Barry, J., Mathern, G. W., Fallah, A., et al. (2018). Cellular antiseizure mechanisms of everolimus in pediatric tuberous sclerosis complex, cortical dysplasia, and non-mTOR-mediated etiologies. *Epil. Open* 3, 180–190. doi: 10.1002/epi4.12253

Chen, G. T., Nair, G., Osorio, A. J., Holley, S. M., Ghassemzadeh, K., Gonzalez, J., et al. (2024). Enhancer-targeted CRISPR-activation rescues Haploinsufficient autism susceptibility genes. *bioRxiv*. doi: 10.1101/2024.03.13.584921

Chung, C., Yang, X., Bae, T., Vong, K. I., Mittal, S., Donkels, C., et al. (2023). Comprehensive multi-omic profiling of somatic mutations in malformations of cortical development. *Nat. Genet.* 55, 209–220. doi: 10.1038/s41588-022-01276-9

Crino, P. B., Trojanowski, J. Q., Dichter, M. A., and Eberwine, J. (1996). Embryonic neuronal markers in tuberous sclerosis: single-cell molecular pathology. *Proc. Natl. Acad. Sci. USA* 93, 14152–14157. doi: 10.1073/pnas.93.24.14152

Crino, P. B., Trojanowski, J. Q., and Eberwine, J. (1997). Internexin, MAP1B, and nestin in cortical dysplasia as markers of developmental maturity. *Acta Neuropathol.* 93, 619–627. doi: 10.1007/s004010050660

De Rosa, M. J., Farrell, M. A., Burke, M. M., Secor, D. L., and Vinters, H. V. (1992). An assessment of the proliferative potential of 'balloon cells' in focal cortical resections performed for childhood epilepsy. *Neuropathol. Appl. Neurobiol.* 18, 566–574. doi: 10.1111/j.1365-2990.1992.tb00827.x

DeBerardinis, R. J., Lum, J. J., Hatzivassiliou, G., and Thompson, C. B. (2008). The biology of cancer: metabolic reprogramming fuels cell growth and proliferation. *Cell Metab.* 7, 11–20. doi: 10.1016/j.cmet.2007.10.002

D'Gama, A. M., Geng, Y., Couto, J. A., Martin, B., Boyle, E. A., LaCoursiere, C. M., et al. (2015). Mammalian target of rapamycin pathway mutations cause hemimegalencephaly and focal cortical dysplasia. *Ann. Neurol.* 77, 720–725. doi: 10.1002/ana.24357

Dodt, H. U., and Zieglgansberger, W. (1990). Visualizing unstained neurons in living brain slices by infrared DIC-videomicroscopy. *Brain Res.* 537, 333–336. doi: 10.1016/0006-8993(90)90380-T

Dooves, S., van Velthoven, A. J. H., Suciati, L. G., and Heine, V. M. (2021). Neuron-glia interactions in Tuberous Sclerosis complex affect the synaptic balance in 2D and organoid cultures. *Cells* 10. doi: 10.3390/cells10010134

Dudek, F. E., Wuarin, J. P., Tasker, J. G., Kim, Y. I., and Peacock, W. J. (1995). Neurophysiology of neocortical slices resected from children undergoing surgical treatment for epilepsy. *J. Neurosci. Methods* 59, 49–58. doi: 10.1016/0165-0270(94)00193-K

Dzhala, V. I., Talos, D. M., Sdrulla, D. A., Brumback, A. C., Mathews, G. C., Benke, T. A., et al. (2005). NKCC1 transporter facilitates seizures in the developing brain. *Nat. Med.* 11, 1205–1213. doi: 10.1038/nm1301

Englund, C., Folkerth, R. D., Born, D., Lacy, J. M., and Hevner, R. F. (2005). Aberrant neuronal-glial differentiation in Taylor-type focal cortical dysplasia (type IIA/B). *Acta Neuropathol.* 109, 519–533. doi: 10.1007/s00401-005-1005-9

European Chromosome 16 Tuberous Sclerosis Consortium (1993). Identification and characterization of the tuberous sclerosis gene on chromosome 16. *Cell* 75, 1305–1315. doi: 10.1016/0092-8674(93)90618-Z

Fauser, S., Becker, A., Schulze-Bonhage, A., Hildebrandt, M., Tuxhorn, I., Pannek, H. W., et al. (2004). CD34-immunoreactive balloon cells in cortical malformations. *Acta Neuropathol.* 108, 272–278. doi: 10.1007/s00401-004-0889-0

Ferrer, I. (2024). Historical review: the golden age of the Golgi method in human neuropathology. *J. Neuropathol. Exp. Neurol.* 83, 375–395. doi: 10.1093/jnen/nlae031

Ferrer, I., Fabregues, I., Coll, J., Ribalta, T., and Rives, A. (1984). Tuberous sclerosis: a Golgi study of cortical tuber. *Clin. Neuropathol.* 3, 47–51

Frauscher, B., Bartolomei, F., Kobayashi, K., Cimbalnik, J., van, M., Rampp, S., et al. (2017). High-frequency oscillations: the state of clinical research. *Epilepsia* 58, 1316–1329. doi: 10.1111/epi.13829

Garbelli, R., Frassoni, C., Condorelli, D. F., Trovato Salinaro, A., Musso, N., Medici, V., et al. (2011). Expression of connexin 43 in the human epileptic and drug-resistant cerebral cortex. *Neurology* 76, 895–902. doi: 10.1212/WNL.0b013e31820f2da6

Garbelli, R., Munari, C., De Biasi, S., Vitellaro-Zuccarello, L., Galli, C., Bramerio, M., et al. (1999). Taylor's cortical dysplasia: a confocal and ultrastructural immunohistochemical study. *Brain Pathol.* 9, 445–461. doi: 10.1111/j.1750-3639.1999.tb00534.x

Gelot, A. B., and Represa, A. (2020). Progression of fetal Brain lesions in Tuberous Sclerosis complex. *Front. Neurosci.* 14:899. doi: 10.3389/fnins.2020.00899

Gerasimenko, A., Baldassari, S., and Baulac, S. (2023). mTOR pathway: insights into an established pathway for brain mosaicism in epilepsy. *Neurobiol. Dis.* 182:106144. doi: 10.1016/j.nbd.2023.106144

Gonzalez-Martinez, J. A., Ying, Z., Prayson, R., Bingaman, W., and Najm, I. (2011). Glutamate clearance mechanisms in resected cortical dysplasia. *J. Neurosurg.* 114, 1195–1202. doi: 10.3171/2010.10.JNS10715

Grajkowska, W., Kotulska, K., Matyja, E., Larysz-Brysz, M., Mandera, M., Roszkowski, M., et al. (2008). Expression of tuberin and hamartin in tuberous sclerosis complex-associated and sporadic cortical dysplasia of Taylor's balloon cell type. *Folia Neuropathol.* 46, 43–48

Gruber, V. E., Lang, J., Endmayr, V., Diehm, R., Pimpel, B., Glatter, S., et al. (2021). Impaired myelin production due to an intrinsic failure of oligodendrocytes in mTORpathies. *Neuropathol. Appl. Neurobiol.* 47, 812–825. doi: 10.1111/nan.12744

Gruner, J. E. (1969). Histopathologie fine de la maladie de Bourneville. *Acta Neurol.* 24:334.

Guerrini, R., and Dobyns, W. B. (2014). Malformations of cortical development: clinical features and genetic causes. *Lancet Neurol.* 13, 710–726. doi: 10.1016/S1474-4422(14)70040-7

Hadouiri, N., Darmency, V., Guibaud, L., Arzimanoglou, A., Sorlin, A., Carmignac, V., et al. (2020). Compassionate use of everolimus for refractory epilepsy in a patient with MTOR mosaic mutation. *Eur. J. Med. Genet.* 63:104036. doi: 10.1016/j.ejmg.2020.104036

He, J. J., Li, S., Shu, H. F., Yu, S. X., Liu, S. Y., Yin, Q., et al. (2013). The interleukin 17 system in cortical lesions in focal cortical dysplasias. *J. Neuropathol. Exp. Neurol.* 72, 152–163. doi: 10.1097/NEN.0b013e318281262e

Hirfanoglu, T., and Gupta, A. (2010). Tuberous sclerosis complex with a single brain lesion on MRI mimicking focal cortical dysplasia. *Pediatr. Neurol.* 42, 343–347. doi: 10.1016/j.pediatrneurol.2010.01.001

Hirose, T., Scheithauer, B. W., Lopes, M. B., Gerber, H. A., Altermatt, H. J., Hukee, M. J., et al. (1995). Tuber and subependymal giant cell astrocytoma associated with tuberous sclerosis: an immunohistochemical, ultrastructural, and immunoelectron and microscopic study. *Acta Neuropathol.* 90, 387–399. doi: 10.1007/BF00315012

Holley, S. M., Reidling, J. C., Cepeda, C., Wu, J., Lim, R. G., Lau, A., et al. (2023). Transplanted human neural stem cells rescue phenotypes in zQ175 Huntington's disease mice and innervate the striatum. *Mol. Ther.* 31, 3545–3563. doi: 10.1016/j.ymthe.2023.10.003

Huang, K., Wang, Z., He, Z., Li, Y., Li, S., Shen, K., et al. (2022). Downregulated formyl peptide receptor 2 expression in the epileptogenic foci of patients with focal cortical dysplasia type IIb and tuberous sclerosis complex. *Immun. Inflamm. Dis.* 10:e706. doi: 10.1002/iid3.706

Huttenlocher, P. R., and Heydemann, P. T. (1984). Fine structure of cortical tubers in tuberous sclerosis: a Golgi study. *Ann. Neurol.* 16, 595–602. doi: 10.1002/ana.410160511

Jozwiak, J., Jozwiak, S., and Skopinski, P. (2005). Immunohistochemical and microscopic studies on giant cells in tuberous sclerosis. *Histol. Histopathol.* 20, 1321–1326. doi: 10.14670/HH-20.1321

Jozwiak, J., Kotulska, K., and Jozwiak, S. (2006). Similarity of balloon cells in focal cortical dysplasia to giant cells in tuberous sclerosis. *Epilepsia* 47:805. doi: 10.1111/j.1528-1167.2006.00531_1.x

Jozwiak, S., Kwiatkowski, D., Kotulska, K., Larysz-Brysz, M., Lewin-Kowalik, J., Grajkowska, W., et al. (2004). Tuberin and hamartin expression is reduced in the majority of subependymal giant cell astrocytomas in tuberous sclerosis complex consistent with a two-hit model of pathogenesis. *J. Child Neurol.* 19, 102–106. doi: 10.1177/088307380401900204O1

Juric-Sekhar, G., and Hevner, R. F. (2019). Malformations of cerebral cortex development: molecules and mechanisms. *Annu. Rev. Pathol.* 14, 293–318. doi: 10.1146/annurev-pathmechdis-012418-012927

Kato, M., Kada, A., Shiraishi, H., Tohyama, J., Nakagawa, E., Takahashi, Y., et al. (2022). Sirolimus for epileptic seizures associated with focal cortical dysplasia type II. *Ann. Clin. Transl. Neurol.* 9, 181–192. doi: 10.1002/acn3.51505

Khanlou, N., Mathern, G. W., Mitchell, W. G., Salamon, N., Pope, W. B., Yong, W. H., et al. (2009). Cortical dysplasia with prominent Rosenthal fiber formation in a case of intractable pediatric epilepsy. *Hum. Pathol.* 40, 1200–1204. doi: 10.1016/j.humpath.2009.02.012

Kimura, Y., Shioya, A., Saito, Y., Oitani, Y., Shigemoto, Y., Morimoto, E., et al. (2019). Radiologic and pathologic features of the Transmantle sign in focal cortical dysplasia: the T1 signal is useful for differentiating subtypes. *AJNR Am. J. Neuroradiol.* 40, 1060–1066. doi: 10.3174/ajnr.A6067

Krueger, D. A., Wilfong, A. A., Holland-Bouley, K., Anderson, A. E., Agricola, K., Tudor, C., et al. (2013). Everolimus treatment of refractory epilepsy in tuberous sclerosis complex. *Ann. Neurol.* 74, 679–687. doi: 10.1002/ana.23960

Kubach, J., Muhlebner-Fahrngruber, A., Soylemezoglu, F., Miyata, H., Niehusmann, P., Honavar, M., et al. (2020). Same same but different: a web-based deep learning application revealed classifying features for the histopathologic distinction of cortical malformations. *Epilepsia* 61, 421–432. doi: 10.1111/epi.16447

Kwiatkowski, D. J., and Manning, B. D. (2005). Tuberous sclerosis: a GAP at the crossroads of multiple signaling pathways. *Hum. Mol. Genet.* 14, R251–R258. doi: 10.1093/hmg/ddi260

Lamparello, P., Baybis, M., Pollard, J., Hol, E. M., Eisenstat, D. D., Aronica, E., et al. (2007). Developmental lineage of cell types in cortical dysplasia with balloon cells. *Brain J. Neurol.* 130, 2267–2276. doi: 10.1093/brain/awm175

Lee, W. S., Baldassari, S., Stephenson, S. E. M., Lockhart, P. J., Baulac, S., and Leventer, R. J. (2022). Cortical dysplasia and the mTOR pathway: How the study of human brain tissue has led to insights into epileptogenesis. *Int. J. Mol. Sci.* 23:1344. doi: 10.3390/ijms23031344

Lee, J. H., Huynh, M., Silhavy, J. L., Kim, S., Dixon-Salazar, T., Heiberg, A., et al. (2012). De novo somatic mutations in components of the PI3K-AKT3-mTOR pathway cause hemimegalencephaly. *Nat. Genet.* 44, 941–945. doi: 10.1038/ng.2329

Lee, A., Maldonado, M., Baybis, M., Walsh, C. A., Scheithauer, B., Yeung, R., et al. (2003). Markers of cellular proliferation are expressed in cortical tubers. *Ann. Neurol.* 53, 668–673. doi: 10.1002/ana.10579

Leitner, D. F., Kanshin, E., Askenazi, M., Siu, Y., Friedman, D., Devore, S., et al. (2022). Pilot study evaluating everolimus molecular mechanisms in tuberous sclerosis complex and focal cortical dysplasia. *PLoS One* 17:e0268597. doi: 10.1371/journal.pone.0268597

Levinson, S., Tran, C. H., Barry, J., Viker, B., Levine, M. S., Vinters, H. V., et al. (2020). Paroxysmal discharges in tissue slices from pediatric epilepsy surgery patients: critical role of GABAB receptors in the generation of ictal activity. *Front. Cell. Neurosci.* 14:54. doi: 10.3389/fncel.2020.00054

Lim, J. S., Kim, W. I., Kang, H. C., Kim, S. H., Park, A. H., Park, E. K., et al. (2015). Brain somatic mutations in MTOR cause focal cortical dysplasia type II leading to intractable epilepsy. *Nat. Med.* 21, 395–400. doi: 10.1038/nm.3824

Lippa, C. F., Pearson, D., and Smith, T. W. (1993). Cortical tubers demonstrate reduced immunoreactivity for synapsin I. *Acta Neuropathol.* 85, 449–451. doi: 10.1007/BF00334458

Liu, G. Y., and Sabatini, D. M. (2020). mTOR at the nexus of nutrition, growth, ageing and disease. *Nat. Rev. Mol. Cell Biol.* 21, 183–203. doi: 10.1038/s41580-019-0199-y

Liu, Z., Shen, X., Lin, K., Wang, F., Gao, J., Yao, Y., et al. (2024). Balloon cells in malformations of cortical development: friends or foes? *Acta Epileptol.* 6:20. doi: 10.1186/s42494-024-00164-5

Liu, Y., Shen, X., Zhang, Y., Zheng, X., Cepeda, C., Wang, Y., et al. (2023). Interactions of glial cells with neuronal synapses, from astrocytes to microglia and oligodendrocyte lineage cells. *Glia* 71, 1383–1401. doi: 10.1002/glia.24343

Lopez-Rivera, J. A., Leu, C., Macnee, M., Khoury, J., Hoffmann, L., Coras, R., et al. (2023). The genomic landscape across 474 surgically accessible epileptogenic human brain lesions. *Brain J. Neurol.* 146, 1342–1356. doi: 10.1093/brain/awac376

Lozovaya, N., Gataullina, S., Tsintsadze, T., Tsintsadze, V., Pallesi-Pocachard, E., Minlebaev, M., et al. (2014). Selective suppression of excessive GluN2C expression rescues early epilepsy in a tuberous sclerosis murine model. *Nat. Commun.* 5:4563. doi: 10.1038/ncomms5563

Luat, A. F., Makki, M., and Chugani, H. T. (2007). Neuroimaging in tuberous sclerosis complex. *Curr. Opin. Neurol.* 20, 142–150. doi: 10.1097/WCO.0b013e3280895d93

Machado-Salas, J. P. (1984). Abnormal dendritic patterns and aberrant spine development in Bourneville's disease--a Golgi survey. *Clin. Neuropathol.* 3, 52–58

Malatesta, P., Hartfuss, E., and Gotz, M. (2000). Isolation of radial glial cells by fluorescent-activated cell sorting reveals a neuronal lineage. *Development* 127, 5253–5263. doi: 10.1242/dev.127.24.5253

Marcotte, L., Aronica, E., Baybis, M., and Crino, P. B. (2012). Cytoarchitectural alterations are widespread in cerebral cortex in tuberous sclerosis complex. *Acta Neuropathol.* 123, 685–693. doi: 10.1007/s00401-012-0950-3

Marin-Valencia, I., Guerrini, R., and Gleeson, J. G. (2014). Pathogenetic mechanisms of focal cortical dysplasia. *Epilepsia* 55, 970–978. doi: 10.1111/epi.12650

Martin, K. R., Zhou, W., Bowman, M. J., Shih, J., Au, K. S., Dittenhafer-Reed, K. E., et al. (2017). The genomic landscape of tuberous sclerosis complex. *Nat. Commun.* 8:15816. doi: 10.1038/ncomms15816

Martinian, L., Boer, K., Middeldorp, J., Hol, E. M., Sisodiya, S. M., Squier, W., et al. (2009). Expression patterns of glial fibrillary acidic protein (GFAP)-delta in epilepsy-associated lesional pathologies. *Neuropathol. Appl. Neurobiol.* 35, 394–405. doi: 10.1111/j.1365-2990.2008.00996.x

Mathern, G. W., Cepeda, C., Hurst, R. S., Flores-Hernandez, J., Mendoza, D., and Levine, M. S. (2000). Neurons recorded from pediatric epilepsy surgery patients with cortical dysplasia. *Epilepsia* 41, S162–S167. doi: 10.1111/j.1528-1157.2000.tb01575.x

Matsuo, T., Fujimoto, S., Komori, T., and Nakata, Y. (2022). Case report: the origin of transmantle-like features. *Front. Radiol.* 2:927764. doi: 10.3389/fradi.2022.927764

Messing, A., Brenner, M., Feany, M. B., Nedergaard, M., and Goldman, J. E. (2012). Alexander disease. *J. Neurosci. Off. J. Soc. Neurosci.* 32, 5017–5023. doi: 10.1523/JNEUROSCI.5384-11.2012

Miyata, H., Chiang, A. C., and Vinters, H. V. (2004). Insulin signaling pathways in cortical dysplasia and TSC-tubers: tissue microarray analysis. *Ann. Neurol.* 56, 510–519. doi: 10.1002/ana.20234

Mizuguchi, M., Yamanouchi, H., Becker, L. E., Itoh, M., and Takashima, S. (2002). Doublecortin immunoreactivity in giant cells of tuberous sclerosis and focal cortical dysplasia. *Acta Neuropathol.* 104, 418–424. doi: 10.1007/s00401-002-0575-z

Mori, K., Mori, T., Toda, Y., Fujii, E., Miyazaki, M., Harada, M., et al. (2012). Decreased benzodiazepine receptor and increased GABA level in cortical tubers in tuberous sclerosis complex. *Brain Dev.* 34, 478–486. doi: 10.1016/j.braindev.2011.09.001

Muhlebner, A., Bongaarts, A., Sarnat, H. B., Scholl, T., and Aronica, E. (2019). New insights into a spectrum of developmental malformations related to mTOR dysregulations: challenges and perspectives. *J. Anat.* 235, 521–542. doi: 10.1111/joa.12956

Munakata, M., Watanabe, M., Otsuki, T., Itoh, M., Uematsu, M., Saito, Y., et al. (2013). Increased Ki-67 immunoreactivity in the white matter in hemimegalencephaly. *Neurosci. Lett.* 548, 244–248. doi: 10.1016/j.neulet.2013.05.033

Muncy, J., Butler, I. J., and Koenig, M. K. (2009). Rapamycin reduces seizure frequency in tuberous sclerosis complex. *J. Child Neurol.* 24, 477. doi: 10.1177/0883073808324535

Najm, I., Lal, D., Alonso Vanegas, M., Cendes, F., Lopes-Cendes, I., Palmini, A., et al. (2022). The ILAE consensus classification of focal cortical dysplasia: An update proposed by an ad hoc task force of the ILAE diagnostic methods commission. *Epilepsia* 63, 1899–1919. doi: 10.1111/epi.17301

Nakashima, M., Saitsu, H., Takei, N., Tohyama, J., Kato, M., Kitaura, H., et al. (2015). Somatic mutations in the MTOR gene cause focal cortical dysplasia type IIb. *Ann. Neurol.* 78, 375–386. doi: 10.1002/ana.24444

Noctor, S. C., Flint, A. C., Weissman, T. A., Dammerman, R. S., and Kriegstein, A. R. (2001). Neurons derived from radial glial cells establish radial units in neocortex. *Nature* 409, 714–720. doi: 10.1038/35055553

Northrup, H., Aronow, M. E., Bebin, E. M., Bissler, J., Darling, T. N., de Vries, P. J., et al. (2021). Updated international Tuberous Sclerosis complex diagnostic criteria and surveillance and management recommendations. *Pediatr. Neurol.* 123, 50–66. doi: 10.1016/j.pediatrneurol.2021.07.011

Oh, H. S., Lee, M. C., Kim, H. S., Lee, J. S., Lee, J. H., Kim, M. K., et al. (2008). Pathophysiologic characteristics of balloon cells in cortical dysplasia. *Child Nerv. Syst.* 24, 175–183. doi: 10.1007/s00381-007-0453-z

Orlova, K. A., Tsai, V., Baybis, M., Heuer, G. G., Sisodiya, S., Thom, M., et al. (2010). Early progenitor cell marker expression distinguishes type II from type I focal cortical dysplasias. *J. Neuropathol. Exp. Neurol.* 69, 850–863. doi: 10.1097/NEN.0b013e3181eac1f5

Panwar, V., Singh, A., Bhatt, M., Tonk, R. K., Azizov, S., Raza, A. S., et al. (2023). Multifaceted role of mTOR (mammalian target of rapamycin) signaling pathway in human health and disease. *Signal Transduct. Target. Ther.* 8:375. doi: 10.1038/s41392-023-01608-z

Park, S. H., Pepkowitz, S. H., Kerfoot, C., De Rosa, M. J., Poukens, V., Wienecke, R., et al. (1997). Tuberous sclerosis in a 20-week gestation fetus: immunohistochemical study. *Acta Neuropathol.* 94, 180–186. doi: 10.1007/s004010050691

Pellizzi, G. B. (1901). Contributo alla istologia ed alla patogenesi dei Tumori di Tessuto nervoso. *Riv. Speriment. Freniat.* 27, 957–995.

Pelorosso, C., Watrin, F., Conti, V., Buhler, E., Gelot, A., Yang, X., et al. (2019). Somatic double-hit in MTOR and RPS6 in hemimegalencephaly with intractable epilepsy. *Hum. Mol. Genet.* 28, 3755–3765. doi: 10.1093/hmg/ddz194

Probst, A., and Ohnacker, H. (1977). Tuberous sclerosis in a premature infant (author's transl). *Acta Neuropathol.* 40, 157–161. doi: 10.1007/BF00688705

Represa, A. (2019). Why malformations of cortical development cause epilepsy. *Front. Neurosci.* 13:250. doi: 10.3389/fnins.2019.00250

Ribadeau Dumas, G. L., Poirier, G., and Escourolle, R. (1973). Etude ultrastructurale des lésions cérébrales de la sclérose tubéreuse de Bourneville. *Acta Neuropathol.* 25, 259–270. doi: 10.1007/BF00691754

Ribierre, T., Bacq, A., Donneger, F., Doladilhe, M., Maletic, M., Roussel, D., et al. (2024). Targeting pathological cells with senolytic drugs reduces seizures in neurodevelopmental mTOR-related epilepsy. *Nat. Neurosci.* 27, 1125–1136. doi: 10.1038/s41593-024-01634-2

Rivera, C., Voipio, J., Payne, J. A., Ruusuvuori, E., Lahtinen, H., Lamsa, K., et al. (1999). The K+/cl- co-transporter KCC2 renders GABA hyperpolarizing during neuronal maturation. *Nature* 397, 251–255. doi: 10.1038/16697

Rossini, L., De Santis, D., Mauceri, R. R., Tesoriero, C., Bentivoglio, M., Maderna, E., et al. (2021). Dendritic pathology, spine loss and synaptic reorganization in human cortex from epilepsy patients. *Brain J. Neurol.* 144, 251–265. doi: 10.1093/brain/awaa387

Rossini, L., Villani, F., Granata, T., Tassi, L., Tringali, G., Cardinale, F., et al. (2017). FCD type II and mTOR pathway: evidence for different mechanisms involved in the pathogenesis of dysmorphic neurons. *Epilepsy Res.* 129, 146–156. doi: 10.1016/j.eplepsyres.2016.12.002

Salamon, N., Andres, M., Chute, D. J., Nguyen, S. T., Chang, J. W., Huynh, M. N., et al. (2006). Contralateral hemimicrencephaly and clinical-pathological correlations in children with hemimegalencephaly. *Brain J. Neurol.* 129, 352–365. doi: 10.1093/brain/awh681

Schick, V., Majores, M., Engels, G., Hartmann, W., Elger, C. E., Schramm, J., et al. (2007a). Differential Pi3K-pathway activation in cortical tubers and focal cortical dysplasias with balloon cells. *Brain Pathol.* 17, 165–173. doi: 10.1111/j.1750-3639.2007.00059.x

Schick, V., Majores, M., Engels, G., Spitoni, S., Koch, A., Elger, C. E., et al. (2006). Activation of Akt independent of PTEN and CTMP tumor-suppressor gene mutations in epilepsy-associated Taylor-type focal cortical dysplasias. *Acta Neuropathol.* 112, 715–725. doi: 10.1007/s00401-006-0128-y

Schick, V., Majores, M., Fassunke, J., Engels, G., Simon, M., Elger, C. E., et al. (2007b). Mutational and expression analysis of CDK1, cyclinA2 and cyclinB1 in epilepsy-associated glioneuronal lesions. *Neuropathol. Appl. Neurobiol.* 33, 152–162. doi: 10.1111/j.1365-2990.2006.00788.x

Schwartzkroin, P. A., and Walsh, C. A. (2000). Cortical malformations and epilepsy. *Ment. Retard. Dev. Disabil. Res. Rev.* 6, 268–280. doi: 10.1002/1098-2779(2000)6:4<268::AID-MRDD6>3.0.CO;2-B

Sharma, M. C., Ralte, A. M., Gaekwad, S., Santosh, V., Shankar, S. K., and Sarkar, C. (2004). Subependymal giant cell astrocytoma--a clinicopathological study of 23 cases with special emphasis on histogenesis. *Pathol. Oncol. Res.* 10, 219–224. doi: 10.1007/BF03033764

Shu, H. F., Zhang, C. Q., Yin, Q., An, N., Liu, S. Y., and Yang, H. (2010). Expression of the interleukin 6 system in cortical lesions from patients with tuberous sclerosis complex and focal cortical dysplasia type IIb. *J. Neuropathol. Exp. Neurol.* 69, 838–849. doi: 10.1097/NEN.0b013e3181eaeae5

Sofroniew, M. V., and Vinters, H. V. (2010). Astrocytes: biology and pathology. *Acta Neuropathol.* 119, 7–35. doi: 10.1007/s00401-009-0619-8

Sosunov, A. A., Wu, X., Weiner, H. L., Mikell, C. B., Goodman, R. R., Crino, P. D., et al. (2008). Tuberous sclerosis: a primary pathology of astrocytes? *Epilepsia* 49, 53–62. doi: 10.1111/j.1528-1167.2008.01493.x

Soul, J. S., Bergin, A. M., Stopp, C., Hayes, B., Singh, A., Fortuno, C. R., et al. (2021). A pilot randomized, controlled, double-blind Trial of bumetanide to treat neonatal seizures. *Ann. Neurol.* 89, 327–340. doi: 10.1002/ana.25959

Spreafico, R., Battaglia, G., Arcelli, P., Andermann, F., Dubeau, F., Palmini, A., et al. (1998). Cortical dysplasia. *Neurology* 50, 27–36. doi: 10.1212/WNL.50.1.27

Stephenson, S. E. M., Maixner, W. J., Barton, S. M., D'Arcy, C., Mandelstam, S. A., Mac Gregor, D., et al. (2021). Resection of tuber centers only for seizure control in tuberous sclerosis complex. *Epilepsy Res.* 171:106572:106572. doi: 10.1016/j.eplepsyres.2021.106572

Sugiura, C., Miyata, H., Ueda, M., Ohama, E., Vinters, H. V., and Ohno, K. (2008). Immunohistochemical expression of fibroblast growth factor (FGF)-2 in epilepsy-associated malformations of cortical development (MCDs). *Neuropathology* 28, 372–381. doi: 10.1111/j.1440-1789.2007.00881.x

Talos, D. M., Kwiatkowski, D. J., Cordero, K., Black, P. M., and Jensen, F. E. (2008). Cell-specific alterations of glutamate receptor expression in tuberous sclerosis complex cortical tubers. *Ann. Neurol.* 63, 454–465. doi: 10.1002/ana.21342

Talos, D. M., Sun, H., Kosaras, B., Joseph, A., Folkerth, R. D., Poduri, A., et al. (2012). Altered inhibition in tuberous sclerosis and type IIb cortical dysplasia. *Ann. Neurol.* 71, 539–551. doi: 10.1002/ana.22696

Taylor, D. C., Falconer, M. A., Bruton, C. J., and Corsellis, J. A. (1971). Focal dysplasia of the cerebral cortex in epilepsy. *J. Neurol. Neurosurg. Psychiatry* 34, 369–387. doi: 10.1136/jnnp.34.4.369

Thom, M., Martinian, L., Sisodiya, S. M., Cross, J. H., Williams, G., Stoeber, K., et al. (2005). Mcm 2 labelling of balloon cells in focal cortical dysplasia. *Neuropathol. Appl. Neurobiol.* 31, 580–588. doi: 10.1111/j.1365-2990.2005.00651.x

Tihan, T., Vohra, P., Berger, M. S., and Keles, G. E. (2006). Definition and diagnostic implications of gemistocytic astrocytomas: a pathological perspective. *J. Neuro-Oncol.* 76, 175–183. doi: 10.1007/s11060-005-4897-2

Toering, S. T., Boer, K., de Groot, M., Troost, D., Heimans, J. J., Spliet, W. G., et al. (2009). Expression patterns of synaptic vesicle protein 2A in focal cortical dysplasia and TSC-cortical tubers. *Epilepsia* 50, 1409–1418. doi: 10.1111/j.1528-1167.2008.01955.x

Trombley, I. K., and Mirra, S. S. (1981). Ultrastructure of tuberous sclerosis: cortical tuber and subependymal tumor. *Ann. Neurol.* 9, 174–181. doi: 10.1002/ana.410090211

Ueda, M., Sugiura, C., Ohno, K., Kakita, A., Hori, A., Ohama, E., et al. (2011). Immunohistochemical expression of fibroblast growth factor-2 in developing human cerebrum and epilepsy-associated malformations of cortical development. *Neuropathology* 31, 589–598. doi: 10.1111/j.1440-1789.2011.01205.x

Urbach, H., Scheffler, B., Heinrichsmeier, T., von Oertzen, J., Kral, T., Wellmer, J., et al. (2002). Focal cortical dysplasia of Taylor's balloon cell type: a clinicopathological entity with characteristic neuroimaging and histopathological features, and favorable postsurgical outcome. *Epilepsia* 43, 33–40. doi: 10.1046/j.1528-1157.2002.38201.x

Van Andel, D. M., Sprengers, J. J., Oranje, B., Scheepers, F. E., Jansen, F. E., and Bruining, H. (2020). Effects of bumetanide on neurodevelopmental impairments in patients with tuberous sclerosis complex: an open-label pilot study. *Mol. Autism.* 11:30. doi: 10.1186/s13229-020-00335-4

Vinters, H. V., De Rosa, M. J., and Farrell, M. A. (1993). Neuropathologic study of resected cerebral tissue from patients with infantile spasms. *Epilepsia* 34, 772–779. doi: 10.1111/j.1528-1157.1993.tb00460.x

Vinters, H. V., Park, S. H., Johnson, M. W., Mischel, P. S., Catania, M., and Kerfoot, C. (1999). Cortical dysplasia, genetic abnormalities and neurocutaneous syndromes. *Dev. Neurosci.* 21, 248–259. doi: 10.1159/000017404

Wang, Y., Greenwood, J. S., Calcagnotto, M. E., Kirsch, H. E., Barbaro, N. M., and Baraban, S. C. (2007). Neocortical hyperexcitability in a human case of tuberous sclerosis complex and mice lacking neuronal expression of TSC1. *Ann. Neurol.* 61, 139–152. doi: 10.1002/ana.21058

Wang, X., Hu, W., Shao, X., Zheng, Z., Ai, L., Sang, L., et al. (2023). Hypometabolic patterns of focal cortical dysplasia in PET-MRI co-registration imaging: a retrospective evaluation in a series of 83 patients. *Front. Neurosci.* 17:1173534. doi: 10.3389/fnins.2023.1173534

White, R., Hua, Y., Scheithauer, B., Lynch, D. R., Henske, E. P., and Crino, P. B. (2001). Selective alterations in glutamate and GABA receptor subunit mRNA expression in dysplastic neurons and giant cells of cortical tubers. *Ann. Neurol.* 49, 67–78. doi: 10.1002/1531-8249(200101)49:1<67::AID-ANA10>3.0.CO;2-L

Wolff, J. R., Rickmann, M., and Chronwall, B. M. (1979). Axo-glial synapses and GABA-accumulating glial cells in the embryonic neocortex of the rat. *Cell Tissue Res.* 201, 239–248. doi: 10.1007/BF00235060

Wu, K., Yue, J., Shen, K., He, J., Zhu, G., Liu, S., et al. (2021a). Expression and cellular distribution of FGF13 in cortical tubers of the tuberous sclerosis complex. *Neurosci. Lett.* 749:135714. doi: 10.1016/j.neulet.2021.135714

Wu, K., Yue, J., Shen, K., He, J., Zhu, G., Liu, S., et al. (2021b). Increased expression of fibroblast growth factor 13 in cortical lesions of the focal cortical dysplasia. *Brain Res. Bull.* 168, 36–44. doi: 10.1016/j.brainresbull.2020.11.023

Wuarin, J. P., Kim, Y. I., Cepeda, C., Tasker, J. G., Walsh, J. P., Peacock, W. J., et al. (1990). Synaptic transmission in human neocortex removed for treatment of intractable epilepsy in children. *Ann. Neurol.* 28, 503–511. doi: 10.1002/ana.410280406

Wuarin, J. P., Peacock, W. J., and Dudek, F. E. (1992). Single-electrode voltage-clamp analysis of the N-methyl-D-aspartate component of synaptic responses in neocortical slices from children with intractable epilepsy. *J. Neurophysiol.* 67, 84–93. doi: 10.1152/jn.1992.67.1.84

Yamanouchi, H., Jay, V., Rutka, J. T., Takashima, S., and Becker, L. E. (1997). Evidence of abnormal differentiation in giant cells of tuberous sclerosis. *Pediatr. Neurol.* 17, 49–53. doi: 10.1016/S0887-8994(97)00036-2

Yasin, S. A., Latak, K., Becherini, F., Ganapathi, A., Miller, K., Campos, O., et al. (2010). Balloon cells in human cortical dysplasia and tuberous sclerosis: isolation of a pathological progenitor-like cell. *Acta Neuropathol.* 120, 85–96. doi: 10.1007/s00401-010-0677-y

Ying, Z., Gonzalez-Martinez, J., Tilelli, C., Bingaman, W., and Najm, I. (2005). Expression of neural stem cell surface marker CD133 in balloon cells of human focal cortical dysplasia. *Epilepsia* 46, 1716–1723. doi: 10.1111/j.1528-1167.2005.00276.x

Yue, J., Zhang, C., Shi, X., Wei, Y., Liu, L., Liu, S., et al. (2019). Activation of leukocyte immunoglobulin-like receptor B2 signaling pathway in cortical lesions of pediatric patients with focal cortical dysplasia type IIb and tuberous sclerosis complex. *Brain Dev.* 41, 829–838. doi: 10.1016/j.braindev.2019.08.002

Zarzor, M. S., Blumcke, I., and Budday, S. (2023). Exploring the role of the outer subventricular zone during cortical folding through a physics-based model. *eLife* 12:12. doi: 10.7554/eLife.82925

Zimmer, T. S., Broekaart, D. W. M., Luinenburg, M., Mijnsbergen, C., Anink, J. J., Sim, N. S., et al. (2021). Balloon cells promote immune system activation in focal cortical dysplasia type 2b. *Neuropathol. Appl. Neurobiol.* 47, 826–839. doi: 10.1111/nan.12736

frontiers | Frontiers in Cellular Neuroscience

TYPE Review
PUBLISHED 06 January 2025
DOI 10.3389/fncel.2024.1478572

OPEN ACCESS

EDITED BY
Enrico Cherubini,
European Brain Research Institute, Italy

REVIEWED BY
Mohammad Hasanain,
University of Miami Health System, United States
Yohei Hayashi,
RIKEN BioResource Research Center (BRC), Japan
Nishant Singhal,
National Centre for Cell Science, India

*CORRESPONDENCE
Lisa M. Julian
✉ ljulian@sfu.ca

RECEIVED 10 August 2024
ACCEPTED 13 December 2024
PUBLISHED 06 January 2025

CITATION
Imani Farahani N, Lin L, Nazir S, Naderi A, Rokos L, McIntosh AR and Julian LM (2025) Advances in physiological and clinical relevance of hiPSC-derived brain models for precision medicine pipelines. *Front. Cell. Neurosci.* 18:1478572. doi: 10.3389/fncel.2024.1478572

Advances in physiological and clinical relevance of hiPSC-derived brain models for precision medicine pipelines

Negin Imani Farahani[1,2,3], Lisa Lin[2,3,4], Shama Nazir[2,3,4], Alireza Naderi[2,3,4], Leanne Rokos[3,5,6], Anthony Randal McIntosh[3,5] and Lisa M. Julian[1,2,3,4]*

[1]Department of Molecular Biology and Biochemistry, Simon Fraser University, Burnaby, BC, Canada, [2]Centre for Cell Biology, Development, and Disease, Simon Fraser University, Burnaby, BC, Canada, [3]Institute for Neuroscience and Neurotechnology, Simon Fraser University, Burnaby, BC, Canada, [4]Department of Biological Sciences, Simon Fraser University, Burnaby, BC, Canada, [5]Department of Biomedical Physiology and Kinesiology, Simon Fraser University, Burnaby, BC, Canada, [6]Rotman Research Institute, Baycrest Health Sciences, University of Toronto, Toronto, ON, Canada

Precision, or personalized, medicine aims to stratify patients based on variable pathogenic signatures to optimize the effectiveness of disease prevention and treatment. This approach is favorable in the context of brain disorders, which are often heterogeneous in their pathophysiological features, patterns of disease progression and treatment response, resulting in limited therapeutic standard-of-care. Here we highlight the transformative role that human induced pluripotent stem cell (hiPSC)-derived neural models are poised to play in advancing precision medicine for brain disorders, particularly emerging innovations that improve the relevance of hiPSC models to human physiology. hiPSCs derived from accessible patient somatic cells can produce various neural cell types and tissues; current efforts to increase the complexity of these models, incorporating region-specific neural tissues and non-neural cell types of the brain microenvironment, are providing increasingly relevant insights into human-specific neurobiology. Continued advances in tissue engineering combined with innovations in genomics, high-throughput screening and imaging strengthen the physiological relevance of hiPSC models and thus their ability to uncover disease mechanisms, therapeutic vulnerabilities, and tissue and fluid-based biomarkers that will have real impact on neurological disease treatment. True physiological understanding, however, necessitates integration of hiPSC-neural models with patient biophysical data, including quantitative neuroimaging representations. We discuss recent innovations in cellular neuroscience that can provide these direct connections through generative AI modeling. Our focus is to highlight the great potential of synergy between these emerging innovations to pave the way for personalized medicine becoming a viable option for patients suffering from neuropathologies, particularly rare epileptic and neurodegenerative disorders.

KEYWORDS

precision medicine, hiPSCs, brain disorders, biomarkers, generative AI, brain organoids, neurophysiology

1 Introduction

Precision medicine is a clinical approach that strives to develop targeted treatment paradigms for individual or specific groups of patients based on their unique genetic, molecular, physiological, environmental, and behavioral signatures (Kosorok and Laber, 2019). The promise of human induced pluripotent stem cells (hiPSCs) (Takahashi and Yamanaka, 2006; Takahashi et al., 2007) to play a central role in precision medicine approaches for the diagnosis and treatment of human diseases has been evident since their initial discovery, given that they reflect the full genomic complement of the patient from which they were derived (Agarwal et al., 2008; Gunaseeli et al., 2010; Marchetto et al., 2010; Chun et al., 2011). The synergistic emergence of advanced genome, tissue engineering, and high-throughput analytical approaches, combined with increased clinical accessibility and depth of genome sequencing technologies, is helping to make the promise of hiPSCs as central agents of precision medicine a reality. These advancing technologies allow researchers to model complex neurodevelopmental processes *in vitro* at cellular and molecular levels and to identify potential pathogenic mechanisms, biomarkers and therapeutic vulnerabilities, all in a patient-specific context. In under two decades (Takahashi and Yamanaka, 2006; Takahashi et al., 2007), hiPSCs have transformed our understanding of human development in both normal and disease contexts and new advances continue to mount at a rapid rate.

hiPSC-based technologies have been particularly impactful for the brain. Given the inaccessibility and scarcity of *ex vivo* human brain tissues available for study, and a relative lack of congruence between humans and animal models (Jucker, 2010; Knock and Julian, 2021), mechanistic investigation of the human brain has historically been challenging. hiPSCs now provide researchers with an invaluable tool to simply produce human neural cells and ever more complex tissues "in a dish." Produced from the nuclear reprogramming of highly accessible sources of somatic cells, hiPSCs can be derived from any individual and strategies to establish these cells are becoming increasingly accessible (Liu et al., 2020). The initial somatic cell source used for hiPSC derivation was dermal fibroblasts obtained by punch biopsy of the donor's skin; however, blood plasma and even urine samples are now more commonly used, making the process simpler and less invasive for donors and clinicians (Sohn et al., 2012). The reprogramming of somatic cells involves the introduction into the donor cells of four transcription factors–OCT4, SOX2, KLF4, and c-MYC–by either nucleofection or, more commonly due to increased efficiency, transduction with viral vectors (Takahashi et al., 2007). As hiPSCs have the same genotype as their somatic cell source obtained from the human donor, they typically carry disease-associated mutations of interest as well as other genetic variants specific to that individual. Isogenic hiPSC lines produced by genomic engineering to repair a disease-causing variant, or hiPSCs obtained from family members with a similar, though typically not identical, germline signature, serve as valuable controls for mechanistic investigations (An et al., 2012; Fujimori et al., 2018; Laperle et al., 2020). These standard methods allow researchers to study the unique impacts of inherited patient-specific mutations in the multiple cell types that can be differentiated from hiPSCs. Although cells and tissues derived from human stem cells cannot, on their own, provide information across all physiological scales, they can illuminate the genetic and molecular features of neurological disorders. With ongoing advances, such as the ability to produce a myriad of neural cell types, more complex region-specific three-dimensional (3D) organoid tissues, and non-neural cell types that are important contributors in the neural niche (Muffat et al., 2016; Abud et al., 2017; Centeno et al., 2018; Wörsdörfer et al., 2019), the mechanisms and causative factors identified will become more likely to serve as valid biomarkers or therapeutic targets. Moreover, the subtle differences in genetic make-up of these cultures makes them the perfect tool to characterize the development and progression of neurological disorders for each patient or specific classes of patients (such as those that share a common rare disease diagnosis).

A wide variety of protocols to generate neural cells and 3D tissues from hiPSCs have been developed (Muratore et al., 2014; Galiakberova and Dashinimaev, 2020; Mayhew and Singhania, 2023), and these vary in their complexity and therefore their degree of fidelity to the molecular, structural and functional heterogeneity of *in vivo* human brain tissue. These engineered models of the human brain are now routinely used to investigate molecular processes that underly key stages of brain development including stem cell maintenance and fate decisions, neuro- and glio-genesis, and neuronal network formation and synaptic properties (Liu and Zhang, 2011). hiPSC models are also increasingly used to elucidate mechanisms of not only neurodevelopmental but also aging-related diseases (Yagi et al., 2011; Stern et al., 2018; Knock and Julian, 2021). In parallel, methods to precisely modify the genome of hiPSCs, for instance to insert or repair disease-relevant mutations or lineage-tracing markers, and to produce neural cells and tissues *in vitro* that reflect the complexity of the native environment, have become increasingly sophisticated. Continued innovation in these areas will greatly enrich our ability to uncover both common mechanisms of disease between distinct disorders and to then determine how each patient population, or individuals within these populations, are unique–a central requirement to achieve precision-level medical care.

As summarized in Figure 1, this review will highlight emerging technologies that together have great potential to center hiPSCs as powerful tools for physiological-level modeling of patient- and disease-specific pathological trajectories, and as agents for drug discovery, in neurological disorders. Efforts to consistently improve the depth and physiological relevance of high-throughput screening, neurophysiological analysis approaches, and the region-specific brain organoids and co-culture models (e.g., multi-region neural organoid models or those incorporating non-neural cell types) that can be established will have a particularly profound impact. We posit that a future exists in which hiPSCs are centered as agents to adequately inform clinical understanding and likely treatment trajectories for patients with genetic neurological disorders. However, to realize this goal the increasing repertoire of iPSC-derived human neural tissues, which elevate our ability to model the human brain with high complexity and fidelity, must continue to develop. Additionally, their integration with patient-derived biophysical data is needed. Personalization that spans cells to neural systems, achieved by integrating high resolution hiPSC-derived phenotyping data with multiscale biophysical models established from patient neuroimaging representations, can deepen our understanding of the underlying features of a patient's disease and clarify complex mechanisms. Measuring cellular

phenotypes across timescales, particularly after integration and validation with neurocognitive physiological parameters, may also uncover tissue and fluid-based biomarkers of bona fide disease trajectories and potential treatment approaches. These powerful emerging approaches and the critical advances that will follow from their integration, will transform the ability of researchers and clinicians to unravel the complexities of brain function and dysfunction and pave the way for personalized medicine becoming a viable and effective option for patients suffering from genetic neuropathologies.

2 A need for increased complexity to improve physiological relevance of hiPSC-based disease models

Human pluripotent stem cell-derived neuronal cultures and organoids have now been used to model numerous neurological disorders with a genetic basis. Early studies were largely focused on common diseases that impact development and aging trajectories like schizophrenia, bipolar disorder, autism syndromes, Alzheimer's disease (AD) and Parkinson's disease (PD) (Murai et al., 2016; Ochalek et al., 2017; Lewis et al., 2019; Bame et al., 2020; Laperle et al., 2020). Though more recently, rare genetic diseases have been increasingly represented in hiPSC disease modeling efforts and this focus promises to be especially impactful, both for our understanding of neuropathology in general and for our ability to effectively treat marginalized patient populations (Hosoya et al., 2017; Saito et al., 2018). Rare diseases frequently impact the brain, are typically genetic, and individually affect a small proportion of the human population (each fewer than 1 in 2000 live births) (Umair and Waqas, 2023). Given the large number of rare diseases that are thought to exist (an estimated ~8000) (Somanadhan et al., 2023) and the small number of patients available for study in each case, there is currently little to no mechanistic understanding for most rare conditions. This reality precludes accurate diagnoses, limits options for effective treatment, and results in a lack of fundamental knowledge about how many genetic disorders impact the form and function of our brains. Though rapid advances in genetic testing are increasingly improving the odds of identifying causative genetic variants for distinct rare conditions, which can then lead to cell and molecular-level mechanistic understanding, this is not always successful. Furthermore, there is often a lack of adequate functional information to validate candidate mutations or determine which gene variant, sometimes among multiple potential candidates, is causing a patient's disease.

Patient-derived hiPSC-neural models (paired with isogenic or familial controls) have already revealed important mechanistic details, and in some cases have elucidated therapeutic vulnerabilities, for many genetic disorders (Paşca et al., 2011; Liu et al., 2013; Barak et al., 2022). Few, however, have led to true clinical translation, and for most rare diseases hiPSC-derived models have yet to be developed at all. hiPSC approaches to model neural diseases have so far been fragmented, where investigations of pathology from individual groups typically emphasize specific aspects of a disease–such as cellular, physiological, cognitive, or clinical presentation–but lack an integrated view across multiple scales. Additionally, hiPSC-based studies typically assess individual cell types or a single brain region at a time, even though many neurological diseases are multifactorial involving contributions from different cell types and brain regions (Allen and Lyons, 2018; Fessel, 2023). This piecemeal strategy is inadequate to fully model and interrogate genetic brain diseases, as they are typically complex and impact multiple scales of brain form and function.

Establishing stem cell-based models for every rare genetic condition of the brain is a tall order. Though easing the burden, it has been promising to see as more studies as reported that specific pathogenic mechanisms often overlap between different genetic conditions. Furthermore, these overlapping mechanisms are often also observed in more common disorders for which mechanistic understanding is more abundant, and center on organelle dysfunction, altered proteostasis, and changes in the balance of excitatory and inhibitory (E/I) neurophysiological parameters (Reddy, 2009; Maestú et al., 2021; Pradhan and Bellingham, 2021; Wingo et al., 2022). Precision medicine approaches harnessing hiPSC technologies may therefore be accelerated by efforts to first group patients together who share similar disease signatures, even if they span distinct conditions. After this initial stratification, unique disease- or patient-specific phenotypic differences can then be more easily identified. This approach could help to put many patients on a promising diagnostic or treatment path more quickly and could greatly streamline mechanistic and therapeutic discovery endeavors, including identification of patient groups for which clinically approved drugs can be repurposed.

Before hiPSC-based technologies can reliably support disease diagnosis, trajectory predictions and treatment validation in the clinic (Figure 1), new paths to increase the throughput, fidelity, complexity, and physiological relevance of the neural cells and tissues they can produce must continue to emerge. Efforts to consistently improve the depth and accuracy of high-throughput screening and neurophysiological analysis approaches, and the region-specific brain organoids and co-culture models (e.g., multi-region neural organoid models or those incorporating non-neural cell types) that can be established from hiPSCs, will have a particularly profound impact. Technical strategies to analyze the impact of gene variants on cell fate decisions and molecular phenotypes, particularly those that are amenable to fluorescent-based imaging (Murai et al., 2016; Ochalek et al., 2017; Yang et al., 2017), are now quite robust. However, neurophysiological understanding at the cellular level requires quantification of the synaptic activity inherent in these cultures. Direct integration of cellular-level data with patient-derived neuroimaging representations (Figure 1) can be achieved by pairing datasets whose E/I balance parameters are closely matched (Figure 1; Schirner et al., 2018). Thus, we will focus our discussion on integrative cells-to-neural systems modeling of neurological disorders that are characterized by epilepsy and neurodegeneration, which consistently display measurable alterations in synaptic E/I balance. Notably, many neurological conditions–both developmental and aging-related–are marked by epileptic activity or neural tissue degeneration and their underlying mechanisms have been extensively investigated in animal and hiPSC disease models (Solodkin et al., 2011; Falcon et al., 2016; Bavassano et al., 2017; Jirsa et al., 2017; Rousseaux et al., 2018; Hashemi et al., 2020; Hommersom et al., 2022; Schirner et al., 2022; Jirsa et al., 2023). Given the prominence of epilepsy and neurodegeneration among neurological conditions, we therefore

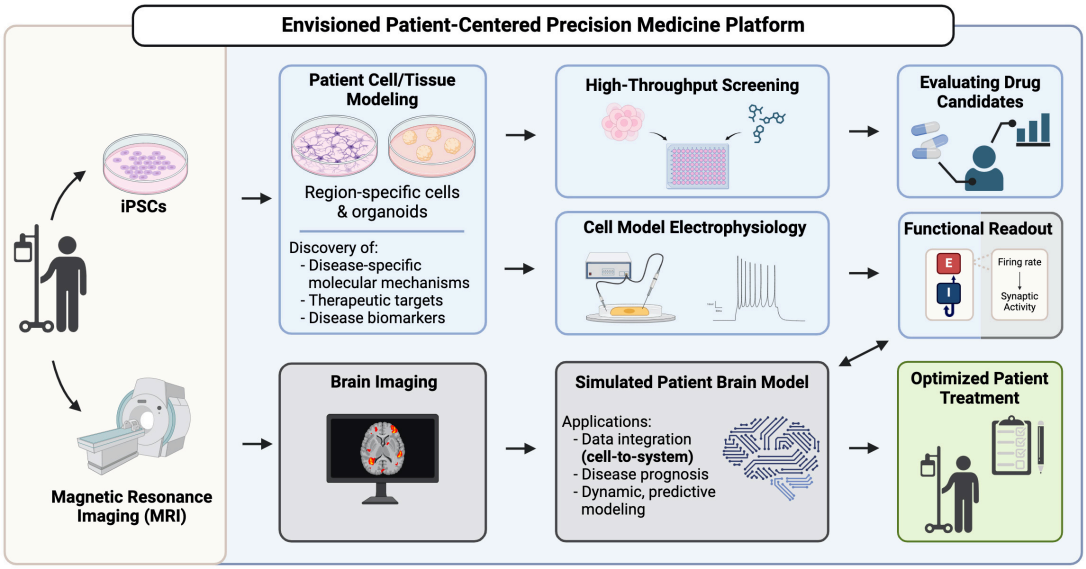

FIGURE 1
A vision for hiPSCs as key contributors in patient-centered precision medicine platforms. Patient-derived iPSCs are generated from patient somatic cells and are differentiated into brain region-specific cells and organoids for profiling, uncovering disease mechanisms and potential therapeutic targets. High-throughput screening using these patient-derived cells can reveal drug candidates that can go on for further evaluation of their efficacy. Functional readouts from electrophysiological assays, such as excitatory/inhibitory (E/I) balance in different neuronal populations can be integrated with brain imaging data in a simulated patient brain model to ultimately generate a predictive model to inform decision-making in patient diagnosis, prognosis and treatment.

predict that the integrated patient-centered modeling platform we envision (Figure 1) will ultimately be amenable to most genetic brain conditions.

2.1 Advances in patient-centered modeling of neurodegenerative disorders

Neurodegenerative diseases (NDDs) are a diverse group of complex conditions characterized by progressive and irreversible dysfunction of the brain due to the continuous loss of specific neuron populations that are susceptible to degeneration (Forman et al., 2004). Animal models of NDDs have enhanced our understanding of the molecular pathogenesis of diseases such as AD, PD, and Huntington's disease (HD) (Savitt et al., 2006; Yang et al., 2017; Dawson et al., 2018), with the hope of facilitating the discovery of multiple points of therapeutic intervention (Zeiss, 2017). However, findings in model organisms are not always translatable as some NDD pathologies are unique to humans. For example, because AD does not occur naturally in rodents, mouse models require genetic modification to cause the overexpression of human amyloid precursor protein (APP) and presenilin genes associated with familial AD (Sasaguri et al., 2017). The disease also manifests differently than in humans, where although the mice will develop amyloid plaques like those found in patients, they do not exhibit tauopathy or neurodegeneration (Selkoe, 2001). Due to the complexity and heterogeneity of NDDs in humans, animal models cannot fully recapitulate all physiological aspects of these disorders. Thus, there is a significant need for the development of advanced model systems that can effectively address the limitations of current animal models to enhance our mechanistic understanding of neurodegenerative diseases.

To address these concerns, many researchers are increasingly using human-based neuronal models to study NDDs. The synergy of novel hiPSC technologies with developments in genome-editing and sequencing has allowed for the investigation of cellular mechanisms during NDD pathogenesis. hiPSCs can also allow for the study of neurological diseases that don't have underlying mutations yet identified, as patient-derived hiPSCs retain the full genetic information of any germline and sometimes somatic mutations, providing researchers with a tool to also study sporadic diseases. In the case of Amyotrophic Lateral Sclerosis (ALS), a heterogenous motor neuron disease which causes the progressive degeneration of motor neurons in the spinal cord and brain (Cluskey and Ramsden, 2001), 90–95% of cases are sporadic (sALS) (Kiernan et al., 2011), meaning they are not inherited unlike familial ALS (fALS). Before the development of hiPSCs, it was difficult to establish useful models of sALS. Now, not only are researchers able to establish human cellular models of sALS, but they have also used them to identify a therapeutic agent, ropinirole, which showed protective effects in both their fALS and sALS cell models (Fujimori et al., 2018). This discovery led to phase 1/2a clinical trials in patients with sALS testing ropinirole (Morimoto et al., 2023), where ropinirole was shown to slow disease progression, resulting in slower functional decline when patients were treated with the drug earlier. While further efforts are required to uncover the precise mechanism of action for ropinirole in ALS, this body of work demonstrates that hiPSC culture models have the capability to be used in precision medicine pipelines to identify drug candidates and predict the responsiveness of patients to treatments (Farkhondeh et al., 2019; Okano and Morimoto, 2022).

The bulk of hiPSC-neural modeling studies to date have centered on models of the forebrain. However, it is well known that *in vivo*, NDDs often involve heterogenous representations across multiple brain regions. The forebrain may be involved in some pathological process, but it is not always the primary tissue region affected with other brain regions often displaying the first signs of the degeneration cascade. This means that many existing human cell models of NDD do not address the appropriate cell and tissue types. Recent innovations that are transforming our ability to produce region-specific brain organoids, particularly the cerebellum, are starting to fill this critical gap (Silva et al., 2020; Atamian et al., 2024). For example, the cerebellum is an important contributor in neural atrophy disorders such as Familial Ataxia Syndromes (Silva et al., 2020), Multiple System Atrophy (MSA) (Ciolli et al., 2014), and Creutzfeldt-Jakob Disease (CJD) (Zerr and Parchi, 2018). New findings suggest that cerebellar gray matter atrophy is also involved in many conditions previously attributed to the degeneration of the cerebral cortex such as AD, PD and Frontotemporal Dementia (FTD) (Guo et al., 2016; Gellersen et al., 2017; Seidel et al., 2017), suggesting that a more thorough investigation of the cerebellum can be insightful for human NDD modeling.

One such example of cerebellar atrophy disorders are the spinocerebellar ataxias (SCAs), a group of over 40 rare hereditary progressive movement disorders that primarily affect neurons in the hindbrain and cerebellum, with involvement in some forms in the spinal cord and cerebral cortex (Klockgether et al., 2019; Chirino-Pérez et al., 2021; Guo et al., 2023; Pilotto et al., 2023). To study this class of NDDs in a human model, researchers can use hiPSCs derived from both healthy individuals and SCA patients to generate cerebellar organoids, which can consistently reproduce multiple types of functional cerebellar neurons (Atamian et al., 2024). This very recent establishment of a functional human model of the cerebellum is an integral step to improving our understanding of human neurophysiology and pathology, as studies have shown that the human cerebellum differs drastically from that of rodents. For example, in contrast to mouse, the human cerebellum has more outer radial glia in an outer subventricular zone during development that drives human cerebellar expansion and gyrification (Nowakowski et al., 2016). Other differences in human cerebellum development are in rhombic lip (RL) morphology and the existence of substructure zones such as ventricular (RL^{VZ}) and subventricular zones (RL^{SVZ}), as well as internalization of the RL into the posterior lobule to form a tightly packed pool of cells (Haldipur et al., 2019). Differences in development ultimately translate to a different mature tissue, highlighting the importance of a human-based model to capture all aspects of neurophysiology and pathology in the cerebellum. While it can be argued that because hiPSC models elucidate mechanisms of disease in an earlier developmental model they might not be well suited for modeling diseases that arise later in adulthood, there is evidence to suggest that events during early prodromal stages in these developmental models can shed light on the acquisition of late-stage syndromic phenotypes (Caldwell et al., 2015; Tremlett and Marrie, 2021). This prodromal window may also be a more suitable therapeutic window to recover brain homeostasis.

The recent development of brainstem organoids (Eura et al., 2020; Lui et al., 2023), an area of extensive atrophy in many patients with SCA, will help to further develop appropriately complex models for this class of NDDs. Incorporating multiple brain region-specific organoids that are relevant to a given NDD–for example forebrain, cerebellum and brainstem–can permit analysis of degenerative mechanisms both within and between distinct affected regions. The rapid advance of brain organoid assembloid technologies (further detailed below), where unique types of organoids are physically connected to permit observation and assessment of neuronal network formation across brain regions, is substantially supporting efforts to improve physiological relevance in neurological disease models.

2.2 Advances in patient-centered epilepsy modeling

Epilepsy, a condition characterized by persistent predisposition to experiencing seizures, is thought to affect a staggering ∼1% of the population, or about 80 million people worldwide (Beghi, 2020). Epilepsy can arise due to one of many genetically defined conditions or, more often, as a secondary feature of other neuropathological conditions or from unknown causes. The exact mechanisms driving the underlying neural network dysfunction in these disorders largely remain to be uncovered (Perucca and Perucca, 2019), but *in vitro* modeling of inherited epilepsy disorders with hiPSCs has opened new doors for mechanistic investigations and drug discovery. The added value emerging from hiPSC-derived neural epilepsy models again highlights the limitations of existing animal models to capture certain human-specific features, which are critical to the establishment of altered brain architecture and synaptic networks that underlie these syndromes (Blair et al., 2018; Knock and Julian, 2021; Eichmuller et al., 2022). As with NDDs, in many epilepsies a genetic cause is presumed but the gene variant is unknown. hiPSC approaches to model brain development and neural network function from epileptic patients can therefore inform pathogenic mechanisms both for patients with well-defined mutations and for those whose genetic cause is not yet identified. In the latter case, the presence of epileptic phenotypes in hiPSC neural models derived from patients, compared to those from familial controls, can help to diagnose individuals by establishing if their syndrome does indeed have a genetic basis.

Many genetic epilepsies exist, but we will focus on a select few for which hiPSC models have provided significant advances–Dravet syndrome, a severe myoclonic epilepsy characterized by febrile seizures that begin in infancy, and the class of disorders termed malformations of cortical development (MCDs) (Chen et al., 2014; Costa et al., 2016; Sun and Dolmetsch, 2018; Majolo et al., 2019; Klofas et al., 2020). MCD describes numerous disorders that are characterized by altered brain development causing architectural and neuronal network abnormalities, which almost invariably lead to altered cognition and severe epilepsy that are typically treatment resistant (Oegema et al., 2020). Tuberous sclerosis, focal cortical dysplasia, and megalencephaly are among the most commonly studied MCDs, and hiPSC-derived *in vitro* models for these conditions continue to improve in their fidelity and capacity to model disease-relevant features (Li et al., 2017; Avansini et al., 2022; Eichmuller et al., 2022).

Given the relative ease of electrophysiological analyses in pure neuronal cultures, hiPSC-based models of epilepsy

have predominantly focused on the derivation and functional assessment of 2D cultures of neurons, sometimes also including astrocytes. Typically, these are telencephalic forebrain neurons given the propensity of basic neuronal differentiation protocols to yield forebrain cells (Muratore et al., 2014). Efforts to model Dravet syndrome with patient-derived hiPSCs, which carry a deleterious mutation in the Nav1.1 sodium channel, indicate that cultures of telencephalic interneurons carrying this variant have reduced sodium current density and action potential output; however, no phenotypic change was observed in excitatory neurons (Sun et al., 2016). These results are in line with previous findings in a mouse model of Dravet syndrome (Yu et al., 2006) and highlight differences in the contribution of distinct neuronal subtypes to the epileptic state in Dravet patients. Although only in 2D culture models, these results showcase the potential of hiPSCs to translate cellular-level phenotypes to clinical presentation, and further suggest the potential to evaluate the efficacy of potential therapeutic compounds at the cellular level. hiPSC models have similarly been used to shed light on the antiepileptic properties of cannabidiol (CBD) in Dravet syndrome and to study its mechanism of action. Researchers administered CBD to telencephalic neurons produced from patient-derived hiPSCs, which increased the excitability of inhibitory neurons and decreased the excitability of excitatory neurons, without altering sodium channel currents in these cell types (Sun and Dolmetsch, 2018). These observations indicate that the effect of CBD is also targeted to specific neuronal subtypes and is independent of sodium channel activity.

MCDs stand as the leading cause of medically refractory epilepsy in children (Oegema et al., 2020). In adults, the MCD Focal Cortical Dysplasia ranks as the third most common cause of medically intractable seizures (Kabat and Król, 2012). Molecular analysis of neurons from patients with Focal Cortical Dysplasia Type II identified dysregulation of several genes associated with neuronal migration during neurogenesis and embryonic neural progenitor cell differentiation, which is a key factor that underlies development of the malformed cortical tissue within the brains of these patients that underlies their epileptic activity (Majolo et al., 2019). hiPSCs carrying loss-of-function mutations in *DEPDC5*, encoding a GATOR1 complex member, show overactivation of the mammalian target of rapamycin complex 1 (mTORC1) signaling node, resulting in epileptic episodes which can be alleviated by administering the mTORC1 inhibitor rapamycin (Klofas et al., 2020). A growing number of studies indicate that mTORC1 plays a significant role in many neurological diseases due to its involvement in autophagy, proteostasis, cell proliferation and migration, and its interactions with multiple signaling pathways that modify the cell's energetic state, neurotransmitters, and growth factors (Cuyàs et al., 2014; Guo et al., 2018).

mTORC1 disruption is heavily implicated in multiple forms of MCDs, including megalencephaly disorders and tuberous sclerosis (TS) which is caused by mutations in the *TSC1* or *TSC2* genes (Hernandez et al., 2007; Kashii et al., 2023), leading to persistent mTORC1 hyperactivation. Disruption of the mTORC1 pathway leads to formation of benign tumors and generalized tissue malformations in multiple organs including the brain (Delaney et al., 2014; Crino, 2020; Delaney et al., 2020; Dhaliwal et al., 2024). Epilepsy manifests in up to 90% of TS patients (Rocktäschel et al., 2019), which is due to the presence of these low grade architecturally abnormal tumors or "cortical tubers" (Delaney et al., 2014; Frost and Hulbert, 2015). Patients with TS inherit a mutation in one allele of *TSC1* or *TSC2* and subsequent loss of heterozygosity in a subset of cells gives rise to focal regions of malformed brain tissue. Complete loss of *TSC1* or *TSC2* is therefore required to observe the full spectrum of disease-relevant phenotypes. Mouse models are not fully sufficient to investigate the molecular mechanisms of tuber formation, since homozygous germline *TSC1* or *TSC2* mutants are embryonic lethal due to failure of neural tube closure (Kobayashi et al., 1999; Møller et al., 2016), and various conditional knockouts fail to recapitulate the architecture of cortical tubers. The approach of differentiating neurons and glia from human pluripotent stem cells has proven to be an ideal and unique tool to investigate how *TSC1* or *TSC2* loss impacts the development of neural precursors, neurons, and glia, and the neural networks that they form, in the human brain (Nadadhur et al., 2019; Delaney et al., 2020). Reports on hiPSC-derived neuronal cultures have shown that deletion of *TSC2* leads to structural abnormalities in neuroectodermal rosettes, reminiscent of the defective neural tube closure observed *in vivo* (Costa et al., 2016; Winden et al., 2019). More directly relevant to epileptic phenotypes, molecular, cellular, and electrophysiological characteristics of dysplastic neurons from cortical tubers induced by deletion of *TSC2* have been routinely measured in forebrain neuronal cultures and rescued by the mTORC1 inhibitor rapamycin, a derivative of the leading pharmaceutical treatment for TS (Costa et al., 2016; Nadadhur et al., 2019; Winden et al., 2019; Delaney et al., 2020). Despite these advances in 2D neuronal cultures, TS is a profound example of the importance of 3D organoid modeling to more accurately reflect human disease phenotypes, as only in cerebral organoids has the architecture of cortical tubers been recapitulated (Blair et al., 2018; Eichmuller et al., 2022). The synergy of these hiPSC-derived neural cultures with advances in the electrophysiological assays discussed in the following section make them an ideal tool to study the impacts of potential drug therapeutics on epilepsy phenotypes *in vitro*.

3 Advancing hiPSC neural circuitry measurements with region-specific brain organoids

Our understanding of the early stages of neural circuitry development in humans has long been impeded by a lack of access to fetal and neonatal brain tissue. Obvious ethical concerns surrounding the use of such tissues to directly observe and manipulate developing neural circuitry have precipitated the use of alternative animal models to uncover key insights into human brain development. Rodents are widely used due to their genetic tractability and well-characterized neuroanatomy (Glowinski and Iversen, 1966). Non-human primate models are also used, albeit more sparingly, as they are closer to humans in terms of brain complexity and behavior (Feng et al., 2020). Additionally, zebrafish have transparent embryos that allow visualization of live early neural development (Sakai et al., 2018), while fruit flies and *C. elegans* have a simple nervous system, providing a more manageable model for exploring neural circuits (Sengupta and Samuel, 2009; Bellen et al., 2010). While the use of animal models

has been essential to understanding the basic nature of brain disorders that impact humans and continue to be an invaluable tool, they also come with their own disadvantages. Confounding factors such as captivity and housing conditions, which can cause stress and impacts on animal welfare, can negatively impact the validity and reproducibility of experimental results. It is also important to note that despite some similarities between humans and animal models, there is a lack of congruence to many features of the developing and adult human brain, which is thought to largely underlie the substantial issue of translational failure as promising therapeutic strategies are moved from experimental models to the clinical domain (Marshall et al., 2023).

The introduction of hiPSC-derived neural models, superseded by human embryonic stem cells (hESCs), in the last 20 years (Takahashi and Yamanaka, 2006; Marchetto et al., 2010; Cheung et al., 2011) has provided a profound tool to study neural circuitry in early human development, when in the past we have mostly been limited to postmortem tissues and neuroimaging data (Manzini et al., 2021). As a result, researchers are now able to use electrophysiological tools to assess the functional attributes of neurons in culture, including: (1) regular and high-density multi-electrode arrays (MEA) for prolonged, non-destructive recordings of electrical activity and network dynamics (Negri et al., 2020; Habibey et al., 2022); (2) patch clamping for direct measurement of neuronal activity (Bardy et al., 2016); (3) calcium imaging using fluorescent calcium indicators to monitor changes in intracellular calcium levels, serving as a proxy of neuronal activity (Estévez-Priego et al., 2023); (4) voltage-sensitive dye imaging using fluorescent dyes that change their fluorescent properties in response to changes in membrane potential (Glover et al., 2008); and (5) optogenetics, harnessing genetically engineered neurons that express light-sensitive proteins called opsins, permitting selective activation or inhibition of neurons by light stimulation to manipulate neuronal activity *in vitro* (Deisseroth et al., 2006). It is important to note that these 2D models lack native tissue architecture and complex intercellular interactions, which poses a challenge to studying neurodevelopment *in vitro* (Adlakha, 2023). The development of the 3D neural organoid culture method has provided a platform for the investigation of brain development in a more complex tissue environment. Many of the previously mentioned electrophysiological assays are now being applied to investigate neuronal function in 3D brain organoid models (Birey et al., 2017; Xiang et al., 2017; Fair et al., 2020; Tasnim and Liu, 2022; Yang et al., 2024). The cellular diversity of brain organoids allows researchers to study the diverse interactions that contribute to neural circuit function. Additionally, as these organoids can be maintained in culture for extended periods, including recent advances with organoid transplantation into mouse brain tissues to permit more advanced human neuronal cell and electrophysiological development (Revah et al., 2022; Kelley et al., 2024) researchers can study the development and maturation of neural circuit network dynamics over time (Fair et al., 2020). These 3D systems have been used to model disorders with known electrophysiological abnormalities, such as epilepsy (Hirose et al., 2020; Nieto-Estévez and Hsieh, 2020; Saberi et al., 2022), and can be further applied to substantiate therapeutic testing via high throughput drug screening applications.

To study the interactions between cells from different brain regions, researchers have developed co-culture methods to combine brain-region specific organoids into a single integrated model (Figure 2A; Bagley et al., 2017; Xiang et al., 2017). Since the introduction of these methods, there have been many multi-region organoid co-culture models generated to enable human neural circuitry studies in a dish to investigate complex neuropathophysiologies. The combination of these various neural organoids has allowed researchers to study key developmental processes in a more physiologically relevant model, such as interneuron migration and various neural circuitry projections. Table 1 lists some of these models that have been developed in recent years.

The electrophysiology data collected from these multi-region assembloid models allows for a detailed assessment of neural cell and circuit interactions between different brain regions, particularly as inhibitory interneurons integrate within excitatory neuron networks in the dorsal and ventral forebrain organoid co-culture model, a phenomenon that is highly reflective of neural circuit development in the human brain.

4 Advancing understanding of the brain microenvironment with co-culture of non-neural cell types

In vitro research on the human brain has primarily centered around neural cell types, including neurons, astrocytes and oligodendrocytes. However, when aiming to establish platforms to facilitate effective precision medicine strategies, which should mirror the *in vivo* condition as closely as possible, it is crucial to acknowledge the critical role that non-neural cells play in brain physiology and pathology. These cells can include pericytes and endothelial cells, which constitute the blood-brain-barrier. One of the most prominent non-neural cell types in the brain, which have emerged as particularly impactful regulatory cells across the lifespan, are brain-specific immune cells called microglia (Colonna and Butovsky, 2017; Mehl et al., 2022). During human brain development, microglia originate from primitive myeloid progenitors derived from the yolk sac. These progenitors migrate into the brain early during development, where they then differentiate into functional microglial cells. Microglia constitute approximately 5–16% of the total cell population in a fully developed brain and are maintained throughout life through self-renewing divisions (Masuda et al., 2020). As brain resident immune cells, microglia play a significant role in normal brain development and homeostasis. They are found to accumulate near dead neurons and are involved in phagocytosis of cell debris and degenerating axons. This role is more evident in a state of neural injury or stroke (Colonna and Butovsky, 2017). Microglia have also been associated with the stem cell niche in the brain at the subventricular zone and neocortex, where they regulate the differentiation of neural stem cells by selective cell engulfment (Xu et al., 2021). Moreover, they regulate the formation of neural circuits and maintain a balance of excitatory and inhibitory neurons by affecting inhibitory interneuron migration (Bohlen et al., 2019; Mehl et al., 2022). In addition to these widespread roles, microglia affect neuronal function through their crosstalk with other glial cells (Thion et al., 2018).

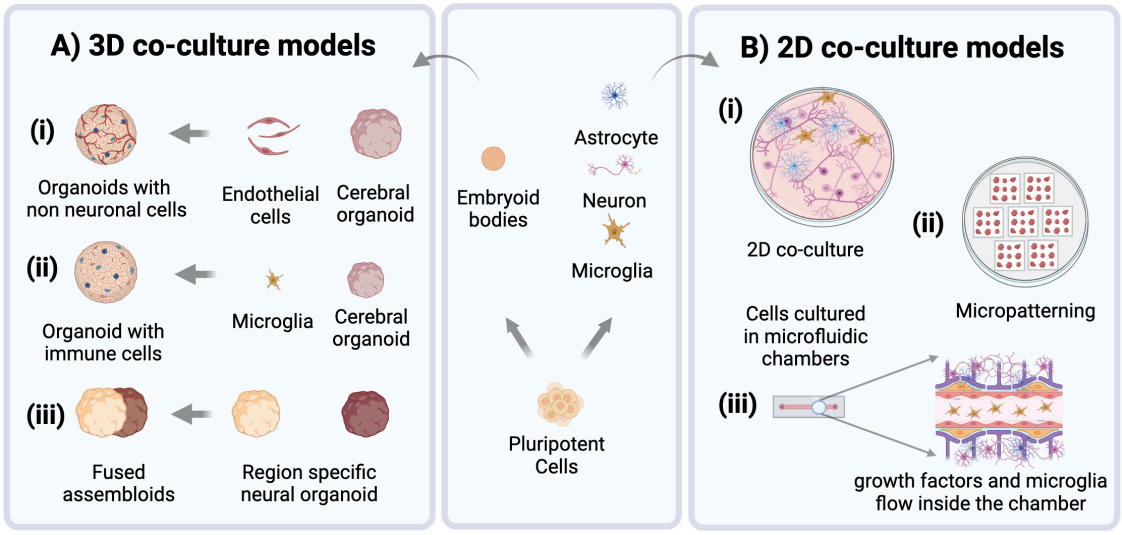

FIGURE 2
Modeling approaches for brain disorders using hiPSCs. Pluripotent stem cells are routinely used to derive embryoid bodies for heterogenous 3D organoid production, or cultures of neural and non-neural (e.g., microglia) cells that can then be combined to establish co-cultures of specified cell types (center panel). **(A)** 3D brain organoid models increasingly use co-culture approaches to enhance their physiological relevance by incorporating non-neural cell types such as (i) endothelial cells (ii) microglia, and (iii) generating region-specific organoids which can be fused to create assembloids. **(B)** 2D co-culture models: (i) culturing neurons, microglia, and astrocytes in a dish. (ii) Micropatterns, Cells are patterned into arrays of specific shapes and sizes to control their spatial organization. (iii) Microfluidic models of brain tissue are created to control the flow of nutrients and incorporate non-neural cell types through small scale channels.

TABLE 1 **Examples of multi-region organoids.**

Multi-region organoid model	Aspect of neural circuitry studied	Disease modeled	Publications
Dorsal forebrain & ventral forebrain	Interneuron migration	Timothy syndrome	Bagley et al., 2017; Birey et al., 2017; Xiang et al., 2017; Sloan et al., 2018
Cortical + thalamic	Thalamo-cortical projections of ascending sensory input	Schizophrenia, bipolar disorder, autism spectrum disorders, epilepsy (Angulo Salavarria et al., 2023)	Xiang et al., 2019
Cortical + striatal	Projections of motor planning circuits	Phelan-McDermid syndrome	Miura et al., 2020
Cortical + spinal + skeletal muscle	Cortico-spinal projections	Amyotrophic lateral sclerosis, spinal muscular dystrophy	Andersen et al., 2020
Retina + cortical + thalamic	Projections of circuitry of the visual pathway	Ocular neurodegeneration	Fligor et al., 2021

Table showing the region-specific organoids necessary to generate the listed multi-region organoid models, including the aspects of neural circuitry and disease that can be investigated with the model, as well as publications that have used these models.

Microglia are morphologically dynamic, ranging from thin, ramified structures under normal physiological conditions and transitioning to an activated state and hypertrophic morphology in response to certain stimuli (such as injury, infection, or neuroinflammation). In the active state, they show increased proliferation while secreting inflammatory factors such as chemokines and cytokines, which profoundly affect brain function [reviewed in Bohlen et al. (2019)]. Their activation, therefore, impacts brain physiology at many levels including neural circuits, cell populations, synapses, and neurotransmitter signaling (Bohlen et al., 2019; Mehl et al., 2022). Considering the many key functions they carry out, it is no surprise that microglia have a significant role in brain disorders spanning psychiatric conditions, such as schizophrenia, bipolar disorder, and autism, to neurodegenerative diseases like AD, PD and ataxias (Willis et al., 2020; Silvin et al., 2022; Tagliatti et al., 2024). *In vitro* models that lack microglia often present clear limitations in their ability to fully elucidate the mechanisms underlying neurological disorders. Thus, integrating immune cells like microglia into human neural cell models is paramount, and overlooking their contribution can result in significant gaps in our understanding of complex regulatory mechanisms in brain development and disease pathogenesis (Ronaldson and Davis, 2020; du Chatinier et al., 2023).

For *ex vivo* studies, researchers typically isolate primary microglia from postmortem human, rodent or non-human primate brain tissue (Roqué and Costa, 2017). The use of primary microglia comes with certain limitations, including inconsistent phenotypes due to the positive disease status of the donor, altered

activation states during the process of isolation, and, in the case of humans, lack of access to high-quality human postmortem tissue (Timmerman et al., 2018). Immortalized microglial cell lines, such as BV2 (derived from mouse), HMC3 (derived from human embryo), and CHME-5 (derived from adult human tissue) are also available (Dello Russo et al., 2018; Tian et al., 2019). While convenient, these cell lines show heterogeneity, genetic instability, and differences in differentiation state, which may impact their relevance to *in vivo* conditions (Das et al., 2016; Aktories et al., 2022). In addition to primary and immortalized microglia, protocols have been designed to differentiate or "induce" microglia (iMG) from embryonic or induced pluripotent stem cells (Speicher et al., 2019). iMG generated by these protocols resemble *in vivo* microglia in the context of their ability to phagocytose exogenous substances and respond to immune stimulation (Abud et al., 2017).

Microglia exhibit distinct responses to their microenvironment when cultured in 3D as opposed to traditional 2D cultures. In 3D environments, microglia display altered morphology, enhanced motility, and differential gene expression profiles compared to their 2D counterparts, reflecting the influence of spatial cues and cell-cell interactions on microglia behavior (Luchena et al., 2022). Therefore, 3D cultures with microglia (Figure 2A) can better recapitulate aspects of tissue architecture and cellular organization, providing a more accurate model for studying microglia behavior and function *in vitro* and their impacts on the developing brain. iMGs have been shown to incorporate into brain organoid tissue when co-cultured with them and show functional relevance to *in vivo* microglia post-integration (Abud et al., 2017). Xu et al. (2021) showed that iMG integrated into cerebral organoids engulf neural progenitor cells (NPCs), apoptotic cells, and neuronal synapses. iMGs when co-cultured with brain-specific organoids (i.e., with dorsal and ventral forebrain organoids), displayed different migration ability, intracellular Ca2 + signaling, and responses to pro-inflammatory stimuli (with higher expression of TNF-α and TREM2 in the ventral organoid-microglia group) (Song et al., 2019). Additionally, the transcriptome profile of iMGs cultured with dorsal brain organoids differs from that of ventral brain organoids, demonstrating that they are capable of responding to different neural niches *in vitro* (Hasselmann et al., 2019).

Microglia are also essential for proper development and function of the retina, and thus play a crucial role in the pathogenesis and progression of retinal disorders. The native state of retinal organoids is not captured accurately if microglia are absent. Therefore, to precisely represent the native retina, hiPSC-derived retinal organoids containing microglia are developed either by direct co-culture or by differentiating microglia in parallel within the organoids (Bartalska et al., 2022; Gao et al., 2022; Usui-Ouchi et al., 2023).

Microglia have also been incorporated into more defined engineered models to study their interaction with neural cells more precisely (Figure 2). These include microfluidic devices that allow dynamic control over microenvironmental factors and replication of *in vivo* nutrient gradients. Organ-on-a-chip models, which incorporate microfluidics to mimic physiological conditions of the brain and involve more intricate modeling of brain tissue, for example components of neural tissue juxtaposed with cells of the blood-brain-barrier (BBB) (Amirifar et al., 2022). Tissue micropatterning harnesses the power of growth restriction to pattern cells into self-assembled structures that reflect *in vivo* tissue organization, and interestingly microglia show structural diversity when grown on different micropatterned surfaces (Amadio et al., 2013). This approach can help to correlate the structural differences of microglia with their distinct functional identities. Co-culturing microglia with micropatterned neural tissue can reveal how microglia respond to different patterns of neural organization, providing insights into various subpopulations and their roles in development (Figure 2B). Simulation models further complement these approaches by enabling the computational study of microglial functions, such as their response to stress or inflammation and integrating that information into predictive models of brain function and disease. Ao et al. (2021) developed an organoid-on-chip model by synthesizing a device in a tubular shape where EBs are cultured to form a tubular organoid with an inner channel for the flow of nutrients and non-neural cells such as microglia, thus offering comprehensive insights into their functions and cellular interactions. Similarly, Pediaditakis et al. (2022) synthesized a microfluidic model to culture neurons, microglia, astrocytes and pericytes together, creating a neurovascular unit to study neuron and glia interactions in the brain microenvironment. Amadio et al. (2013) showed that microglia can move through microfluidic channels and travel up to 55 μm within 12 h. Culturing microglia on micropatterned surfaces and restricting their growth spatially can help to obtain more reproducible phenotypes. It has been shown that microglia possess distinct morphologies when cultured on different biomimetic micropatterned surfaces with different shapes correlating to diverse functional identities (Amadio et al., 2013). Finally, to achieve an integrated understanding of biological processes, computational models are also employed [as reviewed in Anderson and Vadigepalli (2016)]. Modeling studies demonstrate a strong correlation between microglial morphology and their function. The introduction of microglia and cytokine signaling into brain simulation models can further the knowledge of their plasticity and variability and the impact of different microglia states on brain form and function (Anderson and Vadigepalli, 2016). The neuroinflammatory environment can be created by co-culturing microglia with neurons and astrocytes, but to capture physiologically relevant microglial phenotypes more robust models must be created. These models should involve use of vasculature, endothelial cells and spatial cues to understand role of microglia in health and disease (Figure 2).

5 hiPSC-derived models as tools to identify disease-associated biomarkers

Disease-specific biomarkers have a crucial role in precision medicine, as they can help to identify specific characteristics that indicate the presence of progression of a particular disease, allowing clinicians to make accurate diagnoses, categorize patients into subtypes based on their biomarker signature and ultimately develop targeted interventions and treatments. Biomarkers can exist in the form of specific proteins, metabolites, genetic mutations, physiological parameters (e.g., blood pressure) or even brain imaging patterns that indicate a patient's prognosis, in addition to the stage of disease pathogenesis and progression (Chen et al.,

2011). Although the use of biomarkers in precision medicine has been mostly applied in oncological indications, such as estrogen receptor, progesterone receptor, and human epidermal growth factor receptor 2 (ER/PR/HER2) for breast cancer (Gamble et al., 2021), applications to a variety of target organs - including the brain - do exist.

Common neurodegenerative diseases such as AD affect millions of people worldwide and are especially prevalent clinically in the aging population. To make an accurate and differential diagnosis, a combination of structural and functional imaging, genetic, blood-based and cerebrospinal fluid (CSF) biomarkers are used by clinicians. In the case of AD, increased CSF levels of total-tau and phosphorylated-tau protein along with decreased levels of CSF Aβ1−42 create the typical AD biomarker profile found in most AD patients (Bouwman et al., 2022). While these CSF biomarkers represent the gold standard for the molecular characterization of neurodegenerative diseases, collecting CSF from patients for long-term observation is not feasible due to its invasive nature (Koníčková et al., 2022). While blood-based biomarkers exist for these neurological diseases, accurately measuring them poses a challenge as these brain-derived biomarkers are present at low concentrations in this fluid due to the blood-brain barrier (Zetterberg and Burnham, 2019). Additionally, certain biomarkers for AD may have potential interference from heterophilic antibodies and can be at risk of proteolytic degradation by proteases in blood plasma (Zetterberg and Burnham, 2019). Due to these considerations, an alternative source for brain-derived biomarkers is needed to enable further discovery and characterization for patients with rare neuropathophysiologies (Zetterberg and Burnham, 2019).

A recent technology describing the generation of human barrier-forming choroid plexus (ChP) neural organoids capable of producing CSF-like fluid (Pellegrini et al., 2020) may present a potential solution to the challenges with CSF-based biomarkers. Organoids are defined as *in vitro* cellular models formed via self-organization, including multiple organ-specific cell types that demonstrate functional and cytoarchitectural traits associated with a specific organ (Paşca et al., 2022). Fitting this definition, ChP organoids demonstrate key features of the human ChP, forming tight barriers that selectively regulate the entry of small molecules, and secrete a fluid akin to human CSF that contains proteins and known molecular biomarkers in self-contained cystic structures (Pellegrini et al., 2020). The generation of these organoids from hiPSC lines can present an alternative source for patient-derived CSF samples, limiting the need for invasive procedures such as lumbar punctures to collect this fluid. There is evidence to suggest that ChP organoids at day 60 of development and beyond can demonstrate functionality of adult ChP, with the production of a mature hiPSC-derived *in vitro* cerebral spinal fluid (iCSF) by 100 days (Pellegrini et al., 2020). iCSF can be harvested at multiple timepoints to track changes of the presence and levels of proteins and inflammatory cytokines found within the iCSF, providing insight to the progression of disease. For example, mass spectrometry is a commonly used technique to perform intensive proteomic survey of human CSF (Macron et al., 2019; Núñez Galindo et al., 2019), and can be done on iCSF as well to further investigate the iCSF proteome of patients with rare neurological diseases. Proteomic data from iCSF samples can be compared to existing spectral libraries of human CSF (hCSF) proteomes from patients (Schilde et al., 2020), to confirm that iCSF is a valid alternative to hCSF for biomarker research and discovery. As shown in Figure 3, in addition to proteomic analysis, metabolomic (Yan et al., 2021) and lipidomic (Byeon et al., 2021) analyses can be performed on this fluid to provide a comprehensive characterization of the composition of patient-derived CSF, with the aim of detecting unique disease biomarker signatures compared to CSF from healthy patients. The signatures found using this *in vitro* model can also be integrated into generative computer modeling platforms to inform clinicians of patient disease progression, creating a translational bridge by turning these observations into informed patient interventions.

However, while hiPSC-derived neural organoid models provide a promising platform to study the molecular and cellular mechanisms underlying neurological diseases in human cells, they have their limitations. These models are isolated systems that generally do not give rise to cell types of non-neural lineages due to the promotion of neural induction during differentiation, have limited maturation of their existing cell types and possess an atypical physiology that cannot fully recapitulate the complex environment of the human brain (Andrews and Kriegstein, 2022). To address this limitation, researchers have been co-culturing 2D and 3D neural tissues with non-neural cell types (Figure 2A). Neural organoids also lack vascularization, limiting the nutrient and metabolite exchange from the innermost regions of these structures, resulting in cell death in those regions (Lancaster and Knoblich, 2014). In the case of ChP organoids, lack of vascularization also means that this system cannot reproduce one of the key functions of the ChP *in vivo*, the formation of the blood-cerebrospinal fluid barrier (B-CSF) (Solár et al., 2020). There are groups who have vascularized organoids (Solár et al., 2020), and while these approaches create space for passive media flow, it still doesn't fully replicate blood flow. Despite these limitations, the ChP organoid model has the potential to provide a platform to allow further work on the identification and validation of biomarkers for rare neurodegenerative and neurodevelopmental diseases, with the aim of contributing to accurate and differential diagnoses and improved patient outcomes.

6 High-throughput approaches to disease-specific drug discovery

Clinical drug trials notoriously report poor outcomes, in part because drug discovery, development, and pre-clinical research have typically relied on non-mammalian model systems that lack important genetic and physiological features that are unique to the human brain. An important part of the challenge is that human primary cells are challenging to procure and propagate *in vitro*. With the emergence of hiPSCs and the ongoing collective efforts of the scientific community, directed differentiation methods can produce specific cell types which is enabling targeted pharmacological research into different neurodevelopmental and neurodegenerative diseases in which specific cell types are affected (i.e., dopaminergic neurons in PD, GABAergic neurons in Huntington's disease) (HD iPSC Consortium, 2012; Doi et al., 2020). Also possible is the investigation of interactions between cell types [i.e., microglia and motor neurons in amyotrophic

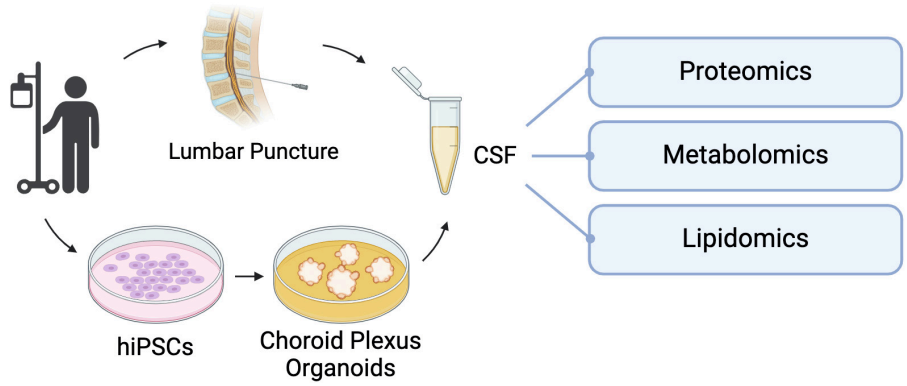

FIGURE 3
hiPSC-derived choroid plexus organoids present an alternative method of collecting CSF for biomarker analysis without the need for invasive lumbar punctures. This *in vitro* CSF-like fluid can be used for targeted investigation of factors of interest or unbiased analyses like proteomic, metabolomic and lipidomic screening to uncover unique molecular signatures that can be used to make differential diagnoses and track disease progression and prognosis.

lateral sclerosis (ALS)] (Sances et al., 2016; Vahsen et al., 2022). Combined with CRISPR-Cas9 technology, the use of hiPSCs has revolutionized drug discovery by allowing the generation of *in vitro* models with much improved relevance to human brain development and cell type fidelity, and by providing a route to gain deeper understanding of the molecular mechanisms that drive human genetic diseases (Takahashi et al., 2007). In this regard, the ability to capture subcellular events in response to pharmacological interventions has been a boon to drug discovery.

High-throughput screening (HTS) is a technique to rapidly assay a range of variables in an automated way that inform cellular phenotypes in relation to genetic mutations or environmental conditions, and is particularly useful as a drug discovery tool. This application was driven by a growing need to find more effective and highly specific drug candidates in a diverse chemical space. In a typical HTS screen, small molecules are tested in parallel against biological targets (e.g., cells or simple tissues) to identify "hit" compounds that can restore normal phenotypes. HTS has been enabled by a confluence of several scientific and technological advances including: (1) the development of large, diverse, and individually characterized compound libraries; (2) improvements to cell-based assays that are cost-effective, involve straightforward protocols, and can probe intra- and inter-cellular events; (3) miniaturization of assays to reduce the cost-prohibitive nature of large screens; (4) advances in engineering of automation robotics to reduce repetitive manual tasks; and (5) development of bioinformatic tools for large dataset management and analysis (Broach and Thorner, 1996; Sittampalam et al., 1997; Fernandes, 1998; Silverman et al., 1998). Each of these fields remains highly active, and ongoing advancements continue to improve HTS and drive its widespread application. Here we will highlight selected areas that could advance drug discovery by harnessing the combined strength of hiPSCs and HTS.

One major advantage of hiPSCs is the continuous and unlimited generation of cells and tissues of interest. However, given the sheer volume of cells required for large screens, which can include 100,000 compounds or more, the manual labor required to culture hiPSCs and downstream cell types is not feasible for most laboratories. Though recently, innovations in automative engineering are addressing this issue by developing automated cell culture systems that entail strictly hands-off and scalable workflows. Liquid handlers and robotic arms can now perform tasks related to tissue culture vessel handling, media exchanges, subculturing, and differentiation protocols (Terstegge et al., 2007; Thomas et al., 2009; Valamehr et al., 2012; Conway et al., 2015; Tristan et al., 2021; Deng et al., 2023). Well-optimized automation can be reliably used to implement standard operating procedures, efficiently manage cell quality control, and reduce random batch-to-batch variability associated with human error. This is important because drug screens are costly assays, and as such it is common practice to have few or no technical or biological replicates. Thus, consistency of cellular and experimental parameters is a key concern as the few (or single) replicate measurements must accurately represent the phenotype(s) of interest.

Due to individual genetic diversity, effective precision medicine platforms will require patient-specific cell lines to appropriately classify both disease-specific cohorts and heterogeneity among patients with a given condition. Thus, scaling up automated cell culture technologies is critical to make this a reality. Efforts have been made to develop automated pipelines for the creation of hiPSC lines from fibroblasts (Paull et al., 2015). In the context of drug discovery, this will improve healthcare efficacy as top drug candidates can be identified before they are administered, thereby minimizing the deleterious side effects of medication optimization.

Despite the current advancements in hiPSC disease modeling, a unique challenge in neuroactive drug discovery using *in vitro* models is the absence of a BBB. The BBB is a layer of endothelial, mural, astrocytic, and immune cells surrounded by a basement membrane. It has a critical role in tightly regulating the transfer of substances between the circulatory system and the central nervous system, and serves to prevent exposure of the brain to harmful substances (Daneman and Prat, 2015). However, because the permeability of the BBB is very selective, most drug candidates are not effectively transported to the brain and only drugs below 400 Da are able to cross via lipid-mediated diffusion (Pardridge, 2012). Strategies have been developed that enhance the ability of drugs to penetrate the BBB, including increasing drug lipid solubility, use

of carrier-mediated transport, or concurrent use of another drug that disrupts BBB permeability (Mikitsh and Chacko, 2014). Thus, consideration and inclusion of models to investigate permeability through the BBB is a critical aspect of *in vitro* drug discovery that needs to be increasingly considered when making predictions for drug efficacy.

Co-culture models that combine distinct hiPSC-derived cell types to replicate key aspects of the BBB exhibit physiologically appropriate characteristics including tube formation, organized tight junctions with acceptable transendothelial electrical resistance (TEER), expression of active transporters, and uptake of low-density lipoprotein (Lippmann et al., 2012; Aday et al., 2016; Qian et al., 2017). This stem-cell derived model, either as a standalone organoid or combined with organ-on-a-chip technology, shows great promise in enhancing drug discovery research by simulating a more physiologically accurate representation of drug delivery (Nzou et al., 2018; Choi et al., 2024). However, the low-volume nature of producing these models presents a challenge in translatability to HTS. Preliminary efforts have started scale up of the system through innovations in multi-chamber chip fabrication, which allows for parallel drug testing, but this technology has yet to be explored with HTS (Fan et al., 2016; Wevers et al., 2018).

Leveraging hiPSC technologies combined with HTS workflows is a cornerstone of translational medicine because it provides a powerful tool to elucidate disease pathways and identify potential pharmacological targets. However, limitations still exist. As described above, the benefits of organoid and assembloid modeling are evident, but incorporating these advances into a HTS workflow remains a barrier due to scalability limitations of 3D tissue models. Additionally, 3D models are typically heterogeneous in composition and size, which introduces high levels of error and thus are intrinsically challenging to characterize with currently available tools (Carragher et al., 2018; Booij et al., 2019). Additionally, compound hit identification relies primarily on a still limited range of fluorescent protein markers. This means that these assays have limited potential for multiplexity due to overlap in excitation and emission wavelengths. Thus, there is an ongoing demand for standardization of 3D tissue models (to produce tissues of reproducible size and architecture) and improved imaging probes, particularly for quantification of functional disease phenotypes and the short- and long-term intra- and inter-cellular responses with drug treatment.

Increasingly advanced hiPSC models have provided a greater understanding of disease pathogenesis, but to improve pharmacological interventions there exists a need for paradigm shifts in strategies for drug discovery. Historically, drug discoveries depended on observations of phenotypic changes of a single known target. To prevent off-target effects, pharmaceutical research aims to develop compounds with low promiscuity. However, this strategy has poor efficacy for complex diseases such as schizophrenia, multiple sclerosis (MS), and cancer. The problem arises because those diseases are polygenic or involve more complex interactions between different cell types or multiple molecular pathways. More recently, research has revealed the benefits of highly specific multi-target compounds in treating such multifactorial diseases, likely due to synergistic effects through secondary off-targets (Peters, 2013; Anighoro et al., 2014; Makhoba et al., 2020). Now coined as polypharmacology, this new approach to drug discovery aims to elucidate new applications of existing and theoretical compounds (Anighoro et al., 2014).

The forefront of drug discovery is moving toward incorporation of deep learning and artificial intelligence (AI) to aid in identifying drug candidates *in silico*. AI-assisted tools are continuously improving predictions and characterizations of cell protein folding and structure, identifying druggable proteomes, and simulating protein-ligand binding behavior (Cichońska et al., 2024). Combined with ultra-large virtual libraries, some with over 116 billion molecules that cover all possible structures within the chemical space, the combination of these powerful resources can generate an unprecedented amount of data for a targeted approach to polypharmacology (Ruddigkeit et al., 2012; Reymond, 2015). Well-characterized mechanisms of action can be invaluable for clinicians making critical treatment decisions and can greatly inform drug design and synthesis. Integration of AI-informed data with hiPSC platforms presents an exciting new frontier of disease modeling and pharmaceutical interventions. In parallel, the advance of high-throughput screening methods, empowered by the scalability of hiPSC-derived systems, holds the promise of expediting identification and validation of novel therapeutic compounds. Thus, with the right applications, hiPSCs are positioned to be particularly powerful clinical tools with outstanding patient-specific precision.

7 Integrating hiPSC-derived cellular data into AI-driven patient biophysical models

Early applications of AI toward hiPSC-derived models centered on image analyses to classify cells and hiPSC colonies based on morphological features, allowing for accurate classifications without human bias and enhancing precision and scalability by automating manual assessments (Vo et al., 2024). This laid the groundwork for the use of machine learning to automate the analysis of more complex data sets, such as RNA sequencing data, morphological and molecular assessment of disease-specific cell types, and cell function monitoring. In the context of disease-modeling, AI algorithms can become trained on large data sets to report alterations in cell morphology (Teles et al., 2021), fluorescent readouts of cell state and function (Nishino et al., 2021) to understand and identify differences in cell differentiation in hiPSCs, ultimately allowing it to predict differentiation outcomes. These predictions can be used to facilitate the high-throughput screening of drug candidates by analyzing cellular responses to treatments, providing insights to drug efficacy and toxicity (Kusumoto et al., 2022). Label-free drug screening systems can be especially useful in cases where no effective molecular markers for a given phenotype are known.

We envision that these achievements in AI around hiPSC-derived brain models can be further expanded to permit integration of meaningful cellular data with other types of patient-derived information that represent brain function or dysfunction on a larger scale. For example, rapid advancements in deep learning and generative AI have also led to the establishment of synthetic replicas

of biophysical entities based on patient-derived neuroimaging data, coined "digital twins" (DT). In its most general sense, DT technology allows for the integration of large volumes of data to simulate a physical system in a digital space and to make predictive models. This concept has been harnessed for a myriad of applications spanning spacecraft navigation simulation (Grieves and Vickers, 2017) to urban planning (Bolton et al., 2018). In the context of biomedical research and precision medicine, there are promising new efforts that leverage the DT technology to integrate subject-derived data to form brain simulations, ultimately with the goal of using this predictive model to inform decision-making in patient diagnosis, prognosis, and therapeutics. For example, consolidation of longitudinal magnetic resonance imaging (MRI) to produce reference data on normal aging can be used to create an algorithm to identify premature development of brain atrophy and predict and monitor disease progression of MS (Voigt et al., 2021; Cen et al., 2023). Electroencephalography (EEG) theta and delta activity can be used as biomarker candidates to classify stroke patients to guide prevention and post-stroke care (Hussain and Park, 2021).

Previous work on a platform built on generative biophysical modeling, The Virtual Brain (TVB), has accurately generated high-fidelity patient brain models that can map trajectories for normative aging (Lavanga et al., 2023) and neurological conditions like neurodegeneration (Zimmermann et al., 2018) idiopathic epilepsy (Jirsa et al., 2014), stroke (Falcon et al., 2016) and cancer (Aerts et al., 2018). TVB has also shown that the excitatory/inhibitory (E/I) balance in different neuronal populations can provide a strong link between cellular and neuroimaging models (Deco et al., 2014; Proix et al., 2017; Schirner et al., 2018; Figure 1). This suggests that electrophysiological modeling can be used as a parameter to determine differences between patient and control iPSC-derived neural cultures. In the context of epilepsy disorders, changes in E/I balance can be used to determine the efficacy of drugs being tested on iPSC-derived neural tissue for treatment of the disease. As most patients have subtle differences in their disease-causing mutations, testing drugs on cultures derived from their own hiPSCs provides the most direct, translatable link if a drug candidate is identified. In further applications, the electrophysiology data collected from the aforementioned multi-region assembloid models allows for a detailed assessment of neural cell and circuit interactions between different brain regions, particularly as inhibitory interneurons integrate within excitatory neuron networks.

The integration of electrophysiological data from hiPSC-derived models into these AI-modeling platforms has the clinical potential to predict how cellular processes and their manipulation can impact the whole brain, providing estimates of brain function across multiple scales–individual cells, and single or interconnected neural networks–on an individualized basis. This integration can allow for the development of a fully personalized platform for rare diseases that can span population-level and patient-specific mechanisms, informing clinical strategies and cross-validated biomarkers. This approach can allow the rapid development of disease-specific diagnostics and individualized treatment plans for patients with rare neurological disorders.

In summary, as hiPSC-derived neural disease models evolve to more accurately reflect the complexity of human neurobiology *in vitro*, their potential to uncover disease mechanisms, identify biomarkers and therapeutic targets will only grow. The integration of hiPSC-derived neural models with advanced tools such as genome engineering, high-throughput screening and AI-modeling platforms offers a promising pathway toward the realization of precision medicine for brain disorders. Together, these innovations hold the promise of transforming the management of complex and rare neurological disorders to hopefully offer more effective and tailored therapeutic approaches.

Author contributions

NF: Conceptualization, Writing – original draft, Writing – review and editing. LL: Writing – original draft, Writing – review and editing, Conceptualization. SN: Writing – original draft, Writing – review and editing, Conceptualization. AN: Writing – original draft, Conceptualization. LR: Writing – original draft. AM: Conceptualization, Writing – original draft, Writing – review and editing. LJ: Conceptualization, Funding acquisition, Writing – original draft, Writing – review and editing.

Funding

The author(s) declare that financial support was received for the research, authorship, and/or publication of this article. LJ is a Tier II Canada Research Chair and a Michael Smith Foundation for Health Research/Parkinson Society BC Scholar. LL is funded by MITACS and the NSERC Alliance program, SN by SFU and Phyllis Carter Burr Graduate Fellowships, and AN by the CIHR Canada Graduate Scholarship-M program. We also acknowledge relevant funding support from Ataxia Canada, Epilepsy Canada, the Cancer Research Society (JULIAN, L-CRS 25551), the Natural Sciences and Engineering Research Council of Canada (JULIAN, L-RGPIN-03965), and AM is funded by the NSERC Discovery Grant RGPIN-2018-04457 and Canadian Institutes of Health Research (CIHR) Project Grant PJT-168980.

Conflict of interest

The authors declare that the research was conducted in the absence of any commercial or financial relationships that could be construed as a potential conflict of interest.

Publisher's note

References

Abud, E. M., Ramirez, R. N., Martinez, E. S., Healy, L. M., Nguyen, C. H. H., Newman, S. A., et al. (2017). iPSC-derived human microglia-like cells to study neurological diseases. *Neuron* 94, 278–293.e9. doi: 10.1016/j.neuron.2017.03.042

Aday, S., Cecchelli, R., Hallier-Vanuxeem, D., Dehouck, M. P., and Ferreira, L. (2016). Stem cell-based human blood–brain barrier models for drug discovery and delivery. *Trends Biotechnol.* 34:382. doi: 10.1016/j.tibtech.2016.01.001

Adlakha, Y. K. (2023). Human 3D brain organoids: steering the demolecularization of brain and neurological diseases. *Cell Death Discov.* 9:221. doi: 10.1038/s41420-023-01523-w

Aerts, H., Schirner, M., Jeurissen, B., Van Roost, D., Achten, E., Ritter, P., et al. (2018). Modeling brain dynamics in brain tumor patients using the virtual brain. *eNeuro* 5, ENEURO.0083-18.2018. doi: 10.1523/ENEURO.0083-18.2018

Agarwal, S., Holton, K. L., and Lanza, R. (2008). Efficient differentiation of functional hepatocytes from human embryonic stem cells. *Stem Cells* 26, 1117–1127. doi: 10.1634/stemcells.2007-1102

Aktories, P., Petry, P., and Kierdorf, K. (2022). Microglia in a dish-which techniques are on the menu for functional studies? *Front. Cell Neurosci.* 16:908315. doi: 10.3389/fncel.2022.908315

Allen, N. J., and Lyons, D. A. (2018). Glia as architects of central nervous system formation and function. *Science* 362, 181–185. doi: 10.1126/science.aat0473

Amadio, S., De Ninno, A., Montilli, C., Businaro, L., Gerardino, A., Volonté, C., et al. (2013). Plasticity of primary microglia on micropatterned geometries and spontaneous long-distance migration in microfluidic channels. *BMC Neurosci.* 14:121. doi: 10.1186/1471-2202-14-121

Amirifar, L., Shamloo, A., Nasiri, R., de Barros, N. R., Wang, Z. Z., Unluturk, B. D., et al. (2022). Brain-on-a-chip: recent advances in design and techniques for microfluidic models of the brain in health and disease. *Biomaterials* 285:121531. doi: 10.1016/j.biomaterials.2022.121531

An, M. C., Zhang, N., Scott, G., Montoro, D., Wittkop, T., Mooney, S., et al. (2012). Genetic correction of Huntington's disease phenotypes in induced pluripotent stem cells. *Cell Stem Cell* 11, 253–263. doi: 10.1016/j.stem.2012.04.026

Andersen, J., Revah, O., Miura, Y., Thom, N., Amin, N. D., Kelley, K. W., et al. (2020). Generation of functional human 3D cortico-motor assembloids. *Cell* 183, 1913–1929.e26. doi: 10.1016/j.cell.2020.11.017

Anderson, W. D., and Vadigepalli, R. (2016). Modeling cytokine regulatory network dynamics driving neuroinflammation in central nervous system disorders. *Drug Discov. Today Dis. Models* 19, 59–67. doi: 10.1016/j.ddmod.2017.01.003

Andrews, M. G., and Kriegstein, A. R. (2022). Challenges of organoid research. *Annu. Rev. Neurosci.* 45, 23–39. doi: 10.1146/annurev-neuro-111020-090812

Angulo Salavarria, M. M., Dell'Amico, C., D'Agostino, A., Conti, L., and Onorati, M. (2023). Cortico-thalamic development and disease: from cells, to circuits, to schizophrenia. *Front. Neuroanat.* 17:1130797. doi: 10.3389/fnana.2023.1130797

Anighoro, A., Bajorath, J., and Rastelli, G. (2014). Polypharmacology: challenges and opportunities in drug discovery. *J. Med. Chem.* 57, 7874–7887. doi: 10.1021/jm5006463

Ao, Z., Cai, H., Wu, Z., Song, S., Karahan, H., Kim, B., et al. (2021). Tubular human brain organoids to model microglia-mediated neuroinflammation. *Lab. Chip* 21, 2751–2762. doi: 10.1039/d1lc00030f

Atamian, A., Birtele, M., Hosseini, N., Nguyen, T., Seth, A., Del Dosso, A., et al. (2024). Human cerebellar organoids with functional Purkinje cells. *Cell Stem Cell* 31, 39–51.e6. doi: 10.1016/j.stem.2023.11.013

Avansini, S. H., Puppo, F., Adams, J. W., Vieira, A. S., Coan, A. C., Rogerio, F., et al. (2022). Junctional instability in neuroepithelium and network hyperexcitability in a focal cortical dysplasia human model. *Brain* 145, 1962–1977. doi: 10.1093/brain/awab479

Bagley, J. A., Reumann, D., Bian, S., Lévi-Strauss, J., and Knoblich, J. A. (2017). Fused cerebral organoids model interactions between brain regions. *Nat. Methods* 14, 743–751. doi: 10.1038/nmeth.4304

Bame, M., McInnis, M. G., and O'Shea, K. S. (2020). MicroRNA alterations in induced pluripotent stem cell-derived neurons from bipolar disorder patients: pathways involved in neuronal differentiation, axon guidance, and plasticity. *Stem Cells Dev.* 29, 1145–1159. doi: 10.1089/scd.2020.0046

Barak, M., Fedorova, V., Pospisilova, V., Raska, J., Vochyanova, S., Sedmik, J., et al. (2022). Human iPSC-derived neural models for studying Alzheimer's disease: from neural stem cells to cerebral organoids. *Stem Cell Rev. Rep.* 18, 792–820. doi: 10.1007/s12015-021-10254-3

Bardy, C., van den Hurk, M., Kakaradov, B., Erwin, J. A., Jaeger, B. N., Hernandez, R. V., et al. (2016). Predicting the functional states of human iPSC-derived neurons with single-cell RNA-seq and electrophysiology. *Mol. Psychiatry* 21, 1573–1588. doi: 10.1038/mp.2016.158

Bartalska, K., Hübschmann, V., Korkut-Demirbaş, M., Cubero, R. J. A., Venturino, A., Rössler, K., et al. (2022). A systematic characterization of microglia-like cell occurrence during retinal organoid differentiation. *iScience* 25:104580. doi: 10.1016/j.isci.2022.104580

Bavassano, C., Eigentler, A., Stanika, R., Obermair, G. J., Boesch, S., Dechant, G., et al. (2017). Bicistronic CACNA1A gene expression in neurons derived from spinocerebellar ataxia type 6 patient-induced pluripotent stem cells. *Stem Cells Dev.* 26, 1612–1625. doi: 10.1089/scd.2017.0085

Beghi, E. (2020). The epidemiology of epilepsy. *Neuroepidemiology* 54, 185–191. doi: 10.1159/000503831

Bellen, H. J., Tong, C., and Tsuda, H. (2010). 100 years of Drosophila research and its impact on vertebrate neuroscience: a history lesson for the future. *Nat. Rev. Neurosci.* 11, 514–522. doi: 10.1038/nrn2839

Birey, F., Andersen, J., Makinson, C. D., Islam, S., Wei, W., Huber, N., et al. (2017). Assembly of functionally integrated human forebrain spheroids. *Nature* 545, 54–59. doi: 10.1038/nature22330

Blair, J. D., Hockemeyer, D., and Bateup, H. S. (2018). Genetically engineered human cortical spheroid models of tuberous sclerosis. *Nat. Med.* 24, 1568–1578. doi: 10.1038/s41591-018-0139-y

Bohlen, C. J., Friedman, B. A., Dejanovic, B., and Sheng, M. (2019). Microglia in brain development, homeostasis, and neurodegeneration. *Annu. Rev. Genet.* 53, 263–288. doi: 10.1146/annurev-genet-112618-043515

Bolton, A., Butler, L., Dabson, I., Enzer, M., Evans, M., Fenemore, T., et al. (2018). Gemini principles. *CDBB*. doi: 10.17863/CAM.32260

Booij, T. H., Price, L. S., and Danen, E. H. J. (2019). 3D Cell-based assays for drug screens: challenges in imaging, image analysis, and high-content analysis. *SLAS Discov.* 24:615. doi: 10.1177/2472555219830087

Bouwman, F. H., Frisoni, G. B., Johnson, S. C., Chen, X., Engelborghs, S., Ikeuchi, T., et al. (2022). Clinical application of CSF biomarkers for Alzheimer's disease: from rationale to ratios. *Alzheimers Dement. (Amst)* 14, e12314. doi: 10.1002/dad2.12314

Broach, J. R., and Thorner, J. (1996). High-throughput screening for drug discovery. *Nature* 384:14.

Byeon, S. K., Madugundu, A. K., Jain, A. P., Bhat, F. A., Jung, J. H., Renuse, S., et al. (2021). Cerebrospinal fluid lipidomics for biomarkers of Alzheimer's disease. *Mol. Omics* 17, 454–463. doi: 10.1039/d0mo00186d

Caldwell, C. C., Yao, J., and Brinton, R. D. (2015). Targeting the prodromal stage of Alzheimer's disease: bioenergetic and mitochondrial opportunities. *Neurotherapeutics* 12, 66–80. doi: 10.1007/s13311-014-0324-8

Carragher, N., Piccinini, F., Tesei, A., Trask, O. J., Bickle, M., Horvath, P., et al. (2018). Concerns, challenges and promises of high-content analysis of 3D cellular models. *Nat. Rev. Drug Discov.* 17:606. doi: 10.1038/nrd.2018.99

Cen, S., Gebregziabher, M., Moazami, S., Azevedo, C., and Pelletier, D. (2023). Toward precision medicine using a "Digital Twin" approach: modeling the onset of disease-specific brain atrophy in individuals with multiple sclerosis. *Res Sq* 13:16279. doi: 10.21203/rs.3.rs-2833532/v1

Centeno, E. G. Z., Cimarosti, H., and Bithell, A. (2018). 2D versus 3D human induced pluripotent stem cell-derived cultures for neurodegenerative disease modelling. *Mol. Neurodegener.* 13:27. doi: 10.1186/s13024-018-0258-4

Chen, W., Liu, J., Zhang, L., Xu, H., Guo, X., Deng, S., et al. (2014). Generation of the SCN1A epilepsy mutation in hiPS cells using the TALEN technique. *Sci. Rep.* 4:5404. doi: 10.1038/srep05404

Chen, X. H., Huang, S., and Kerr, D. (2011). Biomarkers in clinical medicine. *IARC Sci. Publ.* 163, 303–322.

Cheung, A. Y., Horvath, L. M., Grafodatskaya, D., Pasceri, P., Weksberg, R., Hotta, A., et al. (2011). Isolation of MECP2-null Rett Syndrome patient hiPS cells and isogenic controls through X-chromosome inactivation. *Hum. Mol. Genet.* 20, 2103–2115. doi: 10.1093/hmg/ddr093

Chirino-Pérez, A., Vaca-Palomares, I., Torres, D. L., Hernandez-Castillo, C. R., Diaz, R., Ramirez-Garcia, G., et al. (2021). Cognitive impairments in spinocerebellar ataxia type 10 and their relation to cortical thickness. *Mov. Disord.* 36, 2910–2921. doi: 10.1002/mds.28728

Choi, G., Yang, H.-Y., Cho, S., Kwon, D., Kim, D.-W., Ko, S., et al. (2024). Brain-On-A-chip based on human pluripotent stem cell-derived neurons and astrocytes for neurotoxicity testing: Communicative Astrocyte–Neuron DYnamics (CANDY) Chip. *Adv. Mater. Technol.* 9:2400107. doi: 10.1002/admt.202400107

Chun, Y. S., Byun, K., and Lee, B. (2011). Induced pluripotent stem cells and personalized medicine: current progress and future perspectives. *Anat. Cell Biol.* 44, 245–255. doi: 10.5115/acb.2011.44.4.245

Cichońska, A., Ravikumar, B., and Rahman, R. (2024). AI for targeted polypharmacology: the next frontier in drug discovery. *Curr. Opin. Struct. Biol.* 84:102771. doi: 10.1016/j.sbi.2023.102771

Ciolli, L., Krismer, F., Nicoletti, F., and Wenning, G. K. (2014). An update on the cerebellar subtype of multiple system atrophy. *Cerebellum Ataxias* 1:14. doi: 10.1186/s40673-014-0014-7

Cluskey, S., and Ramsden, D. B. (2001). Mechanisms of neurodegeneration in amyotrophic lateral sclerosis. *Mol. Pathol.* 54, 386–392.

Colonna, M., and Butovsky, O. (2017). Microglia function in the central nervous system during health and neurodegeneration. *Annu. Rev. Immunol.* 35, 441–468. doi: 10.1146/annurev-immunol-051116-052358

Conway, M. K., Gerger, M. J., Balay, E. E., O'Connell, R., Hanson, S., Daily, N. J., et al. (2015). Scalable 96-well plate based iPSC culture and production using a robotic liquid handling system. *J. Vis. Exp.* 99:e52755. doi: 10.3791/52755

Costa, V., Aigner, S., Vukcevic, M., Sauter, E., Behr, K., Ebeling, M., et al. (2016). mTORC1 inhibition corrects neurodevelopmental and synaptic alterations in a human stem cell model of tuberous sclerosis. *Cell Rep.* 15, 86–95. doi: 10.1016/j.celrep.2016.02.090

Crino, P. B. (2020). mTORopathies: a road well-traveled. *Epilepsy Curr.* 20, 64S–66S. doi: 10.1177/1535759720959320

Cuyàs, E., Corominas-Faja, B., Joven, J., and Menendez, J. A. (2014). Cell cycle regulation by the nutrient-sensing mammalian target of rapamycin (mTOR) pathway. *Methods Mol. Biol.* 1170, 113–144. doi: 10.1007/978-1-4939-0888-2_7

Daneman, R., and Prat, A. (2015). The blood–brain barrier. *Cold Spring Harb. Perspect. Biol.* 7:a020412. doi: 10.1101/cshperspect.a020412

Das, A., Kim, S. H., Arifuzzaman, S., Yoon, T., Chai, J. C., Lee, Y. S., et al. (2016). Transcriptome sequencing reveals that LPS-triggered transcriptional responses in established microglia BV2 cell lines are poorly representative of primary microglia. *J. Neuroinflamm.* 13:182. doi: 10.1186/s12974-016-0644-1

Dawson, T. M., Golde, T. E., and Lagier-Tourenne, C. (2018). Animal models of neurodegenerative diseases. *Nat. Neurosci.* 21, 1370–1379. doi: 10.1038/s41593-018-0236-8

Deco, G., Ponce-Alvarez, A., Hagmann, P., Romani, G. L., Mantini, D., Corbetta, M., et al. (2014). How local excitation-inhibition ratio impacts the whole brain dynamics. *J. Neurosci.* 34, 7886–7898. doi: 10.1523/JNEUROSCI.5068-13.2014

Deisseroth, K., Feng, G., Majewska, A. K., Miesenböck, G., Ting, A., Schnitzer, M. J., et al. (2006). Next-generation optical technologies for illuminating genetically targeted brain circuits. *J. Neurosci.* 26, 10380–10386. doi: 10.1523/JNEUROSCI.3863-06.2006

Delaney, S. P., Julian, L. M., and Stanford, W. L. (2014). The neural crest lineage as a driver of disease heterogeneity in tuberous sclerosis complex and lymphangioleiomyomatosis. *Front. Cell Dev. Biol.* 2:69. doi: 10.3389/fcell.2014.00069

Delaney, S. P., Julian, L. M., Pietrobon, A., Yockell-Lelièvre, J., Doré, C., Wang, T. T., et al. (2020). Stem cell models identify lineage-specific catabolic signaling, neoplastic mechanisms and therapeutic vulnerabilities in tuberous sclerosis Running title: lineage-specific catabolic signaling in Tuberous Sclerosis. *bioRxiv [Preprint]* doi: 10.1101/683359

Dello Russo, C., Cappoli, N., Coletta, I., Mezzogori, D., Paciello, F., Pozzoli, G., et al. (2018). The human microglial HMC3 cell line: where do we stand? A systematic literature review. *J. Neuroinflamm.* 15:259. doi: 10.1186/s12974-018-1288-0

Deng, T., Jovanovic, V. M., Tristan, C. A., Weber, C., Chu, P. H., Inman, J., et al. (2023). Scalable generation of sensory neurons from human pluripotent stem cells. *Stem Cell Rep.* 18:1030. doi: 10.1016/j.stemcr.2023.03.006

Dhaliwal, N. K., Weng, O. Y., Dong, X., Bhattacharya, A., Ahmed, M., Nishimura, H., et al. (2024). Synergistic hyperactivation of both mTORC1 and mTORC2 underlies the neural abnormalities of PTEN-deficient human neurons and cortical organoids. *Cell Rep.* 43:114173. doi: 10.1016/j.celrep.2024.114173

Doi, D., Magotani, H., Kikuchi, T., Ikeda, M., Hiramatsu, S., Yoshida, K., et al. (2020). Pre-clinical study of induced pluripotent stem cell-derived dopaminergic progenitor cells for Parkinson's disease. *Nat. Commun.* 11:3369. doi: 10.1038/s41467-020-17165-w

du Chatinier, A., Velilla, I. Q., Meel, M. H., Hoving, E. W., Hulleman, E., Metselaar, D. S., et al. (2023). Microglia in pediatric brain tumors: the missing link to successful immunotherapy. *Cell Rep. Med.* 4:101246. doi: 10.1016/j.xcrm.2023.101246

Eichmuller, O. L., Corsini, N. S., Vértesy, Á, Morassut, I., Scholl, T., Gruber, V. E., et al. (2022). Amplification of human interneuron progenitors promotes brain tumors and neurological defects. *Science* 375:eabf5546. doi: 10.1126/science.abf5546

Estévez-Priego, E., Moreno-Fina, M., Monni, E., Kokaia, Z., Soriano, J., Tornero, D., et al. (2023). Long-term calcium imaging reveals functional development in hiPSC-derived cultures comparable to human but not rat primary cultures. *Stem Cell Rep.* 18, 205–219. doi: 10.1016/j.stemcr.2022.11.014

Eura, N., Matsui, T. K., Luginbühl, J., Matsubayashi, M., Nanaura, H., Shiota, T., et al. (2020). Brainstem organoids from human pluripotent stem cells. *Front. Neurosci.* 14:538. doi: 10.3389/fnins.2020.00538

Fair, S. R., Julian, D., Hartlaub, A. M., Pusuluri, S. T., Malik, G., Summerfied, T. L., et al. (2020). Electrophysiological maturation of cerebral organoids correlates with dynamic morphological and cellular development. *Stem Cell Rep.* 15, 855–868. doi: 10.1016/j.stemcr.2020.08.017

Falcon, M. I., Riley, J. D., Jirsa, V., McIntosh, A. R., Chen, E. E., Solodkin, A., et al. (2016). Functional mechanisms of recovery after chronic stroke: modeling with the virtual brain. *eNeuro* 3:ENEURO.158–ENEURO.115. doi: 10.1523/ENEURO.0158-15.2016

Fan, Y., Nguyen, D. T., Akay, Y., Xu, F., and Akay, M. (2016). Engineering a brain cancer chip for high-throughput drug screening. *Sci. Rep.* 6:25062. doi: 10.1038/srep25062

Farkhondeh, A., Li, R., Gorshkov, K., Chen, K. G., Might, M., Rodems, S., et al. (2019). Induced pluripotent stem cells for neural drug discovery. *Drug Discov. Today* 24, 992–999. doi: 10.1016/j.drudis.2019.01.007

Feng, G., Jensen, F. E., Greely, H. T., Okano, H., Treue, S., Roberts, A. C., et al. (2020). Opportunities and limitations of genetically modified nonhuman primate models for neuroscience research. *Proc. Natl. Acad. Sci. U.S.A.* 117, 24022–24031. doi: 10.1073/pnas.2006515117

Fernandes, P. B. (1998). Technological advances in high-throughput screening. *Curr. Opin. Chem. Biol.* 2:597. doi: 10.1016/s1367-5931(98)80089-6

Fessel, J. (2023). Cure of Alzheimer's dementia requires addressing all of the affected brain cell types. *J. Clin. Med.* 12:2049. doi: 10.3390/jcm12052049

Fligor, C. M., Lavekar, S. S., Harkin, J., Shields, P. K., VanderWall, K. B., Huang, K. C., et al. (2021). Extension of retinofugal projections in an assembled model of human pluripotent stem cell-derived organoids. *Stem Cell Rep.* 16, 2228–2241. doi: 10.1016/j.stemcr.2021.05.009

Forman, M. S., Trojanowski, J. Q., and Lee, V. M. (2004). Neurodegenerative diseases: a decade of discoveries paves the way for therapeutic breakthroughs. *Nat. Med.* 10, 1055–1063. doi: 10.1038/nm1113

Frost, M., and Hulbert, J. (2015). Clinical management of tuberous sclerosis complex over the lifetime of a patient. *Pediatr. Health Med. Ther.* 6, 139–146. doi: 10.2147/PHMT.S67342

Fujimori, K., Ishikawa, M., Otomo, A., Atsuta, N., Nakamura, R., Akiyama, T., et al. (2018). Modeling sporadic ALS in iPSC-derived motor neurons identifies a potential therapeutic agent. *Nat. Med.* 24, 1579–1589. doi: 10.1038/s41591-018-0140-5

Galiakberova, A. A., and Dashinimaev, E. B. (2020). Neural stem cells and methods for their generation from induced pluripotent stem cells. *Front. Cell Dev. Biol.* 8:815. doi: 10.3389/fcell.2020.00815

Gamble, P., Jaroensri, R., Wang, H., Tan, F., Moran, M., Brown, T., et al. (2021). Determining breast cancer biomarker status and associated morphological features using deep learning. *Commun. Med. (Lond)* 1:14. doi: 10.1038/s43856-021-00013-3

Gao, M. L., Zhang, X., Han, F., Xu, J., Yu, S. J., Jin, K., et al. (2022). Functional microglia derived from human pluripotent stem cells empower retinal organ. *Sci. China Life Sci.* 65, 1057–1071. doi: 10.1007/s11427-021-2086-0

Gellersen, H. M., Guo, C. C., O'Callaghan, C., Tan, R. H., Sami, S., Hornberger, M., et al. (2017). Cerebellar atrophy in neurodegeneration-a meta-analysis. *J. Neurol. Neurosurg. Psychiatry* 88, 780–788. doi: 10.1136/jnnp-2017-315607

Glover, J. C., Sato, K., and Momose-Sato, Y. (2008). Using voltage-sensitive dye recording to image the functional development of neuronal circuits in vertebrate embryos. *Dev. Neurobiol.* 68, 804–816. doi: 10.1002/dneu.20629

Glowinski, J., and Iversen, L. L. (1966). Regional studies of catecholamines in the rat brain. I. The disposition of [3H]norepinephrine, [3H]dopamine and [3H]dopa in various regions of the brain. *J. Neurochem.* 13, 655–669. doi: 10.1111/j.1471-4159.1966.tb09873.x

Grieves, M., and Vickers, J. (2017). "Digital twin: mitigating unpredictable, undesirable emergent behavior in complex systems," in *Transdisciplinary Perspectives on Complex Systems*, eds J. Kahlen, S. Flumerfelt, and A. Alves (Cham: Springer).

Gunaseeli, I., Doss, M. X., Antzelevitch, C., Hescheler, J., and Sachinidis, A. (2010). Induced pluripotent stem cells as a model for accelerated patient- and disease-specific drug discovery. *Curr. Med. Chem.* 17, 759–766. doi: 10.2174/092986710790514480

Guo, C. C., Tan, R., Hodges, J. R., Hu, X., Sami, S., Hornberger, M., et al. (2016). Network-selective vulnerability of the human cerebellum to Alzheimer's disease and frontotemporal dementia. *Brain* 139, 1527–1538. doi: 10.1093/brain/aww003

Guo, F., Liu, X., Cai, H., and Le, W. (2018). Autophagy in neurodegenerative diseases: pathogenesis and therapy. *Brain Pathol.* 28, 3–13. doi: 10.1111/bpa.12545

Guo, J., Jiang, Z., Liu, X., Li, H., Biswal, B. B., Zhou, B., et al. (2023). Cerebello-cerebral resting-state functional connectivity in spinocerebellar ataxia type 3. *Hum. Brain Mapp.* 44, 927–936. doi: 10.1002/hbm.26113

Habibey, R., Striebel, J., Schmieder, F., Czarske, J., and Busskamp, V. (2022). Long-term morphological and functional dynamics of human stem cell-derived neuronal networks on high-density micro-electrode arrays. *Front. Neurosci.* 16:951964. doi: 10.3389/fnins.2022.951964

Haldipur, P., Aldinger, K. A., Bernardo, S., Deng, M., Timms, A. E., Overman, L. M., et al. (2019). Spatiotemporal expansion of primary progenitor zones in the developing human cerebellum. *Science* 366, 454–460. doi: 10.1126/science.aax7526

Hashemi, M., Vattikonda, A. N., Sip, V., Guye, M., Bartolomei, F., Woodman, M. M., et al. (2020). The Bayesian virtual epileptic patient: a probabilistic framework designed to infer the spatial map of epileptogenicity in a personalized large-scale brain model of epilepsy spread. *Neuroimage* 217:116839. doi: 10.1016/j.neuroimage.2020.116839

Hasselmann, J., Coburn, M. A., England, W., Figueroa Velez, D. X., Kiani Shabestari, S., Tu, C. H., et al. (2019). Development of a chimeric model to study and manipulate human microglia *in vivo*. *Neuron* 103, 1016–1033.e10. doi: 10.1016/j.neuron.2019.07.002

HD iPSC Consortium (2012). Induced Pluripotent Stem Cells from Patients with Huntington's Disease Show CAG-Repeat-Expansion-Associated Phenotypes. *Cell Stem Cell* 11, 264–278. doi: 10.1016/j.stem.2012.04.027

Hernandez, O., Way, S., McKenna, J., and Gambello, M. J. (2007). Generation of a conditional disruption of the Tsc2 gene. *Genesis* 45, 101–106. doi: 10.1002/dvg.20271

Hirose, S., Tanaka, Y., Shibata, M., Kimura, Y., Ishikawa, M., Higurashi, N., et al. (2020). Application of induced pluripotent stem cells in epilepsy. *Mol. Cell Neurosci.* 108:103535. doi: 10.1016/j.mcn.2020.103535

Hommersom, M. P., Buijsen, R. A. M., van Roon-Mom, W. M. C., van de Warrenburg, B. P. C., and van Bokhoven, H. (2022). Human induced pluripotent stem cell-based modelling of spinocerebellar ataxias. *Stem Cell Rev. Rep.* 18, 441–456. doi: 10.1007/s12015-021-10184-0

Hosoya, M., Fujioka, M., Sone, T., Okamoto, S., Akamatsu, W., Ukai, H., et al. (2017). Cochlear cell modeling using disease-specific iPSCs unveils a degenerative phenotype and suggests treatments for congenital progressive hearing loss. *Cell Rep.* 18, 68–81. doi: 10.1016/j.celrep.2016.12.020

Hussain, I., and Park, S. -J. (2021). Prediction of myoelectric biomarkers in post-stroke gait. *Sensors* 21:5334. doi: 10.3390/s21165334

Jirsa, V. K., Proix, T., Perdikis, D., Woodman, M. M., Wang, H., Gonzalez-Martinez, J., et al. (2017). The virtual epileptic patient: individualized whole-brain models of epilepsy spread. *Neuroimage* 145, 377–388. doi: 10.1016/j.neuroimage.2016.04.049

Jirsa, V. K., Stacey, W. C., Quilichini, P. P., Ivanov, A. I., and Bernard, C. (2014). On the nature of seizure dynamics. *Brain* 137, 2210–2230. doi: 10.1093/brain/awu133

Jirsa, V., Wang, H., Triebkorn, P., Hashemi, M., Jha, J., Gonzalez-Martinez, J., et al. (2023). Personalised virtual brain models in epilepsy. *Lancet Neurol.* 22, 443–454. doi: 10.1016/S1474-4422(23)00008-X

Jucker, M. (2010). The benefits and limitations of animal models for translational research in neurodegenerative diseases. *Nat. Med.* 16, 1210–1214. doi: 10.1038/nm.2224

Kabat, J., and Król, P. (2012). Focal cortical dysplasia - review. *Pol. J. Radiol.* 77, 35–43. doi: 10.12659/pjr.882968

Kashii, H., Kasai, S., Sato, A., Hagino, Y., Nishito, Y., Kobayashi, T., et al. (2023). Tsc2 mutation rather than Tsc1 mutation dominantly causes a social deficit in a mouse model of tuberous sclerosis complex. *Hum. Genomics* 17:4. doi: 10.1186/s40246-023-00450-2

Kelley, K. W., Revah, O., Gore, F., Kaganovsky, K., Chen, X., Deisseroth, K., et al. (2024). Host circuit engagement of human cortical organoids transplanted in rodents. *Nat. Protoc.* 19, 3542–5367. doi: 10.1038/s41596-024-01029-4

Kiernan, M. C., Vucic, S., Cheah, B. C., Turner, M. R., Eisen, A., Hardiman, O., et al. (2011). Amyotrophic lateral sclerosis. *Lancet* 377, 942–955. doi: 10.1016/S0140-6736(10)61156-7

Klockgether, T., Mariotti, C., and Paulson, H. L. (2019). Spinocerebellar ataxia. *Nat. Rev. Dis. Primers* 5:24. doi: 10.1038/s41572-019-0074-3

Klofas, L. K., Short, B. P., Snow, J. P., Sinnaeve, J., Rushing, G. V., Westlake, G., et al. (2020). DEPDC5 haploinsufficiency drives increased mTORC1 signaling and abnormal morphology in human iPSC-derived cortical neurons. *Neurobiol. Dis.* 143:104975. doi: 10.1016/j.nbd.2020.104975

Knock, E., and Julian, L. M. (2021). Building on a solid foundation: adding relevance and reproducibility to neurological modeling using human pluripotent stem cells. *Front. Cell Neurosci.* 15:767457. doi: 10.3389/fncel.2021.767457

Kobayashi, T., Minowa, O., Kuno, J., Mitani, H., Hino, O., Noda, T., et al. (1999). Renal carcinogenesis, hepatic hemangiomatosis, and embryonic lethality caused by a germ-line Tsc2 mutation in mice. *Cancer Res.* 59, 1206–1211.

Koníčková, D., Menšíková, K., Tučková, L., Hényková, E., Strnad, M., Friedecký, D., et al. (2022). Biomarkers of neurodegenerative diseases: biology, taxonomy, clinical relevance, and current research status. *Biomedicines* 10:1760. doi: 10.3390/biomedicines10071760

Kosorok, M. R., and Laber, E. B. (2019). Precision medicine. *Annu. Rev. Stat. Appl.* 6, 263–286. doi: 10.1146/annurev-statistics-030718-105251

Kusumoto, D., Yuasa, S., and Fukuda, K. (2022). Induced pluripotent stem cell-based drug screening by use of artificial intelligence. *Pharmaceuticals (Basel)* 15:562. doi: 10.3390/ph15050562

Lancaster, M. A., and Knoblich, J. A. (2014). Generation of cerebral organoids from human pluripotent stem cells. *Nat. Protoc.* 9, 2329–2340. doi: 10.1038/nprot.2014.158

Laperle, A. H., Sances, S., Yucer, N., Dardov, V. J., Garcia, V. J., Ho, R., et al. (2020). iPSC modeling of young-onset Parkinson's disease reveals a molecular signature of disease and novel therapeutic candidates. *Nat. Med.* 26, 289–299. doi: 10.1038/s41591-019-0739-1

Lavanga, M., Stumme, J., Yalcinkaya, B. H., Fousek, J., Jockwitz, C., Sheheitli, H., et al. (2023). The virtual aging brain: causal inference supports interhemispheric dedifferentiation in healthy aging. *Neuroimage* 283:120403. doi: 10.1016/j.neuroimage.2023.120403

Lewis, E. M. A., Meganathan, K., Baldridge, D., Gontarz, P., Zhang, B., Bonni, A., et al. (2019). Cellular and molecular characterization of multiplex autism in human induced pluripotent stem cell-derived neurons. *Mol. Autism* 10:51. doi: 10.1186/s13229-019-0306-0

Li, Y., Muffat, J., Omer, A., Bosch, I., Lancaster, M. A., Sur, M., et al. (2017). Induction of expansion and folding in human cerebral organoids. *Cell Stem Cell* 20, 385–396.e3. doi: 10.1016/j.stem.2016.11.017

Lippmann, E. S., Azarin, S. M., Kay, J. E., Nessler, R. A., Wilson, H. K., Al-Ahmad, A., et al. (2012). Derivation of blood-brain barrier endothelial cells from human pluripotent stem cells. *Nat. Biotechnol.* 30:783. doi: 10.1038/nbt.2247

Liu, G., David, B. T., Trawczynski, M., and Fessler, R. G. (2020). Advances in pluripotent stem cells: history, mechanisms, technologies, and applications. *Stem Cell Rev. Rep.* 16, 3–32. doi: 10.1007/s12015-019-09935-x

Liu, H., and Zhang, S. C. (2011). Specification of neuronal and glial subtypes from human pluripotent stem cells. *Cell Mol. Life Sci.* 68, 3995–4008. doi: 10.1007/s00018-011-0770-y

Liu, Y., Lopez-Santiago, L. F., Yuan, Y., Jones, J. M., Zhang, H., O'Malley, H. A., et al. (2013). Dravet syndrome patient-derived neurons suggest a novel epilepsy mechanism. *Ann. Neurol.* 74, 128–139. doi: 10.1002/ana.23897

Luchena, C., Zuazo-Ibarra, J., Valero, J., Matute, C., Alberdi, E., Capetillo-Zarate, E., et al. (2022). A neuron, microglia, and astrocyte triple co-culture model to study Alzheimer's disease. *Front. Aging Neurosci.* 14:844534. doi: 10.3389/fnagi.2022.844534

Lui, K. N., Li, Z., Lai, F. P., Lau, S. T., and Ngan, E. S. (2023). Organoid models of breathing disorders reveal patterning defect of hindbrain neurons caused by PHOX2B-PARMs. *Stem Cell Rep.* 18, 1500–1515. doi: 10.1016/j.stemcr.2023.05.020

Macron, C., Núñez Galindo, A., Cominetti, O., and Dayon, L. (2019). A versatile workflow for cerebrospinal fluid proteomic analysis with mass spectrometry: a matter of choice between deep coverage and sample throughput. *Methods Mol. Biol.* 2044, 129–154. doi: 10.1007/978-1-4939-9706-0_9

Maestú, F., de Haan, W., Busche, M. A., and DeFelipe, J. (2021). Neuronal excitation/inhibition imbalance: core element of a translational perspective on Alzheimer pathophysiology. *Ageing Res. Rev.* 69:101372. doi: 10.1016/j.arr.2021.101372

Majolo, F., Marinowic, D. R., Palmini, A. L. F., DaCosta, J. C., and Machado, D. C. (2019). Migration and synaptic aspects of neurons derived from human induced pluripotent stem cells from patients with focal cortical dysplasia II. *Neuroscience* 408, 81–90. doi: 10.1016/j.neuroscience.2019.03.025

Makhoba, X. H., Viegas, C., Mosa, R. A., Viegas, F. P. D., and Pooe, O. J. (2020). Potential impact of the multi-target drug approach in the treatment of some complex diseases. *Drug Des. Devel. Ther.* 14, 3235–3249. doi: 10.2147/DDDT.S257494

Manzini, A., Jones, E. J. H., Charman, T., Elsabbagh, M., Johnson, M. H., Singh, I., et al. (2021). Ethical dimensions of translational developmental neuroscience research in autism. *J. Child Psychol. Psychiatry* 62, 1363–1373. doi: 10.1111/jcpp.13494

Marchetto, M. C., Carromeu, C., Acab, A., Yu, D., Yeo, G. W., Mu, Y., et al. (2010). A model for neural development and treatment of Rett syndrome using human induced pluripotent stem cells. *Cell* 143, 527–539. doi: 10.1016/j.cell.2010.10.016

Marshall, L. J., Bailey, J., Cassotta, M., Herrmann, K., and Pistollato, F. (2023). Poor translatability of biomedical research using animals - A narrative review. *Altern. Lab. Anim.* 51, 102–135. doi: 10.1177/02611929231157756

Masuda, T., Sankowski, R., Staszewski, O., and Prinz, M. (2020). Microglia heterogeneity in the single-cell era. *Cell Rep.* 30, 1271–1281. doi: 10.1016/j.celrep.2020.01.010

Mayhew, C. N., and Singhania, R. (2023). A review of protocols for brain organoids and applications for disease modeling. *STAR Protoc.* 4:101860. doi: 10.1016/j.xpro.2022.101860

Mehl, L. C., Manjally, A. V., Bouadi, O., Gibson, E. M., and Tay, T. L. (2022). Microglia in brain development and regeneration. *Development* 149:dev200425. doi: 10.1242/dev.200425

Mikitsh, J. L., and Chacko, A.-M. (2014). Pathways for small molecule delivery to the central nervous system across the blood-brain barrier. *Perspect. Med. Chem.* 6, 11–24. doi: 10.4137/pmc.s13384

Miura, Y., Li, M. Y., Birey, F., Ikeda, K., Revah, O., Thete, M. V., et al. (2020). Generation of human striatal organoids and cortico-striatal assembloids from human pluripotent stem cells. *Nat. Biotechnol.* 38, 1421–1430. doi: 10.1038/s41587-020-00763-w

Møller, R. S., Weckhuysen, S., Chipaux, M., Marsan, E., Taly, V., Bebin, E. M., et al. (2016). Germline and somatic mutations in the MTOR gene in focal cortical dysplasia and epilepsy. *Neurol. Genet.* 2:e118. doi: 10.1212/NXG.0000000000000118

Morimoto, S., Takahashi, S., Ito, D., Daté, Y., Okada, K., Kato, C., et al. (2023). Phase 1/2a clinical trial in ALS with ropinirole, a drug candidate identified by iPSC drug discovery. *Cell Stem Cell* 30, 766–780.e9. doi: 10.1016/j.stem.2023.04.017

Muffat, J., Li, Y., Yuan, B., Mitalipova, M., Omer, A., Corcoran, S., et al. (2016). Efficient derivation of microglia-like cells from human pluripotent stem cells. *Nat. Med.* 22, 1358–1367. doi: 10.1038/nm.4189

Murai, K., Sun, G., Ye, P., Tian, E., Yang, S., Cui, Q., et al. (2016). The TLX-miR-219 cascade regulates neural stem cell proliferation in neurodevelopment and schizophrenia iPSC model. *Nat. Commun.* 7:10965. doi: 10.1038/ncomms10965

Muratore, C. R., Srikanth, P., Callahan, D. G., and Young-Pearse, T. L. (2014). Comparison and optimization of hiPSC forebrain cortical differentiation protocols. *PLoS One* 9:e105807. doi: 10.1371/journal.pone.0105807

Nadadhur, A. G., Alsaqati, M., Gasparotto, L., Cornelissen-Steijger, P., van Hugte, E., Dooves, S., et al. (2019). Neuron-glia interactions increase neuronal phenotypes in tuberous sclerosis complex patient iPSC-derived models. *Stem Cell Rep.* 12, 42–56. doi: 10.1016/j.stemcr.2018.11.019

Negri, J., Menon, V., and Young-Pearse, T. L. (2020). Assessment of spontaneous neuronal activity. *eNeuro* 7: :ENEURO.0080-19.2019. doi: 10.1523/ENEURO.0080-19.2019

Nieto-Estévez, V., and Hsieh, J. (2020). Human brain organoid models of developmental epilepsies. *Epilepsy Curr.* 20, 282–290. doi: 10.1177/1535759720949254

Nishino, K., Takasawa, K., Okamura, K., Arai, Y., Sekiya, A., Akutsu, H., et al. (2021). Identification of an epigenetic signature in human induced pluripotent stem cells using a linear machine learning model. *Hum. Cell* 34, 99–110. doi: 10.1007/s13577-020-00446-3

Nowakowski, T. J., Pollen, A. A., Sandoval-Espinosa, C., and Kriegstein, A. R. (2016). Transformation of the radial glia scaffold demarcates two stages of human cerebral cortex development. *Neuron* 91, 1219–1227. doi: 10.1016/j.neuron.2016.09.005

Núñez Galindo, A., Macron, C., Cominetti, O., and Dayon, L. (2019). Analyzing cerebrospinal fluid proteomes to characterize central nervous system disorders: a highly automated mass spectrometry-based pipeline for biomarker discovery. *Methods Mol. Biol.* 1959, 89–112. doi: 10.1007/978-1-4939-9164-8_6

Nzou, G., Wicks, R. T., Wicks, E. E., Seale, S. A., Sane, C. H., Chen, A., et al. (2018). Human cortex spheroid with a functional blood brain barrier for high-throughput neurotoxicity screening and disease modeling. *Sci. Rep.* 8:7413. doi: 10.1038/s41598-018-25603-5

Ochalek, A., Mihalik, B., Avci, H. X., Chandrasekaran, A., Téglási, A., Bock, I., et al. (2017). Neurons derived from sporadic Alzheimer's disease iPSCs reveal elevated TAU hyperphosphorylation, increased amyloid levels, and GSK3B activation. *Alzheimers Res. Ther.* 9:90. doi: 10.1186/s13195-017-0317-z

Oegema, R., Barakat, T. S., Wilke, M., Stouffs, K., Amrom, D., Aronica, E., et al. (2020). International consensus recommendations on the diagnostic work-up for malformations of cortical development. *Nat. Rev. Neurol.* 16, 618–635. doi: 10.1038/s41582-020-0395-6

Okano, H., and Morimoto, S. (2022). iPSC-based disease modeling and drug discovery in cardinal neurodegenerative disorders. *Cell Stem Cell* 29, 189–208. doi: 10.1016/j.stem.2022.01.007

Pardridge, W. M. (2012). Drug transport across the blood–brain barrier. *J. Cereb. Blood Flow Metab.* 32:1959. doi: 10.1038/jcbfm.2012.126

Paşca, S. P., Arlotta, P., Bateup, H. S., Camp, J. G., Cappello, S., Gage, F. H., et al. (2022). A nomenclature consensus for nervous system organoids and assembloids. *Nature* 609, 907–910. doi: 10.1038/s41586-022-05219-6

Paşca, S. P., Portmann, T., Voineagu, I., Yazawa, M., Shcheglovitov, A., Paşca, A. M., et al. (2011). Using iPSC-derived neurons to uncover cellular phenotypes associated with Timothy syndrome. *Nat. Med.* 17, 1657–1662. doi: 10.1038/nm.2576

Paull, D., Sevilla, A., Zhou, H., Hahn, A. K., Kim, H., Napolitano, C., et al. (2015). Automated, high-throughput derivation, characterization and differentiation of induced pluripotent stem cells. *Nat. Methods* 12:885. doi: 10.1038/nmeth.3507

Pediaditakis, I., Kodella, K. R., Manatakis, D. V., Le, C. Y., Barthakur, S., Sorets, A., et al. (2022). A microengineered Brain-Chip to model neuroinflammation in humans. *iScience* 25:104813. doi: 10.1016/j.isci.2022.104813

Pellegrini, L., Bonfio, C., Chadwick, J., Begum, F., Skehel, M., Lancaster, M. A., et al. (2020). Human CNS barrier-forming organoids with cerebrospinal fluid production. *Science* 369, eaaz5626. doi: 10.1126/science.aaz5626

Perucca, P., and Perucca, E. (2019). Identifying mutations in epilepsy genes: impact on treatment selection. *Epilepsy Res.* 152, 18–30. doi: 10.1016/j.eplepsyres.2019.03.001

Peters, J. U. (2013). Polypharmacology - foe or friend? *J. Med. Chem.* 56, 8955–8971. doi: 10.1021/jm400856t

Pilotto, F., Douthwaite, C., Diab, R., Ye, X., Al Qassab, Z., Tietje, C., et al. (2023). Early molecular layer interneuron hyperactivity triggers Purkinje neuron degeneration in SCA1. *Neuron* 111, 2523–2543.e10. doi: 10.1016/j.neuron.2023.05.016

Pradhan, J., and Bellingham, M. C. (2021). Neurophysiological mechanisms underlying cortical hyper-excitability in amyotrophic lateral sclerosis: a review. *Brain Sci.* 11:549. doi: 10.3390/brainsci11050549

Proix, T., Bartolomei, F., Guye, M., and Jirsa, V. K. (2017). Individual brain structure and modelling predict seizure propagation. *Brain* 140, 641–654. doi: 10.1093/brain/awx004

Qian, T., Maguire, S. E., Canfield, S. G., Bao, X., Olson, W. R., Shusta, E. V., et al. (2017). Directed differentiation of human pluripotent stem cells to blood-brain barrier endothelial cells. *Sci. Adv.* 3:e1701679. doi: 10.1126/sciadv.1701679

Reddy, P. H. (2009). Role of mitochondria in neurodegenerative diseases: mitochondria as a therapeutic target in Alzheimer's disease. *CNS Spectr.* 14, 8–13; discussion 16–18. doi: 10.1017/s1092852900024901

Revah, O., Gore, F., Kelley, K. W., Andersen, J., Sakai, N., Chen, X., et al. (2022). Maturation and circuit integration of transplanted human cortical organoids. *Nature* 610, 319–326. doi: 10.1038/s41586-022-05277-w

Reymond, J. L. (2015). The chemical space project. *Acc. Chem. Res.* 48, 722–730. doi: 10.1021/ar500432k

Rocktäschel, P., Sen, A., and Cader, M. Z. (2019). High glucose concentrations mask cellular phenotypes in a stem cell model of tuberous sclerosis complex. *Epilepsy Behav.* 101:106581. doi: 10.1016/j.yebeh.2019.106581

Ronaldson, P. T., and Davis, T. P. (2020). Regulation of blood-brain barrier integrity by microglia in health and disease: a therapeutic opportunity. *J. Cereb. Blood Flow Metab.* 40, S6–S24. doi: 10.1177/0271678X20951995

Roqué, P. J., and Costa, L. G. (2017). Co-culture of neurons and microglia. *Curr. Protoc. Toxicol.* 74, 11.24.11–11.24.17. doi: 10.1002/cptx.32

Rousseaux, M. W. C., Tschumperlin, T., Lu, H. C., Lackey, E. P., Bondar, V. V., Wan, Y. W., et al. (2018). ATXN1-CIC complex is the primary driver of cerebellar pathology in spinocerebellar ataxia type 1 through a gain-of-function mechanism. *Neuron* 97, 1235–1243.e5. doi: 10.1016/j.neuron.2018.02.013

Ruddigkeit, L., van Deursen, R., Blum, L. C., and Reymond, J. L. (2012). Enumeration of 166 billion organic small molecules in the chemical universe database GDB-17. *J. Chem. Inf. Model.* 52, 2864–2875. doi: 10.1021/ci300415d

Saberi, A., Aldenkamp, A. P., Kurniawan, N. A., and Bouten, C. V. C. (2022). In-vitro engineered human cerebral tissues mimic pathological circuit disturbances in 3D. *Commun. Biol.* 5:254. doi: 10.1038/s42003-022-03203-4

Saito, A., Ooki, A., Nakamura, T., Onodera, S., Hayashi, K., Hasegawa, D., et al. (2018). Targeted reversion of induced pluripotent stem cells from patients with human cleidocranial dysplasia improves bone regeneration in a rat calvarial bone defect model. *Stem Cell Res. Ther.* 9:12. doi: 10.1186/s13287-017-0754-4

Sakai, C., Ijaz, S., and Hoffman, E. J. (2018). Zebrafish models of neurodevelopmental disorders: past, present, and future. *Front. Mol. Neurosci.* 11:294. doi: 10.3389/fnmol.2018.00294

Sances, S., Bruijn, L. I., Chandran, S., Eggan, K., Ho, R., Klim, J. R., et al. (2016). Modeling ALS with motor neurons derived from human induced pluripotent stem cells. *Nat. Neurosci.* 19, 542–553. doi: 10.1038/nn.4273

Sasaguri, H., Nilsson, P., Hashimoto, S., Nagata, K., Saito, T., De Strooper, B., et al. (2017). APP mouse models for Alzheimer's disease preclinical studies. *EMBO J.* 36, 2473–2487. doi: 10.15252/embj.201797397

Savitt, J. M., Dawson, V. L., and Dawson, T. M. (2006). Diagnosis and treatment of Parkinson disease: molecules to medicine. *J. Clin. Invest.* 116, 1744–1754. doi: 10.1172/JCI29178

Schilde, L. M., Steinbach, S., Serschnitzki, B., Maass, F., Bähr, M., Lingor, P., et al. (2020). Human cerebrospinal fluid data for use as spectral library, for biomarker research. *Data Brief.* 32:106048. doi: 10.1016/j.dib.2020.106048

Schirner, M., Domide, L., Perdikis, D., Triebkorn, P., Stefanovski, L., Pai, R., et al. (2022). Brain simulation as a cloud service: the virtual brain on EBRAINS. *Neuroimage* 251:118973. doi: 10.1016/j.neuroimage.2022.118973

Schirner, M., McIntosh, A. R., Jirsa, V., Deco, G., and Ritter, P. (2018). Inferring multi-scale neural mechanisms with brain network modelling. *Elife* 7:e28927. doi: 10.7554/eLife.28927

Seidel, K., Bouzrou, M., Heidemann, N., Krüger, R., Schöls, L., den Dunnen, W. F. A., et al. (2017). Involvement of the cerebellum in Parkinson disease and dementia with Lewy bodies. *Ann. Neurol.* 81, 898–903. doi: 10.1002/ana.24937

Selkoe, D. J. (2001). Alzheimer's disease: genes, proteins, and therapy. *Physiol. Rev.* 81, 741–766. doi: 10.1152/physrev.2001.81.2.741

Sengupta, P., and Samuel, A. D. (2009). Caenorhabditis elegans: a model system for systems neuroscience. *Curr. Opin. Neurobiol.* 19, 637–643. doi: 10.1016/j.conb.2009.09.009

Silva, T. P., Fernandes, T. G., Nogueira, D. E. S., Rodrigues, C. A. V., Bekman, E. P., Hashimura, Y., et al. (2020). Scalable generation of mature cerebellar organoids from human pluripotent stem cells and characterization by immunostaining. 160, *J. Vis. Exp.* doi: 10.3791/61143

Silverman, L., Campbell, R., and Broach, J. R. (1998). New assay technologies for high-throughput screening. *Curr. Opin. Chem. Biol.* 2:397. doi: 10.1016/s1367-5931(98)80015-x

Silvin, A., Uderhardt, S., Piot, C., Da Mesquita, S., Yang, K., Geirsdottir, L., et al. (2022). Dual ontogeny of disease-associated microglia and disease inflammatory macrophages in aging and neurodegeneration. *Immunity* 55, 1448–1465.e6. doi: 10.1016/j.immuni.2022.07.004

Sittampalam, G. S., Kahl, S. D., and Janzen, W. P. (1997). High-throughput screening: advances in assay technologies. *Curr. Opin. Chem. Biol.* 1:384. doi: 10.1016/s1367-5931(97)80078-6

Sloan, S. A., Andersen, J., Paşca, A. M., Birey, F., and Paşca, S. P. (2018). Generation and assembly of human brain region-specific three-dimensional cultures. *Nat. Protoc.* 13, 2062–2085. doi: 10.1038/s41596-018-0032-7

Sohn, Y. D., Han, J. W., and Yoon, Y. S. (2012). Generation of induced pluripotent stem cells from somatic cells. *Prog. Mol. Biol. Transl. Sci.* 111, 1–26. doi: 10.1016/B978-0-12-398459-3.00001-0

Solár, P., Zamani, A., Kubíčková, L., Dubovı, P., and Joukal, M. (2020). Choroid plexus and the blood-cerebrospinal fluid barrier in disease. *Fluids Barriers CNS* 17:35. doi: 10.1186/s12987-020-00196-2

Solodkin, A., Peri, E., Chen, E. E., Ben-Jacob, E., and Gomez, C. M. (2011). Loss of intrinsic organization of cerebellar networks in spinocerebellar ataxia type 1: correlates with disease severity and duration. *Cerebellum* 10, 218–232. doi: 10.1007/s12311-010-0214-5

Somanadhan, S., O'Donnell, R., Bracken, S., McNulty, S., Sweeney, A., O'Toole, D., et al. (2023). Children and young people's experiences of living with rare diseases: an integrative review. *J. Pediatr. Nurs.* 68, e16–e26. doi: 10.1016/j.pedn.2022.10.014

Song, L., Yuan, X., Jones, Z., Vied, C., Miao, Y., Marzano, M., et al. (2019). Functionalization of brain region-specific spheroids with isogenic microglia-like cells. *Sci. Rep.* 9:11055. doi: 10.1038/s41598-019-47444-6

Speicher, A. M., Wiendl, H., Meuth, S. G., and Pawlowski, M. (2019). Generating microglia from human pluripotent stem cells: novel in vitro models for the study of neurodegeneration. *Mol. Neurodegener.* 14:46. doi: 10.1186/s13024-019-0347-z

Stern, S., Santos, R., Marchetto, M. C., Mendes, A. P. D., Rouleau, G. A., Biesmans, S., et al. (2018). Neurons derived from patients with bipolar disorder divide into intrinsically different sub-populations of neurons, predicting the patients' responsiveness to lithium. *Mol. Psychiatry* 23, 1453–1465. doi: 10.1038/mp.2016.260

Sun, Y., and Dolmetsch, R. E. (2018). Investigating the therapeutic mechanism of cannabidiol in a human Induced Pluripotent Stem Cell (iPSC)-based model of dravet syndrome. *Cold Spring Harb. Symp. Quant. Biol.* 83, 185–191. doi: 10.1101/sqb.2018.83.038174

Sun, Y., Paşca, S. P., Portmann, T., Goold, C., Worringer, K. A., Guan, W., et al. (2016). A deleterious Nav1.1 mutation selectively impairs telencephalic inhibitory neurons derived from Dravet Syndrome patients. *Elife* 5:e13073. doi: 10.7554/eLife.13073

Tagliatti, E., Desiato, G., Mancinelli, S., Bizzotto, M., Gagliani, M. C., Faggiani, E., et al. (2024). Trem2 expression in microglia is required to maintain normal neuronal bioenergetics during development. *Immunity* 57, 86–105.e9. doi: 10.1016/j.immuni.2023.12.002

Takahashi, K., and Yamanaka, S. (2006). Induction of pluripotent stem cells from mouse embryonic and adult fibroblast cultures by defined factors. *Cell* 126, 663–676. doi: 10.1016/j.cell.2006.07.024

Takahashi, K., Tanabe, K., Ohnuki, M., Narita, M., Ichisaka, T., Tomoda, K., et al. (2007). Induction of pluripotent stem cells from adult human fibroblasts by defined factors. *Cell* 131, 861–872. doi: 10.1016/j.cell.2007.11.019

Tasnim, K., and Liu, J. (2022). Emerging bioelectronics for brain organoid electrophysiology. *J. Mol. Biol.* 434:167165. doi: 10.1016/j.jmb.2021.167165

Teles, D., Kim, Y., Ronaldson-Bouchard, K., and Vunjak-Novakovic, G. (2021). Machine learning techniques to classify healthy and diseased cardiomyocytes by contractility profile. *ACS Biomater. Sci. Eng.* 7, 3043–3052. doi: 10.1021/acsbiomaterials.1c00418

Terstegge, S., Laufenberg, I., Pochert, J., Schenk, S., Itskovitz-Eldor, J., Endl, E., et al. (2007). Automated maintenance of embryonic stem cell cultures. *Biotechnol. Bioeng.* 96:195. doi: 10.1002/bit.21061

Thion, M. S., Ginhoux, F., and Garel, S. (2018). Microglia and early brain development: an intimate journey. *Science* 362, 185–189. doi: 10.1126/science.aat0474

Thomas, R. J., Anderson, D., Chandra, A., Smith, N. M., Young, L. E., Williams, D., et al. (2009). Automated, scalable culture of human embryonic stem cells in feeder-free conditions. *Biotechnol. Bioeng.* 102:1636. doi: 10.1002/bit.22187

Tian, Y., Zhu, P., Liu, S., Jin, Z., Li, D., Zhao, H., et al. (2019). IL-4-polarized BV2 microglia cells promote angiogenesis by secreting exosomes. *Adv. Clin. Exp. Med.* 28, 421–430. doi: 10.17219/acem/91826

Timmerman, R., Burm, S. M., and Bajramovic, J. J. (2018). An overview of *in vitro* methods to study microglia. *Front. Cell Neurosci.* 12:242. doi: 10.3389/fncel.2018.00242

Tremlett, H., and Marrie, R. A. (2021). The multiple sclerosis prodrome: emerging evidence, challenges, and opportunities. *Mult. Scler.* 27, 6–12. doi: 10.1177/1352458520914844

Tristan, C. A., Ormanoglu, P., Slamecka, J., Malley, C., Chu, P. H., Jovanovic, V. M., et al. (2021). Robotic high-throughput biomanufacturing and functional differentiation of human pluripotent stem cells. *Stem Cell Rep.* 16:3076. doi: 10.1016/j.stemcr.2021.11.004

Umair, M., and Waqas, A. (2023). Undiagnosed rare genetic disorders: importance of functional characterization of variants. *Genes (Basel)* 14:1469. doi: 10.3390/genes14071469

Usui-Ouchi, A., Giles, S., Harkins-Perry, S., Mills, E. A., Bonelli, R., Wei, G., et al. (2023). Integrating human iPSC-derived macrophage progenitors into retinal organoids to generate a mature retinal microglial niche. *Glia* 71, 2372–2382. doi: 10.1002/glia.24428

Vahsen, B., Gray, E., Candalija, A., Cramb, K. M. L., Scaber, J., Dafinca, R., et al. (2022). Human iPSC co-culture model to investigate the interaction between microglia and motor neurons. *Sci. Rep.* 12:12606. doi: 10.1038/s41598-022-16896-8

Valamehr, B., Abujarour, R., Robinson, M., Le, T., Robbins, D., Shoemaker, D., et al. (2012). A novel platform to enable the high-throughput derivation and characterization of feeder-free human iPSCs. *Sci. Rep.* 2:213. doi: 10.1038/srep00213

Vo, Q. D., Saito, Y., Ida, T., Nakamura, K., and Yuasa, S. (2024). The use of artificial intelligence in induced pluripotent stem cell-based technology over 10-year period: a systematic scoping review. *PLoS One* 19:e0302537. doi: 10.1371/journal.pone.0302537

Voigt, I., Inojosa, H., Dillenseger, A., Haase, R., Akgün, K., Ziemssen, T., et al. (2021). Digital twins for multiple sclerosis. *Front. Immunol.* 12:669811. doi: 10.3389/fimmu.2021.669811

Wevers, N. R., Kasi, D. G., Gray, T., Wilschut, K. J., Smith, B., van Vught, R., et al. (2018). A perfused human blood–brain barrier on-a-chip for high-throughput assessment of barrier function and antibody transport. *Fluids Barriers CNS* 15:23. doi: 10.1186/s12987-018-0108-3

Willis, E. F., MacDonald, K. P. A., Nguyen, Q. H., Garrido, A. L., Gillespie, E. R., Harley, S. B. R., et al. (2020). Repopulating microglia promote brain repair in an IL-6-dependent manner. *Cell* 180, 833–846.e16. doi: 10.1016/j.cell.2020.02.013

Winden, K. D., Sundberg, M., Yang, C., Wafa, S. M. A., Dwyer, S., Chen, P. F., et al. (2019). Biallelic mutations in TSC2 lead to abnormalities associated with cortical tubers in human iPSC-derived neurons. *J. Neurosci.* 39, 9294–9305. doi: 10.1523/JNEUROSCI.0642-19.2019

Wingo, T. S., Liu, Y., Gerasimov, E. S., Vattathil, S. M., Wynne, M. E., Liu, J., et al. (2022). Shared mechanisms across the major psychiatric and neurodegenerative diseases. *Nat. Commun.* 13:4314. doi: 10.1038/s41467-022-31873-5

Wörsdörfer, P., Dalda, N., Kern, A., Krüger, S., Wagner, N., Kwok, C. K., et al. (2019). Generation of complex human organoid models including vascular networks by incorporation of mesodermal progenitor cells. *Sci. Rep.* 9:15663. doi: 10.1038/s41598-019-52204-7

Xiang, Y., Tanaka, Y., Cakir, B., Patterson, B., Kim, K. Y., Sun, P., et al. (2019). hESC-derived thalamic organoids form reciprocal projections when fused with cortical organoids. *Cell Stem Cell* 24, 487–497.e7. doi: 10.1016/j.stem.2018.12.015

Xiang, Y., Tanaka, Y., Patterson, B., Kang, Y. J., Govindaiah, G., Roselaar, N., et al. (2017). Fusion of regionally specified hPSC-derived organoids models human brain development and interneuron migration. *Cell Stem Cell* 21, 383–398.e7. doi: 10.1016/j.stem.2017.07.007

Xu, R., Boreland, A. J., Li, X., Erickson, C., Jin, M., Atkins, C., et al. (2021). Developing human pluripotent stem cell-based cerebral organoids with a controllable microglia ratio for modeling brain development and pathology. *Stem Cell Rep.* 16, 1923–1937. doi: 10.1016/j.stemcr.2021.06.011

Yagi, T., Ito, D., Okada, Y., Akamatsu, W., Nihei, Y., Yoshizaki, T., et al. (2011). Modeling familial Alzheimer's disease with induced pluripotent stem cells. *Hum. Mol. Genet.* 20, 4530–4539. doi: 10.1093/hmg/ddr394

Yan, J., Kuzhiumparambil, U., Bandodkar, S., Dale, R. C., and Fu, S. (2021). Cerebrospinal fluid metabolomics: detection of neuroinflammation in human central nervous system disease. *Clin. Transl. Immunol.* 10:e1318. doi: 10.1002/cti2.1318

Yang, S., Chang, R., Yang, H., Zhao, T., Hong, Y., Kong, H. E., et al. (2017). CRISPR/Cas9-mediated gene editing ameliorates neurotoxicity in mouse model of Huntington's disease. *J. Clin. Invest.* 127, 2719–2724. doi: 10.1172/JCI92087

Yang, X., Forró, C., Li, T. L., Miura, Y., Zaluska, T. J., Tsai, C. T., et al. (2024). Kirigami electronics for long-term electrophysiological recording of human neural organoids and assembloids. *Nat. Biotechnol.* 42, 1836–1843. doi: 10.1038/s41587-023-02081-3

Yu, F. H., Mantegazza, M., Westenbroek, R. E., Robbins, C. A., Kalume, F., Burton, K. A., et al. (2006). Reduced sodium current in GABAergic interneurons in a mouse model of severe myoclonic epilepsy in infancy. *Nat. Neurosci.* 9, 1142–1149. doi: 10.1038/nn1754

Zeiss, C. J. (2017). From reproducibility to translation in neurodegenerative disease. *ILAR J.* 58, 106–114. doi: 10.1093/ilar/ilx006

Zerr, I., and Parchi, P. (2018). Sporadic creutzfeldt-jakob disease. *Handb. Clin. Neurol.* 153, 155–174. doi: 10.1016/B978-0-444-63945-5.00009-X

Zetterberg, H., and Burnham, S. C. (2019). Blood-based molecular biomarkers for Alzheimer's disease. *Mol. Brain* 12:26. doi: 10.1186/s13041-019-0448-1

Zimmermann, J., Perry, A., Breakspear, M., Schirner, M., Sachdev, P., Wen, W., et al. (2018). Differentiation of Alzheimer's disease based on local and global parameters in personalized virtual brain models. *Neuroimage Clin.* 19, 240–251. doi: 10.1016/j.nicl.2018.04.017

frontiers | Frontiers in Systems Neuroscience

TYPE Brief Research Report
PUBLISHED 18 June 2025
DOI 10.3389/fnsys.2025.1484769

OPEN ACCESS

EDITED BY
Egidio D'Angelo,
University of Pavia, Italy

REVIEWED BY
John Sharer Allen,
University of Hawaii at Manoa, United States
Glauber T. Silva,
Federal University of Alagoas, Brazil

*CORRESPONDENCE
Pier Francesco Moretti
✉ pierfrancesco.moretti@cnr.it
Giovanni Longo
✉ longo@ism.cnr.it

RECEIVED 28 August 2024
ACCEPTED 26 May 2025
PUBLISHED 18 June 2025

CITATION
Girasole M, Moretti PF, Di Giannatale A, Di Paolo V, Galardi A, Lampis S, Dinarelli S and Longo G (2025) Toward a role for the acoustic field in cells interaction.
Front. Syst. Neurosci. 19:1484769.
doi: 10.3389/fnsys.2025.1484769

Toward a role for the acoustic field in cells interaction

Marco Girasole[1], Pier Francesco Moretti[2]*, Angela Di Giannatale[3], Virginia Di Paolo[3], Angela Galardi[3], Silvia Lampis[3], Simone Dinarelli[1] and Giovanni Longo[1]*

[1]Institute of Matter Structure, Italian National Research Council, ISM-CNR, Rome, Italy, [2]Department of Earth System Sciences and Environmental Technologies, Consiglio Nazionale delle Ricerche, Rome, Italy, [3]Hematology/Oncology and Cell and Gene Therapy Unit, Bambino Gesù Children's Hospital, IRCCS, Rome, Italy

Nanoscale motility of cells is a fundamental phenomenon, closely associated with biological status and response to environmental solicitations, whose investigation has disclosed new perspectives for the comprehension of cell behavior and fate. To investigate intracellular interactions, we designed an experiment to monitor movements of clusters of neuroblastoma cells (SH-SY5Y) growing on a nanomechanical oscillator (nanomotion sensor) suspended few hundreds of microns over the surface of a Petri dish where other neuroblastoma cells are freely moving. We observed that the free-to-move cells feel the presence of cells on the nearby nanosensor (at a distance of up to 300 microns) and migrate toward them, even in presence of environmental hampering factors, such as medium microflows. The interaction is bidirectional since, as evidenced by nanomotion sensing, the cells on the sensor enhance their motion when clusters of freely moving cells approach. Considering the geometry and environmental context, our observations extend beyond what can be explained by sensing of chemical trackers, suggesting the presence of other physical mechanisms. We hypothesize that the acoustic field generated by cell vibrations can have a role in the initial recognition between distant clusters. Integrating our findings with a suitable wave propagation model, we show that mechanical waves produced by cellular activity have sufficient energy to trigger mechanotransduction in target cells hundreds of microns away. This interaction can explain the observed distance-dependent patterns of cellular migration and motion alteration. Our results suggest that acoustic fields generated by cells can mediate cell-cell interaction and contribute to signaling and communication.

KEYWORDS

cell-cell interactions, nanomotion sensor, mechanical waves, acoustic field, neuroblastoma cell, cell behavior

Introduction

Living organisms are composite systems, often formed by a multitude of interconnected organs and components, each with its own intrinsic complexity. Downscaling in the spatial dimension of this chain, we can identify the cell as a major building block of this process. Cells can sense and respond to their environment and their interactions are essential for the proper functioning of complex organisms. This interaction happens *in vivo* through different kinds of mechanisms, including chemical sensing, *via* receptors and ion channels and mechanical sensing, through integrins and cytoskeleton, which allow cells to respond to mechanical stimulation (Ullo and Case, 2023; Dinarelli et al., 2022). These processes are crucial for various physiological functions,

including development, immune response, and tissue maintenance. Among those, the most studied cellular interaction is chemical signaling. Indeed, all cells probe and sense their environment and interact with nearby cells using chemical mediators, raising interest in the metabolic pathways behind these kinds of interactions (SenGupta et al., 2022).

Recent studies have shown that, by using different artificially induced stimulations alongside chemical signaling, a second, mechanical interaction appears as an equally important pathway through which cells sense and respond to the environment (Zhou et al., 2020; Dinarelli et al., 2018b; Wuest et al., 2015; Blaber et al., 2015; Wehland et al., 2013). This is directly translated into aging pathways of red blood cells, changes in the metabolic activity of bacteria, or in the resilience of cardiomyocytes and is a key parameter in the development of cancers (Dinarelli et al., 2018b; Villalba et al., 2021; Craig and Basson, 2009; Dinarelli et al., 2018a). The ability of the cells to perform mechano-sensing and to translate such stimulation into biological patterns has led to the idea that the acoustic field may also play a role in the communication process between cells.

Sound is involved into important aspects of animal behavior and plays a crucial role in a wide range of social and ecological interactions. Sound is an essential component of the environment and fauna have adapted to use sound, developing highly specialized auditory systems to detect and interpret oscillating waves. Acoustic signals can vary in pitch, rhythm, amplitude, and are often highly structured and repeated in patterns, such as drumming or rattling (Longo et al., 2021).

Overall, sound waves can deliver, effectively and rapidly, mechanical signals produced by living systems (or can assist other forms of communication). Cells can produce and respond to mechanical waves through a medium, which propagate as an acoustic field, by involving mechanosensitive ion channels present in the cell membrane that can be sensitive to pressure change, by induction of vibrations in the extracellular matrix (ECM) transmitted to the cell through integrins and other adhesion molecules, or by influencing membrane-bound receptors and producing secondary messengers (Ambattu and Yeo, 2023). These responses are translated into micro- and nano-sized cellular movements, which are directly associated to the cellular status. Indeed, there is a strong correlation between movement and life, between energy consumption and motions or vibrations at various scales, from the level of complex organisms down to single cells, and even further to molecules and macromolecules (Alonso-Sarduy et al., 2014).

Several mechanisms are involved in cellular motility, including cytoskeleton remodeling, environmental signaling and metabolic state (Suresh and Diaz, 2021). For instance, the cell cytoskeleton, composed of actin filaments, microtubules, and intermediate filaments, typically organized into networks, can be reconfigured in response to stimuli, such as forces arising from extracellular matrix degradation, cellular remodeling and pharmacological treatment (Yanes and Rainero, 2022).

Sound has been studied for its potential in NB cell maturation or for a potential therapeutic effect in enhancing tissue regeneration (Lucas et al., 2020; Armand et al., 2025; Cho et al., 2022). The interaction of cells with an acoustic field have been exploited in oncology, exploiting the fact that healthy and cancerous cells exhibit different mechanical properties, with metastatic cells generally being more deformable than primary tumor and normal cells, probably due to alterations in their cytoskeleton (Fraldi et al., 2019; Runel et al., 2021). Theoretical models have predicted that ultrasonic vibrations may differentially affect healthy and cancerous cells, both in single-cell systems and in heterogeneous cell clusters at the mesoscale (Fraldi et al., 2016). Other experiments investigating wave-cell interactions have shown the induction of unidirectional cell migration aligned with the direction of the propagating wave, which increased at a critical wave intensity but was suppressed at higher intensities (Imashiro et al., 2021).

In this work, we investigate the role of the acoustic field in simplified yet complex, living systems such as clusters of NB cells. We designed an experiment focused on the interaction between small clusters of NB cells to study the interaction between smaller complex systems.

To this aim we selected SH-SY5Y cell line, a model in neuroscience research, which can be induced to differentiate into neuron-like cells, both cholinergic and dopaminergic, through treatments with agents such as retinoic acid (RA), Brain-Derived Neurotrophic Factor (BDNF), or cAMP (Shipley et al., 2016; Hoffmann et al., 2023). The neuronal-like differentiation is revealed by the expression of key neuronal markers, including tau protein, synaptophysin, and tyrosine hydroxylase (Lopez-Suarez et al., 2022). Additionally, they also exhibit the ability to form neurites that allow the cells to establish synaptic connections, stimulating cell-cell interactions and forming neuronal networks making them suitable for *in vitro* studies (Angiari et al., 2022; Armingol et al., 2021; Song et al., 2019; Teppola et al., 2016).

It is known that neurons in complex aggregates (such as brains) show a temporal organization of their activity, that can be represented by a system of rhythms, that has been classified for humans and for mammals in a similar way (Buzsáki et al., 2013). Currently, investigation of the neuronal activity is mainly associated by the acquisition of electric signals, while no specific correlation between their mobility and behavior of the organisms has been reported. To study NB's behavior, we coupled optical imaging with time-resolved nanoscale vibration sensors to describe cell behavior at the micro and nanoscale (Aghayee et al., 2013; Zhou et al., 2024; Longo et al., 2013; Ruggeri et al., 2017). In particular, we used the nanomotion sensor to monitor cell's vibrations as a mark of their cellular activity (Zou et al., 2023; Kasas et al., 2015; Lupoli et al., 2018; Wu et al., 2016). This particular geometrical setup, where small clusters of NB cells interact freely with other similar cells placed at a controlled distance, provided a sandbox to investigate alterations in NB activity and movement when cell-cell interactions are underway (Figure 1).

We propose that the distortion of the density field in the environment induced by the vibrations of cells adhering to the sensor can result in an unexpected contribution to communication, even at the single cell level. In fact, while it is known that cell motility is a fundamental parameter in the study of NB cells and has repercussions on the study of brain-related cancers (Ul Islam et al., 2017; Shimizu et al., 2020), we suggest that acoustic waves,

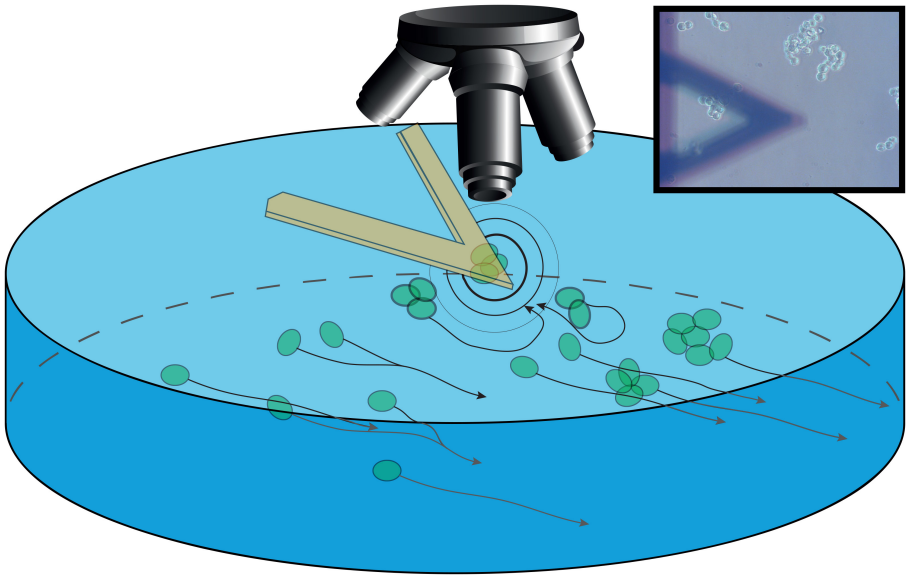

FIGURE 1
Sketch of the setup. The sensor is immersed in the growing medium in a Petri dish with an optical microscope collecting images. The sensor is bearing S-cell NB which are interacting (outward black and gray circles) with P-cells. These cells are aggregating and moving in the background following the medium flow (black arrow lines). Inset: Image of the setup as acquired through the optical microscope, with the sensor in foreground and the aggregated cells in focus on the background.

such as those generated at the nanoscale by cell activity, can have an important role in the cell-cell interactions.

Materials and methods

Materials

DMEM low glucose, 1% penicillin-streptomycin and 1% L-Glutamin were acquired from Euroclone (Pero, MI). 10% Fetal bovine serum and (3-Aminopropyl)triethoxysilane (APTES) 10% v/v were acquired from Thermofisher (Massachusetts, USA). Petri dishes and all laboratory equipment were obtained from Merck (Darmstadt, DE).

Cell preparation

SH-SY5Y Neuroblastoma (NB) cell lines (CRL-2266) derived from metastatic bone tumors, obtained from the cell repository from the OPBG were kindly provided by Dr. Di Giannatale. These cells are known to differentiate in N-type (neuronal) and S-type (substrate-adherent) and have the additional characteristic of being capable of growing in adhesion or in suspension, making them the ideal candidates for our experiments (Kovalevich and Langford, 2013; Bell et al., 2013).

Cells were cultured in DMEM low glucose supplemented with 10% Fetal bovine serum, 1% penicillin-streptomycin and 1% L-Glutamine. Cells were incubated at 37°C in a humidified atmosphere with 5% CO_2. Cells were seeded 24–48 h prior to measurements on plastic Petri dishes. Medium composition, cell culture density and temperature were kept constant throughout all experiments.

Setup description

For all our experiments we have used two interchangeable setups, based on two atomic force microscopes (AFM): a Park NX-12 (Park Systems, Suwon, Korea) and a Nanosurf Flex (Nanosurf AG, Liestal, Switzerland). These microscopes were mounted on an Olympus IX-9 inverted optical microscope (Olympus Corporation, Tokio, Japan) equipped with a high-resolution Progres MFCool digital camera (Jenoptik, Germany) and an active antivibration table, to ensure that environmental noise did not influence the measurements. This setup allowed performing concurrently all the measurements on the chosen cells. To ensure the measured effects were only correlated to cellular behavior and not due to external factors, all experiments were carried out in a controlled environment, kept at 37°C in 5% CO_2 and in a fully humidified environment throughout the entire measurement run.

The optical microscopy images were used to monitor the behavior of the cells both on the sensor and on the Petri dish and were collected every 20 s using a 40x objective. By using a semi-automated cell tracking system [Fiji, a distribution of the freeware ImageJ (Schindelin et al., 2012)], we followed the movements of these P-cells, highlighting the path followed by the cells after every image.

Regarding the nanomotion setup, we chose commercial AFM cantilevers as sensors, namely Bruker ONP-10 tipless AFM cantilevers (Bruker Corporation, Massachusetts, USA), choosing the sensor with a nominal elastic constant of 0.12 N/m. Prior to all experiments, the sensors were calibrated using the built-thermal-noise routines to determine the resonant frequency and the corresponding mechanical properties of the sensor (Hutter and Bechhoefer, 1993). The nanomotion signal was acquired using

custom LabView software to control a NI USB-4431 card (National Instruments, USA) collecting the nanoscale oscillations of the sensor caused by the oscillations of the cells at a 15 kHz rate. We analyzed this data using a custom Labview software, to calculate the variance of the nanomotion signal over small time-chunks (typically 10–60 s) (Venturelli et al., 2020).

Sensor preparation and cell immobilization

Figure 1 shows a sketch view of the setup and, in the inset, the field of view in a typical experiment is shown, with small and large clusters of P-cells passing underneath the sensor.

The setup used to monitor and detect vibrations of neuronal cells is similar to a conventional nanomotion setup, as described in detail in previous works (Longo et al., 2013; Venturelli et al., 2020). At first, the sensors were washed in ultrapure water, functionalized by 10 min exposure to APTES 10% v/v which was followed by thorough rinsing in ultrapure water and immediate transfer to the AFM for immediate use.

Next, we placed growing medium and living NB cells in a Petri dish which was not functionalized. This substrate allows a weak cellular attachment but does not stimulate complete cellular adhesion, thus placing the cells in an environment in which their innate tendency to grow in adhesion is impeded, possibly stimulating environmental sensing and interaction. The sensor was then brought in the near vicinity to the surface by using the AFM's motors, and single cells or small clusters were identified for collection. To do this, we pressed the sensor against chosen specimens allowing the functionalization of the sensor to stimulate the cell's adhesion. After 1 min of pressure (maximum applied pressure 20 nN), we retracted the sensor to a distance from the Petri dish surface of 100 or 200 μm. During this whole procedure, we used the optical microscope first to determine which cells to attach and next to monitor the firm cell adhesion to the sensor. The optical microscope was also used to monitor over time both the sensor bearing the NB cells (which we call S-cells) and the other NB cells present on the Petri dish (the P-cells). Each experiment lasted at least 4 h (with some measurements rounding up to up to 7 h) and was divided into 30- or 40-min chunks for the analysis.

In the typical experiment the motion of the cells, both the P-cells and the S-cells, were combined with the analysis of the time-dependent fluctuations induced by the S-cells on the sensor. The variance of the nanomotion signal was directly related to the activity of the S-cells in the different environmental conditions (Kohler et al., 2019; Girasole et al., 2023), while the movements of the P-cells gave us an insight on the interaction between the NB cells.

Notably, even in a small receptacle such as a Petri dish, the medium underneath the sensor can exhibit a flux, which drives the movements of the P-cells. We were able to identify this flux in terms of speed and direction by following the small particulate in the growing medium. We focused on the alteration of these movements correlated to these medium microcurrents when influenced by the presence of the sensor and of the S-cells, mediated by the oscillations of the S-cells (as depicted in Figure 1).

Cell health estimates

Optical images evidenced that the cells exhibited normal behavior, including formation of filopodia and substrate probing, which were determined to be signals of good viability.

As additional control, other NB cells were kept in the same environmental conditions side-by-side with the cells under investigation, and the viability and wellbeing of these control cells were verified at the end of each experiment.

Statistical analysis

The presented results were replicated in more than 30 independent experiments from distinct preparations, and several different interaction events were collected throughout each experiment. Bearing this in mind, there is a point to be highlighted regarding the variability of each experimental run. The number, position and activity of the P-cells as well as of the S-cells is difficult to control and to categorize. Indeed, even if we can control the position and number of S-cells at the beginning of each experiment, they were free to move, even if on a very small platform, thus we had no control over their displacement during the experiment. Furthermore, we had no control over when and where the P-cells appear and at what distance they will pass in the vicinity of the S-cells. This means that a completely quantitative determination of the cell-cell interaction, a priori, is impossible. The only statistical determination we can provide is a statistical analysis of the average cell-cell distance at which we can determine that an interaction is underway, through which we have estimated the size of the approximate interaction-sphere within which the relative effect can be observed.

Results

Large-scale movements of NB cells

In all the experiments the optical images evidenced how both the cells attached to the sensor (S-cells) and those moving on the surface of the Petri dish (P-cells) shifted and moved, often through a roto-translational pattern. The available space for their motion was very different: while the S-cells were observed vibrating and moving over the nano sensor, the P-cells moved on much larger distances, often entering and exiting the field of view of the optical microscope.

The first and most common behavior of the P-cells was that they moved freely over the Petri dish substrate to find and make contact with other cells (Figure 2). In this way, they typically formed larger clusters. This appears to constitute a major driving force influencing the activity of freely moving NB cells which should be considered in the interpretation of the data. A second effect influencing the movements of P-cells was the micro-dynamics of the growth medium. Small differences in liquid pressure in the Petri dish produced local fluid currents, which can be seen through the drifting of small particulates in the medium. This flow directed the movement of the P-cells, driving them in specific directions. We highlighted such trajectories which were derived

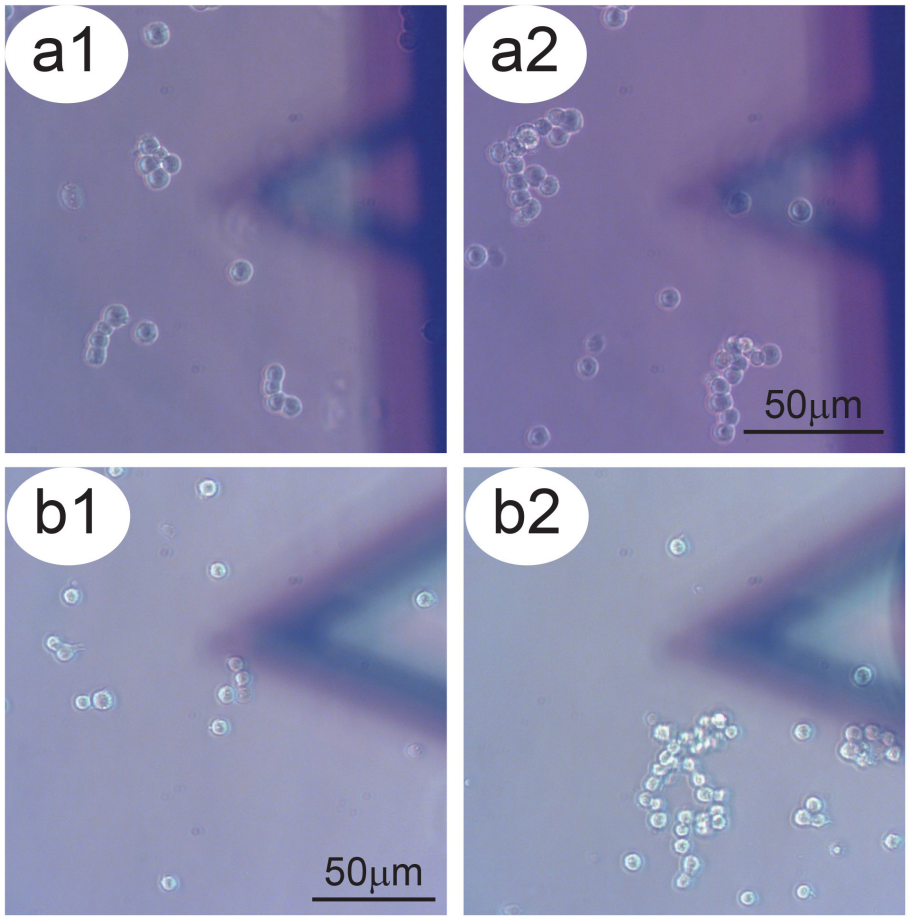

FIGURE 2
Aggregation tendency of P-cells. Panels a1–a2 and b1–b2: Two examples of NB cells which tend, over time, to aggregate to form larger clusters. In the foreground, the sensor bearing S-cells.

from the time-lapse videos of the P-cells in the presence of a sensor. The resulting overlay lines and the corresponding displacement graphs depict a typical scenario in which clusters of P-cells pass in the vicinity and underneath the sensor and allow comparing the behavior of the cells with cases in which the cells pass far from the sensor and from the cells placed on it.

When no S-cells were present (Supplementary Figure 1a), the cells were driven by the microflow of the medium and passed in view with approximately linear paths, unaltered by the presence of the bare sensor (Supplementary Figures 1b–d).

When NB cells were present on the sensor, while P-cells passing far from the S-cells appeared to continue an unaltered path (Figures 3a, a1), the P-cell clusters that passed in the close vicinity and underneath the S-cells experienced a modification of their motion, such as slowing down or brief stops (Figure 3, a2), up to a transient or permanent stop when in close proximity to the sensor (Figures 3b, b1, b2), even against the micro-currents of the growth-medium (see the blue arrows in Figures 3a, b). Some cases exhibit a large deflection of the cell path or a combination of different P-cell clusters to interact with the NB cells on the sensor (Supplementary Figure 2, Supplementary Movie 1).

Remarkably, in most cases, the interaction between the P-cells and the S-cells starts before the former cells pass near the sensor, and in presence of a medium flux, with the P-cells still upwind to the S-cells (Figure 3b, Supplementary Figure 2). Interestingly, there are cases in which the P-cells move against the medium flow, reducing their velocity and even deviating their trajectory to approach the specimens on the sensor. In addition, the time needed for the clusters of P-cells to alter their motion is fast, with changes in speed and direction happening in less than the time between two subsequent optical images (i.e., 20 s).

The observed cell-cell interactions evidence additional peculiar behaviors. In a remarkable experiment, clusters of P-cells have partially detached from the substrate, moving toward direct contact with the cells on the sensor. This is particularly interesting as these S-cells were suspended over the Petri dish surface at 100 microns on the vertical axis (Supplementary Figure 3, Supplementary Movie 2).

These dynamics suggest that the mechanisms underlying the cell-cell interaction point toward the formation of large cell aggregates and are strong enough to produce substantial and unexpected consequences on the cell behavior.

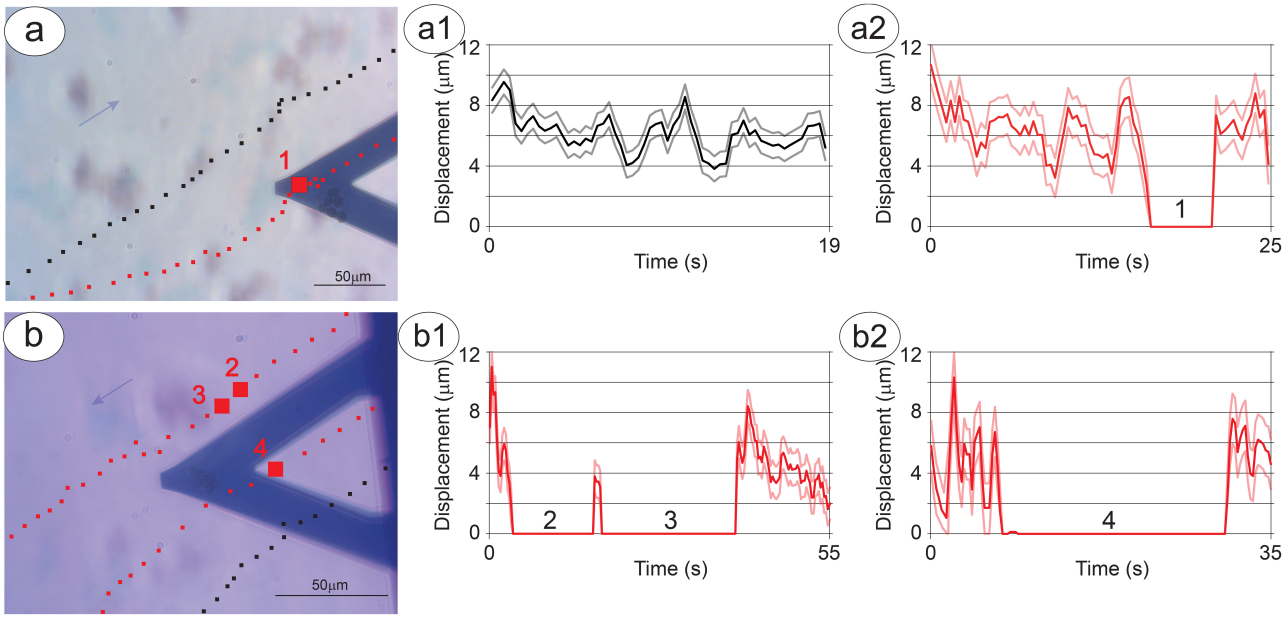

FIGURE 3
Dynamics of the interaction between P-cells and S-cells. The trajectories (series of black or red squares on the optical image) and displacement (corresponding a1–a2 and b1–b2 graphs) of a cell cluster over time. **(A)** Shows a cluster stopping near the S-cells (red squares with a larger square corresponding to the area of cell-cell interaction) and a nearby cluster which does not change its trajectory (black squares). **(B)** Shows two clusters stopping near the S-cells (red squares with larger squares and numbers corresponding to the areas of cell-cell interaction) and a nearby cluster which passes under the sensor but does not change its trajectory (black squares). The scale bar indicates 50 mm and the lighter variance curves indicate the error in the displacement measurements.

Regarding the S-cells, these are limited in their movements by the geometry of our setup but at the same time tend to interact with the P-cells by shifting and moving toward them when they come by (Figure 4, panels 1–4). A very interesting characteristic of these cells is that their behavior depends greatly on their number. In experiments when only one or two cells were loaded on the sensor, they appeared to move on the sensor, exploring the surrounding environment, possibly focused on the search for other cells. This movement pattern of single cells often brought them to detach from the sensor (Supplementary Figure 4), especially when some cluster of P-cells passed in the vicinity, thus showing a preference toward the cell-to-cell contact instead of the functionalized surface of the sensor.

Because of the numerous possible configurations of medium flow, the varying number and positions of S-cells, and the diverse abundance and clustering patterns of P-cells, a full statistical analysis of how sensor and P-cells interact is unfeasible. Therefore, we measured the distance between the cells when a change in their movement, indicating an interaction, could be detected (Supplementary Figure 5a). We used these values to define the range of interaction between the P-cells and the S-cells (Supplementary information 2).

Nanomotion

In experimental conditions where cell-cell interactions occur, the movements recorded by the nanosensor provide an insight into the behavior and status of the S-cells and during their interaction with the P-cells. A typical nanomotion signal of an experiment can be used to compare variance (Figures 4a, b) and amplitude of the oscillations (Figure 4c) with the optical images (Figure 4, time-points 1–4). Through this comparison we can divide the experiment into different sections. At first there are five well-attached cells onto the sensor, resulting in an overall movement transferred to the sensor which has a low amplitude and is constant over time (Figure 4, time-point 1). When a large cluster of P-cells approaches, this excites at least two S-cells which start to shift on the sensor in a roto-translation pattern, causing a slight but measurable increase in the overall fluctuations of the sensor, with peculiar spikes in the detected signals (Figure 4, time-point 2). Even after the departure of the cluster, the cells on the sensor maintain their increased roto-translational activity.

When a second larger cluster arrives near the sensor and interacts with the S-cells, these increase their activity, moving on the sensor and extending filopodia or neurites, and this produces a significant increase of the nanomotion signal (Figure 4, time-point 3). The nanomotion pattern is diverse, with large spikes and an overall large amplitude of the fluctuations. Finally, when a very large cluster of P-cells approaches and stays under the sensor, interacting with the S-cells, the cluster of cells splits, and the motile activity of each cell increases. This causes a further increase in the nanomotion signal with much higher oscillations and eventually resulting in some of the S-cells, at that point no more bound to the sensor cluster, detaching from the sensor to join the larger cluster on the Petri dish (Figure 4, time-point 4).

The alterations in the behavior of S-cells when P-cells are approaching has been consistently observed across multiple

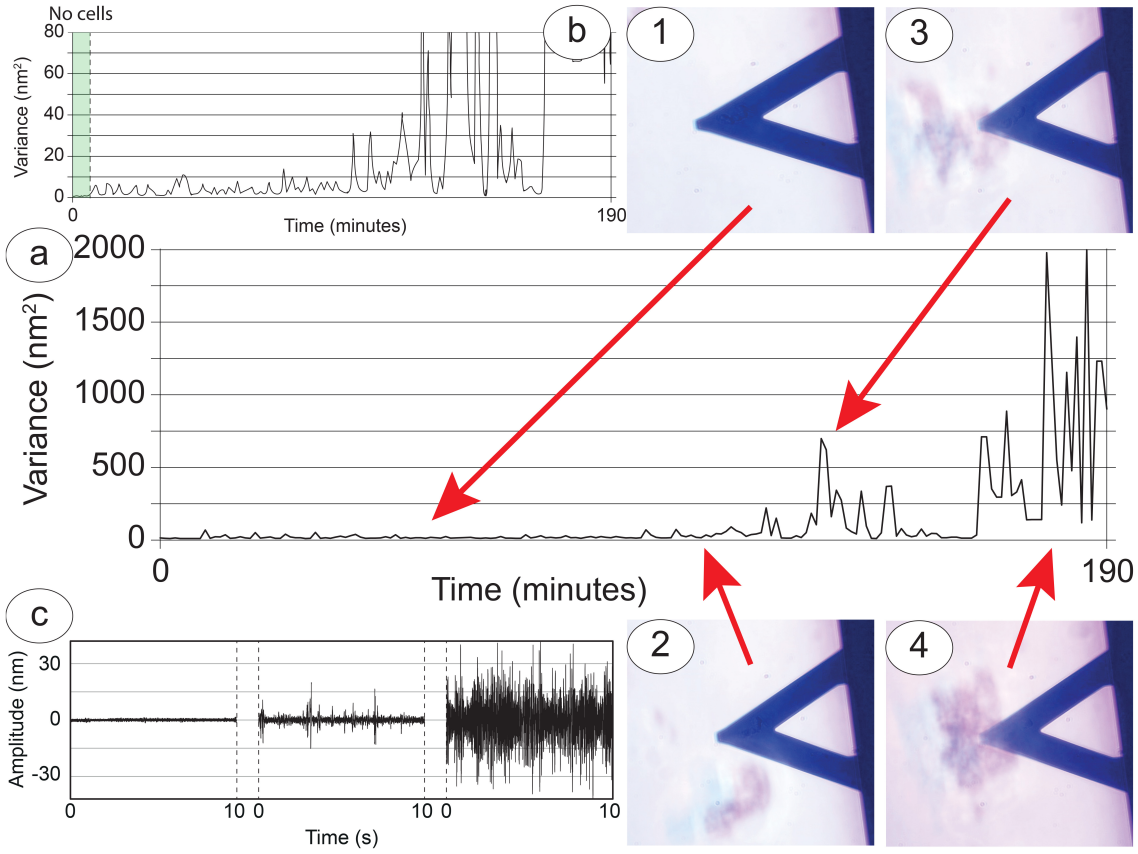

FIGURE 4
Cellular nanoscale vibration response of the S-cells to the nearby presence of the P-cells. **(A)** Nanomotion variance during an entire experiment, lasting more than 3 h. **(B)** Zoom in to highlight the behavior at lower variance values. Panels 1 to 4: Snapshots of interesting cell-cell interactions: the nanomotion variance increases according to the size and distance of the cluster of P-cells which have approached the sensor. **(C)** Typical amplitudes collected from the sensor in correspondence to zones 1 and 2 (right curve), zone 3 (center curve) and zone 4 (right curve).

experiments ($n = 5$), suggesting a reproducible and generalizable cellular response.

Discussion

We presented a series of experiments designed to highlight and characterize, at micro and nanoscale and in a controlled geometry, the interactions between cells. The goal was to estimate the possible role for acoustic fields in the cell-cell interaction process even at the single cell level.

We focused on a simplified nanoscale system consisting of a small cluster of NB cells geometrically constrained to a small flat surface, interacting with a larger number of other NB cells freely moving on a Petri dish which did not favor their adhesion. This condition stimulated in P-cells the need to explore the environment, searching for a surface where to adhere or for other cells to form larger self-sustained clusters and in the S-cells the tendency to communicate with other cells and an amplified activity which was measured by the nanomotion sensor.

Our experiments showed that the activity of the cells is dominated by a general trend leading to the formation of large clusters of NB aggregates. This general behavior must be mediated by forces acting at the cellular scale and is expected to be limited and modulated by biological, physical and environmental factors.

The experimental setup that we propose presents a two-fold advantage. On one side it provides a unique environment to stimulate and observe the cellular interactions. On the other side, the nanomotion sensor has the capability to monitor the cells' activity in real time and to quantify their activity during their homeostasis or during cell-cell interactions.

Indeed, the results shown in Figure 4 point toward a large increase in activity of the S-cells during interaction with P-cell clusters, an interaction that appears to be mediated by relevant cellular communication. In fact, many of our observations have evidenced how, in absence of external measurable forces, P-cells have altered in a large manner their motion in the vicinity of the S-cells, even detaching from the substrate (Supplementary Figure 3). In several cases, such alterations of the free motion of the P-cells occurred against the flow of the medium, that is, against the environmental force gradient (Figure 3, Supplementary Figure 2).

While a purely chemical interaction is commonly considered to be the main actor in cell-cell communication, the upwind directional responses observed in our experiments cannot be simply explained through simple chemical communication. Such a fast, upwind and complex geometry of interaction suggests that the cells could exploit their strong tendency to communicate by tapping into different kinds of communication mechanisms, including those driven by mechanical stimulation.

The data shown in Supplementary Figure 5a indicates that the cell-cell interactions depend on many parameters such as the number of cells, their status and the strength of the medium flow. In any case, we were never able to identify interactions which exceeded 300 microns in distance between clusters. To understand if the S-cells' oscillations were sufficient to produce a mechanical wave that could be detected by the P-cells, we performed a semi-quantitative evaluation of our data (Supplementary information 2). Considering our geometry and the characteristics of the cells and of the medium, we were able to determine that the oscillations generated by the S-cells and integrated by the sensor in a clear and coherent signal, can produce an oscillating mechanical field which has a sufficient amplitude to interact on cells distant even several hundreds of microns. According to the measured value of sensor oscillation, this traveling field has the strength to determine membrane deformation on the target P-cells which, in our experimental condition, can be predicted to activate the mechano-transduction mediated by PIEZO proteins and by integrins (Kumar and Weaver, 2009; Lin et al., 2019; Baratchi et al., 2024; Niu et al., 2022; Wang and Ha, 2013; Jo et al., 2022). Furthermore, our interpretative model includes the viscous behavior of the culture medium (a real fluid) which, through the energy draining occurring in the Stokes layer (Sader, 1998), allows understanding why the effects on the P-cells were observed only within few hundreds of micron from the source.

In fact, the calculated range of such Stokes layer in our experimental conditions, agrees with the maximum distance at which we unambiguously identified cell-cell interactions (Supplementary Figure 5b). It is worth noting that, on a larger scale of biological aggregation, signaling through these kinds of oscillations are associated with acoustic waves, and we can suggest that these can have an impact also on the collective activity of even the smallest building blocks of living organisms (i.e., cell clusters).

Overall, mechanical oscillations produced by cellular vibrations in a fluid environment can generate a distortion of the density/pressure field that can be detected and transduced by target cells through mechano-sensing proteins and result in cellular response. We have presented evidence that suggests that such acoustic waves can be scaled down even to single cell interactions.

While a direct measurement of the acoustic waves is impossible in our setup (acoustic waves in liquids are usually measured by hydrophones, which are bulky and do not have the sensibility to measure waves at very short distances), our model of cell-cell interaction supports this conclusion.

Obviously, the complexity of a real experiment cannot be completely reflected in this simplified model. Indeed, extensive statistical analysis is complex, since our experimental setup welcomes biological variability, heterogeneity in cellular response and the randomness of a real-life scenario to better understand the collective behavior of the NB cells. Furthermore, our model doesn't consider effects associated with multiple reflections of the acoustic fields or the geometrical limitations of the cell-wave interaction, which could modulate the effectiveness of the biological transduction.

Further confirmation of the proposed role for acoustic-based communication would come from dedicated experiments involving fluorescent tags on mechano-transductive proteins to better highlight the chemical signaling pathways and their alterations in presence of acoustic waves. Similarly, investigating the effect of specific protein inhibitors or that of drugs known to alter cell-cell interactions would provide a better biological characterization for this new interaction mechanism.

Within the limits of our setup and model, we propose that an acoustic field can be invoked to justify, directly or indirectly, the counter-intuitive cellular behavior observed in our experiments, especially considering that acoustic fields may act through multiple mechanisms. For instance, the induction of mechanical waves in the liquid may contribute to a greater diffusion of neurotransmitters in the culture medium or it may increase the availability of the signal molecules dispersed in the buffer, contributing to an acoustic enhancement of the "conventional" chemical signaling of the cells.

Data availability statement

The raw data supporting the conclusions of this article will be made available by the authors, without undue reservation.

Ethics statement

Ethical approval was not required for the studies on humans in accordance with the local legislation and institutional requirements because only commercially available established cell lines were used.

Author contributions

MG: Conceptualization, Data curation, Formal analysis, Investigation, Methodology, Supervision, Validation, Visualization, Writing – original draft, Writing – review & editing. PM: Data curation, Formal analysis, Funding acquisition, Methodology, Project administration, Resources, Validation, Writing – review & editing. AD: Methodology, Resources, Supervision, Writing – review & editing. VD: Resources, Writing – review & editing. AG: Resources, Writing – review & editing. SL: Resources, Writing – review & editing. SD: Formal analysis, Resources, Writing – review & editing. GL: Conceptualization, Data curation, Formal analysis, Investigation, Methodology, Resources, Software, Supervision, Validation, Visualization, Writing – original draft, Writing – review & editing.

Funding

The author(s) declare that no financial support was received for the research and/or publication of this article.

Acknowledgments

The authors would like to thank Vasileios Basios for stimulating discussions.

Conflict of interest

The authors declare that the research was conducted in the absence of any commercial or financial relationships that could be construed as a potential conflict of interest.

Publisher's note

All claims expressed in this article are solely those of the authors and do not necessarily represent those of their affiliated organizations, or those of the publisher, the editors and the reviewers. Any product that may be evaluated in this article, or claim that may be made by its manufacturer, is not guaranteed or endorsed by the publisher.

Supplementary material

The Supplementary Material for this article can be found online at: https://www.frontiersin.org/articles/10.3389/fnsys.2025.1484769/full#supplementary-material

References

Aghayee, S., Benadiba, C., Notz, J., Kasas, S., Dietler, G., Longo, G., et al. (2013). Combination of fluorescence microscopy and nanomotion detection to characterize bacteria. *J. Mol. Recognit.* 26, 590–595. doi: 10.1002/jmr.2306

Alonso-Sarduy, L., Los Rios, P., De Benedetti, F., Vobornik, D., Dietler, G., Kasas, S., et al. (2014). Real-time monitoring of protein conformational changes using a nano-mechanical sensor. *PLoS ONE* 9:e103674. doi: 10.1371/journal.pone.0103674

Ambattu, L. A., and Yeo, L. Y. (2023). Sonomechanobiology: Vibrational stimulation of cells and its therapeutic implications. *Biophys Rev (Melville)* 4:021301. doi: 10.1063/5.0127122

Angiari, S., D'Alessandro, G., Paolicelli, R. C., Prada, I., and Vannini, E. (2022). Editorial: Cell-cell interactions controlling neuronal functionality in health and disease. *Front. Integr. Neurosci.* 16:968029. doi: 10.3389/fnint.2022.968029

Armand, A. C., Bikaran, M., Gardner, T. B., and Matthew, M. K. (2025). The role of infrasound and audible acoustic sound in modulating wound healing: a systematic review. *Int. Wound J.* 22:e70243. doi: 10.1111/iwj.70243

Armingol, E., Officer, A., Harismendy, O., and Lewis, N. E. (2021). Deciphering cell–cell interactions and communication from gene expression. *Nat. Rev. Genet.* 22, 71–88. doi: 10.1038/s41576-020-00292-x

Baratchi, S., Danish, H., Chheang, C., Zhou, Y., Huang, A., Lai, A., et al. (2024). Piezo1 expression in neutrophils regulates shear-induced NETosis. *Nat. Commun.* 15:7023. doi: 10.1038/s41467-024-51211-1

Bell, N., Hann, V., Redfern, C. P., and Cheek, T. R. (2013). Store-operated Ca(2+) entry in proliferating and retinoic acid-differentiated N- and S-type neuroblastoma cells. *Biochim. Biophys. Acta* 1833, 643–651. doi: 10.1016/j.bbamcr.2012.11.025

Blaber, E. A., Finkelstein, H., Dvorochkin, N., Sato, K. Y., Yousuf, R., Burns, B. P., et al. (2015). Microgravity reduces the differentiation and regenerative potential of embryonic stem cells. *Stem Cells Dev.* 24, 2605–2621. doi: 10.1089/scd.2015.0218

Buzsáki, G., Logothetis, N., and Singer, W. (2013). Scaling brain size, keeping timing: evolutionary preservation of brain rhythms. *Neuron* 80, 751–764. doi: 10.1016/j.neuron.2013.10.002

Cho, H., Park, H.-J., Choi, J.-H., Nam, M.-H., Jeong, J.-S., and Seo, Y.-K. (2022). Sound affects the neuronal maturation of neuroblastoma cells and the repair of damaged tissues. *Elect. J. Biotechnol.* 57, 1–11. doi: 10.1016/j.ejbt.2022.03.001

Craig, D. H., and Basson, M. D. (2009). Biological impact of mechanical stimuli on tumor metastasis. *Cell Cycle* 8, 828–831. doi: 10.4161/cc.8.6.7940

Dinarelli, S., Girasole, M., Spitalieri, P., Talarico, R. V., Murdocca, M., Botta, A., et al. (2018a). AFM nano-mechanical study of the beating profile of hiPSC-derived cardiomyocytes beating bodies WT and DM1. *J. Mol. Recognit.* 31:e2725. doi: 10.1002/jmr.2725

Dinarelli, S., Longo, G., Dietler, G., Francioso, A., Mosca, L., Pannitteri, G., et al. (2018b). Erythrocyte's aging in microgravity highlights how environmental stimuli shape metabolism and morphology. *Sci. Rep.* 8:5277. doi: 10.1038/s41598-018-22870-0

Dinarelli, S., Longo, G., Francioso, A., Mosca, L., and Girasole, M. (2022). Mechano-transduction boosts the aging effects in human erythrocytes submitted to mechanical stimulation. *Int. J. Mol. Sci.* 23:10180. doi: 10.3390/ijms231710180

Fraldi, M., Cugno, A., Carotenuto, A., Cutolo, A., Pugno, N., Deseri, L., et al. (2016). Small-on-large fractional derivative–based single-cell model incorporating cytoskeleton prestretch. *J. Eng. Mechan.* 143:D4016001. doi: 10.1061/(ASCE)EM.1943-7889.0001178

Fraldi, M., Palumbo, S., Carotenuto, A. R., Cutolo, A., Deseri, L., Pugno, N., et al. (2019). Buckling soft tensegrities: fickle elasticity and configurational switching in living cells. *J. Mech. Phys. Solids* 124, 299–324. doi: 10.1016/j.jmps.2018.10.017

Girasole, M., Dinarelli, S., and Longo, G. (2023). Correlating nanoscale motion and ATP production in healthy and favism erythrocytes: a real-time nanomotion sensor study. *Front. Microbiol.* 14:1196764. doi: 10.3389/fmicb.2023.1196764

Hoffmann, L. F., Martins, A., Majolo, F., Contini, V., Laufer, S., Goettert, M. I., et al. (2023). Neural regeneration research model to be explored: SH-SY5Y human neuroblastoma cells. *Neural Regen. Res.* 18, 1265–1266. doi: 10.4103/1673-5374.358621

Hutter, J. L., and Bechhoefer, J. (1993). Calibration of atomic-force microscope tips. *Rev. Scient. Instrum.* 64, 1868–1873. doi: 10.1063/1.1143970

Imashiro, C., Kang, B., Lee, Y., Hwang, Y.-H., Im, S., Kim, D.-E., et al. (2021). Propagating acoustic waves on a culture substrate regulate the directional collective cell migration. *Microsyst. Nanoeng.* 7:90. doi: 10.1038/s41378-021-00304-8

Jo, M. H., Li, J., Jaumouillé, V., Hao, Y., Coppola, J., Yan, J., et al. (2022). Single-molecule characterization of subtype-specific β1 integrin mechanics. *Nat. Commun.* 13:7471. doi: 10.1038/s41467-022-35173-w

Kasas, S., Ruggeri, F. S., Benadiba, C., Maillard, C., Stupar, P., Tournu, H., et al. (2015). Detecting nanoscale vibrations as signature of life. *Proc. Natl. Acad. Sci. USA.* 112, 378–381. doi: 10.1073/pnas.1415348112

Kohler, A., Venturelli, L., Longo, G., Dietler, G., and Kasas, S. (2019). Nanomotion detection based on Atomic Force Microscopy cantilevers. *Cell Surf.* 5:100021. doi: 10.1016/j.tcsw.2019.100021

Kovalevich, J., and Langford, D. (2013). Considerations for the use of SH-SY5Y neuroblastoma cells in neurobiology. *Methods Mol. Biol.* 1078, 9–21. doi: 10.1007/978-1-62703-640-5_2

Kumar, S., and Weaver, V. M. (2009). Mechanics, malignancy, and metastasis: The force journey of a tumor cell. *Cancer Metast. Rev.* 28, 113–127. doi: 10.1007/s10555-008-9173-4

Lin, Y.-C., Guo, Y. R., Miyagi, A., Levring, J., MacKinnon, R., and Scheuring, S. (2019). Force-induced conformational changes in PIEZO1. *Nature* 573, 230–234. doi: 10.1038/s41586-019-1499-2

Longo, G., Alonso Sarduy, L., Rio, L. M., Bizzini, A., Trampuz, A., Notz, J., et al. (2013). Rapid detection of bacterial resistance to antibiotics using AFM cantilevers as nanomechanical sensors. *Nat Nano* 8, 522–526. doi: 10.1038/nnano.2013.120

Longo, G., Giannatale, A. D., Colletti, M., Moretti, P. F., and Girasole, M. (2021). "COMplexity Analysis in the Simplest Alive Neuronal network," in *A Quest for an Interface Between Information and Action*, eds. P. F. Moretti, and V. Basios (Gaeta: National Research Council of Italy), 43–51.

Lopez-Suarez, L., Awabdh, S. A., Coumoul, X., and Chauvet, C. (2022). The SH-SY5Y human neuroblastoma cell line, a relevant *in vitro* cell model for investigating neurotoxicology in human: Focus on organic pollutants. *Neurotoxicology* 92, 131–155. doi: 10.1016/j.neuro.2022.07.008

Lucas, B., De Pérez, L. M., Bernal, A., and Gálvez, B. G. (2020). Ultrasound therapy: experiences and perspectives for regenerative medicine. *Genes* 11:1086. doi: 10.3390/genes11091086

Lupoli, F., Vannocci, T., Longo, G., Niccolai, N., and Pastore, A. (2018). The role of oxidative stress in Friedreich's ataxia. *FEBS Lett.* 592, 718–727. doi: 10.1002/1873-3468.12928

Niu, L., Cheng, B., Huang, G., Nan, K., Han, S., Ren, H., et al. (2022). A positive mechanobiological feedback loop controls bistable switching of cardiac fibroblast phenotype. *Cell Discov.* 8:84. doi: 10.1038/s41421-022-00427-w

Ruggeri, F. S., Mahul-Mellier, A. L., Kasas, S., Lashuel, H. A., Longo, G., Dietler, G., et al. (2017). Amyloid single-cell cytotoxicity assays by nanomotion detection. *Cell Death Discov.* 3:17053. doi: 10.1038/cddiscovery.2017.53

Runel, G., Lopez-Ramirez, N., Chlasta, J., and Masse, I. (2021). Biomechanical properties of cancer cells. *Cells* 10:887. doi: 10.3390/cells10040887

Sader, J. E. (1998). Frequency response of cantilever beams immersed in viscous fluids with applications to the atomic force microscope. *J. Appl. Phys.* 84, 64–76. doi: 10.1063/1.368002

Schindelin, J., Arganda-Carreras, I., Frise, E., Kaynig, V., Longair, M., Pietzsch, T., et al. (2012). Fiji: an open-source platform for biological-image analysis. *Nat. Methods* 9, 676–682. doi: 10.1038/nmeth.2019

SenGupta, S., Parent, C. A., and Bear, J. E. (2022). The principles of directed cell migration. Nature reviews. *Mol. Cell Biol.* 22, 529–547. doi: 10.1038/s41580-021-00366-6

Shimizu, T., Fujii, T., and Sakai, H. (2020). The relationship between actin cytoskeleton and membrane transporters in cisplatin resistance of cancer cells. *Front. Cell Dev. Biol.* 8:597835. doi: 10.3389/fcell.2020.597835

Shipley, M. M., Mangold, C. A., and Szpara, M. L. (2016). Differentiation of the SH-SY5Y human neuroblastoma cell line. *J. Vis. Exp.* 17:53193. doi: 10.3791/53193

Song, L., Yan, Y., Marzano, M., and Li, Y. (2019). Studying heterotypic cell−cell interactions in the human brain using pluripotent stem cell models for neurodegeneration. *Cells* 8:299. doi: 10.3390/cells8040299

Suresh, R., and Diaz, R. J. (2021). The remodelling of actin composition as a hallmark of cancer. *Transl. Oncol.* 14:101051. doi: 10.1016/j.tranon.2021.101051

Teppola, H., Sarkanen, J. R., Jalonen, T. O., and Linne, M. L. (2016). Morphological differentiation towards neuronal phenotype of SH-SY5Y neuroblastoma cells by estradiol, retinoic acid and cholesterol. *Neurochem. Res.* 41, 731–747. doi: 10.1007/s11064-015-1743-6

Ul Islam, S., Shehzad, A., Kyung Sonn, J., and Sup Lee, Y. (2017). PRPF overexpression induces drug resistance through actin cytoskeleton rearrangement and epithelial-mesenchymal transition. *Oncotarget* 8:17855. doi: 10.18632/oncotarget.17855

Ullo, M. F., and Case, L. B. (2023). How cells sense and integrate information from different sources. *WIREs Mechan. Dis.* 15:e1604. doi: 10.1002/wsbm.1604

Venturelli, L., Kohler, A. C., Stupar, P., Villalba, M. I., Kalauzi, A., Radotic, K., et al. (2020). A perspective view on the nanomotion detection of living organisms and its features. *J. Mol. Recognit.* 33:e2849. doi: 10.1002/jmr.2849

Villalba, M. I., Venturelli, L., Willaert, R., Vela, M. E., Yantorno, O., Dietler, G., et al. (2021). Nanomotion spectroscopy as a new approach to characterize bacterial virulence. *Microorganisms* 9:1545. doi: 10.3390/microorganisms9081545

Wang, X., and Ha, T. (2013). Defining single molecular forces required to activate integrin and notch signaling. *Science* 340, 991–994. doi: 10.1126/science.1231041

Wehland, M., Ma, X., Braun, M., Hauslage, J., Hemmersbach, R., Bauer, J., et al. (2013). The Impact of altered gravity and vibration on endothelial cells during a parabolic flight. *Cellul. Physiol. Biochem.* 31, 432–451. doi: 10.1159/000343380

Wu, S., Liu, X., Zhou, X., Liang, X. M., Gao, D., Liu, H., et al. (2016). Quantification of cell viability and rapid screening anti-cancer drug utilizing nanomechanical fluctuation. *Biosens. Bioelectron.* 77, 164–173. doi: 10.1016/j.bios.2015.09.024

Wuest, S. L., Richard, S., Kopp, S., Grimm, D., and Egli, M. (2015). Simulated microgravity: critical review on the use of random positioning machines for mammalian cell culture. *Biomed Res. Int.* 2015:971474. doi: 10.1155/2015/971474

Yanes, B., and Rainero, E. (2022). The interplay between cell-extracellular matrix interaction and mitochondria dynamics in cancer. *Cancers* 14:1433. doi: 10.3390/cancers14061433

Zhou, J., Liao, C., Zou, M., Villalba, M. I., Xiong, C., Zhao, C., et al. (2024). An optical fiber-based nanomotion sensor for rapid antibiotic and antifungal susceptibility tests. *Nano Lett.* 24, 2980–2988. doi: 10.1021/acs.nanolett.3c03781

Zhou, J., Ruggeri, F. S., Zimmermann, M. R., Meisl, G., Longo, G., Sekatskii, S., et al. (2020). Effects of sedimentation, microgravity hydrodynamic mixing and air-water interface on α-synuclein amyloid formation. *Chem. Sci.* 11, 3687–3693. doi: 10.1039/D0SC00281J

Zou, M., Liao, C., Chen, Y., Xu, L., Tang, S., Xu, G., et al. (2023). 3D printed fiber-optic nanomechanical bioprobe. *Int. J. Extreme Manufact.* 5:015005. doi: 10.1088/2631-7990/acb741

Frontiers in
Cellular Neuroscience

Leading research in cellular mechanisms underlying brain function and development

Part of the world's most cited neuroscience journal series that advances our understanding of the cellular mechanisms underlying cell function in the nervous system across all species.

Discover the latest Research Topics

See more →

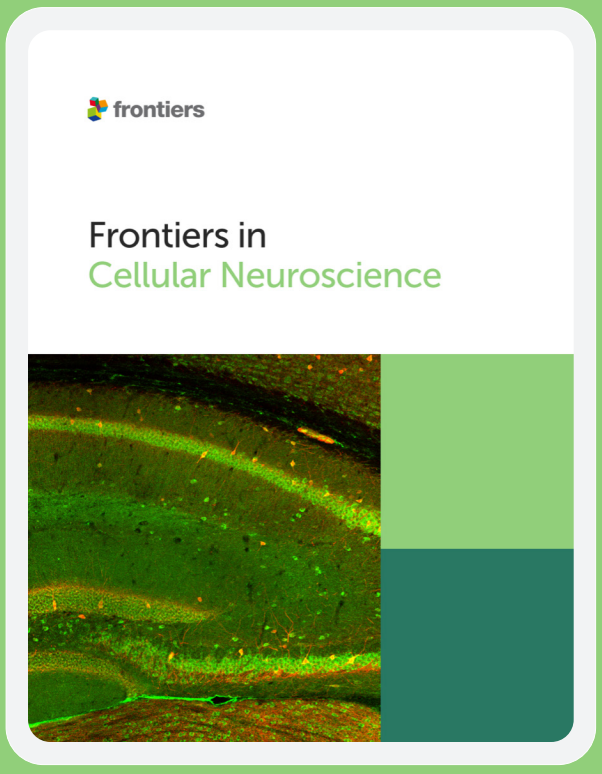

Frontiers

Avenue du Tribunal-Fédéral 34
1005 Lausanne, Switzerland
frontiersin.org

Contact us

+41 (0)21 510 17 00
frontiersin.org/about/contact